An Investigation of the Class C Chemokine Receptor and Ligand and their Potential Role in the Central Nervous System

Jordan Talbot

School of Clinical Dentistry

University of Sheffield

Submitted for the Degree of Doctor of Philosophy (PhD)

September 2018

Acknowledgements

Over the course of this PhD I have received great support from many people. First and foremost this has arisen from my two supervisors Professor Fiona Boissonade and Dr Richard Mead. This project has certainly provided a challenge, one which required the adoption of multiple lines of enquiry. I thank my supervisors for embracing my suggestions and encouraging my independent mode of inquiry whilst also maintaining my focus on the overall objectives. I have learned a great deal from this process. As is sometimes said, "it is the journey, not the destination that matters". This sentiment certainly rings dear when I reflect on this PhD.

There are many others for whom I wish to thank, a list which would require a chapter on its own. However, I would in particular like to thank the contributions of the Mead research group, those of past and present. Dr Jodie Stephenson was a joy to work with and provided a great deal of support and expertise at the start of this project. I would also like to thank Dr Matthew Stopford for his willingness to provide help and advice, as well as his own work to provide further insight to my research. To the rest of the 'Mead Team': it has been a pleasure.

I also wish to thank the tremendous technical assistance provided by Jason Heath and Brenka McCabe throughout my entire time working in the third floor research labs. They do a brilliant job in maintaining the labs for use of all students and staff within the School of Clinical Dentistry. Dr Gareth Richards and his students at the Mellanby Centre for Bone research have also provided excellent advice and technical assistance. In particular, thank you to Dr Paris Avgousto for being a brilliant mentor within the lab and introducing me to some new techniques that contributed greatly to my research.

Finally, a note should be made for my friends and family. They have always been a source of support and advice and are also the first to congratulate me for any of my academic endeavours. This is despite pronouncing their complete lack of understanding over "what it is I actually do" the minute that I begin talking science. Well, now it is written and complete you have no excuse to not understand. Copies will be available upon request!

Convention for protein and gene nomenclature

Gene names have been reported in italics and protein names referred to in standard font. Human proteins and genes are reported in uppercase; proteins and genes of mouse are reported with an uppercase first letter only. For example: XCR1, *XCR1* = protein and gene of human XCR1; Xcr1, *Xcr1* = protein and gene of mouse XCR1 homologue.

Abstract

Background: XCR1 represents the sole member of the class C chemokine receptor family. In humans, this receptor has two exclusive ligands – XCL1 and XCL2. This chemokine signalling axis demonstrates clear conservation of sequence, structure and function between mice and humans. However only a single ligand, Xcl1, exists in mice. In addition, a lack of clarity surrounds the molecular identity of the Xcr1 protein in mice. Recent evidence from a rat model of peripheral nerve injury has demonstrated the expression of Xcr1 within the CNS and suggests this chemokine signalling axis to contribute to the inflammatory response to central and peripheral nerve injury. Further examination of this chemokine signalling axis was sought to characterise the contribution of XCR1 and XCL1 to CNS function.

Aims and Objectives: 1) Determine the molecular identity of mRNA and protein produced by *Xcr1.* 2) Characterise the expression of Xcr1 and Xcl1 within the mouse CNS. 3) Determine the influence of a central inflammatory response on the gene and protein expression of Xcr1 and Xcl1 within the mouse CNS. 4) Attempt the identification of XCR1 presence within the spinal cord of humans in the context of health and disease.

Results: This project provides the first direct functional comparison of the two predicted Xcr1 isoforms and demonstrates higher β-arrestin recruitment to the Xcr1 protein produced from an open reading frame located entirely within exon 2. The expression of *Xcr1* and *Xcl1* was observed to be low within the CNS of NTg animals. However, an increase of *Xcl1* expression within the spinal cords of mice demonstrating prolific glial activation was observed, whilst the expression of *Xcr1* remained unchanged. Attempts to refine the cellular source of *Xcl1* expression identified a low expression of *Xcl1* within primary microglial preparations from NTg, SOD1-G93A and TDP-Q331K mice. The expression of *Xcl1* by these primary cell preparations was not influenced by LPS treatment. Detection of XCR1 within the spinal cord of humans by immunohistochemistry provides the first indication, to our knowledge, of XCR1 expression by glial cells of the white matter.

Conclusions: Further credence has been given to the molecular identity of mouse Xcr1 to arise exclusively from exon 2 of *Xcr1*. The identity of *Xcr1* mRNA however remains inconclusive. This has implications for future investigations of the expression of this chemokine receptor, as well as for the development of methodologies to achieve this. *Xcr1* and *Xcl1* expression is suggested to be low within the CNS of NTg animals. The increased expression of *Xcl1* is in accordance with this chemokine to contribute to a central inflammatory response, however this expression is not supported to arise from microglia. The presence of XCR1 within human spinal cord is indicated to localise to glial cells, however further investigation is required to confirm the cellular identity of this expression.

Table of Contents

List of Figures

List of Tables

Abbreviations

5' RACE	5' Rapid Amplification cDNA ends
ACKRs	Atypical Chemokine Receptors
AD	Alzheimer's Disease
ALS	Amyotrophic Lateral Sclerosis
APC	Antigen Presenting Cell
ATAC	Activation induced And Chemkokine-related molecule
BBB	Blood-Brain Barrier
C9-ALS/FTD	C9ORF72-related ALS/FTD
CA	Corpora Amylacea
cAB-Xcr1	Custom anti-mouse Xcr1 Antibody
CCI	Chronic Constriction Injury
cDC	classical Dendritic Cell
CHO	Chinese Hamster Ovary
CLN	Cervical Lymph Node
CNS	Central Nervous System
CSF	Cerebrospinal Fluid
Cy3	Cyanine Dye 3
DAB	Diaminobenzidine
DAPI	4',6-diamidino-2-phenylindole
DC	Dendritic Cell
DMEM	Dulbecco's Modfied Essential Medium
DMSO	Dimethyl Sulfoxide
EA	Enzyme Acceptor
EAE	Experimental Autoimmune Encephalomyelitis
ED	Enzyme Donor
EDTA	Ethylenediamineteraacetic acid
EFC	Enzyme Fragment Complementation
ELISA	Enzyme Linked Immunosorbant Assay
ER	Endoplasmic Reticulum
fALS	Familial ALS
FBS	Foetal Bovine Serum
FITC	Fluorescein isothiocyanate
FTD	FrontoTemporal Dementia

FUS	Fused in Sarcoma
gDNA	Genomic DNA
GFAP	Glial Fibrillary Acidic Protein
GFP	Green Fluorescent Protein
GM-CSF	Granulocye-Macrophage Colony Stimulating Factor
GPCR	G-protein Coupled Receptor
GRK	G-protein Receptor Kinase
HB9	Homeobox Protein 9
HBSS	Hanks Balanced Salt Solution
HIER	Heat Induced Epitope Retrieval
HIV-1	Human Immunodeficiency Virus-1
HRP	Horseradish Peroxidase
Iba-1	Ionised calcium binding adaptor molecule-1
IBM	Inclusion Body Myopathy
ICAM-1	Intercellular Adhesion Molecule-1
ISF	Interstitial Fluid
L-ARMS2	pCMV-Xcr1L-ARMS2-PK2
LCST	Lateral Corticospinal Tract
L-PK2	pCMV-Xcr1L-PK2
LPS	Lipopolysaccharide
mESC	murine Embryonic Stem Cell
MND	Motor Neuron Disease
MS	Multiple Sclerosis
mTECs	Thymic medullary Epithelial Cells
NGS	Normal Goat Serum
NK	Natural Killer
NSC34	Neuroblastoma Spinal Cord 34
NSCs	Neural Stem Cells
NTg	Non-Transgenic
OPC	Oligodendrocyte Precursor Cell
ORF	Open Reading Frame
PAG	Peri-Aqueductal Grey
PBS	Phosphate Buffered Saline
PCR	Polymerase Chain Reaction

PD	Parkinson's Disease
PFA	Paraformaldehyde
PNI	Peripheral Nerve Injury
qPCR	quantitative PCR
R_f	Relative Migration Distance
RT-PCR	Reverse Transcription-PCR
sALS	Sporadic ALS
SAP	Shrimp Alkaline Phosphatase
S-ARMS2	pCMV-Xcr1S-ARMS2-PK2
SBTB	Sheffield Brain Tissue Bank
SD	Standard Deviation
SDS-PAGE	Sodium Dodecyl Sulphate Polyacrylamide Gel Electrophoresis
SOD1	Cu^{2+}, Zn^{+}, Superoxide Dismutase
SOD1-G93A	SOD1 Glycine to Arginine substitution Amino Acid Position 93
S-PK2	pCMV-Xcr1S-PK2
T_{CM}	Central Memory T-cell
TDP-43	Transactive response DNA binding protein (Protein)
TDP-Q331K	TDP-43 Glutamine to Lysine substitution Amino Acid Position 331
TLR	Toll-Like Receptor
T_{Reg}	Regulatory T-cell
Vc	Subnucleus Caudalis of Trigeminal Nucleus
VCAM-1	Vascular Cell Adhesion Molecule-1
VCST	Ventral Corticospinal Tract

Chapter 1: An Overview of Chemokines and their Roles in the Central Nervous System

This PhD project has sought to investigate the potential expression and function of the Class C chemokine, XCL1, and the class C chemokine receptor, XCR1, in the health and disease of the central nervous system (CNS). To provide a complete background to the potential capacity for XCR1 and XCL1 to function in the CNS, the reader is first introduced to the characteristics of the chemokine superfamily and the existing evidence for those members documented to function within the CNS, in an effort to demonstrate the possible functions for which the studied chemokine signalling axis may be involved. Following this, the existing evidence of XCR1 and XCL1 is discussed and the aim of the project is proposed.

1.1 The Chemokine Superfamily

1.1.1 Chemokine classification and nomenclature

Chemokines (Chemotactic cytokines) are a superfamily of proteins which consists of 48 members within humans. The characteristic function of chemokines is to control cellular migration or arrest of receptor cells and, since the initial description of CXCL8 (Walz *et al.*, 1989; Holmes *et al.*, 1991; Murphy and Tiffany, 1991), represent one of the first molecular superfamilies in mammals to be documented to its entirety. The chemokine superfamily is divided in to four subfamilies- C, CC, CXC, CX_3C - based on the amino acid sequence that separates the first to the possible second cysteine residue of the N-terminal domain. Chemokines may contain up to four cysteine residues in total with the disulphide bond(s) that exists between these also contributing to a canonical 'chemokine fold' structure (Zlotnik and Yoshie, 2012)(Figure 1.1).

Chemokines may exist as secreted or membrane bound proteins (Cardona *et al.*, 2006) and undergo significant post-translational modifications that significantly influence their characteristics (Mortier *et al.*, 2011). Their chemotactic function relies upon interaction with their cognate receptor(s), a group of rhodopsin-like seven transmembrane proteins, although alternative roles for chemokines without receptor engagement have been demonstrated, such as antimicrobial activities (Nevins *et al.*, 2016). A total of 23 Chemokine Receptors have been identified with the majority of receptors exerting their function via a functional intracellular coupling with a trimeric G-protein. However, 5 of these receptors, designated as Atypical ChemoKine Receptors (ACKRs), do not induce any intracellular signalling following chemokine binding and instead act to scavenge extracellular chemokines and modulate their signalling capacity by the internalisation of bound ligand.

Chemokine receptors demonstrate a bias towards the class of chemokine to which they are activated by. The classification of chemokines and chemokine receptors is therefore based on the subgroup of chemokine to which they belong or bind to, with the addition of an 'L' or

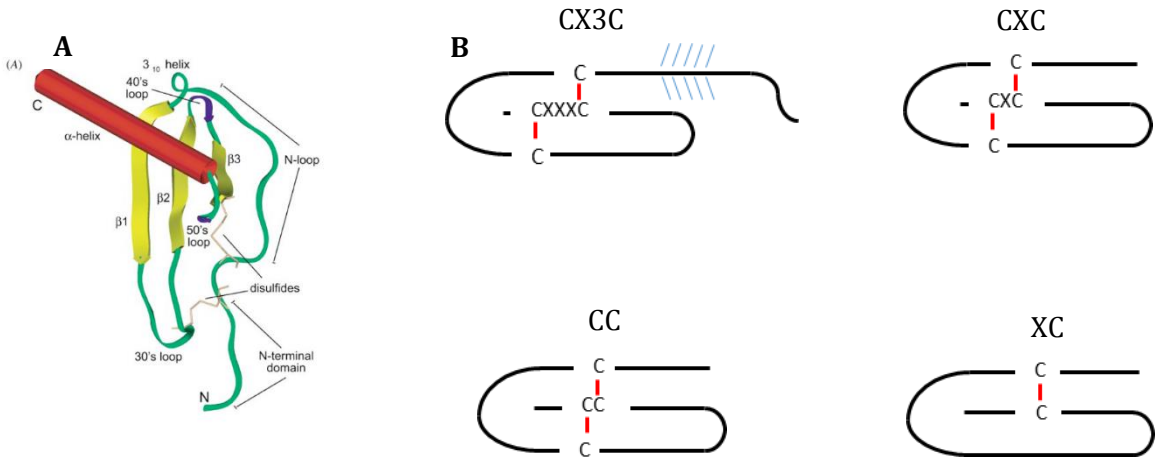

Figure 1.1 *Structural characteristics of Chemokines.* Images used with permission from (Fernandez and Lolis, 2002). The prototypical secondary structure of chemokines is represented by CXCL8 in (A). From N' to C' the protein is composed of; a disordered N-terminal domain which exhibits the least homology, of the chemokine domains, between individual chemokines and is attributed with endowing the chemokine with its respective chemokine receptor(s) affinity; a cysteine motif which is composed of one (XC) or two (CX3C, CXC, CC) cysteine residues. These cysteine residues are responsible for stabilising the chemokine structure via disulphide bridges formed with one (XC) or two (CX3C, CXC, CC) cysteine residues found towards the C-terminus of the protein (see (B)); an N-loop which runs between the N-terminal and the first β-sheet; a series of three interconnected anti-parallel β-sheets; and an α-helical domain at the C-terminus of the protein which overlies the β-sheet surface. (B) The differing number and position of cysteine residues within each chemokine subfamily is illustrated by a schematic overview. Note the mucin-stalk domain of the CX3C class which permits integration with the plasma membrane. XC chemokines contain only two cysteine residues and hence only have a single disulphide bridge. The tertiary and quaternary structure of these chemokines is thought to be stabilised by extensive glycosylation.

'R' suffix to denote 'Ligand' or 'Receptor', respectively. Due to their seemingly unorthodox lack of bias towards chemokine subfamilies and their lack of intracellular signalling activation following chemokine binding, ACKRs are excluded from this systematic nomenclature. Furthermore, this approach does not capture the qualities of chemokines that may have antagonistic effects on the receptor, a property of chemokines that appears to lack any congruent feature (Zlotnik and Yoshie, 2000; Zlotnik and Yoshie, 2012).

1.1.2 Functional classification of chemokines

An abundance of chemokine discovery occurred throughout the late 1980's and throughout the 1990's. These discoveries were biased towards chemokines that are highly expressed in activated leukocytes, due to the relatively high quantity of these transcripts allowing more reliable isolation and characterisation according to the available methods of the time. Early understanding was therefore dominated by evidence of chemokine contributions to the innate immune response and their capacity to induce cellular migration as a consequence of interaction with their respective chemokine receptor(s) during inflammatory states.

A second round of discovery of chemokine genes was achieved as a consequence of the development of more elaborate genetic databases. Subsequent investigation of these chemokines has since illuminated the capacity of some chemokines to function during homeostatic states, display more restricted receptor affinities and to have greater exclusivity to the tissue and cellular origin of expression (Zlotnik and Yoshie, 2000). Despite these differences, all chemokines consistently demonstrate the capacity to induce chemotaxis and as such have been referred to as 'master regulators' of cellular migration.

As a consequence of this divergence in observed function, chemokines have been functionally categorised as inflammatory, homeostatic and dual function. Dual function chemokines are an example of those which have recognised roles in both inflammation and homeostasis. Furthermore, additional subgroups of inflammatory chemokines have been proposed. Platelet and Plasma chemokines are those that require proteolytic cleavage for their activation in serum and/or are stored in the α-granules of platelets (Flad and Brandt, 2010; Nomiyama, Osada and Yoshie, 2010), typically acting as early mediators of the inflammatory response to vascular injury.

The recognition that chemokines can participate in homeostatic as well as inflammatory processes makes an important distinction which has aided the appreciation of the broader roles that chemokines occupy. However, this method of classification is considered operational and doesn't capture the elementary properties of individual chemokines. A further caveat is the promiscuous and redundant binding properties of chemokines that allow some chemokine

Chemokine Receptor	Ligand(s)	
	Agonist	Antagonist
CXC family		
CXCR1	CXCL6, CXCL7, CXCL8	
CXCR2	CXCL1, CXCL2, CXCL3, CXCL5, CXCL6, CXCL7, CXCL8	
CXCR3	CXCL4, CXCL9, CXCL10, CXCL11, CXCL13	CCL11
CXCR4	CXCL12	
CXCR5	CXCL13	
CXCR6	CXCL16	
CXCR7	CXCL11, CXCL12	
CC family		
CCR1	CCL3, CCL3L1, CCL5, CCL7, CCL8, CCL13, CCL14, CCL15, CCL16, CCL23	CCL26
CCR2	CCL2, CCL7, CCL8, CCL13, CCL16	CCL11, CCL26
CCR3	CCL3L1, CCL5, CCL7, CCL11, CCL13, CCL14, CCL15, CCL24, CCL26, CCL28	CXCL9, CXCL10, CXCL11, CCL18
CCR4	CCL17, CCL22	
CCR5	CCL3, CCL3L1, CCL4, CCL4L1, CCL5, CCL8, CCL11, CCL16	CCL7, CXCL11, CCL26
CCR6	CCL20	
CCR7	CCL19, CCL21	
CCR8	CCL1, CCL16	
CCR9	CCL25	
CCR10	CCL27, CCL28	
XC family		
XCR1	XCL1, XCL2	
CX3C family		
CX3CR1	CX3CL1, CCL26	
ACKRs		
CCBP2	CCL2, CCL3, CCL3L1, CCL4, CCL4L1, CCL5, CCL7, CCL8, CCL11, CCL13, CCL14, CCL17, CCL22, CCL23, CCL24	
CCRL1	CCL19, CCL21, CCL25, CXCL13	
CCRL2	CCL19	
DARC	CXCL1, CXCL2, CXCL3, CXCL7, CXCL8, CCL2, CCL5, CCL11, CCL13, CCL14, CCL17	

Table 1.1 *Human Chemokine Receptors and their ligands*. Ligands are colour coded according to their chromosomal location. This illustrates how agonists of individual chemokine receptors originate from the same chromosomal location. The affinity of 'atypical' chemokine receptors shows greater promiscuity to that of 'typical' chemokine receptors. This likely reflects greater functional redundancy. Table created from evidence presented in (Zlotnik, Yoshie and Nomiyama, 2006; Zlotnik and Yoshie, 2012; Nomiyama, Osada and Yoshie, 2013).

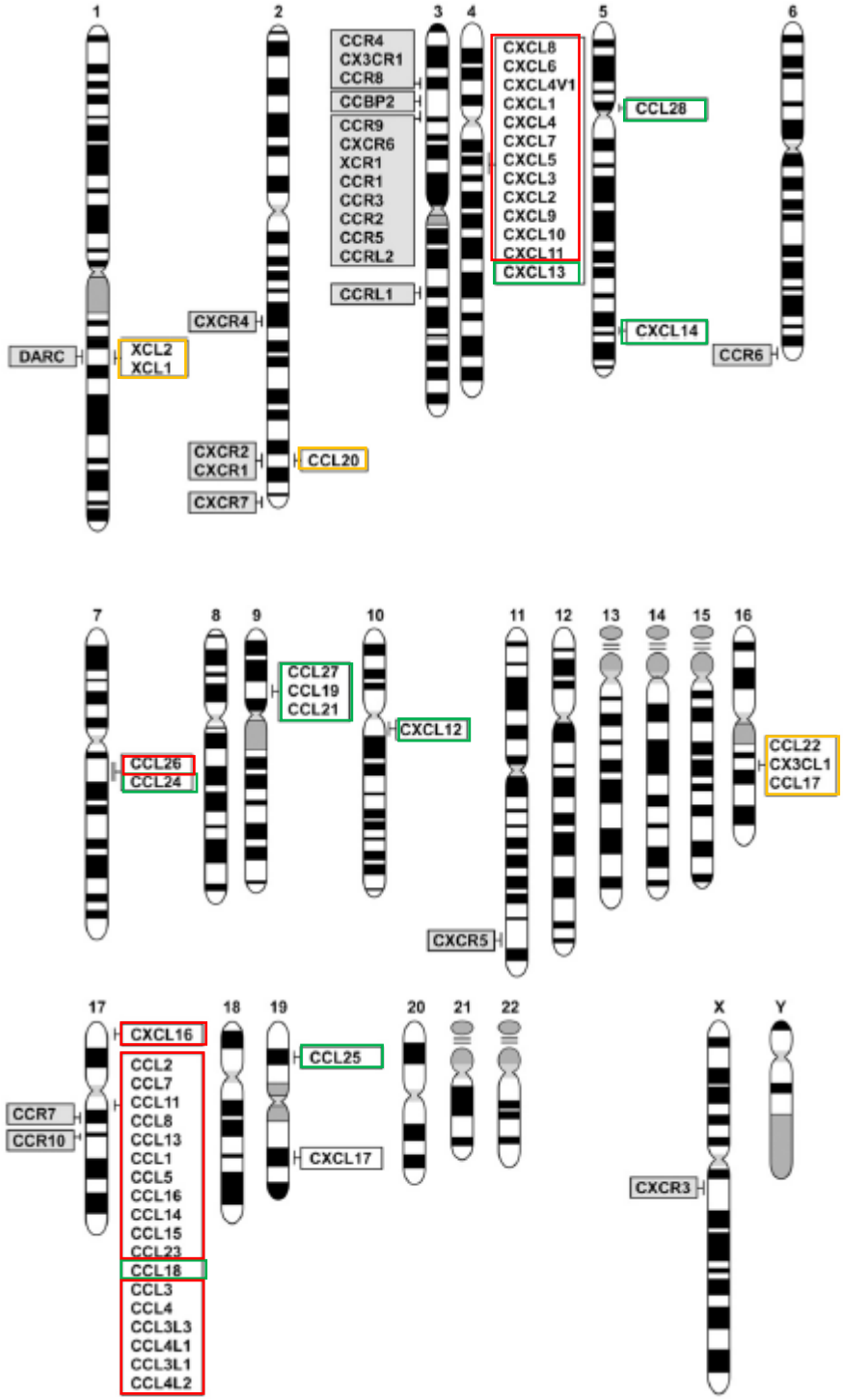

Figure 1.2 *Chromosomal mapping of Human Chemokines and Chemokine Receptors*. Chemokines are highlighted to indicate their functional category: Red = Inflammatory; Yellow = Dual Function; Green = Homeostatic. Note that all inflammatory chemokines are found as part of a cluster, whilst dual function and homeostatic chemokines are found in isolated genomic locations.

ligands to bind multiple chemokine receptors and some chemokine receptors to bind several chemokine ligands. This can lead to oversimplification of individual chemokines based on their grouping with other chemokines that bind that receptor, particularly when evaluating chemokine function by the use of heterologous expression systems *in vitro*.

A milestone in understanding the fundamental bases to chemokine function has been to take an evolutionary approach to the conceptualisation of chemokine function. This approach has rationalised the understanding of this superfamily by identifying molecular characteristics of individual chemokines according to their phylogeny. Table 1.1 and Figure 1.2 illustrate how the genomic mapping of human chemokines has identified traits that correspond with the observed affinity to chemokine receptors. Chemokines that reside close to one another in a genomic context have similar receptor targets and hence have related functions, whilst those identified in isolated genomic regions have more specific receptor affinities and hence have more restricted functional roles. Moreover, those which reside as clusters are most likely to participate in inflammatory roles whilst those which exist in isolation are most likely to perform homeostatic or dual function roles (Nomiyama, Osada and Yoshie, 2013; Zlotnik, Yoshie and Nomiyama, 2006; Zlotnik and Yoshie, 2012). Thus, the genetic properties of an individual chemokine in tandem with their physical homology to other chemokines can strongly inform their likely function.

1.2 Chemokines and the Central Nervous System

Chemokine research has centred on their role within the immune system. However, there is now substantial evidence that demonstrates the capacity of chemokines to function within the nervous system and, although their defining function, this is not just as mediators of cellular migration. Chemokines have now been described to be expressed by neurons, astrocytes, microglia and oligodendrocytes. Perhaps most importantly, several of these chemokines are expressed constitutively and perform homeostatic functions, indicating essential roles within the CNS. This is in addition to the more expected function in mediating immunological recruitment to sites of inflammation.

1.2.1 Immunological privilege of the CNS parenchyma

Under physiologic conditions the CNS parenchyma is immunologically privileged. This is characterised by a low presence of peripheral immune cells within the tissue, a feature that is most strongly associated with the presence of the blood-brain barrier (BBB) that surrounds the majority of CNS capillaries that serve the brain and spinal cord. Immune cells are, however, found in specific regions of the CNS in which the permeability of vessels supplying blood and cerebrospinal fluid (CSF) is reduced or compromised. This includes (i) fenestrated blood vessels of the

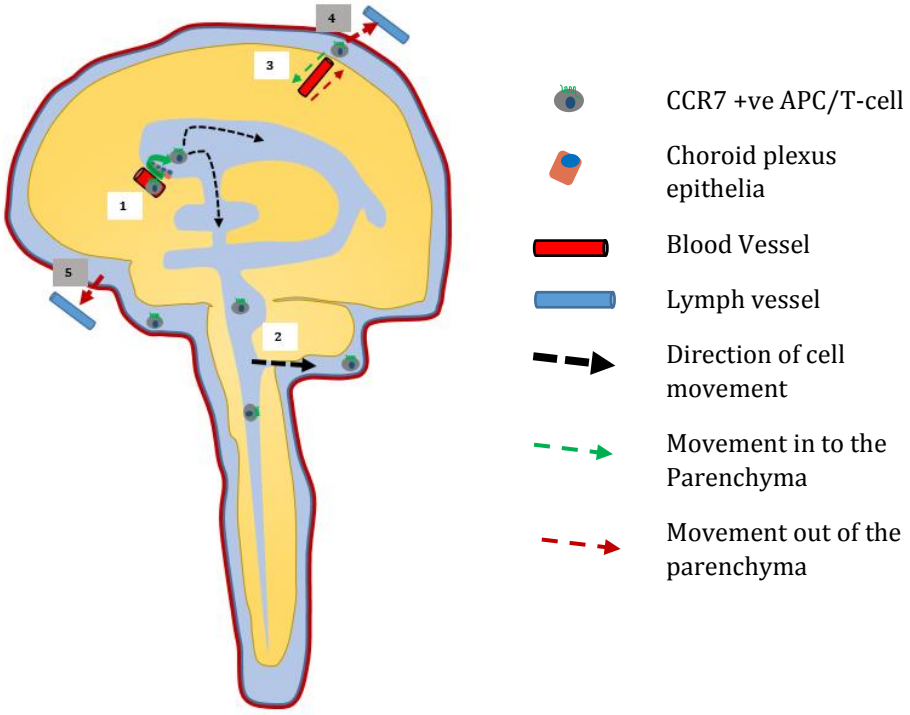

Figure 1.3. *Schematic overview of Antigen Presenting Cell (APC) and T-cell circulation within the CSF.* 1) Entry to the CSF is suggested to occur via chemotactic gradients established by choroid plexus epithelia which permit the transmigration of immune cells from the underlying capillary in to the CSF. 2) Within the CSF, immune cells are able to circulate within the ventricles of the brain and throughout the spinal cord central canal. The presence of small openings (foramina) within the fourth ventricle permit the movement of cells in to the subarachnoid space that surrounds the brain and spinal cord. 3) The turnover of perivascular immune cells within specific 'Virchow-Robin' spaces enables the constant surveillance of CSF antigen. 4, 5) Immune cells home to the lymphoid network following the entrance in to lymphatic vessels within the dura matter (4) and along peri-neural lymph vessels that exit the cranium via the cribiform plate (5). Chemokine signalling via CCR7 appears to be particularly important for the circulation of immune cells within the CNS. The chemokine ligands CCL21 and CCL19 are indicated to be make essential contributions to the migration of CCR7-positive cells due to their enrichment within specific CSF and lymph entry points (see text for details).

choroid plexus; (ii) Virchow-Robin spaces - a perivascular niche that surrounds some meningeal arteries that infiltrate the CNS brain parenchyma (a component of the "glymphatic" system (Ma *et al.*, 2017)); and (iii) post-capillary venules (Ousman and Kubes, 2012). In all three of these regions, without the presence of inflammation, peripheral immune cells are maintained in perivascular spaces which provide a cellular niche for co-ordinating immune surveillance or activation (Abbott *et al.*, 2010; Williams *et al.*, 2014). Importantly there is a broad distinction in the presence of immune cells between the two main fluid compartments of the CNS: the CSF and the interstitial fluid (ISF). This results from the intricate passage of these fluids at specific gateways to the CNS parenchyma as well as the distinct access that they each have to recirculating lymph (Figure 1.3). CSF is separated from the brain and spinal cord parenchyma by the pial membrane and contains circulating T-lymphocytes and also Dendritic Cells (DCs). These immune cells are recycled via lymphatic drainage, in particular via the newly discovered lymphatic network within the dura matter (Louveau *et al.*, 2015; Absinta *et al.*, 2017) and via perineural routes from the olfactory bulb to the nasal lymphatics (Engelhardt *et al.*, 2016; Louyeau, Harris and Kipnis, 2015). A small percentage of CSF may be exchanged with ISF at paravascular gateways to the CNS parenchyma (Abbott *et al.*, 2010; Ma *et al.*, 2017).

The constitutive presence of immune cells within the CSF permits the surveillance of antigens within the cranial and vertebral cavities, fulfilling the previously proposed function of a surrounding 'lymph' of CNS tissue (Ransohoff, Kivisakk and Kidd, 2003). The growing evidence of this more extensive immunological function has made it more recognised now than ever before that the immune privilege of the CNS is not absolute but is instead strategically and intricately controlled.

1.2.2 Chemokine contribution to immunological coordination within the CNS

Chemokines make an essential contributions to the control of immune cell migration in all vascular regions of the CNS during both homeostatic and inflammatory conditions. In the absence of inflammation, localised chemokine expression is associated with recruitment and turnover of leukocytes within the perivascular and leptomeningeal spaces containing immune cells (Ousman and Kubes, 2012; Engelhardt *et al.*, 2016; Louyeau, Harris and Kipnis, 2015; Absinta *et al.*, 2017).

One of the most prominent chemokine signalling axis for controlling immune cell surveillance of the CNS is the CCL19/CCL21/CCR7 signalling axis. It is now demonstrated that within the CNS the expression of CCR7 is essential to direct the migration of central memory T-lymphocytes (T_{CM}) and DCs from the entry point of the CSF at choroid plexus epithelia, through the leptomeningeal spaces that surround the brain and spinal cord and facilitate their return to circulating lymph via nasal and dural lymphatics (Figure 1.3)

(Absinta *et al.*, 2017; Kida, Pantazis and Weller, 1993). CCR7 therefore permits the surveillance of CNS antigen within the CSF and allows the homing of activated DCs through the chemotactic gradients established by CCL21 and CCL19 within lymphatic vessels (Absinta *et al.*, 2017; Clarkson *et al.*, 2017) as has been described for the function of CCR7 in the periphery (Forster, Davalos-Misslitz and Rot, 2008). The subsequent circulation to cervical lymph nodes (CLNs) of T_{CM} and DCs is essential for the presentation of antigen and to facilitate appropriate immune responses. CCL19 also allows the physiologic recruitment and retention of CCR7+ immune cells at the level of post-capillary venules, one of the key sites for immune cell retention within the CNS (Ousman and Kubes, 2012; Williams *et al.*, 2014).

In contrast to migratory surveillance of antigen within the fluid compartment of the CNS, the CCL2/CCR2 signalling axis has been shown to be essential for maintaining homeostatic populations of perivascular macrophages (Schilling *et al.*, 2009). Under physiological conditions, there is a constant turnover of macrophages between the blood and the perivascular regions of CNS blood vessels (Bechmann *et al.*, 2001). The CCL2-CCR2 axis also has a well characterised role in the recruitment of monocytes and macrophages during inflammatory conditions to the CNS (Conductier *et al.*, 2010). CCR2 is responsible for the migration of a specific population of peripheral Ly6-C^{high} monocytes in to the brain parenchyma via the chemotactic gradient established by CCL2. The CCL2-CCR2 axis therefore contributes to the physiological turnover of perivascular macrophages as well being an essential inflammatory mediator that permits entrance of peripheral monocytes in to the CNS parenchyma, functions which are determined by the source and level of its expression (Stowe *et al.*, 2012; Reaux-Le Goazigo *et al.*, 2013).

CXCL12 also exerts control of immune cell migration within the CNS. One of the receptors for CXCL12, CXCR7, is an ACKR that regulates the turnover and polarity of CXCL12 expression (Cruz-Orengo *et al.*, 2011). At the BBB, CXCL12 is associated with maintaining the localisation of CXCR4+ leukocytes at a perivascular location due to its abluminal expression by brain microvasculature endothelial cells (BMEC's) (McCandless *et al.*, 2006). However, in response to pro-inflammatory cytokines, CXCL12 is internalised by CXCR7 and redistributed to the luminal surface of BMEC's. Consequently, the loss of abluminal CXCL12 disrupts perivascular leukocyte retention and promotes CXCR4+ leukocyte extravasation and infiltration, a phenomenon observed in post-mortem examination of patients with Multiple sclerosis (MS) and in the murine model of MS, Experimental Autoimmune Encephalomyelitis (EAE) (Cruz-Orengo *et al.*, 2011; McCandless *et al.*, 2008). Therefore, as well as increasing inflammatory chemokine expression, subtle changes in the expression and distribution of homeostatic chemokines can also make

A

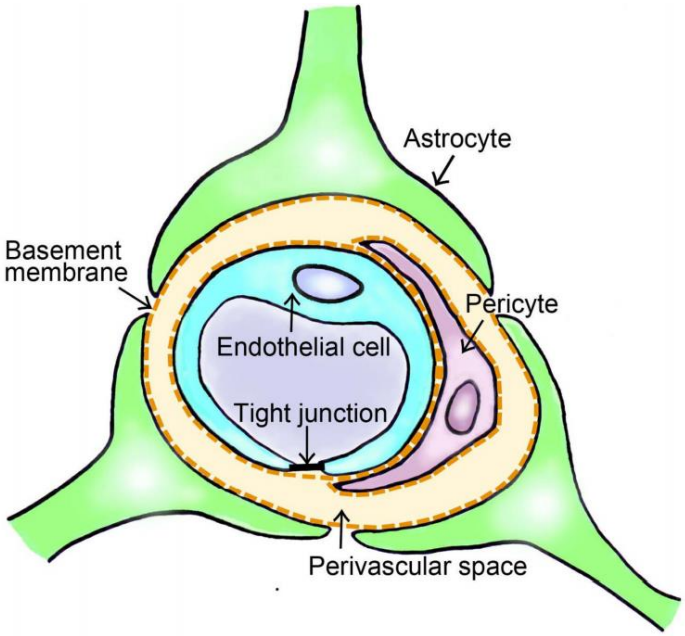

B

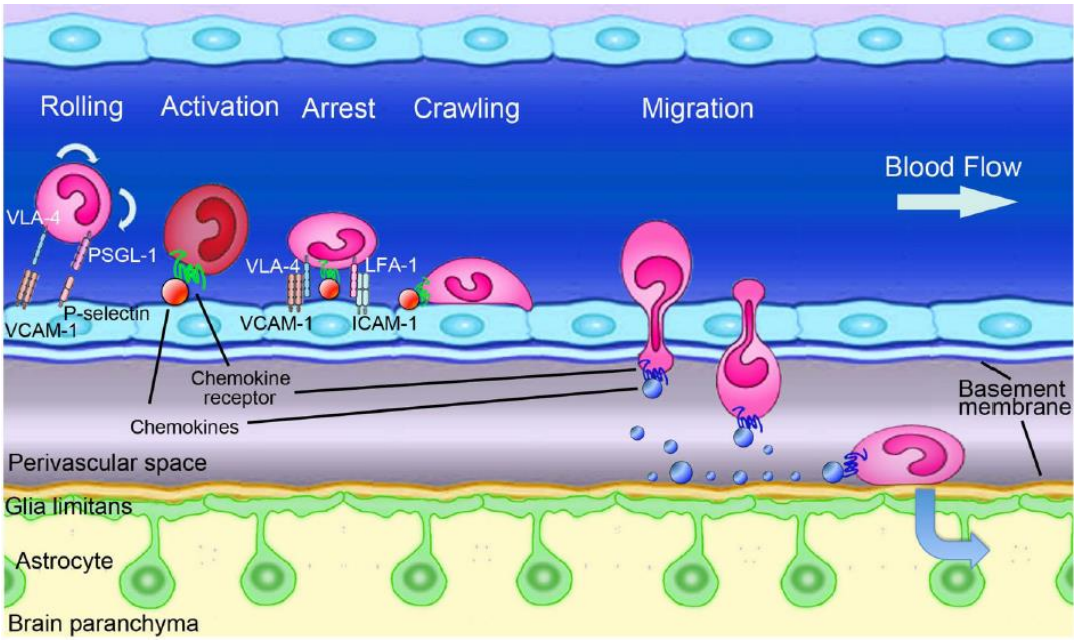

Figure 1.4 *The Blood-Brain Barrier and leukocyte migration*. Images sourced with permission from (Takeshita and Ransohoff, 2012). (A) The abluminal side of the CNS microvasculature is encapsulated by the endothelial basement membrane in which pericyte cells reside. Pericyte secretory factors such as TGF-β inhibit endothelial cell activation and disruption to tight junction formation. More distal from the abluminal surface to this are astrocytic endfeet, defining the glia limitans and the parenchymal aspect of the perivascular space. These processes extend from astrocytes and encapsulate the vessel structure providing trophic factors which are essential for the development and maintenance of BBB integrity. (B) Extravasation of leukocytes involves 5 steps: rolling, activation, arrest, crawling and migration. Chemokines expressed on the endothelial surface stimulate activation and arrest of leukocytes, facilitating subsequent para- or trans-cellular migration.

significant contributions to the inflammatory state of the CNS. In response to inflammation, chemokines provide directional chemotactic gradients which are essential for the extravasation and migration of leukocytes to sites of injury or infection. In comparison to peripheral and lymphoid vasculature, there is little known about the exact expression patterns and identities of chemokine expression within the CNS microvasculature, particularly for inflammatory chemokines (Holman, Klein and Ransohoff, 2011). Although the stages of leukocyte migration through the vascular wall has been well documented (figure 1.4) the direct relevance of this to leukocyte migration in the CNS is unclear due to a lack of in vitro models capable of replicating BBB physiology and allowing more in depth characterisation (Takeshita and Ransohoff, 2012). However, it has been observed that several chemokines expressed by activated endothelial cells, including CXCL12, CCL11 and CCL21, are capable of inducing integrin activation of rolling leukocytes via interaction with their cognate receptors. This facilitates interaction with endothelial cell adhesion molecules, such as intercellular adhesion molecule-1 (ICAM1) and vascular cell adhesion molecule-1 (VCAM-1), and promotes the strong adhesion of leukocytes to the endothelial surface that is necessary for subsequent transmigration in to the perivascular space (Laudanna *et al.*, 2002; Engelhardt, 2006). In addition to their luminal expression, transcellular and perivascular chemokine localisation is ideally situated for providing haptotactic guidance for this extravasation (Holman, Klein and Ransohoff, 2011). Indeed, the release of inflammatory chemokines by resident glial cells of the CNS is strongly implicated in establishing a chemotactic gradient for leukocyte recruitment (Babcock *et al.*, 2003). Chemokines can also promote extravasation by inducing the degradation of tight junction proteins and increasing BBB permeability (Stamatovic *et al.*, 2006; Stamatovic *et al.*, 2009).

CX3CL1 and its receptor CX3CR1 exemplify an additional mode by which chemokines influence immunological activity within the CNS. Within the CNS, CX3CL1 is expressed predominantly by neurons whereas CX3CR1 is expressed almost exclusively by microglia (Cardona *et al.*, 2006; Clark and Malcangio, 2012). As the resident macrophage of the CNS, microglia sample the extracellular environment of the CNS parenchyma and exhibit rapid activation in response to inflammatory stimuli. However, under physiological conditions microglia are maintained in a resting state, a phenotype which is strongly influenced by CX3CL1 release from neurons (Cardona *et al.*, 2006). Although the mechanism for this remains unclear, the CX3CL1-CX3CR1 signalling axis is an essential mediator for regulating microglial neurotoxicity and provides an additional example of how chemokines contribute to immune functions within the CNS. Importantly, it provides an example of chemokines acting independently of the peripheral immune system.

1.2.3 Chemokines and CNS Development

Chemokines and their receptors are expressed throughout development and maturity within the CNS. Their expression is highly regionalised, often exclusive to specific cell types and, in tandem with their capacity to modulate cellular migration, it is perhaps unsurprising that chemokines are strongly implicated in cellular patterning and morphogenesis of the CNS.

The CXCL12-CXCR4 is currently believed to be the ancestral chemokine signalling axis (Nomiyama, Osada and Yoshie, 2010) and has the earliest expression of any chemokine during embryogenesis. Genetic knockout of either CXCL12 or CXCR4 leads to perinatal death (Ma *et al.*, 1998) and causes abnormalities of neuronal positioning within the cerebellum, dentate gyrus, trigeminal ganglia, dorsal root ganglia and cortical interneurons as well as deviation of axonal projections from spinal motor neurons (Lazarini *et al.*, 2003; Ransohoff, 2009; Bajetto *et al.*, 2001). During adulthood, CXCL12 expression in the granule cell layer of the dentate gyrus maintains proliferation of neural progenitor cells and guides their migration for subsequent differentiation in to mature granule neurons (Schultheiss *et al.*, 2013). Furthermore, CXCL12 expression within the vascular plexus and by ependymal cells is essential for the homing of CXCR4+ Neural Stem Cells (NSCs) to the neurogenic niche that surrounds the subventricular zone of rodents (Kokovay *et al.*, 2010), a function analogous to the role of CXCL12-CXCR4 in the homing and colonisation of the bone marrow by hematopoietic stem cells (Sugiyama *et al.*, 2006). Indeed, chemotactic guidance of NSCs by CXCL12 is a component of the neurovascular niche that contributes to functional recovery following cerebral ischemia (Ohab *et al.*, 2006; Robin *et al.*, 2006).

Chemokines are also indicated to coordinate synapse remodelling during development. In the cerebellum, cells including microglia, Bergmann glia, astrocytes and neighbouring neurons all transiently express peak levels of CCR1 at independent time points during which they each show close interaction with CCL3-expressing purkinje cells, suggesting a functional role in the extensive elaboration of purkinje-cell connectivity (Cowell and Silverstein, 2003). CX3CL1 and CX3CR1 are also implicated in homeostatic synaptic pruning within the mature hippocampus by facilitating microglial-neuronal interaction. This may also be contributed to by modulatory effects of CX3CR1 signalling on synaptic activity and Long Term Potentiation (Murphy, 2013).

Chemokine signalling also contributes to glial development. During the formation of presumptive white matter, the expression of CXCL1 by white matter astrocytes provides a chemotactic and proliferative cue for oligodendrocyte precursor cells (OPCs) via CXCR2 (Tsai *et al.*, 2002). *In vitro* characterisation has extended the involvement of other CXC

chemokines in oligodendrocyte development, with CXCL12 and CXCL8 displaying the capacity to induce proliferation and differentiation of rat OPCs (Kadi *et al.*, 2006).

Thus, although maintaining the central function of guiding chemotaxis, chemokine signalling provides migrational cues that contribute to the maintenance of essential processes for CNS development, maturation and regeneration following injury. This is a result of the divergent targets downstream of chemokine receptor binding and G-protein activation which can simultaneously promote cellular migration and cellular survival, for example. The presence of additional external mediators which signal via convergent downstream signalling cascades to chemokine receptors will therefore also influence the outcome of chemokine signalling. An example of this is given by the role of chemokines in activity dependent neuromodulation, discussed below.

1.2.4 Neuromodulatory functions of chemokines

The identification of chemokine and chemokine receptor expression by neurons and their localisation to nerve terminals and synaptic vesicles prompted an altogether different perspective on chemokine function (Rostene, Kitabgi and Melik-Parsadaniantz, 2007). Several chemokines, including CCL2 (Gosselin *et al.*, 2005), CXCL12 (Banisadr *et al.*, 2003), CX3CL1 (Ragozzino *et al.*, 2006), CCL21 (de Jong *et al.*, 2005) and CXCL8 (Puma *et al.*, 2001), have demonstrated characteristics that are consistent with chemokines performing neuromodulatory functions (Figure 1.5).

The concept of neuromodulation centres on the capacity of an agent to modulate neuronal sensitivity as a consequence of altering the permeability of neuronal membranes (both internal and external membranes) to ionic flux. Neuromodulators can act at synaptic or extra-synaptic locations and, as a general summary of action, influence the thresholds required for a neuron to generate an action potential or release presynaptic vesicles (Nadim and Bucher, 2014).

As a distinct subfamily of G-Protein Coupled Receptors (GPCRs), chemokine receptors are capable of influencing cellular properties that are consistent with affecting neuronal activity. Indeed, their specific anatomical distribution within the CNS, amongst other characteristics discussed below, have led some to speculate chemokines and their receptors to represent the third major signalling system of the CNS, after neurotransmitters and neuropeptides (Adler and Rogers, 2005).

An important feature to this evidence of neuromodulation is the consistent colocalisation of individual chemokines to neuronal populations with distinct neurochemical phenotypes, in particular the association with neuronal populations and networks that are associated with diffuse neuromodulation. Immunohistochemical detection has found CXCL12 to localise to

A

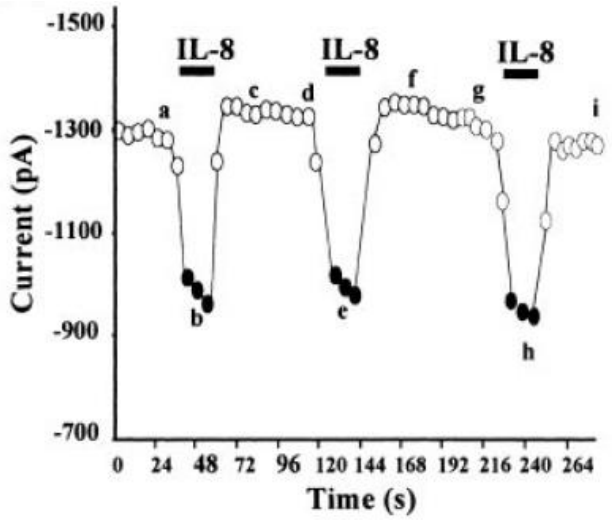

B

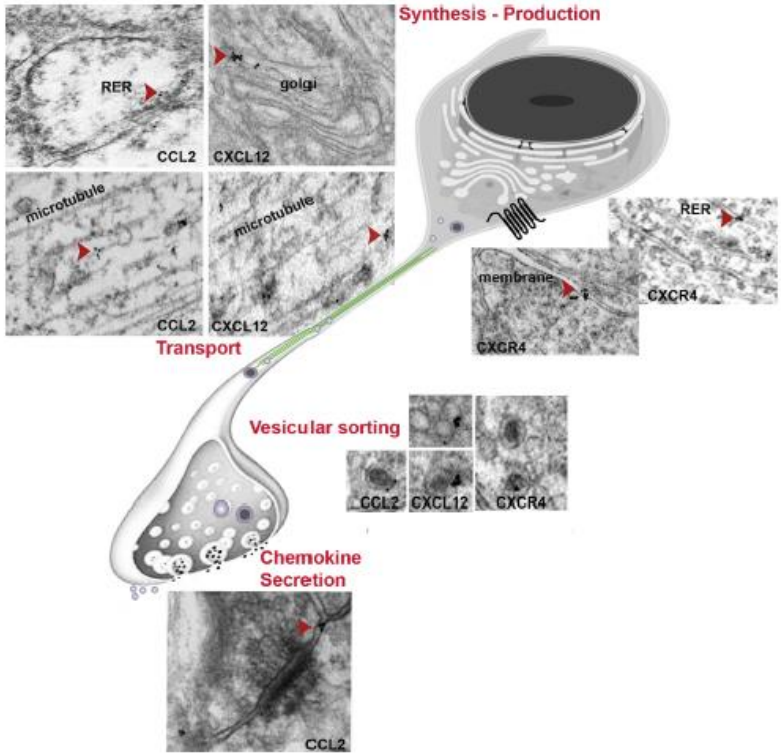

Figure 1.5. *Chemokines as Neuromodulators.* A) Plot of whole cell recordings from septal cholinergic neuron illustrating modulation of Ca^{2+} current by IL-8 (CXCL8). Image used with permission from (Puma *et al.*, 2001). Before (a), during (b) and after (c) application of 10mM IL-8 clearly shows reversible modulation of Ca^{2+} currents. Inhibition of Ca^{2+} currents by IL-8 was found to be mediated by closure of N- and L-type Ca^{2+} channels, due to reduced inhibition following application of nimodipine and ω-CgTX-GVIA, respectively. Furthermore, inhibition of Ca^{2+} currents was sensitive to application of $G_{i/o}$ inhibitor, NEM, demonstrating a G-protein-dependant mechanism of IL-8-mediated Ca^{2+} current inhibition. B) Subcellular localisation of CCL2, CXCL12 and CXCR4. Electron micrograph shows synthesis, microtubule transport and loading in to large dense-core vesicles, within the synaptic bouton, of both chemokines and the chemokine receptor. Image used with permission from (Reaux-Le Goazigo *et al.*, 2013).

dopaminergic, cholinergic and vasopressinergic neurons (Banisadr *et al.*, 2003), whilst CCL2 and it's receptor CCR2 have been localised to cholinergic and dopaminergic neurons (Banisadr *et al.*, 2005). Furthermore, administration of both CXCL12 and CCL2 to the dorsal striatum is capable of increasing dopamine release and promoting circling behaviour in rats (Skrzydelski *et al.*, 2007; Guyon *et al.*, 2009). CCR2 is also expressed throughout the spinal cord, particularly within the dorsal horn. Signalling via this receptor is strongly implicated in the development of pain following acute and chronic insult (Abbadie *et al.*, 2003) as a result of reducing GABA-mediated currents in spinal neurons by CCL2-induced CCR2 and $GABA_A$ receptor interaction (Gosselin *et al.*, 2005). Chemokines are also able to modulate neuronal activity by influencing the composition of post-synaptic receptors (Ragozzino *et al.*, 2006) (Nicolai *et al.*, 2010). Perhaps most importantly of all, both CXCL12 and CCL2 are demonstrated to be present within large dense-core vesicles of neuronal synapses (Jung *et al.*, 2008) (Callewaere *et al.*, 2008). This localisation is characteristic of molecules, such as neuropeptides, that act in a modulatory capacity and supports the capacity of these chemokines to act as neuromodulators.

The neuromodulatory capacity of chemokines, using such diverse mechanisms, highlights the numerous intracellular pathways that chemokines may exploit to exert their function. This is an important consideration to be made when evaluating experimental evidence of chemokine function. *In vitro* expression systems, for example, may utilise cellular models which do not include the intracellular substrate which these signalling systems would normally target *in vivo*.

1.3 Chemokine Expression and CNS Disease

Neuroinflammation is characterised by activation of glial cells, recruitment of leukocytes and the release of inflammatory mediators and is a common component of CNS pathology. Given the role of chemokines in many of these processes they are therefore implicated in the pathophysiology of disease and trauma of the CNS.

1.3.1 Chemokines and Pain

The development of pain is a cardinal feature of inflammation. Inflammation of the CNS can ensue as a result of direct injury or disease of the organ or as a consequence of peripheral nerve damage also. It is now recognised that activation of central glial cells, particularly microglia, is a key contributor for the development of chronic pain following central and peripheral nerve injury (PNI) (Watkins, Milligan and Maier, 2001). As essential signalling peptides, chemokines including CX3CL1, CXCL1, CCL2, CCL21 and CCL7 have been shown to contribute to this process (Ji, Xu and Gao, 2014). CX3CR1 expression is upregulated in chronic pain conditions (Verge *et al.*, 2004) and likely responds to increased CX3CL1

signalling as a consequence of cleavage of this chemokine from the membrane of injured neurons. Activation of CX3CR1 in spinal microglia is associated with activation of p38 MAPK signalling which likely drives neuropathic pain symptoms through the increased release of pro-inflammatory mediators such as IL-1b and TNF-a that can directly lead to hyperexcitability of surrounding neurons (Zhuang *et al.*, 2007; Kawasaki *et al.*, 2008). This is supported by the observed analgesic effect of CX3CR1 antibody administration that is capable of reducing mechanical allodynia in models of neuropathic pain (Zhuang *et al.*, 2007). The evidence for a role of CCL21 is similar in nature, indicating that neuronal release of CCL21 following PNI upregulates P2X4 expression in microglia. The absence or block of CCL21 signalling abrogates tactile allodynia, with concomitant reduction of microglial P2X4 expression (Biber *et al.*, 2011) suggesting a causal link between neuronal CCL21 release, microglial P2X4 expression and the development of neuropathic pain.

An alternative mechanism by which chemokines may modulate sensitivity to pain relates to their capacity as neuromodulators. Descending activity of opioid-sensitive neurons of the peri-aqueductal grey matter (PAG) is associated with the analgesic effects of opioid compounds which are able to suppress ascending activity of peripheral nociceptive afferents. Within the PAG it has been shown that the administration of chemokines CXCL12, CX_3CL1 or CCL5 prior to the administration of opioids was sufficient to diminish the anti-nociceptive activity of such compounds (Szabo *et al.*, 2002; Chen *et al.*, 2007; Heinisch, Palma and Kirby, 2011). This inhibition of the anti-nociceptive effect by chemokines is associated with the activity of their receptors, which are each expressed within the PAG, to inhibit opioid receptors following ligand activation by heterologous desensitisation. CXCR4 and CCR5 have both been shown to cross-desensitise opioid receptors via targeted phosphorylation of GPCRs by downstream protein kinases or by the formation of GPCR heterodimers (Szabo *et al.*, 2002; Chen *et al.*, 2004). Therefore the coexpression of chemokine receptors, including CCR5, CXCR4 and CX_3CR1, with opioid receptors by neurons within the PAG underlie the capability of CCL5, CX_3CL1 and CXCL12 to inhibit the anti-nociceptive capacity of descending opioid-sensitive neurons.

Chemokine release by astrocytes also contributes to chronic pain symptoms. Following spinal nerve ligation (SNL) the expression of CCL2 was observed to be increased in astrocytes and application of CCL2 to ex-vivo spinal cord slices potentiated glutamatergic currents in lamina II neurons that express CCR2 (Gao *et al.*, 2009). In addition, transgenic mouse models that overexpress CCL2, specifically within astrocytes, display hypersensitive nociception (Menetski *et al.*, 2007) strongly indicating a role for CCL2-mediated neuromodulation underlying behavioural symptoms of chronic pain. Increases in CXCL1 and CXCR2 expression in astrocytes and dorsal horn neurons, respectively, is also observed

following spinal nerve ligation. Blocking either ligand or receptor with specific antibodies is capable of attenuating behavioural symptoms of neuropathic pain (Zhang *et al.*, 2013) lending further credence to the role of chemokine cross-talk between astrocytes and neurons as important mediators in the development of chronic pain.

Another important aspect of the contribution of chemokines to the development of pain, is the recruitment of peripheral immune cells following central or peripheral nerve injury. Like surrounding glia in the CNS, the release of pro-inflammatory mediators by activated immune cells heighten neuronal excitability, increasing afferent nociceptive input that facilitate plastic changes within the local synaptic environment of the dorsal horn. Both of these consequences are key mechanisms of central sensitisation that is intimately linked to the development of chronic neuropathic pain (Latremoliere and Woolf, 2009; Ren and Dubner, 2010).

Chemokines can therefore directly contribute to acute and chronic pain symptoms by modulating the activity of neurons in multiple domains of the CNS that are responsible for the transmission and integration of nociceptive sensory information. This includes primary afferent terminals of the dorsal horn and supraspinal centres such as the PAG. Additionally, chemokines can indirectly contribute to neuronal sensitisation by facilitating the recruitment and activation of glial and immune cells following peripheral and central nerve injury that can further perpetuate inflammatory signals that heighten neuronal sensitivity. The breadth of mechanisms by which chemokines and their receptors can modulate neuronal sensitivities is therefore wide and reflects their activity to not only contribute to immunological function during disease, but to also facilitate adaptive behaviours by providing a neurophysiological substrate within specific CNS domains.

1.3.2 Chemokines and Neurodegenerative Disease

Many of the functions of chemokines that contribute to neurodegenerative disease have been eluded to throughout this review. Most prominently, chemokines are implicated in almost all neurodegenerative diseases due to the important neuroinflammatory component of these disorders.

MS is an autoimmune disorder characterised by chronic inflammation and lesions of neuronal white matter that is associated with demyelination of axonal tracts (Hoglund and Maghazachi, 2014). Within the inflammatory lesions are substantial numbers of peripheral lymphocytes and macrophages as well as activated microglia and astrocytes. Numerous inflammatory chemokines have therefore been implicated in the pathogenesis of the disease by contributing to the recruitment and activation of these cells. The expression of CCL2, as seen following peripheral and central nerve injury, is again localised to hypertrophic

astrocytes that surround demyelinating lesions (Simpson *et al.*, 1998) and probably represents the most important chemotactic mediator for the recruitment of peripheral monocytes in MS (Bose and Cho, 2013).

In contrast to promoting the migration of immune cells, other astrocyte-derived chemokines may contribute to the pathogenesis of MS by inhibiting the migration of oligodendrocytes. Around the edge of white matter lesions, oligodendrocytes expressing CXCR2 are found in close apposition to astrocytes expressing CXCL1. This signalling axis is known to promote proliferation of oligodendrocyte precursor cells and inhibit their migration (Tsai *et al.*, 2002). Indeed, oligodendrocyte hyperplasia is observed within this region, but in inhibiting their migration CXCL1 release by astrocytes may actually inhibit remyelination also (Omari *et al.*, 2005; Omari *et al.*, 2006).

Amyotrophic Lateral Sclerosis (ALS) is a neurodegenerative disease that is characterised by the loss of upper and/or lower motor neurons of the motor cortex and ventral spinal cord. The aetiology of this disease is unclear although numerous genetic and environmental factors have been implicated in the pathogenesis (Ling, Polymenidou and Cleveland, 2013). However, an important progression in the understanding of ALS was the recognition of non-cell autonomous pathology; that is the disease is not simply a disorder of motor neurons and in fact is strongly influenced by surrounding microglia and astrocytes (Clement *et al.*, 2003; Di Giorgio *et al.*, 2008; Haidet-Phillips *et al.*, 2011). Indeed, the role of central neuroinflammation in disease pathogenesis is strongly associated with the production of a toxic neuronal environment and the presence of activated astrocytes and microglia is considered a pathological hallmark of the disease (Barber and Shaw, 2010). In addition, there is clear infiltration of immune cells within areas of motor neuron degeneration including macrophages, mast cells and T-cells (Graves *et al.*, 2004; Henkel *et al.*, 2004; Henkel *et al.*, 2006).

Direct evidence for a role of chemokines in ALS is indicated from observations of elevated chemokine levels within the CSF of ALS patients in comparison to controls. Increased CCL2 and CXCL8 CSF levels negatively correlate with survival time of affected individuals, whilst CCL4 and CXCL10 have a positive correlation with the ALS functional rating score, indicative of a better clinical prognosis (Tateishi *et al.*, 2010; Kuhle *et al.*, 2009). Although a functional explanation for these correlations is lacking it is suggested that elevated CCL2 and CXCL8 levels reflect greater glial activation and also contribute to greater monocyte recruitment (Kuhle *et al.*, 2009). CCL4 and CXCL10 on the other hand can provide neuroprotection from excitotoxicity, a mechanism that has been heavily implicated in ALS pathology (Tateishi *et al.*, 2010; Foran and Trotti, 2009). Therefore, chemokines may provide a useful avenue for

the development of biomarkers for this disease, however further investigation is clearly needed to characterise their contribution to the pathophysiology of ALS.

Chemokines have also been implicated in Alzheimer's disease (Liu *et al.*, 2014) and Parkinson's disease (Kalkonde *et al.*, 2007) and this is again due to their contribution in neuroinflammatory mechanisms. Indeed this is the predominant role suggested for chemokines in the pathogenesis of neurodegenerative diseases. However, it should be appreciated that these signalling networks may well contribute to other aspects of disease pathology via alternative mechanisms, as has been discussed.

1.4 Summary and Perspectives

Chemokines represent a diverse repertoire of proteins which have been extensively characterised for their role in the immune system but are now becoming increasingly relevant to the CNS. The sheer number of these proteins makes elucidating their individual biology difficult, time consuming and may lead to contradictory conclusions - a result of physiologically redundant expression patterns and signalling pathways.

Recent bioinformatic investigation of chemokine evolution has significantly improved the understanding of this superfamily however, by refining chemokine classification according to their principle genetic characteristics. This has distinguished chemokine function and allowed a global perspective that has identified common features within chemokine groups, whilst further delineating chemokines that show distinct sequence, structural and physiological characteristics. As a framework to guide future hypotheses, the molecular evolution of chemokines can provide important clues to the primary aspects of individual chemokines due to the logical relationship between evolutionary pressures, chemokine function and genomic organisation. Indeed, this method has been suggested to represent an important method for investigating gene superfamilies in the future (Zlotnik and Yoshie, 2000; Zlotnik, Yoshie and Nomiyama, 2006).

The identification of chemokines and their receptors within the CNS represents an important milestone in the understanding of chemokine biology; principally it has highlighted the capacity of these signalling networks to participate in functions outside of the immune system. Despite this, chemokines retain their central characteristics as master regulators of cellular migration. Chemokines participate in the development and regeneration of the CNS whilst simultaneously contributing to immunological surveillance both in concert with, and independently to, the peripheral immune system. Furthermore, it is perhaps unsurprising that the diverse downstream signalling pathways which chemokines propagate are exploited by cells of the CNS to perform novel functions, most notably in the modulation of neuronal excitability.

In the context of disease chemokines are unanimously implicated regardless of the affected tissue due to their fundamental role in coordinating the immune response. The CNS is no exception for this, but the immunological privilege of the CNS is an important aspect to consider under any inflammatory state. Additionally, the immunological capacity of resident CNS cells exerts a profound influence on the immune response. As essential components of intercellular communication chemokines therefore participate in the inflammatory response by both controlling the immediate response of resident glia and providing the essential bridge of communication that can facilitate the recruitment of peripheral immune cells. Currently, there is no evidence to suggest that chemokines directly underlie the pathology of CNS disease. However, as a result of their universal participation in numerous pathophysiologies chemokines are sure to represent important future targets for therapeutic intervention or as disease biomarkers. The purpose of this work is to investigate a novel role for the class C chemokine, XCL1, and its receptor, XCR1, within the CNS.

1.5 A Potential Role for XCR1 and XCL1 in the CNS

1.5.1 XCR1 and XCL1

XCR1 and XCL1 represent the exclusive ligand and receptor signalling axis for the class C subfamily of dual-function chemokines. In humans, there are two highly homologous ligands, XCL1 and XCL2, which differ at only 2 amino acid positions within the N-Terminal domain. XCL1 exhibits an Aspartate (D7) and Lysine (K8) at amino acid positions 7 and 8, whilst XCL2 exhibits a substituted Histidine (H7) and Arginine (R8) at these positions (Yoshida *et al.*, 1995). Both *XCL1* and *XCL2* genes are located in chromosome 1 of humans. For mice, only a single isoform, Xcl1, exists for the class C chemokine family and also resides on chromosome 1 of *mus musculus*.

Currently, the functional consequences of the amino acid changes between XCL1 and XCL2 are unknown. However, both ligands demonstrate a structural dichotomy that is unique amongst chemokines. At physiological temperatures and salt concentrations, both XCL1 and XCL2 demonstrate a dynamic conformational equilibrium within which they exist in monomeric form (LTN10) or as a highly interactive dimer (LTN40) (Kuloglu *et al.*, 2001; Kuloglu *et al.*, 2002). LTN10 demonstrates the canonical chemokine fold structure (illustrated in figure 1.1) and is capable of binding XCR1. LTN40, however, does not exhibit XCR1 binding and instead binds with high affinity to extracellular glycosaminoglycans and may confer antimicrobial activity (Nevins *et al.*, 2016). Regardless of the adopted structure for either XCL1 or XCL2 however, functional comparisons suggest both proteins demonstrate almost identical characteristics and the difference in physiological role for the two isoforms is likely mediated by alternative transcriptional regulation and expression

patterns (Fox *et al.*, 2015). For example, both XCL1 and XCL2 are constitutively expressed by Natural Killer (NK) cells, but only XCL1 demonstrates an upregulation in response to Interleukin-2 (Fox *et al.*, 2015). In contrast, CD8+ T-cells exhibit constitutive expression of both ligands and induce the upregulation of both ligands following activation (Yamazaki *et al.*, 2010).

XCR1 is a seven transmembrane GPCR that was originally identified from the functional characterisation of the orphan GPCR, GPR5. It was found that application of recombinant XCL1 and XCL2 to murine L1.2 cells stably expressing GPR5 was capable of inducing intracellular Ca^{2+} mobilisation and chemotaxis. The observed sensitivity to the class C chemokines therefore led to GPR5 being designated as XCR1 (Yoshida *et al.*, 1998).

1.5.2 XCR1 and XCL1 in health and disease

The *XCR1* gene is located on chromosome 3 of humans and encodes a 333aa protein. Phylogenetic analyses demonstrates *XCR1* to be evolutionary conserved from fish to humans (Nomiyama, Osada and Yoshie, 2011) with XCL1 residing within an isolated chromosomal location for both human and mouse genomes (Figure 1.2), suggesting an essential and conserved functional role of this chemokine axis. Indeed, investigations have demonstrated XCR1 to define an evolutionary conserved population of classical dendritic cells (cDCs) between mice and humans (Yamazaki *et al.*, 2010; Bachem *et al.*, 2010; Crozat *et al.*, 2011; Dorner *et al.*, 2009) that are distinct from the other category of cDCs which are defined by their expression of CD11b. Xcr1+ cDCs are categorised as lymphoid (CD8α+) or non-lymphoid resident (CD103+) DCs and are found in all primary, secondary and tertiary lymphoid organs as well as laying resident in non-lymphoid organs/tissues where they perform antigen surveillance during physiological states. They are distinguished by their function to cross present exogenous antigen in complex with Major Histocompatibility Protein-I protein, an essential component for immune response to non-cytosolic proteins arising from viruses and intracellular bacteria (Bedoui *et al.*, 2009). This XCR1+ cDC population in both mice and humans therefore perform essential roles in mediating a cytotoxic, Th1-type immune response. In support of this, the co-release of XCL1 alongside CCL3, CCL4, CCL5 and IFN-γ by Th1-polarised CD4+ and CD8+ T-cells (Dorner *et al.*, 2002; Dorner *et al.*, 2004) is considered to represent an archetypal protein secretion that defines a Th1 immune response (Moser and Loetscher, 2001).

In addition to this role during the Th-1 type immune response, the expression of XCL1 by thymic medullary epithelial cells (mTECs) is an essential component for the homeostatic maintenance and development of regulatory T-cells in the thymus. Expression of XCL1 by mTECs is required for the recruitment of XCR1+ DCs to the central region of the thymic

medulla where the interaction between mTECs, XCR1+ DCs and developing thymocytes mediate antigen presentation and the development of self-tolerance (Lei and Takahama, 2012).

Investigations of XCL1 in the context of disease has demonstrated XCL1 expression to be elevated in several autoimmune diseases including rheumatoid arthritis (Endres *et al.*, 2010), Crohn's disease (Middel *et al.*, 2001) and Th-1 cells that infiltrate the pancreas and cause insulin-dependent diabetes mellitus (Bradley *et al.*, 1999). The capacity of XCR1+ DCs to mediate cross-presentation to cytotoxic CD8+ T-cells also implicates this chemokine signalling axis in anti-tumour immunity, through the co-ordination of DC migration and the facilitation of cell-cell interactions within lymphoid tissues (Lei and Takahama, 2012).

XCR1 and XCL1 may also contribute to other functions of the body outside of the immune system. Immunohistochemical analysis demonstrated constitutive expression of XCR1 by healthy oral epithelial cells *in vivo* that was upregulated in epithelial cells collected from subjects diagnosed with inflammatory or metastatic disease, in addition to the upregulation of XCL1 also. Furthermore, *in vitro* analysis of normal oral keratinocytes supported the constitutive surface expression of XCR1 observed *in vivo,* with XCR1 and XCL1 expression observed to be increased within several cancer cell lines. This increased expression of XCR1 was associated with increased cellular proliferation, migration and invasion in response to XCL1 by cancer cell lines. Moreover, the examined cancer cell lines also demonstrated a qualitatively different response to XCL1 than normal keratinocytes, with enhanced adhesive capacity and a differential expression profile of matrix metalloproteinase enzymes. In tandem with the observed increase of XCL1 by surrounding cells *in vivo,* this together suggests that increased expression of XCR1 may contribute to the enhanced survival and potential metastatic capacity of malignant oral epithelia (Khurram 2010).

1.5.3 Evidence for a role of XCR1-XCL1 signalling in the CNS

The evidence for a role of XCL1-XCR1 within the CNS is scarce. Protein expression profiles have indicated the expression of XCL1 to be induced within whole brain homogenates up to 120 hours post-infection with Pneumococcal meningitis (Klein *et al.*, 2006) and XCL1 is also upregulated in the cornea and trigeminal ganglion of mice following infection with herpes simplex virus type 1 (Araki-Sasaki *et al.*, 2006). Additionally, in a transgenic mouse model overexpressing the Human Immunodeficiency Virus-1 (HIV-1) Tat protein specifically within the CNS, XCL1 transcript and protein levels were significantly upregulated, with expression predominating within astrocytes and to a lesser extent in microglia (Kim *et al.*, 2004). However, the function of this upregulation has not been tested and has instead not been commented upon or incorrectly assumed to represent an additional signal for the

chemotactic recruitment of T-cells (Kim *et al.*, 2004; Dorner *et al.*, 2009; Lei and Takahama, 2012).

During the course of this project, a publication by Zychowska and colleagues reported a contribution of Xcl1 to the development of symptoms observed within a mouse model of diabetic neuropathy. From this investigation, the authors concluded that the central expression of Xcr1 by neurons of the mouse spinal cord mediated increased sensitisation of streptozotocin-treated mice (Zychowska *et al.*, 2016). The details of this investigation are discussed in depth throughout this thesis and at this point, to our knowledge, represents the sole investigation of Xcr1 expression and function within the CNS of mice.

In addition to the data by Zychowska *et al.,* investigations by the Oral Neuroscience research group at the University of Sheffield, in collaboration with colleagues at the University of Leeds, has demonstrated Xcl1-Xcr1 signalling to enhance neuronal excitability within the rat trigeminal nucleus (Bird *et al.*, 2018). This study observed Xcr1 to be expressed within the subnucleus caudalis (Vc) of the trigeminal brainstem nucleus, a region containing the synaptic terminals of nociceptive neurons that innervate the facial region. Application of Xcl1 to *ex-vivo* slices of rat brainstem was demonstrated to enhance spontaneous neuronal excitability and increase expression of c-Fos, pERK and pp38 by Vc neurons. The effect of Xcl1 was blocked following the application of viral Macrophage Inflammatory Protein-II, a viral protein that acts as an antagonist at the XCR1 receptor. In addition, the expression of Xcr1 along peripheral axons of the mental nerve was observed by immunohistochemistry to be increased in rats at 3 days following chronic constriction injury (CCI) in comparison to a complete lack of Xcr1 reactivity along the peripheral axons of sham animals. Xcr1 reactivity within the brainstem demonstrated colocalisation to oligodendrocyte markers and also localised to superficial regions of Vc. However, this reactivity was unable to be colocalised with a particular cellular marker but was observed to demonstrate colocalisation with vGlut2 (Bird *et al.*, 2018).

Together this data suggests a contribution of XCL1-XCR1 signalling to the neuroinflammatory response to peripheral nerve injury. In addition, it suggests that the activation of Xcr1 by Xcl1 is capable of modulating neuronal activity, a feature that has been described for other chemokine receptor and neuromodulators.

1.5.4 Project aims and objectives

Despite the relative lack of evidence for a function of XCR1 and XCL1 within the CNS in comparison to that for other chemokines (see above), the emerging and current evidence, in addition to the molecular characteristics of this chemokine signalling axis, provides a rational basis to investigate the potential function of XCR1 and XCL1 in the CNS. The

molecular evolution of this chemokine axis indicates an evolutionary conserved function that, based on chromosomal location, is highly specific, as has been demonstrated for its expression by a specific population of cDCs. Such ancient phylogeny and functional characteristics associated with homoestasis, are qualities that some have used to debate the evolution of chemokines to have arisen within the primitive nervous system (Huising *et al.*, 2003a; Huising *et al.*, 2003b; Shields, 2003). Indeed, as discussed for other chemokines such as CXCL12 and CCL2 (section 1.2), there is now a consistent body of evidence to suggest that chemokines perform independent functions within the CNS to those that they perform within the periphery and immune system. Recent evidence now supports the capacity of XCR1 and XCL1 modulate neuronal activity (Bird et al. 2018; Zychowska et al 2016). However, the link of XCR1 to define a specific cDC population, and the known capacity for DC surveillance of the CNS (Section 1.2.2) provides another route by which the Class C chemokine axis may contribute to the function of the CNS in health and disease.

The overall objective of this project was to investigate the expression of Xcr1 and Xcl1 within the CNS of mice. Due to the significant contribution of murine models to the understanding of the human CNS and to the development of novel therapeutic strategies it was therefore aimed to provide a comprehensive detail of the expression of this chemokine receptor and ligand within the mouse CNS. This would inform further characterisation of the potential role for this chemokine signalling axis within the nervous system. In particular, three main objectives were sought to be obtained in the mouse which could inform subsequent investigation within humans.

1. Determine the molecular identity of mRNA and protein produced by *Xcr1.*
2. Characterise the expression of Xcr1 and Xcl1 within the CNS.
3. Determine the influence of a central inflammatory response on the gene and protein expression of Xcr1 and Xcl1 within the CNS.
4. Investigate the expression of XCR1 within the CNS of humans.

Chapter 2: Materials and Methods

2.1 Animal Procedures and Sample collection

All samples of mouse tissue were collected from mice that were cared for and housed under the terms of the UK Animals (Scientific Procedures) Act 1986 and under a UK Home Office project License. Procedures of tissue collection were performed following the designated Schedule 1 Appropriate Methods of Humane Killing of the UK Animals (Scientific Procedures) Act 1986.

2.1.1 Collection of Tissue

Animals were sacrificed by terminal anaesthesia following intraperitoneal sodium pentobarbital injection. Conformation of sufficient anaesthetic depth was achieved by observing the absence of a withdrawal reflex following pinching of hind paws.

Animals were subsequently transcardially perfused with 0.01M Phosphate Buffered Saline (PBS), to clear residual blood, and 4% (w/v) Paraformaldehyde (PFA, BDH chemicals Ltd.) in PBS. To do this, a horizontal incision was made along the subcostal plane to allow vertical retraction of the dermis and expose the underlying viscera. A horizontal incision was then made immediately below the thorax to reveal the diaphragm which was then pierced and the blade drawn horizontally to the lateral edge of the bottom ribs. The blade was then drawn upwards to sever the ribs and allow the ribcage to be lifted to expose the heart. The vena cavae were severed above the right atrium and a 25 gauge catheter inserted to the left ventricle. 8-10ml of PBS was then perfused until returning fluid to right atrium was clear of blood. The syringe of PBS was then replaced with 4% PFA and tissue perfused for fixation.

2.1.1.1 Collection of Spinal cord

For collection of spinal cord, the head was first decapitated by a single cut with scissors. An incision was then made along the entire sagittal plane of the spinal column to allow resection of the dermis. This was then peeled away to expose the vertebral column. Scissors were then placed immediately lateral to the spinal column and cut all along this axis, parallel to the column, stopping once the cut had severed hips. This was repeated for both lateral sides of the spinal column. A cut was then made horizontally, just below the hip, severing the most caudal spinal cord regions. These three cuts isolated the spinal column and allowed its removal from the body.

To isolate the spinal cord, laminectomy was performed using microsurgical scissors to break each vertebra independently along the entire vertebral column. The bottom blade was inserted underneath both lateral sides of the vertebra, starting at the rostral end of the spinal column. The scissors were then closed and pulled upwards, away from the dorsal

aspect of the column, to break the vertebra. Once severed on both sides the vertebra was pulled away from the spinal canal using forceps. Repeating this along the entire dorsal aspect of the spinal column allows exposure of the spinal cord located within the spinal canal. For isolation of the spinal cord only, microsurgical scissors were ran along the spinal canal immediately adjacent to the spinal cord in order to sever fibres of the dorsal and ventral roots. The cord was then removed by lifting away from the spinal canal.

2.1.1.2 Collection of Spleen

For isolation of spleen, a vertical incision was drawn along the midline towards the hind limbs from the subcostal incision used for the initial transcardial perfusion. This fully exposed the abdominal cavity. The spleen was identified within an anterodorsal lateral position to the liver, below the stomach. The major vessels supplying the spleen were severed with a pair of microsurgical scissors and the spleen removed with forceps.

2.1.2 Preparation of Tissue for histological processing

Following collection, tissue was fully immersed within 4% PFA solution and left to incubate at 4°C for 24 hours to permit a complete fixation of the tissue. The tissue was then treated in sucrose solutions of ascending concentration (5%, 10%, 15%) for 5 minutes each before incubation for 24 hours in 20% sucrose at 4°C in order to protect the tissue during cryopreservation.

The whole tissue was then immersed within optimal cutting temperature (OCT) compound (ThermoScientific) within a rubber mould. The tissue and OCT was frozen above a cold plate at -50°C before transfer to a -80°C freezer. Tissue was frozen for at least 24 hours at -80°C before sectioning.

2.1.3 Immunohistochemistry

Immunohistochemistry was performed using free-floating sections of sample tissue. All tissue sections were cut at 30um using a chilled microtome at -20°C within a cryostat and then immersed within PBS. For the long-term storage of sectioned tissue, sections were immersed within a 60% glycerol (v/v) solution within PBS and chilled to -20°C.

2.1.3.1 Chromogenic immunohistochemistry

Detection of primary antibody (see table 2.1, A for details) was visualised using the chromogenic Diaminobenzidine (DAB) Horseradish peroxidase (HRP) substrate following primary antibody detection using the VectaStain® ABC HRP kit (Vector Labs). Sections were washed 2x in PBS before a 30 minute incubation with 0.3% H_2O_2 in PBS to quench endogenous peroxidase activity. This was followed by 2 further washes for 10 minutes in

PBS and a 1 hour block in 10% normal goat serum (NGS) in PBS. NGS was then removed from test sections and primary antibody added overnight at 4°C. Negative controls without primary antibody were left in NGS or had primary antibody added that had been pre-incubated for 24 hours with the antigenic peptide. Sections were then washed 3x for 10 minutes in PBS and incubated with a biotinylated goat anti-rabbit secondary antibody. A further 2 washes for 10 minutes in PBS was then performed before a 30 minute incubation with the vectastain avidin-biotin HRP-complex. A final 2 washes for 10 minutes in PBS was performed before addition of DAB. The reaction was allowed for up to 10 minutes after which the sections were flooded with PBS to quench peroxidase activity. Sections were subsequently dehydrated by sequential dehydration through 70%, 90% and 100% EtOH followed by 1 minute incubation in histo-clear (ThermoFisher). Sections were then mounted on to glass slides and covered in Pertex solution (CellPath Ltd).

2.1.3.2 Fluorescent immunohistochemistry

Free-floating tissue sections (30µm) were washed 3x for 10 minutes in PBS. Sections were then blocked for 1 hour in appropriate blocking buffer (10% serum/PBS) at room temperature (RT). Blocking buffer was removed and primary antibody was added to sections overnight at 4°C (see table 2.1 for antibody preparation). Negative controls had primary antibody omitted and sections were left in blocking buffer or had primary antibody added that had been pre-incubated for 24 hours with the antigenic peptide. After incubation overnight, sections were washed 3x for 10 minutes in PBS and then secondary antibody(ies) was added for 2 hours at RT on an orbital rotor. Sections were washed for a final 3 times, each for 10 minutes, with PBS and subsequently mounted on to glass slides. Excess PBS was removed from slides and then sections were covered with Vectashield® mounting reagent (Vector Labs) or Prolong® Gold mounting reagent with 4',6-diamidino-2-phenylindole (DAPI) (ThermoFisher) with glass coverslips placed over the top in preparation for imaging.

2.1.4 Collection of RNA from Tissue

Prior to the collection of RNA, all mice were culled according to the designated Schedule 1 Appropriate Methods of Humane Killing of the UK Animals (Scientific Procedures) Act 1986.

2.1.4.1 Spinal Cord

For the collection of RNA from spinal cord, the animal was first decapitated by a single horizontal cut at the rostral end of the cervical region. Spinal column was exposed by a vertical incision through the dermis along the entire midline. Horizontal retraction of the dermis then permitted the exposure of the underlying spinal column. A horizontal cut was then made at the rostral end of the spinal column, anterior to the line of the hips. In combination with decapitation, this exposed the spinal canal containing the spinal cord at

both rostral and caudal ends of the column. In order to retrieve the entire spinal cord, a 200ul pipette (and associated tip) was filled with PBS and inserted firmly in to the rostral end of the spinal column to form a complete a seal as possible between tip and spinal column. Extraction of the cord was achieved by aspiration of the pipette and PBS with sufficient pressure to eject the cord from the column. The ejected spinal cord was collected within a sterile petri dish filled with ice cold PBS and stored over ice. The tissue was then transferred to 1ml TRIzol ® reagent in a 1.5ml Eppendorf tube.

2.1.4.2 Spleen

For collection of RNA from spleen, the spleen was identified within the animal located within an anterodorsal lateral position to the liver, below the stomach. To enable efficient homogenisation, spleen tissue was cut in to smaller pieces before transferring 50-90mg to 1ml of TRIzol ® reagent. For some samples prepared from frozen spleen tissue, tissue was first prepared using RNAlater ®-Ice Frozen Tissue Transition Solution (Ambion) according to manufacturer's instructions.

2.1.4.3 Tissue homogenisation and RNA extraction

Spinal cord and spleen tissue was homogenised using either a hand-held tissue homogeniser (Argos Technologies) or dissociated completely by sonication at 25-30 kHz using a hand-held ultrasonicator (Jencons Scientific Ltd). Homogenised samples in TRIzol ® were then processed according to manufacturer recommendations for RNA isolation. Following isolation, RNA was resuspended in RNase and DNase-free H_2O to achieved a concentration of <1000ng/µl. RNA samples were then used immediately for Reverse Transcription-PCR (RT-PCR) (see below) or stored at -80°C until further use.

2.1.5 Primary microglia collection and cell seeding

A method for the collection and culture of brain-derived primary microglia was deduced from a method kindly provided by Dr Laura Ferraiuolo and further optimised according to protocols published in the literature (Saura, Tusell and Serratosa, 2003; Moussaud and Draheim, 2010).

Each microglial preparation was performed using the brains of 3 age and gender-matched mice from the same genetic background. Brain from each mouse was removed following cervical dislocation and decapitation of the mouse. A sagittal incision was made from the posterior of the head along the dorsal aspect to the midline. This allowed the dermis to be peeled away to expose the cranium. Three breaks to the skull were then made on the dorsal and both lateral sides of the foramen magnum by inserting the tips of scissors and drawing backwards, ensuring the direction of the break did not compromise the integrity of the

A)

Antibody (Catalogue number)	Manufacturer	Immunogen	Host	Clonality	Concentration (ICC and IHC)	Concentration (Immunoblot)
Anti-XCR1 (LS-A158)	LifeSpan Biosciences	3rd extracellular domain (Human) 19aa, position not specified	Rabbit	Polyclonal	2.5 – 10ug/ml	2ug/ml
Anti-XCR1 (HPA013169)	Atlas Antibodies Inc.	Extracellular N-Terminal domain (Human) 34aa, position 1-34	Rabbit	Polyclonal	1-4ug/ml	0.4ug/ml
Anti-XCR1 (188896)	Abcam	2nd cytoplasmic domain (Human) 19aa, position not specified	Rabbit	Polyclonal	2.5-10ug/ml	2ug/ml
Anti-Xcr1 (LS-C37380)	LifeSpan Biosciences	N-terminus to 3rd cytoplasmic (Mouse) 180aa, position 43-222	Rabbit	Polyclonal	5-20ug/ml	3ug/ml
Custom Anti-Xcr1 (cAb-Xcr1)	Eurogentec	3rd cytoplasmic domain (Mouse) position 222-236	Rabbit	Polyclonal	2.5-10ug	1ug/ml
Anti- C-myc (9B11)	Cell Signalling Technologies	C-myc (Human), EQKLISEEDL	Mouse	Monoclonal	1ug/ml	1ug/ml
Anti-β-Actin (A1978)	Sigma	N-terminus, (DDDIAALVIDNGSGK)	Mouse	Monoclonal	N/A	1ug/ml
Anti-Iba-1 (Ab5076)	Abcam	-	Goat	Polyclonal	1ug/ml	-
Anti-GFAP (Ab7260)	Abcam	-	Rabbit	Polyclonal	1ug/ml	

B)

Secondary Antibody	Manufacturer (Catalague number)	Fluorophore	Excitation Peak (nm)	Emission Peak (nm)	Concentration	Primary antibody Diluent	Secondary antibody diluent
Donkey anti-Rabbit IgG	Jackson (711-165-152)	Cy3	550	570	1:500	5% NDS, PBS (ICC) or PBS-T (IHC)	1.5% NDS, PBS
Donkey anti-mouse IgG	Jackson (715-095-156)	FITC	495	520	1:500	5% NDS, PBS (ICC) or PBS-T (IHC)	1.5% NDS, PBS
Donkey anti-Goat IgG	Jackson (705-165-147)	Cy3	550	570	1:500	5% NDS, PBS (ICC) or PBS-T (IHC)	1.5% NDS, PBS

Table 2.1. *Details of primary and secondary antibodies used for immunocytochemistry and immunohistochemistry.* A) Details of primary antibodies and their respective preparation. Determination of antibody concentration was based upon manufacturer's recommendations. B) Details of fluorescent secondary antibodies used for the detection of primary antibodies raised in Rabbit, Mouse and Goat. Cy3 = Cyanine Dye 3; FITC = Fluorescein Isothiocyanate; NDS = Normal Donkey Serum; PBS at 0.01M concentration. PBS-T = 0.2% Triton™ X-100, 0.01M PBS. ICC = Immunocytochemistry; IHC = Immunohistochemistry.

underlying brain tissue. The skull was then peeled away to reveal the brain. To remove the brain, the tissue was lifted and the optic nerve severed and then pulled upwards and backwards. Collected brains were placed immediately in to ice cold PBS and stored over ice until all 3 brains were collected. Following collection, the cerebellum was removed and the remaining tissue washed thoroughly with ice cold PBS. Brains were then thoroughly fragmented using a scalpel to provide a homogenous tissue devoid of large tissue clumps. This was performed for all 3 brains and the collective brain tissue then added to 6ml papain enzyme solution (dissolved in dH_2O: papain (20 units/ml, Sigma), 1000 units/ml penicillin and 0.01mg/ml streptomycin (Sigma), 116mM NaCl, 1M KCl, 26mM $NaHCO_3$, 1mM NaH_2PO_4, 1.5mM $CaCl_2$, 1mM $MgSO_4$, 25mM glucose, 1mM cysteine). Note that the addition of papain enzyme to the solution was made after the addition of brain tissue. Inclusion of pen/strep antibiotic was made in response to bacterial infections that were experienced during preliminary attempts of the method and was found to aid the prevention of any contamination during subsequent preparations.

Tissue was dissociated by incubation in papain enzyme solution for 1 hour at 37°C within a water bath, with agitation of the sample every 10-15 minutes to maximise dissociative activity. After 1 hour, any clumps of tissue were dissociated by aspiration with a p1000 pipette. Papain enzyme activity was quenched by the addition of a 1:1 volume of 40% Fetal Bovine Serum (FBS) (ThermoFisher) in Hanks Balanced Salt Solution (-Ca^{2+}/Mg^{2+}) (HBSS) to papain enzyme solution. The solution was mixed and then centrifuged at 200xg for 4 minutes. The resulting supernatant was removed and the pellet resuspended in 2ml DNase I solution (0.5mg/ml DNase I (Sigma), 1x HBSS) and incubated at room temperature for 5 minutes. Tissue was then filter dissociated through a 70µm cell strainer (strainer was washed with an additional 1ml 1x HBSS to improve cellular yield). The sample was then centrifuged for 4 minutes at 200xg to pellet the collected cell dissociate. The cell pellet was then resuspended in 10 ml 20% isotonic Percoll (Sigma) (2ml isotonic percoll (200µl 10x HBSS, 1.8ml Percoll), 8ml 1x HBSS). To isolate the cells by centrifugation, 10ml 1x HBSS was dispensed carefully above the cell/Percoll suspension. Addition of the overlying HBSS was done without disrupting the cell/Percoll suspension. The combined cell/Percoll suspension and overlying HBSS solution was then centrifuged for 20 minutes at 200xg using the slowest acceleration and no brake. The resultant solution demonstrated a large interphase layer containing cell debris and myelin (visible white band in solution). Cells were contained within a pellet at the bottom of the tube. The entire solution above the cell pellet was removed and the pellet washed by the application of 2ml 1x HBSS and gentle agitation. Cells were then re-pelleted by centrifugation for 4 minutes at 200xg. The overlying supernatant was removed and purified cells resuspended in 8ml of complete glial cell media (DMEM/F12 (ThermoFisher), 10% FBS (ThermoFisher), 4000 units/ml penicillin and

0.04mg/ml streptomycin (Sigma), 5ng/ml Granulocye-Macrophage Colony Stimulating Factor (GM-CSF) (Peprotech). Cells were seeded to poly-L-ornithine-coated T25 flasks (incubated for 18-24 hours with 1:200 0.01% poly-L-ornithine (dH_2O) at room temperature) following a single wash of the flask with PBS.

2.1.5.1 Primary microglia cell culture

Following cell seeding, cells were monitored daily. 48 hours post-seeding, half of the cell media was replaced with complete glial cell media (note GM-CSF concentration was doubled to maintain effective concentration). From 48 hours post-seeding, unless cell numbers and growth was particularly high (judged according to appearance of media), only half the volume of complete glial cell media was replaced at 48-72 hour intervals. Note that GM-CSF concentration was adjusted to maintain a constant 5ng/ml concentration in the total media volume. This was performed until confluence was achieved in the T25 flask (typically after 10-14 days). Complete glial cell media was prepared on the day of use.

To achieve appropriate cell numbers for the desired applications, once cells had reached confluence within the T25 flask the entire cell population was dissociated and re-seeded in to a T75 flask coated in Poly-L-ornithine, as described above. To do this, total media (containing dissociated, floating microglia), was removed and stored. 5ml of 0.25% Trypsin-Ethylenediamineteraacetic acid (EDTA) (ThermoFisher) was then added and incubated at 37°C for 10 minutes. Vigorous tapping and pipetting of the flask was required to dissociate cells. Previously collected media was then added back to trypsinised cells to maximise collection of microglia. The solution was then centrifuged for 5 minutes at 200xg and the resulting cell pellet resuspended in complete glia cell media and seeded to a T75 flask. Cells were maintained in T75 flasks until further use, by 50% media replacement with complete glia cell media every 2-3 days.

2.1.5.2 LPS treatment of primary brain-derived microglia

Lipopolysaccharide (LPS) treatment of primary brain-derived microglia was performed according to protocol described by Zychowska et al., 2016. Following culture and expansion of primary brain-derived microglia, cells contained within T75 flasks were treated with 8ml 0.25% Trypsin-EDTA (ThermoFisher) and dissociated and centrifuged as described in 2.1.5.1. Cell pellets were resuspended in 5ml complete glial cell media (without GM-CSF) and counted using a hemocytometer. For cells to be evaluated by immunocytochemistry, 60, 000 cells were seeded to each well of a 24 well plate. The seeded well was first covered with sterile 12mm^2 glass slides. Cells were seeded in 1ml complete glial cell media, without GM-CSF. For cells to be used for RNA collection, 200,000 cells were seeded to 6 well plates in 2ml complete glial cell media (- GM-CSF). Note that seeding to both 6 and 24 well plates was

preceded by poly-L-ornithine coating of wells and glass coverslips for 24 hours. 72 hours after cell seeding, cells were treated with complete glial cell media (- GM-CSF) or complete glial cell media (- GM-CSF) with the addition of 100ng/ml LPS derived from *E. Coli* (ThermoFisher) and incubated for 24 hours. RNA was then collected from cells, as described in section 2.2.7. For immunocytochemistry, cells were processed as described in section 2.2.6.

2.1.5.3 Evaluation of microglial purity: Iba-1 and GFAP immunocytochemistry

The presence of microglia and astrocytes were identified in primary cell cultures by the detection of Ionised calcium binding adaptor molecule-1 (Iba-1) and Glial Fibrillary Acidic Protein (GFAP) proteins, respectively, using double immunocytochemistry (section 2.2.6).

Images were obtained at magnifications of 10x and 40x and analysed as described in section 2.3. Microglial purity was estimated by counting the number of Iba-1-positive and GFAP-positive cells and determining their relative abundance to total cell numbers as determined by DAPI staining. Semi-quantitative analysis of Iba-1 reactivity was determined from the RawIntDensity of the corresponding colour channel to the fluorophore conjugated to the desired secondary antibody.

2.2 Cell Culture

2.2.1 HeLa cells

HeLa cells were obtained from frozen stocks kindly donated by Dr Yolanda Gibson. Cells were resurrected and cultured in a complete HeLa growth media composed of high glucose (+ sodium pyruvate) Dulbecco's Modified Essential Medium (DMEM, ThermoFisher), 10% FBS (ThermoFisher), 1000 units/ml penicillin and 0.01mg/ml streptomycin (Sigma). Cells were incubated in T75 flasks at 37°C supplemented with 5% CO_2.

2.2.2 Parental EA-CHO cells

A parental CHO cell line for the use in the DiscoverX ® PathHunter™ β-arrestin assay were maintained in complete CHO cell media (Ham's F12-K media (ThermoFisher), 10% FBS, Penicillin (1000 units/ml) Streptomycin (0.01mg/ml)), unless otherwise stated.

2.2.3 Subculture of Cells

Upon confluency of cells, both CHO and HeLa cells were subcultured by incubation with 5ml 0.05% Trypsin-EDTA (ThermoFisher) and resuspended in 5ml Complete growth media. 1ml of this cell suspension was then added to 15ml of Complete growth media and the cells reseeded to a T75 flask to maintain cell stocks.

2.2.4 Cryopreservation of cells

Cell stocks were created by the cryopreservation of existing cell lines. Cells were initially dissociated and centrifuged at 200xg for 5 minutes. Cells were then resuspended in complete growth media and counted using a hemocytometer. Cells were centrifuged at 200xg for 5 minutes and then resuspended to achieve a concentration of $1x10^6$ cells/ml in Cell freezing media composed of the respective cell complete growth media with an additional 10% concentration of FBS and a 10% concentration of dimethyl sulfoxide (DMSO). Cells were then frozen at a steady rate to -80°c from room temperature within a Mr. Frosty™ freezing container (Nalgene).

2.2.5 Cell Transfection

2.2.5.1 Lipojet™ Transfection of HeLa cells

Cells were seeded the day before transfection (at least 18 hours prior) at a density aimed to achieve ~80% by the time of transfection (table 2.2). For cells to be tested by immunocytochemistry, cells were seeded in 24 well plates containing 12mm circular glass slides or in glass-bottomed 96-well plates (Greiner, Merck). For cells to be used for the collection of cell lysate for western blot, cells were seeded to 6 well plates. Plasmid transfection of HeLa cells was performed using the LipoJet™ In Vitro DNA and siRNA Transfection Kit (SignaGen Laboratories). 1 hour prior to transfection a fresh volume of complete HeLa growth media (including serum) was added to the wells. 15 minutes prior to transfection the designated amount of plasmid DNA was added to the 1x LipoJet™ transfection buffer and vortexed briefly. The determined amount of LipoJet™ reagent was then added to the 1x buffer plus plasmid solution and vortexed. After incubating these three components for 15 minutes the plasmid-transfection reagent solution was added dropwise to the overlying cell media and the plate gently shaken to maximise transfection coverage. An equal number of wells to the number that were transfected were left untransfected as negative controls. Cells were then incubated for 24 hours at 37°C in 5% CO_2 before preparation for immunocytochemistry (2.2.6) or western blot (2.4.2 and 2.4.3).

Final LipoJet™ and plasmid concentrations were made to achieve a 1:1, 2:1, or 3:1 ratio of LipoJet™ reagent (µl): plasmid DNA (µg), with plasmid concentrations tested at 1ng/µl, 2ng/ul and 3ng/ul of total transfection volume (transfection solution + cell media). See table 2.2 for details of transfection solution composition.

2.2.5.2 PolyPlus PEIpro® transfection of CHO cells

$1x10^6$ EA-expressing CHO cells were seeded to T25 flasks 16-24 hours prior to transfection to achieve 60-80% confluency. On the day of transfection, cells were washed twice with PBS and complete CHO cell media was replaced with 5ml Opti-MEM serum-free medium (ThermoFisher). pCMV-ProLink2 vectors were prepared by the addition of the desired

amount of plasmid to 250µl Opti-MEM media. The corresponding amount of PEIpro transfection reagent (Polyplus-transfection Inc.) was prepared in a separate 250µl volume of OptiMEM media. Plasmid amounts were calculated based on achieving a plasmid concentration of 750ng/ml of total cell media volume. PEIpro transfection volume was determined based on a 2:1 ratio of PEIpro (µl): plasmid DNA (µg). Both plasmid and PEIpro solutions were then gently vortexed, mixed together and vortexed once more, with the combined plasmid-PEIpro solution then allowed to incubate at room-temperature for 15 minutes. Plasmid-PEIpro solution was then added to the T25 flask and incubated with the cells for 24 hours. After this time, cell media was replaced with complete CHO cell media and left to incubate for a further 24 hours, following which cells were either seeded for ligand application, or underwent antibiotic selection.

2.2.5.2.1 Antibiotic selection of CHO Cells stably expressing pCMV-Prolink2 plasmids

Cells successfully transfected with pCMV-ProLink2 vectors were selected for by culturing of cells in G418-CHO cell media (Ham's F12-K medium (Sigma), 10% FBS, 2mg/ml G418 (Insight). 24 hours after cell transfection, G418-CHO cell media was replaced every 2-3 days for 8-12 days prior to ligand application. Conformation of G418 efficacy was determined by the use of non-transfected CHO cells.

2.2.6 Immunocytochemistry

Cells were washed twice in PBS and fixed in 4% PFA for 60 minutes at 4°C. Cells were then washed a further 2 times in PBS and stored in PBS at 4°C until use.

Cells were washed 3x for 10 minutes in PBS and 1x for 10 minutes in PBS containing 0.2% Triton x-100 (Sigma) (PBS-T). Cells were then blocked for 1 hour in appropriate blocking serum at room temperature (RT) on an orbital rotor. The blocking serum was removed and primary antibody was added to coverslips overnight at 4°C on an orbital rotor (for details of antibodies used see table 2.1). Negative controls had primary antibody omitted and left in blocking serum or had primary antibody added that had been pre-incubated for 24 hours with the antigenic peptide. The following day, coverslips were washed 3x for 10 minutes in PBS. Secondary antibody(ies) were then added for 2 hours at RT on an orbital rotor (see table 2.1 for details of antibodies used and their concentrations). Cell nuclei were stained with 1:2000 DAPI in PBS for 10 minutes. This was followed by a final 3 washes for 10 minutes with PBS. For cells in 24 well plates, excess PBS was removed from wells and then coverslips were removed and placed on to glass slides with Vectashield® mounting reagent. Cells in 96 well plates were left in PBS until imaging.

Culture plate (surface area mm^2)	Intended Use	Cell seeding density/well	Plasmid DNA/µl Total transfection volume	LipoJet™ Reagent Volume (µl): Plasmid DNA (µg)	LipoJet™ Transfection buffer per well	Cell media volume
6	Protein analysis	300,000	1-3ng/µl	1:2	200µl	2ml
24	Immuno-cytochemistry	100,000	0.4-3ng/µl	1:2	50µl	0.5ml
96	Immuno-cytochemistry	20,000	1-3ng/µl	1:2	5µl	0.05ml

Table 2.2. *Composition of LipoJet™ transfection solutions used for transient transfection of HeLa cells with RC221929 or MR225748 plasmids.* The composition of transfection solution was based on manufacturer's recommendations and optimised according to Green Fluorescent Protein (GFP) transfection efficiency, C-myc reactivity and Cell viability.

In addition to the standard protocol above, antibody reactivity was also tested by immunocytochemistry following Heat Induced Epitope Retrieval (HIER). This was performed following cell fixation by heating the cells in a pH 6 sodium citrate buffer (10mM Sodium citrate, 0.05% Tween-20, pH 6.0) at 95°C for 10 minutes and then allowing the samples to cool to room temperature.

2.2.6.1 Custom Ab design

A custom polyclonal anti-Xcr1 antibody was designed under consultation with representatives from Eurogentec Ltd. The protein sequence of mouse Xcr1 corresponding to NCBI reference sequence NP_035928.2 was used for antigen identification and peptide design (Figure 2.1). A 16-amino acid region corresponding to the 3rd cytoplasmic region of the receptor was produced for immunisation in conjugation with a Keyhole limpet hemocyanin (KLH) carrier protein (Figure 2.1). Polyclonal antibody production was achieved by an 87 day immunisation protocol of two Rabbits. Immunisations with the antigenic peptide plus carrier was performed at day 0, 21, 49 and 77. A final bleed was performed at day 87 and the antibody provided following affinity-purification to the antigenic peptide. Confirmation of antibody specificity and affinity was evaluated by Enzyme Linked Immunosorbant Assay (ELISA) to the antigenic peptide. For an illustration of Xcr1 epitopes targeted by the anti-Xcr1 antibodies used, please see figure 2.1.

2.2.7 RNA collection from cells

Preparation of RNA from cell samples was performed using TRIzol ® reagent. For all preparations from cells, samples were prepared from ≤ 1 x 10^6 cells. Provided frozen cell pellets were immersed in 1ml TRIzol ® reagent immediately from storage and then incubated for 5 minutes at room temperature prior to resuspension of the cells by aspiration of the solution. For adherent cell monolayers collected from culture, 1ml TRIzol ® reagent was added to the cell culture container. Cells were completely dissociated in to the reagent by use of a rubber cell scraper. Samples were then aspirated and collected in to a sterile 1.5ml Eppendorf tube. From the homogenised cell samples RNA was collected using the Direct-Zol RNA microprep kit (ZymoResearch) following the associated manufacturer protocol WITHOUT the optional DNase treatment. RNA samples were then quantitatively and qualitatively analysed by NanoDrop Spectrophotometer (ThermoFisher) to ensure sufficient RNA quantity and purity according to 260/230 and 260/280 ratios of >2.0 and >1.8, respectively. RNA samples were then used immediately for RT-PCR or stored at -80°C until further use.

2.2.8 Collection of cell lysate and purification of protein

A)

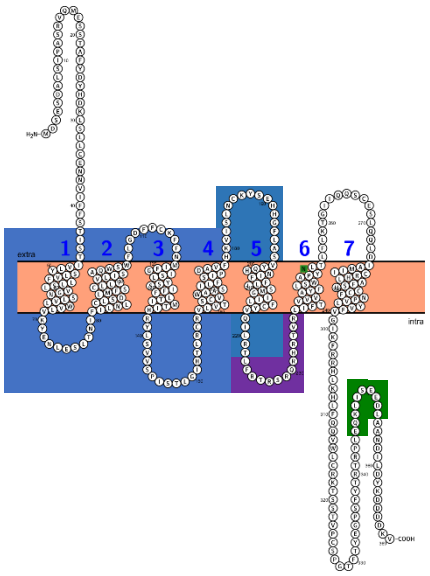

B)

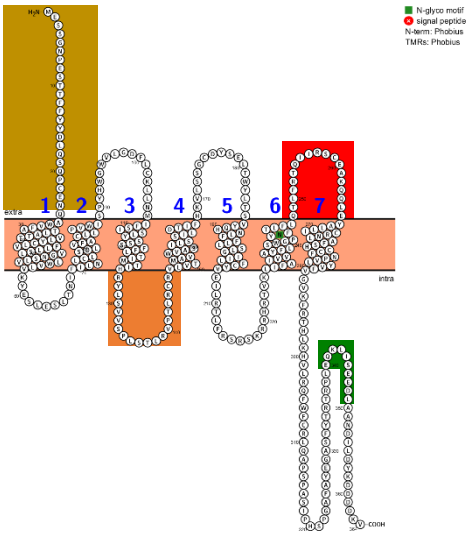

C)

```
                                                                LS-C373870 (43-222)
Xcr1-myc 1    MDSESDALSIPASRVQMESSTAFYDYHDKLSLLCENNVIFFSTISTIVLYSLVFLLSLVG  60
                        :|:: :| || |: |:|::|::|||::  | |: | |||:|||||||||
XCR1-myc 1    ----------MESSGNPE-STTFF-YYDLQSQPCENQAWVFATLATTVLYCLVFLLSLVG  48
                         Atlas HPA013169 (1-34)

Xcr1-myc 61   NSLVLWVLVKYENLESLTNIFILNLCLSDLMFSC-LLPVLISAQWSWFLGDFFCKFFNMI  119
              |||||||||||| ||||||||||||||||:| | |:::::  :|:|:|||||:||::|||
XCR1-myc 49   NSLVLWVLVKYESLESLTNIFILNLCLSDLVFACLLPVWISPYHWGWVLGDFLCKLLNMI  108


Xcr1-myc 120  FGISLYSSIFFLTIMTIHRYLSVVSPISTLGIHTLRCRVLVTSCVWAASILFSIPDAVFH  179
              |:||||||:|||||||||||||||||:|||:: |||||||||: ||:||||:||:|  ||
XCR1-myc 109  FSISLYSSSFFLTIMTIHRYLSVVSPLSTLRVPTLRCRVLVTMAVWVASILSSILDTIFH  168
                                Abcam188896 (127-146)
                                                              CustomAb (222-236)
Xcr1-myc 180  KVISLNCKYSEHHGFLASVYQHNIFFLLSMGIILFCYVQILRTLFRTRSRQRHRTVRLIF  239
              ||:|::|:||| : :| ||||||:|||| |||||||:|||||| ||::||||||:|||
XCR1-myc 169  KVLSSGCDYSELTWYLTSVYQHNLFFLLSLGIILFCYVEILRTLFRSRSKRRHRTVKLIF  228


Xcr1-myc 240  TVVVAYFLSWAPYNLTLFLKTGIIQQSCESLQQLDIAM---IICRHLAFSHCCFNPVLYV  296
                |||||||| |||:|||| | :::|  :|:::: :     :|||:|||||||||||||
XCR1-myc 229  AIVVAYFLSWGPYNFTLFLQTLFRTQIIRSCEAKQQLEYALLICRNLAFSHCCFNPVLYV  288
                                LS-A158 248-266
                                                              Anti-myc (345-354)
Xcr1-myc 297  FVGIKFRRHLKHLFQQVWLCRKTSSTVPCS-PGTFTYE---GPSFYTRTRPLEQKLISEE  352
                |||:||| ||||:::| |:||      : | |  :  :   |:||||||||||||||||
XCR1-myc 289  FVGVKFRTHLKHVLRQFWFCRLQAPSPA-SIPHSPGAFAYEGASFYTRTRPLEQKLISEE  347
                                                              Anti-myc (340-349)
Xcr1-myc 353  DLAANDILDYKDDDDKV  369
              |||||||||||||||||
XCR1-myc 348  DLAANDILDYKDDDDKV  364
```

Figure 2.1. *Epitopes of human and mouse XCR1 homologues.* Schematic overview of structures of protein produced from MR225748 (Xcr1-myc, A) and RC221929 (XCR1-myc, B) with highlighted regions of antibody epitopes detailed in C. C) Sequence alignment of XCR1-myc and Xcr1-myc. Annotated regions correspond to epitopes of tested antibodies (table 2.1 (A)). Annotations above = antibody raised to immunogen of Xcr1; annotations below = antibody raised to immunogen of XCR1. Protein schematics provided by Protter (Omasits 2014).

Cell lysates were collected from 6 well plates by the addition of 300ul RIPA buffer (Sigma) plus complete protease and phosphatase inhibitor (Roche). Cells were removed from the well surface using a cell scraper and then the cell solution aspirated several times before loading in to a sterile 1.5ml Eppendorf tube. Samples were stored on ice and vortexed every 5 minutes for 6 repeats. Protein was then separated from larger cell debris by centrifugation at 14,000xg for 15 minutes. The resultant supernatant was then transferred to a sterile vessel and evaluated for protein content by BCA assay. Protein concentrations were calculated based on absorbance in reference to a standard curve established from bovine serum albumin concentrations between 0 and 2mg/ml.

2.2.8.1 PNGase F treatment of protein

For the removal of N-linked oligosaccharides, 15µg cell lysate was treated by denaturing and non-denaturing deglycosylation with PNGase F (NEB) according to manufacturer's instruction. For the non-denaturing protocol, PNGase F was added for 24 hours at 37°C before preparation for western blot. The total amount of enzyme used was limited to prevent glycerol concentration exceeding 5% of the total reaction volume. A positive control was established via the use of WFDC2 protein that was kindly donated by Miss Hannah Armes (University of Sheffield).

2.3 Microscopy and image analysis

2.3.1 Microscopy

Fluorescent and chromogenic samples were inspected with a Zeiss Axioplan 2 imaging microscope (Carl Zeiss International). For fluorescent samples, a Lumen 200 Fluorescent illumination system (Prior Inc.) was used to illuminate samples. Microscopy filters were applied to select the appropriate wavelength for excitation of FITC, DAPI and Cy3 fluorophores. Digital images were obtained with a QI Click colour CCD camera (Q-Imaging) and processed using Image Pro-plus software (Media Cybernetics Inc.). For images used for semi-quantitative comparison, identical exposure times were used for the target fluorophore(s).

2.3.2 Image analysis with Fiji

2.3.2.1 Quantification of antibody binding: Manual image analysis with Fiji

For the manual assessment of antibody specificity and reactivity, the image analysis software Fiji (Schindelin *et al.*, 2012) was used. RawIntensity values were measured from each channel corresponding to the desired fluorophore for semi-quantitative evaluation of

antibody binding. Cell numbers were manually counted based on DAPI reactivity or estimated based on RawIntensity values of the DAPI (blue) channel. To eliminate background signal from samples the RawIntensity values for each channel from a secondary only control was subtracted from the test images. All evaluations were based on analysis of at least 3 images per condition. Quantitative evaluation of cell number and transfection positive cells (judged according to presence of appropriate reactivity within cell cytoplasm) were used to evaluate total cell counts and transfection efficiency (number of fluorescent cells/Total cells).

In order to evaluate antibody binding, two methods were devised. The first method aims to determine the antibody reactivity per cell based on manual counting of cells according to DAPI reactivity and morphology. An alternative and more objective method, approximates cell number according to DAPI RawIntensity of the image. Due to comparative images being taken with identical exposure times, this method offered the opportunity to make the analysis more efficient. A relative measure of antibody binding to cell presence was then calculated according to the RawIntensity values of signal obtained from the fluorescent secondary antibody (used for the detection of the test primary antibody) and the RawIntensity of DAPI signal(Antibody/DAPI Rawintensity). This measure could then be used to compare antibody binding to non-transfected and transfected cells to establish antibody binding to the test protein (Xcr1-myc or XCR1-myc).

2.3.2.2. Area of antibody binding

2.3.2.2.1 Quantification of area of Fluorescently labelled antibodies

The area of antibody presence was identified as a percentage of the total measure of the image area or selected Region of Interest (ROI). ROIs were delineated by freehand selection of the desired area. To identify specific staining each image was split to RGB channels. The channel corresponding to the fluorophore used for detection of the desired antibody was then used. The 'Subtract background' removed background staining, according to a rolling ball radius of 25 pixels. The threshold of the greyscale image was then adjusted to reflect specific staining and the % Area of specific staining relative to the total ROI area was used for analysis. Measurements were collected using Microsoft Excel (2013) and then analysed using Prism 7.0 (Graphpad Inc.).

2.3.2.2.2 Quantification of DAB staining Area

The area of DAB reactivity was quantified as a percentage of total image area. DAB staining was identified within the image using the Colour Deconvolution process of Fiji according to the appropriate "H DAB" colour vectors. The threshold of detected DAB staining was then adjusted to permit identification of positive staining and %Area of staining measured.

Quantified DAB area (as a percentage of the total image area) was then exported to Microsoft Excel (2013) for subsequent data processing.

2.3.3. Opera Phenix™ High Content Screening system

For the analysis of antibody specificity to XCR1 proteins expressed in transfected HeLa, cells seeded and treated in 96 well plates were evaluated by automated image capture and analysis using the Opera Phenix High Content Confocal Screening system (PerkinElmer). Images were captured at 20x for each fluorophore and analysed using Harmony image acquisition and analysis software (PerkinElmer). Cell nuclei and cell cytoplasm were identified using the most suitable algorithm available within the Harmony software. Semi-quantitative evaluation of antibody binding was performed for all cells within the test image. Quantification was based upon the Mean Cell Intensity of the signal emitted from the corresponding secondary antibody used for detection of the respective primary antibody.

Colocalisation of test antibody reactivity with C-myc reactivity was performed to support antibody specificity. This was achieved by specifying regions of the individual image that demonstrated the highest intensity of signal corresponding to C-myc binding. Quantification of the emitted signal arising from the test antibody within this specified region was then used as a measure of colocalisation.

Raw data from Harmony analysis was exported to Microsoft Excel (2013) and subsequently analysed as described in section 2.9. Automated image acquisition provided images that were auto-contrasted according to individual images. To display a consistent display range of pixel intensity and accurately represent differences in antibody signal, the display range of images used for comparison presented in the Results section were adjusted using Fiji Image analysis software (Schindelin *et al.*, 2012).

2.4 Molecular Biology Methods

2.4.1 BCA assay

Protein concentrations of collected samples were determined using the Pierce™ bicinchoninic acid (BCA) assay (ThermoFisher). The protein concentration of unknown samples was determined from the standard curve of optical density at 560nm for a series of protein samples of known concentration between 0 and 2000µg/ml of Albumin.

2.4.2 SDS-Polyacrylamide Gel electrophoresis

15-30µg of protein was diluted in 6x protein loading buffer (National Diagnostics) and incubated for at least 30 minutes at room temperature or heated to 95°C for 10 minutes

before cooling to room temperature. Samples were then loaded in to a 12-15% sodium dodecyl sulphate-polyacrylamide gel along with the Ez-run Rec protein molecular weight ladder (ThermoFisher) and separated by electrophoresis (SDS-PAGE) at 100 – 150V until the desired travel of protein was achieved.

2.4.3 Immunoblotting

Following SDS-PAGE, protein was transferred from the gel to a nitrocellulose membrane (GE Healthcare) using the Trans-Blot® Turbo™ blotting system (BioRad). Protein transfer was evaluated by ponceau S (ThermoFisher) staining before incubating the membrane in blocking buffer (0.1% Tween-20, Tris Buffered Saline (50mM Tris-Cl, pH 7.5, 150mM NaCl) (TBS-T), 5% dried non-fat milk powder) for 1 hour. Primary antibodies were then added at concentrations as detailed in table 2.1 in blocking buffer and incubated at 4°C whilst rolling overnight. The membrane was then washed 2x for 5 minutes and 2x for 10 minutes in TBS-T before adding the desired HRP-conjugated secondary antibody for 2 hours whilst rolling at RT. A further 3x 10 minute washes of the membrane in TBS-T was then performed. Localisation of HRP-conjugated secondary antibody was then identified by the addition of the Clarity™ Western ECL chemiluminescent substrate (BioRad) for 1 minute. Chemiluminscence was then detected by exposure to light-sensitive film for the desired time period. The exposed film was then developed using the automated Compact X4 Film developer (Xograph Imaging Systems).

Estimation of molecular weight of proteins identified by western blot was made based on the relative migration distance of protein standards loaded within the same gel. For each protein standard a relative migration distance (R_f) was calculated based upon the following equation:

$$Rf = \frac{migration\ distance\ of\ protein}{migration\ distance\ of\ dye\ front}$$

Rf values of each protein standard were plotted against the Log_{10}(molecular weight) of the protein standards and linear regression was performed using Prism 7.0 (Graphpad Inc.) to determine the standard curve formula. The Rf value of an identified (unknown) protein was then used to calculate the molecular weight according to the standard curve formula:

$Log_{10}(Molecular\ Weight) = (A*R_f) + C$

2.4.4 Polymerase Chain Reaction

2.4.4.1 Primer Design

The design of primers was performed using the NCBI Primer-Blast Tool (Ye *et al.*, 2012) in combination with the manual selection of primer targets according to the recorded gene

sequences detailed on the NCBI Nucleotide and Ensemble Gene databases. Selected primer pairs were then chosen according to the matching of primer melting temperatures, calculated from the Online Custom Oligo Ordering Tool (Merck).

2.4.4.2 DreamTaq Hot Start Green PCR

Polymerase Chain Reaction (PCR) amplification of target amplicons ≤1kb was performed using DreamTaq Hot Start Green PCR Master Mix (ThermoFisher). Primers were prepared to a concentration of 1µM and cDNA was used at a concentration of 50-100ng per 50µl Reaction. PCR was performed according to a three step protocol consisting of primer annealing at (Tm-5)°C, amplicon extension at 72°C and denaturation at 95°C. The performed time parameters for each step were determined according to the size of target amplicon as described by the manufacturer.

2.4.4.3 Phusion PCR

For the amplification of PCR inserts for subsequent cloning in to a host vector (section 2.4.6) the high fidelity Phusion DNA polymerase (NEB) was used. Reaction components and buffers were determined according to manufacturers recommendation for the size and quality of target amplicon. An internal control to confirm efficiency of PCR amplification of large (10kb) amplicons was included with each reaction, using the provided bacteriophage lambda DNA template.

2.4.5 Agarose Gel electrophoresis

DNA fragments produced by PCR or restriction endonuclease digest were separated by agarose gel electrophoresis. The desired concentration of agarose powder was added to 200ml 1x TAE buffer (40mM Tris-Acetate, 1mM EDTA (dH_2O)) and heated in a microwave until the agarose powder had completely dissolved. EtBr was added to achieve a concentration of 0.003% (v/v) and then the solution was poured in to a cassette to cool with an inserted comb to permit sample aspiration to the gel. The gel was placed in to a tank of 1x TAE and samples loaded along with a desired molecular weight ladder. Samples were ran at 100V until the desired separation of fragments had been achieved. Separated fragments were then imaged using the InGenius 3 Gel documentation system (SynGene).

2.4.6 Plasmid Cloning

2.4.6.1 Plasmids

Two plasmids were purchased from Origene. Origene RC221929 is a plasmid composed of a pCMV6 entry vector with an insert containing the Human *XCR1* protein coding sequence (NCBI reference NM_001024644) with a C-terminal Myc-DDK tag. Origene MR225748 is

A)

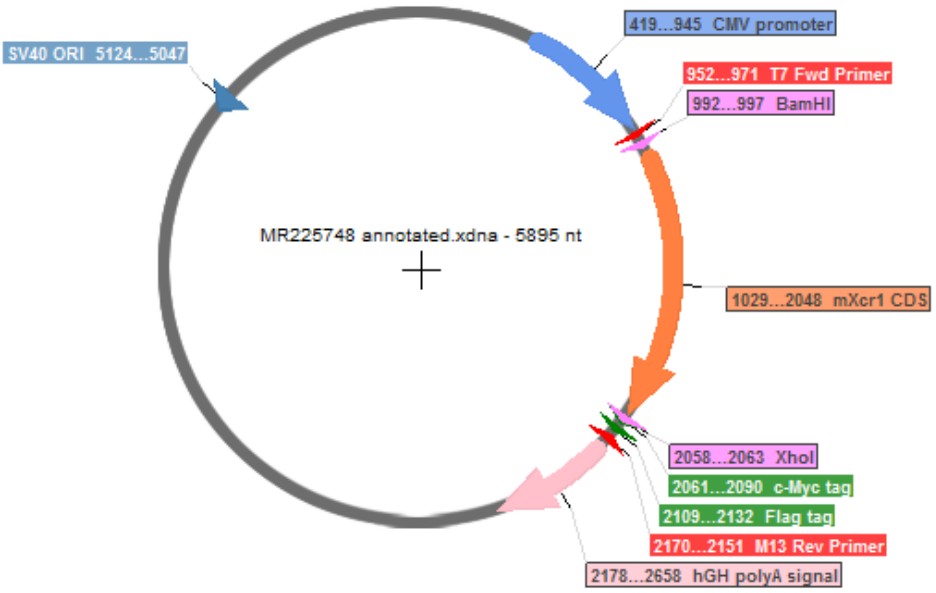
SV40 ORI 5124...5047
419...945 CMV promoter
952...971 T7 Fwd Primer
992...997 BamHI
MR225748 annotated.xdna - 5895 nt
1029...2048 mXcr1 CDS
2058...2063 XhoI
2061...2090 c-Myc tag
2109...2132 Flag tag
2170...2151 M13 Rev Primer
2178...2658 hGH polyA signal

B)

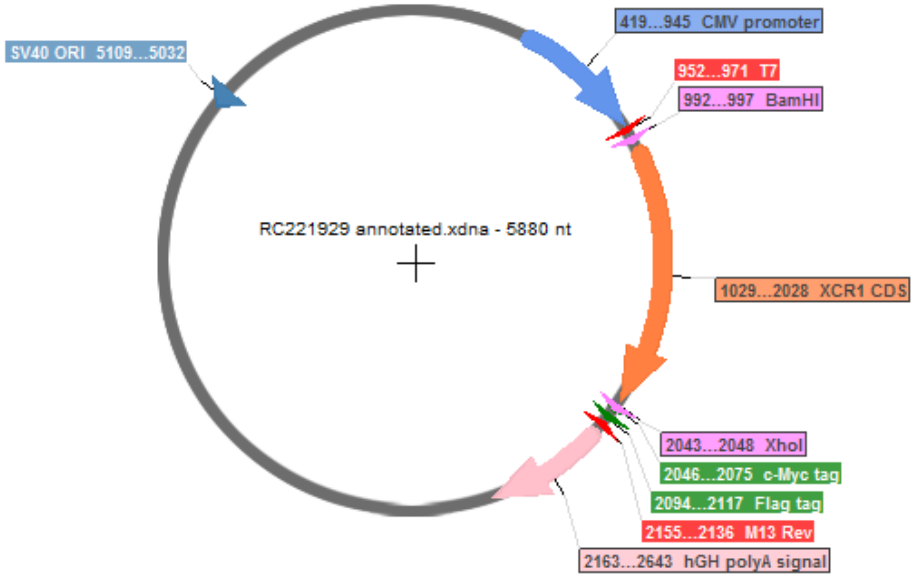
SV40 ORI 5109...5032
419...945 CMV promoter
952...971 T7
992...997 BamHI
RC221929 annotated.xdna - 5880 nt
1029...2028 XCR1 CDS
2043...2048 XhoI
2046...2075 c-Myc tag
2094...2117 Flag tag
2155...2136 M13 Rev
2163...2643 hGH polyA signal

C)

D)

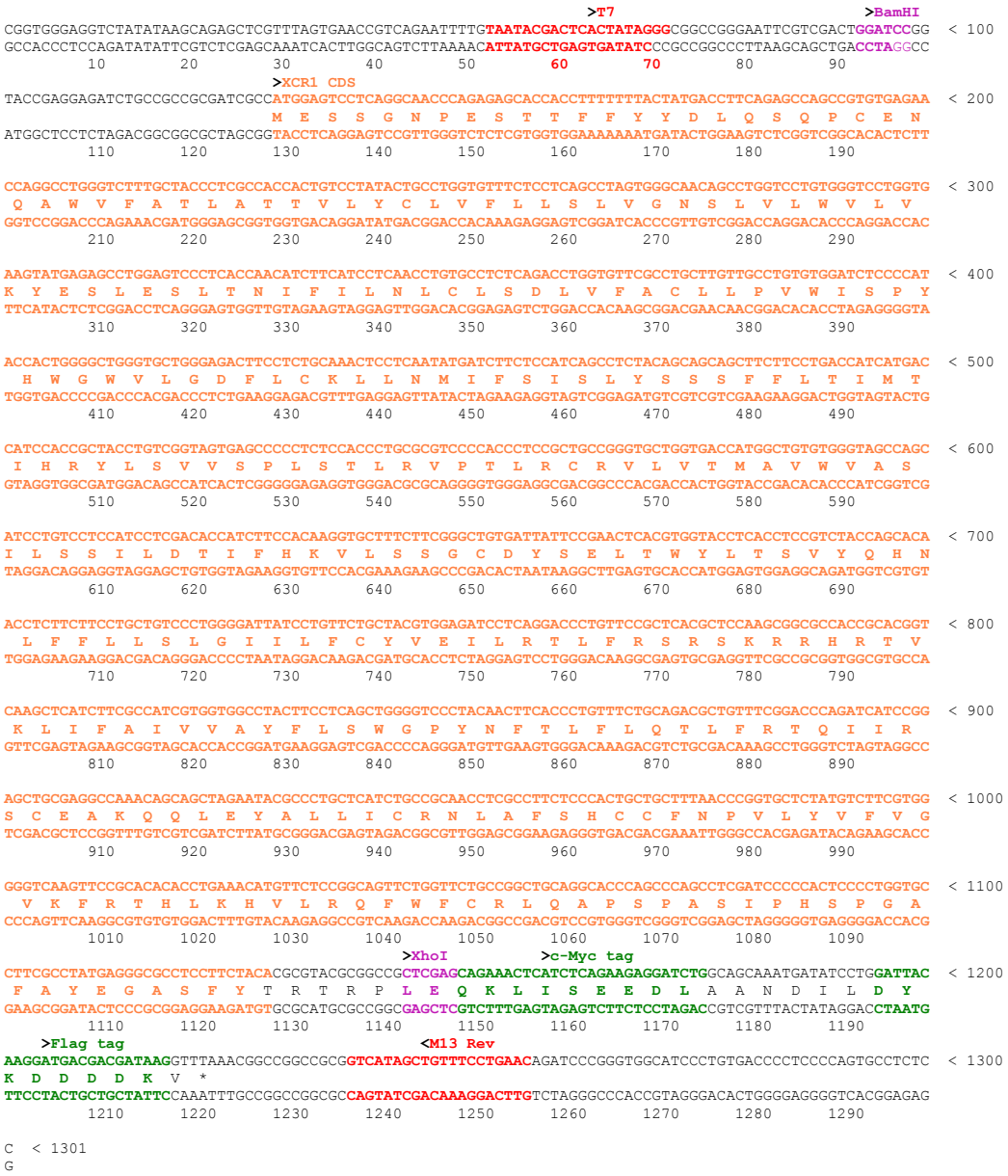

Figure 2.2. *Schematic and sequence data of plasmids used for antibody testing containing myc-tagged Xcr1 and XCR1 inserts.* A,B) Schematic overview of A) MR225748 plasmid containing the Xcr1-myc coding sequence and B) RC221929 plasmid containing the XCR1-myc coding sequence. C, D) Sequences of C) MR225748 and D) RC221929 inserts as provided by manufacturer (Origene). Highlighted regions: Blue – SV40 origin of replication and CMV promoter; Red- primers used for sequencing of plasmids (T7 and M13 Rev); Purple - Restriction endonuclease sites used for confirming plasmid size following E.Coli amplification (BamHI and XhoI); Orange – Coding sequence of desired Xcr1 (MR225748) or XCR1 (RC221929) proteins; Green – C-terminal sequences coding for Myc and Flag tag peptides; Pink – hGH termination sequence for 3' polyadenylation and termination of expressed mRNA.

also a pCMV6 entry vector with an insert containing the Murine *Xcr1* protein coding sequence (NCBI reference NM_011798.4) with a C-terminal Myc-DDK tag (Figure 2.2). Transfection with pcDNA5/FRT/TO GFP (Addgene #1944), kindly donated by Dr Adrian Higginbottom (University of Sheffield), and a TDP-43-C-myc plasmid, kindly donated by Dr Yolanda Gibson (University of Sheffield), were also used to evaluate transfection efficiency and optimise transfection conditions. pCMV-PK2 and pCMV-ARMS2-PK2 vectors for use in the DiscoverX® PathHunter™ β-arrestin assay were kindly provided by the laboratory of Dr Gareth Richards (University of Sheffield).

2.4.6.2 DH5α E.Coli Transformation and Selection

To amplify plasmid stock, transformation of competent DH5α *E.Coli* cells (Invitrogen) was performed. *E.Coli* bacteria stocks were thawed on ice. 50µl of thawed *E.Coli* was then aspirated gently using a 200µl pipette with the pipette tip cut with scissors to minimise shear forces introduced to the bacteria during pipetting. This was done to ensure collection of cells within the suspension that may have deposited to the bottom of the vial. 50µl of *E.Coli* was then aliquoted in to a pre-chilled (on ice) 1.5ml Eppendorf tube. 1-5µl of plasmid (up to 50ng) was then added dropwise to the top of the cells and incubated in ice for 30 minutes. As a positive control for transformation, 2.5µl (250pg) of the supplied pUC19 control plasmid (Invitrogen) was added to a separate 1.5ml Eppendorf tube containing 50µl of DH5α *E.Coli* cells. After 30 minutes on ice cells were heat shocked at 42°C, in a pre-heated heat block, for 40-45 seconds and then returned immediately to ice for 2 minutes. 950µl of pre-warmed (37°C) Super Optimal Broth with Catabolite suppression (SOC) media was then added to the 1.5ml Eppendorf tube. Eppendorf tubes were shaken at 225RPM at 37°C for 90 minutes before 100µl of each transformed culture was streaked across a pre-warmed (37°C) agar selection plate containing the appropriate concentration of selective antibiotic (Ampicillin 100µg/ml, Kanamycin 50µg/ml). Agar plates were then incubated for 24-72 hours at 37°C. Individual colonies were then selected and transferred to 5ml lysogeny broth (LB) containing the appropriate concentration of antibiotic (Ampicillin 100µg/ml, Kanamycin 50µg/ml) within a falcon tube. Transformed *E.Coli* cultures were then incubated overnight (16-18 hours) at 37°C whilst shaking at 225RPM on a rotator plate.

2.4.6.3 Plasmid Mini-prep and MaxiPrep

After overnight culture, plasmids were isolated from 1ml transformed *E.Coli* using the Isolate II Plasmid mini-kit (Bioline) according to manufacturer's instructions for isolation of low-copy plasmids. Plasmids from each colony were then preliminarily identified by restriction endonuclease digest (see 2.4.6.4). Following confirmation of identity, 500ml of LB containing the appropriate concentration of antibiotic (50µg/ml Kanamycin, 100µg/ml Ampicillin) was inoculated with 1ml from one of the cultures of *E.Coli* to provide a larger

bacterial stock. This 500ml culture was then incubated for 18-20 hours at 37°C whilst shaking at 225RPM on a rotator plate. Plasmids were isolated from this 500ml culture using the Plasmid Maxi kit (Qiagen) using a high speed Avanti J-26 XP centrifuge (Beckman Coulter™). Isolated plasmids prepared using the Isolate II Plasmid mini-kit (Bioline) or Plasmid Maxi kit (Qiagen) were eluted or resuspended with RNase and DNase free water. 1µl of each sample was then quantitatively and qualitatively analysed using a NanoDrop 1000 spectrophotometer (ThermoScientific, USA) and then stored at -80°C until subsequent use.

2.4.6.4 Restriction Endonuclease Digest

Plasmids isolated from *E.Coli* were identified by a preliminary restriction endonuclease digest to determine the presence of predicted DNA fragment sizes and to provide DNA fragments for the subsequent directional cloning of plasmids. Restriction endonuclease sites were first identified using the online NEBcutter tool (Vincze, Posfai and Roberts, 2003). 500ng of plasmid DNA was incubated with the chosen restriction enzymes according to manufacturer's instruction. 10µl of digested plasmid DNA was then loaded in to a 1% agarose gel with 2µl 6x protein loading buffer (ThermoFisher). 5µl of GeneRuler 1kb DNA ladder (ThermoFisher) was loaded for fragment size reference. Fragments were then separated by agarose gel electrophoresis. The separated fragments were imaged within the agarose gel using InGenius 3 Gel documentation system (SynGene).

2.4.6.5 Plasmid Subcloning

The production pCMV-PK2 plasmids containing the coding sequences of either Xcr1L or Xcr1S proteins was achieved by directional cloning of *Xcr1L* and *Xcr1S* nucleotide inserts in to pCMV-PK2 and pCMV-ARMS2-PK2 vectors.

Xcr1L and *Xcr1S* inserts were generated by PCR amplification of the target coding sequences from the OriGene MR225748. Coding inserts were cloned in to pCMV-PK2 and pCMV-ARMS2-PK2 vectors by directional cloning to the vector multiple cloning site as detailed in Figure 2.3. PCR of target insert amplicons was performed using the High Fidelity Phusion PCR kit (NEB). Due to the high melting temperatures of the primers used, cycling parameters were performed using a 2 step PCR protocol composed of a 98°C denaturation step for 1 minute, followed by 40 cycles of 98°C for 10 seconds to 72°C for 30 seconds. A final elongation step was performed for 10 minutes at 72°C and then returned to 4°C for storage. Confirmation of amplicon production was determined by agarose gel electrophoresis.

PCR inserts and vectors were digested with BgIII and HindIII restriction enzymes for 4 hours at 37°C using 3.1 buffer (NEB). A total of 1µg vector and insert were used for digestion.

To prevent autoligation, shrimp alkaline phosphatase (SAP) (NEB) was added to digested inserts for 30 minutes at 37°C at a concentration of 1.5µl SAP/µg of insert DNA. All samples digested with BgIII and HindIII were then heated to 80°C to inactivate the enzymes. Following digestion, vector backbone and inserts were separated by agarose gel electrophoresis and purified using the Isolate II PCR and gel kit (Bioline) according to manufacturer's instruction. Target insert and vector were then ligated at a 2:1 molar ratio of insert to vector by overnight incubation at 16-18°C with T4 DNA ligase (NEB) according to manufacturer's instruction.

Recombinant plasmid vectors were then transformed to competent *E.Coli* for the production of plasmid stocks, as detailed in section 2.4.6.1 and 2.4.6.2. Produced plasmids are referred to collectively as 'pCMV-Prolink2 vectors' and individually as follows: pCMV-Xcr1L-PK2 (L-PK2); pCMV-Xcr1S-PK2 (S-PK2); pCMV-Xcr1L-ARMS2-PK2 (L-ARMS2); pCMV-Xcr1S-ARMS2-PK2 (S-ARMS2).

2.4.6.6 DNA sequencing

Conservation of Plasmid coding sequences were determined by DNA sequencing by the Core Genomics Facility (University of Sheffield). Sequencing of plasmids obtained from Origene was performed using the T7 forward (5'-TAATACGACTCACTATAGGG-3') and M13 Reverse (5'-CAGGAAACAGCTATGACC-3') primers (Figure 2.2). Sequencing of pCMV-Prolink2 vectors was performed using a combination of primers targeted to the *Xcr1* sequence. Confirmation of nucleotide identity was evaluated by FinchTV (GeoSpiza Inc.). Pairwise sequence alignment was performed using EMBOSS Needle Nucleotide pairwise alignment tool (Rice, Longden and Bleasby, 2000) and/or Serial Cloner Software (http://serialbasics.free.fr/Serial_Cloner.html).

2.5 Gene Expression profiling

2.5.1 DNase Treatment of RNA

Prior to preparation of cDNA, all RNA samples underwent DNase I treatment after RNA isolation. The appropriate RNA quantity required for analysis was treated by DNase I (amplification grade; specific activity >10,000 units/mg, ThermoFisher) at a concentration ratio of 1µg RNA to 1µl DNase I and prepared according to manufacturer's instruction.

DNase-treated RNA was then heated at 72°C for 10 minutes before being placed immediately on ice for at least 5 minutes. This ensured sufficient denaturation of RNA secondary structure prior to cDNA synthesis and was found to significantly improve the reliability and consistency of subsequent cDNA production.

A

```
                                BgIII      HindIII   >ProLink
                                  |          |       |
ATCCGCTAGCGCTACCGGACTCAGATCTCGAGCTCAAGCTTCGAATTGGGAGGT
TAGGCGATCGCGATGGCCTGAGTCTAGAGCTCGAGTTCGAAGCTTAACCCTCCA
          10        20        30        40        50
```

B

> Xcr1L pCMV-ProLink2 insert, 1014bp, stop codon omitted

```
ATGGACTCAGAGTCAGATGCTCTCAGTATCCCTGCATCCCGCGTCCAGATGGAGTCCTCTACAGCCTTTTATGATTATCATGATAAAT
TGAGTCTTCTATGTGAGAACAATGTCATCTTCTTTTCCACCATCTCTACCATTGTCCTGTACTCTCTGGTATTTCTCCTCAGCCTTGT
GGGTAACAGCCTGGTTTTGTGGGTCTTGGTGAAGTATGAGAATCTAGAGTCACTCACCAATATCTTCATCCTCAACCTGTGTCTCTCA
GACCTGATGTTCTCCTGTCTACTGCCTGTGTTGATCTCAGCACAATGGAGTTGGTTTCTAGGTGACTTCTTCTGCAAGTTCTTCAACA
TGATCTTCGGCATCAGCCTCTACAGCAGCATCTTCTTCCTTACCATCATGACCATCCACCGATACCTGTCTGTAGTGAGCCCCATCTC
TACTCTGGGTATCCATACCCTCCGCTGCCGTGTGCTGGTGACATCATGTGTGTGGGCAGCCAGCATCCTGTTCTCCATCCCTGATGCT
GTCTTCCACAAAGTGATCTCCTTAAATTGTAAATATTCTGAACATCATGGGTTCTTGGCCTCAGTCTACCAGCACAACATCTTCTTCC
TCCTCTCCATGGGAATCATCCTATTCTGTTATGTACAGATTCTCAGGACTTTGTTTCGCACAAGGTCCAGACAGAGACACCGAACAGT
CAGGCTCATCTTCACCGTCGTGGTAGCATACTTCCTCAGCTGGGCTCCCTACAACCTCACACTCTTCCTGAAAACTGGAATCATCCAG
CAGAGCTGTGAGAGCCTTCAGCAACTGGACATTGCTATGATTATCTGTCGCCATTTGGCCTTCTCTCATTGCTGTTTCAACCCAGTGC
TTTATGTCTTTGTTGGGATCAAGTTCCGCAGACACCTAAAACATCTCTTCCAGCAGGTCTGGCTGTGCCGGAAGACATCCAGCACTGT
TCCCTGCTCCCCTGGTACCTTTACATATGAGGGACCCTCCTTCTAC
```

C

> Xcr1S pCMV-Prolink2 insert, 966bp, stop codon omitted

```
ATGGAGTCCTCTACAGCCTTTTATGATTATCATGATAAATTGAGTCTTCTATGTGAGAACAATGTCATCTTCTTTTCCACCATCTCTA
CCATTGTCCTGTACTCTCTGGTATTTCTCCTCAGCCTTGTGGGTAACAGCCTGGTTTTGTGGGTCTTGGTGAAGTATGAGAATCTAGA
GTCACTCACCAATATCTTCATCCTCAACCTGTGTCTCTCAGACCTGATGTTCTCCTGTCTACTGCCTGTGTTGATCTCAGCACAATGG
AGTTGGTTTCTAGGTGACTTCTTCTGCAAGTTCTTCAACATGATCTTCGGCATCAGCCTCTACAGCAGCATCTTCTTCCTTACCATCA
TGACCATCCACCGATACCTGTCTGTAGTGAGCCCCATCTCTACTCTGGGTATCCATACCCTCCGCTGCCGTGTGCTGGTGACATCATG
TGTGTGGGCAGCCAGCATCCTGTTCTCCATCCCTGATGCTGTCTTCCACAAAGTGATCTCCTTAAATTGTAAATATTCTGAACATCAT
GGGTTCTTGGCCTCAGTCTACCAGCACAACATCTTCTTCCTCCTCTCCATGGGAATCATCCTATTCTGTTATGTACAGATTCTCAGGA
CTTTGTTTCGCACAAGGTCCAGACAGAGACACCGAACAGTCAGGCTCATCTTCACCGTCGTGGTAGCATACTTCCTCAGCTGGGCTCC
CTACAACCTCACACTCTTCCTGAAAACTGGAATCATCCAGCAGAGCTGTGAGAGCCTTCAGCAACTGGACATTGCTATGATTATCTGT
CGCCATTTGGCCTTCTCTCATTGCTGTTTCAACCCAGTGCTTTATGTCTTTGTTGGGATCAAGTTCCGCAGACACCTAAAACATCTCT
TCCAGCAGGTCTGGCTGTGCCGGAAGACATCCAGCACTGTTCCCTGCTCCCCTGGTACCTTTACATATGAGGGACCCTCCTTCTAC
```

D

pCMV-ProLink Insert	**Forward Primer (BgIII + Kozak)**	**Reverse Primer (HindIII)**
BgIII-*Xcr1L*-HindIII	5'-GGGCGGAGATCTGCCACC***ATG***GACTCAGAGTCAGATGC-3'	5'-GGGCCGAAGCTTGC*GTAGAAGGAGGGTCCCTCAT*-3'
BgIII-*Xcr1S*-HindIII	5'-GGGCCGAGATCTGCCACC***ATG***GAGTCCTCTACAGCCTT-3'	5'-GGGCCGAAGCTTGT*GTAGAAGGAGGGTCCCTCAT*-3'

Figure 2.3. *Directional cloning of Xcr1L and Xcr1S PCR inserts in to pCMV-Prolink2 vectors.* A) Multiple cloning site of pCMV-ProLink2 vectors, as provided by manufacturer. BgIII and HindIII restriction sites were used for cloning of inserts. ProLink sequence highlighted in red conferred coding sequence for either ProLink2 or ARMS2-ProLink2 enzyme donor (ED) tags. B) Coding sequence of Xcr1L protein to be amplified by PCR from Origene MR225748 plasmid. Sequence in Red highlights 5' Sequence that distinguishes *Xcr1L* from *Xcr1S*. C) Coding sequence of Xcr1S protein to be amplified by PCR from Origene MR225748 plasmid. D) Details of primers used for PCR amplification of *Xcr1L* and *Xcr1S* inserts. Underlined sequence corresponds to sequence for restriction enzyme recognition. Sequence in italics represents complementary sequence to target amplicon. Start codons of *Xcr1L* and *Xcr1S* coding sequences are highlighted in bold.

2.5.2 Reverse Transcription-PCR

cDNA was prepared using the High Capacity RNA to cDNA kit (ThermoFisher) according to manufacturer's instruction. RNA samples of ≤1µg/µl of RT enzyme were used. Note that the reverse transcription mixture was thoroughly chilled prior to addition to the DNase-treated RNA sample. Reverse transcription was performed for 1 hour at 37°C followed by inactivation of the transcriptase enzyme for 5 minutes at 95°C. Samples were then stored at 4° until use or at -80° for long term storage.

2.5.3 Quantitative Polymerase Chain reaction

Assessment of mRNA expression was performed via quantitative evaluation of cDNA presence by quatitative-PCR (qPCR) using Power SYBR ® master mix (ThermoFisher). Primers were designed for the amplification of sequences from *Gapdh, Xcr1, Xcl1, Tmem119, Cg-Tmed2* and *Cg-Xcl1* (Table 2.3). All primers were designed to achieve a melting temperature (Tm) of between 61°C and 63°C. qPCR was performed using the Rotor Gene Q (Qiagen) Thermal Cycler and associated Rotor Gene Q Series Software (Qiagen). Cycling parameters were performed using a two-step protocol that included an initial 10 minute incubation at 95°C followed by 40 cycles of 95°C to primer (Tm-5)°C. Cycle threshold (Ct) values were obtained by setting a threshold fluorescence that was above the observed fluorescent background for each experiment. After cDNA quantification, melt curve analysis was performed to determine the specificity of primer amplification by heating the samples from 50°C to 99°C at a rate of 10 seconds per 1°C and measuring the associated fluorescence. Melt curve analysis is presented by dF/dT, corresponding to the rate of change of Fluorescence per change in Temperature. The production of specific amplicons was also evaluated by agarose gel electrophoresis.

2.5.3.1 qPCR analysis

Ct values of the target amplicons were exported from the provided report of the Rotor Gene Q Series Software (Qiagen) to Microsoft Excel (2013). Gene expression was quantified according to the relative expression level of the target gene to an internal reference gene, otherwise known as the delta Ct method. For evaluation of mouse transcripts the internal reference gene used was *Gapdh*, whilst for evaluation of transcripts from Chinese Hamster Ovary (CHO) cells the internal reference gene used was *Cg-Tmed2* according to published recommendations (Brown 2017). Comparative expression of target genes between samples were calculated according to the difference of the relative target gene expression between samples, otherwise known as the delta-delta Ct method (Pfaffl 2001).

2.5.3.2 Accounting for non-detects

Target	Fwd sequence (Location)	Rev Sequence (Location)	Amplicon Size
Xcr1L	5'-GAAACCCTGACATGGACTCA-3' (Exon 1)	5' – CTTCACCAAGACCCACAAA – 3' (Exon 2)	221bp
Xcr1S	5'-CCAGATGGAGTCCTCTACAGC-3' (Exon 2)	5' – CTTCACCAAGACCCACAAA – 3' (Exon 2)	164bp
Xcl1	5'-CCTATATCATCTGGGAGGGG-3' (Exon 2)	5'-GCTTCTGGATCAGCACAAAT-3' (Exon 3)	82bp
Gapdh	5'-GTGGAGTCATACTGGAACATGTAG-3' (Exon 2)	5'-AATGGTGAAGGTCGGTGTG-3' (Exon 3)	130bp
Cg-Tmed2 (Brown 2017)	5'-GCCCACATGGATGGGACATAC-3'	5'-TGATGAGCTTCTGTCTCCATGTC-3'	131bp
Cg-Xcl1 (Designed to XM_007613998.1)	5'-ACCTATACCATCAGGGAGGG-3' (Exon 2)	5'-ATCTGTGCAGATCCACACG-3' (Exon 3)	82bp

Table 2.3. *Primer sequences used for quantitation of associated genes by qPCR.* All primer sequences are designed to nucleotide sequences corresponding to mouse genes unless indicated by Cg-prefix to denote targeting of primers to associated gene of *Cricetulus griseus* (Chinese Hamster). Primers targeting *Cg-Tmed2* were taken from those optimised previously and are documented to amplify an intron-spanning product (Brown 2017).

For some samples, due to the low presence of associated transcripts, the generation of amplicons failed to reach the detection threshold. These non-detects were dealt in accordance with previous recommendations (McCall *et al.*, 2014). From these recommendations it was determined that non-detects would be accounted for by assigning a Ct value of 35.

2.5.3.3 Comparison of Xcr1L and Xcr1S expression

Due to the structure of *Xcr1* and its potential mRNA sequences, amplicons detected by the amplification of cDNA by *Xcr1S* primers also detect the same cDNA as *Xcr1L* primers. Therefore, in order to calculate the difference in expression of *Xcr1S*-specific to *Xcr1L* amplicons, the component of *Xcr1S* amplicons that shared the same cDNA origin as that of *Xcr1L* amplicons had to be first subtracted from the total *Xcr1S* expression. Assuming 100% efficient PCR amplification, the expression of *Xcr1S*-specific amplicons can be determined by the subtraction of *Xcr1L* amplicon expression from *Xcr1S* amplicon expression. Hence the expression of *Xcr1S*-specific amplicons is determined as follows:

Xcr1S-specific expression = *Xcr1S expression – Xcr1L expression*

Where the expression of *Xcr1S* and *Xcr1L* amplicons is determined by the delta Ct method with reference to the internal GAPDH reference gene. For all comparisons between *Xcr1S* and *Xcr1L* expression this correction to *Xcr1S* expression was first applied. For clarity, all references to *Xcr1S* expression in result sections refers to this *Xcr1S*-specific calculation. The relative expression of *Xcr1S* amplicons to *Xcr1L* amplicons has therefore been calculated as follows:

$$\text{Relative } Xcr1S/Xcr1L \text{ expression} = \frac{(Xcr1S \text{ expression} - Xcr1L \text{ expression})}{Xcr1L \text{ expression}}$$

2.5.3.4 Comparison of gene expression changes between biological replicates

For the evaluation of *Xcl1* expression between control primary microglial cultures and primary microglial cultures treated with LPS, data was first processed according to the recommendations by Willems *et al*., 2008. This method provides a method to correct for the variability in gene expression quantification that typically arises between biological replicates. To provide a more robust comparison between control and LPS-treated primary microglia, mean Ct values of *Xcl1* and the internal *Gapdh* reference, calculated from their respective technical triplicates, were inputted to the supplementary spreadsheet provided (Willems, Leyns and Vandesompele, 2008). Mean, SEM and N values from Ct values that were log-transformed and mean-centred were then inputted to Prism 7.0 (Graphpad Inc.). Statistical comparisons were made by independent T-test.

2.5.4 Retrospective microarray analysis

Microarray data collected from Neuroblastoma Spinal Cord 34 (NSC-34) cells was kindly provided by Dr Matthew Stopford. To evaluate the differential expression of RNA arising from *Xcr1* exon 1 or *Xcr1* exon 2, the provided RMA-ALT-SPLICE CHP files were opened with the Transcriptomics Analysis Console (Affymetrix). For all data analysed, the performance of each array had been evaluated according to quality control metrics recommended by the manufacturer using the Affymetrix ® Expression Console™ (Stopford, 2016). The comparison between each of the arrays compared by retrospective analysis was therefore considered valid according to the assessment of quality control demonstrating consistent metrics from each array that did not occur outside the two SD threshold for more than one metric.

Individual probe intensities corresponding to the detection of each exon were then collected and averaged to determine the mean probe intensity for the detection of exon 1 and exon 2 of *Xcr1* from 9 independent microarray replicates. The relative difference in expression of each exon was then compared by normalisation of mean exon probe intensity to the mean exon probe intensity of exon 1. Statistical comparisons were then made by independent t-test using Prism 7.0 (Graphpad Inc.)

2.6 Investigation of *Xcr1* mRNA sequence composition

2.6.1 5' Rapid Amplification of cDNA ends

mRNA sequences were analysed by 5' Rapid Amplification of cDNA Ends (RACE) using the 5'/3' RACE kit (Sigma) according to manufacturer's instruction. Target transcripts were amplified by two rounds of PCR amplification. The first round of PCR amplification was performed using the High Fidelity Phusion PCR kit (NEB). The second round of PCR was performed using DreamTaq Hot Start Green PCR master mix. Details of primers used and their location in respect to *Xcr1* mRNA are detailed in Figure 2.4.

Produced amplicons were provided to the Core Genomics Facility at the University of Sheffield for DNA sequencing with the Sp3 primer. Resultant sequences were inspected using FinchTV, with provided sequences deduced from the most prominent nucleotide peak at each position.

2.6.2 Testing of Xcr1 intron retention

To evaluate the retention of intron 1 within *Xcr1* mRNA, PCR was performed using reverse-transcribed and RT-negative samples of DNase I-treated RNA from 3 x spleen. Forward PCR primers tested were located as follows within the *Xcr1* intron (for bp location, see appendix 1) and used in conjunction with the Sp2 Rev primer (figure 2.4):

> *Xcr1* Coding sequence (ENSMUST00000182350.1)

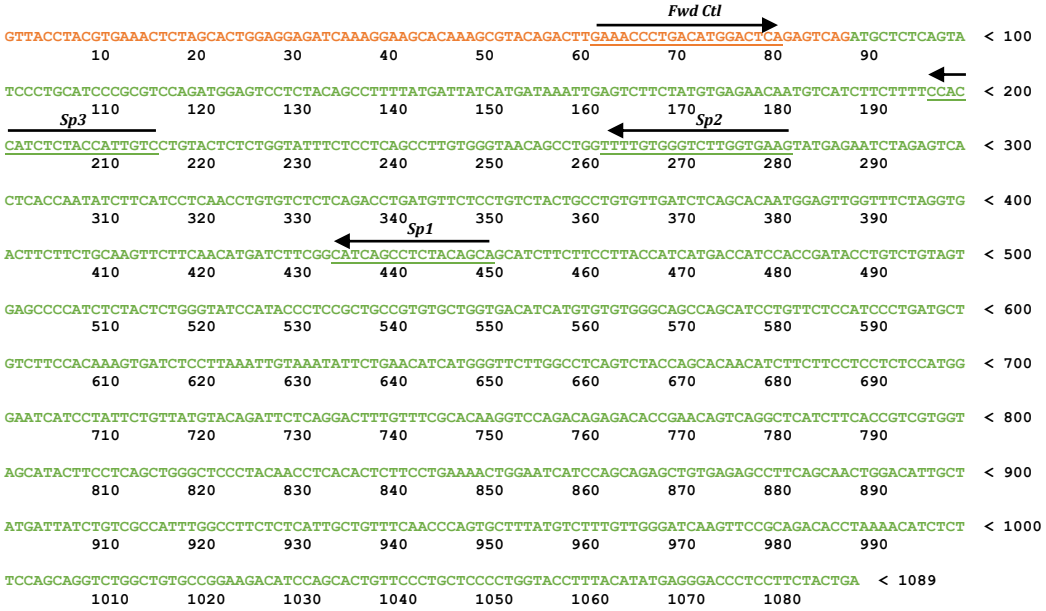

Figure 2.4. *Primer design for detection of Xcr1 mRNA sequence by 5' RACE.* Detailed sequence corresponds to coding sequence of *Xcr1* mRNA as described by Ensemble Transcript ID ENSMUST00000182350.1 (Assembly GRCm38.p6). 5' RACE was achieved by first strand cDNA synthesis using primer Sp1 (5' – TGCTGCTGTAGAGGCTGATG – 3') followed by two subsequent PCR amplifications. The first PCR amplification of cDNA utilised Sp2 primer (5' – CTTCACCAAGACCCACAAAA – 3') with the oligo-DT primer provided with the 5'/3' RACE kit (Sigma). The second PCR amplification utilised Sp3 primer (5' – GACAATGGTAGAGATGGTGG – 3') with the provided PCR anchor primer. A control PCR amplification utilised a Fwd Ctl primer (5' – GAAACCCTGACATGGACTCA – 3') in combination with primer Sp3 to confirm successful production of cDNA product that was specific to *Xcr1* mRNA. Underlined sequences indicate location of sequences to which primers Fwd Ctl, Sp1, Sp2 and Sp3 were designed to recognise. Arrows indicate direction of PCR amplification from the respective primers.

Xcr1 Intron Fwd1 5' - GGATTTAAACCCAACATGTCTATCA – 3' Location 5799 – 5824bp

Xcr1 Intron Fwd2 5' – AGCCCAATTCTCAATCTTGTTA – 3' Location 5696 – 5618bp

Xcr1 Intron Fwd3 5' – TTGATTTCAAGCCTTTCGGT – 3' Location 5504 – 5523bp

Xcr1 Intron Fwd4 5' – GAAAGTGATAGCCAGAAAGGG – 3' Location 5328 – 5348bp

Xcr1 Intron Fwd5 5' – GATGTTCAAGCTTCCTGGTTT – 3' Location 5192 – 5212bp

2.7 DiscoverX ™ PathHunter ® β-Arrestin Assay

To evaluate ligand binding to Xcr1L and Xcr1S isoforms, the DiscoverX ® PathHunter β-arrestin assay was used (Figure 2.5). Donor Enzyme-Acceptor (EA) expressing parental CHO cell lines and pCMV-ProLink 2 (pCMV-PK2) mammalian cloning vectors were kindly provided by the laboratory of Dr Gareth Richards. An overall workflow of the assay is presented in Figure 2.6.

2.7.1 Xcl1 *application and evaluation of β-arrestin recruitment to Xcr1 isoforms*

After transfection (2.2.5.2) and (where specified) antibiotic selection (2.2.5.2.1), cells were dissociated from the flask using cell dissociation buffer (Sigma) and counted in trypan blue using Countess II Automated cell counter (ThermoFisher). 5 x 10^3 cells were then seeded to each well of a 384 well plate (details) in 20µl of complete CHO cell media and briefly centrifuged to collect cells at the bottom of each well. A sample of 1 x 10^6 cells were also collected and used for RNA collection. Cells were then left for 18-24 hours prior to the addition of ligand.

Recombinant Xcl1 (R&D systems) and his-tagged recombinant Xcl1 (his-Xcl1) (Sino Biological) were prepared by serial half-Log_{10} dilutions in 1x HBSS to achieve concentrations between 1 x 10^{-6} M and 1 x 10^{-12}M final concentration. Recombinant Xcl1 protein was applied to CHO cells and incubated for 20, 40, 60 or 90 minutes at 37°C. Each application was performed in quadruplicate. The PathHunter ® Detection Kit (DiscoverX) was then prepared and applied to cells according to manufacturer's instruction. Chemiluminescent detection was performed using an Ensight™ MultiMode Plate Reader (Perkin Elmer). Collected luminescence data was exported to Microsoft Excel (2013) and subsequently analysed using Prism 7.0 (Graphpad Inc.).

2.8 Detection of XCR1 within Human Cervical Cord

All cervical cord sections were obtained from Autopsy donations to the Sheffield Brain Tissue Bank (SBTB) that were made with the written consent of the next of kin for the use of tissues for scientific research. Sections of cervical cord were obtained from 6 sporadic-ALS (sALS)

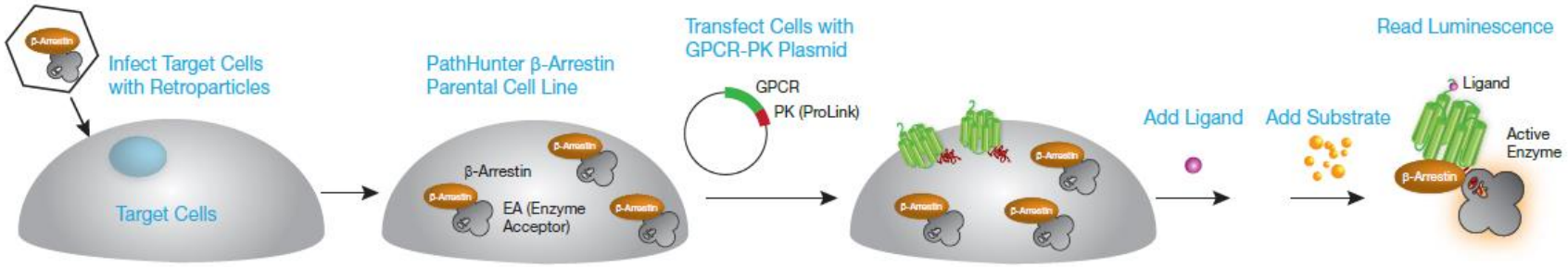

Figure 2.5. *DiscoverX® PathHunter™ β-arrestin assay.* Schematic illustration of the process by which ligand binding to GPCRs is assayed by the PathHunter™ β-arrestin assay. The assay provides a method to measure β-arrestin recruitment to the target GPCR through enzyme fragment complementation (EFC). Parental cell lines constitutively expressing β-arrestin conjugated to an enzyme acceptor (EA) were transfected with Prolink™2 (PK2) vectors containing a nucleotide insert corresponding to the coding sequence of Xcr1L or Xcr1S proteins that reside in-frame with a C-terminal enzyme donor (ED) fragment. EFC of the EA and ED domains of the β-galactosidase enzyme occurs as a consequence of ligand binding and β-arrestin-EA conjugate recruitment to the ED-tagged GPCR. β-arrestin recruitment to the GPCR is then measured from the production of a chemiluminescent product from β-galactosidase catabolism of the provided substrate. Illustrated figure is the property of EuroFins DiscoverX and is used with permission.

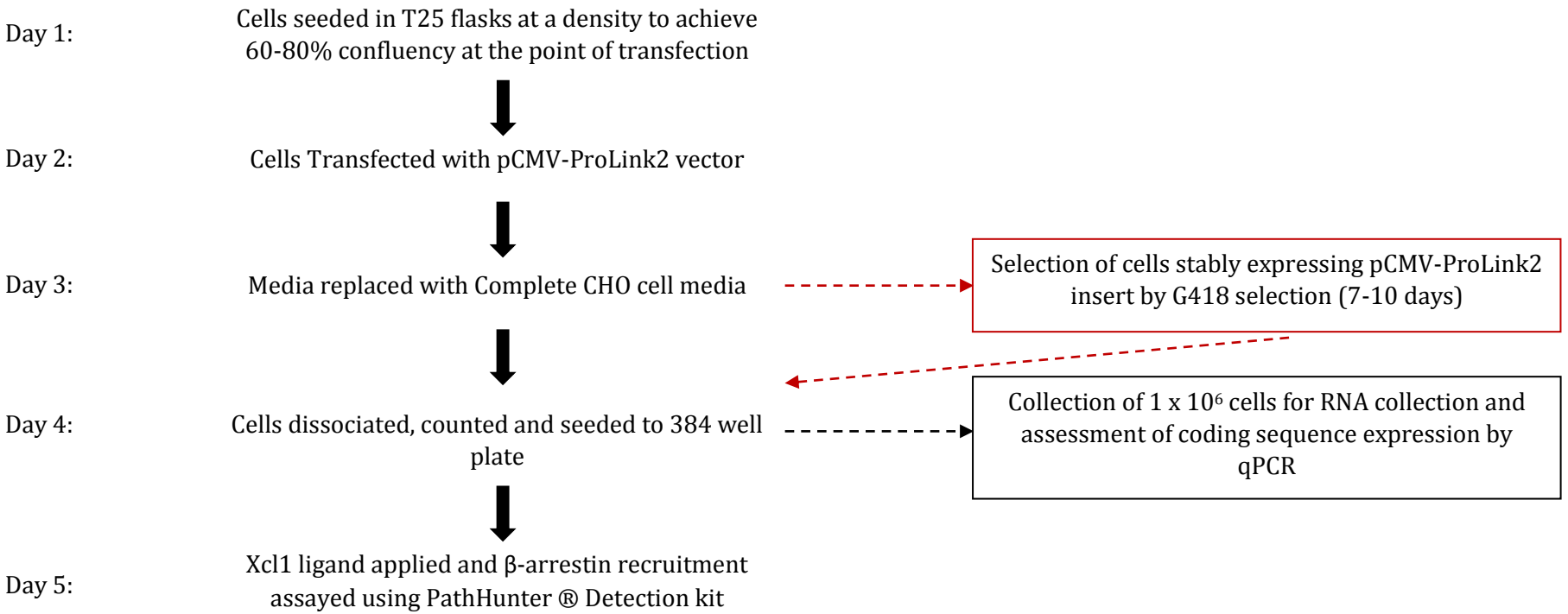

Figure 2.6. *Workflow of cell preparation and treatment for DiscoverX® PathHunter™ β-arrestin assay.* Solid black arrows indicate standard workflow. Red arrows and boxes indicate additional, optional cell treatment. Dashed black arrow indicates simultaneous preparation of cells for RNA collection and for seeding to 384 well plate.

patients and 5 age and gender-matched neurological controls. The SBTB Management Board gave ethical approval for use of tissue in this study under the provision to act as a Research Tissue Bank as approved by the Scotland A Research Ethics Committee (ref. 08/MRE00/103).

Reactivity of the HPA013169 anti-XCR1 antibody (Atlas) within the human cervical cord was identified by chromogenic immunohistochemistry using 14μm paraffin-embedded sections mounted on to glass slides. Immunohistochemistry was optimised by testing antibody concentrations between 0.5μg/ml and 4μg/ml following antigen retrieval. Antigen retrieval was tested using a pH6 or a pH9 buffer with heat HIER by pressure cooker or by microwaving for 10 minutes at 800W.

The optimised protocol for the detection of XCR1 by HPA013169 was determined to consist of the following steps, using the Rabbit Vectastain ABC detection kit (Vector Labs). Sections were first washed with xylene for 2x 5 minutes to remove wax. Sections were then rehydrated through sequential 5 minute incubations in absolute ethanol (repeat x2), 95% ethanol, 70% ethanol and then in to H_2O. Endogenous peroxidase activity was minimised by incubation of samples in 3% H_2O_2 dissolved in methanol, for 20 minutes. Sections were then washed for 5 minutes within running tap water. HIER was then performed using a pH6 antigen retrieval buffer and heated for 10 minutes at full power using an 800W microwave. The buffer was then rinsed from sections using tap water until sections were cooled and all buffer had been removed and for a further 1 minute beyond this. Sections were then incubated in TBS for 5 minutes and then blocked using the normal serum provided with the Vectastain ABC kit, prepared according to manufacturer's instruction, for 30 minutes. Blocking solution was then drained from the sections and the HPA013169 antibody added to the sections at a concentration of 4μg/ml overnight at 4°C. To maximise section coverage, sections were covered with parafilm to prevent loss of the antibody solution. Sections were then washed in TBS twice for 5 minutes. The biotinylated anti-Rabbit IgG secondary antibody provided with the Vectastain ABC kit and prepared according to manufacturer's instruction, was then added to sections for 30 minutes. Sections were then washed twice in TBS for 5 minutes followed by a 30 minute incubation with the prepared ABC reagent. Sections were then washed in TBS twice for 5 minutes. The addition of a DAB solution (vector labs) was then made to permit the localisation of the HRP-conjugated streptavidin used for the detection of primary antibody. This was added to the samples for 10 minutes before rinsing continuously with tap water for 5 minutes to stop the production of coloured staining produced by DAB oxidation. Cell nuclei were then counterstained by a 60 second incubation in Gills Hematoxylin followed by a further 1 minute wash with tap water. Nuclei were then coloured blue by immersion in Scott's tap water for 10 seconds. Sections were

then washed once more in tap water for 1 minute before dehydrating the sections by sequential 1 minute incubation in 70%, 95% and 100% (twice) ethanol. Sections were then transferred to xylene for 5 minutes prior to the addition of coverslips with DPX mountant. Prepared slides were then incubated at 37°C to facilitate the setting of the DPX mountant prior to imaging.

Following optimisation, chromogenic immunohistochemistry for the detection of XCR1 within the cervical cord of sALS patients and neurological controls was performed by the histology team at the Sheffield Institute for Translational Neuroscience (SITraN), University of Sheffield. Provided sections were then qualitatively examined and analysed for DAB staining as described in section 2.3.2.2.2.

2.9 Statistical analysis and Data Presentation

Statistical analysis was performed with GraphPad prism v7.03. Comparisons between three or more independent groups were made using Ordinary One-Way ANOVA. Post-hoc Tukey's multiple comparison test was performed to compare means between individual groups with significance reported as multiplicity adjusted P values. Comparisons between two independent groups were performed using the independent T-test. Two-tailed P-values are reported and corrected for multiple comparisons using the Holm-Sidak method. Statistical significance for all comparisons are based on a family-wise error rate of 0.05. (*, $p<0.05$; **, $p<0.01$; ***, $p<0.001$).

Chapter 3: An Investigation of *Xcr1* and *Xcl1* Gene Expression and the Functional Assessment of Potential Xcr1 Isoforms

3.1 Introduction

To provide an insight in to the presence and expression of Xcr1 and Xcl1 within the mouse CNS, this study has focussed on the characterisation of the expression of *Xcr1* and *Xcl1* transcripts. An important consideration for the evaluation of *Xcr1* expression is the current lack of clarity surrounding the functional isoform of the Xcr1 protein (see below). Therefore, in addition to assessing *Xcr1* gene expression, the functional capacity of proposed Xcr1 isoforms was also evaluated.

3.1.1 Xcr1 and Xcl1 gene expression

The identification of *Xcr1* and *Xcl1* genes were simultaneously described by several research groups during the 1990s. Identification of the mRNA sequence and corresponding proteins were achieved by the screening of cDNA libraries produced from a variety of murine lymphocyte cell lines. The identification of murine *Xcr1* and *Xcl1* was supported by the parallel description of their Human homologues following similar investigational methods in Human cell samples.

Xcl1 was provisionally described as Lymphotactin based on its capacity to induce chemotaxis and Ca^{2+}-flux in a $CD8^{+}$-enriched lymphoid cell population. Expression of *Xcl1* was localised to a collection of mature and precursor $CD8^{+}$ thymocyte populations following their activation. The *Xcl1* sequence corresponded to a 345bp clone, producing a 115aa protein (Kelner *et al.*, 1994). Adherence to the systematic nomenclature proposed by Zlotnik *et al*, led to the classification of Lymphotactin as Xcl1 due to the protein representing the sole member of the Class C chemokine family in mice (Zlotnik and Yoshie, 2000). The relevance of this preliminary biochemical and functional characterisation of Lymphotactin was given credence by the original descriptions of the Human XCL1 homologues, provisionally described as AcTivation induced And Chemokine-related molecule (ATAC) (Muller 1995) and Single Cysteine Molecule-1 (SCM-1) (Yoshida *et al.*, 1995). These two descriptions identified expression in activated CD8+ T-cell populations but did not define any T-cell population that were sensitive, based on either chemotaxis or Ca^{2+}-flux assays, to ATAC (Muller *et al.*, 1995). However, the recognition that homologous *XCL1* gene sequences were well conserved across mammalian species, including mice, was confirmed (Yoshida *et al.*, 1995).

Subsequent investigations have demonstrated Xcl1 expression to be primarily associated with a Th1-type immune response, with *Xcl1* expression identified by $CD8^{+}$ (Kelner *et al.*, 1994), $CD4^{-}$ $CD8^{-}$T-Cell Receptor (TCR-)$\alpha\beta^{+}$, $TCR\gamma\delta^{+}$ (Boismenu *et al.*, 1996; Ohta *et al.*,

2016) lymphocytes, NK cells (Dorner *et al.*, 2004) and Thymic Medullary Epithelial cells (mTECs) (Lei *et al.*, 2011). Based on this cellular expression, *Xcl1* expression is therefore most readily observed within the large intestine, thymus and spleen (Yue *et al.*, 2014). The *Xcl1* gene is localised to chromosome 9 in mice and is composed of 3 exons.

Xcr1 was originally identified following the observation of migratory responses by a murine pre-B cell line stably expressing *Xcr1* (Yoshida *et al.*, 1999). The coding sequence of *Xcr1* was identified by hybridisation of genomic DNA from C57BL/6 mice with the previously characterised Human XCR1 cDNA (Yoshida *et al.*, 1998). The identified coding sequence produced a predicted protein of 322aa protein, arising from a 966bp coding sequence, which demonstrated a 71% homology to XCR1 (Figure 3.1.1) (Yoshida *et al.*, 1999). The authors proposed this coding sequence to lie entirely within a single exon. RT-PCR using primers designed within this exon was then used to determine the expression of *Xcr1* within a $CD8^+$-enriched cell population, isolated from spleen.

More recent analysis of *Xcr1* expression has recognised the presence of 2 exons within the *Xcr1* gene (Dorner *et al.*, 2009)(Figure 3.1.2). Previous studies had determined the expression of *Xcr1* within a variety of cell types, with claims of cellular effects being assumed based upon the interdependence of functional evidence obtained from both Murine and Human cell lines. Evidence included expression of *Xcr1* by neutrophils, T-lymphocytes (Cairns *et al.*, 2001; Huang *et al.*, 2001; Kurt *et al.*, 2001), NK cells, $CD8^+$-spleen cells (Yoshida *et al.*, 1999) and B-cells (Huang *et al.*, 2001).However, all of these studies used primers that amplified a sequence located entirely within exon 2. Hence, these studies were susceptible to detection of amplicons arising from genomic DNA, something later identified as leading to the inaccurate documentation of *Xcr1* expression (Dorner *et al.*, 2009). The recognition of an additional exon within the *Xcr1* gene has since enabled a more reliable assessment of *Xcr1* mRNA that was not susceptible to genomic DNA contamination due to the intron-spanning design of primers. This genomic organisation was used to greater refine the expression of *Xcr1* in specific cell types and tissues and indicated splenic $CD8^+$ DCs (and associated non-lymphoid populations) to be the principal expressor of *Xcr1 (Dorner et al., 2002)*. This evidence has since been expanded to demonstrate the expression of *Xcr1* to define a distinct population of resident-lymphoid ($CD8^+$) and migratory non-lymphoid ($CD103^+$) cross-presenting cDCs in mice (Crozat *et al.*, 2011; Dorner *et al.*, 2009; Kroczek and Henn, 2012). A homologous cell population is also supported in Humans, with XCR1 expression associated with CD141+ cross-presenting DCs (Crozat *et al.*, 2010; Bachem *et al.*, 2010; Yamazaki *et al.*, 2013). Therefore it should be noted that the previous descriptions of Lymphotactin function at T-cells (Kelner *et al.*, 1994) and *Xcr1* expression by several cell types (see above) were erroneous. Instead, these seminal studies utilising the two-exon

>ENA|AB028459|AB028459.1 Mus musculus gene for SCM1 receptor mXCR1, complete cds

```
GG AAA AAA AAA TGT TCC TTA ATG ACT TTT ATG TAG TAG CCC AAT TCT CAA TCT TGT TAT AAA TAG TTC ACT AGT GGA ATC  < 80
           10          20          30          40          50          60          70
                                                                                  1
TGG CCC ACA GAC TTT ACT TTT TTG CAG CAT GGA TAA TAA TGA TCC CCA TTC CAA CTA TGT GGA TTT AAA CCC AAC ATG TC  < 160
                                                                                    M   S
          90          100         110         120         130         140         150
                                  2
T ATC ATT TCA GAT GCT CTC AGT ATC CCT GCA TCC CGC GTC CAG ATG GAG TCC TCT ACA GCC TTT TAT GAT TAT CAT GAT A  < 240
  I   I   S   D   A   L   S   I   P   A   S   R   V   Q   M   E   S   S   T   A   F   Y   D   Y   H   D   K
        170         180         190         200         210         220         230

AA TTG AGT CTT CTA TGT GAG AAC AAT GTC ATC TTC TTT TCC ACC ATC TCT ACC ATT GTC CTG TAC TCT CTG GTA TTT CTC  < 320
    L   S   L   L   C   E   N   N   V   I   F   F   S   T   I   S   T   I   V   L   Y   S   L   V   F   L
        250         260         270         280         290         300         310

CTC AGC CTT GTG GGT AAC AGC CTG GTT TTG TGG GTC TTG GTG AAG TAT GAG AAT CTA GAG TCA CTC ACC AAT ATC TTC AT  < 400
L   S   L   V   G   N   S   L   V   L   W   V   L   V   K   Y   E   N   L   E   S   L   T   N   I   F   I
        330         340         350         360         370         380         390

C CTC AAC CTG TGT CTC TCA GAC CTG ATG TTC TCC TGT CTA CTG CCT GTG TTG ATC TCA GCA CAA TGG AGT TGG TTT CTA G  < 480
  L   N   L   C   L   S   D   L   M   F   S   C   L   L   P   V   L   I   S   A   Q   W   S   W   F   L   G
        410         420         430         440         450         460         470

GT GAC TTC TTC TGC AAG TTC TTC AAC ATG ATC TTC GGC ATC AGC CTC TAC AGC AGC ATC TTC TTC CTT ACC ATC ATG ACC  < 560
   D   F   F   C   K   F   F   N   M   I   F   G   I   S   L   Y   S   S   I   F   F   L   T   I   M   T
        490         500         510         520         530         540         550

ATC CAC CGA TAC CTG TCT GTA GTG AGC CCC ATC TCT ACT CTG GGT ATC CAT ACC CTC CGC TGC CGT GTG CTG GTG ACA TC  < 640
I   H   R   Y   L   S   V   V   S   P   I   S   T   L   G   I   H   T   L   R   C   R   V   L   V   T   S
        570         580         590         600         610         620         630

A TGT GTG TGG GCA GCC AGC ATC CTG TTC TCC ATC CCT GAT GCT GTC TTC CAC AAA GTG ATC TCC TTA AAT TGT AAA TAT T  < 720
  C   V   W   A   A   S   I   L   F   S   I   P   D   A   V   F   H   K   V   I   S   L   N   C   K   Y   S
        650         660         670         680         690         700         710

CT GAA CAT CAT GGG TTC TTG GCC TCA GTC TAC CAG CAC AAC ATC TTC TTC CTC CTC TCC ATG GGA ATC ATC CTA TTC TGT  < 800
   E   H   H   G   F   L   A   S   V   Y   Q   H   N   I   F   F   L   L   S   M   G   I   I   L   F   C
        730         740         750         760         770         780         790

TAT GTA CAG ATT CTC AGG ACT TTG TTT CGC ACA AGG TCC AGA CAG AGA CAC CGA ACA GTC AGG CTC ATC TTC ACC GTC GT  < 880
Y   V   Q   I   L   R   T   L   F   R   T   R   S   R   Q   R   H   R   T   V   R   L   I   F   T   V   V
        810         820         830         840         850         860         870

G GTA GCA TAC TTC CTC AGC TGG GCT CCC TAC AAC CTC ACA CTC TTC CTG AAA ACT GGA ATC ATC CAG CAG AGC TGT GAG A  < 960
  V   A   Y   F   L   S   W   A   P   Y   N   L   T   L   F   L   K   T   G   I   I   Q   Q   S   C   E   S
        890         900         910         920         930         940         950

GC CTT CAG CAA CTG GAC ATT GCT ATG ATT ATC TGT CGC CAT TTG GCC TTC TCT CAT TGC TGT TTC AAC CCA GTG CTT TAT  < 1040
   L   Q   Q   L   D   I   A   M   I   I   C   R   H   L   A   F   S   H   C   C   F   N   P   V   L   Y
        970         980         990         1000        1010        1020        1030

GTC TTT GTT GGG ATC AAG TTC CGC AGA CAC CTA AAA CAT CTC TTC CAG CAG GTC TGG CTG TGC CGG AAG ACA TCC AGC AC  < 1120
V   F   V   G   I   K   F   R   R   H   L   K   H   L   F   Q   Q   V   W   L   C   R   K   T   S   S   T
        1050        1060        1070        1080        1090        1100        1110

T GTT CCC TGC TCC CCT GGT ACC TTT ACA TAT GAG GGA CCC TCC TTC TAC TGA GAG GAG AGG ATG GGC ACA TGG AGA TGA C  < 1200
  V   P   C   S   P   G   T   F   T   Y   E   G   P   S   F   Y   *
        1130        1140        1150        1160        1170        1180        1190

TA TGG GAG GTA AAG GAA GAC AAG GAG AAG TGG ATC AGG AAG GAA AAT ATA ACT GAA GAT ACT ACA GAG GTG TGG AGG AAA  < 1280
        1210        1220        1230        1240        1250        1260        1270

GAC ATG ATA CCT ATG GGA AAG TGG CTT CCA GCT GGG CAA GCC AAA GCA ACA CTT TGT GCA CTC AGT TCA TCA TTT ATT CT  < 1360
        1290        1300        1310        1320        1330        1340        1350

C TTA CGT AGA CAT AGA TTG CTT GTT AGT GAT GGT CAG AAG ATC CTA AAT AGA AGG ATT TCT AGA CTT TAG AGG GCT TGA A  < 1440
        1370        1380        1390        1400        1410        1420        1430

GC TTA TAG TAT GTG CTA ACT GTG CAG TGA TGT TGC TGG TAC ATA GGG  < 1487
        1450        1460        1470        1480
```

Figure 3.1.1. *Original description of Xcr1 mRNA and coding sequence.* The entire sequence corresponding to the detection of *Xcr1* mRNA as identified by Yoshida et al., 1999 is presented (obtained from the European Nucleotide Archive, access number AB028459). Highlighted in green is the total predicted coding sequence. Two alternative start codons are located at position 156 and 204 (indicated by red arrows). Both start codons are present in-frame with a Stop Codon at position 1170, producing two potential proteins of 338aa (Start Codon 1) and 322aa (Start Codon 2). Start Codon 2 was assumed to represent the canonical start site. The sequence arising from Start Codon 2 was used for cloning and initial functional characterisation of the Xcr1 receptor (Yoshida et al., 1999).

A

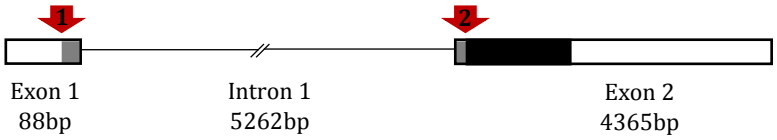

B

> ENSMUST00000182350.1

```
                                                                                1
GTT ACC TAC GTG AAA CTC TAG CAC TGG AGG AGA TCA AAG GAA GCA CAA AGC GTA CAG ACT TGA AAC CCT GAC ATG GAC TC  < 80
                                                                                M   D   S
          10          20          30          40          50          60          70
                                                2
A GAG TCA GAT GCT CTC AGT ATC CCT GCA TCC CGC GTC CAG ATG GAG TCC TCT ACA GCC TTT TAT GAT TAT CAT GAT AAA T  < 160
  E   S   D   A   L   S   I   P   A   S   R   V   Q   M   E   S   S   S   T   A   F   Y   D   Y   H   D   K   L
          90          100         110         120         130         140         150

TG AGT CTT CTA TGT GAG AAC AAT GTC ATC TTC TTT TCC ACC ATC TCT ACC ATT GTC CTG TAC TCT CTG GTA TTT CTC CTC  < 240
    S   L   L   C   E   N   N   V   I   F   F   S   T   I   S   T   I   V   L   Y   S   L   V   F   L   L
          170         180         190         200         210         220         230

AGC CTT GTG GGT AAC AGC CTG GTT TTG TGG GTC TTG GTG AAG TAT GAG AAT CTA GAG TCA CTC ACC AAT ATC TTC ATC CT  < 320
S   L   V   G   N   S   L   V   L   W   V   L   V   K   Y   E   N   L   E   S   L   T   N   I   F   I   L
          250         260         270         280         290         300         310

C AAC CTG TGT CTC TCA GAC CTG ATG TTC TCC TGT CTA CTG CCT GTG TTG ATC TCA GCA CAA TGG AGT TGG TTT CTA GGT G  < 400
  N   L   C   L   S   D   L   M   F   S   C   L   L   P   V   L   I   S   A   Q   W   S   W   F   L   G   D
          330         340         350         360         370         380         390

AC TTC TTC TGC AAG TTC TTC AAC ATG ATC TTC GGC ATC AGC CTC TAC AGC AGC ATC TTC TTC CTT ACC ATC ATG ACC ATC  < 480
    F   F   C   K   F   F   N   M   I   F   G   I   S   L   Y   S   S   I   F   F   L   T   I   M   T   I
          410         420         430         440         450         460         470

CAC CGA TAC CTG TCT GTA GTG AGC CCC ATC TCT ACT CTG GGT ATC CAT ACC CTC CGC TGC CGT GTG CTG GTG ACA TCA TG  < 560
H   R   Y   L   S   V   V   S   P   I   S   T   L   G   I   H   T   L   R   C   R   V   L   V   T   S   C
          490         500         510         520         530         540         550

T GTG TGG GCA GCC AGC ATC CTG TTC TCC ATC CCT GAT GCT GTC TTC CAC AAA GTG ATC TCC TTA AAT TGT AAA TAT TCT G  < 640
  V   W   A   A   S   I   L   F   S   I   P   D   A   V   F   H   K   V   I   S   L   N   C   K   Y   S   E
          570         580         590         600         610         620         630

AA CAT CAT GGG TTC TTG GCC TCA GTC TAC CAG CAC AAC ATC TTC TTC CTC CTC TCC ATG GGA ATC ATC CTA TTC TGT TAT  < 720
    H   H   G   F   L   A   S   V   Y   Q   H   N   I   F   F   L   L   S   M   G   I   I   L   F   C   Y
          650         660         670         680         690         700         710

GTA CAG ATT CTC AGG ACT TTG TTT CGC ACA AGG TCC AGA CAG AGA CAC CGA ACA GTC AGG CTC ATC TTC ACC GTC GTG GT  < 800
V   Q   I   L   R   T   L   F   R   T   R   S   R   Q   R   H   R   T   V   R   L   I   F   T   V   V   V
          730         740         750         760         770         780         790

A GCA TAC TTC CTC AGC TGG GCT CCC TAC AAC CTC ACA CTC TTC CTG AAA ACT GGA ATC ATC CAG CAG AGC TGT GAG AGC C  < 880
  A   Y   F   L   S   W   A   P   Y   N   L   T   L   F   L   K   T   G   I   I   Q   Q   S   C   E   S   L
          810         820         830         840         850         860         870

TT CAG CAA CTG GAC ATT GCT ATG ATT ATC TGT CGC CAT TTG GCC TTC TCT CAT TGC TGT TTC AAC CCA GTG CTT TAT GTC  < 960
    Q   Q   L   D   I   A   M   I   I   C   R   H   L   A   F   S   H   C   C   F   N   P   V   L   Y   V
          890         900         910         920         930         940         950

TTT GTT GGG ATC AAG TTC CGC AGA CAC CTA AAA CAT CTC TTC CAG CAG GTC TGG CTG TGC CGG AAG ACA TCC AGC ACT GT  < 1040
F   V   G   I   K   F   R   R   H   L   K   H   L   F   Q   Q   V   W   L   C   R   K   T   S   S   T   V
          970         980         990         1000        1010        1020        1030

T CCC TGC TCC CCT GGT ACC TTT ACA TAT GAG GGA CCC TCC TTC TAC TGA  < 1089
  P   C   S   P   G   T   F   T   Y   E   G   P   S   F   Y   *
          1050        1060        1070        1080
```

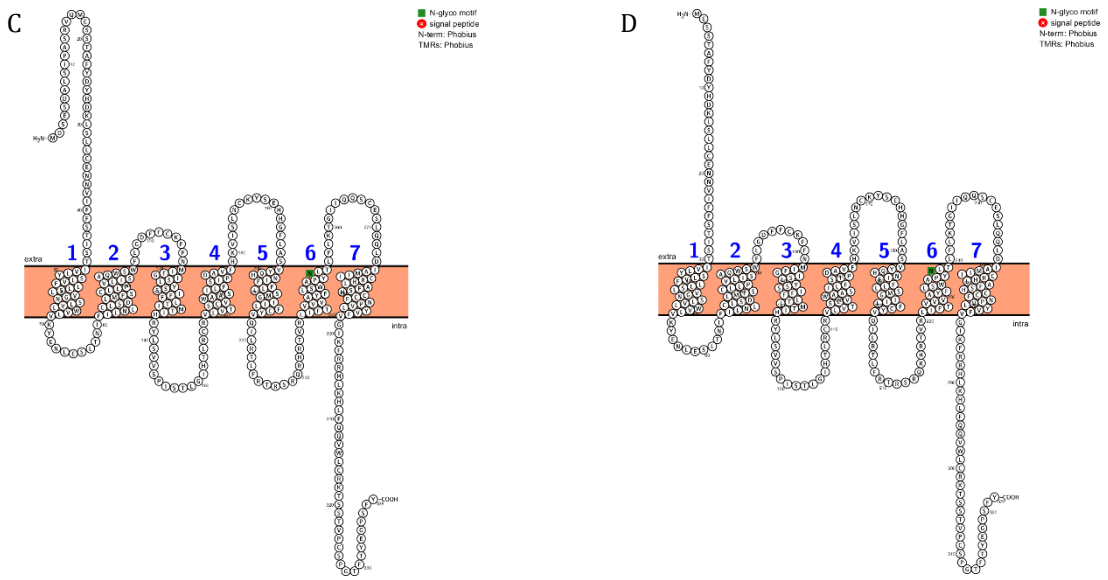

Figure 3.1.2. *Current description of Xcr1 and potential* Xcr1 *isoforms.* A) Schematic illustration of *Xcr1* gene structure as detailed by Ensemble (Assembly GRCm38.6). Black boxes represent exons separated by intron 1. Xcr1 coding sequence highlighted by grey and black solid fill regions. Grey fill = coding sequence from start codon 1 to start codon 2; Black fill = coding sequence from start codon 2 to stop codon. B) Coding sequences arising from Exon 1 (Orange) and Exon 2 (Green) of *Xcr1* mRNA as described by Ensemble database (Assembly GRCm38.6, Transcript ID ENSMUST00000182350.1). Alternative Start Codons 1 (position 74) and 2 (position 122) of *Xcr1* mRNA are highlighted with Red Arrows and represent Start Codons of two alternative, in-frame sequences of 1014bp (Start codon 1 to Stop codon, *Xcr1L*) and 966bp (Start Codon 2 to Stop codon, *Xcr1S*). Translated sequence of Xcr1L (338aa) = Blue + Red Amino Acid sequence; Translated Sequence of Xcr1S (322aa) = Red Amino Acid sequence. C, D) Schematic illustration of predicted protein structures of Xcr1L (C) and Xcr1S (D).

structure of *Xcr1* have determined the expression of this chemokine receptor to be exclusive to the above cross-presenting population of cDCs.

3.1.2 Xcl1 and Xcr1 expression by cells of the CNS

Prior to the start of this project there was a scarce amount of published information regarding the expression of *Xcr1* or *Xcl1* transcripts in the CNS. The expression of *Xcl1* had been investigated in a murine model of neuroinflammation, as a consequence of CNS-specific expression of the HIV-1 Tat protein (Kim *et al.*, 2004). In this model, an inducible HIV-1 *Tat* sequence was inserted downstream of the astrocyte-specific GFAP promoter. At 7 days post-induction of *Tat* expression, *Xcl1* expression was evaluated by In-Situ Hybridisation (ISH) and by RT-PCR. The expression of *Xcl1* was significantly increased to ~4x that observed in controls within whole brain total RNA samples according to RT-PCR. This correlated to an increased production of Xcl1 protein within whole brain homogenates, as determined by ELISA. Furthermore, ISH of *Xcl1* was colocalised to astrocytes, monocytes and macrophage/microglia by dual ISH-IHC for the respective cell markers. Notably, *Xcl1* hybridisation to the ISH probe was not identified in neuronal cells identified by MAP-2 reactivity. As a further measure of the capacity for *XCL1* expression by astrocytes, the authors also demonstrated the capacity of Tat expression to activate the XCL1 promoter and increase constitutive XCL1 protein secretion in a Human astrocyte cell line (Kim *et al.*, 2004).

Further to this evidence, the recent study performed by Zychowska *et al.*, provided a further basis to support *Xcl1* and *Xcr1* mRNA expression by cells of the CNS. In particular, this study investigated *Rn-Xcl1 (Rattus norvegicus-Xcl1)* and *Rn-Xcr1 (Rattus norvegicus-Xcr1)* expression by primary microglial and astrocyte cells obtained from the cortex of rat pups at postnatal day 1, following LPS and minocycline treatment. Evidence from quantitative RT-PCR demonstrated *Rn-Xcl1* expression to increase by an average of 400x following LPS treatment of primary microglia and an average of 15x following LPS treatment of primary astrocytes, in comparison to untreated cells. For both cell types, treatment with minocycline caused a reduction in the magnitude of *Rn-Xcl1* mRNA increase following LPS treatment. In contrast to the increases observed for *Rn-Xcl1,* evaluation of *Rn-Xcr1* expression demonstrated a reduction in primary microglia and no change of expression in primary astrocytes, following LPS treatment. Interestingly, the decrease in *Rn-Xcr1* expression observed in microglia was associated with a ~3x increase of Xcr1 protein expression, as determined by western blot. No detection of *Rn*-Xcr1 protein was identified from the lysate of primary astrocytes under any experimental condition (Zychowska *et al.*, 2016). However, the relevance of this evidence to *Xcr1* and *Xcl1* expression in the murine CNS remains to be established.

From the little published information that is available, the expression of *Xcr1* and *Xcl1* by cells of the CNS is so far generally indicated as a consequence of inflammatory stimuli. This is further supported by the lack of detection of either *Xcl1* or *Xcr1* related transcripts within the CNS of healthy mice, as documented by online transcriptomic databases (see e.g. (Yue *et al.*, 2014; Lein *et al.*, 2007). It should be noted, however, that neither of these databases evaluates gene expression within the spinal cord. Despite this evidence, the documentation of *Xcr1* and *Xcl1* expression in the CNS is extremely limited.

3.1.3 The Xcr1 *protein has two potential isoforms*

A survey of the available protein databases reveals a conflict in the consensus of Xcr1 amino acid sequence identity. This conflict has arisen as a consequence of the recent identification of an additional exon to the *Xcr1* gene, as discussed above. Prior to this identification, the coding sequence of Xcr1 was assumed to be located entirely within a single exon and represent a protein of 322 amino acids (Uniprot Accession no. Q9R0M1; Yoshida *et al*., 1999). The annotation of *Xcr1* to include an additional exon has led to bioinformatic databases to subsequently document Xcr1 to be instead composed of 338 amino acids, as a result of the presence of an additional, in-frame, alternative start codon in Exon 1 (see Ensembl CCDS23665; NCBI RefSeq NP_035928.2; UniProt S4R1K3). However, bioinformatic records still include the documentation of *Xcr1* coding sequences to lie entirely within exon 2 as determined from cDNA libraries (European Nucleotide Archive Sequence BC141369.1, (Strausberg *et al.*, 2002)). Figure 3.1.2 illustrates this evidence of the two potential Xcr1 isoforms which will from hereafter be referred to as 'Xcr1L' (Xcr1-Long, representing the 338 amino acid protein encoded by the coding sequence beginning at Start Codon 1 (Figure 3.1.2, C)) and 'Xcr1S' (Xcr1-Short, representing the 322 amino acid protein encoded by the coding sequence beginning at Start Codon 2 (Figure 3.1.2, D)). The corresponding nucleotide sequences that encode the potential Xcr1L and Xcr1S protein isoforms will be referred to as *Xcr1L* and *Xcr1S*, respectively.

The first functional evaluation of Xcr1 was based upon the stable expression of Xcr1S within a Murine Precursor B-cell line. Application of Xcl1 demonstrated this to be a specific ligand for Xcr1S based on the induction of chemotaxis and Ca^{2+} mobilisation (Yoshida et al., 1999). The only subsequent publication to document Xcr1 function was performed by Luttichau (Luttichau, 2008). In this article, the function of both Murine and Human XCL1 homologues, along with two viral chemokine mimics (vCCL2 and vCCL3), were evaluated against XCR1 and Xcr1 which were transiently expressed by COS-7 cells. Importantly, the sequence of insert used for the transient transfection of these cells represented a nucleotide sequence that included exon 1 of *Xcr1* mRNA (GenBank Accession number AK089908.1). Without clarification in the article regarding the protein identity produced from this cDNA insert, it

is not clear whether the expressed protein used for functional analysis represented Xcr1L or Xcr1S. This investigation demonstrated efficacy of XCL1 only when tested with cells expressing XCR1 and not for cells transfected with the *Xcr1* insert. In contrast, Xcl1 demonstrated efficacy at both XCR1 and Xcr1. However, it was noted that relatively high concentrations of Xcl1 were required to elicit a response in cells transfected with the *Xcr1* insert, suggesting that Xcl1 had a low potency at the expressed Xcr1 protein. The author attributed this feature to the potential impact of an additional N-terminal methionine or the lack of appropriate glycosylation to the recombinant Xcl1 protein used for evaluation (Luttichau, 2008). However, without clarification of the protein identity produced from the transfected *Xcr1* vector, the expression of alternate Xcr1 isoforms may also have contributed to the lack of Xcl1 potency.

3.1.4 Functional consequences of proposed Xcr1 *isoforms*

Due to the proposed difference in Xcr1L and Xcr1S amino acid sequences to lie within the N-terminal domain, there is the potential that such changes could impact various aspects of receptor function. The N-terminal domain of GPCRs has been implicated in several essential processes that are required for the effective translation, export, trafficking and ligand binding of the receptor. These functions rely on the presence of consensus motifs within the N-terminal sequence. For example, N-terminal domains may contain hydrophobic signal peptide sequences that provide essential signals for the effective export of some GPCRs from the endoplasmic reticulum (ER) (Schuelein *et al.*, 2012). In addition, post-translational modification of the receptor by N-linked glycosylation at NxS/T motifs can also facilitate the integration of the receptor in to the cell membrane (Dong *et al.*, 2007). However, just as the N-terminal domain can facilitate efficient transport to the cell membrane, important examples have demonstrated how some N-terminal domains actually prevent receptor translocation to the cell membrane (Kochl *et al.*, 2002; Alken *et al.*, 2009; Coleman, Ngo and Smith, 2017). For these receptors, the lack of signal peptide cleavage reduces presentation at the cell membrane whilst also mediating other functions, such as to inhibit receptor dimerization or increasing the competency of ligand binding (Jahnsen and Uhlen, 2012; Coleman, Ngo and Smith, 2017).

In relation to ligand binding and receptor activation, N-terminal domains of GPCRs display an array of functions. Most typical of these functions is for the N-terminus to mediate receptor activation via the provision of essential ligand binding sites. However, yet other mechanisms exist by which the N-terminus can modulate receptor activation due to qualities that are intrinsic to the N-terminus, or their associated metabolites. This has been well documented for the GPCR sub-family of protease activated receptors for which the proteolytic cleavage of the N-terminus liberates a signal peptide that is then capable of

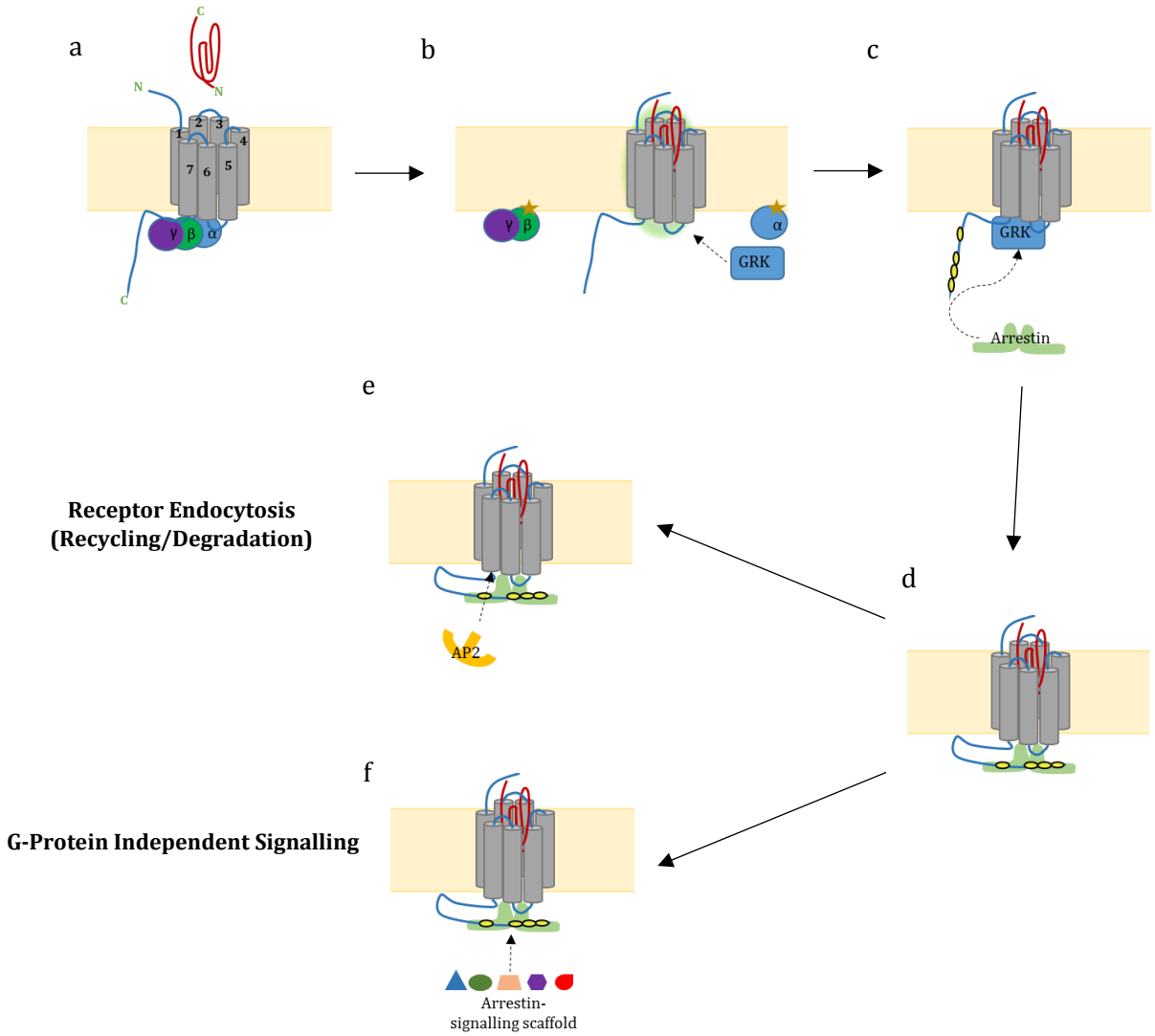

Figure 3.1.3. *Chemokine receptors: ligand binding and receptor activation.* Schematic diagrams have been made with reference to motifs found within the Xcr1L sequence according to previous descriptions of GPCR and chemokine receptor consensus motifs (Bohm, Grady and Bunnett, 1997). a) In resting state, chemokine receptors, like other GPCRs, exist as a heptahelical transmembrane bundle that associates with an inactive GDP-bound heterotrimeric G-protein. For Xcr1, the associated G-protein α-subunit is a member of the pertussis-sensitive $G_{\alpha i}$ subclass. Chemokines (red schematic) demonstrate a secondary topology consisting of a disordered N-terminal domain, that is followed by a succession of three β-strands and a C-terminal alpha helix (Fernandez and Lolis, 2002). For Xcr1, a Cysteine residue (aa316) located within the C-terminal domain is consistent with that described to be sensitive to palmitoylation and may faciliate membrane anchoring of the C-terminus. b) Chemokine binding and signal transduction relies on a two-step binding interaction (see text), following which the receptor is stabilised to an active conformation that facilitates the exchange of GDP for GTP to the Gα-subunit. This leads to the dissociation of the α and β/γ subunits which then mediate their respective downstream signalling cascades. Exposure of intracellular motifs as a consequence of receptor activation permits the association of G-protein Receptor Kinases (GRKs). c) GRKs phosphorylate specific motifs, particularly Serine/Threonine residues within the intracellular C-terminus (yellow circles). For Xcr1L, 8 such residues exist

(between residues 319 and 336). Phosphorylation of these residues may also be mediated by Protein Kinase C and/or Protein Kinase A to exert regulation of receptor activity by heterologous desensitisation. Phosphorylation of these residues is associated with a conformation the permits the association with arrestins. d) Following arrestin recruitment, the interaction between the receptor and any trimeric G-proteins is blocked, thereby inhibiting any subsequent G-protein signalling. Arrestin recruitment results in two primary outcomes for the membrane-bound GPCR: internalisation or G-protein independent signalling. e) The binding of arrestin and stabilisation of the receptor in a particular conformation is thought to expose specific tyrosine containing motifs that interact with the clathrin associated protein, AP-2. For GPCRs, an NPxxxY motif is highly conserved within transmembrane domain seven and is indeed identified within the Xcr1L sequence. Association of the AP-2 protein is essential for the subsequent recruitment of clathrin subunits that encapsulate the membrane and results in internalisation and subsequent degradation or recycling of the receptor following unbinding of the chemokine ligand. f) Arrestin proteins are also capable of stabilising an array of signalling proteins at the membrane following binding to the GPCR. This results in the formation of an Arrestin-signalling scaffold that can subsequently initiate diverse intracellular, G-protein independent, signalling (Bohm, Grady and Bunnett, 1997; Allen, Crown and Handel, 2007; Scheerert and Sommer, 2017) .

agonising the receptor from which it was released (Ossovskaya and Bunnett, 2004). N-terminal domains may also exhibit constitutive agonist activity at the receptor without any prior proteolytic processing (Srinivasan *et al.*, 2004). This 'tethered-agonist' mechanism results in basal activation of the receptor that can be inhibited by the presence of antagonistic ligands (Ersoy *et al.*, 2012). In direct contrast to these 'tethered-agonists' GPCR N-terminal domains may also demonstrate intrinsic suppressive activity that are required to constrain agonist-induced and constitutive receptor activation (Belmer *et al.*, 2014). Thus, the N-terminal domain contributes to a myriad of receptor functions via an array of mechanisms, many of which are only beginning to be appreciated. In direct relation to chemokine receptors, current evidence that has been gathered from a select number of the chemokine receptor family, indicates a two-step binding mechanism for chemokines at their cognate receptor(s) (Allen, Crown and Handel, 2007). In this model, the C-terminal domain of the chemokine first binds to the N-terminus and extracellular loops of the receptor. This first step of binding precedes a subsequent interaction between the transmembrane helical bundle of the receptor and the N-terminal domain of the chemokine ligand. This results in the stabilisation of the receptor in an active conformation that is capable of inducing subsequent downstream intracellular signalling cascades, via the dissociation of activated G-proteins and/or the recruitment of arrestins that can mediate G-protein independent signalling (Figure 3.1.3) (Bohm, Grady and Bunnett, 1997; Allen, Crown and Handel, 2007; Scheerert and Sommer, 2017).

In the absence of a resolved, crystallised structure of Xcr1 there is a clear conflict in the foundation to the evidence of Xcr1 function: that is, there is no consensus to the amino acid sequence of the Xcr1 protein. Xcr1L differs from Xcr1S by the presence of an additional 16 amino acids within the N-terminal domain. In light of the essential and divergent mechanisms by which this domain can contribute to receptor function, the differences between these two potential isoforms may therefore have important consequences on receptor function. Moreover, the validity of these two potential isoforms is difficult to conclude based on sequence analysis alone and has not yet been tested. This is primarily due to the small change in sequence length between the two isoforms and because of the two alternative start codons lying in-frame with one another within *Xcr1* mRNA. Hence the two isoforms exhibit highly similar amino acid sequences. Furthermore, whilst functional evaluations of Xcr1S have been performed, the evidence provided by Luttichau provides some inconsistencies of Xcl1 efficacy at this receptor, a result that may be associated with the use of a coding sequence that is capable of producing both of the potential Xcr1 isoforms.

In reviewing this evidence, it cannot be discounted that the initial functional characterisation of Xcr1 (Yoshida et al., 1999) may have provided evidence for a protein

that does not accurately reflect the Xcr1 receptor expressed endogenously *in vivo*. The more recent identification of an additional exon to the *Xcr1* gene, provides an alternative start codon that lies upstream and in-frame to that assumed for *Xcr1S*. Consequently, the endogenously produced protein arising from the translation of *Xcr1* mRNA may therefore represent either Xcr1S, Xcr1L or a combination of the two. Further complexity to this arises from the potential array of mechanisms that regulate the transcriptional identity of *Xcr1* mRNA itself, as has been observed for other chemokine receptors (Mummidi *et al.*, 2007; Wierda and van den Elsen, 2012). Consequently transcriptional regulation that may influence the composition of *Xcr1* mRNA may therefore influence the amino acid composition of the produced Xcr1 protein. An investigation in to the function of Xcr1L and Xcr1S and an interrogation of their associated genetic transcripts is therefore necessary to validate the existing description of Xcr1.

3.1.5 Aims

The focus of this study has been to determine a method to examine the expression of both *Xcr1* and *Xcl1* transcripts. In particular, the aim was to provide a method that would accurately quantify the expression of *Xcr1* transcripts that reflects the expression of the potential Xcr1 isoforms. This assessment of *Xcr1*-related transcripts was performed in a variety of cell types and tissues from the CNS, alongside the evaluation of *Xcl1* expression, to further validate and expand upon the expression patterns of *Xcr1* and *Xcl1* observed by others. In order to clarify the functional isoform of the Xcr1 protein, an *in vitro* assay of β-arrestin recruitment was utilised in order to test the ligand binding and receptor activation of Xcr1L and Xcr1S, with the aim of providing clear evidence regarding the functional isoform of this chemokine receptor.

3.2 Results

3.2.1 Assessment of *Xcr1* and *Xcl1* expression in the CNS

3.2.1.1 Optimisation of Xcr1- and Xcl1- specific primers

To reliably detect the expression of target mRNA transcripts, primers were evaluated for specificity to the target cDNA by agarose gel electrophoresis and melt-curve analysis of the produced DNA amplicons following the determined qPCR protocol. Primers designed to *Xcr1*-related transcripts were either designed to produce an amplicon that spanned intron 1 (*Xcr1L)* or an amplicon that corresponded to exon 2 only (*Xcr1S*). These two primer pairs utilised the same reverse primer with an alternative forward primer located either in exon 1 (*Xcr1L*) or exon 2 (*Xcr1S*). For the evaluation of *Xcl1* mRNA expression, a single, intron-spanning, primer pair was utilised with the forward primer located in exon 2 and the reverse primer located in exon 3 of the *Xcl1* gene. To facilitate the simultaneous evaluation of *Xcr1*- and *Xcl1*-related transcripts from the sample using the same qPCR protocol, each primer was designed to achieve a melting temperature within 1°C of one another.

Testing of primer efficiency was done by serial dilution of spleen cDNA over five Log_{10} concentrations using primer concentrations between 0.1µM and 1µM. Primers were assessed to achieve an efficiency of 90-100% and an R^2 value of >0.98 (Svec *et al.*, 2015). Figure 3.2.1 and figure 3.2.2 illustrate the specificity and efficiencies of the primers used for the detection of *Xcr1L, Xcr1S* and *Xcl1* cDNA. *Xcl1* primers were observed to generate competing amplicons at concentrations of 0.5µM and 1µM. These likely arose from primer dimerisation based on the presence of these amplicons in negative controls that did not contain any cDNA. However, adequate efficiency and a lack of competing amplicon production was achieved by reducing the primer concentrations to 0.1µM. Evaluation of *Xcl1* cDNA was therefore performed using the primers at 0.1µM. Primers used for the detection of *Xcr1S* and *Xcr1L* sequences were observed to achieve the desired criteria of performance at all primer concentrations tested. The produced amplicons using *Xcr1L, Xcr1S* and *Xcl1* primers were determined to produce specific amplicons according to melt-curve analysis and agarose gel electrophoresis.

3.2.1.2 Validation of DNA-free preparations for cDNA synthesis

A key consideration to be made for the evaluation of *Xcr1S* amplicons was the presence of contaminating genomic DNA (gDNA) within RNA preparations. Due the intra-exon design of *Xcr1S* primers, gDNA contamination would lead to the false-positive detection of *Xcr1S* mRNA. This contaminating factor was previously identified as leading to the erroneous description of *Xcr1* expression within various cell types following PCR analysis (Dorner *et al.*, 2009; Lei and Takahama, 2012).

A

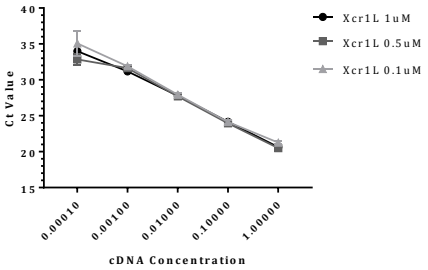

B

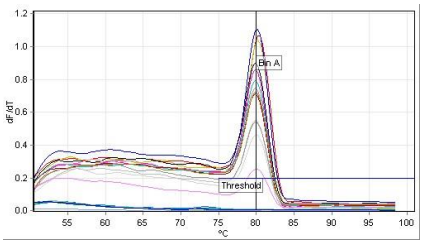

C

Xcr1L Primer Conc.	R^2	M
1µM	0.997	-3.437
0.5µM	0.973	-3.237
0.1µM	0.986	-3.537

D

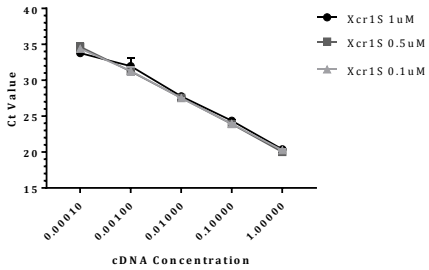

E

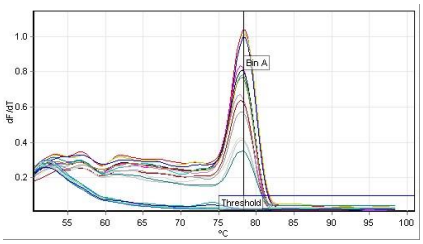

Xcr1S Primer Conc.	R^2	M
1µM	0.981	-3.607
0.5µM	0.997	-3.662
0.1µM	0.997	-3.599

G

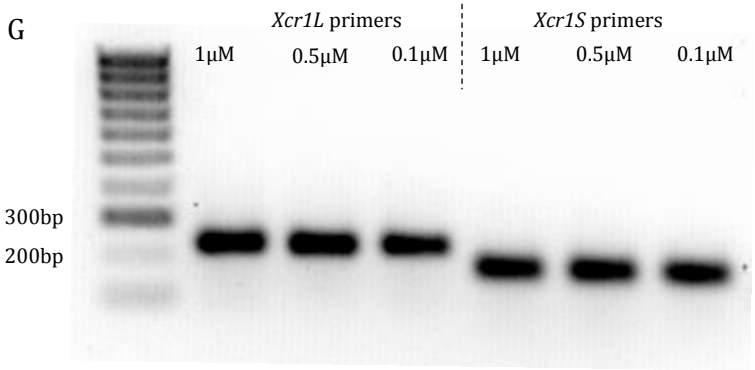

Figure 3.2.1. *Validation of primers for the detection of Xcr1 cDNA.* Forward and reverse primers for the detection of cDNA containing *Xcr1L* (A-C, G) and *Xcr1S* sequences (D-F, G) were tested at concentrations of 1μM, 0.5μM and 0.1μM using serially diluted cDNA prepared from spleen. Ct values obtained following qPCR of serially diluted spleen cDNA is displayed for the *Xcr1L* (A) and *Xcr1S* (D) primers. Melt curve analysis of amplicons produced from *Xcr1L* (B) and *Xcr1S* (E) primers demonstrate the production of dsDNA that displays a peak of fluorescence at a temperature of 80°C (*Xcr1L*) and 78°C (*Xcr1S*). (C, F) Linear regression analysis demonstrates the linear amplification of amplicons with an efficiency close to that expected (M = -3.332) for the serial Log_{10} dilution of cDNA. R^2 values demonstrate a strong correspondence of both *Xcr1L* (C) and *Xcr1S* (F) data to the linear regression model applied. G) Agarose gel electrophoresis illustrates production of amplicons with expected size for the respective primer pair (Xcr1L = 221bp; Xcr1S = 164bp) at all primer concentrations tested.

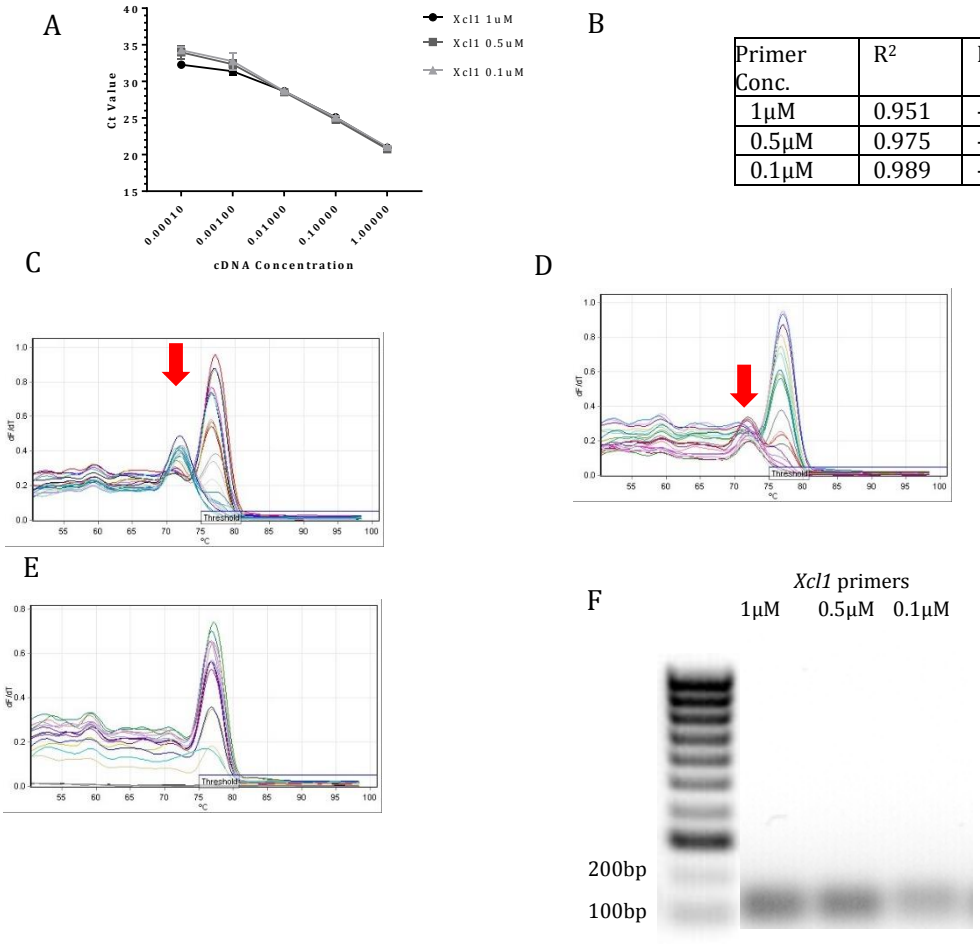

Primer Conc.	R^2	M
1µM	0.951	-2.895
0.5µM	0.975	-3.401
0.1µM	0.989	-3.379

Figure 3.2.2. *Validation of primers for the detection of Xcl1 cDNA.* A) Ct plots obtained from the amplification of cDNA produced from spleen using primers specific for *Xcl1* cDNA at concentrations of 1µM, 0.5µM and 0.1µM. B) Linear regression analysis demonstrates the linear amplification of product to correspond well to the observed data, as supported by R^2 values. However, the amplification efficiency is above that expected, at concentrations of 1µM. Amplicon production using *Xcl1* primers at 0.5µM and 0.1µM more closely resembles the amplification expected. Melt curve analysis (C, D, E) suggests the production of a non-specific amplicon when using primers at 1µM and 0.5µM concentrations (red arrows). Importantly, this amplicon was produced in negative controls and accounts for the lack of expected linearity of amplification at these concentrations. Melt curve analysis for primers used at 0.1µM, demonstrates a lack of this additional product in all samples, including negative controls (E) . F) Agarose gel electrophoresis demonstrates the production of an amplicon within the expected size range for the *Xcl1* primers used (82bp).

However, based on the conflicting evidence as to the location of Xcr1 coding sequences and also a lack of conformation as to whether *Xcr1* mRNA can be composed of only exon 2 or exon 1 plus exon 2, or potentially both, the evaluation of *Xcr1L* and *Xcr1S* sequences was performed independently using the corresponding primers described above (section 3.2.1.1). In order to support the valid assessment of cDNA sequences arising from mRNA only by *Xcr1S* primers, conformation that the protocol for the production of cDNA lacked any genomic DNA contamination was essential.

A combination of evidence has been used for this. Firstly, confirmation of DNase efficacy was determined by incubating cDNA samples produced from spleen with DNase I. Subsequent qPCR evaluation demonstrated a complete lack of amplicon expression that was supported by absence of amplicon presence following agarose gel electrophoresis of the sample. This supported the capacity of DNase I treatment to efficiently eliminate any DNA within the RNA sample that would subsequently be used for cDNA production. Secondly, reverse transcription negative (RT-) controls were included for each experiment. These controls corresponded to the DNase-treated RNA sample that was used for cDNA production. Use of this control would indicate the presence of any DNA contamination, gDNA or otherwise, that could generate false-positive detection of *Xcr1S* mRNA. Where amplicons were produced, the validity of these amplicons to relate to the specific amplification of an *Xcr1S* sequence was tested by melt curve analysis and/or agarose gel electrophoresis (see below). Preliminary evaluations also tested the capacity of the untreated RNA sample, collected from spleen, to produce amplicons that were detectable by qPCR and hence determine if the RNA collection protocol was capable of providing an RNA sample that was devoid of any DNA contamination. This analysis failed to detect any amplicon produced by *Xcr1S* primers demonstrating the RNA collection protocol to provide a DNA-free sample, even without DNase treatment. Thirdly, post-hoc analysis of amplicon identity by melt curve analysis and/or agarose gel electrophoresis provided additional verification that the fluorescent signal detected by qPCR corresponded to the amplification of the specific amplicon by confirming the melting temperature and/or amplicon length.

By combining these three sources of evidence, each experiment to evaluate *Xcr1S* amplicons was confirmed to assess *Xcr1S* mRNA presence and not reflect the presence of gDNA based on the evidence that: i) DNase efficacy was sufficient to abolish any contaminating DNA prior to cDNA production; ii) RT- controls lacked the capacity to provide a substrate for *Xcr1S* amplicon production; iii) the RNA collection protocol provided an RNA sample that was free of DNA contamination; and iv) post-hoc analysis of amplicon identity could confirm the specificity of amplicon production in test cDNA samples whilst also verifying the identity of any amplicon produced from RT- controls.

Extensive controls have therefore been made to ensure the validity of amplicon production from *Xcr1S* primers to reflect the production of amplicons from RNA only. Consequently, unless otherwise stated, all qPCR data presented can be assumed to be free of contaminating gDNA and all assessments of *Xcr1S* expression represent a true indicator of *Xcr1S* RNA presence.

3.2.1.3 Evaluation of Xcr1L, Xcr1S and Xcl1 expression in whole spinal cord

Examination of *Xcr1L* and *Xcr1S* expression was performed using RNA extracted from the whole spinal cord of non-transgenic (NTg) male and female mice at the age of 6 and 10 months (Figure 3.2.3). This demonstrated a low expression of both *Xcr1* isoforms in the spinal cord. Considerable variation in the detection of *Xcr1L* arose from the lack of detected amplicons within a number of samples. However, the detection of *Xcr1S* was more reliable and was relatively higher than *Xcr1L* expression in all samples evaluated. Interestingly, within the spinal cord of 6 month mice, particularly for males, this relative increase was much higher than that seen for samples collected at 10 months. Indeed, *Xcr1S* expression was observed to be 4.01x and 6.17x higher than *Xcr1L* for females and males at 6 months of age, respectively. This increase was statistically significant for male *Xcr1S* vs *Xcr1L* expression ($p = 0.011$) at 6 months. The validity of this relative increase of *Xcr1S* to *Xcr1L* amplicon detection to reflect a genuine relative change in mRNA expression is supported by the observed expression of the two mRNA isoforms in mouse spleen (Figure 3.2.3, A). Analysis of the expression of the two *Xcr1* isoforms in this sample demonstrates a decreased expression of *Xcr1S* in comparison to *Xcr1L,* corresponding to a 4.23x higher expression of *Xcr1L* to *Xcr1S*. Correlation analysis between *Xcl1* expression and the expression of the two *Xcr1* isoforms indicates a very similar correlation of *Xcl1* expression with both *Xcr1S* and *Xcr1L*.

Evaluation of *Xcl1* expression identified a higher and more consistent expression of this mRNA than *Xcr1* in whole spinal cord RNA. *Xcl1* expression was not identified to be statistically different between any of the groups tested, suggesting a consistent expression of this chemokine for both genders at both 6 and 10 months.

3.2.1.4 Evaluation of Xcr1L, Xcr1S and Xcl1 expression in mouse motor neurons

In order to refine the identification of *Xcr1* or *Xcl1* expression to a particular cell type in the CNS, analysis of gene expression was conducted using RNA collected from *in vitro* samples of neurons, astrocytes and microglia.

Analysis of both *Xcr1* isoforms in neurons was performed by qPCR using RNA collected from cell cultures of mouse embryonic stem cell (mESC)-derived motor neurons kindly donated by Dr Matthew Stopford (University of Sheffield). These cells express Green Fluorescent

Protein (GFP) under the transcriptional control of the motor neuron-specific Homeobox Protein-9 (HB9) promoter. Motor neurons were obtained by the differentiation of mESCs according to the protocol described previously (Haidet-Phillips *et al.*, 2011; Meyer *et al.*, 2014) to generate a cell sample that was enriched with mouse motor neurons. Cells were provided as a cell pellet and processed as described in section 2.2.7. qPCR analysis demonstrated an 82x relative expression of *Xcr1S* in comparison to *Xcr1L*, however this did not achieve statistical significance (Figure 3.2.4). Further support for the higher expression of *Xcr1* mRNA that does not contain exon 1 arose from the retrospective analysis of microarray data collected from NSC-34 cells. In these cells, the signal arising from oligonucleotide probes that were specific to exon 2 was 44% higher than that observed for probes specific to exon 1. This increase was consistent across analysis of 9 cell samples and obtained statistical significance. Moreover, signals arising from oligonucleotide probes that spanned exon 1 and exon 2 were not identified within these cells, suggesting that the expression of *Xcr1* mRNA by NSC-34 cells did not include exon 1 and exon 2 together.

The expression of *Xcl1* mRNA was also identified by qPCR analysis of mESC-derived motor neurons. This expression was consistent but low across the 3 samples analysed.

3.2.1.5 Evaluation of Xcr1L, Xcr1S and Xcl1 in Astrocytes

qPCR analysis was also performed to evaluate the presence of *Xcr1L, Xcr1S* and *Xcl1* within the RNA prepared from primary cortical astrocytes collected from P1 mouse pups, kindly donated by Dr Scott Allen (University of Sheffield). Although the cDNA prepared was from viable RNA and the results obtained from a valid qPCR protocol, as determined by assessment of *GAPDH* expression and according to positive amplification of control cDNA, no detection of *Xcr1L, Xcr1S* or *Xcl1* was observed within these cell samples.

3.2.1.6 Evaluation of Xcl1 expression in microglia

Xcl1 was recently described to be expressed by microglia, with this expression being sensitive to treatment by LPS and minocycline (Zychowska *et al.*, 2016). However, this evidence formed part of a study investigating the function of Xcl1 and Xcr1 within the Mouse CNS, but the evaluation of *Xcl1* in primary cells was restricted to evidence from primary Rat microglial cells collected from P1 rat pups. In order to reconcile the evidence of *Xcl1* expression by primary Rat microglial cells with the proposed expression of *Xcl1* by Mouse microglia *in vivo*, primary cultures of Mouse microglia were prepared from NTg mouse brains at 10 months of age. To further investigate the proposed sensitivity of microglial *Xcl1* expression, these cells were treated with LPS, according to the protocol performed by Zychowska *et al*., 2016.

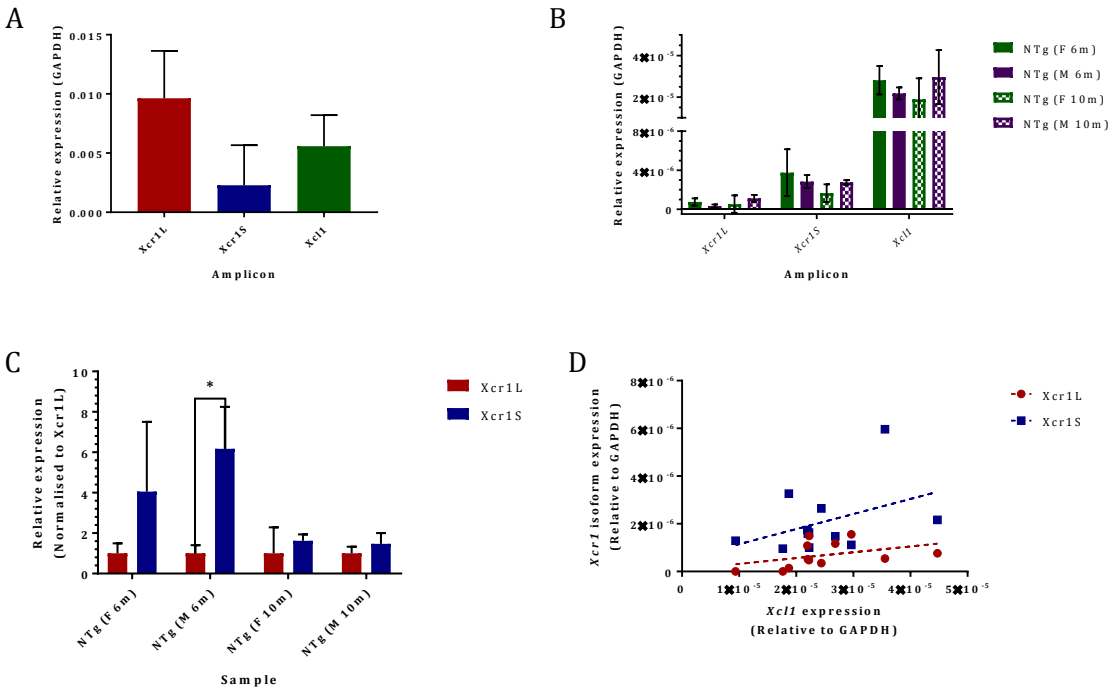

Figure 3.2.3. *Xcr1L, Xcr1S and Xcl1 expression in the spinal cord.* A) Expression of *Xcr1L, Xcr1S* and *Xcl1* in mouse spleen (N=3). No statistically significant difference between *Xcr1L* and *Xcr1S* expression is observed. B) Expression of *Xcr1L, Xcr1S* and *Xcl1* in RNA collected from whole spinal cords of Male and Female NTg mice at 6 and 10 months of age. No statistically significant difference in expression for either transcript was observed following comparison between groups by one-way ANOVA with post-hoc Tukey's multiple comparison. N = 3 for all groups. C) Relative expression of *Xcr1S* to *Xcr1L* in whole spinal cord of NTg mice. *Xcr1S* demonstrates 6.17x higher expression than *Xcr1L* in NTg male mice at 6 months (*, p = 0.013). N=3 for all groups. D) Pearson correlation identifies a non-significant positive correlation between *Xcr1L* (dashed red line: r = 0.408, p = 0.188) and *Xcr1S* (dashed blue line: r= 0.4055, p = 0.191) expression to *Xcl1* expression. N = 12 for both groups. Error bars for all graphs = ±SD.

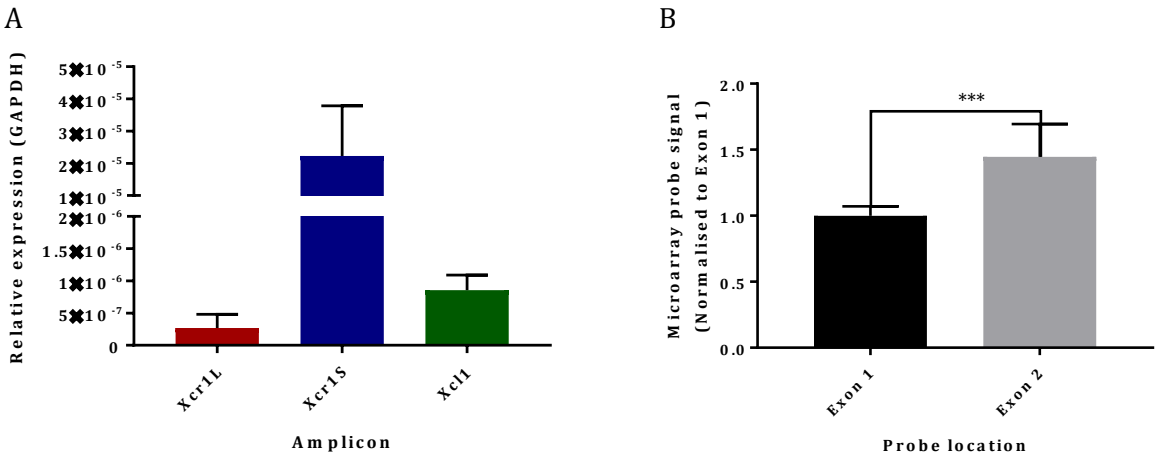

Figure 3.2.4. *Evaluation of Xcr1L, Xcr1S and Xcl1 in neuronal cells.* A) qPCR analysis of *Xcr1L, Xcr1S* and *Xcl1* in RNA isolated from mESC-derived mouse motor neurons demonstrates *Xcr1S* expression to be 82.77x higher than *Xcr1L* ($p = 0.071$). A low but consistent amount of *Xcl1* expression is also identified. N=3 for each amplicon; Error bars = ±SD B) Retrospective analysis of microarray data prepared using RNA collected from NSC-34 cells indicates a significantly higher detection of RNA originating from exon 2 than exon 1 of *Xcr1* (***, mean difference = 0.445, $p < 0.001$) . N=9; Error bars = ±SD.

3.2.1.6.1 Characterisation of microglia

In order to characterise the purity of microglial cells, immunocytochemical detection of Iba-1 was performed using control treated primary microglial cultures. As a further consideration, due to the protocol of primary cell preparation, cell expression of GFAP was also tested by immunocytochemistry.

Figure 3.2.5 (A, a-c) illustrates the typical composition of the primary cell cultures obtained. The cell numbers demonstrating Iba-1 reactivity varied between preparations, suggesting the presence of a number of other cells. A low number of these cells (~2%) were astrocytes, as indicated by GFAP reactivity. These cells were not numerous and did not distribute homogenously, in comparison to Iba-1 positive cells. Overall the cells were therefore considered to be composed of mainly microglial cells and supported later analysis to evaluate changes that primarily related to that of microglia.

3.2.1.6.2 Evaluation of Xcl1 expression in primary microglial cultures: Control vs LPS treatment

LPS treatment represents one of the most potent methods to elicit microglial activation (Chhor *et al.*, 2013). Quantification of *Xcl1* expression by control and LPS-treated primary microglial cultures demonstrated a statistically significant reduction in *Xcl1* expression following LPS treatment, in comparison to their respective controls, in all 3 primary microglial cultures evaluated. This reduction corresponded to an expression, following LPS treatment, that was 26% lower than that observed for untreated controls (figure 3.2.5, D).

To further support this change in *Xcl1* expression to relate to the activation of microglia, semi-quantitative evaluation of Iba-1 reactivity was performed for untreated and LPS treated microglial cultures. This demonstrated a 50% increase in Iba-1 reactivity by cells treated with LPS in comparison to untreated cells (figure 3.2.5, C). Furthermore, Iba-1-positive cells treated with LPS adopted a rounded, amoeboid morphology (Figure 3.2.5, A(d)) in comparison to the ramified structure of untreated, Iba-1-positive, microglial cells (Figure 3.2.5, A(a)).

3.2.2. Assessment of Xcr1 mRNA sequence : 5' RACE

From the data gathered, the discrepancy in detection of amplicons arising from *Xcr1S* and *Xcr1L* primers suggests an additional component of *Xcr1* mRNA that includes exon 2 and not exon 1. If *Xcr1* mRNA was composed of a single type, it would be expected that qPCR detection by *Xcr1S* and *Xcr1L* primers would be consistent between one another. Furthermore, every effort has been made to eradicate the potential for gDNA contamination

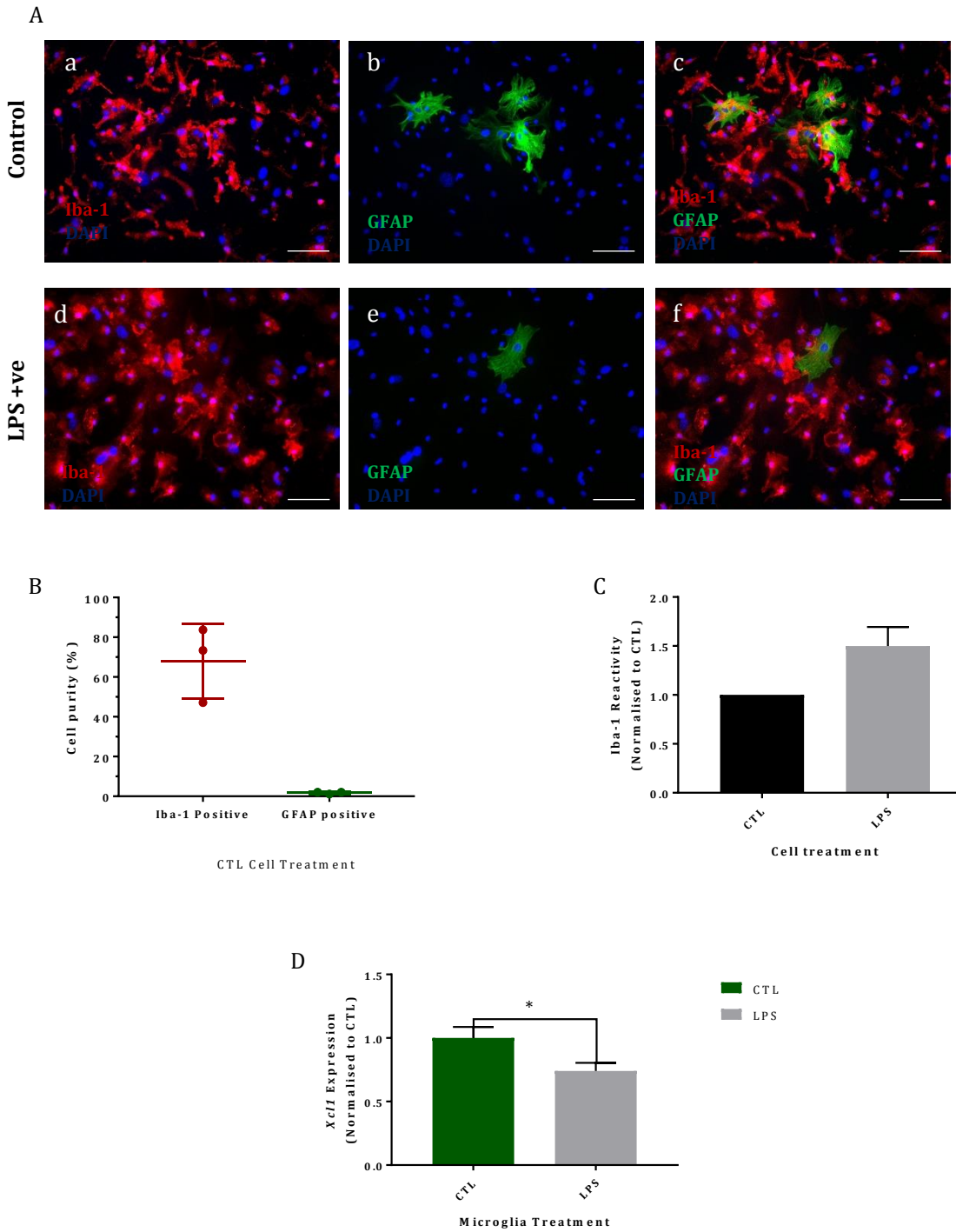

Figure 3.2.5. *Evaluation of Xcl1 expression by primary microglial cell cultures.* A) Immunocytochemical detection of Iba-1 (red) and GFAP (green) was performed to determine the presence of microglia and astrocytes, respectively, in control (CTL) cell cultures (a-c) and in cultures treated for 24 hours with LPS. Note the morphological change in Iba-1-positive cells as a consequence of LPS treatment (d) in comparison to CTL (a). B) Quantification of Iba-1-positive and GFAP-positive cells in three preparations of primary glia cultures. Iba-1 positive cells account for the majority of cells within these cultures. C) Semi-quantitative analysis of Iba-1 reactivity demonstrates a 50% increase by cultures treated for 24 hours with LPS in comparison to their respective controls that were treated with media only. D) Evaluation of *Xcl1* expression indicates a small but consistent decrease as a consequence of LPS treatment by primary microglial cultures in comparison to control (*, Mean difference vs CTL = -0.26, p = 0.014). N=3 for both LPS and CTL groups.

A

> *Xcr1* Coding sequence (ENSMUST00000182350.1)

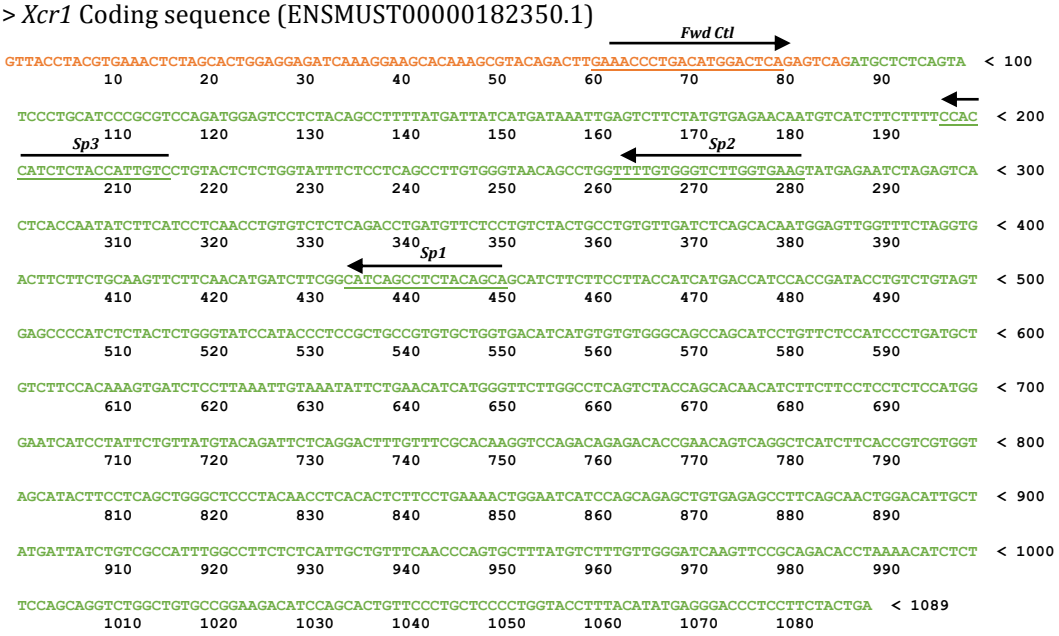

B

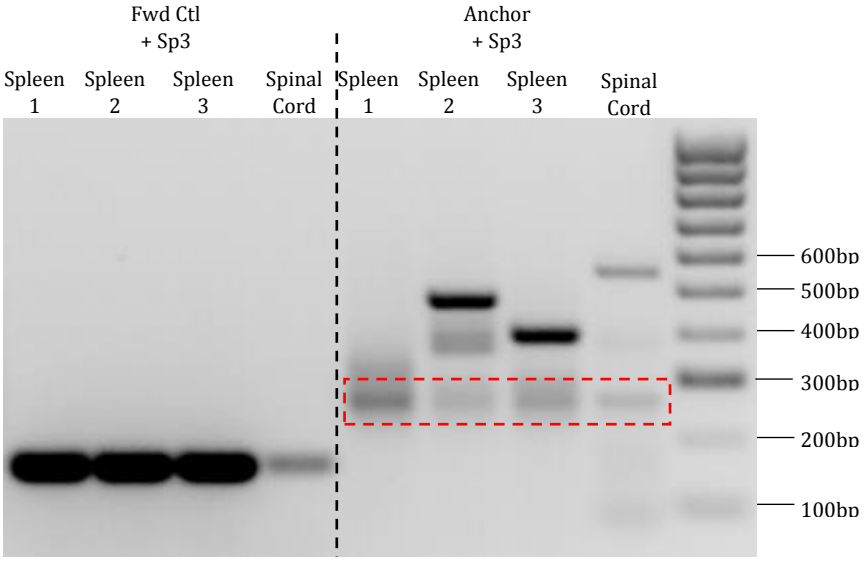

C

> Spleen 1 sequenced product

```
                          >Unidentified sequence
                          |
TTTTTTGGCCTTCCGAAAGGGGTGGGCAAAATGCCGATTTTTAAATGTGCCGTTTTTTGTTACCTACGTGAAACTCTAGCACTGGAGGAGATCAAAGGAA  < 100
        10        20        30        40        50        60        70        80        90
 >Exon1                                                                    >Exon 2
 |                                                                         |
GCACAAAGCGTACAGACTTGAAACCCTGACATGGACTCAGAGTCAGATGCTCTCAGTATCCCTGCATCCCGCGTCCAGATGGAGTCCTCTACAGCCTTTT  < 200
        110       120       130       140       150       160       170       180       190

ATGATTATCATGATAAATTGAGTCTTCTAA  < 230
        210       220
```

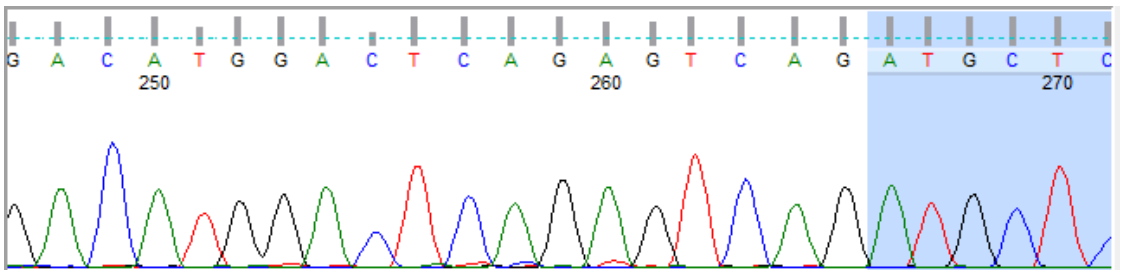

D

> Spleen 2 sequenced product

```
                                                  >5' Flanking
                                                  |
TTAAAAAAAAAAACTTTAGTCCAAAATTTCATTTTAAGAAGGGGAAGTTTGAGGCCAGCCTAGACAATTTAATAGAACCTTTATCAAGCTAGGGTTACCT  < 100
        10        20        30        40        50        60        70        80        90
                  >Exon 1
                  |
ACGTGAAACTCTAGCACTGGAGGAGATCAAAGGAAGCACAAAGCGTACAGACTTGAAACCCTGACATGGACTCAGAGTCAGATGCTCTCAGTATCCCTGC  < 200
        110       120       130       140       150       160       170       180       190
            >Exon 2
            |
ATCCCGCGTCCAGATGGAGTCCTCTACAGCCTTTTATGATTATCATGATAAATTGAGTCTAAGA  < 264
        210       220       230       240       250       260
```

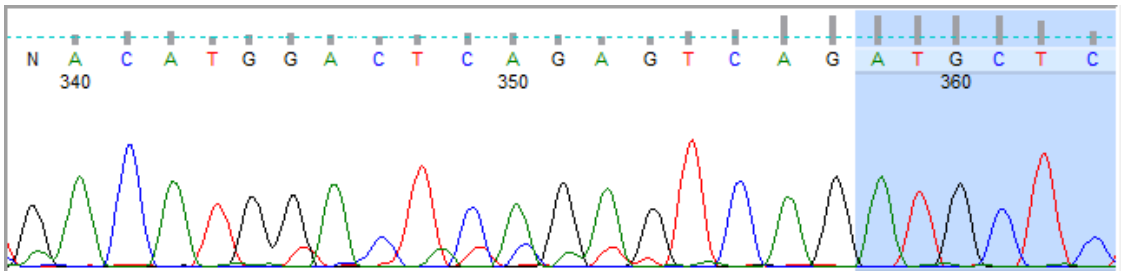

E

> Spleen 3 sequenced product

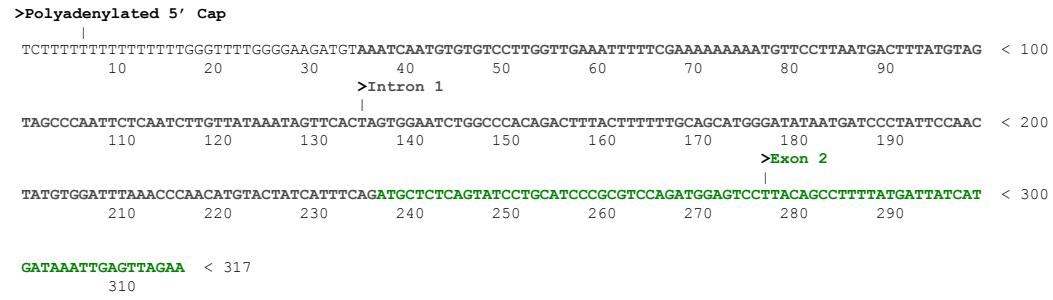

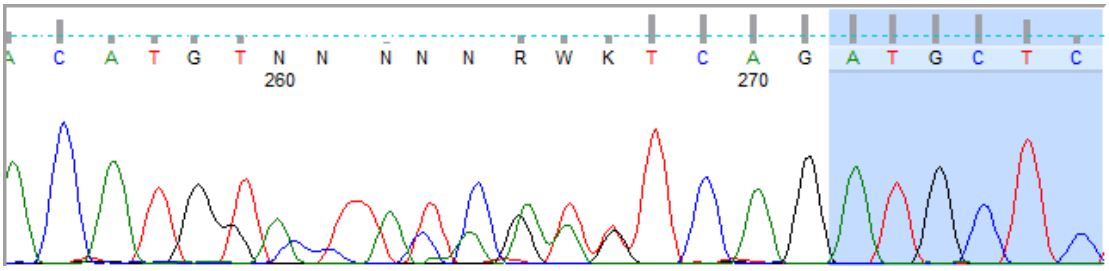

F

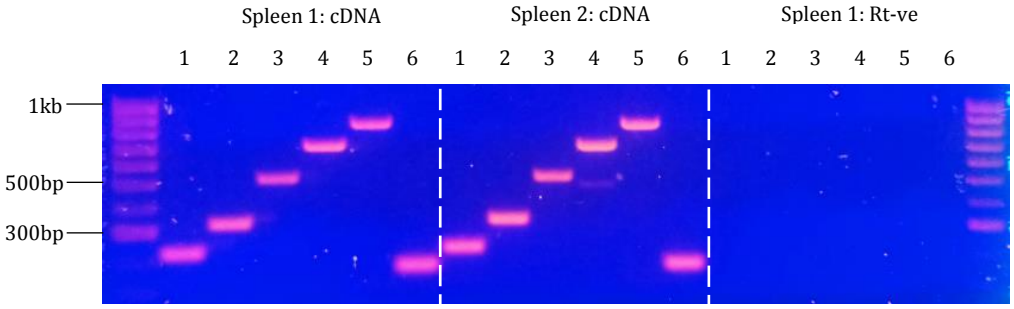

Figure 3.2.6. *Xcr1 mRNA sequence analysis by 5' RACE.* A) Proposed *Xcr1* mRNA sequence with annotated locations of primers used for 5' RACE. B) PCR amplification of produced cDNA following 5' RACE of total RNA from 3x spleen and 1x spinal cord samples. A control PCR amplification (Fwd Ctl + Sp3) was used to confirm specific reverse transcription of target *Xcr1* mRNA by the 5' RACE protocol. Anchor + Sp3 amplification produced amplicons corresponding to sequences that lie upstream to Sp3 binding sequences and are located within the 5' region of *Xcr1* mRNA. Region highlighted (dashed red box) corresponds to predicted amplicon size produced from 5' RACE Anchor primer being located at 5' end of Exon 1 to Sp3 primer. C, D, E) Sequenced products of 5' RACE from spleen 1, 2 and 3. Highlighted regions are confirmed following sequence alignment to *Xcr1* mRNA as detailed by Ensembl. Nucleotide chromatogram provided below each sequence corresponds to region immediately preceding exon 2 (highlighted in blue). F) Agarose gel electrophoresis of amplicons produced following PCR amplification of cDNA and RT- RNA samples using exon 2 Sp2 reverse primer in conjunction with: Xcr1 intron Fwd 1 (lanes 1) Fwd2 (lanes 2) Fwd3 (Lanes 3) Fwd 4 (lanes 4) Fwd 5 (lanes 5) and Fwd Ctl (Lanes 6). Predicted amplicon sizes: Lanes 1, 225bp; Lanes 2, 329bp; Lanes 3, 521bp; Lanes 4, 697bp; Lanes 5, 833bp; Lanes 6, 121bp.

from these comparisons. Based on evaluation of these methods and according to internal controls of qPCR experiments, gDNA contamination does not account for the observed discrepancies of *Xcr1S* and *Xcr1L* amplicon production. In order to investigate the potential sequence of *Xcr1* mRNA and provide further clarity for its quantification, RNA was collected from spleen and spinal cord and evaluated by 5' Rapid Amplification of cDNA Ends (5' RACE, see section 2.7). This method allows the evaluation of mRNA sequence identity by sequence specific cDNA production from a sequence that is located downstream (3') to the unknown mRNA transcriptional start site. Subsequent capping of this unknown sequence by polyadenylation then permits PCR amplification of the unknown cDNA sequence that can be subsequently provided for sequencing. The predicted amplicon size produced from PCR amplification of *Xcr1*, assuming *Xcr1* mRNA to be composed of Exon 1 and exon 2, is 255bp (anchor primer + exon 1 + exon 2 (to 3' complement of Sp3)). Any alternative mRNA composed of exon 2 only would have to be determined from DNA sequencing.

Figure 3.2.6 illustrates the results obtained following 5' RACE of RNA collected from 3x spleen and 1x spinal cord samples. All samples were collected from NTg 10 month female mice. Preliminary attempts were also made to analyse RNA from spleen that was enriched with mRNA, however this was unsuccessful (data not shown). Following 5' RACE, all samples were confirmed to contain *Xcr1* mRNA that included both exon 1 and exon 2 by PCR amplification of the produced cDNA using a Ctl forward primer located in exon 1 and the test Sp3 primer located in exon 2 (Figure 3.2.6, B). This confirmed the capacity of the 5' RACE protocol to produce cDNA that was specific to *Xcr1* mRNA. Notably, the expression of this mRNA was considerably lower in spinal cord, as reflected by the intensity of produced amplicon from spinal cord RNA. Testing of amplicons produced by the use of the 5' RACE anchor primer in conjunction with the test Sp3 primer, produced a varied composition of amplicon sizes. Spleens 2 and 3 demonstrate the most prominent band at an amplicon length that far exceeds that expected from the amplification of a sequence composed of exon 1 and exon 2. For both samples 2 and 3 an amplicon of ~400bp is produced, with an additional band of approximately 450bp observed from spleen 2. For the spinal cord sample, the most prominent band lies at between 500 and 600bp, which is again far larger than would be expected for *Xcr1* mRNA that is composed of Exon 1 and exon 2 only. However, consistent to all samples was an amplicon with a size of ~250bp. For spleen 1, this amplicon was the only observable amplicon. This size corresponds to the predicted amplicon size produced from *Xcr1* mRNA composed of exon 1 and part of exon 2 (as detailed above).

Subsequent sequencing of the produced amplicons from 5' RACE reflected the observed amplicon production following agarose gel electrophoresis. Sequencing products from

spleen corresponded to identifiable regions of the *Xcr1* gene sequence, however sequencing of products from spinal cord were unable to be clarified due to poor consistency of nucleotide sequences and have not been reported.

For two of the spleen samples characterised, both exon 1 and exon 2 sequences are observed as a continuous sequence, supporting *Xcr1* mRNA to be composed of exon 1 and exon 2. As suggested from the observable amplicon produced by agarose gel electrophoresis, sequencing of samples from spleen 1 produced a product that corresponded to exon 1 and exon 2. This sequence was well conserved and corresponds to the reported mature *Xcr1* mRNA sequence (ENSMUST00000182350.1). Furthermore, for sequencing of Spleen 2, a sequence that corresponded to the described 5' flanking sequence (located upstream of Exon 1 within *Xcr1*) plus exon 1 plus exon 2 was identified. However, for both spleen 2 and spleen 3 samples it can be seen from the nucleotide chromatogram that the sequence immediately preceding exon 2 has competing nucleotide signals, suggesting alternative sequences to exist. For sequencing of samples from spleen 3, this preceding sequence corresponds to the sequence originating from intron 1 of the *Xcr1* gene. Although the entire sequence was not discernible due to low sequencing fidelity, particularly within the 3' region of DNA, the sequencing product of spleen 3 had a length of ~370bp. This corresponds well with the most prominent amplicon observed by agarose gel electrophoresis. Moreover, the sequencing reaction provided a clear indication of where the polyadenylated cap was added, as indicated by the 5' poly-T sequence highlighted in figure 3.2.6, E. The presence of this capping sequence is indicative of a consistent point at which reverse transcription ends and provides a putative 5' terminus to an alternative *Xcr1* RNA species.

Due to the sequencing reactions providing an indication that *Xcr1* mRNA may include an intron sequence, PCR was performed using Reverse Transcribed (RT+) and RT- DNase-treated RNA samples from the test spleens to support the sequenced products to arise from RNA sequences only (Figure 3.2.6, F). PCR utilised forward primers located within the 3' region of intron 1 and were coupled with the Sp2 reverse primer in exon 2. In support of the detailed sequencing products to arise solely from the amplification of cDNA arising from the reverse transcription of RNA and to not include genomic DNA contamination, no amplicons were produced in any of the 3 spleen RNA samples without reverse transcription. This provides further confidence in the identified sequences to reflect only RNA sequences arising from *Xcr1.* Furthermore, it adds additional support to the use of DNase treatment as a method to eradicate gDNA contamination of RNA samples used for genetic analyses (as discussed in section 3.2.1.2).

3.2.3 Functional evaluation of proposed Xcr1 isoforms

There currently exists two proposed proteins arising from the *Xcr1* gene. The first of these proteins, Xcr1L, is encoded from a sequence arising from exon 1 and exon 2. Xcr1L is composed of 338 amino acids and has an estimated molecular weight of 39 kDA. The second proposed protein, referred to here as Xcr1S, is translated from a sequence that lies exclusively within exon 2. Xcr1S is composed of 322 amino acids and has an estimated molecular weight of 37.3 kDA. Confirmation of which of these proteins is expressed *in vivo* has not yet been determined.

Suggestive evidence for the production of both of these proteins from *Xcr1* RNA has been provided during the process of this investigation following the transfection of HeLa cells with the MR225748 plasmid. Western Blot detection of C-myc from cell lysates prepared from these cells, demonstrates the production of two proteins that have very similar molecular weights. Treatment of this protein with PNGase was performed to test if these proteins may represent a glycosylated and non-glycosylated form of the Xcr1 protein. However, conclusive evidence from this treatment could not be made due to enzyme treatment resulting in receptor aggregation (Figure 3.2.7).

To functionally evaluate the two Xcr1 protein isoforms, Xcr1L and Xcr1S, the PathHunter ® β-arrestin assay was used to assess ligand binding and receptor activation. The use of this assay was used in order to provide an indication of any difference in ligand binding and/or receptor activation as a consequence of the divergence in N-terminal amino acid sequences between the two receptor isoforms. The assay relies on the transient transfection of parental CHO cells with plasmids containing enzyme-donor (ED)-tagged receptor coding sequences. The expression of an enzyme-acceptor (EA)-conjugated β-arrestin by the parental CHO cell permits assessment of β-arrestin recruitment to the receptor. This is achieved by the measurement of luminescence as a consequence of substrate metabolism following enzyme fragment complementation (EFC) between the EA and ED. Hence, luminescence is only produced following recruitment of β-arrestin to the receptor.

In order to perform the assay, molecular cloning of insert sequences corresponding to the coding sequences of either Xcr1L or Xcr1S in to the desired Prolink cloning vectors first had to be achieved. For this investigation, two of the Prolink vectors were used: pCMV-Prolink2 (PK2) and pCMV-ARMS2-Prolink2 (ARMS2). The two vectors produce alternative C-terminal ED tags that have different affinities for the EA: proteins produced from ARMS2 vectors contain a C-terminal ED tag that has a higher affinity for the EA tag than proteins produced from PK2 plasmids.

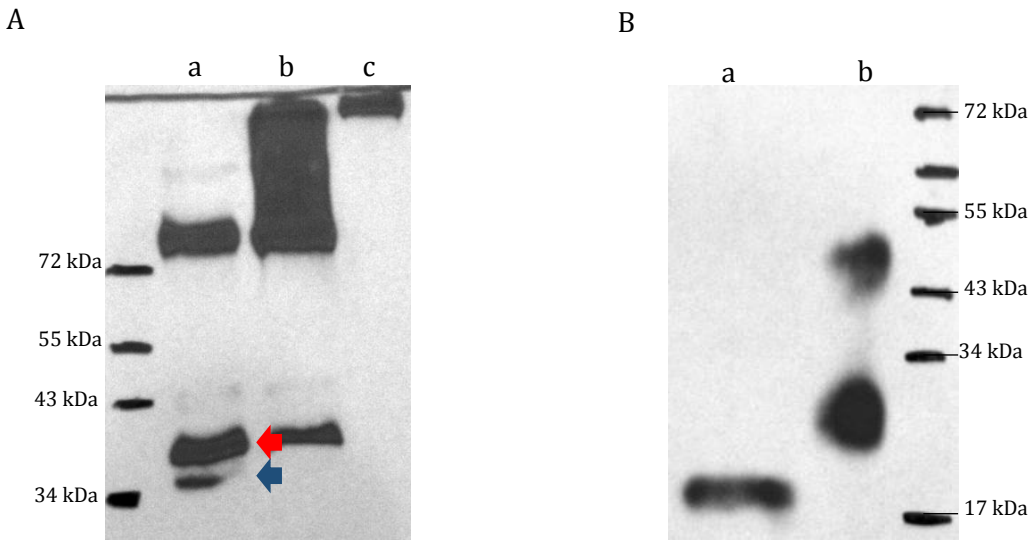

Figure 3.2.7. *C-myc detection of alternative Xcr1 proteins within transfected HeLa cells.* A) C-myc detection of lysate collected from HeLa cells transfected with MR225748 plasmid demonstrates the production of two proteins that have a very similar molecular weight. Calculated molecular weights: Red arrow = 41.78kDA; Blue arrow = 38.8kDA. Predicted molecular weight of Xcr1L-myc = 42.53 kDa; Xcr1S-myc = 40.84 kDa. Lane a: untreated HeLa cell lysate. Lane b: HeLa cell lysate treated by non-denaturing PNGase F deglycosylation. Lane c: HeLa cell lystate treated by denaturing PNGase F deglycosylation. The glycosylated nature of these proteins could not be concluded due to lack of confirmation of PNGase efficacy that arose from protein aggregation of the Xcr1 protein. Aggregation of the protein occurs as a consequence of lysate heating as displayed in Lane c and Lane b. B) The capacity of non-denaturing PNGase F treatment to deglycosylate proteins at N-linked glycosyslation motifs is confirmed by treatment of the FLAG-tagged WFDC2 protein. Lane a: WFDC2 treated by non-denaturing PNGase F treatment results in the expected 19kDA size of the unglycosylated protein. Lane b: Untreated WFDC2 protein. Observed sizes for glycosylated and non-glycosylated products were validated according to previous observations (Drapkin *et al.*, 2005) and personal correspondence with Ms Hannah Armes (University of Sheffield).

3.2.3.1 Assessment of ligand binding and β-arrestin recruitment to Xcr1S-ARMS2 *and* Xcr1L-ARMS2

Initial tests of ligand binding to Xcr1L and Xcr1S proteins were performed using L-ARMS2 and S-ARMS2 plasmids that express the higher affinity C-terminal ARMS2 tag in-frame with the respective Xcr1 isoforms. Figure 3.2.8 and Figure 3.2.9 demonstrate the presence of *Xcr1L* and *Xcr1S* inserts within L-ARMS2 and S-ARMS2 plasmids, respectively.

Tests were performed using a recombinant mouse Xcl1 protein (produced in *E.Coli*) and a recombinant his-tagged Xcl1 protein (his-Xcl1, produced by Baculovirus-insect cell expression). Representative examples of results from the β-arrestin assay are presented in figure 3.2.10. Luminescent signal was produced by cells transfected with L-ARMS2 or S-ARMS2, suggesting recruitment of β-arrestin to both of the receptor isoforms. No luminescent signal was observed from non-transfected cells or from cells transfected with the empty vector. This supported the luminescent signal observed from cells transfected with L-ARMS2 and S-ARMS2 to arise as a consequence of EFC following the valid expression of ED-tagged Xcr1L and Xcr1S proteins from the respective plasmids.

Despite evidence to support the valid expression of the two Xcr1 isoforms, no reproducible response was observed following the application of the ligand at any concentration. Instead, the level of luminescent signal arising from transfected cells treated with Xcl1 at all concentrations remained at a level that was consistent with cells without ligand application. Furthermore, sensitivity to the ligand was not influenced by increasing the incubation time with Xcl1.

A consistent observation however, was the significant difference in luminescent signal produced by cells transfected with S-ARMS2 and L-ARMS2. For all repeats performed (n=4 with Xcl1, n=3 with his-Xcl1), regardless of the ligand incubation time or concentration of ligand applied, cells transfected with S-ARMS2 produced a consistently higher baseline level of luminescence than cells transfected with L-ARMS2. To confirm that this difference in luminescence was not a consequence of a difference in the transfection efficiency or expression of the associated vector inserts, qPCR was performed to evaluate the expression of RNA arising from the transcription of plasmids within transfected cells. This analysis demonstrated a high expression of *Xcr1* RNA within cells transfected with L-ARMS2 or S-ARMS2 that was multiple times higher than that observed for the internal reference control, *TMED2.* Cells transfected with L-ARMS2 were indicated to express a lower amount of *Xcr1* mRNA, corresponding to 78% of that observed for cells transfected with S-ARMS2. Given the extremely high expression within cells transfected with both plasmids this difference was not considered sufficient to account for the higher luminescent signal that was consistently observed for cells transfected with S-ARMS2 in comparison to L-ARMS2.

A

B

> Sequenced L-ARMS2 plasmid start codon aligned to predicted L-ARMS2 plasmid sequence (Restored BgIII site; Start codon)

```
Predicted       ----------------ATCCGCTAGCGCTACCGGACTCAGATCTGCCACCATGGACTCAG
5'-L-ARMS2      TTTAGTGAACCGTCAGATCCGCTAGCGCTACCGGACTCAGATCTGCCACCATGGACTCAG
                          ******************************************

Predicted       AGTCAGATGCTCTCAGTATCCCTGCATCCCGCGTCCAGATGGAGTCCTCTACAGCCTTTT
5'-L-ARMS2      AGTCAGATGCTCTCAGTATCCCTGCATCCCGCGTCCAGATGGAGTCCTCTACAGCCTTTT
                ************************************************************

Predicted       ATGATTATCATGATAAATTGAGTCTTCTATGTGAGAACAATGTCATCTTCTTTTCCACCA
5'-L-ARMS2      ATGATTATCATGATAAATTGAGTCTTCTATGTGAGAACAATGTCATCTTCTTTTCCACCA
                ************************************************************

Predicted       TCTCTACCATTGTCCTGTACTCTCTGGTATTTCTCCTCAGCCTTGTGGGTAACAGCCTGG
5'-L-ARMS2      TCTCTACCATTGTCCTGTACTCTCTGGTATTTCTCCTCAGCCTTGTGGGTAACAGCCTGG
                ************************************************************

Predicted       TTTTGTGGGTCTTGGTGAAGTATGAGAATCTAGAGTCACTCACCAATATCTTCATCCTCA
5'-L-ARMS2      TTTTGTGGGTCTTGGTGAAGTATGAGAATCTAGAGTCACTCACCAATATCTTCATCCTCA
                ************************************************************

Predicted       ACCTGTGTCTCTCAGACCTGATGTTCTCCTGTCTACTGCCTGTGTTGATCTCAGCACAAT
5'-L-ARMS2      ACCTGTGTCTCTCAGACCTGATGTTCTCCTGTCTACTGCCTGTGTTGATCTCAGCACAAT
                ************************************************************

Predicted       GGAGTTGGTTTCTAGGTGACTTCTTCTGCAAGTTCTTCAACATGATCTTCGGCATCAGCC
5'-L-ARMS2      GGAGTTGGTTTCTAGGTGACTTCTTCTGCAAGTTCTTCAACATGATCTTCGGCATCAGCC
                ************************************************************
```

C

> Translated product of sequenced L-ARMS2 plasmid (From start codon) aligned to predicted translated product of L-ARMS2 plasmid

```
Predicted       MDSESDALSIPASRVQMESSTAFYDYHDKLSLLCENNVIFFSTISTIVLYSLVFLLSLVG
5'-L-PKII       MDSESDALSIPASRVQMESSTAFYDYHDKLSLLCENNVIFFSTISTIVLYSLVFLLSLVG
                ************************************************************

Predicted       NSLVLWVLVKYENLESLTNIFILNLCLSDLMFSCLLPVLISAQWSWFLGDFFCKFFNMIF
5'-L-PKII       NSLVLWVLVKYENLESLTNIFILNLCLSDLMFSCLLPVLISAQWSWFLGDFFCKFFNMIF
                ************************************************************
```

D

>Sequenced L-ARMS2 plasmid stop codon aligned to predicted L-ARMS2 plasmid sequence(restored hindIII site; C-terminal prolink tag)

```
3'-Predicted      TATCTGTCGCCATTTGGCCTTCTCTCATTGCTGTTTCAACCCAGTGCTTTATGTCTTTGT
3'-L-PKII         ----------------------------------NNNNNNNNNNNNGCTTTATGTCTTTGT
                                                     ***************

3'-Predicted      TGGGATCAAGTTCCGCAGACACCTAAAACATCTCTTCCAGCAGGTCTGGCTGTGCCGGAA
3'-L-PKII         TGGGATCAAGTTCCGCAGACACCTAAAACATCTCTTCCAGCAGGTCTGGCTGTGCCGGAA
                  ************************************************************

3'-Predicted      GACATCCAGCACTGTTCCCTGCTCCCCTGGTACCTTTACATATGAGGGACCCTCCTTCTA
3'-L-PKII         GACATCCAGCACTGTTCCCTGCTCCCCTGGTACCTTTACATATGAGGGACCCTCCTTCTA
                  ************************************************************

3'-Predicted      CGCAAGCTTCGAAT----------------------------------------------
3'-L-PKII         CGCAAGCTTGAGAGGATCCGTGCCATCAAGGGAGACAACCAACCTGTCTGCTCTGACAGC
                  ********* ..*
```

E

> Translated product of sequenced L-ARMS2 plasmid surrounding stop codon aligned to predicted translated product (Xcr1L coding sequence; in-frame Prolink tag)

```
3'-predicted      GIIQQSCESLQQLDIAMIICRHLAFSHCCFNPVLYVFVGIKFRRHLKHLFQQVWLCRKTS
3'-L-PKII         ----------------------------------LYVFVGIKFRRHLKHLFQQVWLCRKTS
                                                    **************************

3'-predicted      STVPCSPGTFTYEGPSFYASFELGG-----------------------------------
3'-L-PKII         STVPCSPGTFTYEGPSFYASLRGSVPSRETTNLSALTAPGGGGSGGGGSLELAVVLQRRD
                  ********************:. .

3'-predicted      ----------------------------
3'-L-PKII         WENPGVTQLNRLAAHPPFASWRNSEEAR
```

F

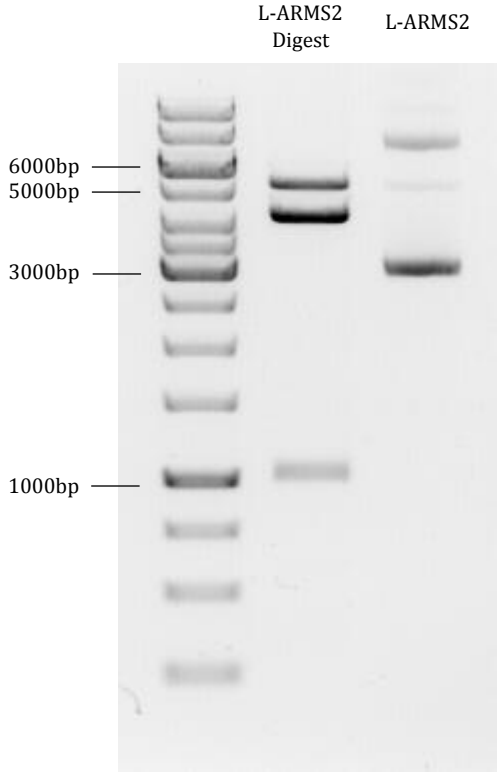

Figure 3.2.8. *Sequencing of L-ARMS2 plasmid*. A) Multiple cloning site of prolink2 vectors as provided by manufacturer. B) Sequenced region of L-ARMS2 plasmid surrounding start codon. C) Translated product of sequenced region from L-ARMS2 start codon. D) Sequenced region of L-ARMS2 surrounding stop codon. Note that sequence corresponding to ARMS2-tag sequence (red) does not align as provided sequence from manufacturer contains Prolink-tag sequence and not ARMS2 sequence. E) Translated product of sequenced region surrounding L-ARMS2 stop codon. F) L-ARMS2 digest with BgIII and HindIII enzymes demonstrate products of ~5500bp, ~4500bp and ~1000bp, corresponding to the undigested plasmid, vector backbone and *Xcr1L* insert, respectively.

A

```
          BglII   HindIII >ProLink
            |     | |
ATCCGCTAGCGCTACCGGACTCAGATCTCGAGCTCAAGCTTCGAATTGGGAGGT
TAGGCGATCGCGATGGCCTGAGTCTAGAGCTCGAGTTCGAAGCTTAACCCTCCA
          10        20        30        40        50
```

B

> Sequenced S-ARMS2 plasmid aligned to predicted S-ARMS2 plasmid sequence (restored HindIII site; in-frame Prolink Tag)

```
predicted          1 ATCCGCTAGCGCTACCGGACTCAGATCTGCCACCATGGAGTCCTCTACAG     50

S-ARMS2            1 --------------------------------------------------       0

predicted         51 CCTTTTATGATTATCATGATAAATT----------------GAGTCTTCT     84
                                                              |||||||||
S-ARMS2            1 ------------------------CCNNNNNNNNNNNNNNGAGTCTTCT     25

predicted         85 ATGTGAGAACAATGTCATCTTCTTTTCCACCATCTCTACCATTGTCCTGT    134
                     ||||||||||||||||||||||||||||||||||||||||||||||||||
S-ARMS2           26 ATGTGAGAACAATGTCATCTTCTTTTCCACCATCTCTACCATTGTCCTGT     75

predicted        135 ACTCTCTGGTATTTCTCCTCAGCCTTGTGGGTAACAGCCTGGTTTTGTGG    184
                     ||||||||||||||||||||||||||||||||||||||||||||||||||
S-ARMS2           76 ACTCTCTGGTATTTCTCCTCAGCCTTGTGGGTAACAGCCTGGTTTTGTGG    125

predicted        185 GTCTTGGTGAAGTATGAGAATCTAGAGTCACTCACCAATATCTTCATCCT    234
                     ||||||||||||||||||||||||||||||||||||||||||||||||||
S-ARMS2          126 GTCTTGGTGAAGTATGAGAATCTAGAGTCACTCACCAATATCTTCATCCT    175

predicted        235 CAACCTGTGTCTCTCAGACCTGATGTTCTCCTGTCTACTGCCTGTGTTGA    284
                     ||||||||||||||||||||||||||||||||||||||||||||||||||
S-ARMS2          176 CAACCTGTGTCTCTCAGACCTGATGTTCTCCTGTCTACTGCCTGTGTTGA    225

predicted        285 TCTCAGCACAATGGAGTTGGTTTCTAGGTGACTTCTTCTGCAAGTTCTTC    334
                     ||||||||||||||||||||||||||||||||||||||||||||||||||
S-ARMS2          226 TCTCAGCACAATGGAGTTGGTTTCTAGGTGACTTCTTCTGCAAGTTCTTC    275

predicted        335 AACATGATCTTCGGCATCAGCCTCTACAGCAGCATCTTCTTCCTTACCAT    384
                     ||||||||||||||||||||||||||||||||||||||||||||||||||
S-ARMS2          276 AACATGATCTTCGGCATCAGCCTCTACAGCAGCATCTTCTTCCTTACCAT    325

predicted        385 CATGACCATCCACCGATACCTGTCTGTAGTGAGCCCCATCTCTACTCTGG    434
                     ||||||||||||||||||||||||||||||||||||||||||||||||||
S-ARMS2          326 CATGACCATCCACCGATACCTGTCTGTAGTGAGCCCCATCTCTACTCTGG    375

predicted        435 GTATCCATACCCTCCGCTGCCGTGTGCTGGTGACATCATGTGTGTGGGCA    484
                     ||||||||||||||||||||||||||||||||||||||||||||||||||
S-ARMS2          376 GTATCCATACCCTCCGCTGCCGTGTGCTGGTGACATCATGTGTGTGGGCA    425

predicted        485 GCCAGCATCCTGTTCTCCATCCCTGATGCTGTCTTCCACAAAGTGATCTC    534
                     ||||||||||||||||||||||||||||||||||||||||||||||||||
S-ARMS2          426 GCCAGCATCCTGTTCTCCATCCCTGATGCTGTCTTCCACAAAGTGATCTC    475

predicted        535 CTTAAATTGTAAATATTCTGAACATCATGGGTTCTTGGCCTCAGTCTACC    584
                     ||||||||||||||||||||||||||||||||||||||||||||||||||
S-ARMS2          476 CTTAAATTGTAAATATTCTGAACATCATGGGTTCTTGGCCTCAGTCTACC    525

predicted        585 AGCACAACATCTTCTTCCTCCTCTCCATGGGAATCATCCTATTCTGTTAT    634
                     ||||||||||||||||||||||||||||||||||||||||||||||||||
S-ARMS2          526 AGCACAACATCTTCTTCCTCCTCTCCATGGGAATCATCCTATTCTGTTAT    575

predicted        635 GTACAGATTCTCAGGACTTTGTTTCGCACAAGGTCCAGACAGAGACACCG    684
                     ||||||||||||||||||||||||||||||||||||||||||||||||||
```

```
S-ARMS2          576 GTACAGATTCTCAGGACTTTGTTTCGCACAAGGTCCAGACAGAGACACCG    625

predicted        685 AACAGTCAGGCTCATCTTCACCGTCGTGGTAGCATACTTCCTCAGCTGGG    734
                     ||||||||||||||||||||||||||||||||||||||||||||||||||||
S-ARMS2          626 AACAGTCAGGCTCATCTTCACCGTCGTGGTAGCATACTTCCTCAGCTGGG    675

predicted        735 CTCCCTACAACCTCACACTCTTCCTGAAAACTGGAATCATCCAGCAGAGC    784
                     ||||||||||||||||||||||||||||||||||||||||||||||||||||
S-ARMS2          676 CTCCCTACAACCTCACACTCTTCCTGAAAACTGGAATCATCCAGCAGAGC    725

predicted        785 TGTGAGAGCCTTCAGCAACTGGACATTGCTATGATTATCTGTCGCCATTT    834
                     ||||||||||||||||||||||||||||||||||||||||||||||||||||
S-ARMS2          726 TGTGAGAGCCTTCAGCAACTGGACATTGCTATGATTATCTGTCGCCATTT    775

predicted        835 GGCCTTCTCTCATTGCTGTTTCAACCCAGTGCTTTATGTCTTTGTTGGGA    884
                     ||||||||||||||||||||||||||||||||||||||||||||||||||||
S-ARMS2          776 GGCCTTCTCTCATTGCTGTTTCAACCCAGTGCTTTATGTCTTTGTTGGGA    825

predicted        885 TCAAGTTCCGCAGACACCTAAAACATCTCTTCCAGCAGGTCTGGCTGTGC    934
                     ||||||||||||||||||||||||||||||||||||||||||||||||||||
S-ARMS2          826 TCAAGTTCCGCAGACACCTAAAACATCTCTTCCAGCAGGTCTGGCTGTGC    875

predicted        935 CGGAAGACATCCAGCACTGTTCCCTGCTCCCCTGGTACCTTTACATATGA    984
                     ||||||||||||||||||||||||||||||||||||||||||||||||||||
S-ARMS2          876 CGGAAGACATCCAGCACTGTTCCCTGCTCCCCTGGTACCTTTACATATGA    925

predicted        985 GGGACCCTCCTTCTACACAAGCTTCGAAT---------------   1021
                     |||||||||||||||||||||||| ..|
S-ARMS2          926 GGGACCCTCCTTCTACACAAGCTTGAGAGGATNCGTGNCATCAN    969
```

C

> Translated product of sequenced S-ARMS2 plasmid aligned to predicted S-ARMS2 plasmid sequence (Xcr1S coding sequence; in-frame prolink tag)

```
Predicted          1 MESSTAFYDYHDKLSLLCENNVIFFSTISTIVLYSLVFLLSLVGNSLVLW     50
                           .....||||||||||||||||||||||||||||||||||||||
S-ARMS2            1 ---------XXXXXSLLCENNVIFFSTISTIVLYSLVFLLSLVGNSLVLW     41

Predicted         51 VLVKYENLESLTNIFILNLCLSDLMFSCLLPVLISAQWSWFLGDFFCKFF    100
                     ||||||||||||||||||||||||||||||||||||||||||||||||||||
S-ARMS2           42 VLVKYENLESLTNIFILNLCLSDLMFSCLLPVLISAQWSWFLGDFFCKFF     91

Predicted        101 NMIFGISLYSSIFFLTIMTIHRYLSVVSPISTLGIHTLRCRVLVTSCVWA    150
                     ||||||||||||||||||||||||||||||||||||||||||||||||||||
S-ARMS2           92 NMIFGISLYSSIFFLTIMTIHRYLSVVSPISTLGIHTLRCRVLVTSCVWA    141

Predicted        151 ASILFSIPDAVFHKVISLNCKYSEHHGFLASVYQHNIFFLLSMGIILFCY    200
                     ||||||||||||||||||||||||||||||||||||||||||||||||||||
S-ARMS2          142 ASILFSIPDAVFHKVISLNCKYSEHHGFLASVYQHNIFFLLSMGIILFCY    191

Predicted        201 VQILRTLFRTRSRQRHRTVRLIFTVVVAYFLSWAPYNLTLFLKTGIIQQS    250
                     ||||||||||||||||||||||||||||||||||||||||||||||||||||
S-ARMS2          192 VQILRTLFRTRSRQRHRTVRLIFTVVVAYFLSWAPYNLTLFLKTGIIQQS    241

Predicted        251 CESLQQLDIAMIICRHLAFSHCCFNPVLYVFVGIKFRRHLKHLFQQVWLC    300
                     ||||||||||||||||||||||||||||||||||||||||||||||||||||
S-ARMS2          242 CESLQQLDIAMIICRHLAFSHCCFNPVLYVFVGIKFRRHLKHLFQQVWLC    291

Predicted        301 RKTSSTVPCSPGTFTYEGPSFYTSFELGG----------------------    329
                     |||||||||||||||||||||||:.
S-ARMS2          292 RKTSSTVPCSPGTFTYEGPSFYTSLRGXVXSXXTTXXSALTXXXXXXXXX    339
```

D

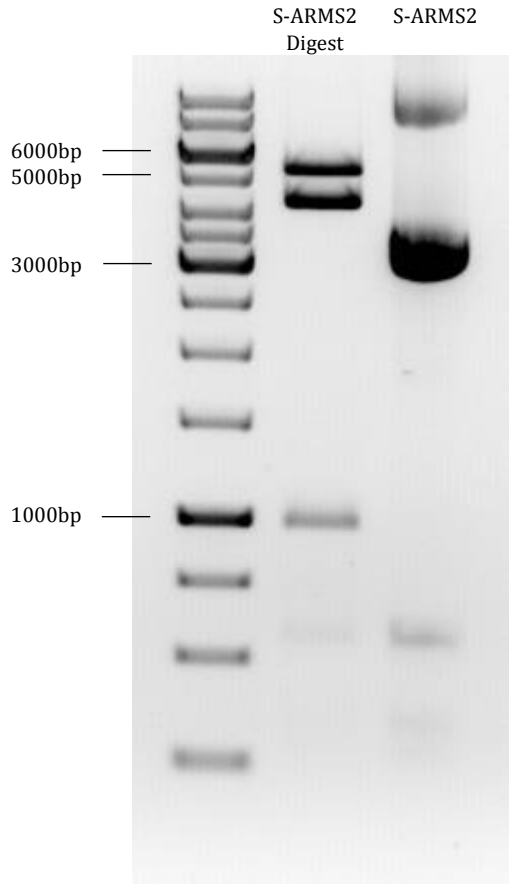

Figure 3.2.9. *Sequencing of S-ARMS2 plasmid*. A) Multiple cloning site of prolink2 vectors as provided by manufacturer. B) Sequenced region of S-ARMS2 plasmid. Note that sequence corresponding to ARMS2-tag sequence (red) does not align as provided sequence from manufacturer contains Prolink-tag sequence. C) Translated product of sequenced region from S-ARMS2 plasmid. D) S-ARMS2 digest with BgIII and HindIII enzymes demonstrate products of ~5500bp, ~4500bp and ~1000bp, corresponding to the undigested plasmid, vector backbone and *Xcr1S* insert, respectively.

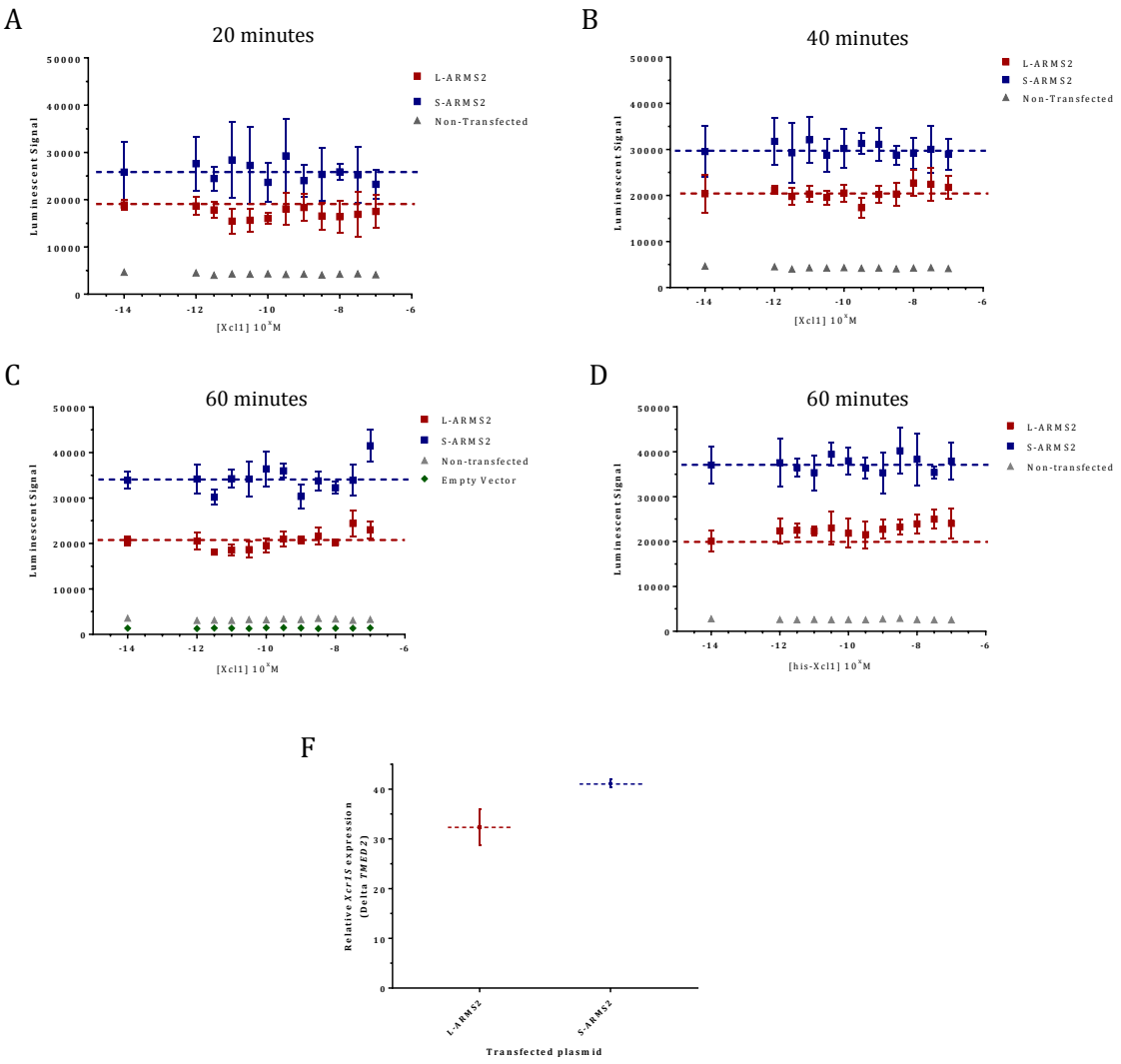

Figure 3.2.10. *Evaluation of β-arrestin recruitment to ARMS2-PK2 conjugated* Xcr1L *and* Xcr1S. A-C) Representative examples of measured luminescence following application of recombinant Xcl1 at half-Log_{10} concentrations between 10^{-7}M and 10^{-12}M. Luminescence from cells treated without ligand is plotted at 10^{-14}M. Xcl1 ligand was applied for 20 (A), 40 (B) or 60 (C) minutes to CHO cells transfected with L-ARMS2 (red) or S-ARMS2 (blue). Error bars = ±SD. D) Measured luminescence following application of his-Xcl1 for 60 minutes. F) qPCR evaluation (n=1) of relative abundance of mRNA arising from L-ARMS2 (red) or S-ARMS2 (blue) plasmids. Error bars = ±SD.

3.2.3.2 Assessment of ligand binding and β-arrestin recruitment to Xcr1S-PK2 *and* Xcr1L-PK2

Despite the consistent observation that S-ARMS2 transfected cells produced a higher luminescent signal, suggestive of increased β-arrestin recruitment, than cells transfected with L-ARMS2, a specific luminescent response to the application of ligand could not be determined. Due to the high expression observed by qPCR, it was decided that the high affinity ARMS2-ED tag produced by the ARMS2 plasmids may be generating too high of a background signal. Therefore, *Xcr1L* and *Xcr1S* coding sequences were next cloned in to PK2 plasmids that express an ED-tag with a lower affinity to the endogenous EA expressed by host CHO cells. Figures 3.2.11 and 3.2.12 detail the successful cloning of *Xcr1S* and *Xcr1L* coding sequences in to S-PK2 and L-PK2 plasmids, respectively. By lowering the affinity, the use of PK2 plasmids aimed to maximise the signal-to-noise ratio and aid the identification of β-arrestin recruitment that was specific to Xcl1 binding to the respective Xcr1 isoforms.

As was observed following the use of L-ARMS2 and S-ARMS2 plasmids, no dose-response of luminescent signal could be observed to the application of recombinant Xcl1 or his-Xcl1 from cells transfected with either L-PK2 or S-PK2 plasmids. However, the use of these plasmids expressing a lower affinity ED C-terminal tag did reduce background luminescent signal. In comparison to cells transfected with ARMS2 plasmids (Figure 3.2.10) the luminescent signal obtained from PK2 plasmids (Figure 3.2.13) was much reduced. Notably, despite this reduction of background signal the basal level of luminescent signal remained significantly higher for cells transfected with S-PK2 plasmid in comparison to L-PK2.

qPCR analysis sought to determine if this discrepancy in basal luminescent signal could be attributed to a variation in expression of the two receptor isoforms within cells transfected with S-PK2 or L-PK2 plasmids. Cells transfected with both plasmids demonstrated a high and consistent expression of *Xcr1* RNA arising from the respective plasmids (figure 3.2.13, C). This demonstrated a significant difference between cells transfected with S-PK2 and L-PK2 plasmids, corresponding to a 1.79x higher expression of *Xcr1S* within cells transfected with S-PK2 in comparison to L-PK2. However, basal luminescent signal remained largely consistent despite the variation in relative *Xcr1* RNA presence observed between replicates of transfection with the same plasmid (figure 3.2.13, D). Moreover, for those cells transfected with L-PK2 and S-PK2 plasmids which showed the closest relative *Xcr1S* RNA expression, the difference in basal luminescent signal remained the same as that for those with relatively larger differences in RNA expression levels. This suggests that the differences in expression of *Xcr1* RNA arising from the transcription of plasmid DNA by transfected cells does not account for the differences in basal luminescent signal observed for cells treated with L-PK2 or S-PK2.

A

B

```
Predicted          1 ATCCGCTAGCGCTACCGGACTCAGATCTGCCACCATGGACTCAGAGTCAG     50
                     ||||||||||||||||||||||||||||||||||||||||||||||||||
L-PK2              1 ATCCGCTAGCGCTACCGGACTCAGATCTGCCACCATGGACTCAGAGTCAG     50

Predicted         51 ATGCTCTCAGTATCCCTGCATCCCGCGTCCAGATGGAGTCCTCTACAGCC    100
                     ||||||||||||||||||||||||||||||||||||||||||||||||||
L-PK2             51 ATGCTCTCAGTATCCCTGCATCCCGCGTCCAGATGGAGTCCTCTACAGCC    100

Predicted        101 TTTTATGATTATCATGATAAATTGAGTCTTCTATGTGAGAACAATGTCAT    150
                     ||||||||||||||||||||||||||||||||||||||||||||||||||
L-PK2            101 TTTTATGATTATCATGATAAATTGAGTCTTCTATGTGAGAACAATGTCAT    150

Predicted        151 CTTCTTTTCCACCATCTCTACCATTGTCCTGTACTCTCTGGTATTTCTCC    200
                     ||||||||||||||||||||||||||||||||||||||||||||||||||
L-PK2            151 CTTCTTTTCCACCATCTCTACCATTGTCCTGTACTCTCTGGTATTTCTCC    200

Predicted        201 TCAGCCTTGTGGGTAACAGCCTGGTTTTGTGGGTCTTGGTGAAGTATGAG    250
                     ||||||||||||||||||||||||||||||||||||||||||||||||||
L-PK2            201 TCAGCCTTGTGGGTAACAGCCTGGTTTTGTGGGTCTTGGTGAAGTATGAG    250

Predicted        251 AATCTAGAGTCACTCACCAATATCTTCATCCTCAACCTGTGTCTCTCAGA    300
                     ||||||||||||||||||||||||||||||||||||||||||||||||||
L-PK2            251 AATCTAGAGTCACTCACCAATATCTTCATCCTCAACCTGTGTCTCTCAGA    300

Predicted        301 CCTGATGTTCTCCTGTCTACTGCCTGTGTTGATCTCAGCACAATGGAGTT    350
                     ||||||||||||||||||||||||||||||||||||||||||||||||||
L-PK2            301 CCTGATGTTCTCCTGTCTACTGCCTGTGTTGATCTCAGCACAATGGAGTT    350

Predicted        351 GGTTTCTAGGTGACTTCTTCTGCAAGTTCTTCAACATGATCTTCGGCATC    400
                     ||||||||||||||||||||||||||||||||||||||||||||||||||
L-PK2            351 GGTTTCTAGGTGACTTCTTCTGCAAGTTCTTCAACATGATCTTCGGCATC    400

Predicted        401 AGCCTCTACAGCAGCATCTTCTTCCTTACCATCATGACCATCCACCGATA    450
                     ||||||||||||||||||||||||||||||||||||||||||||||||||
L-PK2            401 AGCCTCTACAGCAGCATCTTCTTCCTTACCATCATGACCATCCACCGATA    450

Predicted        451 CCTGTCTGTAGTGAGCCCCATCTCTACTCTGGGTATCCATACCCTCCGCT    500
                     ||||||||||||||||||||||||||||||||||||||||||||||||||
L-PK2            451 CCTGTCTGTAGTGAGCCCCATCTCTACTCTGGGTATCCATACCCTCCGCT    500

Predicted        501 GCCGTGTGCTGGTGACATCATGTGTGTGGGCAGCCAGCATCCTGTTCTCC    550
                     ||||||||||||||||||||||||||||||||||||||||||||||||||
L-PK2            501 GCCGTGTGCTGGTGACATCATGTGTGTGGGCAGCCAGCATCCTGTTCTCC    550

Predicted        551 ATCCCTGATGCTGTCTTCCACAAAGTGATCTCCTTAAATTGTAAATATTC    600
                     ||||||||||||||||||||||||||||||||||||||||||||||||||
L-PK2            551 ATCCCTGATGCTGTCTTCCACAAAGTGATCTCCTTAAATTGTAAATATTC    600

Predicted        601 TGAACATCATGGGTTCTTGGCCTCAGTCTACCAGCACAACATCTTCTTCC    650
                     ||||||||||||||||||||||||||||||||||||||||||||||||||
L-PK2            601 TGAACATCATGGGTTCTTGGCCTCAGTCTACCAGCACAACATCTTCTTCC    650

Predicted        651 TCCTCTCCATGGGAATCATCCTATTCTGTTATGTACAGATTCTCAGGACT    700
                     ||||||||||||||||||||||||||||||||||||||||||||||||||
L-PK2            651 TCCTCTCCATGGGAATCATCCTATTCTGTTATGTACAGATTCTCAGGACT    700
```

```
Predicted        701 TTGTTTCGCACAAGGTCCAGACAGAGACACCGAACAGTCAGGCTCATCTT    750
                     ||||||||||||||||||||||||||||||||||||||||||||||||||||
L-PK2            701 TTGTTTCGCACAAGGTCCAGACAGAGACACCGAACAGTCAGGCTCATCTT    750

Predicted        751 CACCGTCGTGGTAGCATACTTCCTCAGCTGGGCTCCCTACAACCTCACAC    800
                     ||||||||||||||||||||||||||||||||||||||||||||||||||||
L-PK2            751 CACCGTCGTGGTAGCATACTTCCTCAGCTGGGCTCCCTACAACCTCACAC    800

Predicted        801 TCTTCCTGAAAACTGGAATCATCCAGCAGAGCTGTGAGAGCCTTCAGCAA    850
                     ||||||||||||||||||||||||||||||||||||||||||||||||||||
L-PK2            801 TCTTCCTGAAAACTGGAATCATCCAGCAGAGCTGTGAGAGCCTTCAGCAA    850

Predicted        851 CTGGACATTGCTATGATTATCTGTCGCCATTTGGCCTTCTCTCATTGCTG    900
                     ||||||||||||||||||||||||||||||||||||||||||||||||||||
L-PK2            851 CTGGACATTGCTATGATTATCTGTCGCCATTTGGCCTTCTCTCATTGCTG    900

Predicted        901 TTTCAACCCAGTGCTTTATGTCTTTGTTGGGATCAAGTTCCGCAGACACC    950
                     ||||||||||||||||||||||||||||||||||||||||||||||||||||
L-PK2            901 TTTCAACCCAGTGCTTTATGTCTTTGTTGGGATCAAGTTCCGCAGACACC    950

Predicted        951 TAAAACATCTCTTCCAGCAGGTCTGGCTGTGCCGGAAGACATCCAGCACT   1000
                     ||||||||||||||||||||||||||||||||||||||||||||||||||||
L-PK2            951 TAAAACATCTCTTCCAGCAGGTCTGGCTGTGCCGGAAGACATCCAGCACT   1000

Predicted       1001 GTTCCCTGCTCCCCTGGTACCTTTACATATGAGGGACCCTCCTTCTACGC   1050
                     ||||||||||||||||||||||||||||||||||||||||||||||||||||
L-PK2           1001 GTTCCCTGCTCCCCTGGTACCTTTACATATGAGGGACCCTCCTTCTACGC   1050

Predicted       1051 AAGCTTCGAATTGGGAGGT   1069
                     ||||||||||||||||||||
L-PK2           1051 AAGCTTCGAATTGGGAGGT   1069
```

C

```
Xcr1               1 MDSESDALSIPASRVQMESSTAFYDYHDKLSLLCENNVIFFSTISTIVLY     50
                     ||||||||||||||||||||||||||||||||||||||||||||||||||||
L-PK2              1 MDSESDALSIPASRVQMESSTAFYDYHDKLSLLCENNVIFFSTISTIVLY     50

Xcr1              51 SLVFLLSLVGNSLVLWVLVKYENLESLTNIFILNLCLSDLMFSCLLPVLI    100
                     ||||||||||||||||||||||||||||||||||||||||||||||||||||
L-PK2             51 SLVFLLSLVGNSLVLWVLVKYENLESLTNIFILNLCLSDLMFSCLLPVLI    100

Xcr1             101 SAQWSWFLGDFFCKFFNMIFGISLYSSIFFLTIMTIHRYLSVVSPISTLG    150
                     ||||||||||||||||||||||||||||||||||||||||||||||||||||
L-PK2            101 SAQWSWFLGDFFCKFFNMIFGISLYSSIFFLTIMTIHRYLSVVSPISTLG    150

Xcr1             151 IHTLRCRVLVTSCVWAASILFSIPDAVFHKVISLNCKYSEHHGFLASVYQ    200
                     ||||||||||||||||||||||||||||||||||||||||||||||||||||
L-PK2            151 IHTLRCRVLVTSCVWAASILFSIPDAVFHKVISLNCKYSEHHGFLASVYQ    200

Xcr1             201 HNIFFLLSMGIILFCYVQILRTLFRTRSRQRHRTVRLIFTVVVAYFLSWA    250
                     ||||||||||||||||||||||||||||||||||||||||||||||||||||
L-PK2            201 HNIFFLLSMGIILFCYVQILRTLFRTRSRQRHRTVRLIFTVVVAYFLSWA    250

Xcr1             251 PYNLTLFLKTGIIQQSCESLQQLDIAMIICRHLAFSHCCFNPVLYVFVGI    300
                     ||||||||||||||||||||||||||||||||||||||||||||||||||||
L-PK2            251 PYNLTLFLKTGIIQQSCESLQQLDIAMIICRHLAFSHCCFNPVLYVFVGI    300

Xcr1             301 KFRRHLKHLFQQVWLCRKTSSTVPCSPGTFTYEGPSFY-------    338
                     ||||||||||||||||||||||||||||||||||||||
L-PK2            301 KFRRHLKHLFQQVWLCRKTSSTVPCSPGTFTYEGPSFYASFELGG    345
```

D

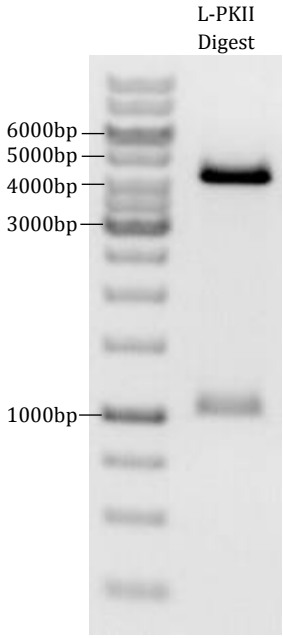

Figure 3.2.11. *Characterisation of L-PK2 plasmid.* A) Sequence of pCMV-PK2 multiple cloning site, as provided by manufacturer. B) Characterised sequence of L-PK2 plasmid following sequencing. Determined sequence of plasmid (L-PK2) has been aligned to predicted L-PK2 sequence (Predicted). Restored sites for BgIII and HindIII digest (blue) and in-frame PK2 C-terminal tag (red) is confirmed. ORF start codon is highlighted in green. C) Predicted translated product from sequenced L-PK2 plasmid (L-PK2) was determined using NCBI ORFfinder and aligned to Xcr1 protein sequence (NCBI protein accession number NP_035928.2). In-frame translated PK2 tag is highlighted in red. D) Restriction digest of L-PK2 plasmid with BgIII and HindIII enzymes produces two products of ~4500bp and ~1000bp, corresponding to pCMV-PK2 backbone and *Xcr1L* insert, respectively following agarose gel electrophoresis.

A

B

```
Predicted           1 ATCCGCTAGCGCTACCGGACTCAGATCTGCCACCATGGAGTCCTCTACAG     50
                      ||||||||||||||||||||||||||||||||||||||||||||||||||
S-PK2               1 ATCCGCTAGCGCTACCGGACTCAGATCTGCCACCATGGAGTCCTCTACAG     50

Predicted          51 CCTTTTATGATTATCATGATAAATTGAGTCTTCTATGTGAGAACAATGTC    100
                      ||||||||||||||||||||||||||||||||||||||||||||||||||
S-PK2              51 CCTTTTATGATTATCATGATAAATTGAGTCTTCTATGTGAGAACAATGTC    100

Predicted         101 ATCTTCTTTTCCACCATCTCTACCATTGTCCTGTACTCTCTGGTATTTCT    150
                      ||||||||||||||||||||||||||||||||||||||||||||||||||
S-PK2             101 ATCTTCTTTTCCACCATCTCTACCATTGTCCTGTACTCTCTGGTATTTCT    150

Predicted         151 CCTCAGCCTTGTGGGTAACAGCCTGGTTTTGTGGGTCTTGGTGAAGTATG    200
                      ||||||||||||||||||||||||||||||||||||||||||||||||||
S-PK2             151 CCTCAGCCTTGTGGGTAACAGCCTGGTTTTGTGGGTCTTGGTGAAGTATG    200

Predicted         201 AGAATCTAGAGTCACTCACCAATATCTTCATCCTCAACCTGTGTCTCTCA    250
                      ||||||||||||||||||||||||||||||||||||||||||||||||||
S-PK2             201 AGAATCTAGAGTCACTCACCAATATCTTCATCCTCAACCTGTGTCTCTCA    250

Predicted         251 GACCTGATGTTCTCCTGTCTACTGCCTGTGTTGATCTCAGCACAATGGAG    300
                      ||||||||||||||||||||||||||||||||||||||||||||||||||
S-PK2             251 GACCTGATGTTCTCCTGTCTACTGCCTGTGTTGATCTCAGCACAATGGAG    300

Predicted         301 TTGGTTTCTAGGTGACTTCTTCTGCAAGTTCTTCAACATGATCTTCGGCA    350
                      ||||||||||||||||||||||||||||||||||||||||||||||||||
S-PK2             301 TTGGTTTCTAGGTGACTTCTTCTGCAAGTTCTTCAACATGATCTTCGGCA    350

Predicted         351 TCAGCCTCTACAGCAGCATCTTCTTCCTTACCATCATGACCATCCACCGA    400
                      ||||||||||||||||||||||||||||||||||||||||||||||||||
S-PK2             351 TCAGCCTCTACAGCAGCATCTTCTTCCTTACCATCATGACCATCCACCGA    400

Predicted         401 TACCTGTCTGTAGTGAGCCCCATCTCTACTCTGGGTATCCATACCCTCCG    450
                      ||||||||||||||||||||||||||||||||||||||||||||||||||
S-PK2             401 TACCTGTCTGTAGTGAGCCCCATCTCTACTCTGGGTATCCATACCCTCCG    450

Predicted         451 CTGCCGTGTGCTGGTGACATCATGTGTGTGGGCAGCCAGCATCCTGTTCT    500
                      ||||||||||||||||||||||||||||||||||||||||||||||||||
S-PK2             451 CTGCCGTGTGCTGGTGACATCATGTGTGTGGGCAGCCAGCATCCTGTTCT    500

Predicted         501 CCATCCCTGATGCTGTCTTCCACAAAGTGATCTCCTTAAATTGTAAATAT    550
                      ||||||||||||||||||||||||||||||||||||||||||||||||||
S-PK2             501 CCATCCCTGATGCTGTCTTCCACAAAGTGATCTCCTTAAATTGTAAATAT    550

Predicted         551 TCTGAACATCATGGGTTCTTGGCCTCAGTCTACCAGCACAACATCTTCTT    600
                      ||||||||||||||||||||||||||||||||||||||||||||||||||
S-PK2             551 TCTGAACATCATGGGTTCTTGGCCTCAGTCTACCAGCACAACATCTTCTT    600

Predicted         601 CCTCCTCTCCATGGGAATCATCCTATTCTGTTATGTACAGATTCTCAGGA    650
                      ||||||||||||||||||||||||||||||||||||||||||||||||||
S-PK2             601 CCTCCTCTCCATGGGAATCATCCTATTCTGTTATGTACAGATTCTCAGGA    650

Predicted         651 CTTTGTTTCGCACAAGGTCCAGACAGAGACACCGAACAGTCAGGCTCATC    700
                      ||||||||||||||||||||||||||||||||||||||||||||||||||
S-PK2             651 CTTTGTTTCGCACAAGGTCCAGACAGAGACACCGAACAGTCAGGCTCATC    700

Predicted         701 TTCACCGTCGTGGTAGCATACTTCCTCAGCTGGGCTCCCTACAACCTCAC    750
                      ||||||||||||||||||||||||||||||||||||||||||||||||||
S-PK2             701 TTCACCGTCGTGGTAGCATACTTCCTCAGCTGGGCTCCCTACAACCTCAC    750
```

```
Predicted        751 ACTCTTCCTGAAAACTGGAATCATCCAGCAGAGCTGTGAGAGCCTTCAGC    800
                     ||||||||||||||||||||||||||||||||||||||||||||||||||||
S-PK2            751 ACTCTTCCTGAAAACTGGAATCATCCAGCAGAGCTGTGAGAGCCTTCAGC    800

Predicted        801 AACTGGACATTGCTATGATTATCTGTCGCCATTTGGCCTTCTCTCATTGC    850
                     ||||||||||||||||||||||||||||||||||||||||||||||||||||
S-PK2            801 AACTGGACATTGCTATGATTATCTGTCGCCATTTGGCCTTCTCTCATTGC    850

Predicted        851 TGTTTCAACCCAGTGCTTTATGTCTTTGTTGGGATCAAGTTCCGCAGACA    900
                     ||||||||||||||||||||||||||||||||||||||||||||||||||||
S-PK2            851 TGTTTCAACCCAGTGCTTTATGTCTTTGTTGGGATCAAGTTCCGCAGACA    900

Predicted        901 CCTAAAACATCTCTTCCAGCAGGTCTGGCTGTGCCGGAAGACATCCAGCA    950
                     ||||||||||||||||||||||||||||||||||||||||||||||||||||
S-PK2            901 CCTAAAACATCTCTTCCAGCAGGTCTGGCTGTGCCGGAAGACATCCAGCA    950

Predicted        951 CTGTTCCCTGCTCCCCTGGTACCTTTACATATGAGGGACCCTCCTTCTAC   1000
                     ||||||||||||||||||||||||||||||||||||||||||||||||||||
S-PK2            951 CTGTTCCCTGCTCCCCTGGTACCTTTACATATGAGGGACCCTCCTTCTAC   1000

Predicted       1001 ACAAGCTTCGAATTGGGAGGT   1021
                     |||||||||||||||||||||
S-PK2           1001 ACAAGCTTCGAATTGGGAGGT   1021
```

C

```
Xcr1               1 MDSESDALSIPASRVQMESSTAFYDYHDKLSLLCENNVIFFSTISTIVLY     50
                                 ||||||||||||||||||||||||||||||||||
S-PK2              1 ----------------MESSTAFYDYHDKLSLLCENNVIFFSTISTIVLY     34

Xcr1              51 SLVFLLSLVGNSLVLWVLVKYENLESLTNIFILNLCLSDLMFSCLLPVLI    100
                     ||||||||||||||||||||||||||||||||||||||||||||||||||||
S-PK2             35 SLVFLLSLVGNSLVLWVLVKYENLESLTNIFILNLCLSDLMFSCLLPVLI     84

Xcr1             101 SAQWSWFLGDFFCKFFNMIFGISLYSSIFFLTIMTIHRYLSVVSPISTLG    150
                     ||||||||||||||||||||||||||||||||||||||||||||||||||||
S-PK2             85 SAQWSWFLGDFFCKFFNMIFGISLYSSIFFLTIMTIHRYLSVVSPISTLG    134

Xcr1             151 IHTLRCRVLVTSCVWAASILFSIPDAVFHKVISLNCKYSEHHGFLASVYQ    200
                     ||||||||||||||||||||||||||||||||||||||||||||||||||||
S-PK2            135 IHTLRCRVLVTSCVWAASILFSIPDAVFHKVISLNCKYSEHHGFLASVYQ    184

Xcr1             201 HNIFFLLSMGIILFCYVQILRTLFRTRSRQRHRTVRLIFTVVVAYFLSWA    250
                     ||||||||||||||||||||||||||||||||||||||||||||||||||||
S-PK2            185 HNIFFLLSMGIILFCYVQILRTLFRTRSRQRHRTVRLIFTVVVAYFLSWA    234

Xcr1             251 PYNLTLFLKTGIIQQSCESLQQLDIAMIICRHLAFSHCCFNPVLYVFVGI    300
                     ||||||||||||||||||||||||||||||||||||||||||||||||||||
S-PK2            235 PYNLTLFLKTGIIQQSCESLQQLDIAMIICRHLAFSHCCFNPVLYVFVGI    284

Xcr1             301 KFRRHLKHLFQQVWLCRKTSSTVPCSPGTFTYEGPSFY-------    338
                     ||||||||||||||||||||||||||||||||||||||
S-PK2            285 KFRRHLKHLFQQVWLCRKTSSTVPCSPGTFTYEGPSFYTSFELGG    329
```

D

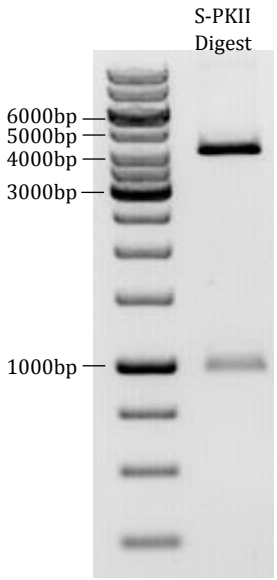

Figure 3.2.12. *Characterisation of S-PK2 plasmid.* A) Sequence of pCMV-PK2 multiple cloning site, as provided by manufacturer. B) Characterised sequence of S-PK2 plasmid following sequencing. Determined sequence of plasmid (S-PK2) has been aligned to predicted S-PK2 sequence (Predicted). Restored sites for BgIII and HindIII digest (blue) and in-frame PK2 C-terminal tag (red) is confirmed. ORF start codon is highlighted in green. C) Predicted translated product from sequenced S-PK2 plasmid (L-PK2) was determined using NCBI ORFfinder and aligned to Xcr1 protein sequence (NCBI protein accession number NP_035928.2). In-frame translated PK2 tag is highlighted in red. D) Restriction digest of S-PK2 plasmid with BgIII and HindIII enzymes produces two products of ~4500bp and ~1000bp, corresponding to pCMV-PK2 backbone and *Xcr1S* insert, respectively following agarose gel electrophoresis.

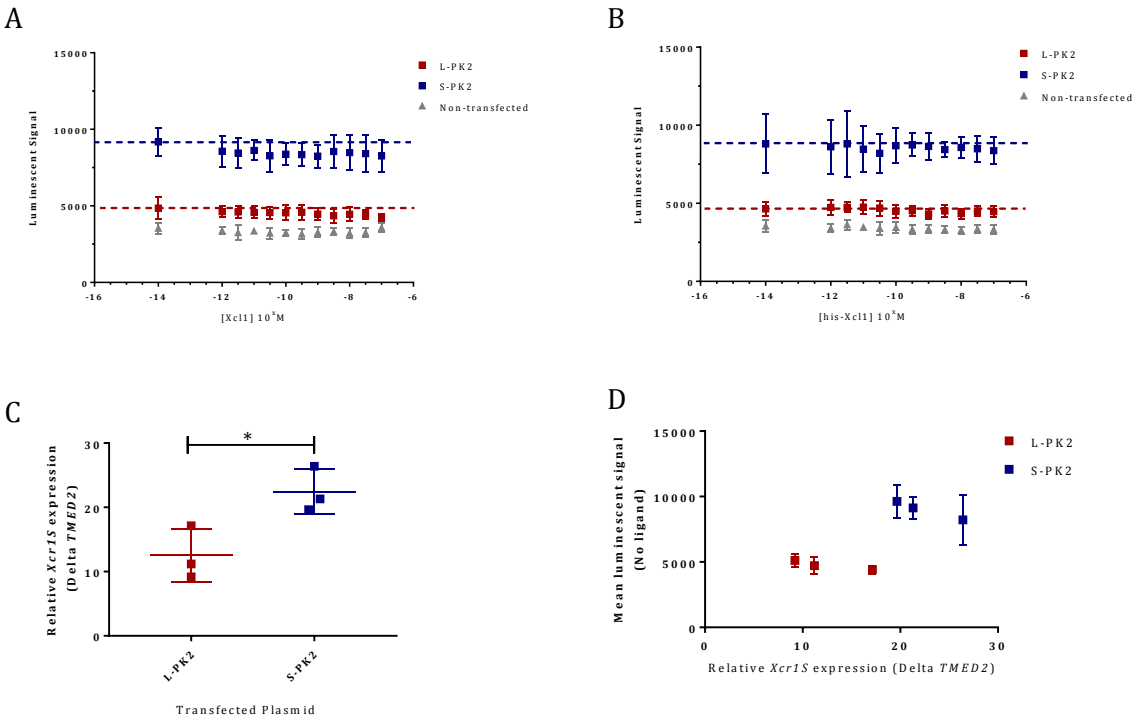

Figure 3.2.13. *Evaluation of β-arrestin recruitment to PK2 conjugated* Xcr1L *and* Xcr1S. A,B) Mean Luminescent signal obtained following the application of recombinant Xcl1 (n=3) (A) or recombinant his-Xcl1 (n=3) (B) to CHO cells transfected with L-PK2 and S-PK2 plasmids. Error bars = ±SD. C) qPCR evaluation of *Xcr1* RNA produced by cells transfected with L-PK2 and S-PK2 plasmids (*, mean difference = 9.93, p = 0.034) n=3, Error bars = ±SD. qPCR evaluation was performed using stock cells used for the evaluation of β-arrestin recruitment in A and B. D) Plot of mean luminescent signal from cells untreated with ligand against relative *Xcr1* RNA expression by cells from 3 independent β-arrestin assays of cells transfected with L-PK2 or S-PK2 plasmids. Error bars = ±SD.

The use of PK2 plasmids was therefore effective in reducing background luminescent signal, yet was still unable to provide a specific luminescent signal that was indicative of β-arrestin recruitment to the respective Xcr1 isoforms as a consequence of ligand binding. Furthermore, luminescent signal arising from cells transfected with S-PK2 maintained a consistently higher level of basal luminescent signal than that observed for cells transfected with the L-PK2 plasmid in all repeats performed. This is consistent with the evidence obtained from cells transfected with ARMS2-plasmids and suggests that despite the reduction in background luminescent signal an alternative mechanism was preventing the observation of ligand-specific induction of β-arrestin recruitment to Xcr1L or Xcr1S.

3.2.3.3 Assessment of ligand binding and β-arrestin recruitment to CHO cells stably expressing Xcr1L-PK2 or Xcr1S-PK2

Given the high expression, demonstrated by qPCR, of the two Xcr1 isoforms expressed by cells transfected with S-PK2 or L-PK2, CHO cells were next selected for the stable expression of plasmid coding sequence by antibiotic selection with G418. By selecting cells with G418 it was aimed to establish a population of cells that expressed a stable and lower level of the plasmid insert. This would permit a lower level of protein expression and reduce the possibility for receptor aggregation that may have inhibited the sensitivity of expressed Xcr1 isoforms to the applied ligand when using transiently transfected cells, as performed previously.

Successful transfection and expression of the desired plasmids was confirmed by G418 selection for 10-12 days prior to performing the β-arrestin assay (figure 3.2.14). Untransfected cells were typically lost after 5-7 days of antibiotic treatment. In contrast, cells transfected with L-PK2 or S-PK2 demonstrated continued cell viability throughout this period suggestive of a maintained and stable expression of the plasmid.

Evaluation of chemiluminescent production from cells transfected with L-PK2 or S-PK2 plasmids, following G418 selection, did indeed demonstrate the eradication of background luminescent signal by cells transfected with L-PK2. Furthermore, the basal level of luminescence produced by cells transfected with S-PK2 was also reduced, in comparison to cells transfected with the two plasmids that did not undergo G418 selection (Figure 3.2.13). This suggested a reduction in the overall expression of the two receptor isoforms within cells transfected with L-PK2 and S-PK2 as a consequence of G418 selection.

This observation is substantiated by the observed reduction of relative *Xcr1* RNA presence within RNA samples as compared to that observed for cells without G418 selection (Figure 3.2.14, C vs Figure 3.2.13, C). This corresponded to a mean reduction in *Xcr1* RNA expression

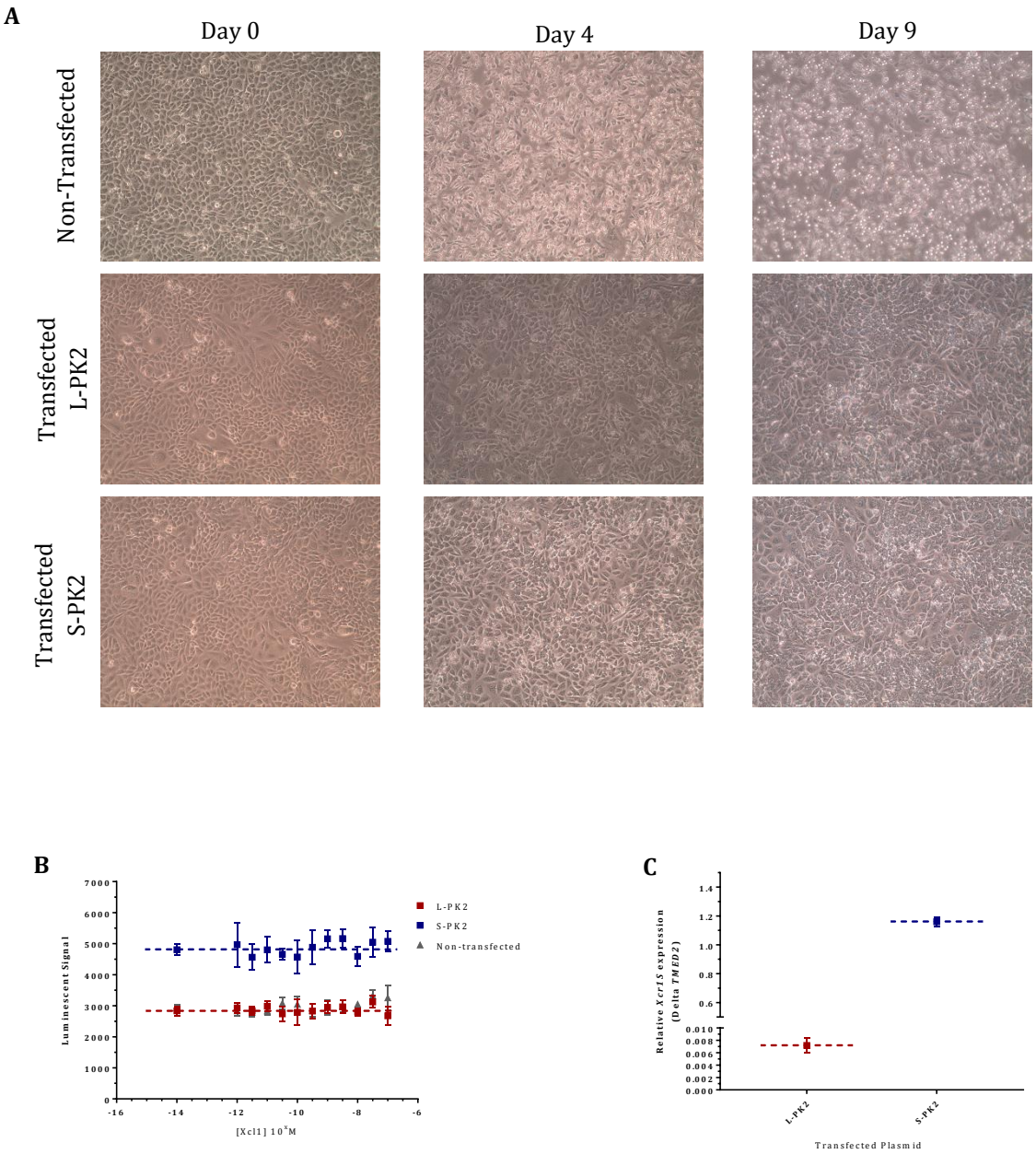

Figure 3.2.14. *Evaluation of β-arrestin recruitment to PK2-conjugated* Xcr1L *and* Xcr1S *following G418 selection of CHO cells.* A) G418 selection of CHO cells. Microscope images demonstrate survival of cells transfected with L-PK2 and S-PK2 plasmids following 9 days of G418 treatment at 2mg/ml. Complete cell death of non-transfected CHO cells confirms the efficacy of G418 treatment. Transfected cells were subsequently dissociated and seeded to 384 well plates for evaluation of β-arrestin recruitment following the application of recombinant ligands. B) Assay of β-arrestin recruitment (n=1) to cells transfected with L-PK2 and S-PK2 following G418 selection as shown in A. Error bars = ±SD C) qPCR evaluation (n=1) of Relative *Xcr1S* expression in RNA extracted from cells transfected with L-PK2 and S-PK2 plasmids following G418 selection. Error bars = ±SD.

of 1787x for cells transfected with L-PK2 and 19x for cells transfected with S-PK2, in comparison to cells transfected with these plasmids that did not undergo G418 selection. As suggested by such substantial reductions in cells transfected with L-PK2, cells transfected with L-PK2 demonstrated a 164x lower expression of *Xcr1* RNA in comparison to cells transfected with S-PK2, following G418 selection. Overall, the evaluation of luminescent signal and RNA expression confirms the process of G418 selection to successfully reduce the expression of both RNA and protein from associated plasmids, although the reduction in *Xcr1* RNA expression is significantly more prominent in cells transfected with L-PK2.

Despite the capacity for G418 selection to successfully reduce expression from associated plasmids, no dose-response was observed by the cells in response to the application of Xcl1 ligand. Therefore, despite every effort being made to refine the sensitivity of the assay by reducing background luminescence and by reducing expression of receptor isoforms within transfected cells, no specific response of either receptor isoform was observed to the application of ligand. However, a consistent observation in all experiments was the higher level of basal luminescence observed in cells expressing the Xcr1S receptor isoform in comparison to cells expressing the Xcr1L isoform. This suggests a higher constitutive recruitment of β-arrestin by Xcr1S in comparison to Xcr1L.

3.3 Discussion

The results presented in this chapter have sought to provide some clarity regarding the expression of *Xcr1* and *Xcl1* within the murine CNS. As a consequence of the conflicting evidence currently available for *Xcr1* mRNA, evaluation of *Xcr1* expression has targeted two alternative amplicons, namely *Xcr1L* and *Xcr1S*. This method aimed to provide an insight as to the relative proportion of *Xcr1* mRNA arising from exon 1 and exon 2 sequences or exon 2 sequences only. Furthermore, this study sought to provide the first direct functional comparison between the two proposed Xcr1 isoforms and provide evidence to substantiate which isoform reflects the Xcr1 protein produced *in vivo*.

3.3.1 Xcr1 and Xcl1 expression is low in the murine CNS

In line with one of the primary objectives of this project the expression of *Xcr1* and *Xcl1* was investigated in whole spinal cord samples. Evaluation of *Xcr1* expression within the spinal cord of male and female mice at six and 10 months indicated a low expression of *Xcr1* RNA within these samples. This was regardless of whether evaluation of *Xcr1S* or *Xcr1L* amplicons was used to determine the expression of this gene. For all investigations performed of *Xcr1* expression in RNA samples collected from cells or tissue of the CNS, Ct values were consistently low (≥ 30). In comparison, evaluation of *Xcl1* expression indicated the expression of the chemokine ligand to be consistently higher than that obtained for *Xcr1* in whole spinal cord regardless of the age or gender of the sample. This low expression of associated RNA was expected based on the lack of previous evidence to suggest that this chemokine and its receptor were expressed prominently within the CNS. Indeed, with the exception of CXCL12/CXCR4, CX3CL1/CX3CR1, this low expression is in correspondence with evidence for other chemokines, for which the expression within cells specific to the CNS parenchyma, is typically made in response to inflammatory stimuli with low, if any, expression during physiological conditions (Reaux-Le Goazigo *et al.*, 2013).

Despite the low expression in whole spinal cord samples, it was sought to refine the cellular source of *Xcr1* and *Xcl1* expression using *in vitro* samples of CNS cells. Evaluation of *Xcr1* expression demonstrated the expression in neuronal cells, a feature that was not observed for samples collected from primary astrocytes. This is in concordance with previous evidence suggesting a low expression of *Xcr1* by primary astrocytes collected from rats (Zychowska *et al.*, 2016). Furthermore, no detection of *Xcl1* expression was observed by primary astrocytes. Should neuronal cells express the Xcr1 protein, this suggests the source of Xcl1 to originate from cells other than astrocytes. The results provided here collected from a primary cell population enriched with microglia suggest that these cells may represent a source of *Xcl1* expression within the CNS. Again, this supports the recent suggestion that microglia express this chemokine ligand (Zychowska *et al.*, 2016) and is in

line with other reports demonstrating the expression of chemokine ligands, most prominently of the CC family, by microglia (Lee, Nagai and Kim, 2002; Babcock *et al.*, 2003; Kremlev, Roberts and Palmer, 2004).

3.3.2 Xcl1 expression in NTg primary mouse microglia is only moderately influenced by LPS

Following on from the recent identification of microglial *Xcl1* expression to be significantly increased in response to LPS stimuli (Zychowska *et al.*, 2016), this study sought evidence to clarify the expression of *Xcl1* by murine microglia. LPS treatment has become the standard treatment used to induce a potent innate immune response by many cells. The presence of LPS leads to the induction of several intracellular signalling cascades as a result of Toll-like Receptor 4 (TLR4) engagement. A key outcome of these TLR4-induced cascades is the resultant translocation of NF-κβ and AP-1 transcription factors to the nucleus where they act as potent inducers of transcription from the genes of pro-inflammatory mediators, including chemokines (Lu, Yeh and Ohashi, 2008). LPS treatment of microglia is associated with a polarisation towards an activated, cytotoxic (previously referred to as 'M1') cellular phenotype (Chhor *et al.*, 2013). As such, the influence of LPS stimulation on the expression of *Xcl1* by microglia was used to provide an indication to the role of this chemokine in the innate immune response by microglia. By adopting the same method of LPS treatment for the treatment of primary Mouse microglia to that performed by Zychowska et al. for the treatment of primary Rat microglia, it was aimed to provide the first characterisation of the *Xcl1* response to LPS by Mouse microglia. Furthermore, we sought to test the validity of evidence from primary Rat microglia to suggest the expression of *Xcl1* by Mouse microglia *in vivo* (Zychowska *et al.*, 2016).

The primary cell populations used for evaluation of *Xcl1* expression were observed to predominantly contain microglial cells, as indicated by Iba-1 immunoreactivity, whilst the presence of astrocyte cells was limited. The presence of other cells within the culture was made necessary according to preliminary attempts that demonstrated the lack of microglial cell numbers and viability in cultures from which these additional cells were removed. Evaluation of *Xcl1* expression in untreated cells suggest that *Xcl1* expression is very low under physiological conditions. However, a small but consistent change in expression as a consequence of LPS treatment was identified in all biological replicates. This equated to an observed reduction of ~22% from that of untreated cells and was supported to arise from the activation of microglia following LPS treatment according to quantitative analysis of Iba-1 reactivity and qualitative assessment of cellular morphology. This small reduction in *Xcl1* expression following LPS treatment is in contrast to the observed magnitude of increase in *Xcl1* expression observed previously (Zychowska *et al.*, 2016).

An important distinction of the microglial cells studied here was their origin from adult mouse brains in comparison to those collected by Zychowska et al., from neonatal Rat brains. This difference in the age and method of cell preparation is likely to influence the behaviour of primary microglial cells. Indeed, the contrast in microglial phenotypes between neonates and adults suggests a contrast in their behaviour in response to stimuli. It has been indicated for example, that the recently described microglial-specific marker TMEM119, does not achieve an expression that is characteristic of mature microglia until postnatal day 14 in mice (Bennett *et al.*, 2016). This is alongside the changes observed for a myriad of other microglial proteins that are dynamically regulated within these cells as a consequence of both intrinsic regulatory mechanisms and as a function of cellular cross-talk during CNS development and maturation (Tuan Leng *et al.*, 2017). A further consideration to this is the sex of animal from which microglial cells are collected. It has been demonstrated that the presence of testosterone can influence the contribution of microglia to pathological mechanisms within a mouse model of neuropathic pain *in vivo* (Sorge *et al.*, 2015), although the influence of sex within *in vitro* preparations of microglia remains unclear. Furthermore, contemporary studies of primary microglia function still include preparations from animals of both sexes (see e.g. (Chhor *et al.*, 2013)). For the evidence collected here, each preparation was prepared from a group of animals of the same sex. However, of the three biological replicates performed, two were collected from female animals and one was collected from male animals. Despite this, the consistency of *Xcl1* expression observed suggests that the sex of animal does not influence the expression of this gene, either constitutively or in response to LPS. In support of this, levels of *Xcl1* expression observed from RNA samples collected from whole spinal cord did not display any significant changes between sexes at either 6 or 10 months of age. Overall, the evidence collected here to evaluate *Xcl1* expression in primary microglia suggests that these cells express a low level of *Xcl1* mRNA that is very moderately influenced following LPS treatment.

3.3.3 Evaluation of Xcr1 mRNA composition and expression in the CNS

The *Xcr1* gene is composed of two exons, in comparison to three exons for human *XCR1* (Shinkai *et al.*, 2005). Currently, there is a conflict of evidence regarding both the coding sequence and mRNA sequence of *Xcr1*. Documented cDNA arising from exon 1 and exon 2, or exon 2 only does exist. Therefore, we have performed quantitative analysis of *Xcr1* RNA expression utilising primers that either span exon 1 and exon 2 (*Xcr1L*) or are located within exon 2 only (*Xcr1S*).

In an effort to identify if there is the potential for the alternative expression of mRNA transcripts arising from *Xcr1*, a comparative expression of *Xcr1L* and *Xcr1S* has been

performed. Due to the nature of this analysis and the potential for confounding factors to influence the expression of each transcript, this analysis has been problematic. However, evidence has been provided which indicates the differential expression of *Xcr1L* and *Xcr1S* amplicons within certain samples. For RNA samples collected from whole spinal cord of male and female mice at 6 months of age, the relative expression of *Xcr1S* was higher than that observed for *Xcr1L*, a feature that was not observed for the same samples collected at 10 months of age. In addition, a more substantial difference was observed between *Xcr1S* and *Xcr1L* expression in RNA samples collected from mouse motor neurons derived from mESCs. Although substantial, this difference did not achieve statistical significance, a feature which arose from the prominence of *Xcr1L* non-detects. A method was employed to counter this issue based on recommendations to provide a more reasonable estimation of gene expression from non-detects. Following this, the Ct value presumed for non-detects has been reduced to 35 in comparison to the value of 40 that is suggested by some methods (McCall *et al.*, 2014). Indeed, use of a higher Ct value for *Xcr1L* non-detects identified from this investigation would have led to more substantial differences and resulted in statistically significant differences in expression in comparison to that identified from *Xcr1S*. However, according to the recommendations provided (McCall *et al.*, 2014) and the results obtained from primer optimisations, a Ct value of 35 was deemed most appropriate.

Despite these difficulties, the relative differences in *Xcr1L* and *Xcr1S* expression identified by qPCR in ESC-derived mouse motor neurons were substantiated by the retrospective analysis of microarray data collected from NSC-34 cells, an immortalised mouse motor neuron-like cell line. This data provided consistent and statistically significant support for the higher relative abundance of RNA derived from exon 2 of *Xcr1,* than exon 1. Together this suggests that motor neurons may express low quantities of *Xcr1* mRNA that is composed primarily from the transcription of exon 2.

3.3.4 5' RACE analysis reveals the potential for intron 1 retention in Xcr1 mRNA

To provide further clarity to the composition of *Xcr1* mRNA within both spleen and spinal cord, 5' RACE analysis was employed with the aim of identifying potential alternative start codons. 5' RACE of *Xcr1* has previously been performed for mouse RNA collected from spleen (Shinkai *et al.*, 2005). Despite efforts to evaluate this sequence within the spinal cord, evidence could only be reliably determined from RNA samples from spleen. These results provided a varied sequence arising from the 5' region of *Xcr1* RNA. Evidence from two samples provided validation for the existing descriptions of *Xcr1* mRNA to include both exons 1 and 2 and supported that which had been previously characterised (Shinkai *et al.*, 2005). However sequencing from one sample also demonstrated the most prominent sequence that lies 5' to exon 2 to arise from intron 1. Furthermore, assessment of amplicons

following agarose gel electrophoresis indicated the presence of amplicons that were far larger than the expected size of amplicons generated from *Xcr1* RNA composed of exon 1 and exon 2 as documented by bioinformatics databases. In addition, PCR evaluation of cDNA produced from spleen RNA demonstrated the consistent retention of intron 1 sequences.

The retention of intron sequences as a mechanism of alternative splicing has been well documented for GPCRs and can arise from the use of alternative promoters (Markovic and Challiss, 2009). The presence of a large intron within the *Xcr1* gene presents the possibility that certain sequences within this region may give rise to transcriptional regulation of exon 2. In support of this, bioinformatics records and annotation, provided by Ensembl (ENSMUST00000182350.1), demonstrate the presence of two promoter sequences to lie in the region of *Xcr1* (Figure 3.3.1). One of these promoters lies 5' to exon 1, whilst the second is located within intron 1. There is also an additional enhancer located within intron 1. This presents a plausible mechanism by which the transcription of exon 1 and exon 2 sequences from *Xcr1* could be independently regulated. Moreover, the tissue and cell-specific nature of transcriptional regulators have the capacity to explain the observed differences in *Xcr1L* and *Xcr1S* expression that appear to be more prominent within the CNS. However, it cannot be discounted that the observed intron 1 sequence from 5' RACE could have arisen from the sequencing of *Xcr1* pre-mRNA. Therefore, although this method offers the insight that the most prominent RNA sequences arising from the *Xcr1* gene can arise from the transcription of intron 1, the reason for this may be due to the method detecting samples of pre-mRNA and not mRNA only. Whilst the presence of mature mRNA species is suggested to vastly exceed that of pre-mRNA (Zeisel *et al.*, 2011), the source of this result to arise exclusively from *Xcr1* mRNA cannot be confirmed. Consequently, although suggested by qPCR and microarray data, conclusive evidence of an alternative *Xcr1* mRNA that does not include exon 1 has not been obtained. However, evidence to support the current consensus of *Xcr1* mRNA to be derived from exon 1 and exon 2 has been provided.

3.3.5 The two potential Xcr1 protein isoforms demonstrate distinct capacities for the interaction with β-arrestin

The corresponding amino acid sequence to the Xcr1 protein has yet to be confirmed. Current assumptions of this are based on the predicted Open Reading Frame (ORF) arising from *Xcr1* mRNA and has resulted in the prediction of two potential isoforms, referred to here as Xcr1L and Xcr1S. This study provided the first functional comparison of these two isoforms and aimed to validate the amino acid sequence of Xcr1 expressed *in vivo* according to the recruitment of β-arrestin following binding of the Xcl1 ligand.

The evidence accrued from these investigations has provided a consistent demonstration that cells expressing Xcr1S recruited β-arrestin at a higher constitutive level than cells

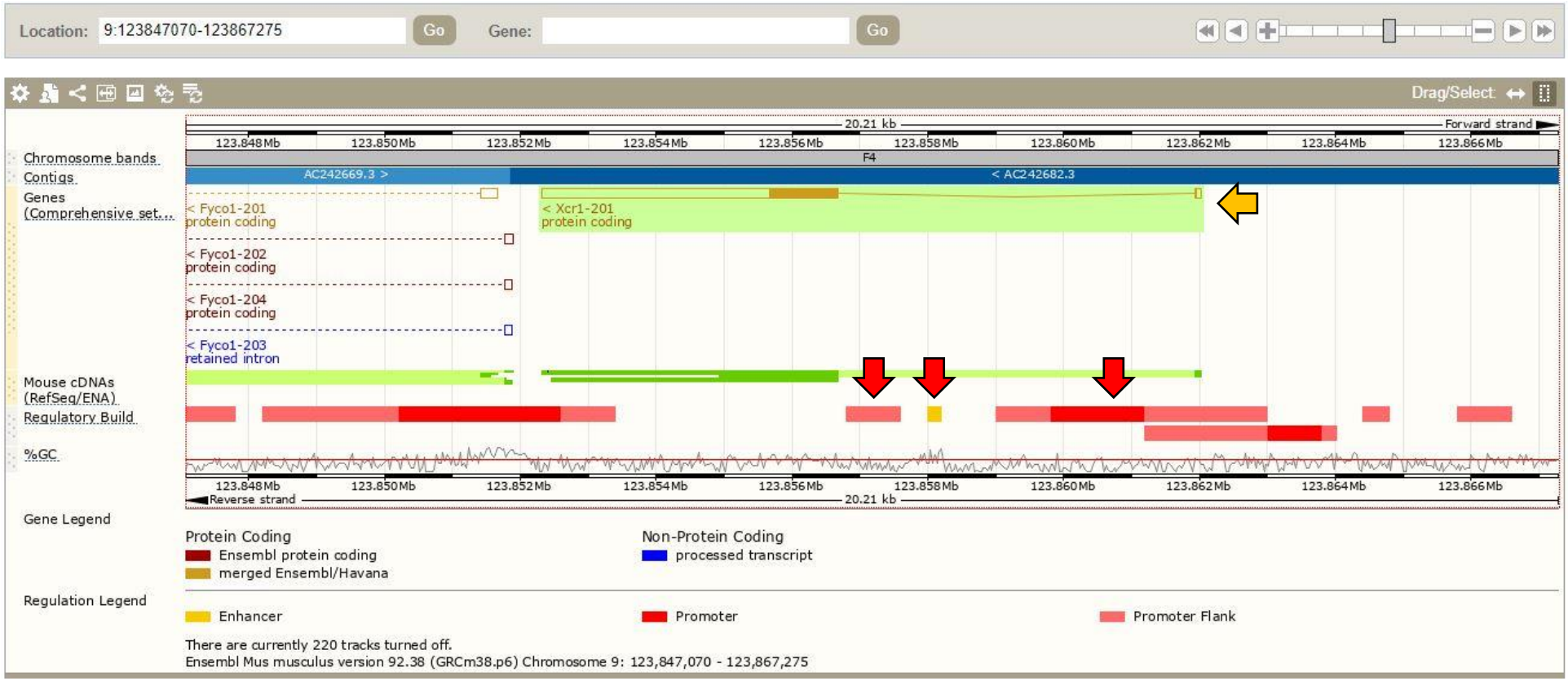

Figure 3.3.1. *Screenshot of online annotation of promoter sequences within and surrounding Xcr1 mRNA according to Ensembl record ENSMUST00000182350.1.* Annotation of predicted sites for promoter regions within *Xcr1* mRNA suggests the existence of promoters that lie upstream of *Xcr1* exon 1 and exon 2. Promoter regions (Red arrows) are highlighted in red and pink (bottom row); Xcr1 coding (Yellow arrow) sequence is highlighted in yellow (top row).

expressing Xcr1L, according to the luminescent signal detected as a consequence of EFC. Unfortunately, it has not been possible to achieve a luminescent signal that demonstrated a dose response to the presence of Xcl1. However, the consistently higher basal interaction of β-arrestin to the Xcr1S isoform is suggestive of functional protein expression and higher turnover of the protein from the cell membrane. Moreover, chemokine receptors are known to undergo basal levels of receptor internalisation and recycling in the absence of ligand (Neel *et al.*, 2005) a feature that has been reported more broadly for the GPCR family as a whole (Seifert and Wenzel-Seifert, 2002).

The consequence of this constitutive β-arrestin recruitment is highlighted by studies of both classical, signalling competent chemokine receptors and ACKRs. It has been previously reported for the D6 ACKR that the interaction with β-arrestin maintains receptor stability and prevents receptor degradation following internalisation, but is not necessary for initial receptor internalisation (Weber *et al.*, 2004). D6 has the closest homology to the CC chemokine receptors CCR1-5 and serves to scavenge extracellular CCL3. Interaction with β-arrestin is prevented by the mutation or loss of a serine-rich domain within the C-terminus. The loss of β-arrestin interaction does not prevent initial ligand binding and internalisation, but instead leads to subsequent receptor degradation and inhibition of progressive scavenging (McCulloch *et al.*, 2008). Hence, for some non-classical chemokine receptors, the interaction of this intracellular adaptor protein is instead required for essential functions that are mediated after receptor internalisation and permit enhanced receptor stability.

The increased stability of receptors afforded by the constitutive interaction with β-arrestin is also suggested for signalling-competent chemokine receptors. CCR1 has been demonstrated to perform basal levels of ligand-independent intracellular G-protein signalling and β-arrestin recruitment that is associated with constitutive levels of receptor phosphorylation and receptor internalisation, a characteristic that is not observed for the homologous CCR2 or CCR5 receptors. Moreover, this basal activity is associated with the formation of a CCR1-$G\alpha_i$-β-arrestin complex that remains stably associated following ligand binding. However, the formation of this complex to occur to individual receptors or following receptor oligomerisation was unclear. Together, this basal activity of CCR1 was suggested to contribute to a previously undescribed chemokine scavenging activity of the receptor. Furthermore, this was a function considered to be reliant upon the constitutive interaction of the receptor with β-arrestin (Gilliland *et al.*, 2013). Although this function of chemokine scavenging appears to be a relatively new, and potentially unusual, addition to the repertoire of chemokine function, a function for Xcr1 in relation to this cannot be excluded. In fact, considering the exclusive binding of Xcl1 to Xcr1, it may not only be plausible, but also a necessary function of Xcr1 to regulate extracellular Xcl1 concentrations

through constitutive receptor activity. Furthermore, the phylogenetic analysis of *Xcr1* suggests this receptor to be most closely related to the CC chemokine receptor family (Nomiyama, Osada and Yoshie, 2011). *XCR1* is also located adjacently to human and mouse *CCR1* genes within their respective genomic locations, indicative of an evolutionary conserved function (Chapter 1).

Although such functions remain intriguing, further analysis and investigation is clearly required to interrogate this potential function of the Xcr1S protein. Most notable for this study however, is the outcome of the PathHunter™ β-arrestin assay to provide evidence that the Xcr1S protein exhibits a greater association to β-arrestin than the Xcr1L protein. The implications of this will also require further investigation, but it provides a further premise to suggest that the produced protein arising from *Xcr1* is encoded entirely within exon 2 as previously suggested (Yoshida *et al.*, 1998; Shinkai *et al.*, 2005). The reasons for the divergent β-arrestin activity between Xcr1L and Xcr1S can only be speculated upon, particularly considering the extensive functions that are associated with the N-terminal domain of chemokine receptors (see section 3.1). Furthermore, sequence analysis and alignments were unable to identify any functional motifs within the longer amino acid sequence found at the N-terminal of Xcr1L in comparison to Xcr1S, suggesting that this additional sequence does not convey any positive functional characteristics to the Xcr1 protein. However, in correspondence with identified *Xcr1* mRNA sequence identified here and by others (Dorner *et al.*, 2009; Shinkai *et al.*, 2005) the translation of Xcr1L from this mRNA cannot be excluded.

To progress this work further and provide a more reliable and physiologically relevant expression system to evaluate the activity of Xcr1L and Xcr1S proteins, it will be essential to generate stably expressing cell lines. The evidence provided here has demonstrated a consistent difference in β-arrestin recruitment between Xcr1L and Xcr1S proteins when qPCR analysis confirmed a similar expression of RNA arising from the two plasmid inserts. However, attempts at reducing insert expression by antibiotic treatment did introduce more substantial differences in RNA presence from the 2 inserts. Use of stably expressing cell lines will permit a more balanced evaluation of protein function that will allow the assessment of protein function under expression levels that more closely resemble that *in vivo*. A principal outcome that should be sought to be achieved from this will be to attain a dose-response to an appropriate ligand. Despite extensive attempts and the use of 2 recombinant Xcl1 ligands, and a recombinant human XCL1 ligand (data not shown) a specific response by the expressed receptor isoforms was not observed in this study. This will be of utmost importance to provide further certainty as to the identity of the functional Xcr1 protein.

Chapter 4: Validation of antibody specificity and reliability

4.1 Introduction

One of the key aims of this project was to identify the localisation and cellular source of XCR1 protein expression within the CNS by immunohistochemistry. The principal aim was to first determine Xcr1 expression within the murine CNS as this would permit greater exploration of receptor expression and potential function in various physiological contexts. The information gleaned from such investigations could then be used to inform the choice of Human samples for investigation of XCR1 within the Human CNS.

At the beginning of this project, no documented evidence of Xcr1 expression within the murine CNS was available within the literature. Furthermore, no evidence of immunohistochemical detection of Xcr1 expression *in situ*, within any tissue type, was identified within the published literature. The presence of Xcr1-expressing cells was instead limited to the use of methods involving genetic recombination of a reporter protein to the *Xcr1* locus (see e.g. (Dorner *et al.*, 2009; Yamazaki *et al.*, 2013)). However, in the process of this investigation, evidence of Xcr1 expression within the murine CNS emerged from a study performed by Zychowska *et al*. In this study, Xcr1 presence was investigated within the lumbar spinal cord of a murine model of diabetic neuropathy. Following 7-days treatment of streptozotocin treatment, Xcr1 was determined to be co-localised to the soma of NeuN-positive neurons located throughout the dorsal laminae of the lumbar spinal cord when evaluated by immunohistochemistry. In addition, Western blot protein analysis was performed to provide a quantitative comparison of Xcr1 presence within the lumbar spinal cord of streptozotocin-treated mice and untreated mice. This demonstrated an increase of Xcr1 protein expression within the protein samples from lumbar spinal cord of streptozotocin-treated mice. The magnitude of this increase in Xcr1 presence was decreased when administered minocycline vs vehicle (Zychowska *et al*., 2016). However, the reliability of this evidence is called in to question, particularly for the detection of Xcr1 by immunohistochemistry, as the antibody used is specified for the detection of Human XCR1 and not Xcr1. No additional details were provided in relation to the validity of this antibody's specificity to Xcr1. The specificity of the other antibody used in this study was also not characterised and could also not be validated in-house due to discontinued production by the manufacturer.

Based on the paucity of available evidence for the use of any particular antibody to detect Xcr1, a valid method for the assessment of Xcr1 expression in the murine CNS by immunohistochemistry would first require the validation of an antibody (or antibodies) to provide a reliable, reproducible and specific detection of Xcr1. An antibody of the same nature would also be required for the detection of XCR1 within Human tissue.

There are numerous methods suggested for the validation of antibody specificity. However, no established standard practice is universally applied. This arises from the unique requirements from each antibody investigation and the methods by which both the antibody and sample are prepared. The characterisation detail for antibodies provided by commercial sources also varies considerably and is often not translatable to the use of the antibody for the detection of the protein expressed endogenously *in vitro* or *in vivo* (Bordeaux *et al.,* 2010). However, a key requirement for the validation of antibody specificity is the use of samples that have proven expression of the desired protein target. This is in contrast to some methods of validation that rely on assessing antibody affinity to the peptide immunogen to which the antibody is raised. These immunogens represent short peptides that may not accurately reflect the 3-dimensional conformation of that peptide amino acid sequence when produced as part of the larger tertiary structure of the target protein. Moreover, this tertiary structure is also influenced by the method of sample preparation. Hence, use of samples that produce the entire target protein provide a presentation of antibody epitope that can therefore more reliably validate the use of the antibody for detection of endogenous protein (Bordeaux *et al.,* 2010). Such samples can then be prepared by various methods according to the intended application that the antibody will be used for the detection of protein in test samples.

The traditional method of establishing a positive antibody control is to use a sample of tissue that is documented to contain the target protein. This method has a major flaw however, in that it doesn't provide an accurate measure of antibody binding to alternative proteins as a consequence of cross-reactivity to competing epitopes. When using biological samples such as tissue specimens, the presence of such competing epitopes is high. This has typically been overcome by the use of pre-incubation controls, for which the antibody is first saturated with its specific immunogen prior to the application to test samples. Although this provides effective control for determining antibody binding to epitopes that correspond to the peptide immunogen, due to the impact of tertiary folding, as discussed above, this does not necessarily prove specificity of the antibody to native target protein. Furthermore, blocking of antibody binding by the immunogen will equally prevent binding of the antibody to both on- and off-target epitopes and is not necessary for antibodies that have been affinity purified to the immunogen. Indeed, the insufficient evidence that immunogen pre-incubation provides in relation to antibody specificity has been criticised for validating the specificity of antibodies to several GPCRs (Michel, Wieland and Tsujimoto, 2009).

A more contemporary method to provide samples with the reliable presence of desired protein is to transfect non-expressing cells with an appropriate vector construct to produce the protein of interest. Testing of antibody specificity can then be determined from the

observed reactivity to transfected cells. In addition, a lack of antibody reactivity to non-transfected cells of the same cell line provides an intrinsic negative control that gives additional conformation of antibody specificity by testing for the presence of non-specific binding (Bordeaux *et al.,* 2010).

The use of transfected cells also enables an additional mode of validation to support antibody specificity by adding an N- or C- terminal molecular tag to the vector protein coding sequence. Antibody specificity for the application of immunohistochemistry can then be determined based upon co-localisation of the test antibody with the antibody used for detection of the protein tag. Furthermore, preparation of cell lysates from transfected cells can also be used to assess antibody specificity to the denatured target protein by western blot. This method has been used for the evaluation of antibody specificity to GPCRs such as the cannabinoid-1 receptor (Grimsey *et al.*, 2008) and GPR120 (Miyauchi *et al.*, 2009). Both studies were able to accurately demonstrate the specificity of certain antibodies to the target protein based on the corresponding signals obtained from the test antibodies and the anti-tag antibodies when applied to samples prepared from transfected cells. This was in addition to demonstrating the lack of non-specific binding to non-transfected cells. Moreover, the flexibility by which samples could be prepared from transfected cells and their corresponding non-transfected controls enabled the specificity of the antibodies to be determined for a variety of methods, including immunohistochemistry and western blot.

4.1.1 Aims

The principal aim of this study was to determine the specificity of available antibodies to Xcr1 and XCR1. An *in vitro* assay of antibody binding that would utilise the benefits of cellular transfection with a plasmid encoding Xcr1 or XCR1 with an appropriate molecular tag was therefore sought. For the validation of antibody specificity to Xcr1, this *in vitro* assay would be used in addition to the use of tissue samples that were expected to provide a relatively high endogenous expression of Xcr1. The method devised has been demonstrated to provide a reliable source of target protein that can then be used to validate antibody specificity by both immunohistochemistry and western blot.

4.2 Results

4.2.1 Preliminary optimisation of Xcr1 detection by immunohistochemistry

Initial tests of antibody specificity were made using spleen tissue from NTg mice. Spleen, along with thymus and other secondary lymphoid organs, demonstrates a high expression of Xcr1 in mice due to the expression of the receptor by CD8+ dendritic cells that localise most prominently in the marginal zones, red pulp and central regions of the spleen (Dorner *et al.,* 2009).

Preliminary attempts of Xcr1 detection within spleen were made using LS-A158 and LS-C37380. LS-A158, although raised against an immunogen arising from XCR1, was used based on the positive reactivity identified in rat, previously established by colleagues within our lab (Bird *et al*., 2018). LS-C37380 was used due to the stated reactivity of this antibody to an immunogen arising from Xcr1. Therefore, despite targeting separate epitopes of human and mouse XCR1 isoforms (Figure 2.1), the use of spleen tissue was used in order to i) identify Xcr1 localisation within mouse spleen based on LS-C37380 reactivity and ii) compare LS-A158 reactivity with that identified by LS-C37380 and determine LS-A158 specificity to Xcr1. Ultimately, identification of Xcr1 reactivity within spleen would serve as an appropriate positive control for subsequent investigations of Xcr1 localisation within the CNS.

Figure 4.2.1 illustrates the reactivity of LS-A158 and LS-C37380 within mouse spleen. Both antibodies demonstrate a high amount of DAB reactivity that declined with decreasing antibody concentration, supporting the notion that the reactivity observed was specific to the presence of antibody. However, evidence of a consistent staining pattern, either based on cellular localisation or anatomical region, was not observed suggesting a lack of antibody specificity to a particular epitope. A lack of antibody specificity by LS-A158 was supported by the same pattern of staining in sections treated with LS-A158 that had been pre-incubated for 24 hours with its respective immunogenic peptide. Moreover, the addition of rabbit IgG at the same concentration as the antibody resulted in high background staining, further adding to the difficulty of distinguishing any antibody-specific reactivity from that contributed to by background staining as a result of rabbit IgG accumulation within the tissue. Overall, the specificity of LS-A158 and LS-C37380 to Xcr1 was not supported by reactivity observed in spleen.

4.2.2 In vitro assessment of antibody specificity to Xcr1 and XCR1 : HeLa transfection assay

Due to the difficulties in establishing a reliable positive control using mouse spleen tissue, it was decided to develop an *in vitro* method of Xcr1 and XCR1 overexpression in order to

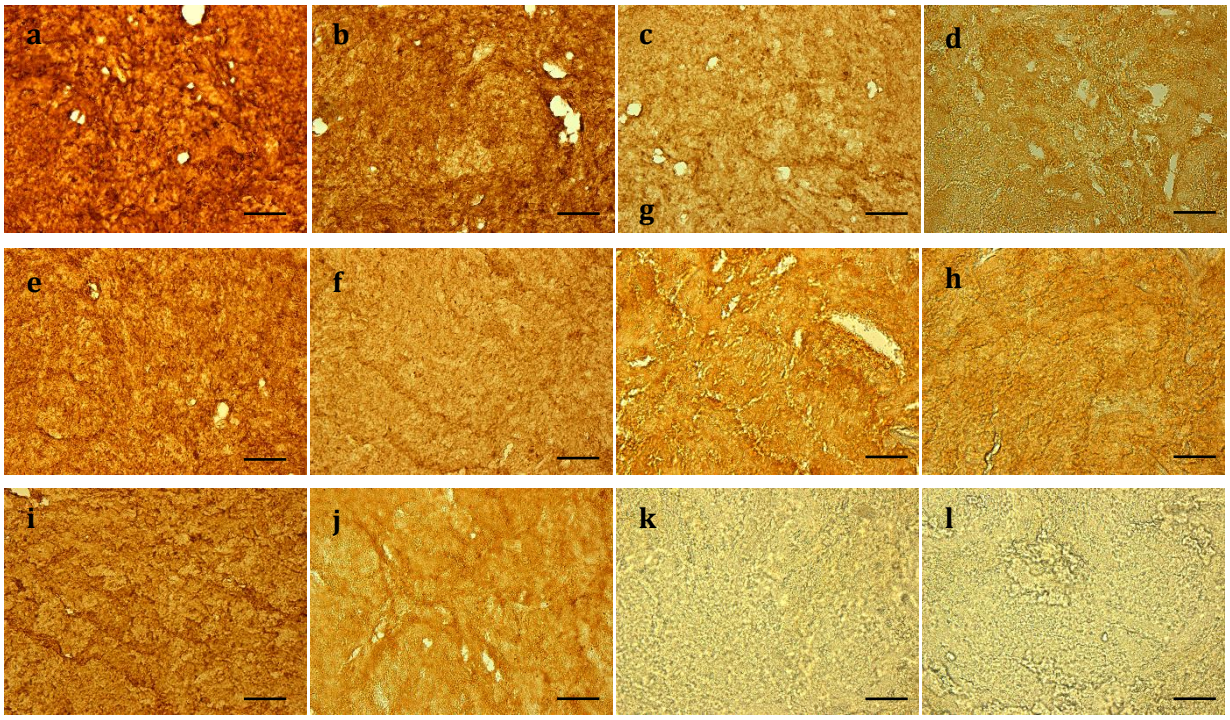

Figure 4.2.1. *Test reactivity of LS-A158 and LS-C37380 in mouse spleen.* LS-A158 was applied at concentrations of 5µg/ml (a), 2.5µg/ml (b), 1.25µg/ml (c) and 0.75µg/ml (d). LS-C37380 was applied at concentrations of 5µg/ml (e), 2.5µg/ml (f), 1.25µg/ml (g) and 0.75µg/ml (h). i) 5µg/ml Rabbit IgG; j) LS-A158 pre-incubation control; k) Primary antibody omitted; l) Blank spleen tissue. Scale bar = 100µm.

characterise antibody reactivity to the respective proteins. Transient transfection of HeLa cells was used to achieve this by transfection with plasmids containing an open reading frame encoding a C-myc tagged human XCR1 protein (XCR1-myc) or a C-myc tagged mouse Xcr1 protein (Xcr1-myc) (Figure 2.2). The addition of a myc tag to the proteins would enable a confirmation of transfection and protein expression. Importantly, double immunocytochemistry using the test and anti-C-myc antibodies would enable the colocalisation of the tested antibodies to cellular regions with a confirmed presence of XCR1 or Xcr1 epitope.

4.2.2.1 Amplification and confirmation of RC221929 and MR225478 plasmid sequence identity

Plasmids encoding XCR1-myc (RC221929) and Xcr1-myc (MR225748) were amplified, isolated and characterised by restriction digest and DNA sequencing as described in section 2.5.6. Isolation of plasmids from a 500ml culture of *E.Coli* transformants using the Plasmid Maxi-prep kit (Qiagen) typically resulted in a yield of 0.5-0.8mg plasmid DNA of high purity as determined by spectrophotometric ratios of $260/230 \geq 2.0$ and $260/280 \geq 1.8$, indicating low contamination by phenolic substances and proteins, respectively.

Preliminary confirmation of plasmid identity and sequence conservation was provided by restriction endonuclease digest of the plasmids by BamHI and XhoI. Digest of the plasmids with these enzymes resulted in the production of DNA fragments at the predicted sizes (RC221929 = 4829bp + 1051bp ; MR225748 = 4829bp + 1066bp), demonstrating the presence of plasmids with a conservation of restriction site and fragments corresponding to the presence of backbone vector plus the respective coding sequence insert (Figure 4.2.2). Definitive evidence of sequence conservation within the plasmid insert was provided by DNA sequencing with T7 Fwd and M13 Rev primers (Figure 4.2.2, Appendix 4.2). Together this evidence supported the successful amplification of RC221929 and MR225478 plasmids that would provide a valid plasmid stock for transfection of HeLa cells to express XCR1-myc or Xcr1-myc proteins for the evaluation of antibody specificity.

4.2.2.2 Optimisation of transfection conditions and manual analysis methods for assessment of antibody specificity by immunocytochemistry

Transient transfection of HeLa cells using LipoJet™ transfection reagent was first optimised with the use of a pCDNA5/FRT/TO GFP plasmid (GFP-plasmid) (Figure 4.2.3, A-E). This plasmid, like the plasmids encoding XCR1-myc and Xcr1-myc, contains a coding sequence that is under the transcriptional control of a CMV promoter. In addition, the expression of the GFP protein generates a luminescent signal that provides a more reliable indication of

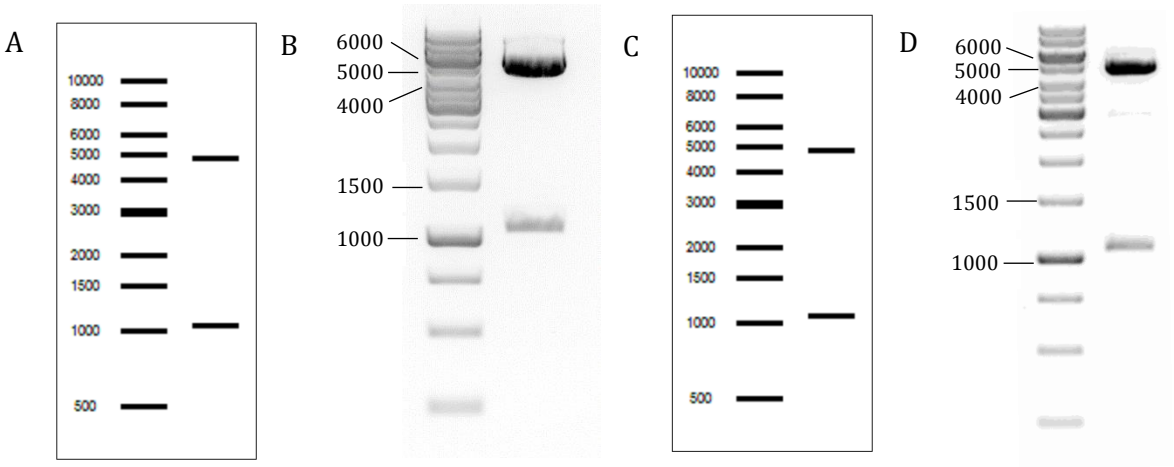

Figure 4.2.2. *Characterisation of RC221929 and MR225748 plasmid clones following amplification and isolation.* Predicted fragment sizes following BamHI + XhoI digest of RC221929 (A) and MR225748 (C). Agarose gel electrophoresis of RC221929 (B) and MR225748 (D) plasmid clones following isolation by Plasmid Maxi Kit and BamHI + XhoI digest.

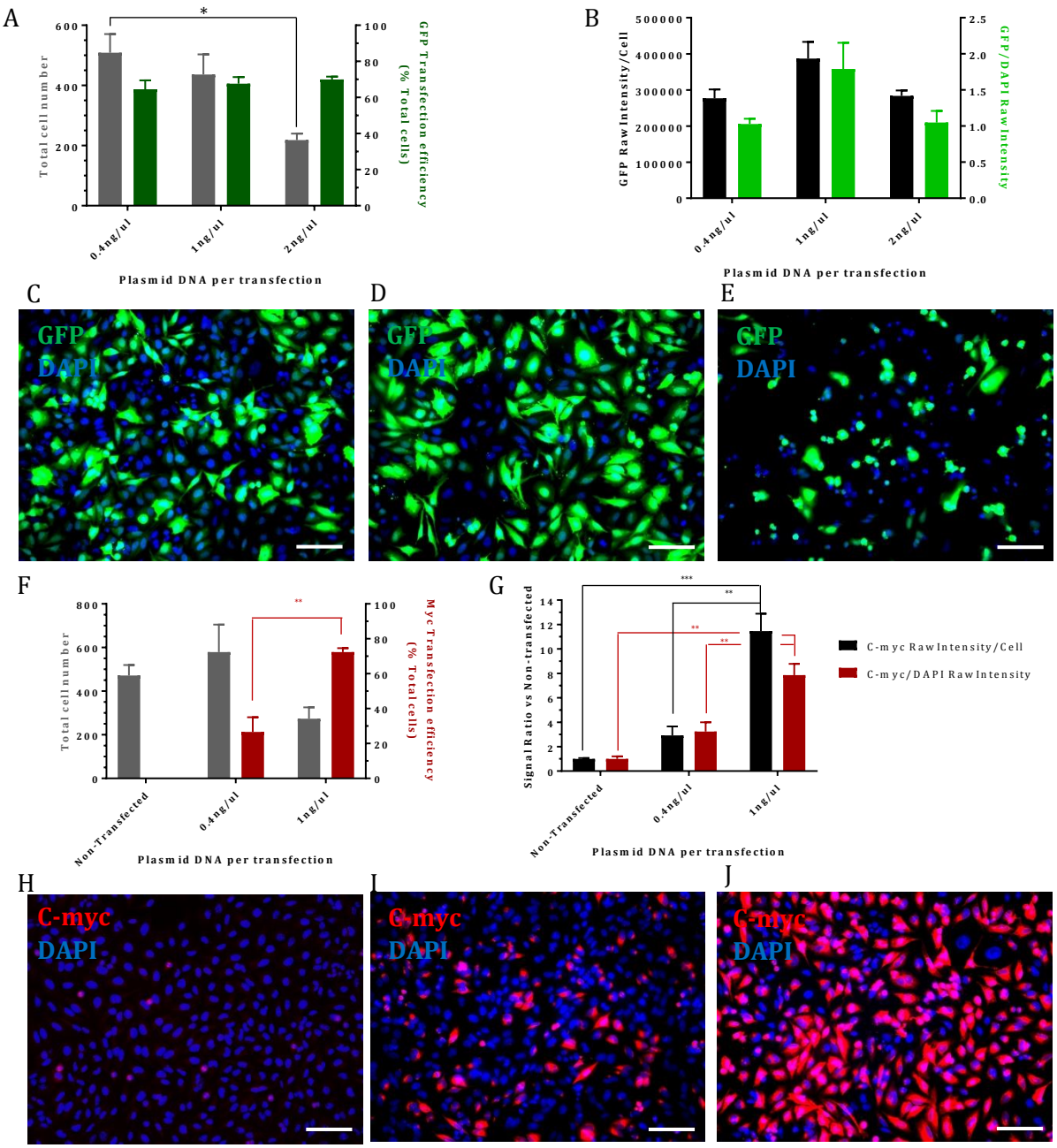

Figure 4.2.3. *Optimisation of transfection parameters with LipoJet™ transfection reagent in 24 well plate.* HeLa cells were transfected with pCDNA5/FRT/TO GFP plasmid (A-E) and MR225748 (F-J) to evaluate optimal transfection conditions for cellular expression of plasmid insert. A) Cell number and GFP transfection efficiency of cells transfected with 0.4-2ng/µl of pCDNA5/FRT/TO GFP plasmid. Cell numbers significantly decrease between 0.4ng/µl and 1ng/µl (* p =0.0211). B) Semi-quantitative evaluation of plasmid insert expression as determined by GFP RawIntensity/cell and GFP/DAPI RawIntensity. C-E) Images of HeLa cells transfected with 0.4ng/µl (C), 1ng/µl (D) and 2ng/µl (E) pCDNA5/FRT/TO GFP plasmid. F) Cell number and transfection efficiency of HeLa cells transfected with 0.4ng/µl and 1ng/µl MR225748 plasmid and non-transfected controls, as determined by RawIntensity values corresponding to detection of C-myc primary antibody. G) Semi-quantitative evaluation of MR225748 plasmid insert expression as determined by associated RawIntensity values of C-myc primary antibody detection per cell (C-myc RawIntensity/Cell) or in relation to RawIntensity of DAPI channel (C-myc/DAPI RawIntensity). H-J) Images of immunocytochemical detection of Myc expression in: H) Non-transfected HeLa cells; I) HeLa cells transfected with 0.4ng/µl MR225748; J) HeLa cells transfected with 1ng/µl MR225478 plasmid. N=3 for all groups. Scale bars = 100µm. * p <0.05, ** p<0.01, ***p<0.001.

transfection efficiency than antibody mediated protein detection, as a consequence of the linear relationship between GFP expression and luminescent signal (Soboleski, Oaks and Halford, 2005). Therefore, initial testing of transfection efficiency with the GFP-plasmid was performed in order to evaluate the optimum transfection conditions that would permit the greatest expression of a plasmid coding sequence under the transcriptional control of a CMV promoter.

Manual image analysis of images taken from cells transfected with 0.4ng/µl, 1ng/µl and 2ng/µl GFP plasmid DNA demonstrated a consistent transfection efficiency regardless of the amount of plasmid used for transfection. However, cell numbers significantly declined as a consequence of increasing plasmid concentration to 2ng/µl, suggesting that although the proportion of transfected to total cells remained consistent with all plasmid amounts, at 2ng/µl this became toxic to the cells either due to the high expression of GFP protein or because of the higher amount of LipoJet™ transfection reagent. Cell numbers of wells treated with 0.4ng/µl and 1ng/µl of plasmid remained consistent indicating a similar tolerance of the cells to these transfection conditions. GFP expression however, as indicated by RawIntensity per cell, was highest in cells transfected with 1ng/µl plasmid. Overall, this supported the use of 0.4 – 1ng/µl plasmid DNA for transfection of HeLa cells, with 1ng/µl plasmid indicated to generate the optimum transfection conditions according to cell viability and cell expression of plasmid insert.

Indeed, for HeLa cells transfected with 0.4ng/µl and 1ng/µl MR225748, transfection with 1ng/µl plasmid demonstrated a significantly higher transfection efficiency and C-myc reactivity per cell (Figure 4.2.3). Although cell numbers do decrease at 1ng/µl of plasmid in comparison to non-transfected and 0.4ng/µl of plasmid (Figure 4.2.3, F), this was not statistically significant. Furthermore, for the purpose of this assay, the viability of protein production was paramount for antibody testing. Therefore, 1ng/µl of plasmid was used for future transfections to evaluate antibody specificity for immunocytochemistry, based on effective protein production and cell viability.

In support of the use of a more efficient method of manual analysis to assess antibody binding (as detailed in section 2.3.2.1) the results displayed in Figure 4.2.3 B and G demonstrate the correspondence in values obtained from analysis based on manual cell counting and analysis based on DAPI RawIntensity as a measure of cell presence. Due to the variation of cell number in each image, it is not suitable to simply approximate antibody binding and specificity based on RawIntensity values of the associated channel from the entire image. This is because antibody binding is dependent on the presence of the target protein that is, of course, expressed by cells. In particular, evaluation of antibody binding to a transmembrane protein such as Xcr1 requires expression within a cellular membrane and

therefore cellular number will directly influence the capacity of antibody binding due to the effect of cell number on epitope presence.

Statistical testing identified no significant differences in the normalised changes in C-myc reactivity, determined by quantifying C-myc RawIntensity per cell or C-myc/DAPI RawIntensity, within the same sample population (Figure 4.2.3, G). Moreover, this correspondence of the two methods in evaluating C-myc antibody binding in relation to cell presence permitted both methods to identify similar statistical differences in C-myc reactivity between non-transfected HeLa and those transfected with the test plasmid amounts. In addition, comparison of GFP RawIntensity per cell to GFP/DAPI RawIntensity highlights the strong correlation in these two measurements (Figure 4.2.3, A). Overall, this supports the manual analysis method which calculates the Rawintensity values of the test antibody channel divided by the Rawintensity values of DAPI (i.e. Antibody/DAPI Rawintensity) to provide a reliable measure of antibody binding per cell. This measure, in conjunction with the primary measure of antibody specificity according to C-myc colocalisation, can therefore be used as a semi-quantitative evaluation of antibody binding and used to support the specificity of the tested antibodies.

4.2.2.3 Optimisation of transfection conditions and automated analysis methods for assessment of antibody specificity by immunocytochemistry

In addition to manual image acquisition and analysis, some antibodies were also evaluated by automated image acquisition and analysis as described in section 2.3.3. The advantage of this method to the manual analysis methods is that the analysis software is capable of identifying cells within an image, allowing analysis of antibody reactivity to be performed on pixel intensity values from regions that correspond specifically to the total area of an image occupied by cells. Thus, this method specifically identifies the cellular area to account for the impact of cellular presence on total availability of epitope presentation, rather than using DAPI assessment (either by counting nuclei or quantifying Rawintensity) as performed for manual image analysis methods. The automated image acquisition and analysis therefore refines the quantification of pixel intensity, corresponding to antibody binding, to the specific image region that contains the cell and its cytoplasm, providing a more accurate estimation of antibody binding to the specific Xcr1 epitopes expressed by transfected cells.

As performed for 24 well plates used for manual image acquisition and analysis, optimisation of transfection conditions within 96 well plates that were used for automated image acquisition and analysis was also performed using the GFP and MR225748 plasmids (Figure 4.2.4). Direct comparison of analysis outcomes using automated and manual analysis methods was performed to test the reliability and accuracy of each method to

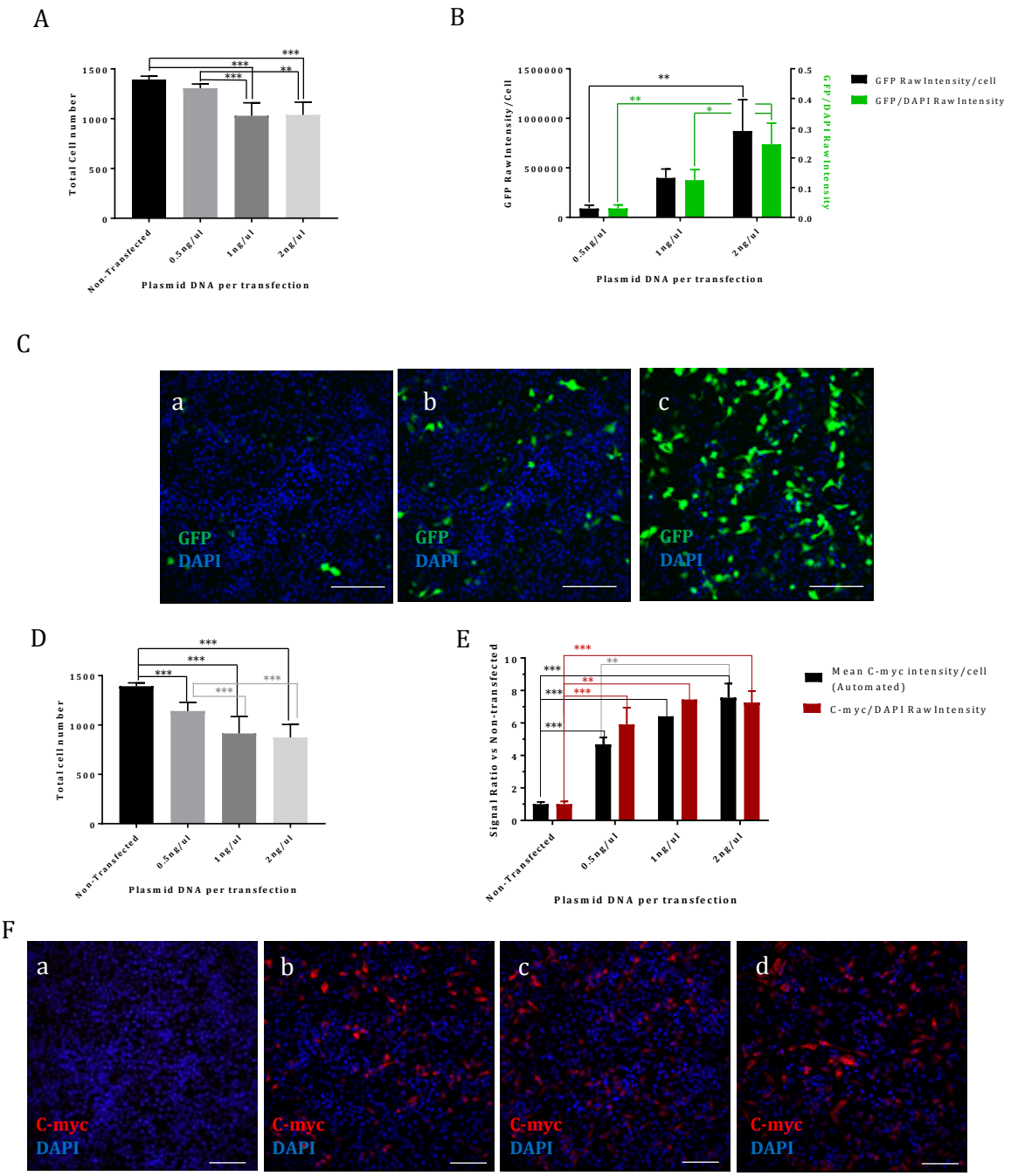

Figure 4.2.4. *Optimisation of transfection conditions for LipoJet™ transfection reagent in 96 well plate for automated analysis.* Evaluation of transfection efficiency and effect on cell viability following transfection with GFP (A-C) and MR225748 (D-F) plasmids. A) Quantification of cell viability when transfected with 0.5ng/ul, 1ng/ul and 2ng/ul of GFP-Plasmid. No statistical difference in cell numbers between cells treated with 1ng/ul or 2ng/ul was observed. **, $p < 0.01$; ***, $p < 0.001$ B) Comparison of manual (GFP/DAPI RawIntensity) and automated (GFP RawIntensity/Cell) analysis to evaluate optimum transfection conditions for GFP-plasmid.. D) Viability of non-transfected cells and cells transfected with 0.5ng/ul, 1ng/ul and 2ng/ul. No significant differences were observed between cell numbers transfected with 1ng/ul and 2ng/ul. E) Comparison of signal ratios obtained by manual (C-myc/DAPI RawIntensity) and automated (Mean C-myc intensity/cell) analysis of cells transfected with 0.5ng/ul, 1ng/ul and 2ng/ul of MR225748 in comparison to non-transfected cells. F) Representative images acquired by Opera Phenix High Content Screening System of HeLa cells non-transfected (a) or transfected with MR225748 plasmid at 0.5ng/ul (b), 1ng/ul (c) and 2ng/ul (d). N=3 for all quantitative comparisons (#, N=1). *, $p<0.05$; **, $p<0.01$; ***, $p<0.001$. Error bars = ±SD.

quantify antibody binding (Figure 4.2.4, B and D). In particular, comparison to the automated analysis outcomes was done to support the validity of the manual analysis method for the assessment of antibody binding, which has been used to assess the specificity of some antibodies (see later sections).

To determine the optimum concentration of plasmid to use for transfection, GFP and C-myc reactivity were assessed following transfection with 0.5ng/µl, 1ng/µl and 2ng/µl. Despite GFP reactivity demonstrating a clear increase in reactivity per cell using transfection at 2ng/µl in comparison to 1ng/µl (Figure 4.2.4, B), C-myc reactivity demonstrated no significant difference between these two conditions (Figure 4.2.4, E). Moreover, there was no impact on cell viability by increasing the concentration of either plasmid from 1ng/µl to 2ng/µl (Figure 4.2.4, A and D). Therefore the transfection of cells using 1ng/µl was used for future transfection protocols in 96 well plates.

Comparison of manual and automated analysis methods to quantify antibody reactivity, demonstrated a strong correlation in the outcomes for both methods. Evaluations of GFP expression in relation to cell number supported both GFP RawIntensity/cell (Automated) and GFP/DAPI RawIntensity (Manual) to identify similar relative quantification of GFP expression and similar statistical differences in GFP expression between the transfection conditions (Figure 4.2.4, B). Similarly, automated and manual image analysis methods were able to identify almost identical quantitative and statistical changes of C-myc reactivity between non-transfected cells and cells transfected with MR225748 at 0.5ng/µl, 1ng/µl and 2ng/µl (Figure 4.2.4, E). Together, this supported both manual and automated image analysis methods to effectively evaluate antibody binding to transfected cells evaluated by immunocytochemistry.

4.2.2.4 Confirmation of desired protein expression by Western Blot

To confirm that the C-myc reactivity observed by immunocytochemistry represented the detection of a C-myc tagged protein of the expected size and hence to support the valid expression of Xcr1 or XCR1, protein content from the cell lysate extracted from transfected and non-transfected HeLa was evaluated by western blot (Figure 4.2.5). Initial efforts using cell lysate from cells transfected with MR225748 suggested the presence of a particularly large protein. Subsequent efforts utilised a transfection control with a plasmid encoding a myc-tagged TAR DNA Binding protein 43-kDa (TDP-43-myc) to confirm that the developed method was suitable for the detection and separation of protein by SDS-PAGE. Indeed, the 43-kDa protein was observed following C-myc detection by western blot (Figure 4.2.5, B,C). However, despite detection of TDP-43-myc validating the protocol, detection of Xcr1-myc remained in a region far higher than the expected ~42kDa size. This suggested that the protein produced from MR225748 plasmid was aggregating as a consequence of protein

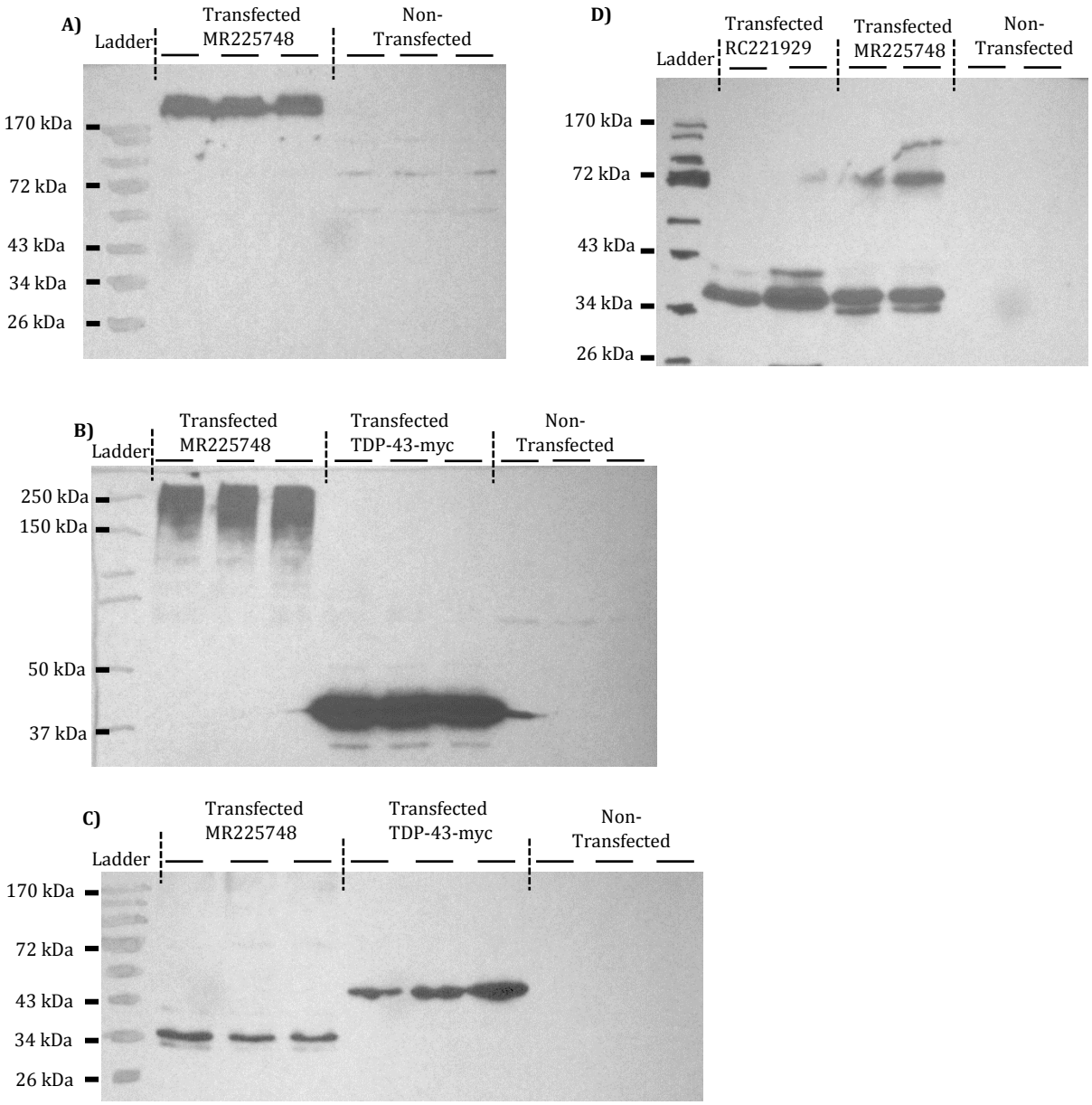

Figure 4.2.5. *C-myc detection of protein from HeLa cell lysate by Western Blot.* Initial attempts to detect a single band corresponding to Xcr1-myc within the lysate of HeLa cells transfected with MR225748 presented a band at a much higher molecular weight than the predicted 39.4 kDA (A and B). This band of higher molecular weight was not a result of a failed western blot protocol as demonstrated by the successful identification of TDP-43-myc within the lysate of HeLa cells overexpressing this protein (B). Excluding sample heating to 95°C from western blot protocol resulted in the identification of C-myc reactivity within the appropriate size range expected of Xcr1-myc (C, D) and XCR1-myc (D) within lysate of HeLa cells transfected with MR225748 or RC221929.

denaturation. Confirmation of c-myc detection of a protein within an appropriate size range of the predicted molecular weight was achieved by the use of a cell lysate preparation that did not include heating to 95°C prior to loading of the sample. Use of this protocol was also used to confirm the molecular size of XCR1-myc produced from the RC221929 plasmid (Figure 4.2.5, D).

The predicted molecular weights of Xcr1-myc and XCR1-myc are 42.6kDa and 42.0 kDa, respectively. The detection of these proteins by western blot (Figure 4.2.5, C, D) with the anti-C-myc antibody demonstrates the presence of proteins that, according to the molecular weight standards, is of a much smaller size than anticipated. This is further highlighted by the discrepancy in size between Xcr1-myc and TDP-43-myc which has a molecular weight of 44kDa (Figure 4.2.5, C). However, the anomalous migration of transmembrane proteins has been well documented in the literature, with a recently proposed correction factor for a more accurate quantification of molecular weight based on the relative molecular mass identified following SDS-PAGE (Rath and Deber, 2013). Following the application of the correction factor proposed for sample proteins migrating faster than the predicted molecular weight (Rath and Deber, 2013), the estimated molecular weight of proteins identified by C-myc reactivity was: Xcr1-myc 41.7kDa and 43.6kDa (Figure 4.2.5, C and D); XCR1-myc 42.9kDa (Figure 4.2.5 D). Taking this correction in to consideration provides an estimated molecular weight that much more closely resembles the predicted values.

In summary, C-myc detection of protein within the lysate of HeLa cells transfected with MR225748 and RC221929 supports the production of proteins with the molecular characteristics that are consistent with the production of Xcr1-myc and XCR1-myc, respectively. The overexpression of Xcr1-myc and XCR1-myc by HeLa will therefore provide a reliable production of appropriate epitope for testing antibody specificity against the respective Mouse and Human XCR1 homologues.

4.2.3 Evaluation of antibody specificity to Mouse Xcr1 by immunocytochemistry

Using the optimised method for transfection and analysis of Xcr1-myc expression by immunocytochemistry (section 4.2.2.2), the HeLa transfection assay was next used to evaluate the specificity of LS-A158, LS-C37380, Ab188896, cAb-Xcr1 and HPA013169 to Xcr1-myc. Confirmation of antibody specificity using this method was used as a pre-requisite to validate the detection of Mouse Xcr1 expressed endogenously within tissue samples.

4.2.3.1 Evaluation of LS-A158 specificity to Mouse Xcr1 by immunocytochemistry

LS-A158 reactivity to HeLa cells expressing Xcr1-myc was tested across a range of concentrations between 5µg/ml and 1.25µg/ml according to the recommended working

concentration supplied by the manufacturer (Figure 4.2.6). LS-A158 reactivity demonstrated diffuse staining across all cells regardless of the antibody concentration used and this reactivity pattern was maintained between transfected and non-transfected cells. Semi-quantitative evaluation of antibody binding was made based on the raw intensity values obtained from the RGB channel corresponding to the fluorescent secondary antibody used for detection of LS-A158. At the highest concentration of LS-A158 tested (5µg/ml) antibody reactivity was indicated to decline in HeLa cells expressing Xcr1-myc, with no significant changes in antibody reactivity observed between transfected and non-transfected cells at lower antibody concentrations. Qualitative examination of LS-A158 colocalisation with C-myc was failed to be consistently observed, with the small amounts that were identified deemed to be a result of the diffuse background staining of all cells.

In an attempt to provide greater exposure of Xcr1 antigen for antibody binding, cells underwent HIER treatment (Figure 4.2.7). LS-A158 testing at 5µg/ml was excluded based on the high background reactivity observed in non-transfected cells above. Despite HIER treatment, LS-A158 reactivity remained diffuse, as seen for cells left untreated prior to the addition of primary antibody (see above) and again this reactivity pattern was consistent between transfected and non-transfected cells. Semi-quantitative evaluation also failed to identify any changes in antibody reactivity against HeLa cells expressing Xcr1-myc in comparison to non-transfected cells. Furthermore, no specific colocalisation of LS-A158 reactivity with C-myc was observed. Overall, this data suggested that LS-A158 does not demonstrate specific binding to Mouse Xcr1.

4.2.3.2 Evaluation of LS-C37380 specificity to Mouse Xcr1 by immunocytochemistry

LS-C37380 was tested at concentrations between 5µg/ml and 20µg/ml as recommended by the manufacturer. Initial testing was performed without antigen retrieval (Figure 4.2.8) and demonstrated a diffuse cellular signal that was consistent for all cells, regardless of Xcr1-myc expression, as demonstrated by C-myc reactivity, in transfected cells. This staining pattern was observed for all concentrations used and therefore clear colocalisation of LS-C37380 with C-myc was not evident above the background reactivity demonstrated for cells transfected with MR225748. Semi-quantitative evaluation of antibody binding supported a clear increase in C-myc reactivity within transfected cells, confirming the qualitative evaluation of Xcr1-myc expression. Despite this, comparisons in LS-C37380 reactivity were inconsistent – at the highest concentration tested (20µg/ml), a statistically significant decrease in LS-C3780/DAPI RawIntensity was observed. LS-C37380/DAPI reactivity remained almost identical between cells treated with 10µg/ml, whilst antibody binding was suggested to increase in cells treated with 5µg/ml, but did not reach statistical significance.

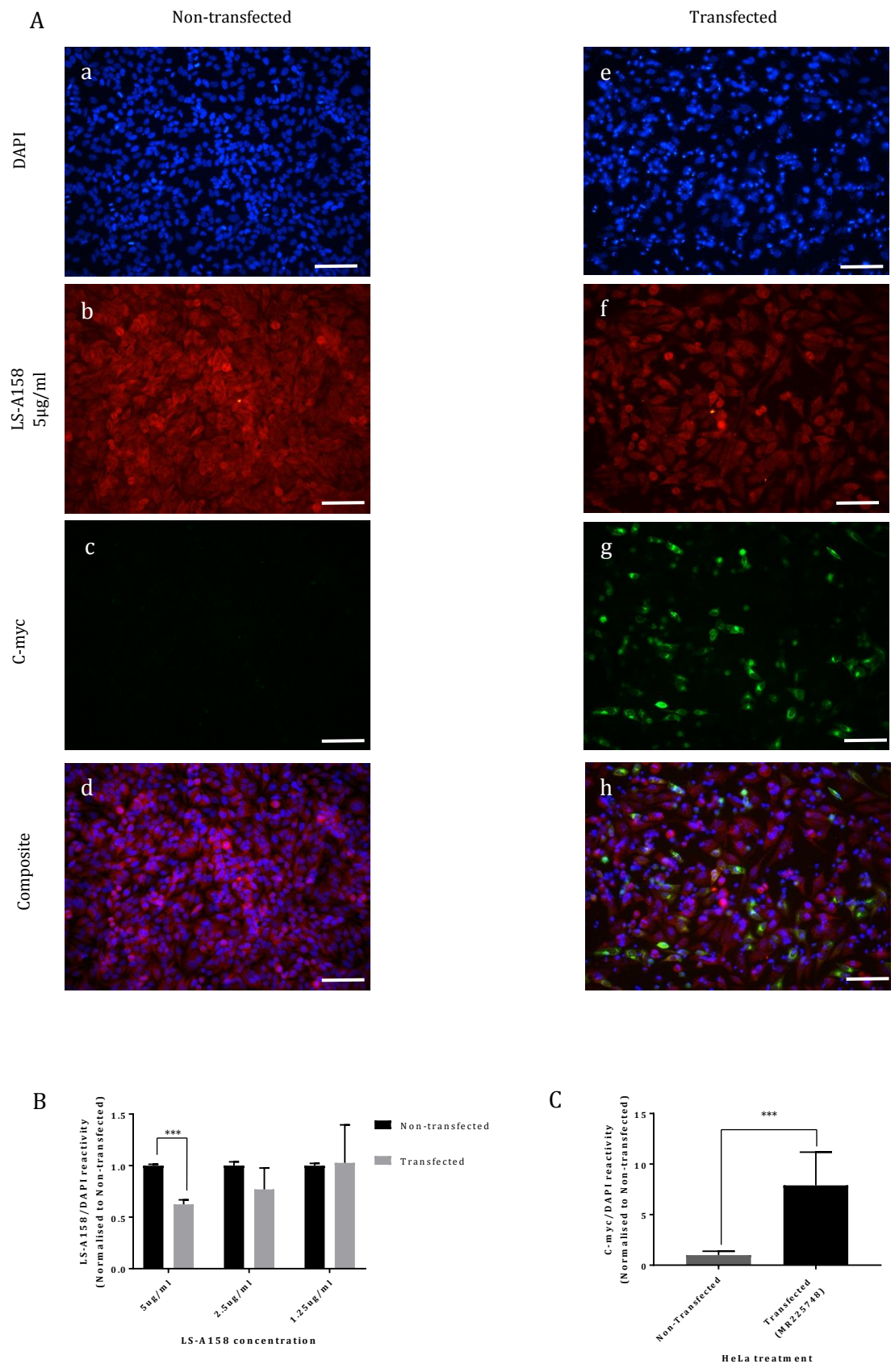
A
Non-transfected
Transfected
DAPI
LS-A158 5µg/ml
C-myc
Composite
a
b
c
d
e
f
g
h
B
LS-A158/DAPI reactivity (Normalised to Non-transfected)
1.5
1.0
0.5
0.0
***
5ug/ml
2.5ug/ml
1.25ug/ml
LS-A158 concentration
Non-transfected
Transfected
C
C-myc/DAPI reactivity (Normalised to Non-transfected)
15
10
5
0
***
Non-Transfected
Transfected (MR225748)
HeLa treatment

Figure 4.2.6. *Test of LS-A158 specificity to HeLa cells expressing Xcr1-myc by immunocytochemistry.* A) Representative images of HeLa cells either transfected with MR225748 or non-transfected controls following double immunocytochemistry with LS-A158 (red) and anti-C-myc (green). a-d = LS-A158 5µg/ml non-transfected; e-h = LS-A158 5µg/ml transfected. Scale bars =100µm. B) Semi-quantitative evaluation of LS-A158/DAPI reactivity demonstrates no change in antibody binding to transfected cells regardless of LS-A158 concentration. A significant reduction in LS-A158/DAPI reactivity is observed for transfected cells treated with 5µg/ml LS-A158 in comparison to non-transfected cells (***, $p < 0.001$). N=3 for all groups. C) C-myc/DAPI RawIntensity demonstrates a significant increase (***, $p < 0.001$) in cells transfected with MR225748, supporting viable expression of Xcr1-myc. N = 9 for both groups. Error Bars = ±SD.

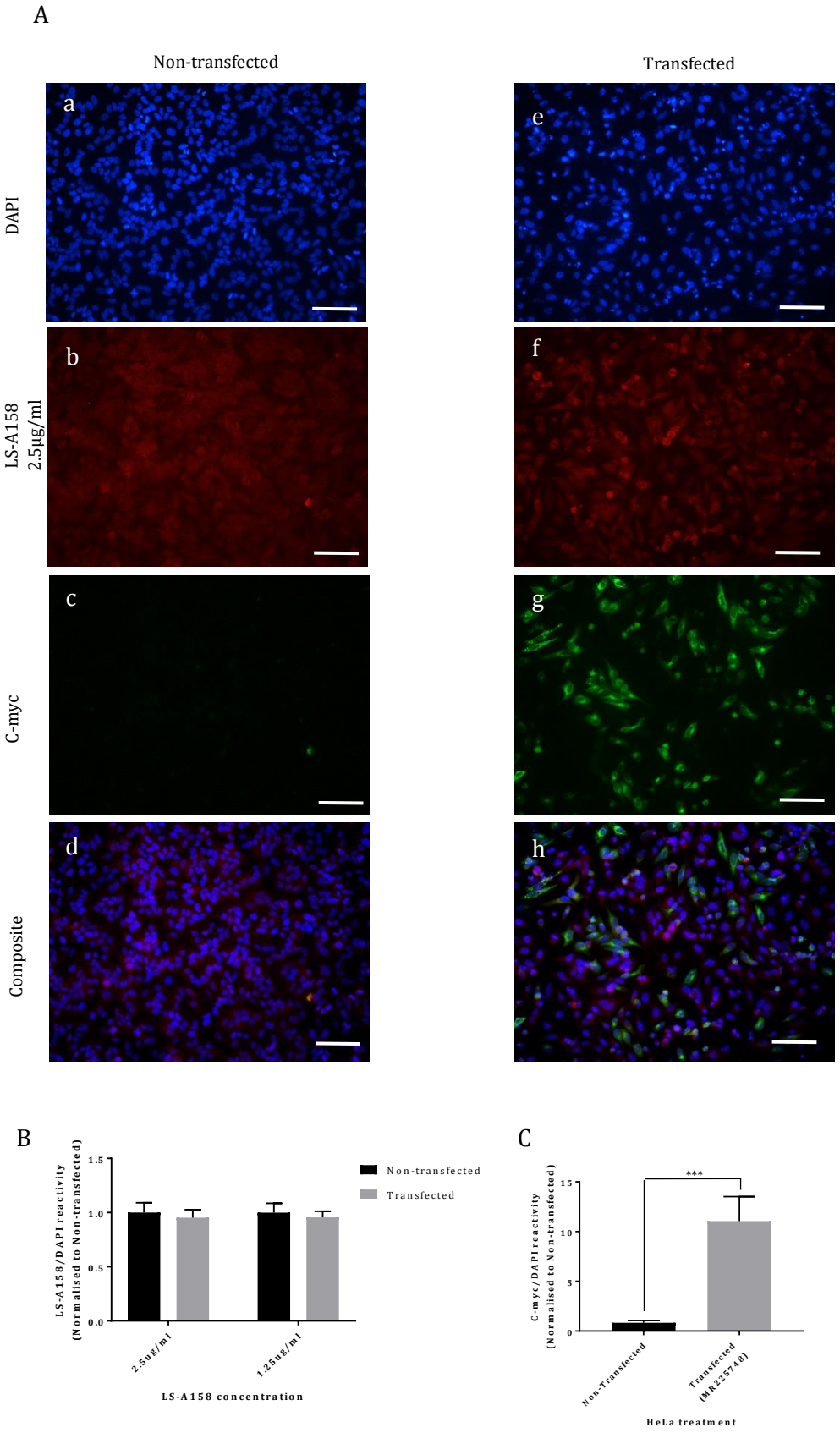
A
Non-transfected
Transfected
DAPI
LS-A158 2.5µg/ml
C-myc
Composite
a
b
c
d
e
f
g
h
B
LS-A158/DAPI reactivity (Normalised to Non-transfected)
1.5
1.0
0.5
0.0
Non-transfected
Transfected
2.5ug/ml
1.25ug/ml
LS-A158 concentration
C
C-myc/DAPI reactivity (Normalised to Non-transfected)
15
10
5
0
***
Non-Transfected
Transfected (MR225748)
HeLa treatment

Figure 4.2.7. *Evaluation of LS-A158 specificity to Xcr1-myc by immunocytochemistry following HIER.* A) Representative images of HeLa cells either transfected with MR225748 or non-transfected controls following double immunocytochemistry with LS-A158 (red) and anti-C-myc (green). a-d = LS-A158 2.5µg/ml non-transfected; e-h = LS-A158 2.5µg/ml transfected. Scale bars =100µm. B) Semi-quantitative evaluation of LS-A158/DAPI reactivity demonstrates no effect of Xcr1-myc expression within HeLa cells on LS-A158 binding in comparison to non-transfected cells (N=3 for all groups). C) Semi-quantitative evaluation of C-myc/DAPI reactivity demonstrates a significant increase in C-myc reactivity in cells transfected with MR225748 (***, $p < 0.001$) supporting the valid expression of the Xcr1-myc protein in transfected cells. N=9 for both groups. Error Bars = ±SD.

In tandem with the lack of colocalisation to C-myc, this evidence did not support the specificity of LS-C37380 to Xcr1.

Further attempts via the use of antigen retrieval (Figure 4.2.9) also failed to improve the specificity by which LS-C37380 appeared to bind to cells; reactivity was again diffuse in all cells whether they were transfected or not. Colocalisation of LS-C37380 with C-myc was also absent, with LS-C37380 reactivity again failing to demonstrate a reactivity higher than background in cells expressing Xcr1-myc. This lack of increased reactivity in transfected cells, as observed by qualitative inspection, was supported by semi-quantitative evaluation failing to demonstrate any significant increases in LS-C3730/DAPI reactivity in cells expressing Xcr1-myc in comparison to non-transfected cells, despite the clear evidence of Xcr1-myc expression as evidenced by semi-quantitative evaluation of C-myc/DAPI RawIntensity (Figure 4.2.9, B and C).

Overall, despite LS-C37380 being raised to an immunogen corresponding to a peptide that is specific to mouse Xcr1, the lack of specific colocalisation with C-myc and a lack of clear semi-quantitative increase in antibody binding does not support the specificity of LS-C37380 to Xcr1.

4.2.3.3 Evaluation of Abcam 188896 specificity to Mouse Xcr1

Although raised to an immunogen with a peptide sequence that corresponds to the Human XCR1 protein, Abcam 188896 has been previously used to support the presence of Xcr1 in the mouse spinal cord by Zychowska *et al.,* 2016. In an attempt to validate the use of this antibody for further characterisation of Xcr1 in the Mouse CNS, Abcam188896 was tested by single immunocytochemistry against HeLa cells expressing Xcr1-myc (Figure 4.2.10). The signal obtained from this antibody was very low in both transfected and non-transfected cells, with fluorescent reactivity specific to the antibody difficult to observe above background at both 10µg/ml and 2.5µg/ml. C-myc reactivity observed by independent immunocytochemistry, but from the same transfection procedure, demonstrated the clear presence of Xcr1-myc in transfected cells. In addition to qualitative evidence demonstrating a lack of reactivity by Abcam188896, semi-quantitative evaluation also demonstrated no significant differences in Abcam188896/DAPI reactivity between cells expressing Xcr1-myc and non-transfected cells. Due to the extremely low reactivity observed, further characterisation of Abcam 188896 was instead based upon testing against Human XCR1 (see section 4.2.4.2). Although further characterisation is needed, this evidence suggests that Abcam188896 does not exhibit specific reactivity to Mouse Xcr1.

A

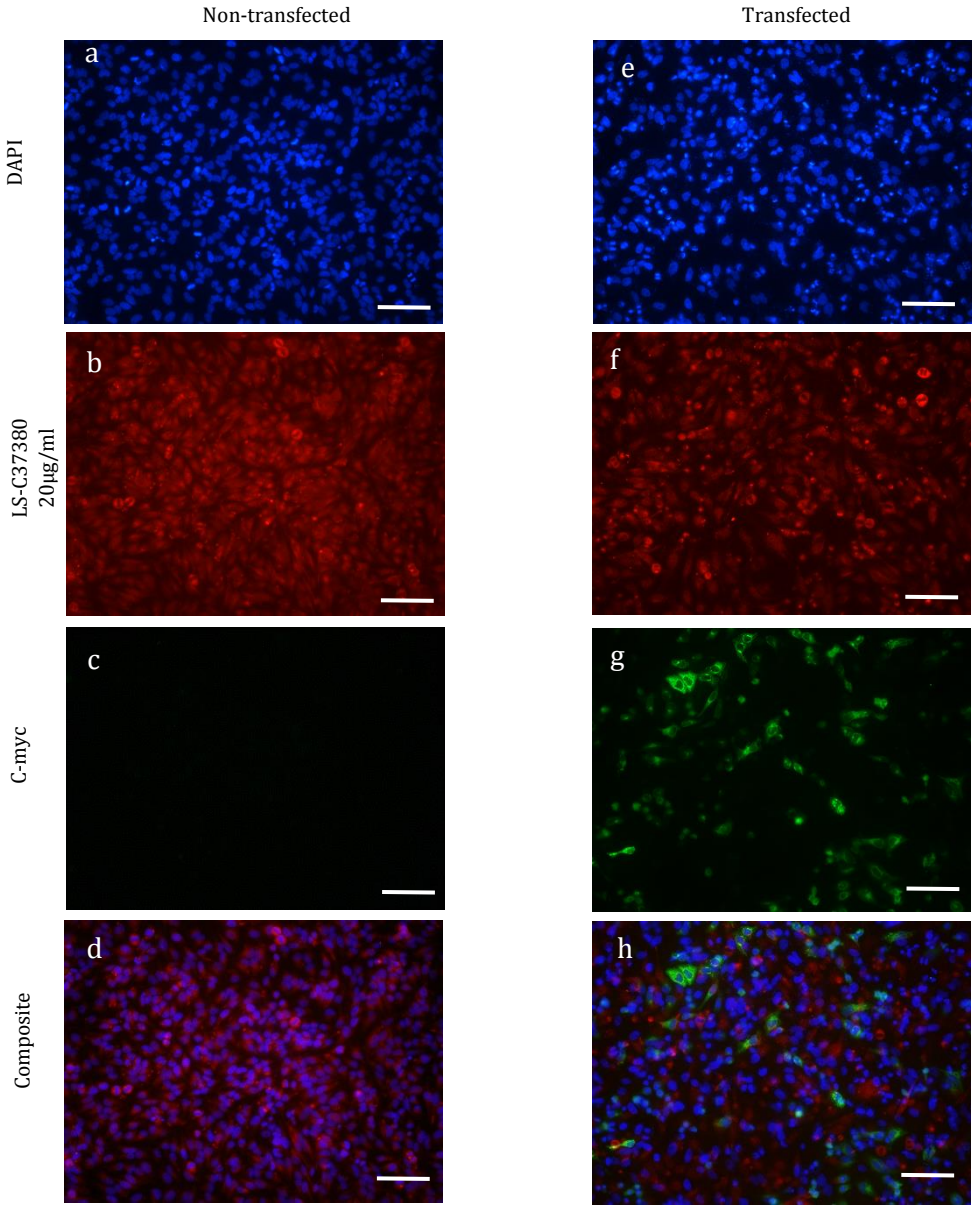
Non-transfected
Transfected
DAPI
LS-C37380 20µg/ml
C-myc
Composite
a
b
c
d
e
f
g
h

B

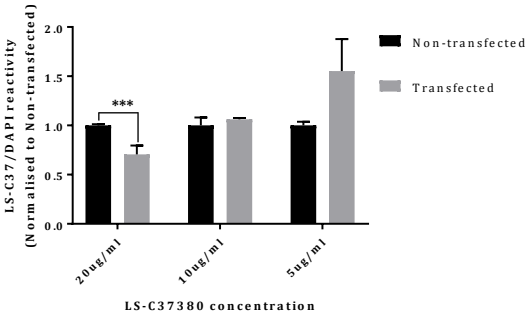
LS-C37/DAPI reactivity (Normalised to Non-transfected)
2.0
1.5
1.0
0.5
0.0
***
20ug/ml
10ug/ml
5ug/ml
LS-C37380 concentration
Non-transfected
Transfected

C

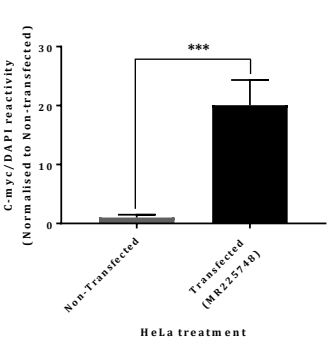
C-myc/DAPI reactivity (Normalised to Non-transfected)
30
20
10
0
***
Non-Transfected
Transfected (MR225748)
HeLa treatment

Figure 4.2.8. *Evaluation of LS-C37380 reactivity to Xcr1-myc by immunocytochemistry.* A) Representative images of HeLa cells either transfected with MR225748 or non-transfected controls following double immunocytochemistry with LS-C37380 (red) and anti-C-myc (green). a-d = LS-C37380 20µg/ml non-transfected; e-h = LS-C37380 20µg/ml transfected. Scale bars =100µm. C) Semi-quantitative evaluation of LS-C37380 binding to cells expressing Xcr1-myc and non-transfected cells. A statistically significant reduction in LS-C37380/DAPI RawIntensity was observed at cells treated with 20µg/ml (***, p=0.004) of LS-C37380 in comparison to non-transfected cells. Data is normalised to non-transfected mean. N=3 for all groups. D) Semi-quantitative evaluation of C-myc/DAPI reactivity demonstrates a significant increase in C-myc reactivity in cells transfected with MR225748 (***, p <0.001) supporting the valid expression of the Xcr1-myc protein in transfected cells. N=9 for both groups. Error Bars = ±SD.

A

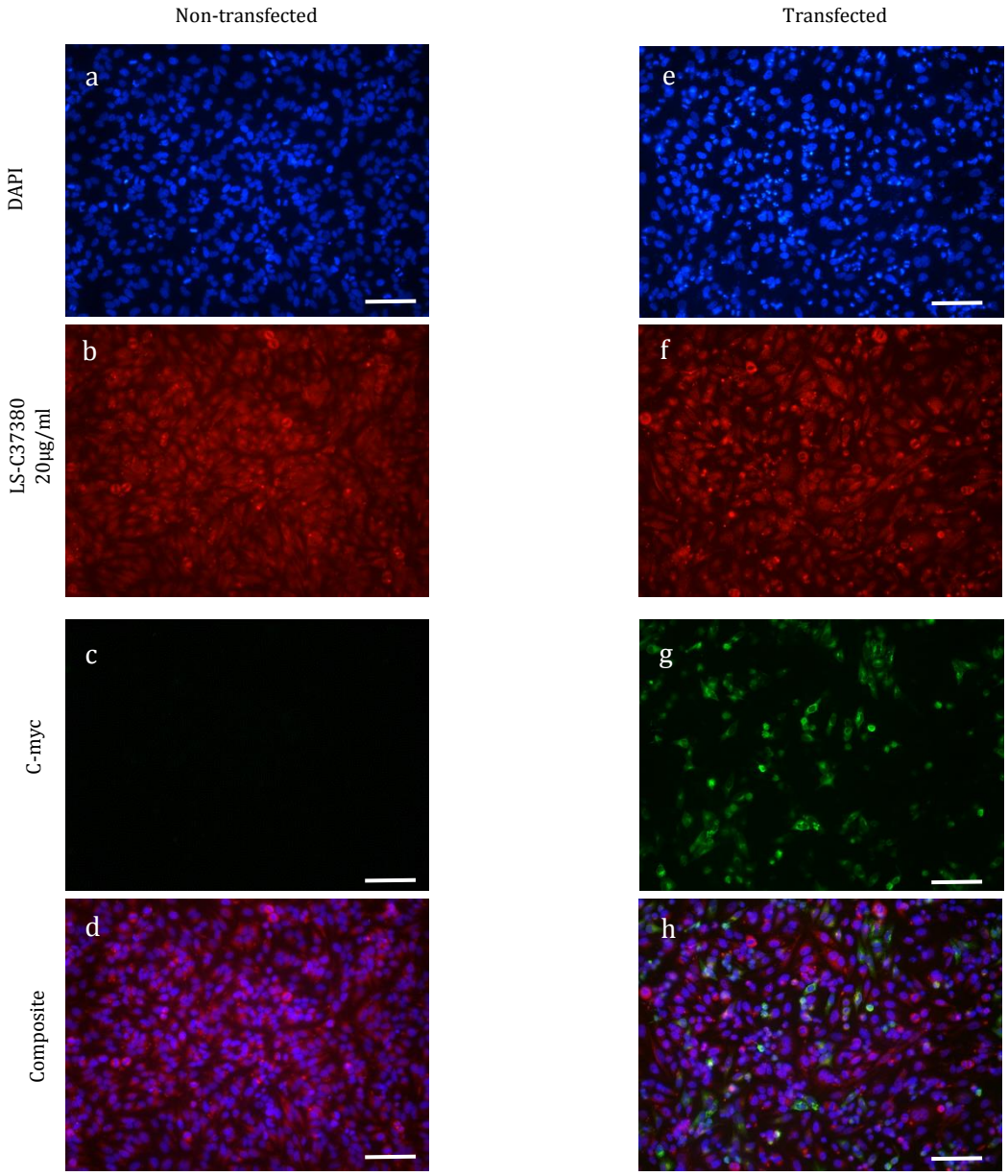
Non-transfected
Transfected
DAPI
LS-C37380 20µg/ml
C-myc
Composite
a
b
c
d
e
f
g
h

B

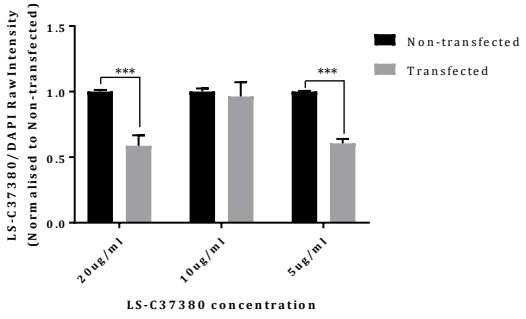
LS-C37380/DAPI Raw Intensity (Normalised to Non-transfected)
1.5
1.0
0.5
0.0
***
***
20ug/ml
10ug/ml
5ug/ml
LS-C37380 concentration
Non-transfected
Transfected

C

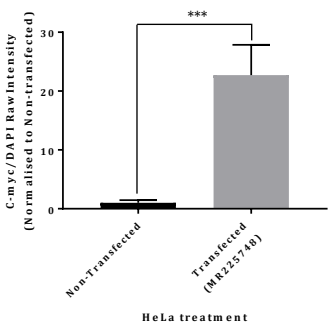
C-myc/DAPI Raw Intensity (Normalised to Non-transfected)
30
20
10
0
***
Non-Transfected
Transfected (MR225748)
HeLa treatment

Figure 4.2.9. *Evaluation of LS-C37380 binding to Xcr1-myc by immunocytochemistry following HIER.* A) Representative images of HeLa cells either transfected with MR225748 or non-transfected controls following double immunocytochemistry with LS-C37380 (red) and anti-C-myc (green). a-d = LS-C37380 20µg/ml non-transfected; e-h = LS-C37380 20µg/ml transfected. Scale bars =100µm. B) Semi-quantitative evaluation of LS-C37380 binding to cells expressing Xcr1-myc and non-transfected cells. A statistically significant reduction in LS-C37380/DAPI RawIntensity was observed for cells treated with 20µg/ml and 5µg/ml of LS-C37380 in comparison to non-transfected cells. Data is normalised to non-transfected mean. N=3 for all groups. C) Semi-quantitative evaluation of C-myc binding to cells expressing Xcr1-myc and non-transfected cells demonstrates a large and significant increase of C-myc/DAPI reactivity as a consequence of transfection and supports the qualitative evaluation of C-myc presence to confirm the high expression of Xcr1-myc. Data is normalised to non-transfected mean. N = 9 per group; ***, $p < 0.001$. Error Bars = ±SD.

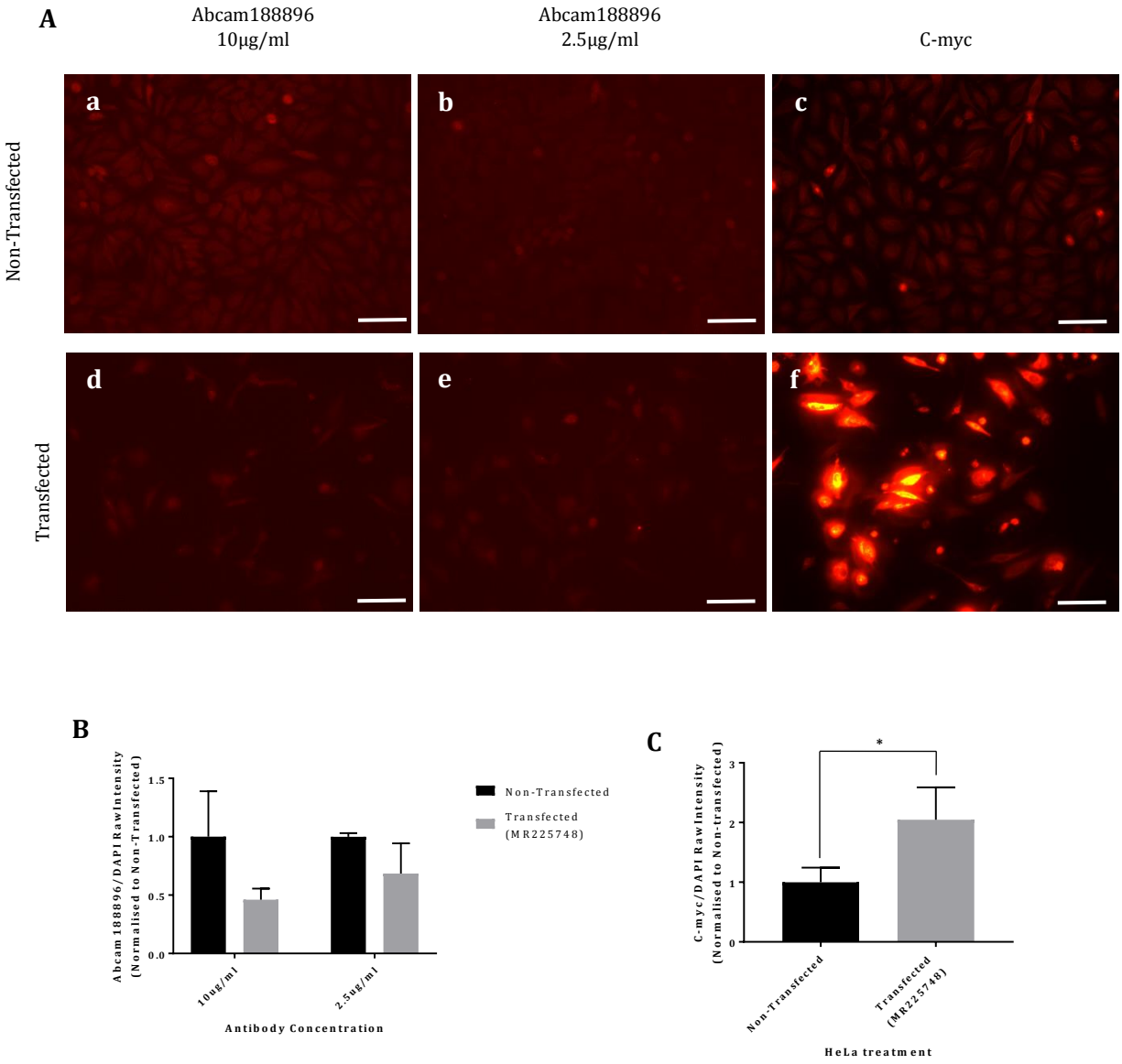

Figure 4.2.10. *Evaluation of Abcam188896 specificity to* Xcr1 *by immunocytochemistry.* A) Immunocytochemistry performed with Abcam188896 or anti-C-myc against Non-Transfected HeLa cells (a-c) or HeLa cells transfected with MR225748 (d-f) (DAPI signal not shown due to loss of data). B) Semi-quantitative evaluation of Abcam188896 antibody binding as calculated by Abcam188896/DAPI RawIntensity. N=3 per group. C) Semi-quantitative evaluation of C-myc/DAPI RawIntensity demonstrates a significant increase of C-myc binding in cells transfected with MR225748 and supports the qualitative evaluation of C-myc presence to confirm the high expression of Xcr1-myc. N = 6 per group; *, $p < 0.05$. Error Bars = ±SD.

4.2.3.4 Evaluation of cAb-Xcr1 specificity to Mouse Xcr1

To overcome the lack of available antibodies that demonstrated specificity to Mouse Xcr1, a custom designed polyclonal antibody (cAb-Xcr1) was produced using a 19 amino acid peptide derived from the 3rd intracellular loop of Mouse Xcr1 (Figure 2.1). This antibody was prepared by affinity-purification to the peptide immunogen and tested by ELISA for specificity alongside total serum and purification column flow-through (Ft), collected following affinity-purification (Figure 4.2.11). The purified antibody that was received from the manufacturer and used for testing by immunocytochemistry demonstrated a sigmoidal binding curve to the immunogenic peptide, with binding evident over 3 $\log_{10}$ concentrations from a 1:100 dilution to a 1:100000 dilution. A similar sigmoidal binding to that of the purified antibody was also observed following application of total serum (Figure 4.2.11, A). Binding of Ft also demonstrated a sigmoidal response, with statistical testing demonstrating significantly less binding to the peptide, in comparison to purified antibody, at all dilutions apart from 1:72900 and 1:218700 (Figure 4.2.11, B). This binding characteristic of Ft suggests the presence of a significant amount of low affinity antibodies within the serum that are able to bind the immunogenic peptide. However, in support of a higher specificity than Ft to the immunogenic peptide, the purified antibody demonstrates a much lower binding affinity to the carrier protein than that demonstrated for total serum and column flow through, although there is some residual binding at higher concentrations of the purified antibody. Together, the results obtained by ELISA to the immunogenic peptide suggest that the purified antibody does exhibit specificity for the peptide, but that this specificity may not be a result of the immunisation producing antigen-specific antibody. Rather, the immunogenic peptide appears to bind multiple antibodies contained within the serum and the purified antibody provided by the manufacturer simply reflects an enriched population of antibodies with a higher relative affinity.

In order to examine the potential use of cAb-Xcr1 for the detection of Mouse Xcr1 by immunohistochemistry, this antibody was then tested by immunocytochemistry at 10µg/ml, 5µg/ml and 2.5µg/ml against cells expressing Xcr1-myc and their non-transfected controls. In addition to manual analysis using ImageJ (Section 2.3.2.1; Figure 4.2.12), the evaluation of cAb-Xcr1 reactivity to cells transfected with MR225748 and non-transfected cells was also evaluated by automated image capture and analysis as described in Section 2.3.3 (Figure 4.2.13). As observed for the previous antibodies, cAb-Xcr1 demonstrated a diffuse signalling pattern that was observed in all cells of the culture, irrespective of the expression of Xcr1-myc that was confirmed by qualitative and semi-quantitative evaluation of C-myc binding by both manual and automated analyses. This diffuse staining pattern was

A

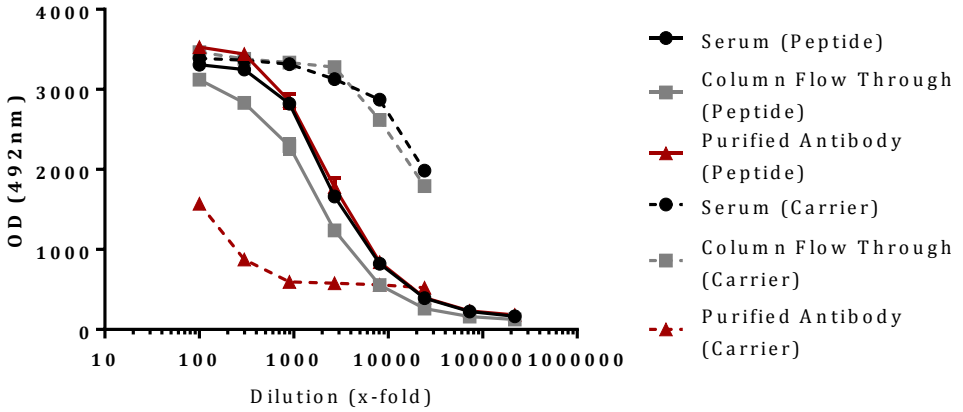

B

	Mean OD 492nm			Statistical comparison (vs PA)	
Dilution	**PA**	**Serum**	**Ft**	**Serum**	**Ft**
1:100	3527	3308	3122	-219, ***	-405, ***
1:300	3442	3247	2833	-195,***	-609, ***
1:900	2857	2820	2290	-36, ns	-567, ***
1:2700	1777	1660	1238	-117, **	-538, ***
1:8100	840	821	556	-19, ns	-284, ***
1:24300	397	393	260	-4, ns	-137, **
1:72900	231	226	160	-5, ns	-71, ns
1:218700	180	164	124	-16, ns	-56, ns

Figure 4.2.11. *Characterisation of cAb-Xcr1 binding to immunogenic peptide by ELISA.* A) Colorimetric measurements obtained following assessment of binding to immunogen by Indirect Enzyme-Linked ImmunoSorbant Assay (ELISA). Total serum (black), purified antibody (red) and column flow through (grey) were tested for binding to the immunogen designed for the production of cAb-Xcr1 (peptide, solid line) and the carrier protein used for host immunisation (carrier, dashed line). Error bars = ±SD. B) Numerical and statistical comparison of semi-quantitative assessment of binding to immunogenic peptide, according to optical density at 492nm, between purified antibody (PA), Serum and purification column flow-through (Ft). Data was compared by Two-Way ANOVA with post-hoc Dunnett's multiple comparisons test. ***, $p < 0.001$; **, $p < 0.01$; *, $p < 0.05$.

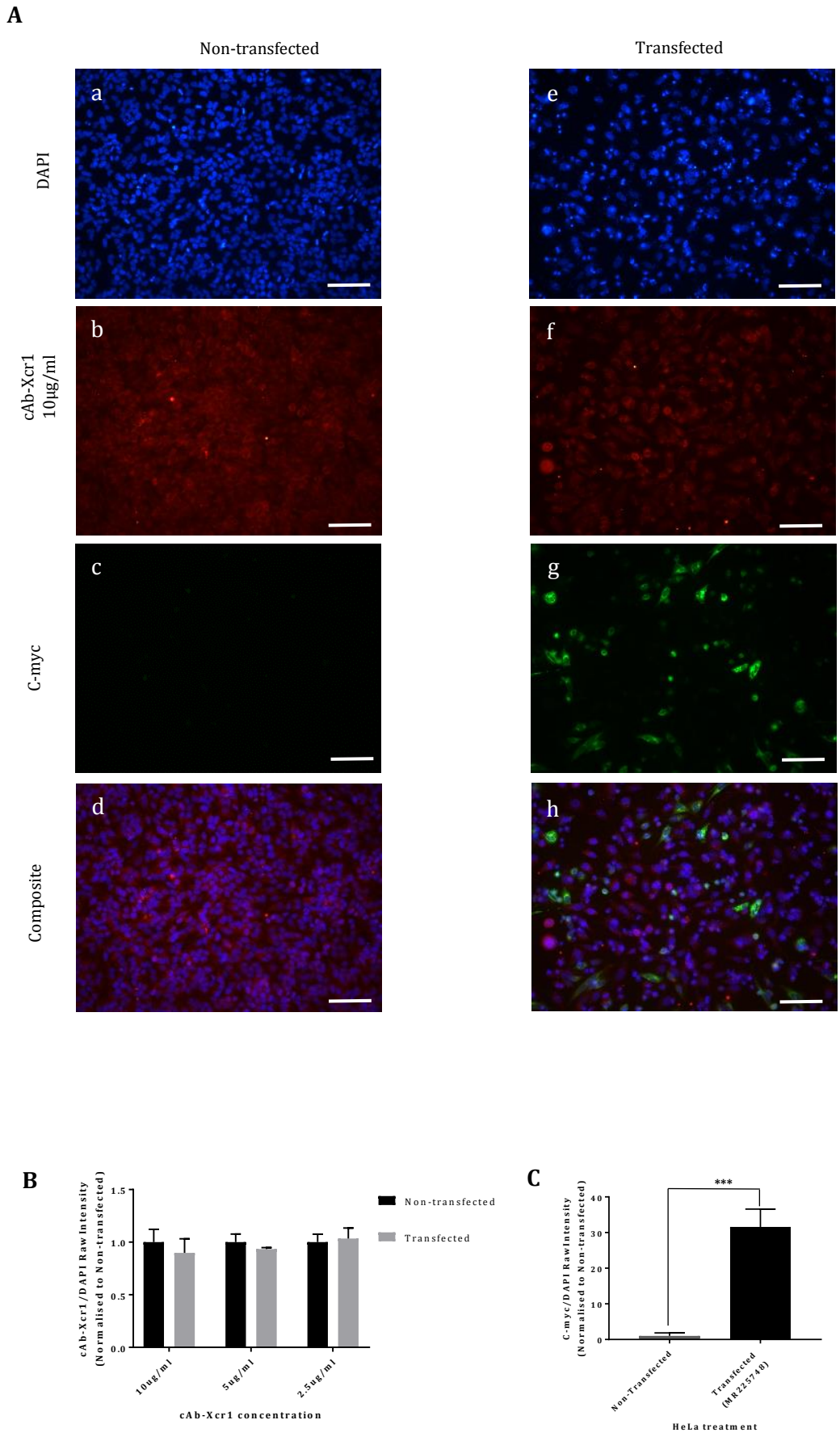
A
Non-transfected
Transfected
DAPI
cAb-Xcr1 10µg/ml
C-myc
Composite
a
b
c
d
e
f
g
h
B
cAb-Xcr1/DAPI Raw Intensity (Normalised to Non-transfected)
1.5
1.0
0.5
0.0
10ug/ml
5ug/ml
2.5ug/ml
cAb-Xcr1 concentration
Non-transfected
Transfected
C
C-myc/DAPI Raw Intensity (Normalised to Non-transfected)
***
40
30
20
10
0
Non-Transfected
Transfected (MR225748)
HeLa treatment

Figure 4.2.12. *Evaluation of cAb-Xcr1 reactivity to* Xcr1-myc *by immunocytochemistry.* A) Representative images of HeLa cells either transfected with MR225748 or non-transfected controls following double immunocytochemistry with cAb-Xcr1 (red) and anti-C-myc (green). a-d = cAb-Xcr1 10µg/ml non-transfected; e-h = cAb-Xcr1 10µg/ml transfected. Scale bars =100µm. B) Semi-quantitative evaluation of cAb-Xcr1 binding to cells expressing Xcr1-myc and non-transfected cells. cAb-Xcr1/DAPI RawIntensity demonstrates a consistent level of signal in cells regardless of Xcr1-myc presence. N = 3 for each group. C) Semi-quantitative evaluation of C-myc binding to cells expressing Xcr1-myc and non-transfected cells demonstrates a large and significant increase of C-myc/DAPI reactivity as a consequence of transfection. This supports the qualitative evaluation of C-myc presence demonstrating the high expression of Xcr1-myc. N = 9 for each group; ***, $p < 0.001$. Error bars = ±SD.

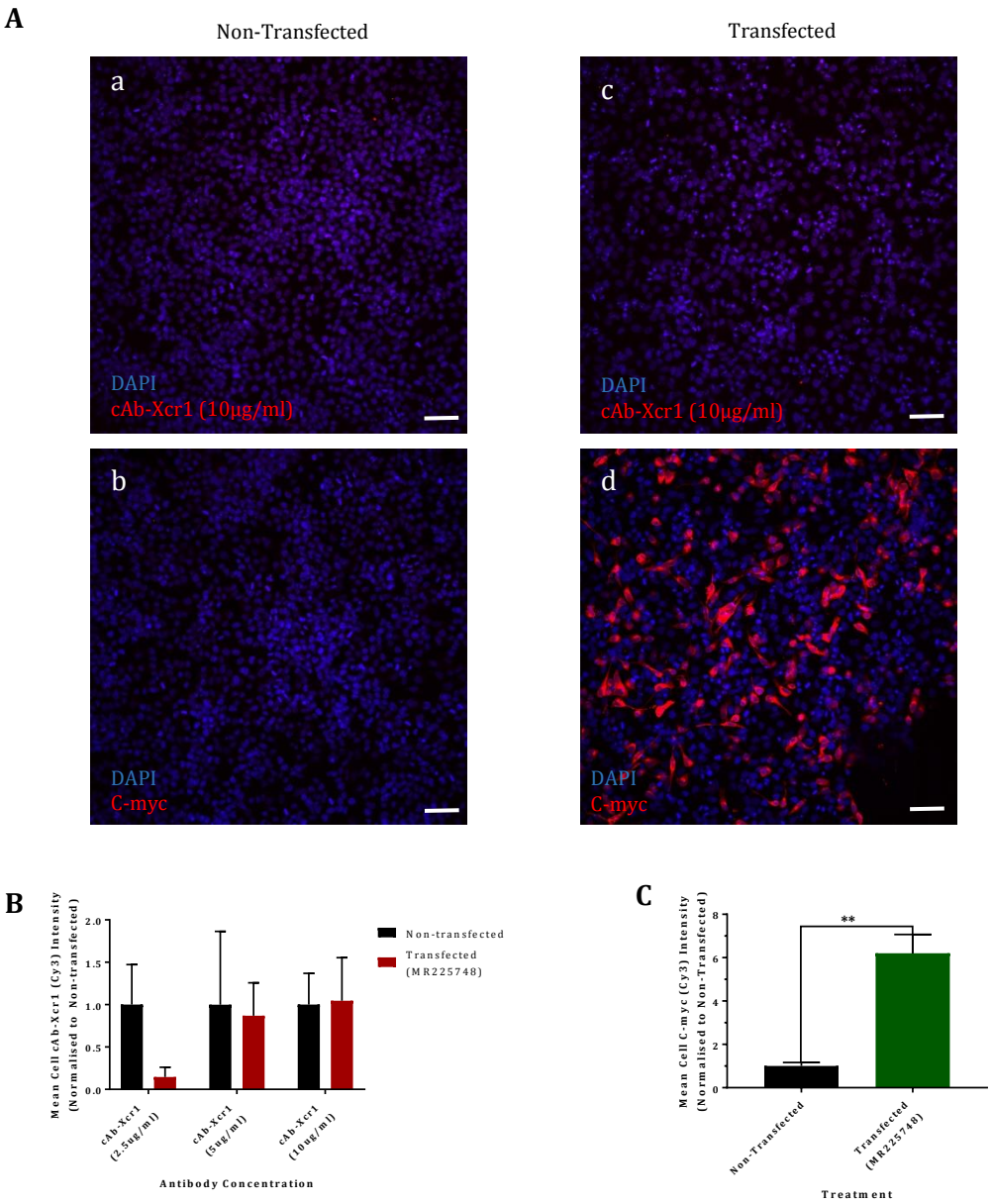

Figure 4.2.13. *Evaluation of cAb-Xcr1 binding to Xcr1-myc by immunocytochemistry using automated image analysis.* A) Representative images acquired by Opera Phenix following single immunocytochemistry using anti-C-myc (b, d) and cAb-Xcr1 (a, c) antibodies with non-transfected cells or cells transfected with MR225748 (Transfected) and visualised by the application of a Cy3-conjugated secondary antibody. The display range of each image has been standardised between non-transfected and transfected samples for each antibody condition to allow qualitative evaluation of antibody binding. No difference in cAb-Xcr1 reactivity was observed as a consequence of transfection with MR225748. Scale bars = 100µm. B) Semi-quantitative evaluation of cAb-Xcr1 antibody binding at all concentrations tested, according to mean Cy3 Intensity per cell, demonstrates no significant difference between cells transfected with MR225748 and their respective non-transfected controls. N=3 per group C) C-myc binding significantly increases as a consequence of transfection in comparison to non-transfected cells (**, mean difference = 5.203; p = 0.008). N=9 per group; **, p<0.01. Error bars = ±SD.

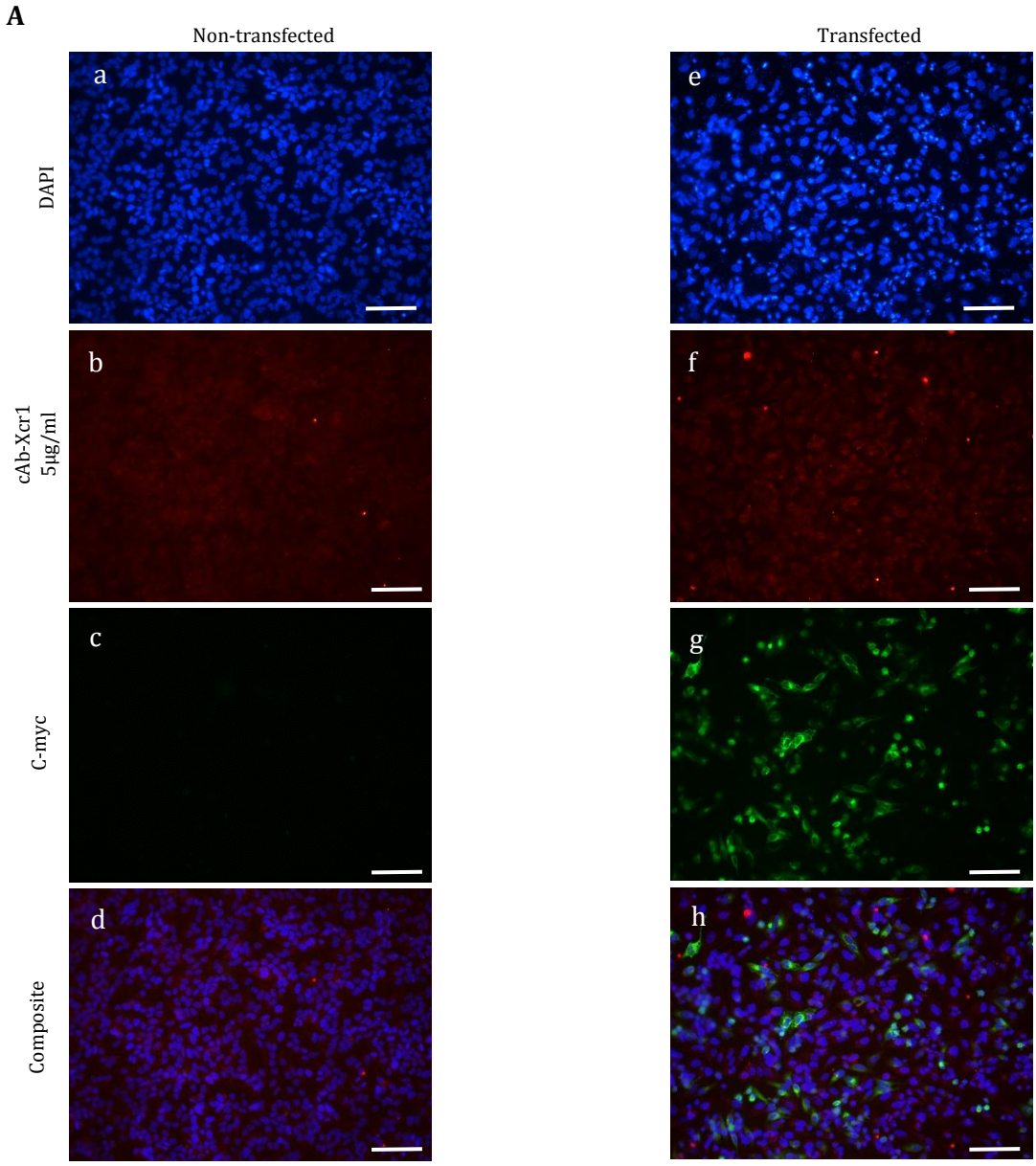
A
Non-transfected
Transfected
DAPI
cAb-Xcr1 5µg/ml
C-myc
Composite
a
b
c
d
e
f
g
h

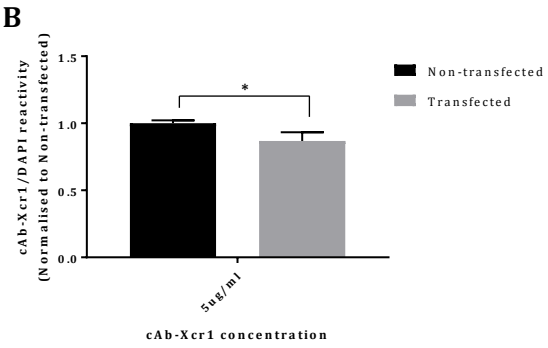
B
cAb-Xcr1/DAPI reactivity (Normalised to Non-transfected)
1.5
1.0
0.5
0.0
*
5ug/ml
cAb-Xcr1 concentration
Non-transfected
Transfected

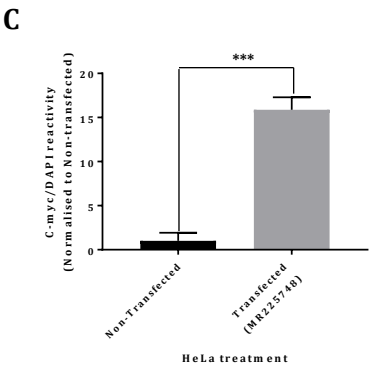
C
C-myc/DAPI reactivity (Normalised to Non-transfected)
20
15
10
5
0
***
Non-Transfected
Transfected (MR225740)
HeLa treatment

Figure 4.2.14. *Evaluation of cAb-Xcr1 specificity to Mouse* Xcr1 *by immunocytochemistry following HIER.* A) Double immunocytochemistry following HIER of HeLa cells transfected with MR225748 and non-transfected controls with cAb-Xcr1 (red) and anti-C-myc (green) primary antibodies. a-d = cAb-Xcr1 5µg/ml non-transfected; e-h cAb-Xcr1 5µg/ml transfected; Scale bars = 100µm B) Semi-quantitative evaluation of cAb-Xcr1 binding to transfected cells expressing Xcr1-myc and non-transfected cells. cAb-Xcr1/DAPI RawIntensity demonstrates a significant decrease in transfected cells in comparison to non-transfected cells. N=3 per group; *, $p<0.05$. C) Semi-quantitative evaluation of C-myc binding to cells expressing Xcr1-myc and non-transfected cells demonstrates a large and significant increase of C-myc/DAPI reactivity as a consequence of transfection and supports the qualitative evaluation of C-myc presence demonstrating the high expression of Xcr1-myc. N=3 per group; ***, $p<0.001$. Error bars = ±SD.

evident at all concentrations used. Moreover, no distinct changes in mean cell Cy3 Intensity was observed between cells treated with cAb-Xcr1 and cells which were treated with secondary antibodies only. Overall, this suggests the antibody to be non-specific to Mouse Xcr1 and to show little, if any, non-specific binding that was not influenced by antibody titer.

The use of HIER prior to immunocytochemistry (Figure 4.2.14) failed to improve antibody binding when applied at 5µg/ml, with antibody reactivity demonstrating a similarly diffuse pattern to that obtained without HIER. Furthermore, no clear colocalisation between the signal obtained from cAb-Xcr1 and C-myc could be identified that was consistently above the background staining observed for all cells.

In summary, cAb-Xcr1 was developed with the aim of providing an antibody that would specifically recognise Mouse Xcr1 based on specific binding to the 3rd intracellular loop of the protein. However, despite showing obvious binding and specificity to the immunogenic peptide, cAb-Xcr1 was unable to demonstrate binding and reactivity to Xcr1 by immunocytochemistry when overexpressed by cells *in vitro.* Overall, this evidence was unable to support the use of cAb-Xcr1 for the specific binding and localisation of Xcr1 by immunohistochemistry.

4.2.4 Evaluation of antibody specificity to Human XCR1 by immunocytochemistry

It was next sought to evaluate antibody specificity to Human XCR1 by utilising the optimised HeLa transfection assay to overexpress XCR1-myc. As for the testing of antibody specificity to Mouse Xcr1, this assessment aimed to confirm antibody specificity to support their use for the detection of endogenous XCR1 expression by immunohistochemistry in the Human CNS.

4.2.4.1 Evaluation of Atlas HPA013169 specificity to Human XCR1

Evaluation of Atlas HPA013169 to Human XCR1 was performed using both manual (Figure 4.2.15) and automated (Figure 4.2.16) analysis. Initial testing utilised single immunocytochemistry with HPA013169 over a range of concentrations to establish antibody reactivity in non-transfected cells and cells expressing XCR1-myc. As established with testing against Mouse XCR1, anti-C-myc reactivity provided clear evidence of transfected cells expressing XCR1-myc as demonstrated by both qualitative (Figure 4.2.15, A (d vs i)) and semi-quantitative evaluation of normalised C-myc/DAPI RawIntensity (Figure 4.2.15, D). HPA013169 also demonstrated a clear and significant increase in binding to cells transfected with RC221929 in comparison to non-transfected cells (Figure 4.2.15, A (a-c vs f-h)). This was supported by semi-quantitative evaluation of antibody binding demonstrating a statistically significant increase in HPA013169/DAPI RawIntensity in comparison to non-transfected cells for all antibody concentrations tested. Normalised to

their respective non-transfected controls, HPA013169 binding increased by 29.86x, 85.07x and 15.47x in cells transfected with RC221929 and treated with 1μg/ml, 2.5μg/ml or 4μg/ml of antibody, respectively (Figure 4.2.15, B). This lack of consistency in relative amounts of antibody binding when normalised to their respective non-transfected controls suggests a poor relationship between antibody concentration and specific epitope binding. However, absolute values of HPA013169/DAPI RawIntensity demonstrate a dose-dependent increase in antibody binding (Figure 4.2.15, C). This supports the specificity of the antibody and indicates that the variation in normalised results is a consequence of variability between corresponding non-transfected values that were used for normalisation. Indeed, for non-transfected cells treated with 4μg/ml HPA013169, the mean HPA013169/DAPI RawIntensity was ~10x higher than that for cells treated with 1μg/ml or 2.5μg/ml. This therefore reduced the relative magnitude of increase in HPA013169/DAPI RawIntensity in transfected cells treated with 4μg/ml HPA013169. Overall, this supported the use of HPA013169 at a concentration of 2.5μg/ml for further investigations as this provided a signal with a greater distinction to background than that observed for 1μg/ml, but did not suffer from the apparent increase in background reactivity observed at 4μg/ml.

Further to semi-quantitative evaluation demonstrating the increase of HPA013169 binding to cells expressing XCR1-myc, double immunocytochemistry provided a clear indication of HPA013169 specificity to XCR1-myc. Figure 4.2.15, E illustrates the colocalisation of HPA013169 and anti-C-myc, providing strong evidence of the specificity of HPA013169 to Human XCR1.

The evidence of HPA013169 specificity to Human XCR1 provided by manual image analysis was further supported by automated analysis (Figure 4.2.16). Images obtained following double immunocytochemistry of cells transfected with RC221929 and non-transfected cells (Figure 4.2.16, A) using anti-C-myc and HPA013169, demonstrate the increased presence of HPA013169 binding to transfected cells. This binding of HPA013169 localises, in particular, to peri-nuclear regions of the cell cytoplasm. There is a small but notable presence of HPA013169 binding in non-transfected cells also. C-myc binding clearly illustrates the expression of XCR1-myc by cells successfully transfected with the RC221929. The clearest evidence of HPA013169 specificity to XCR1-myc is provided by the observed colocalisation of HPA013169 signal to that of the anti-C-myc antibody. This colocalisation is consistent to all cells identified to have XCR1-myc expression by anti-C-myc binding and demonstrates the localisation of HPA013169 binding to XCR1-myc.

Semi-quantitative analysis supports the successful transfection, XCR1-myc expression and HPA013169 specificity to XCR1. Quantitation of C-myc binding (Figure 4.2.16, B) supported the qualitative evidence of transfection efficiency and determined a mean increase of 4.4x

of anti-C-myc binding per cell following transfection with RC221929 in comparison to non-transfected cells. Semi-quantitative analysis also supported the qualitative demonstration of increased HPA013169 binding to transfected cells (Figure 4.2.16, C), with a 3.1x mean increase of Cy3 intensity per cell, for cells transfected with RC221929 in comparison to non-transfected cells. Moreover, this increase in HPA013169 binding is resilient to the presence of the anti-C-myc antibody and demonstrates almost identical increases in binding to transfected cells expressing XCR1-myc when used in isolation or as part of a double immunocytochemical protocol (images of single immunocytochemistry not shown).

As an additional mode of analysis to support the specificity of HPA013169 to XCR1-myc, the intensity of signal corresponding to HPA013169 binding within regions of the test image demonstrating the highest anti-C-myc binding was performed. In cell populations used for transfection with RC221929, the intensity of signal arising from anti-C-myc binding provided a clear distinction between cells that were or were not successfully transfected. Therefore, selection of image regions displaying the highest FITC intensity would identify regions of the image corresponding to transfected cells with the highest XCR1-myc expression. The same method was also applied to non-transfected cells, but rather than identify regions of XCR1-myc expression this method would simply identify the regions that displayed the highest amount of background anti-C-myc binding. As displayed in Figure 4.2.16, D, HPA013169 signal intensity within regions of highest anti-C-myc binding was significantly higher in transfected cells, demonstrating a 108% increase in signal intensity in comparison to the corresponding image regions identified in non-transfected cells.

Together, the evidence provided by manual and automated image analysis provides a clear validation of Atlas HPA013169 specificity to Human XCR1. This evidence is most clearly appreciated by qualitative inspection of HPA013169 colocalisation to anti-C-myc reactivity, but is further supported by semi-quantitative analysis that demonstrates a measurable increase of HPA013169 binding to cells expressing XCR1-myc that is of a large and statistically reliable magnitude in comparison to non-transfected controls.

4.2.4.2 Evaluation of Abcam 188896 specificity to Human XCR1

The specificity of Abcam 188896 was tested against Human XCR1 using both manual (Figure 4.2.17) and automated (Figure 4.2.18) image acquisition and analysis following immunocytochemistry with 5µg/ml Abcam188896 using non-transfected HeLa and HeLa transfected with RC221929.

Manual image acquisition and analysis of Abcam 188896 binding was performed using samples that were prepared using a standard immunocytochemistry protocol (Figure

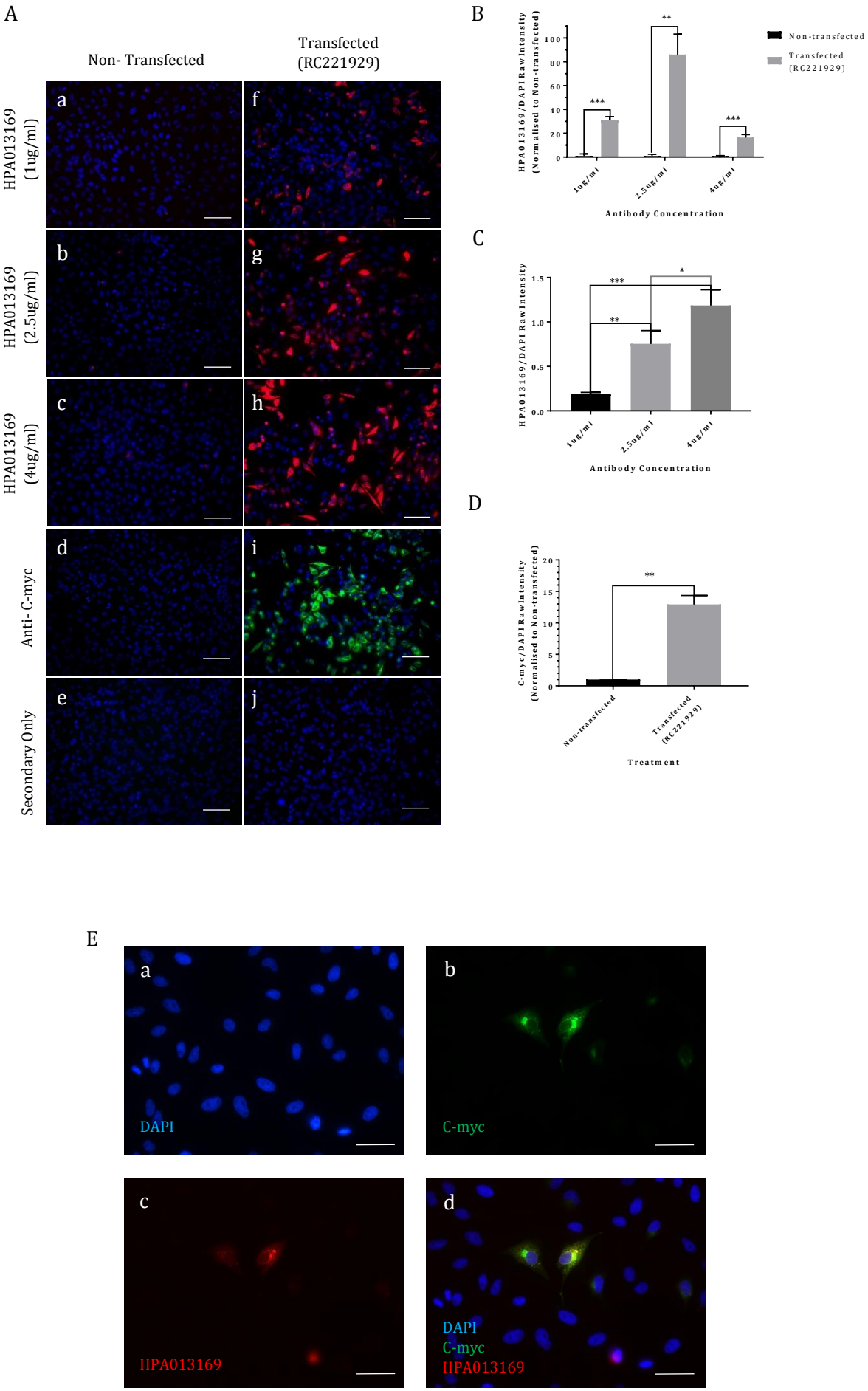
A
Non- Transfected
Transfected (RC221929)
HPA013169 (1ug/ml)
HPA013169 (2.5ug/ml)
HPA013169 (4ug/ml)
Anti- C-myc
Secondary Only
a
b
c
d
e
f
g
h
i
j
B
HPA013169/DAPI Raw Intensity (Normalised to Non-transfected)
Non-transfected
Transfected (RC221929)
1ug/ml
2.5ug/ml
4ug/ml
Antibody Concentration
C
HPA013169/DAPI Raw Intensity
Antibody Concentration
D
C-myc/DAPI Raw Intensity (Normalised to Non-transfected)
Non-transfected
Transfected (RC221929)
Treatment
E
a
DAPI
b
C-myc
c
HPA013169
d
DAPI
C-myc
HPA013169

Figure 4.2.15. *Evaluation of Atlas HPA013169 specificity to XCR1 by immunocytochemistry.* A) Test of Atlas HPA013169 (Red) specificity to Non-transfected HeLa cells (a-e) and HeLa cells expressing XCR1-myc (f-j). Anti-C-myc reactivity (Green, d vs i) was used to confirm expression of XCR1-myc in transfected cells. Scale bars = 100μm. B) Semi-quantitative comparison of HPA013169 binding (normalised to non-transfected values) in transfected and non-transfected cells demonstrate a large and significant increase in antibody binding in cells expressing XCR1-myc in comparison to non-transfected cells. C) HPA013169 demonstrates a dose-dependent increase in antibody/DAPI RawIntensity values in cells transfected with RC221929. D) Semi-quantitative evaluation of C-myc/DAPI RawIntensity (normalised to Non-transfected values) supports qualitative evidence (A, d vs i) of XCR1-myc expression in transfected cells. E) Double immunohistochemistry using anti-C-myc (Green, b) and Atlas HPA013169 (2.5μg/ml, Red, c) of HeLa cells transfected with RC221929 demonstrates clear colocalisation of the two antibodies (d) at a higher magnification. Scale bars = 50μm. Error bars = ± SD. N=3 per group; *, $p<0.05$; **, $p<0.01$; ***, $p<0.001$.

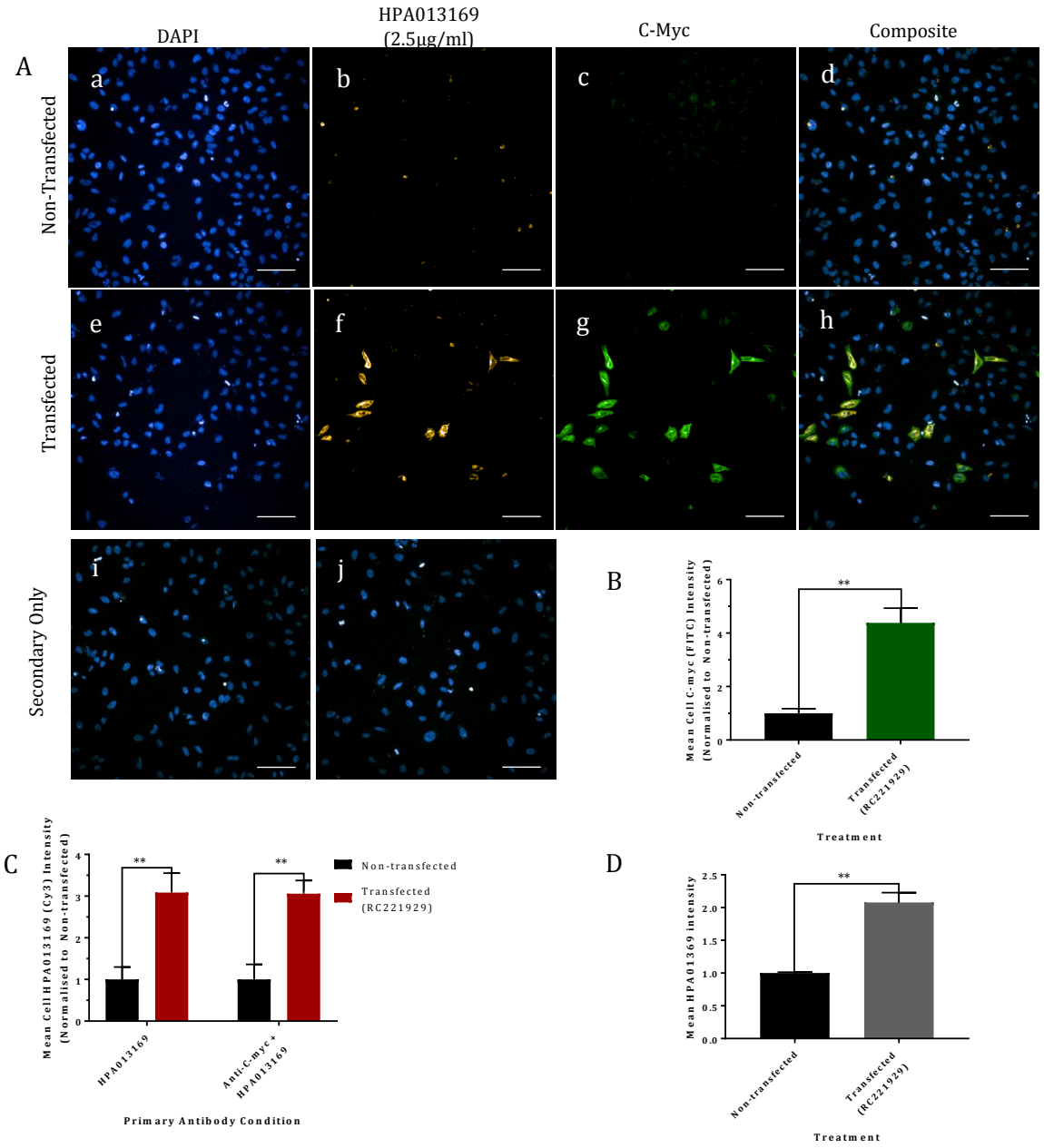

Figure 4.2.16. *Evaluation of HPA013169 specificity to* XCR1-myc *by immunocytochemistry using automated image analysis.* A) Images acquired by Opera Phenix following double immunocytochemistry with HPA013169 (2.5µg/ml) and C-myc. Antibodies were tested against non-transfected cells (a-d) and cells transfected with RC221929 (e-h). Secondary only controls of non-transfected (i) and transfected (j) cells.. In comparison to non-transfected cells (d), colocalisation of signals from C-myc and HPA013169 antibodies is clearly evident throughout cytoplasm of successfully transfected cells (h). Scale bars = 100µm. B) Semi-quantitative evaluation of fluorescent signal corresponding to detection of anti-C-myc supports transfection efficiency and identifies a consistent and significant increase in C-myc binding to transfected cells in comparison to non-transfected cells. N=6 per group;**, $p < 0.01$. C) Semi-quantitative evaluation of Cy3 signal corresponding to detection of HPA013169 demonstrates a consistent and significant increase in HPA013169 binding to transfected cells in comparison to non-transfected cells. The magnitude of this difference remains consistent during both single (HPA013169) and double (Anti-C-myc + HPA013169) immunocytochemical procedures. N=3 per group; **, $p<0.01$. D) HPA013169 binding in regions of highest C-myc binding. Signal intensity arising from HPA013169 within regions of highest C-myc binding demonstrates a mean increase of 108% in cells transfected with RC221929 in comparison to non-transfected cells. N=3 per group; **, $p<0.01$. Error bars = ±SD.

4.2.17, A-C) and immunocytochemistry protocols that included HIER (Figure 4.2.17, D-F). Following the standard immunocytochemistry protocol, qualitative inspection demonstrated a diffuse pattern of cellular staining for all cells treated with Abcam 188896, a feature that did not demonstrate any change as a consequence of transfection with RC221929. Semi-quantitative evaluation identified a small but significant increase in Abcam188896 binding by transfected, in comparison to non-transfected, HeLa. This corresponded to a 1.49x increase in Abcam188896/DAPI RawIntensity in cells transfected with RC221929. This relatively small increase is despite the obviously high expression of XCR1-myc by HeLa transfected with RC221929, as supported by anti-C-myc binding.

The capacity for Abcam188896 binding to XCR1-myc did not appear to improve as a consequence of HIER (Figure 4.2.17, D-F). Despite semi-quantitative evaluation suggesting a small increase in Abcam188896 binding in comparison to non-transfected cells, the quality of Abcam188896 binding remained diffuse and did not demonstrate a localisation pattern that resembled that identified by anti-C-myc. Moreover, the small increase in Abcam188896/DAPI RawIntensity identified for transfected HeLa in comparison to non-transfected HeLa, did not achieve statistical significance. This is despite a 6.31x increase of C-myc presence, as indicated by C-myc/DAPI RawIntensity, supporting the reliable presence of XCR1-myc in HeLa cells transfected with RC221929. Overall, manual analysis of Abcam188896 binding to XCR1-myc, following immunocytochemistry both with and without HIER, was unable to support the specificity of Abcam188896 to Human XCR1.

Further confirmation of a lack of Abcam188896 specificity was provided via automated image acquisition and analysis (Figure 4.2.18). Both qualitative and semi-quantitative evidence failed to provide support for Abcam188896 binding to XCR1-myc expressed by HeLa cells transfected with RC221929. Instead, a small but significant decrease of Abcam188896/DAPI RawIntensity was identified for HeLa cells transfected with RC221929, corresponding to 0.82x the value obtained for non-transfected cells. Based on this evidence demonstrating a lack of specificity by Abcam18896 to Human XCR1, the use of this antibody for the detection of endogenous XCR1 in Human tissue could not be supported.

4.2.5 Evaluation of Antibody specificity by Western Blot

4.2.5.1 Evaluation of antibody specificity to Mouse Xcr1 *by Western Blot*

Based on the confirmed production of a myc-tagged murine Xcr1 protein by HeLa cells transfected with MR225748 (section 4.2.2.3), it was possible to reliably evaluate antibody specificity to Mouse Xcr1 by Western Blot. A total of 5 antibodies were tested for specificity

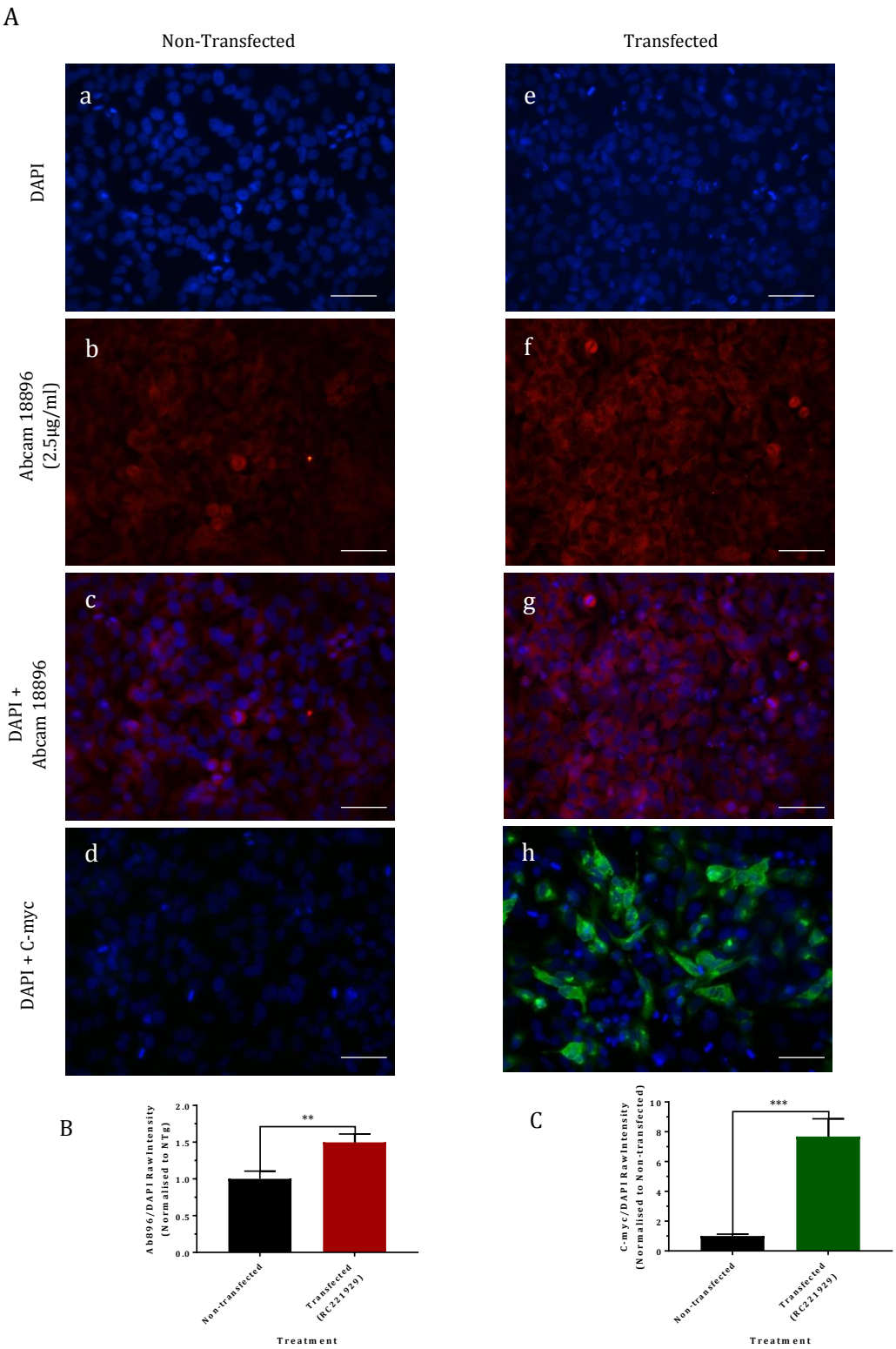

Figure 4.2.17. *Evaluation of Abcam188896 specificity to* XCR1-myc *by immunocytochemistry*. A) Images obtained of single immunocytochemistry protocol to test the specificity of Abcam 188896 to XCR1-myc. Abcam188896 was applied to non-transfected cells (a-c) and cells transfected with RC221929 (e-g). Anti-C-myc antibody was applied independently to confirm expression of XCR1-myc in transfected cells (d vs h). Scale bars = 50µm. B) Semi-quantitative evaluation of Abcam 188896 binding demonstrated a statistically significant increase when applied to transfected cells in comparison to non-transfected cells. C) Semi-quantitative evaluation of C-myc reactivity demonstrated a large and significant increase when applied to transfected cells in comparison to non-transfected cells. N=3 per group; **, $p<0.01$; ***, $p<0.001$. Error bars = ±SD.

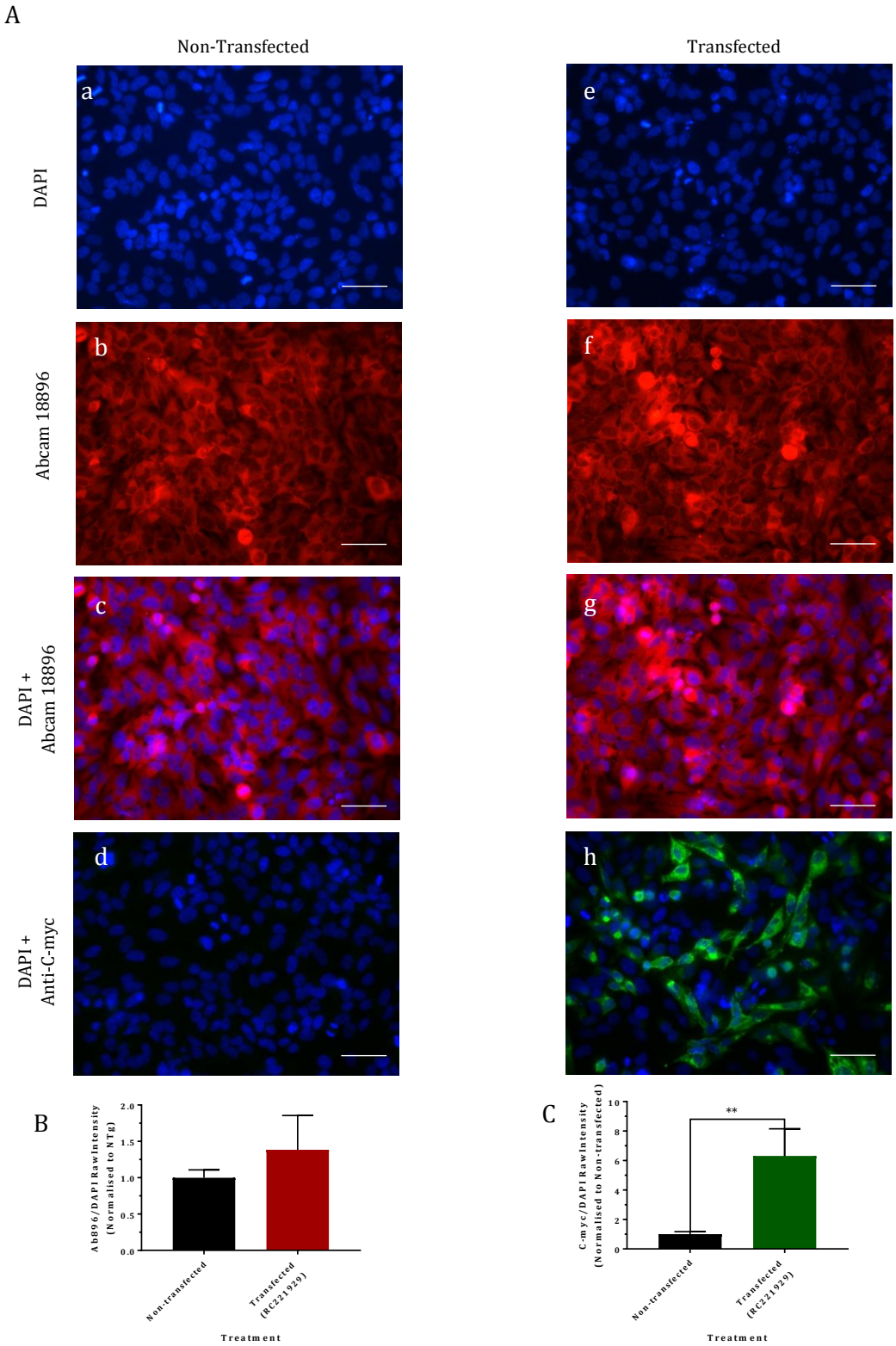

Figure 4.2.18. *Evaluation of Abcam188896 specificity to* XCR1-myc *by immunocytochemistry following HIER*. A) Abcam188896 was applied to non-transfected cells (a-c) and cells transfected with RC221929 (e-g). Anti-C-myc antibody was applied independently to confirm expression of XCR1-myc in transfected cells (d vs h). Scale bars = 50µm. B) Semi-quantitative evaluation of Abcam 188896 binding demonstrated no statistically significant changes to Abcam18896 binding when applied to transfected cells in comparison to non-transfected cells. C) Semi-quantitative evaluation of C-myc reactivity demonstrated a large and significant increase when applied to transfected cells in comparison to non-transfected cells. N=3 per group. **, $p<0.01$. Error bars = ±SD.

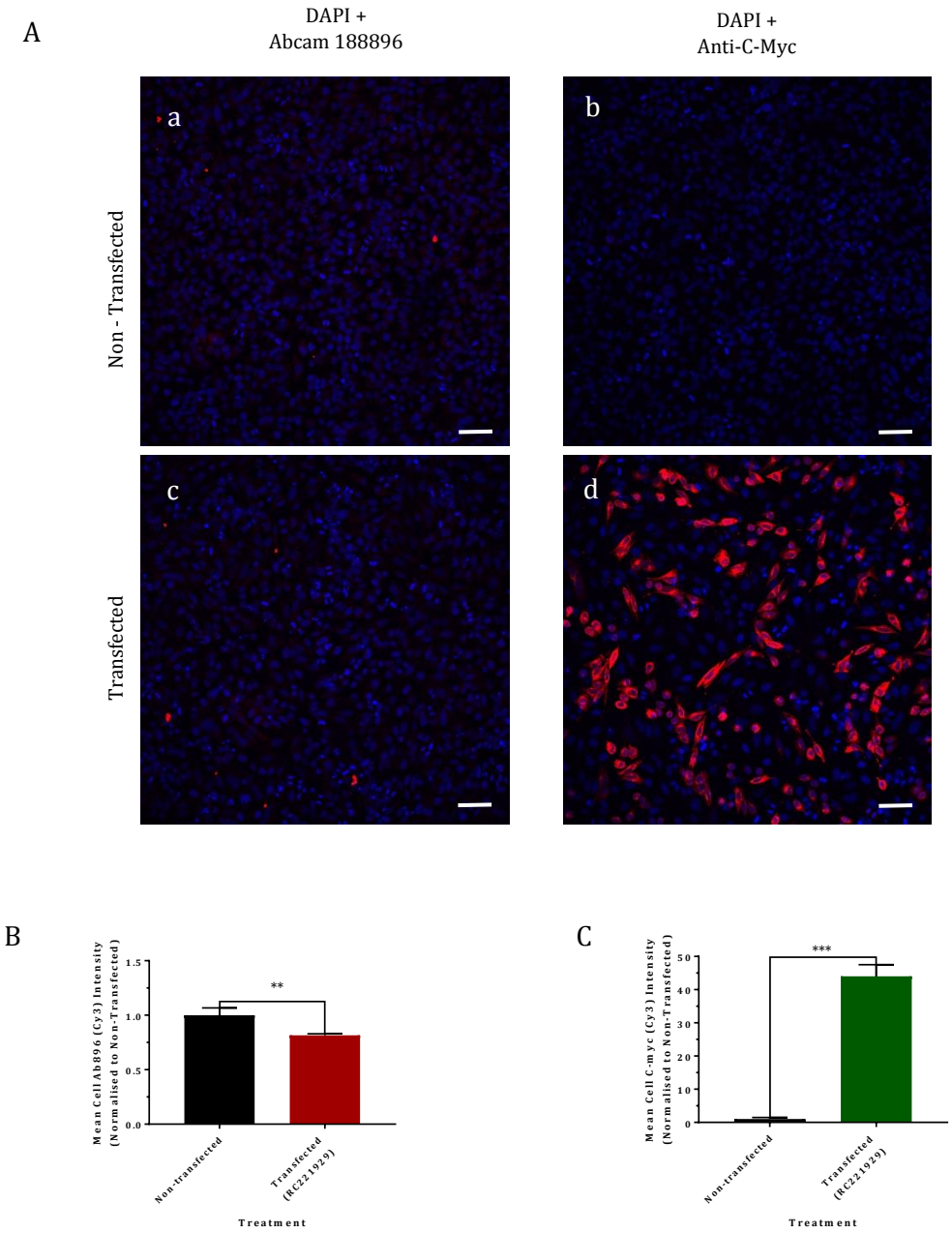

Figure 4.2.19. *Evaluation of Abcam 188896 specificity to* XCR1-myc *by immunocytochemistry using automated image acquisition and analysis.* A) Images obtained from the Opera Phenix™ High Content Screening System following single immunocytochemistry protocols using Abcam 188896 (a, c) and anti-C-myc (b, d) antibodies with non-transfected cells and cells transfected with RC221929. Image contrast thresholds were manually adjusted to provide a display range that accommodated the maximum signal range from non-transfected and transfected samples for each antibody. Scale bars = 100µm. B, C) Comparison of Mean Cell signal intensity arising from the Cy3-conjugated secondary antibody used for the detection of Abcam 188896 (Ab896) (B) and anti-C-myc (C) between transfected and non-transfected cells. N = 3 per group; **, $p<0.01$; ***, $p < 0.001$. Error bars = ±SD.

to Xcr1-myc: LS-A158, LS-C37380, Ab188896, cAb-Xcr1 and HPA013169. For details of antibody concentrations used, see Table 2.1. Of the 5 antibodies tested, only LS-A158 and LS-C37380 demonstrated any binding to the nitrocellulose membrane following protein transfer that could be identified from the associated chemiluminescent detection (Figure 4.2.19). The reactivity arising from both antibodies however, did not correspond to the region of C-myc reactivity used to confirm Xcr1-myc within the protein sample (Figure 4.2.19, E). LS-A158 instead identified an alternative protein with a molecular weight of ~17kDa. Moreover, the detection of this alternative protein was not specific to transfected cells, further suggesting that the epitope identified by LS-A158 did not correspond to those present on Xcr1. LS-C37380 similarly detected proteins consistently within lysates prepared from both non-transfected and transfected HeLa. This corresponded to 3 distinct bands of binding, all of which resided at a higher molecular weight than that identified for Xcr1-myc. All other antibodies were not detected (data not shown), suggesting a complete lack of binding to the nitrocellulose membrane. This evidence suggested that the use of these commercial and custom antibodies were unable to specifically detect Mouse Xcr1 by western blot.

4.2.5.2 Evaluation of Atlas HPA013169 specificity to Human XCR1 *by Western Blot*

Using the lysate of HeLa cells transfected with RC221929 that were previously demonstrated to contain a myc-tagged protein with the molecular characteristics consistent with the presence of XCR1-myc (section 4.2.2.3), it was possible to reliably test the specificity of Atlas HPA013169 to Human XCR1 by western blot.

Figure 4.2.20 demonstrates the capacity of HPA013169 to detect a protein at a molecular weight that is consistent with predicted molecular weight of XCR1-myc and corresponds to the molecular weight of the protein identified by anti-C-myc detection. Of note, HPA013169 was also tested against cell lysate prepared from HeLa cells transfected with MR225748, but did not demonstrate any reactivity. Prolonged exposure of the film to the membrane following HPA013169 incubation, also demonstrated the detection of a protein with a lower molecular weight than XCR1-myc (data not shown). This additional protein was present in lysate obtained from both non-transfected HeLa and HeLa transfected with RC221929. The test of HPA013169 specificity to XCR1-myc therefore demonstrated the capacity of HPA013169 to reliably bind to XCR1-myc, but also demonstrate a degree of non-specificity based on the lower affinity observed for an additional protein within HeLa cell lysate.

4.2.6 LS-A158 reactivity in mouse spinal cord

Exemplary images of that obtained following both chromogenic and fluorescent immunohistochemistry with LS-A158 are provided in Figure 4.2.21.

As was observed in non-transfected HeLa and HeLa expressing Xcr1-myc, LS-A158 demonstrated a diffuse reactivity that appeared to localise to cells, as indicated by the most prominent reactivity being observed in the grey matter of the spinal cord by fluorescent immunohistochemistry. Indeed, double immunohistochemistry of LS-A158 and NeuN resulted in significant overlap of the signals, suggesting that LS-A158 reactivity did localise to neurons, amongst other cell types (Figure 4.2.21, A). Closer inspection of LS-A158 reactivity reveals the antibody to localise to cell membranes, as evidenced by the reactivity to surround regions of NeuN binding that localise to neuronal nuclei.

Further evidence of LS-A158 non-specific binding is demonstrated by the reactivity observed following chromogenic immunohistochemistry protocols (Figure 4.2.21, B). Again, LS-A158 reactivity was widespread within the tissue, particularly within the grey matter. This non-specific labelling of cells reflects the LS-A158 signal obtained following immunohistochemical processing of the spleen (Figure 4.2.1). Low background chromogenic signal obtained from the control section supports the identified signal to be specific to the presence of LS-A158.

Tests on other spinal cord sections (not shown) demonstrated the antibody to consistently provide widespread reactivity that was particularly evident within the grey matter. These evaluations of LS-A158 binding within the mouse spinal cord demonstrate the antibody to exhibit significant non-specific binding.

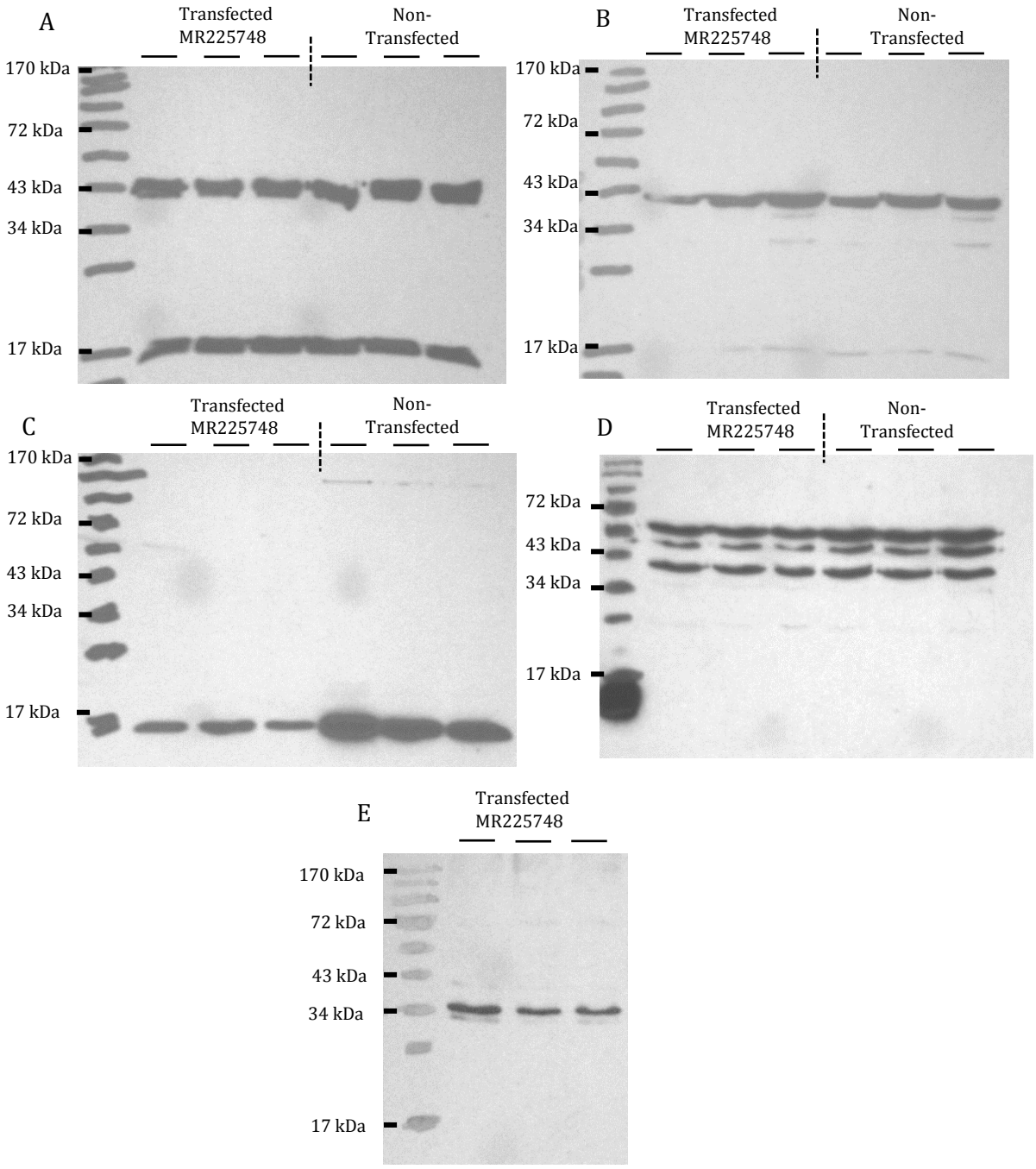

Figure 4.2.20. *Evaluation of LS-A158 and LS-C37380 reactivity to* Xcr1-myc *by western blot.* A) LS-A158 detected a protein with an approximate 17kDA molecular weight. Detection of β-actin was used as a loading control and confirmed consistent levels of protein loading between transfected and non-transfected cells based on reactivity at 42kDa. B) Pre-incubation of LS-A158 with the immunogenic peptide diminished reactivity against the 17kDa protein. β-actin again confirmed a consistent amount of protein between samples based on reactivity observed at 42kDa. C) Without use of β-actin control, reactivity to a protein with an approximate 17kDa molecular weight by LS-A158 was still observed. The discrepancy of reactivity intensities against transfected and non-transfected lysates is likely a result of inconsistent levels of protein loading. D) Chemiluminescent detection of LS-C37380 demonstrates the detection of proteins at 3 distinctive molecular weights, in particular, within the lysate of both non-transfected HeLa and HeLa transfected with MR225748. E) C-myc reactivity confirms presence of Xcr1-myc within test sample used in A, B and C.

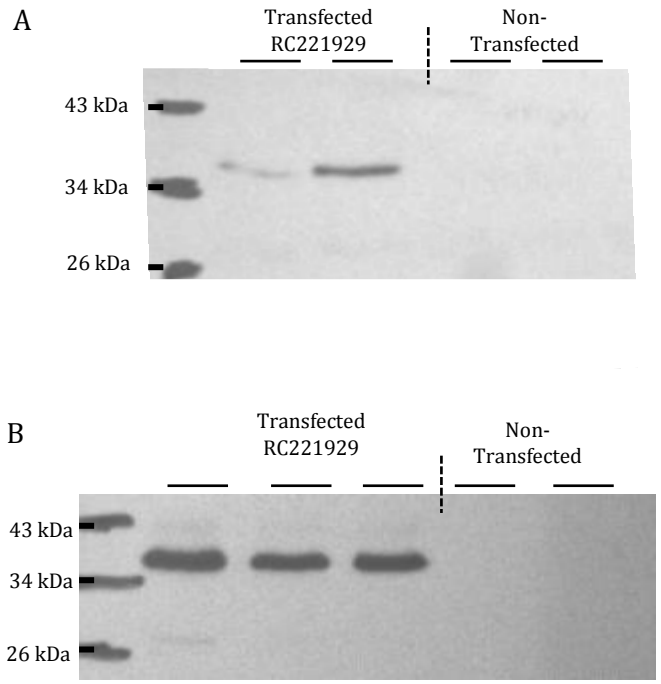

Figure 4.2.21. *Evaluation of HPA013169 specificity to* XCR1-myc *by Western Blot.* A) HPA013169 demonstrates the detection of a protein within the lysate of HeLa cells transfected with RC221929. This protein resides at the molecular weight consistent with the presence of XCR1-myc. B) Anti-C-myc demonstrates the presence of XCR1-myc specifically within the lysate of HeLa cells transfected with RC221929, also used for the evaluation of HPA013169 in A.

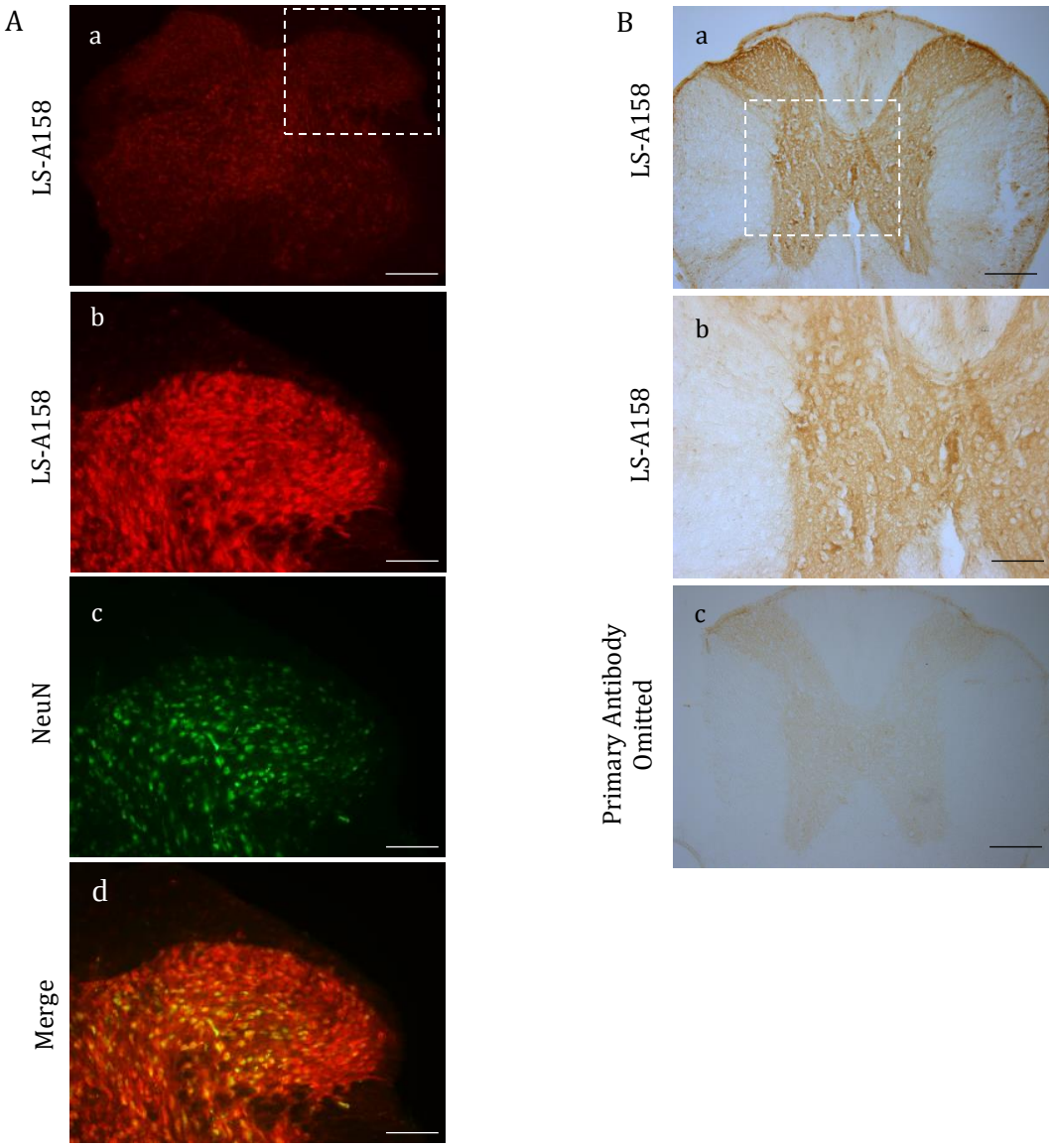

Figure 4.2.22. *Representative images of LS-A158 reactivity in Mouse spinal cord identified by fluorescent and chromogenic immunohistochemistry.* A) LS-A158 reactivity within the sacral spinal cord of a WT mouse following double immunohistochemistry with NeuN. Lower power magnification image (a) illustrates the widespread reactivity of LS-A158 within grey matter of both spinal cord regions. LS-A158 reactivity demonstrates colocalisation to many NeuN-positive cells, but also demonstrates reactivity to a lower level within white matter. Dashed white box in (a) highlights regions focussed upon by higher magnification in b,c,d. Scale bars: a = 200µm; b-d = 100µm. B) LS-A158 reactivity as detected by chromogenic immunohistochemistry within the thoracic cord of a WT mouse. Application of LS-A158 results in background reactivity that is particularly strong within the grey matter, with some reactivity observed within the white matter also (a). At higher magnification (b), LS-A158 reactivity in grey matter does not show any specific localisation within the tissue, although this reactivity is higher than observed for control sections (c) suggesting that the signal is specific to the presence of LS-A158. Scale bars: a, c = 200µm; b = 100µm.

4.4 Discussion

This investigation aimed to establish the specificity of commercially and custom designed antibodies to both XCR1 and Xcr1. In particular, we sought an antibody capable of specifically recognising and binding to murine Xcr1. An important limitation of the method used, that should be immediately acknowledged, is that the tested antibodies were not all raised to immunogens that were specifically designed to detect the protein for which they were evaluated here. Figure 2.1 illustrates the epitopes for which the tested antibodies are specified to bind and illustrates how the use of some these antibodies are specific to XCR1 rather than Xcr1, and vice versa. Therefore, in testing the specificity of antibodies to Xcr1 that were designed to recognise epitopes of XCR1, it is perhaps unsurprising that these antibodies were unable to reliably bind to the protein of our interest.

The reasons for evaluating these antibodies in spite of their specified reactivity was twofold. Firstly, user experience within our lab had demonstrated that LS-A158, despite having a specified reactivity to Human XCR1, had given a reliable reactivity to samples prepared from Rat (Bird *et al.,* 2018). Secondly, the homology of amino acid sequences for the two XCR1 protein homologues in Mouse and Human show a high degree of conservation (70% amino acid identity; 81% amino acid positives (identity according to amino acid functional group properties) (Altschul *et al.*, 1990). In particular, the immunogen sequence used for the production of Abcam188896, which was tested against both XCR1 homologues, has a high conservation of amino acid sequence between Mouse and Human homologues (80% amino acid identity; 95% amino acid positives (Altschul *et al.,* 1990), Figure 2.1). It could therefore be predicted that the two XCR1 homologues share a similarity in i) global protein tertiary structures and ii) conformation of epitopes for which the antibodies tested here were specified to bind. In tandem with the lack of available antibodies that were raised specifically to Xcr1, these two reasons provided the premise for testing of these antibodies according to the potential cross reactivity to both homologues. Further justification arose from the published use of Abcam 188896 to determine Xcr1 expression within the Mouse spinal cord, despite being specified for the detection of Human XCR1 (Zychowska *et al.,* 2016).

4.4.1 Transient expression of XCR1 *homologues provide a reliable sample for validation of antibody specificity*

Initially, testing of antibody specificity was based upon reactivity to the Mouse spleen, for which the expression of Xcr1 has been previously documented (Dorner *et al.*, 2009). The testing of both LS-A158 and LS-C37380 aimed to provide evidence of specific binding to Xcr1 based upon the accepted method of demonstrating consistent reactivity between distinct antibodies (Michel, Wieland and Tsujimoto, 2009; Saper, 2009). This consistency

could then be used to support specificity to Xcr1 according to the stated specificity of LS-C37380 to Xcr1 by the manufacturer. Despite the stated specificity of LS-C37380 to Xcr1, a reactivity of the antibody that was consistent with Xcr1 detection could not be identified. This was also the case when evaluating reactivity by LS-A158. Instead, both antibodies demonstrated a large background of staining that was widespread within the tissue. The level of staining did correlate with the concentration of antibody, but qualitative comparison of antibody reactivity between the different concentrations did not achieve a refinement to antibody localisation, as would be expected for an antibody that targets a specific epitope. Despite this, there was no way of confirming that this lack of antibody reactivity was a consequence of poor antibody specificity or a lack of appropriate epitope availability according to the endogenous expression of Xcr1.

In response to this evidence it became clear that a reliable source of target protein was required to overcome the lack of reliability arising from the use of tissue sample to validate antibody specificity. To achieve this, a method was developed which utilised the transient transfection of HeLa cells to express XCR1-myc or Xcr1-myc, in line with recommendations provided for antibody validation (Bordeaux *et al.,* 2010; Saper, 2009) and which had been successfully used by prior studies to test the specificity of antibodies to other GPCRs (Grimsey *et al.*, 2008; Miyauchi *et al.*, 2009). This method was demonstrated to provide a reliable source of the target protein, the presence of which was confirmed via the use of a monoclonal anti-C-myc antibody using both immunocytochemistry and western blot protein analysis. Moreover, by expressing the target protein in mammalian cells, the target protein was subject to intracellular processing that resembles that experienced by the protein within cells *in situ.* This is an important consideration for the testing of antibodies to target proteins due to the impact of intracellular processing on protein conformation and hence epitope presentation.

The developed *in vitro* assay therefore provided distinct advantages over the use of tissue samples in that it provided a sample of target protein that could be simultaneously confirmed and localised by immunocytochemistry. In addition, the use of non-transfected cells served as a true negative control. This enables the confirmation of antibody specificity by both demonstrating the specific binding to the target protein and supporting a lack of non-specific binding to samples without expression of the target. This is in contrast to the use of tissue samples for which the signal obtained from an antibody is extremely difficult to determine as being a consequence of specific, on-target binding (Rhodes and Trimmer, 2006). An additional benefit is the variety of methods in sample processing that can be applied to the *in vitro* sample to mimic the intended application of the antibody for detection of antigen in tissue. This permitted the evaluation of all test antibodies by both Western Blot

and by immunocytochemistry with and without antigen retrieval treatment. This was a key consideration for the development of the *in vitro* HeLa transfection assay, as it provided a sample that could be processed in near identical conditions to that which the test tissue sample was subjected to. Use of other methods to test antibody specificity, such as flow cytometry, would require different sample preparation conditions and hence may lead to discrepancies of antibody behaviour when testing against tissue samples. Moreover, the use of double immunocytochemistry enables visual confirmation of colocalisation between the test antibody and the anti-tag antibody, thus supporting any antibody signal to arise from the specific detection of the target protein in transfected cells. In this project, the use of a monoclonal anti-C-myc antibody was demonstrated to provide a consistent and specific detection of the target protein. Use of an EGFP tag may provide a yet more reliable colocalisation signal, as has been performed elsewhere (Skogs *et al.*, 2017).

4.4.2 Methods of analysis to support antibody binding and specificity

To provide support of antibody binding and specificity it was sought to provide an objective and quantitative method of analysis to further support qualitative evidence. In using polyclonal antibodies that were not specifically designed for the detection of the XCR1 homologue to which it was being tested, there was the potential for the test antibodies to demonstrate specific binding but at a low affinity. This would result in a correspondingly low signal. Providing an accurate method to quantify and compare antibody binding was therefore important to deduce if the antibody sample contained only a small fraction of antibody clones that were capable of binding the target and hence identify a correspondingly small change in signal between transfected and non-transfected cells. Furthermore, there was potential for the anti-c-myc antibody to block the binding of the test antibody to the target protein when performing dual immunocytochemistry protocols due to the proximity of the potential epitopes and the C-terminal myc-tag. Therefore, for the results presented in this investigation that were collected following assessment by single immunocytochemistry only, the intention was to support any observed differences identified by quantitative analysis by subsequent evidence of colocalisation to anti-C-myc binding.

To provide the quantitative assessment of antibody binding, two methods were adopted. For both of these methods, normalisation to the associated non-transfected control was an essential measure to identify the specific impact of target protein expression on antibody binding. In addition it was essential to provide a measure of antibody binding that was proportional to cell presence. The first method of manual analysis achieved this by providing a proportional measure of antibody binding to the presence of DAPI. This method relied upon the correlation of DAPI presence to the number of cells present in the sample

and indeed demonstrated good correspondence in results when compared to manual cell counting. However, due to evaluation of global DAPI reactivity to the entire image, this method was sensitive to variation in the DAPI signal that may arise from components of the image that were not cell specific. Despite this, this method showed a consistent capacity to identify changes in anti-c-myc binding for all comparisons between transfected and non-transfected cells, supporting its use in providing quantitative evidence to support specific antibody binding when comparing between transfected and non-transfected cells.

In addition, the manual method of analysis showed strong consistency in identifying similar changes in antibody binding between non-transfected and transfected cells to that identified by automated analysis by the Opera Phenix™ High Content Imaging System. This method provided an analysis that made a greater refinement to the identification of cells within the image and was capable of imaging a much greater number of cells in comparison to that performed for manual analysis. Consequently, the variation of data from individual samples was much reduced and provided a more reliable comparison of antibody binding between transfected and non-transfected cells. Furthermore, this method offered the capacity to colocalise test antibody signal with the signal obtained from anti-C-myc binding. This feature proved valuable when analysing samples that, for unknown reasons, demonstrated particularly low transfection efficiency and target protein expression and provided a quantitative measure that related directly to specific binding of the test antibody to the target protein. Furthermore, it suits previous assessment criteria for the evaluation of antibody specificity to other GPCRs (Grimsey *et al.*, 2008).

4.4.3 Limitations to the Method of analysis for antibody binding between transfected and non-transfected cells

Regardless of the method of analysis used, the results collected were sensitive to both the efficiency of cell transfection and the variability of background signal within non-transfected controls. Due to the typically low signal obtained from non-transfected cells, even relatively small changes in background signal could lead to drastic changes in the differences in antibody binding between non-transfected and transfected cells when represented by normalised values. Similarly, a low transfection efficiency would result in mean antibody signals that were unable to reliably differentiate from non-transfected controls, due to the averaging of mean antibody signal from the entire image (manual analysis) or by total cell number (automated analysis). However, restricting the quantification of antibody signal to individual cells expressing the target protein according to C-myc reactivity, as achieved by automated analysis, did improve the tolerance to these limitations as only cell-specific signals contributed to the resulting data.

Antibody Antigen (Catalogue Number)	Specificity to Mouse Xcr1		Specificity to Human XCR1	
	Immunocytochemistry	Western Blot	Immunocytochemistry	Western Blot
Anti-XCR1 (LS-A158)	No (Section 4.2.3.1)	No (Section 4.2.5.1)	N/A	N/A
Anti-XCR1 (Abcam 188896)	No (Section 4.2.3.3)	No (Section 4.2.5.1)	No (Section 4.2.4.2)	N/A
Anti-XCR1 (HPA013169)	No (Data Not Shown)	No (Section 4.2.5.1)	Yes (Section 4.2.4.1)	Yes (Section 4.2.5.2)
Anti-Xcr1 (LS-C37380)	No (Section 4.2.3.2)	No (Section 4.2.5.1)	N/A	N/A
Anti-Xcr1 (cAb-Xcr1)	No (Section 4.2.3.4)	No (Section 4.2.5.1)	N/A	N/A

Table 4.1. *A summary of outcomes investigating antibody specificity to XCR1 and Xcr1 by immunocytochemistry and Western Blot.* All antibodies were tested against cell or protein samples containing Xcr1-myc or XCR1-myc, produced according to the *in vitro* HeLa transfection assay.

Taking these two limitations in to account provides some explanation as to the variation in antibody binding signal obtained for transfected and non-transfected cells when testing an antibody that clearly demonstrated no specificity to the expressed target protein. In these examples it would be expected that a non-specific antibody would demonstrate the same amount of binding, per cell, irrespective of transfection. Indeed, these limitations are why the majority of measures of antibody binding that were identified to be statistically significant were not considered to accurately reflect a change in antibody binding. Instead, these statistical differences, which were also of low magnitude, reflected a variation of normalised fluorescent signal obtained as a consequence of the limitations that were intrinsic to the methods used.

The use of stably-transfected cell lines would overcome the limitation of transfection efficiency, as demonstrated for the testing of antibodies to both human and mouse CB1 receptor homologues (Grimsey *et al.,* 2008). The use of cell lines stably-expressing a tagged target protein has also been recently used to validate the specificity of 197 antibodies (Skogs *et al.*, 2017). The results presented here therefore further support the requirement of achieving consistent levels of target protein expression by all cells for reliable antibody validation.

4.4.4 In vitro HeLa transfection assay as a method to support antibody specificity

Despite the limitations of this method, analysis of HPA013169 vividly demonstrated the capacity of this method to provide strong evidence to support antibody specificity to a target protein. Qualitative inspection of HPA013169 localisation in transfected and non-transfected cells alone, clearly illustrates an increase of antibody binding to transfected cells that demonstrates a subcellular localisation that is consistent with XCR1-myc expression by transfected cells. The difference in antibody binding as a consequence of antibody titer, as identified by manual image analysis, lacked clarity due to the method of evaluation relying upon signal normalisation to the corresponding non-transfected controls. Direct comparison of HPA013169/DAPI RawIntensity between transfected cell samples treated with 1µg/ml, 2.5µg/ml and 4µg/ml, however, clearly illustrated the dose-dependent increase in antibody binding consistent with a specific reactivity of the antibody. Further, and most conclusive, evidence of HPA013169 specificity was provided by the clear localisation of HPA013169 to specific cellular regions of XCR1-myc presence, as evidenced by colocalisation to regions of binding by the monoclonal anti-C-myc antibody.

The evidence of HPA013169 obtained by manual analysis was further supported by automated analysis. As observed for the manual analysis, the results from the automated analysis provided clear evidence of: i) XCR1-myc expression by cells transfected with RC221929 as evidenced by the increase in Mean cell anti-C-myc binding ; ii) a relative

quantitative increase of HPA013169 binding to cells transfected with RC221929 in comparison to non-transfected cells that was consistent when used as part of both single and double immunocytochemistry protocols; and iii) a quantitative increase in HPA013169 signal intensity within specific image regions that correspond to the expression of XCR1-myc within transfected cell populations.

However, it should be noted that a higher amount of background signal was observed for HPA013169 in some samples of non-transfected cells. This background signal appeared when using a separate vial of the antibody to that used for manual analysis. Although from the same lot of antibody, this does call in to question whether this antibody demonstrates non-specific binding when used for immunocytochemistry. Indeed, although HPA013169 demonstrated the capacity to bind to the XCR1-myc protein by western blot, an additional band could also be observed following prolonged exposure. Therefore, whilst providing evidence of HPA013169 to reliably bind to XCR1, this analysis suggests that this antibody may also bind off-target epitopes, albeit with lower affinity.

4.4.5 A lack of available antibodies specific to Mouse Xcr1

Other results from this analysis however, failed to demonstrate the specificity of any other of the tested antibodies. Although the specificity of these antibodies to the XCR1 homologues tested here was not necessarily expected due to the inconsistency between the stated and tested target proteins (discussed above), two antibodies (LS-C37380 and Abcam188896) did not demonstrate specificity to the protein stated by the vendor. In addition, the specificity of a custom-designed antibody to Xcr1 could not be supported. This is despite clear evidence of specific recognition by this custom antibody to the target immunogen by ELISA. In sum, no evidence was provided to support the specificity of any of the five antibodies tested, by both immunocytochemistry and western blot, to Xcr1.

This lack of available antibodies has provided an obstacle to future investigations of Xcr1 presence in the Mouse CNS as it has not been possible to reliably determine the presence and localisation of Xcr1 protein *in situ*. Preliminary attempts were made to use LS-A158 within the mouse CNS and here it was observed that the reactivity from LS-A158 demonstrated widespread reactivity, particularly within the grey matter of spinal cord. Double immunohistochemistry suggested colocalisation of LS-A158 binding to NeuN-positive neurons within both thoracic and sacral regions. However, as evidenced by the *in vitro* assay of LS-A158, this antibody demonstrated large background staining that was observed for both transfected and non-transfected HeLa cells. Therefore, in addition to the lack of evidence for LS-A158 specificity to Xcr1, the background signal identified in spinal cord sections suggests that this antibody exhibits promiscuous binding to multiple cellular

epitopes. Consequently, the signal observed from LS-A158 in the mouse spinal cord could not be supported in any way to represent the localisation of Xcr1.

Furthermore, the specificity of Abcam 188896 to Xcr1 was not supported by this investigation and calls in to question the current evidence of Xcr1 presence within the mouse spinal cord (Zychowska *et al*., 2016). Assessment of this antibody by the *in vitro* HeLa transfection assay also failed to demonstrate specificity of Abcam 188896 to XCR1. This is the protein for which the manufacturer has claimed specificity. According to the results presented here however, this antibody does not provide a reliable or specific recognition of either Human or Mouse XCR1 homologues.

It is noteworthy to add that there are several other sources of anti-Xcr1 antibodies available, for example a monoclonal anti-mouse/rat Xcr1 antibody is now available from Biolegend and has been extensively tested for specificity using flow cytometry. Use of the *in vitro* HeLa transfection assay described here would provide a useful validation to test the specificity of this antibody to mouse Xcr1 following IHC and ICC protocols.

4.4.6 Summary

A primary objective of this project was to identify if Xcr1 was expressed in the mouse CNS. An essential requirement for this objective is the use of reagents that provide a reliable and specific measure of Xcr1 presence. In line with previous (Michel, Wieland and Tsujimoto, 2009; Bordeaux *et al.*, 2010; Saper, 2009) and current (Skogs *et al.,* 2017) recommendations, a method was established to utilise the expression of tagged target proteins for the evaluation of antibody specificity. This method was found to provide a reliable source of target protein that could be used to assess antibody binding to both native and denatured conformations. Via the application of this method, it has not been possible to identify any antibody that demonstrates specificity to Mouse Xcr1. However, it has provided validation for the use of HPA013169 for the detection of Human XCR1 by both immunohistological and Western Blot protein analyses. This evidence has provided the basis to perform immunohistochemical detection of XCR1 within the Human spinal cord and gives credence to any identified reactivity of this antibody to be a result of the specific detection of XCR1.

Chapter 5: Investigation of Xcr1 and Xcl1 expression in Amyotrophic lateral sclerosis

5.1 Introduction

As suggested by previous investigation (Zychowska *et al.*, 2016; Bird *et al.*, 2018) the expression of Xcr1 and Xcl1 within the CNS is likely modulated by the presence of inflammation. Therefore, to provide an assessment of Xcr1 and Xcl1 expression within the context of a disease that demonstrates a prominent central inflammatory response, this study has evaluated *Xcr1* and *Xcl1* expression within mouse models of Amyotrophic Lateral Sclerosis (ALS). In addition, based on the success of antibody validation to detect human XCR1, a preliminary investigation has been made in to the expression of XCR1 within the spinal cord of human subjects.

5.1.1 Amyotrophic Lateral Sclerosis

ALS, also known as Motor Neuron Disease (MND), is a progressive neurodegenerative disorder that is typically fatal within 3-5 years of diagnosis. The disease was originally described in the late 19th century by Jean-Martin Charcot and was so named according to the observed muscle wastage (amyotrophic) and scarring of the lateral spinal tracts (lateral sclerosis) in post-mortem patient tissue. The disease presents an incidence of between 1-3 persons per 100,000 people per year with an estimated prevalence of disease to be 5 per 100,000 people (Al-Chalabi and Hardiman, 2013; Taylor, Brown and Cleveland, 2016), statistics which vividly illustrate the rapid fatality of the disease.

ALS is characterised by the loss of lower motor neurons within the ventral horn of the spinal cord with concomitant degeneration of descending corticospinal tracts that arise from upper motor neurons that reside within layer V of the primary motor cortex. The primary bias of pathology can vary between upper and lower motor neurons, resulting in variability of initial symptom presentation. Primary degeneration of upper motor neurons is associated within increased limb tone, hyperreflexia and spasticity; degeneration of lower motor neurons is associated with muscle weakness and reduced voluntary muscle control. Hence, the disease presents with a variable focus of onset that is typically classified as spinal or bulbar-onset and is associated with symptoms of the body innervated by these respective regions (Al-Chalabi and Hardiman, 2013). Irrespective of the focus of disease onset, ALS results in the contiguous transmission of disease throughout the CNS (Ravits, Paul and Jorg, 2007). The resultant fatality of ALS is most commonly a consequence of motor neuron degeneration within the brainstem, leading to difficulties in speaking, swallowing and breathing that ultimately leads to respiratory failure.

ALS has been broadly categorised as sporadic (sALS) and familial ALS (fALS) to reflect the presence or absence of inheritability. Approximately 10% of ALS cases exhibit transmission

within families, whilst the majority of cases occur sporadically (Ling, Polymenidou and Cleveland, 2013). However, this categorisation has sometimes been confused with the presence or absence of a genetic causation to the disease. Since the discovery of mutations in the *SOD1* gene to cause ALS (Rosen, 1993), there are now more than 100 identified genomic loci that associate with the disease (alsod.iop.kcl.ac.uk). Whilst a causative link between all of these loci and the disease is not yet present ALS is now considered to arise from a complex interaction between genetic and environmental factors, with a predisposing genetic vulnerability considered essential to the precipitation of the disease.

5.1.2 ALS pathology

The pathological mechanisms of ALS are varied and only beginning to be elucidated. This is due to the relatively recent discovery of a key pathological hallmark of the disease, relating to the aggregation of the Transactive response DNA binding protein 43kDa (TDP-43) protein, and the capacity of contemporary techniques to illuminate the genetic underpinnings of the disease. Indeed, over the past decade, a tremendous progress has been made in the understanding of ALS. The associated pathological mechanisms are diverse and include: dysregulation of RNA processing; prion-like protein misfolding and aggregation; oxidative stress; defective autophagy, protein degradation and ER stress; exicitotoxicity; dysfunctional axonal transport; mitochondrial abnormalities; and neuroinflammation (for excellent reviews see e.g. (Barber and Shaw, 2010; Ferraiuolo *et al.*, 2011; Ilieva, Polymenidou and Cleveland, 2009; Ling, Polymenidou and Cleveland, 2013; Taylor, Brown and Cleveland, 2016).

Previous to the identification of TDP-43-positive inclusions, the major understanding of ALS revolved around investigations relating to Cu^{2+}-Zn^{2+}-Superoxide Dismutase (SOD1). SOD1 is a cytoplasmic antioxidant enzyme that catalyses the reduction of superoxide metabolites. In 1993, mutations of the *SOD1* gene, including that leading to a G>A mutation at position 93 of the SOD1 protein, was identified to associate with ALS (Rosen, 1993). The mechanistic link between mutations of SOD1 and ALS is still unclear, but is suggested to arise independent to the dismutase activity of the enzyme. The pathological consequences of mutant SOD1 is instead associated with a toxic gain of function which, among other suggestions, includes the misfolding of mutant SOD1 protein and the formation of ubiquitinated aggregates that accrue with the progress of disease (Bruijn *et al.*, 1998; Banci *et al.*, 2008). Importantly, aggregations of SOD1 protein have so far not been observed to occur in patients without *SOD1* mutation and represents a specific component to such mutations (Mackenzie *et al.*, 2007). Moreover, the pathology caused by mutations in *SOD1* is almost exclusively associated with upper and lower motor neurons unlike that observed for other genetic mutations (Joyce *et al.*, 2015). Mutations of the *SOD1* gene demonstrate an

extremely high penetrance in causing ALS and account for approximately 20% of fALS cases (Rosen, 1993).

The recognition that TDP-43, a protein arising from the *TARDBP* gene, is present within neuronal and glial cytoplasmic inclusions (Neumann *et al.*, 2006) has prompted an altogether different understanding of the pathology of ALS. TDP-43 inclusions are estimated to occur in 97% of all ALS cases, with the remaining 3% of cases demonstrating aggregations of SOD1 and Fused-in Sarcoma (FUS) protein (Ling, Polymenidou and Cleveland, 2013). Moreover, mutations of *TARDBP* have now been identified to cause ALS (Sreedharan *et al.*, 2008). Thus, the *TARDBP* gene and its translated protein contribute to the major convergent pathology observed in the vast majority of ALS cases. Furthermore, the aggregated presence of either TDP-43 or other proteins (including SOD1) support the capacity for distinctive pathophysiology to cause ALS.

TDP-43 is an RNA binding nuclear factor that contributes to the processing and alternative splicing of numerous mRNAs (Sephton *et al.*, 2012). Mutations have been identified throughout the protein which are associated with causing ALS (alsod.iop.kcl.ac.uk). Importantly, *TARDBP* mutations can also result in inclusion body myopathy (IBM) and frontotemporal dementia (FTD), with aggregations of TDP-43 also being a pathological hallmark of these diseases (Salajegheh *et al.*, 2009; Neumann *et al.*, 2006). This observation, along with growing characterisation of the molecular pathology associated with these diseases, suggests that some forms of ALS represent a spectrum of disease. Indeed, the presence of ALS symptoms is often observed in conjunction with symptoms of FTD. Furthermore, post-mortem assessment has demonstrated the concomitant presence of TDP-43 pathology more widely within the brain including frontal, temporal and limbic regions, alongside that observed within the motor system for some ALS patients (Cooper-Knock *et al.*, 2012).

A further seminal discovery in the understanding of ALS, was the identification of a hexanucleotide repeat expansion within a non-coding region of *C9ORF72* to cause ALS, FTD, or both (C9-ALS/FTD) (DeJesus-Hernandez *et al.*, 2011). The presence of this expansion is suggested to account for a significant proportion of patients suffering from ALS and FTD, with one study demonstrating 40% of fALS, 25% of familial FTD, 7% of sALS and 6% of sporadic FTD cases to arise from this mutation (Majounie *et al.*, 2012). The function of C9orf72 is currently unclear, but C9-ALS/FTD is suggested to be a consequence of a toxic gain of function that results in repeat associated non-AUG (RAN)-translation of dipeptide repeats, formation of RNA foci and the sequestration of RNA binding proteins (DeJesus-Hernandez *et al.*, 2011; La Spada and Taylor, 2010; Mori *et al.*, 2013) as well as the potential for age-related disturbances to microglial activation (O'Rourke *et al.*, 2016). Like the

majority of other genetic mutations linked with ALS, TDP-43 neuronal and glial cytoplasmic inclusions are evident within the CNS of patients expressing a pathological C9ORF72 hexanucleotide expansion.

The consistency of TDP-43 pathology has led to the proposal that for the majority of ALS cases, irrespective of the underlying genetic mutation, a disruption to the function of this protein is a cornerstone of ALS pathology. Both *in vitro* and *in vivo* studies have demonstrated the maintenance of TDP-43 expression to a specific level to be essential to cell viability and the integrity of motor function in animal models (Wils *et al.*, 2010; Johnson *et al.*, 2008). The reason for this is suggested to relate to the phase-separation of TDP-43 and associated proteins. When bound to RNA, TDP-43 and associated RNA binding proteins coalesce and form membraneless organelles within the surrounding media. The phase separation of such structures is positively correlated with the concentration of associated proteins and arise from the interaction of low-complexity domains of RNA binding proteins. The most common ALS-associated mutations in *TARDBP* occur within coding regions of TDP-43 low complexity domains, with a much lower frequency of ALS-associated mutations found within in other domains (Chiang *et al.*, 2016). Thus, the formation of TDP-43 inclusions can be envisaged to occur either as a consequence of mutations within the low complexity domain or from mutations in which the nuclear localisation of the protein is disrupted. Such mutations would therefore promote the phase separation and subsequent fibrillisation of TDP-43 and associated RNA binding partners either as a consequence of increasing the endogenous capacity for this or by generating an excessive cytoplasmic concentration that results in precipitation of aggregates (Taylor, Brown and Cleveland, 2016). Moreover, these mutations may not be necessary within TDP-43 itself but instead within the proteins with which TDP-43 interacts. A similar mechanism may also be evident for other proteins, as mutation within the low complexity domains of other RNA binding proteins such as FUS and hnRNP-A1 results in ALS and IBM (Shang and Huang, 2016). Why TDP-43 represents the predominant protein identified within inclusions will require further characterisation of its binding partners and also of the RNA species that it processes. However, it is becoming apparent that a number of ALS-associated genes are processed by TDP-43 (White *et al.*, 2018).

In summary, examination of TDP-43 biology illustrates several concepts that are associated with ALS pathology, namely dysregulation of RNA processing and the prion-like formation of protein aggregates. The multitude of associated pathologies likely reflect the downstream consequences of these initial factors which manifest within the unique environment of the CNS. It is important to recognise that, although leading to the aggregation of a distinct protein, mutations in *SOD1* also recapitulate many of the pathologies observed in patients

that display TDP-43 pathology. However, a major distinction appears to arise from the prevalent role of TDP-43 in RNA processing, for which SOD1 is not involved.

5.1.3 Inflammatory and non-cell autonomous mechanisms of ALS

A unanimous feature of ALS is the activation of resident microglia and astrocytes and the recruitment of peripheral immune cells to sites of degeneration within the CNS. In addition to the cell autonomous mechanisms of disease exemplified by TDP-43 pathology discussed above, the contribution of non-cell autonomous mechanisms to the loss of motor neurons is an essential feature of ALS pathology.

Seminal work to demonstrate this was achieved by the generation of chimeric mice, in which mutant *SOD1* was heterogeneously expressed by cells throughout the animal. It was observed that the presence of mutant *SOD1*-expressing non-neuronal cells could induce SOD1 pathology within adjacent wild-type neuronal cells. Conversely, mutant *SOD1*-expressing neuronal cells demonstrated limited signs of pathology and survived much longer when surrounded by wild-type non-neuronal cells (Clement *et al.*, 2003).

Subsequent work has since refined this evidence and demonstrated the essential role of non-neuronal cells to the onset and progression of neurodegeneration. In particular, it is evident that the activation and/or dysfunction of surrounding microglia, astrocytes and oligodendrocytes drives the progression of the disease (Boillee, Vande Velde and Cleveland, 2006; Yamanaka *et al.*, 2008; Frakes *et al.*, 2014; Ferraiuolo *et al.*, 2011). These cells contribute to the loss of motor neurons by reducing trophic support (Hughes *et al.*, 2013), enhancing excitoxicity and the release of soluble toxic factors (Di Giorgio *et al.*, 2008; Haidet-Phillips *et al.*, 2011; Frakes *et al.*, 2014) . These include pro-inflammatory molecules that exacerbate the inflammatory response, as well as highly reactive oxidative species (Barber and Shaw, 2010; Hensley *et al.*, 2006). It is important to recognise that the phenotype adopted by these glial cells is specific to the presence of disease (Chiu *et al.*, 2013; Phatnani *et al.*, 2013). The functions and expression profiles of these cells are therefore intricately related to the surrounding environment and cannot be easily categorised according to models of polarised states of activation.

In addition to glia, peripheral immune cells are also recruited to sites of pathology (Henkel *et al.*, 2004). These cells play diverse roles dependent on the stage of disease. For example, regulatory T-cells (T_{Reg}) are indicated to down regulate glial activation and promote the expression of immunomodulatory cytokines and neurotrophic factors (Beers *et al.*, 2008; Mantovani *et al.*, 2009) and support neuronal function during early stages of disease. As the disease progresses however this adaptive immune response contributes to neuronal loss and decreased survival following the recruitment of phagocytic and cytotoxic cells, as well

as intercellular signalling pathways, such as that mediated by TNF-α, decreasing cellular viability (Henkel *et al.*, 2004; Phani, Re and Przedborski, 2012; Mantovani *et al.*, 2009). Moreover, the recruitment of peripheral immune cells contributes to the adoption of specific activation states by resident glial cells in a mutant *SOD1* mouse model. Specifically, there appears to be a distinction in the time and activity of CD4+ and CD8+ T cells, in which the recruitment of CD4+ T-cells during disease onset and progression appeared to confer a protective role for neuronal survival via the modulation of microglial and astrocyte activation. The recruitment of CD8+ T-cells was instead observed at the end-stage of disease only and suggested to be associated with neuronal injury (Beers *et al.*, 2008).

5.1.4 The role of chemokines in ALS

Specific roles pertaining to the pathology of ALS by chemokines has not been demonstrated. However, there has been little focus of their role in the disease. One method that has sought to provide an insight to the role of cytokines in the disease, and overcome the limitations of tissue access during the disease progression, has been to assess the presence of cytokines within the blood of ALS patients. A recent meta-analysis of these studies compared the expression of 14 inflammatory cytokines between 812 ALS patients and 639 controls (Hu *et al.*, 2017). This indicated a consistent increase of TNF-α, CXCL8, VEGF, IL-1β and IL-6. Elevations of TNF-α, IL-1β and IL-6 appear to be ubiquitous to neurodegenerative disease as they are also observed to be elevated in the blood collected from patients with Alzheimer's (AD) and Parkinson's Disease (PD). In contrast, CXCL8 demonstrated consistent and robust differences to controls across several studies of ALS patients. Interestingly, CXCL8 elevations also appear to be unique to ALS in comparison to AD and PD samples (Qin *et al.*, 2016), suggesting CXCL8 to reflect a specific component to the inflammatory response in ALS (Hu *et al.*, 2017).

With the exception of CCL2 and its receptor CCR2, there has been minimal investigations to the contribution of chemokines and their receptors to the pathology of ALS within the CNS parenchyma. CCL2 is considered the principal chemotactic protein for the recruitment of monocytes and its expression by cells of the CNS is observed only in response to inflammation. Specifically, the upregulation of CCL2 by glial, endothelial and neuronal cells is observed in the spinal cords of ALS patients (Baron *et al.*, 2005; Henkel *et al.*, 2004) and is considered a component of the innate immune response to the onset of ALS (Jara *et al.*, 2017). Indeed, the increased expression of Ccl2 is observed as early as postnatal day 15 in a mutant *SOD1* mouse model (Henkel *et al.*, 2006) and contributes to the significant migration of peripheral immune cells that accumulate within the spinal cord and motor cortex as the disease progresses (Jara *et al.*, 2017). Moreover, CCL2 levels are elevated

within the CSF and serum of ALS patients in comparison to control samples (Baron *et al.*, 2005; Henkel *et al.*, 2004).

5.1.5 A potential role for XCR1 and XCL1 in ALS

To the best of our knowledge, there has been no documented evidence for the contribution of XCR1 or XCL1 to the pathology of ALS. However, ALS demonstrates a consistent neuroinflammatory response irrespective of the underlying aetiology. This is characterised by a pronounced activation of resident glial cells and the recruitment of peripheral immune cells, including dendritic cells (Henkel *et al.*, 2004).

According to the previous observations of our group (Bird *et al.*, 2018) XCR1 and XCL1 may participate in the central inflammatory response to peripheral nerve injury. Moreover, it has been suggested that the production of Xcl1 by activated microglia in a mouse model of diabetic neuropathy may contribute to the pathological hyperalgesia and allodynia observed in model animals through intercellular communication with resident neurons (Zychowska *et al.*, 2016). As such, the pathophysiology of ALS lends itself to the previous suggestions of XCR1 and XCL1 function in the CNS in that it presents a disease in which there is significant damage to central neurons and their efferent axons that is accompanied by the consistent and prolific activation of resident glial cells.

In this study, we sought to evaluate the expression of *Xcr1* and *Xcl1* within the CNS using two distinct mouse models of ALS. The first, and primary model used (referred to as the TDP-Q331K model), represents a recently characterised mouse colony (Arnold *et al.*, 2013) that expresses a mutant *TARDBP* under the transcriptional control of the mouse prion promoter within a C57BL/6NJ genetic background. This mutation results in the substitution of glutamine (Q) to lysine (K) at position 331 of the TDP-43 protein and was detailed to be expressed with a copy number of 3 in transgenic mice. This model therefore represents the expression of mutant *TARDBP* primarily within motor neurons and astrocytes at an expression level that was aimed to more closely reflect endogenous expression levels of the gene. Previous to this study, these mice were demonstrated to exhibit several pathologies that reflected that observed in ALS patients, including widespread alterations to gene expression and mRNA splicing, motor neuron and motor axon loss and glial activation. However, the disease course of this model is comparatively mild to that observed from other models, with symptom severity reaching a plateau at ~10 months of age (Arnold *et al.*, 2013). Throughout the course of this project, available tissue was collected from and alongside the ongoing characterisation of the model by Dr Jodie Stephenson (University of Sheffield).

Samples were also collected from a second model which utilises overexpression of *SOD1*^{G93A} by an inbred C57BL/6 mouse colony (referred to as the SOD1-G93A model) (Mead *et al.*, 2011). This model demonstrates a comparatively rapid and aggressive disease course and has been extensively characterised by numerous groups, including those located at the University of Sheffield under the supervision of Dr Richard Mead and others. As observed for patients with this mutation, the SOD1-G93A model demonstrates extensive motor neuron loss, SOD1 aggregation and glial activation.

5.1.6 Aims

In accordance with the objective of this project to identify and characterise the expression of Xcr1 and Xcl1 within the mouse CNS, this study aims to evaluate the expression of *Xcr1* and *Xcl1* within the spinal cord of control, TDP-Q331K and SOD1-G93A mice. Furthermore, primary microglial cultures were prepared from TDP-Q331K and SOD1-G93A mice in order to evaluate the expression of *Xcl1* within microglia, in line with the suggestions proposed by Zychowska *et al*. By utilising these models with a contrasting genetic underpinning it was aimed to capture the expression of *Xcr1* and *Xcl1* across a spectrum of pathophysiology that reflects that observed in ALS.

In line with previous suggestions that Xcr1 and Xcl1 expression in the CNS is influenced by an inflammatory stat, a key pathology to examine within the mouse models used was the presence of activated glial cells. In particular, examination of microglial activation according to Iba-1 reactivity and morphology (Beynon and Walker, 2012) was performed. This was key to identify any association between microglial activation and Xcr1 and Xcl1 expression, as these cells were suggested to represent the key source of Xcl1 in a mouse model of diabetic neuropathy (Zychowska *et al.,* 2016).

In light of the failure to obtain a reliable antibody to determine Xcr1 expression (Chapter 4), characterisation of Xcr1 protein localisation within the CNS of mice has not been possible. However, based on the success of identifying a reliable antibody for the detection of human XCR1, a preliminary investigation of XCR1 expression has been performed using spinal cord samples obtained from ALS patients and neurological controls. This study has therefore aimed to provide an insight to the expression of XCR1 and XCL1 within the CNS of mouse and man and identify any potential contributions of this chemokine signalling axis to the pathophysiology of ALS.

5.2 Results

5.2.1 Xcr1 and Xcl1 expression: Mouse Models of ALS

As has been observed for other chemokines within the CNS, should Xcr1 and Xcl1 be expressed by resident cells of the CNS parenchyma, the presence of an inflammatory response is likely to influence their expression. By utilising the TDP-Q331K and SOD1-G93A models, it was aimed to assess the expression of *Xcr1* and *Xcl1* at the level of mRNA in the context of a central inflammatory response. Samples of thoracic cord from each of the models were collected and processed for the detection of Iba-1 and GFAP in order to assess the response of resident microglia and astrocytes test for the presence of central inflammation. RNA samples were also collected from whole spinal cord and assessed by qPCR for the presence of *Xcr1* and *Xcl1* transcripts.

5.2.1.1 Glial reactivity within thoracic cord of ALS mouse models

The thoracic region of the spinal cord represents the largest subdivision of the spinal cord vertebrae. In mice there are 13 thoracic cord segments. In comparison to the cervical and lumbar enlargements of the spinal cord, comparatively little investigation of the thoracic cord has been made within mouse models of ALS. This is primarily due to the more obvious pathology of lower motor neurons within the cervical and lumbar regions that innervate the forelimbs and hindlimbs, respectively. Due to the collection of the lumbar and cervical regions for other projects, thoracic cord was used to characterise glial reactivity within the spinal cord of the mouse models used here. To do this, double immunohistochemistry to detect the reactivity of microglia and astrocytes using Iba-1 and GFAP, respectively, was performed according to the protocol described in section 2.1.3.2.

5.2.1.1.1 Glial reactivity within the thoracic cord of 6 month TDP-Q331K and NTg mice

For the analysis of TDP-Q331K mice, thoracic cord was collected from mice at age 6 months and 10 months, along with the same sample from age-matched controls. For each characterisation it was aimed to evaluate glial reactivity using at least 3 NTg and 3 TDP-Q331K mice. C-myc reactivity of each cord was also evaluated to confirm the expression of myc-tagged Human TDP-Q331K within transgenic animals.

Analysis of thoracic cord from NTg and TDP-Q331K mice demonstrates the consistent localisation of TDP-Q331K expression within neurons throughout the grey matter and white matter of the thoracic cord. This is in accordance with the expected expression of human TDP-Q331K within neurons and astrocytes of transgenic TDP-Q331K mice. A representative example of this is demonstrated for mice aged 6 months (Figure 5.2.1) in which no such C-myc reactivity is observed for NTg mice.

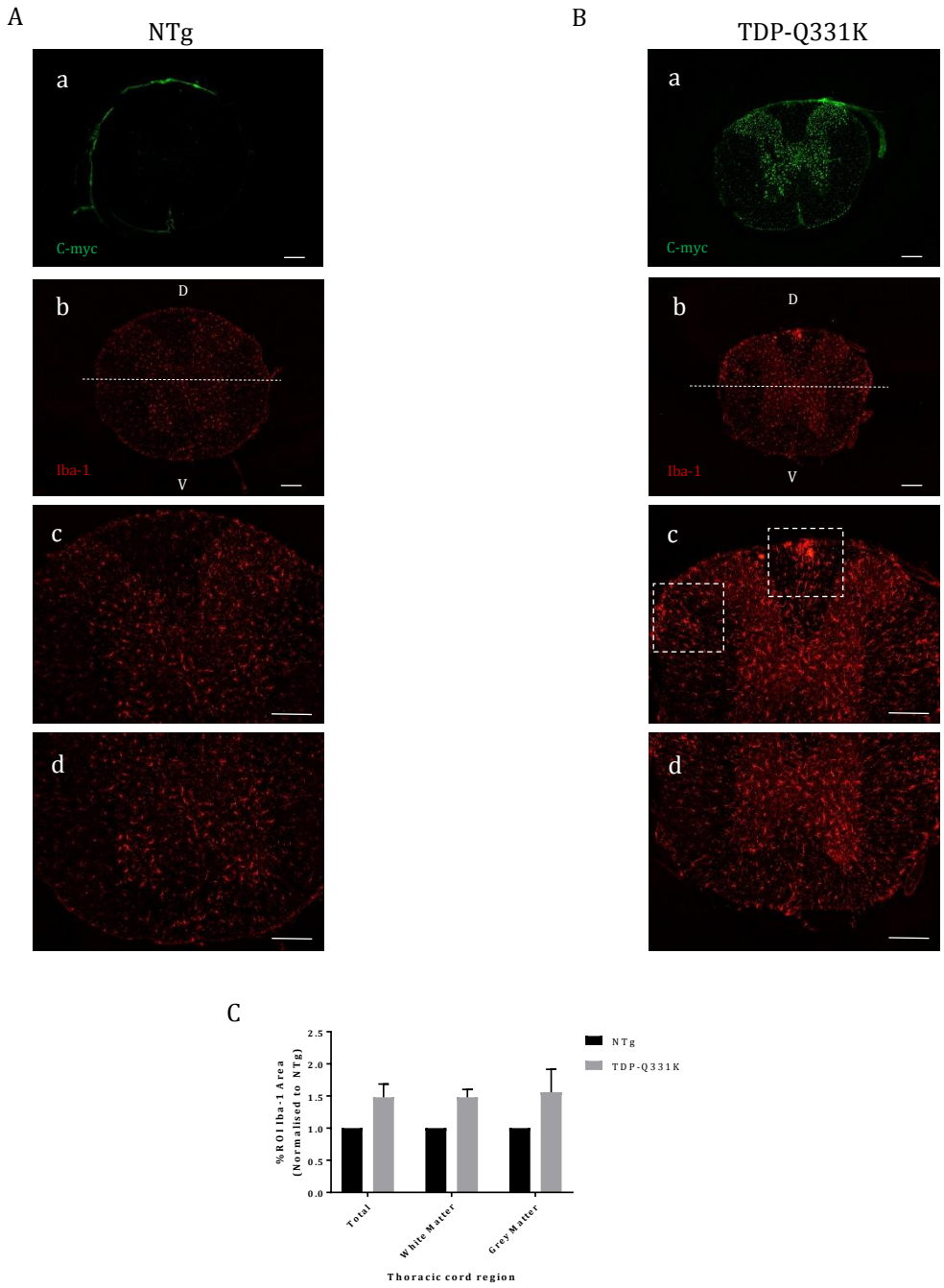

Figure 5.2.1. *Iba-1 reactivity in the thoracic cord of NTg and TDP-Q331K at age 6 months.* Representative images of Iba-1 reactivity in the thoracic cord of NTg (A) and TDP-Q331K (B) mice at age 6 months. Images display C-myc (a) and Iba-1 (b) reactivity of entire coronal thoracic cord section. White dashed line of (b) used to identify dorsal and ventral regions of thoracic cord. Higher magnification of dorsal (c) and ventral (d) regions of thoracic cord. White dashed boxes in B (c) highlight prominent regions of Iba-1 reactivity that are distinct from that observed in NTg. Scale bars = 200μm. C) Semi-quantitative comparison of Iba-1 area of reactivity in thoracic cord. Iba-1 area increases proportionally in both white and grey matter regions for TDP-Q331K mice, relative to NTg (NTg, n = 1; TDP-Q331K, n = 3). Error bars = ±SD.

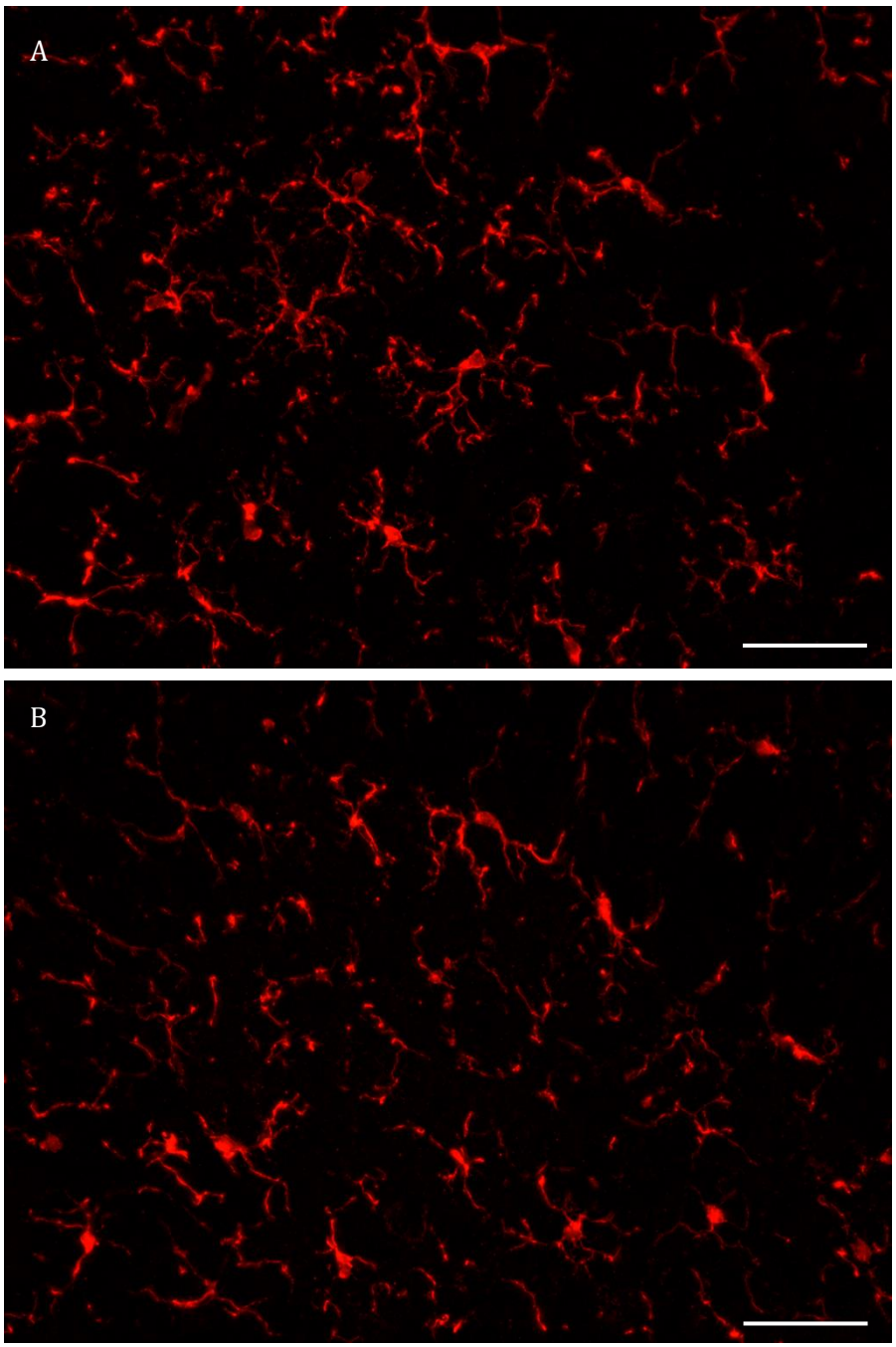

Figure 5.2.2. *Iba-1 reactivity in the ventral horn of a female NTg* (A) *and Q331K* (B) *mouse at 6 months.* Images are a 30µm Z-stack composed of 30 images taken at an interval of 1µm. Scale bars = 50µm.

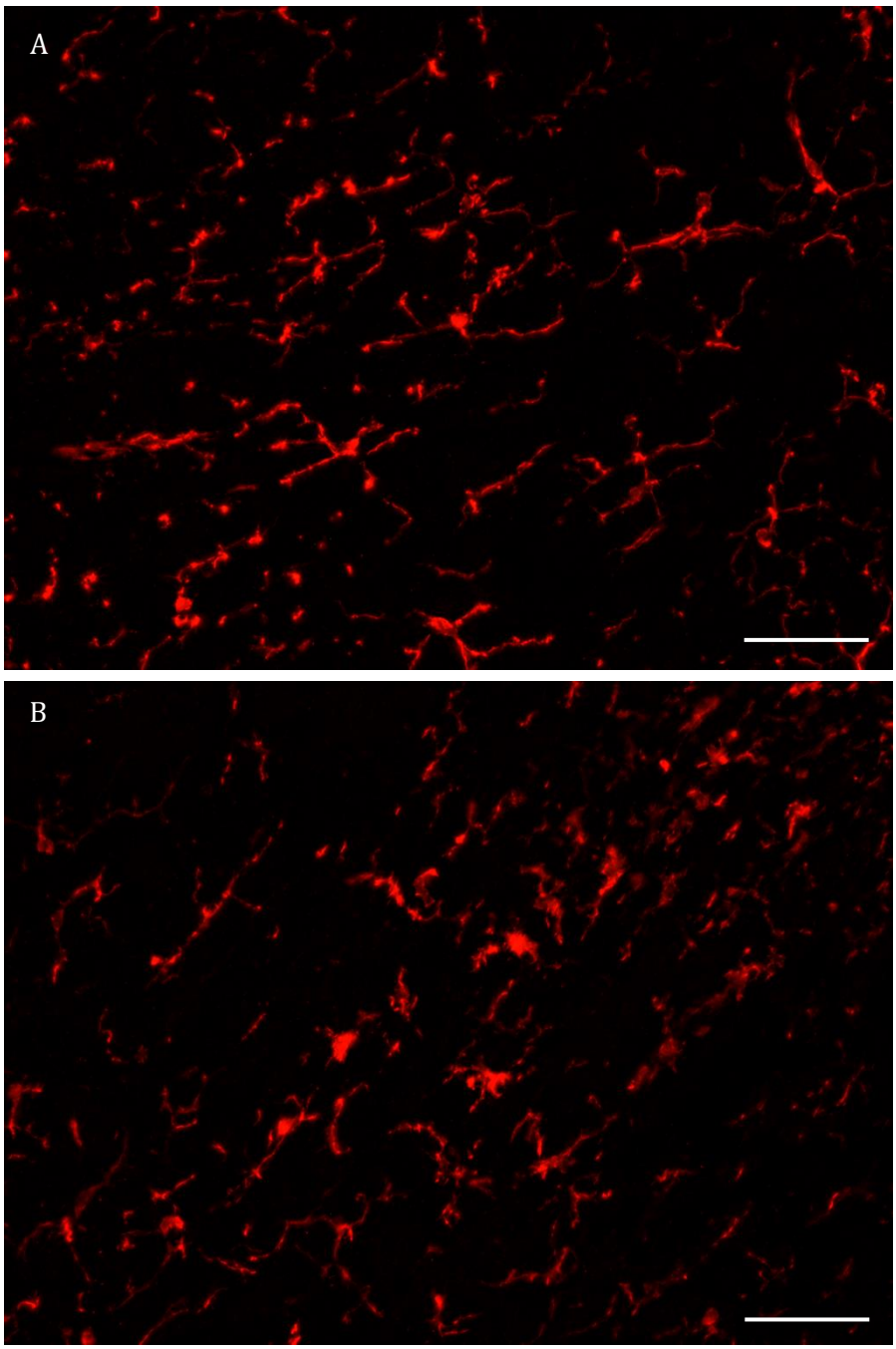

Figure 5.2.3 *Iba-1 reactivity in the lateral white matter of a female NTg* (A) *and Q331K* (B) *mouse at 6 months.* Images are a 30μm Z-stack composed of 30 images taken at an interval of 1μm. Scale bars = 50μm.

Iba-1 reactivity demonstrated a uniform distribution throughout the thoracic cord of NTg animals, and identified the homogeneous presence of ramified microglial cells across the entire thoracic cord region. In contrast, Iba-1 reactivity in TDP-Q331K animals demonstrated an enhanced level of reactivity and also detected the presence of distinct sites of reactivity increase. This was most prominent within the dorsal and lateral regions of the thoracic cord white matter. In addition, the morphology of Iba-1 positive cells within the grey matter of cord becomes more constricted, demonstrating processes which are thicker and more compact in comparison to those observed from NTg mice (Figure 5.2.2 and 5.3.3).

The enhanced reactivity of microglia is supported by quantification of Iba-1 area across the thoracic cord. For this analysis, 6 sections of thoracic cord were analysed from 3 TDP-Q331K mice and 1 NTg mouse. Collection of three NTg mice was performed but Iba-1 reactivity could not be determined from 2 of these mice due to disruption of thoracic cord integrity. In comparison to the NTg mouse, Iba-1 area is increased across the entire thoracic cord of TDP-Q331K mice by an average of 49%. This increase is consistent within both white (55%) and grey matter (48%) regions, supporting the global activation of microglia within the spinal cord of TDP-Q331K mice at 6 months of age.

To provide an indication of how microglial activation occurs throughout the entire spinal cord, Iba-1 reactivity along the entire rostral-caudal axis of thoracic cord was analysed at intervals of 180μm for a 6 month TDP-Q331K mouse. The increased Iba-1 reactivity seen within the dorsal region of thoracic cord in figure 5.2.1 (B, b) was observed for every section. Reactivity in the lateral regions however was less consistent and observed more prevalently within some sections than others, suggesting distinct regions of microglial activation within lateral regions of the white matter.

5.2.1.1.2 Glial reactivity within the thoracic cord of 10 month TDP-Q331K and NTg mice

As performed for 6 month mice, Iba-1 reactivity was assessed in 10 month TDP-Q331K and NTg mice to evaluate microglial activation. In addition, GFAP reactivity was also analysed to evaluate the activation of astrocytes (Figure 5.2.4).

As observed for mice at 6 months of age, TDP-Q331K mice demonstrate Iba-1 reactivity that is indicative of the global activation of microglia. In comparison to NTg mice, Iba-1 reactivity was observed to be increased and this was particularly evident in white matter regions (Figure 5.2.6) in comparison to grey matter regions (Figure 5.2.5). Distinct to NTg mice, TDP-Q331K mice demonstrated increased Iba-1 reactivity predominantly within dorsal and lateral regions of the white matter. This is associated with the presence of numerous, highly reactive cells that exhibit a contracted morphology (Figure 5.2.6).

A

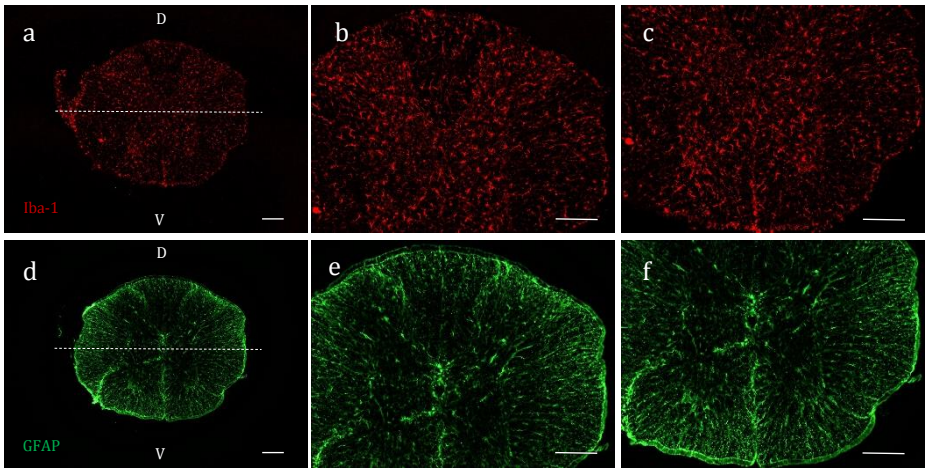

B

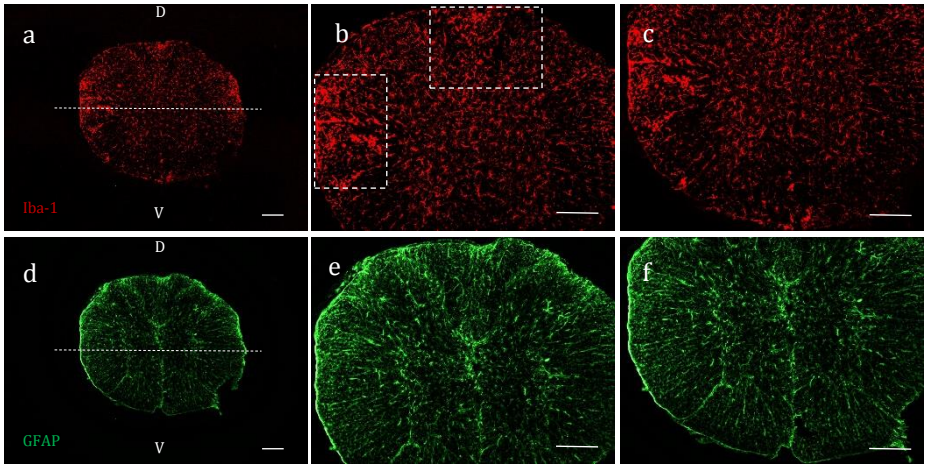

C

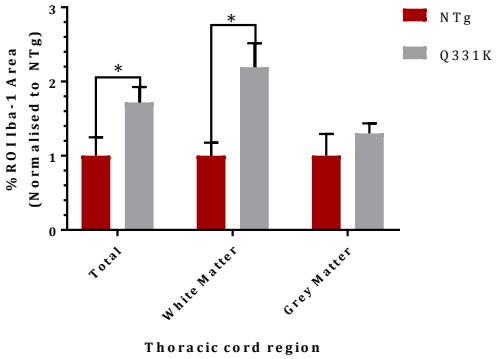

D

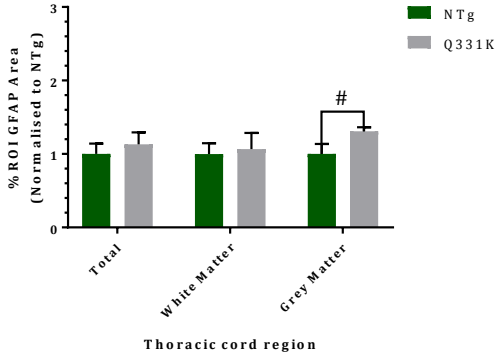

Figure 5.2.4. *Glial reactivity within the thoracic cord of NTg and TDP-Q331K mice at 10 months.* Iba-1 (red) and GFAP (green) reactivity were used to identify microglia and astrocytes, respectively, in thoracic cord of NTg (A) and TDP-Q331K (B) mice at 10 months of age. White dashed line in a and d used to distinguish Dorsal and Ventral regions of thoracic cord. Higher magnification of dorsal region in b and e; higher magnification of ventral region in c and f. White dashed box in B, b used to highlight regions of Iba-1 reactivity in thoracic cord of 10 month

TDP-Q331K that is distinct to NTg. Scale bars = 200μm. C) Quantitative evaluation of Iba-1 Area in total, white matter and grey matter regions of thoracic cord. Iba-1 area is significantly increased in total area of thoracic cord (*, mean difference = 0.719, p = 0.014) and White matter (*, mean difference = 1.193, p = 0.036) of TDP-Q331K mice in comparison to NTg. D) Quantitative evaluation of GFAP area in total, white matter and grey matter regions of thoracic cord of NTg and TDP-Q331K mice. GFAP reactivity is increased in grey matter of TDP-Q331K mice in comparison to NTg, although this does not achieve statistical significance after Holm-Sidak Correction (#, mean difference = 0.308, p = 0.064). NTg N = 3; TDP-Q331K N = 3. Error bars = ± SD.

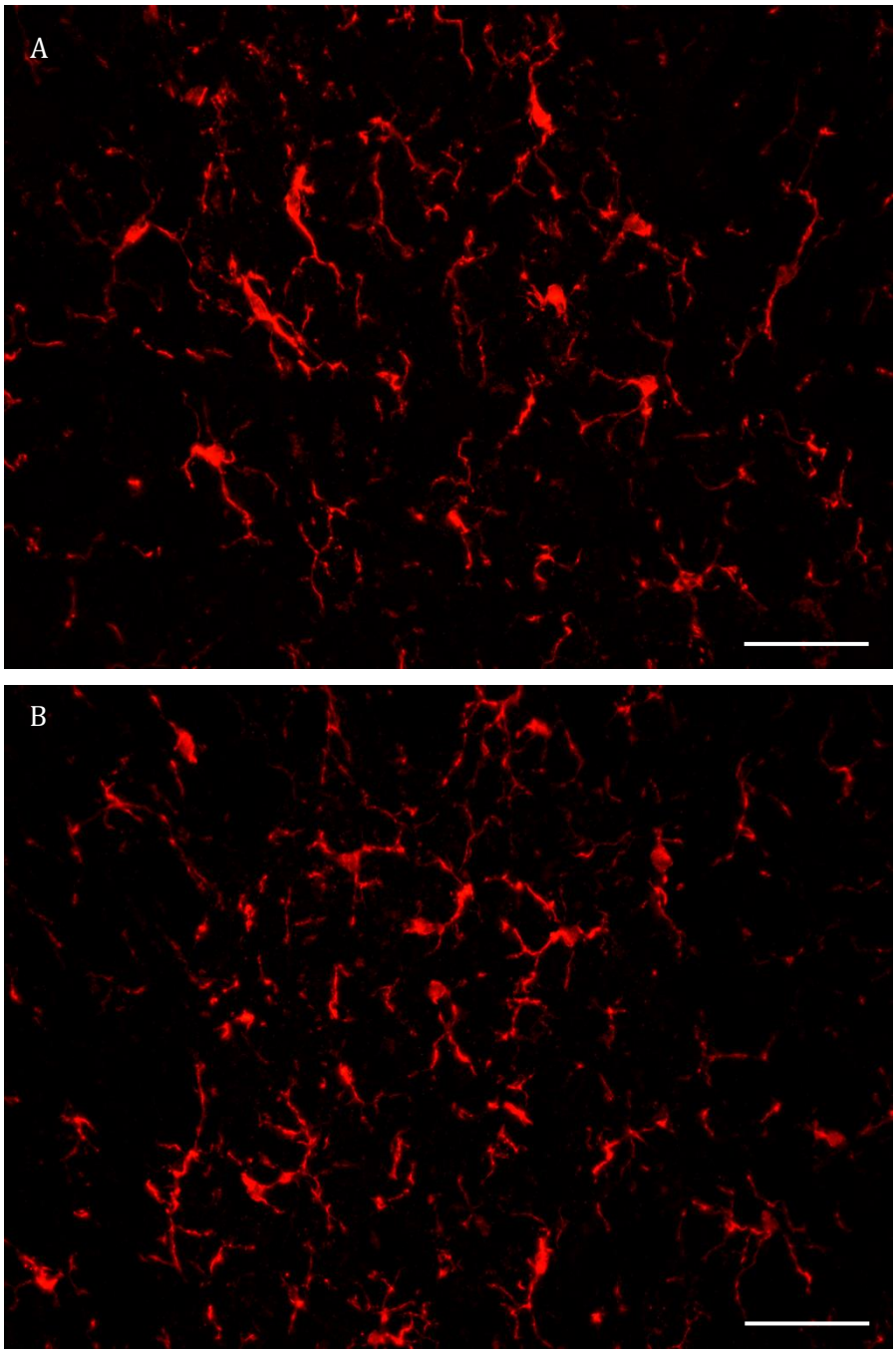

Figure 5.2.5. *Iba-1 reactivity in the ventral horn of a female NTg* (A) *and Q331K* (B) *mouse at 10 months.* Images are a 30µm Z-stack composed of 30 images taken at an interval of 1µm. Scale bars = 50µm.

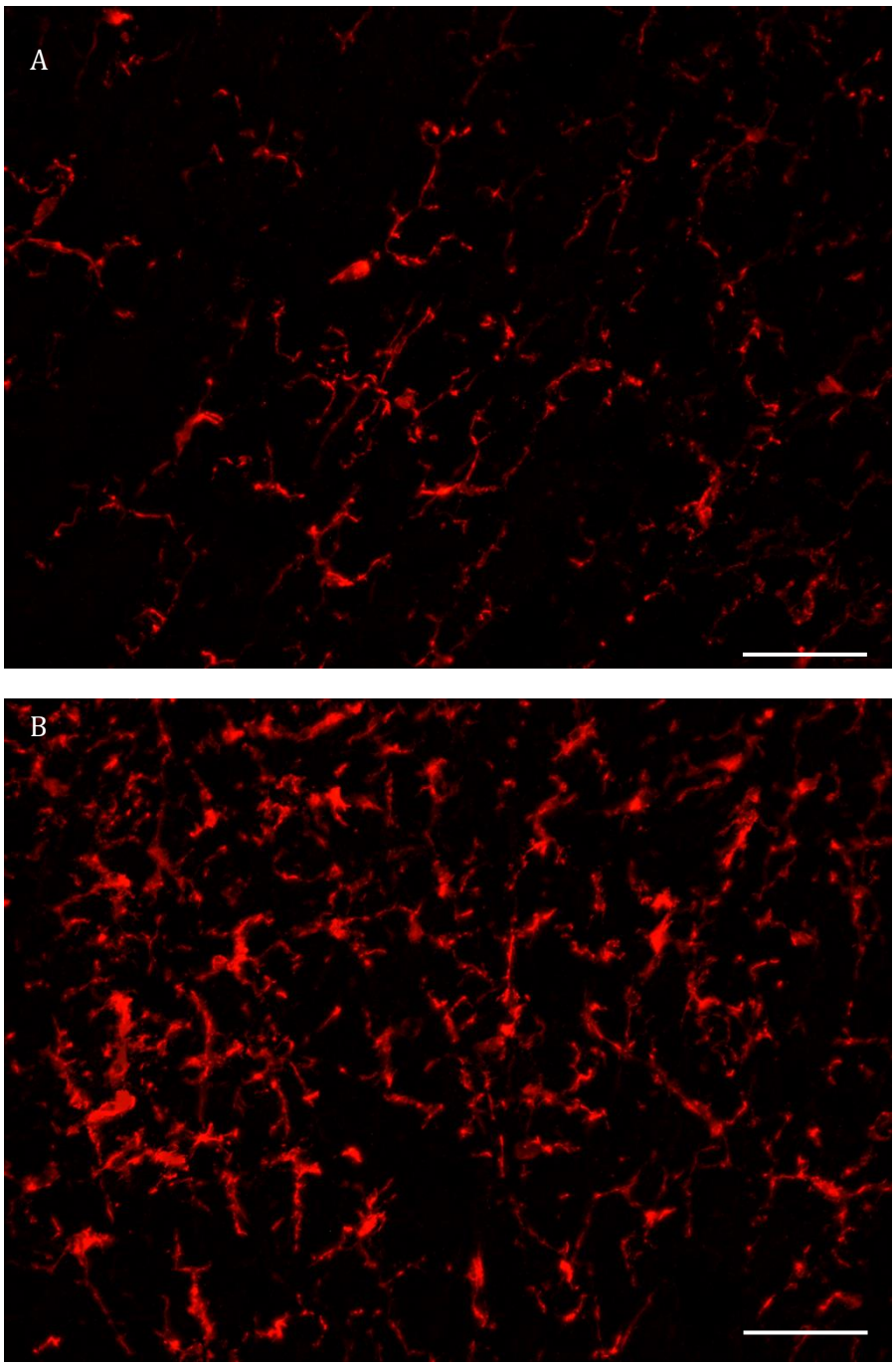

Figure 5.2.6. *Iba-1 reactivity in the lateral white matter of a female NTg* (A) *and Q331K* (B) *mouse at 10 months.* Images are a 30μm Z-stack composed of 30 images taken at an interval of 1μm. Scale bars = 50μm.

Differences in Iba-1 reactivity within grey matter were less distinct than that observed at 6 months. This appears to arise from changes in the microglial state of NTg mice rather than a decreased activation of microglia within TDP-Q331K mice. Indeed, Iba-1 reactivity within microglia of NTg mice demonstrates the presence of cells with a more constricted morphology, indicative of a more activated phenotype.

In support of these qualitative examinations, quantitative assessment of Iba-1 area demonstrated a significant increase of Iba-1 presence within the thoracic cord of TDP-Q331K mice. This corresponded to an increase of 72% across the entire cord, in comparison to NTg mice. However, independent assessment of Iba-1 area within grey and white matter regions demonstrates this increase to arise predominantly from increases of Iba-1 presence within the white matter. Here, Iba-1 area was significantly increased by an average of more than 2-fold (119%) in comparison to NTg mice. In comparison, the increase of Iba-1 area in grey matter was less obvious, corresponding to an increase of 30% within thoracic cord of TDP-Q331K mice compared to NTg. However, this difference did not achieve statistical significance.

The consistency of increased Iba-1 reactivity within the white matter of TDP-Q331K mice at 10 months of age was supported by evaluation of Iba-1 reactivity along the entire rostro-caudal axis of the thoracic cord of a single TDP-Q331K mouse (Appendix 5). As performed for mice at 6 months, Iba-1 reactivity was assessed at 180μm along the thoracic cord. In contrast to that observed for the 6 month mouse, Iba-1 reactivity within the thoracic cord white matter was observed to be consistently increased within both dorsal and lateral regions for every section. This suggests a more widespread activation of microglia within the white matter of spinal cords from TDP-Q331K mice at age 10 months in comparison to 6 months.

In comparison to the activation of microglia, changes in GFAP reactivity were less obvious between TDP-Q331K mice and NTg. Visual inspection shows GFAP reactivity within NTg mice to be most prominent within the white matter, with less consistent astrocyte presence within the grey matter. In comparison, GFAP reactivity within TDP-Q331K indicates astrocytes to be distributed more uniformly within the grey matter of TDP-Q331K mice, suggesting a recruitment of these cells to the grey matter. Indeed, quantitative examination of GFAP area suggests little change across the entire thoracic cord region of TDP-Q331K mice in comparison to NTg. Small increases in GFAP area were observed across total (13%) and white matter (7%) regions. However, in support of a greater astrocyte presence within the grey matter of TDP-Q331K mice, GFAP area was found to be increased by 31% in comparison to NTg mice, although this difference did not achieve statistical significance.

Overall, these data support a global activation of glial cells within the thoracic cord of TDP-Q331K mice. This is most prominently observed for microglia which demonstrate progressively increased reactivity as the disease progresses, a feature that is most apparent within the white matter of thoracic cord.

5.2.1.1.3 Glial reactivity within the thoracic cord of SOD1-G93A mice at 90 days

The predominant focus on lumbar regions of the spinal cord in murine models expressing SOD1 has led to extensive characterisation of glial activation within these regions and is often the principal region for investigation. This is due to the bias of pathology caused by *SOD1* mutations to be focussed predominantly towards the lower motor neurons of the spinal cord. However, it has been recognised that such mutations cause impairments of the autonomic nervous system in mice expressing mutant SOD1. This feature is associated with the degeneration of preganglionic sympathetic motor neurons within the thoracic cord (Kandinov *et al.*, 2013; Kandinov *et al.*, 2011). As such, the activation of glia within the thoracic cord was expected, but for the purposes of this study evidence of glial reactivity within thoracic cord would support the prevalence of glial activation throughout the spinal cord of SOD1-G93A mice.

As performed for TDP-Q331K mice, the activation of microglia and astrocytes were evaluated by assessing Iba-1 and GFAP reactivity. For the assessment of mice at 90 days, sections of thoracic cord were obtained from 5 NTg mice and 6 SOD1-G93A mice.

As displayed in figure 5.2.7, Iba-1 reactivity demonstrates an aggressive and widespread increase across the entire thoracic cord of SOD1-G93A samples. This is in comparison to the homogeneous distribution of ramified microglia observed for NTg animals. In particular, increased Iba-1 reactivity can be seen in dorsal and lateral regions of the thoracic cord white matter (representative images are shown in Figure 5.2.9). Highly reactive Iba-1 cells can be observed in multiple regions across the cord. However, it should be noted that, in comparison to the Iba-1 reactivity observed in TDP-Q331K mice, Iba-1 reactivity within the dorsal white matter was not consistently observed for every section of SOD1-G93A mice. A further contrast to that observed in TDP-Q331K and also NTg mice, is that Iba-1 reactivity within the thoracic cord of SOD1-G93A mice demonstrates increased reactivity and microglial numbers within the ventral horn (Figure 5.2.8) and also within the medioventral pole of the white matter. However, the magnitude of this was observed to fluctuate between different sections of thoracic cord obtained from the same animal.

In line with these observations, quantitative evaluation shows Iba-1 area to be significantly increased by 44% across the entire thoracic cord sections of SOD1-G93A mice in comparison to NTg. This increase arises from the significant increases in both white matter

A

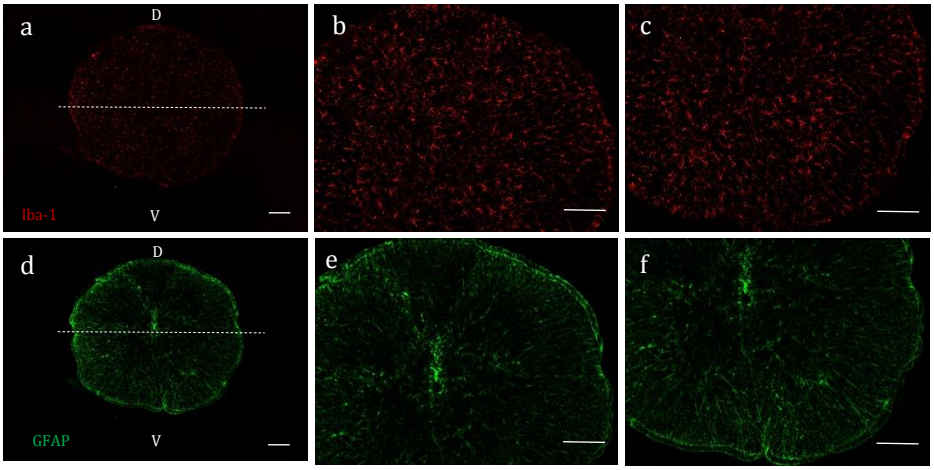

B

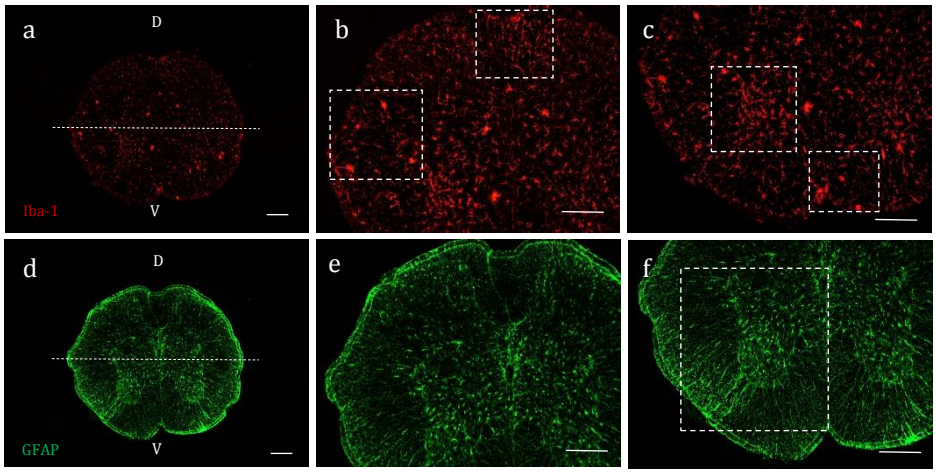

C

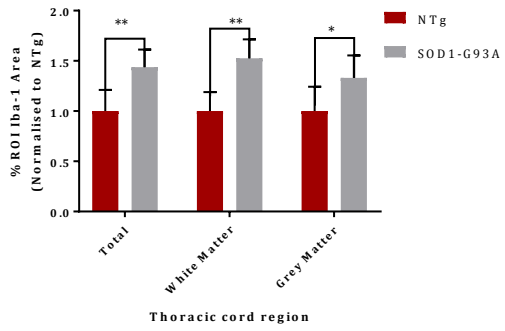

D

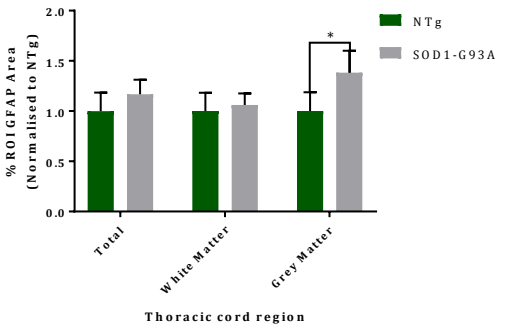

Figure 5.2.7. *Glial reactivity within the thoracic cord of NTg and SOD1-G93A mice at 90 days.* Iba-1 (red) and GFAP (green) reactivity were used to identify microglia and astrocytes, respectively, in thoracic cord of NTg (A) and SOD1-G93A (B) mice at 90 days of age. White dashed line in a and d distinguish Dorsal and Ventral regions of thoracic cord. Higher magnification of dorsal region in b and e; higher magnification of ventral region in c and f. White dashed box in B, b,c and f used to highlight regions of Iba-1 and GFAP reactivity in thoracic cord of SOD1-G93A that is distinct to NTg. Scale bars = 200µm. C) Quantitative assessment of Iba-1 presence demonstrates

significant increase of Iba-1 area in Total (**, mean difference = 0.438, p = 0.008), White Matter (**, mean difference = 0.525, p = 0.003) and grey matter (*, mean difference = 0.332, p = 0.04) regions of thoracic cord for SOD1-G93A mice in comparison to NTg. D) Quantitative assessment of GFAP presence demonstrates significant increase of GFAP area in grey matter (*, mean difference = 0.382, p = 0.041). NTg N = 5 (female); SOD1-G93A N = 6 (female). Error bars = ± SD.

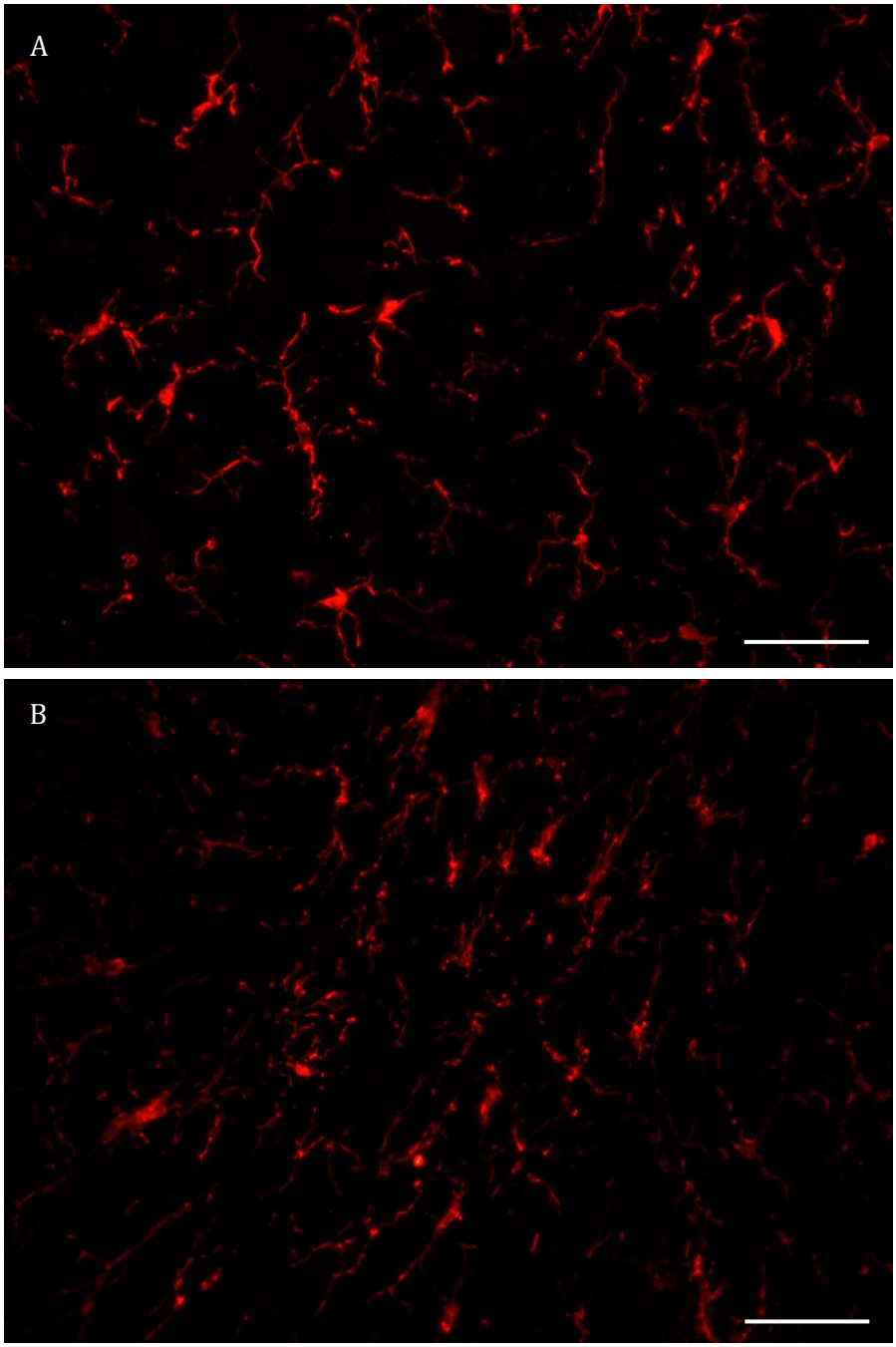

Figure 5.2.8. *Iba-1 reactivity in the ventral horn of a female NTg* (A) *and SOD1-G93A* (B) *mouse at 90 days.* Images are a 30μm Z-stack composed of 30 images taken at an interval of 1μm. Scale bars = 50μm.

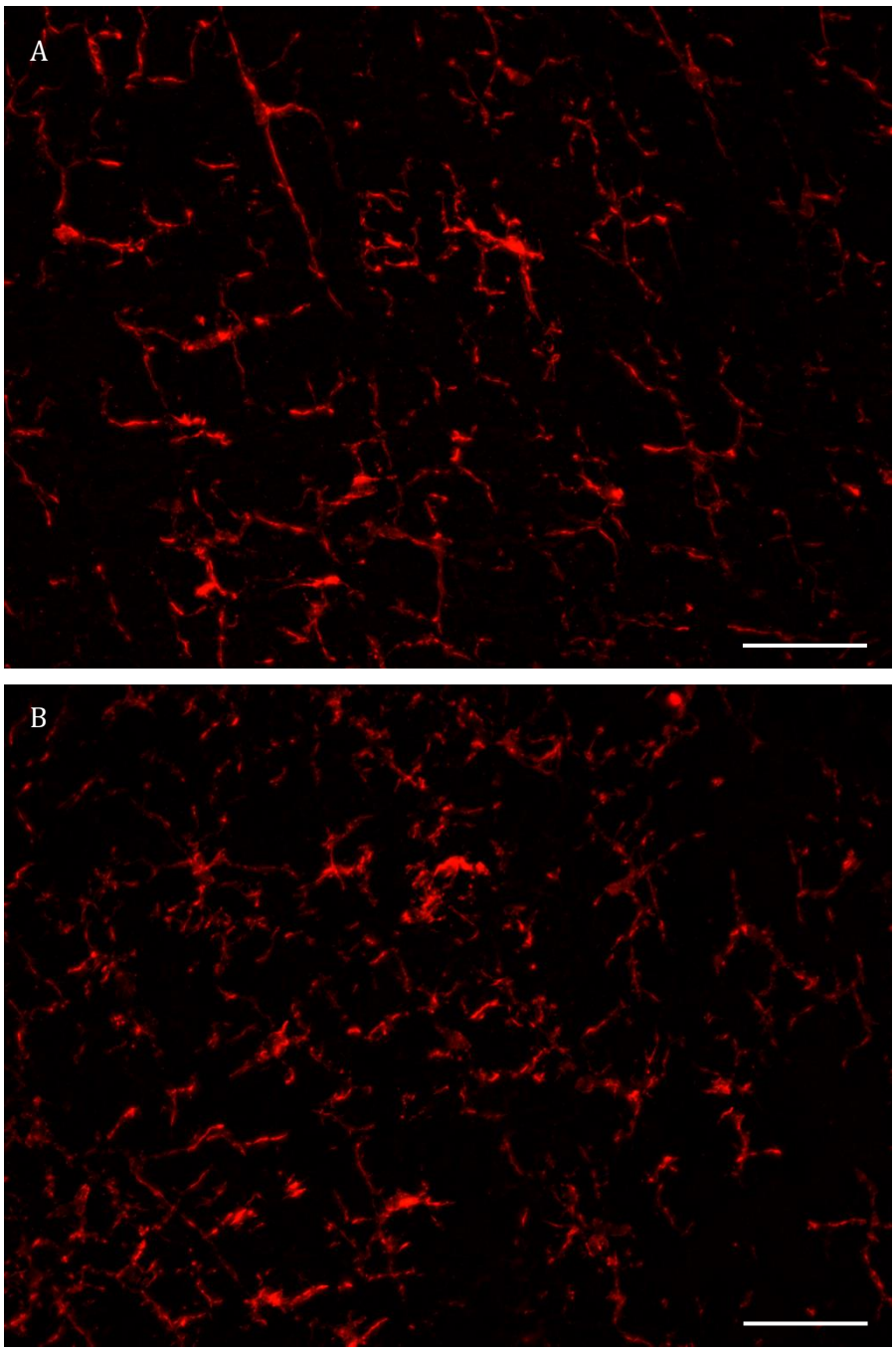

Figure 5.2.9. *Iba-1 reactivity in the lateral white matter of a female NTg* (A) *and SOD1-G93A* (B) *mouse at 90 days.* Images are a 30µm Z-stack composed of 30 images taken at an interval of 1µm. Scale bars = 50µm.

(53%) and grey matter (33%) regions of SOD1-G93A sections, relative to that observed for NTg animals. GFAP reactivity also supports the activation of astrocytes within the thoracic cord of SOD1-G93A mice. The most obvious change, in comparison to NTg mice, is the increased GFAP reactivity within the grey matter of the thoracic cord. Whilst increases can be observed in dorsal regions, the increased GFAP reactivity within the grey matter of SOD1-G93A mice is most clearly apparent within the ventral horn of thoracic cord and also extends from the anterior tip of the ventral horn along the efferent axonal tracts that arise from resident motor neurons. Indeed, quantitative evaluation of GFAP area supports the most obvious differences between NTg and SOD1-G93A mice to exist within the grey matter. Evaluation of GFAP reactivity across the entire thoracic cord section demonstrated a 16% increase within sections of SOD1-G93A mice, although this was not considered a statistically significant change from NTg samples. However, whilst reactivity in the white matter of SOD1-G93A mice is very similar to NTg (demonstrating an increase of 6%), GFAP reactivity within the grey matter is significantly increased by 38% in comparison to NTg animals.

5.2.1.1.4 Glial reactivity within the thoracic cord of SOD1-G93A mice at 120 days

To further extend the evidence of glial activation within thoracic cord, Iba-1 and GFAP reactivity was also evaluated at 120 days for 4 NTg and 4 SOD1-G93A mice (Figure 5.2.10).

Iba-1 reactivity demonstrated the widespread presence of microglial cells with increased reactivity and a morphology consistent with an activated phenotype, in sections obtained from SOD1-G93A mice. These features were most prominent within the grey matter, lateral and ventral regions of the white matter (figures 5.2.11 and 5.2.12). As was detailed for mice at 90 days, the prevalence of reactivity within the mediodorsal regions of white matter was less consistent between sections of the same animal. Indeed, in comparison to the grey matter, lateral and ventral regions of white matter, the Iba-1 reactivity observed within the mediodorsal white matter of the sections analysed from SOD1-G93A mice suggests a much lower prevalence of microglial activation within this area.

In support of the most prevalent difference in Iba-1 reactivity between SOD1-G93A and NTg mice to reside within the white matter, quantitative evaluations of Iba-1 area demonstrated a significant increase of 88% within the white matter of SOD1-G93A mice. This contributed to a significant increase of Iba-1 area across the entire thoracic cord region of 44%. An increase of 37% in Iba-1 area was also observed within the grey matter of SOD1-G93A mice, in comparison to NTg. Whilst this did not achieve statistical significance ($p = 0.058$), this does support an increased microglia activation within the grey matter of SOD1-G93A mice at 120 days.

A

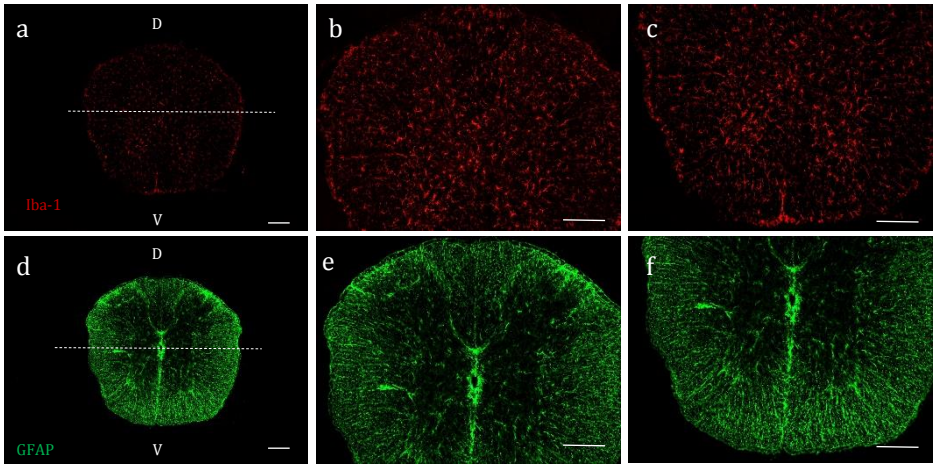

B

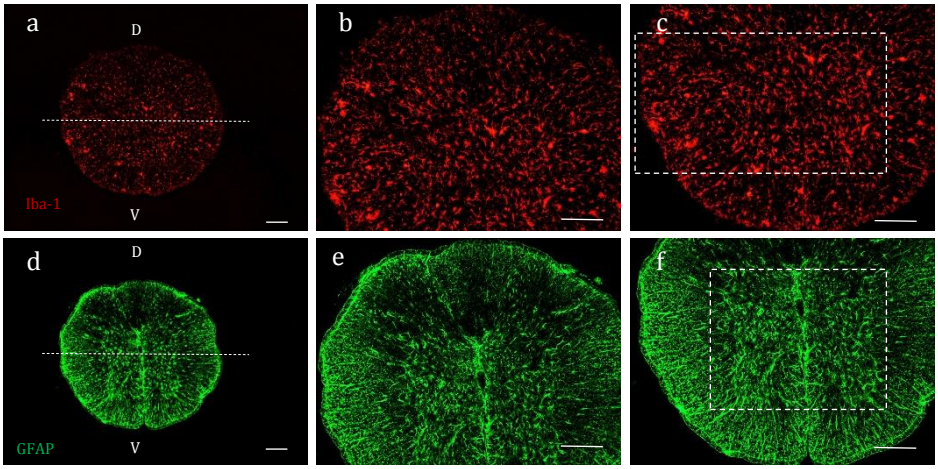

C

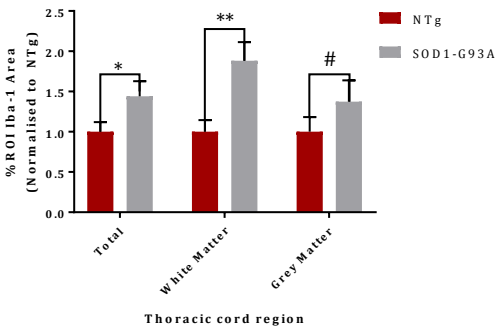

D

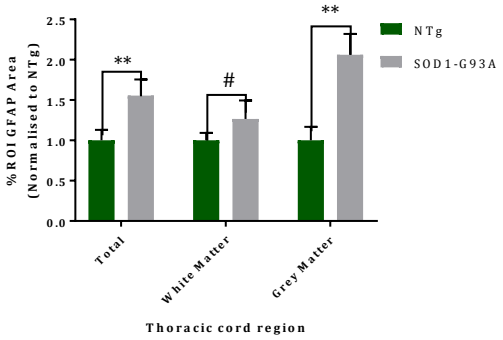

Figure 5.2.10. *Glial reactivity within thoracic cord of NTg and SOD1-G93A mice at 120 days.* Iba-1 (red) and GFAP (green) reactivity were used to identify microglia and astrocytes, respectively, in thoracic cord of NTg (A) and SOD1-G93A (B) mice at 120 days of age. White dashed line in a and d distinguish Dorsal and Ventral regions of thoracic cord. Higher magnification of dorsal region in b and e; higher magnification of ventral region in c and f. White dashed box in B, f used to highlight regions of GFAP reactivity in thoracic cord of SOD1-G93A that is distinct to NTg. Scale bars = 200µm. C) Iba-1 Area of total (*, Mean difference = 0.441, p = 0.015) and White matter (**, Mean difference = 0.882 , p = 0.002) regions of thoracic cord is significantly increased in SOD1-G93A

mice in comparison to NTg. Iba-1 area in grey matter is also increased but does not achieve statistical significance (#, mean difference = 0.375, p = 0.058). D) GFAP area of total (**, mean difference = 0.554 , p = 0.007) and grey matter (**, mean difference = 1.062, p = 0.001) regions is significantly increased within thoracic cord of SOD1-G93A mice in comparison to NTg. GFAP area is also increased within white matter region of SOD1-G93A mice, but to a lower degree that does not achieve statistical significance (#, mean difference = 0.266 , p = 0.07). NTg N = 4 (females); SOD1-G93A N = 4 (Females). Error bars = ± SD.

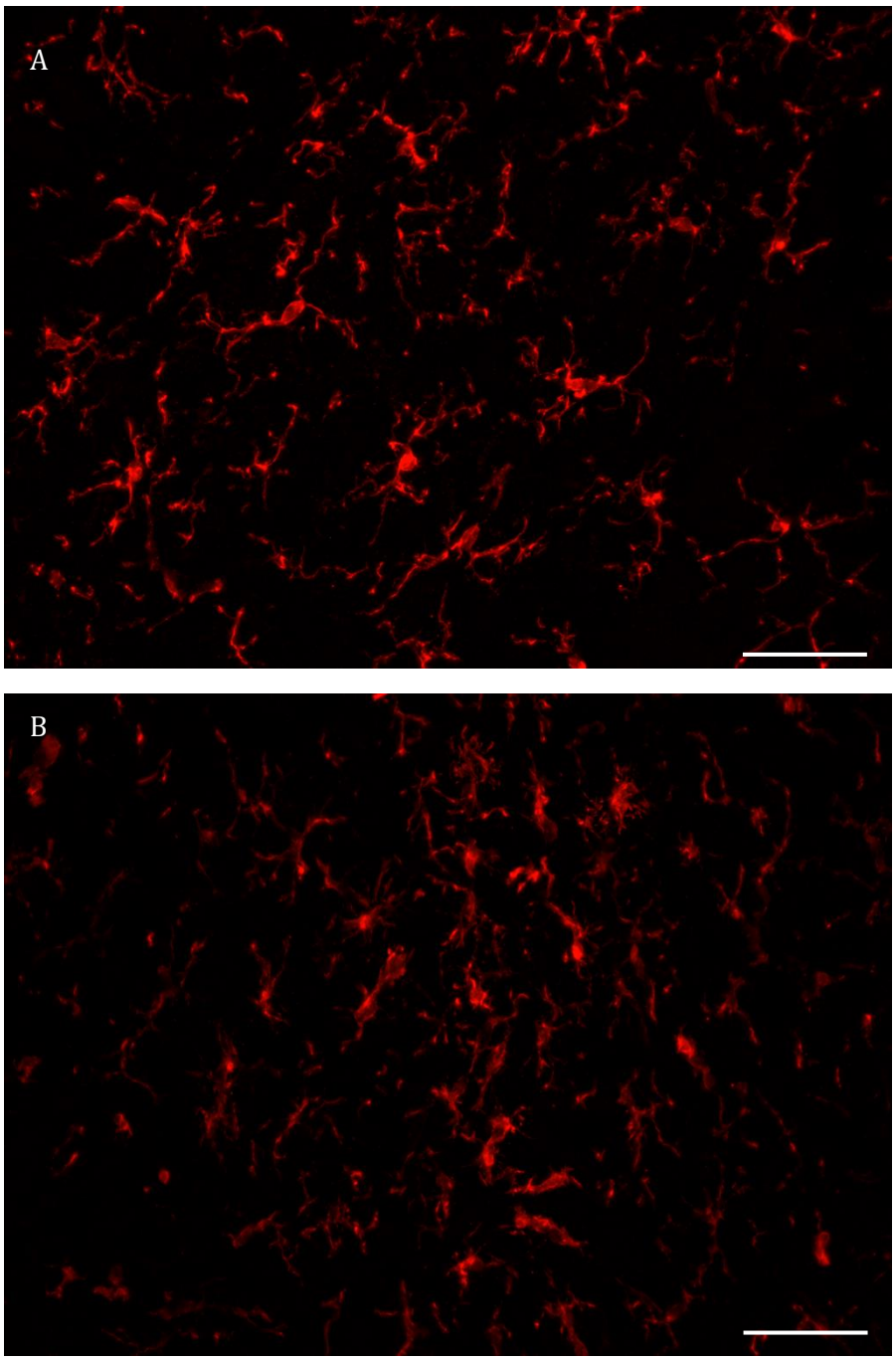

Figure 5.2.11. *Iba-1 reactivity in the ventral horn of a female NTg* (A) *and SOD1-G93A* (B) *mouse at 120 days.* Images are a 30μm Z-stack composed of 30 images taken at an interval of 1μm. Scale bars = 50μm.

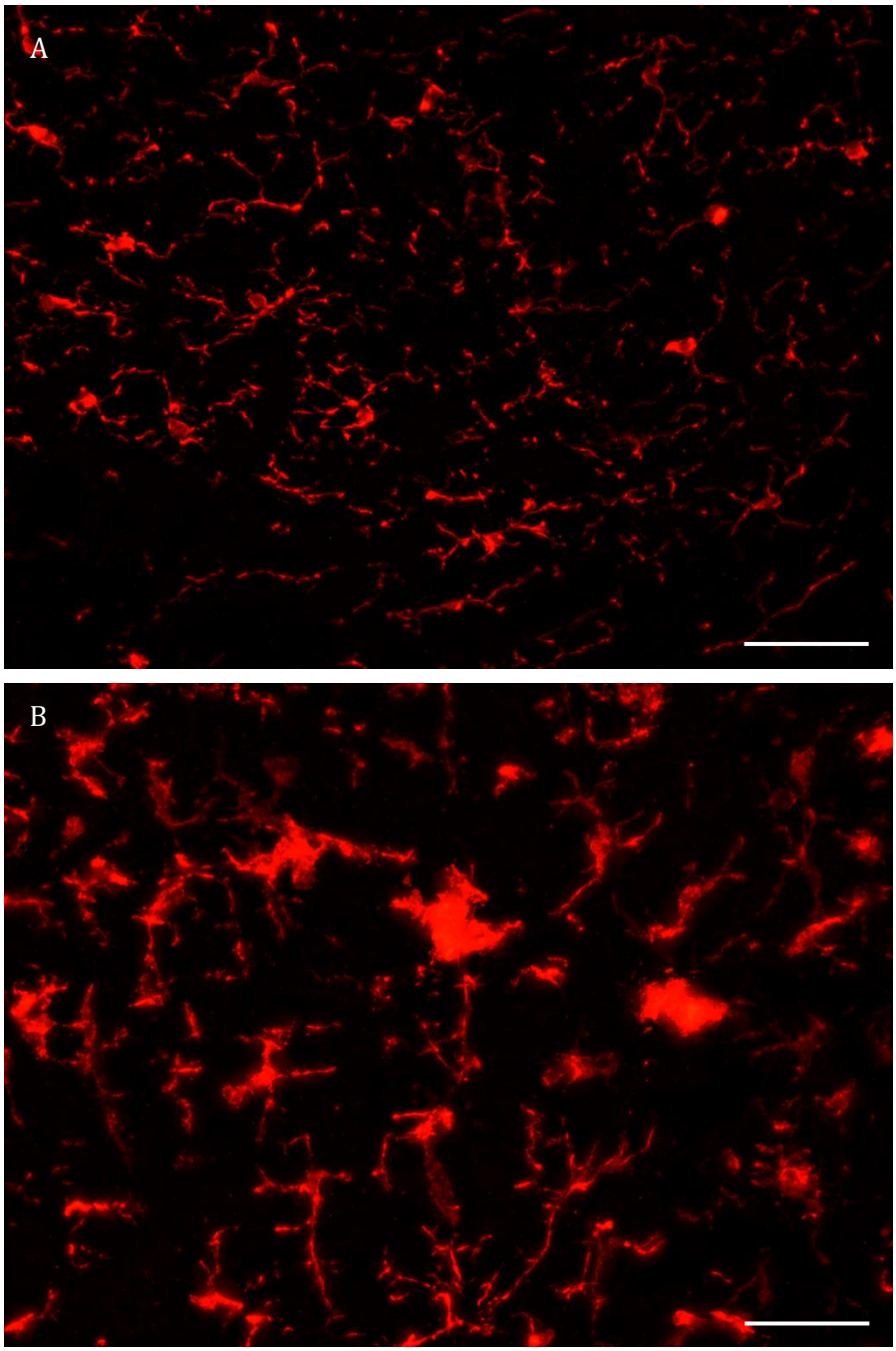

Figure 5.2.12. *Iba-1 reactivity in the lateral white matter of a female NTg* (A) *and SOD1-G93A* (B) *mouse at 120 days.* Images are a 30μm Z-stack composed of 30 images taken at an interval of 1μm. Scale bars = 50μm.

GFAP reactivity within the thoracic cord of SOD1-G93A mice also supported the prevalent activation of astrocytes. As demonstrated for SOD1-G93A mice at 90 days, a notable increase of GFAP reactivity was observed within the grey matter of thoracic cord at 120 days. This increase of GFAP reactivity appeared to predominate within the ventral, rather than dorsal regions of the grey matter. In addition, reactivity within the white matter also appeared more prominent than that observed at 90 days. This was supported by quantitative evaluation of GFAP area within the thoracic cord of SOD1-G93A mice, in which a significant increase of 106% and 55% were observed across the grey matter and total area, respectively, in comparison to NTg sections. A 27% increase was also observed for the white matter of SOD1-G93A sections in comparison to NTg, however this did not achieve statistical significance ($p = 0.074$).

5.2.1.2 Xcr1 and Xcl1 expression in the spinal cord of ALS mouse models

Based on the above evidence of consistent and extensive activation of microglia and astrocytes, spinal cord samples of SOD1-G93A and TDP-Q331K mice provided samples in which there was prevalent neuroinflammation. Evaluation of *Xcr1* and *Xcl1* expression within RNA samples collected from whole spinal cords of these mice was therefore performed in order to provide an insight in to the potential contribution of this chemokine signalling axis to the central inflammatory response generated within these two ALS mouse models.

For the reported *Xcr1* expression detailed here, the presence of *Xcr1* mRNA has been evaluated using *Xcr1S* primers. This has been done due to the consistency of these primers to provide a detectable signal of *Xcr1* mRNA presence by qPCR. In contrast, *Xcr1L* primers provided a less reliable detection and, as was described in chapter 3, this introduced difficulties for the evaluation of mRNA expression due to the confounding influence of non-detects in providing accurate quantification of amplicon presence from qPCR investigations. In addition, the method of preparation of cDNA was demonstrated to reliably minimise contamination of RNA samples with genomic DNA, supporting the reliable detection of *Xcr1* mRNA by *Xcr1S* primers.

5.2.1.2.1 Xcr1 and Xcl1 expression in the spinal cord of 6 month TDP-Q331K mice

Xcr1 and *Xcl1* expression was evaluated within total RNA samples collected from whole spinal cords of 6 NTg mice (3 males; 3 females) and 6 Q331K mice (3 males; 3 females) at both 6 months and 10 months of age (Figure 5.2.13).

At 6 months, evaluation of *Xcr1* expression demonstrated a low and consistent presence of *Xcr1* for both male and female mice of both NTg and TDP-Q331K genotypes, suggesting no change in *Xcr1* expression within the spinal cord of TDP-Q331K mice in comparison to age-

matched NTg controls. In addition, no difference of *Xcr1* expression was identified between sexes.

Assessment of *Xcl1* expression demonstrated a significant increase of expression for both male and female TDP-Q331K mice in comparison to their respective NTg controls. For males, this corresponded to a level of expression that was 2.02x that of male NTg samples. For females this corresponded to a level of expression that was 1.79x that of female NTg samples. No differences in *Xcl1* expression were identified between male and female mice from either genotype. This suggests that at 6 months of age, *Xcl1* levels are increased within the spinal cord of TDP-Q331K mice in comparison to NTg mice. Moreover, this feature is consistent between sexes.

5.2.1.2.2 Xcr1 and Xcl1 expression in the spinal cord of 10 month TDP-Q331K mice

In comparison to the differences observed at 6 months, *Xcr1* expression was indicated to be higher within male than female samples at 10 months of age. For male NTg mice, this corresponded to a mean increase of 1.67x in comparison to females. For male Q331K mice, this corresponded to a mean increase of 1.82x in comparison to females. However these differences did not achieve statistical significance.

Evaluation of *Xcl1* expression indicated an increased expression within TDP-Q331K mice for both sexes. For male mice, this corresponded to an increase in *Xcl1* expression that was 1.81x that of male NTg samples. Female TDP-Q331K mice demonstrated an increase in *Xcl1* expression that was 1.68x that of NTg samples. Neither of these increases achieved statistical significance.

In addition, similar to the trend observed for *Xcr1* expression, *Xcl1* expression also demonstrated a trend to be increased within RNA samples from males in comparison to females. This corresponded to an increase of *Xcl1* expression in male NTg mice that was 1.56x that observed in female NTg mice. Male TDP-Q331K mice demonstrated a larger difference in *Xcl1* expression, corresponding to a mean increase of 1.73x that observed for female TDP-Q331K mice. However, neither of these differences were considered statistically significant.

5.2.1.2.3 Xcr1 and Xcl1 expression in the spinal cord of SOD1-G93A mice at 90 days

Xcr1 and *Xcl1* expression was also investigated within the spinal cords of 3 SOD1-G93A mice and 3 age-matched NTg controls. Unlike for TDP-Q331K evaluations, all of these mice were female.

In comparison to NTg controls, SOD1-G93A samples were indicated to contain a lower level of *Xcr1* mRNA, although there was considerable overlap in the expression levels. For *Xcl1*

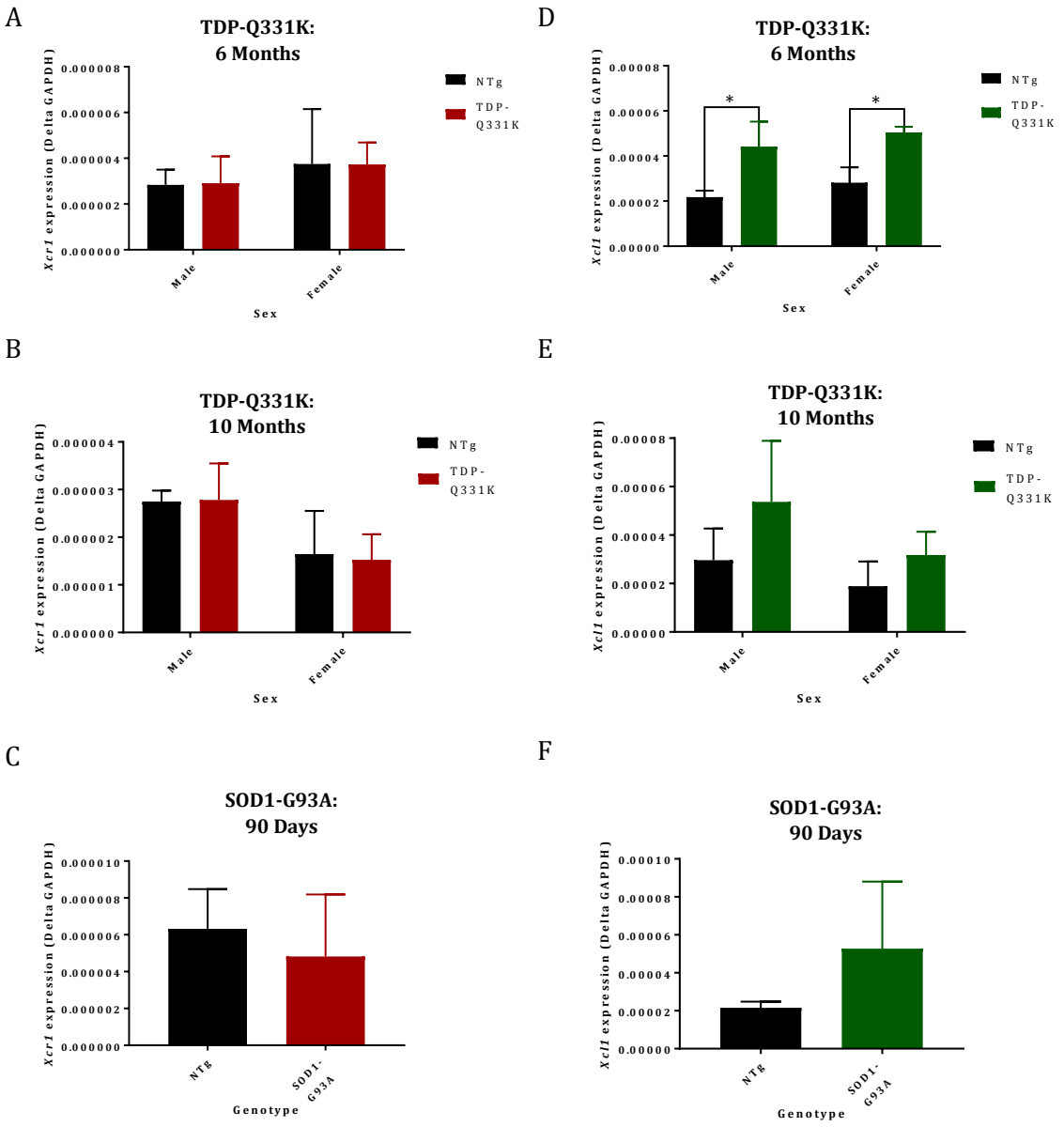

Figure 5.2.13. *Xcr1 and Xcl1 expression in the spinal cord of TDP-Q331K and SOD1-G93A mouse models of ALS.* Evaluation of *Xcr1* expression (A, B and C) and *Xcl1* expression (D, E and F) in TDP-Q331K and age-matched NTg controls at 6 months (A, D) and 10 months (B, E) and in SOD1-G93A mice at 90 days (C, F). Absolute levels of gene expression (relative to GAPDH) have been shown for clarity. No differences were observed for *Xcr1* expression under any condition. *Xcl1* expression was observed to be significantly increased by TDP-Q331K mice at 6 months in comparison to controls for both male (*, mean difference = 2.237x 10^{-5} (2.02x NTg), p = 0.028) and female (*, mean difference = 2.229 x 10^{-5} (1.79x NTg), p = 0.012) mice. Error bars = ±SD. N=3 for all groups.

expression, SOD1-G93A mice demonstrated a 2.45x increase relative to NTg controls. However, this difference was not considered statistically significant.

5.2.1.3 Evaluation of Xcl1 expression in primary microglial cultures from ALS mouse models

As performed for NTg mice in chapter 3, primary microglial cultures were prepared from the brains of 10 month TDP-Q331K mice and 90-100day old SOD1-G93A mice. Unfortunately, due to infection, one of the SOD1-G93A primary cultures had to be destroyed and therefore comparison presented here are made between 3 primary cell cultures prepared from NTg mice; 3 primary cultures from TDP-Q331K mice; and 2 primary cultures prepared from SOD1-G93A mice. Preliminary attempts were made for the preparation of microglial cultures from the spinal cords of mice, however these were unsuccessful due to low cells numbers decreasing cell viability and preventing the culture of sufficient cell numbers for downstream analysis.

The preparations of these cells were made in order to test the capacity for primary microglia to express *Xcl1,* and to see whether the microglia obtained from ALS mouse models differed in this capacity, in comparison to microglia from NTg mice. Furthermore, treatment with LPS was performed in order to evaluate the response of *Xcl1* expression by microglia from the different mouse genotypes to a stimulus that has been demonstrated to induce an inflammatory response.

5.2.1.3.1 Purity of primary microglia cultures

The purity of primary cultures was determined by immunocytochemical detection of Iba-1 and GFAP within cells to provide an indication of microglial and astrocyte presence, respectively (Figure 5.2.14, A, B). The presence of Iba-1 positive cells did vary considerably between cultures obtained from TDP-Q331K and SOD1-G93A mice. For cultures prepared from TDP-Q331K mice, the presence of Iba-1 cells was significantly lower than that obtained from SOD1-G93A mice, indicating a mean microglial presence of 35% of the total cell number, as determined by DAPI cell counts. In comparison, microglial presence was indicated to account for 67% of cells from SOD1-G93A mice, a proportion that demonstrated very strong consistency between the two cultures used for analysis. Microglial presence was therefore comparable between NTg and SOD1-G93A cultures. However, the lower presence of Iba-1 positive cells within TDP-Q331K cultures does compromise the reliability of analyses from these cultures to reflect changes primarily within microglial cells.

5.2.1.3.2 Evaluation of Xcl1 expression in primary microglial cultures from NTg and ALS mouse models

To evaluate the influence of disease on *Xcl1* expression by primary microglia from the two ALS models, *Xcl1* expression was quantified and compared between untreated primary cultures from NTg, TDP-Q331K and SOD1-G93A mice. As demonstrated in Figure 5.2.14, E, the expression of *Xcl1* within the primary microglial cultures, although low, were indicated to differ between cultures from mice of different genotypes. Of particular note was the consistency of *Xcl1* expression identified within SOD1-G93A cultures, supporting the consistency of cell composition within the two independent primary cultures evaluated. Furthermore, *Xcl1* expression demonstrated a mean increase in SOD1-G93A cultures that was 1.93x greater than NTg cultures and 2.56x greater than TDP-Q331K cultures. Indeed, *Xcl1* expression within TDP-Q331K cultures was slightly lower, corresponding to a mean expression that was 0.75x that observed for NTg cultures.

Whilst neither of these differences were determined to be statistically significant, the observed *Xcl1* expression in tandem with the observed Iba-1 reactivity within cultures provides some credence to the association of *Xcl1* expression by microglia. First of all, the lowest mean *Xcl1* expression was observed within TDP-Q331K cultures that also demonstrated the lowest number of Iba-1 positive cells and hence lowest microglial presence. Secondly, the observed consistency of Iba-1 positive cells within primary cultures from SOD1-G93A mice was reflected by a consistent detection of *Xcl1* expression within the two cultures. Thirdly, the observed Iba-1 reactivity within untreated primary cultures from SOD1-G93A mice (Figure 5.2.14 B, control images) is indicative of cells with a higher state of activation than that observed from Q331K or NTg cultures. Therefore, despite having a slightly lower mean microglial purity than NTg cultures, this suggests that the endogenous activation state of microglial cells obtained from SOD1-G93A mice may contribute to the observed increase in expression. This suggests an association of microglia presence and also, potentially, the endogenous activation state of primary microglia to associate with *Xcl1* expression. Moreover, the increased *Xcl1* expression observed within primary microglial cultures of SOD1-G93A cultures in comparison to NTg cultures is reminiscent of that observed for the evaluation of *Xcl1* expression within whole spinal cord RNA samples from the two groups (Figure 5.2.13, F).

5.2.1.3.3 Evaluation of Xcl1 expression following LPS treatment of primary microglial cultures from SOD1-G93A and TDP-Q331K mice

Treatment of primary microglia with LPS was performed in order to test the capacity for such treatment to influence *Xcl1* expression, but also to determine if the response from microglial cells prepared from the two ALS models would differ from control.

A

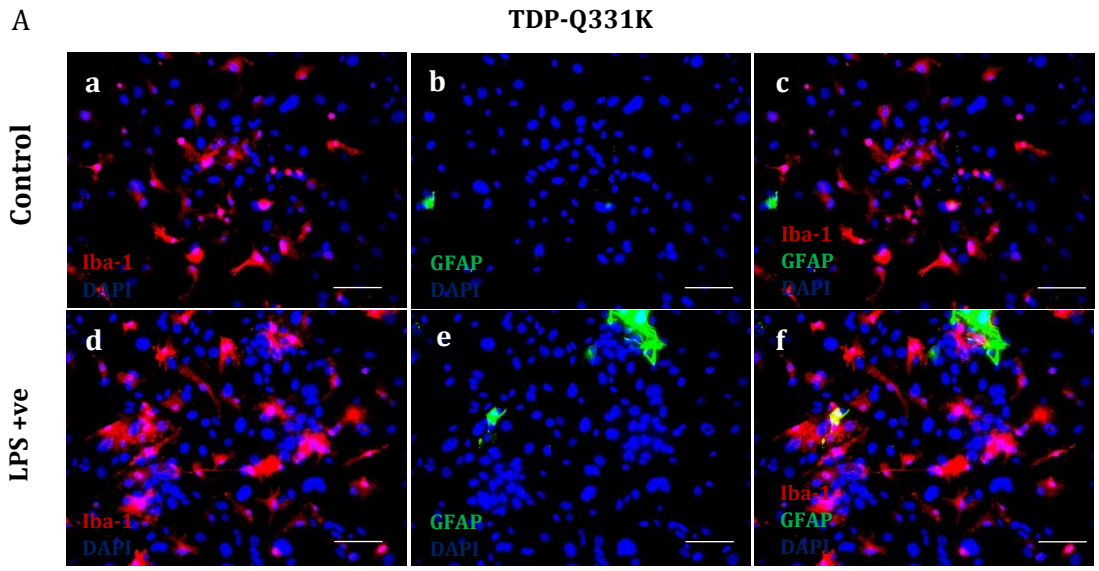
TDP-Q331K
Control
LPS +ve
a
b
c
d
e
f
Iba-1
DAPI
GFAP
DAPI
Iba-1
GFAP
DAPI

B

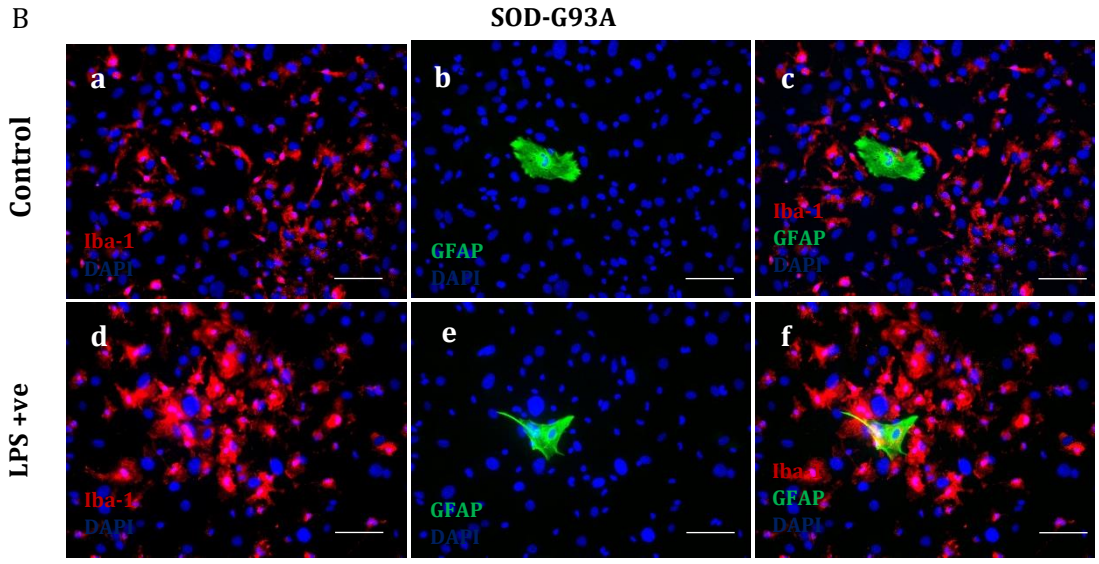
SOD-G93A
Control
LPS +ve
a
b
c
d
e
f
Iba-1
DAPI
GFAP
DAPI
Iba-1
GFAP
DAPI

C

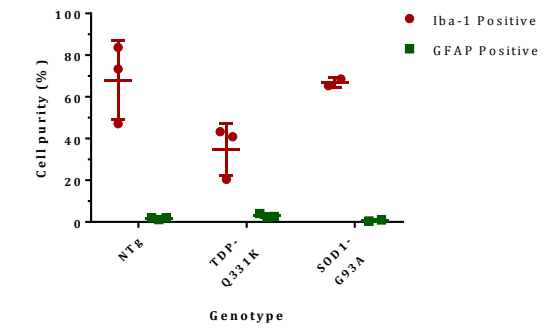
Cell purity (%)
100
80
60
40
20
0
Iba-1 Positive
GFAP Positive
NTg
TDP-Q331K
SOD1-G93A
Genotype

D

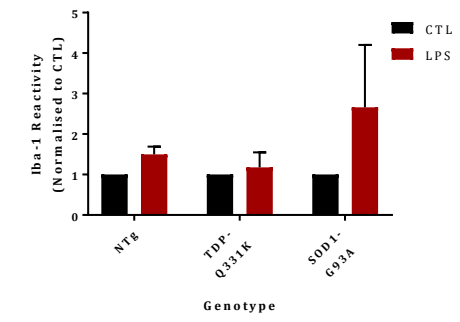
Iba-1 Reactivity (Normalised to CTL)
5
4
3
2
1
0
CTL
LPS
NTg
TDP-Q331K
SOD1-G93A
Genotype

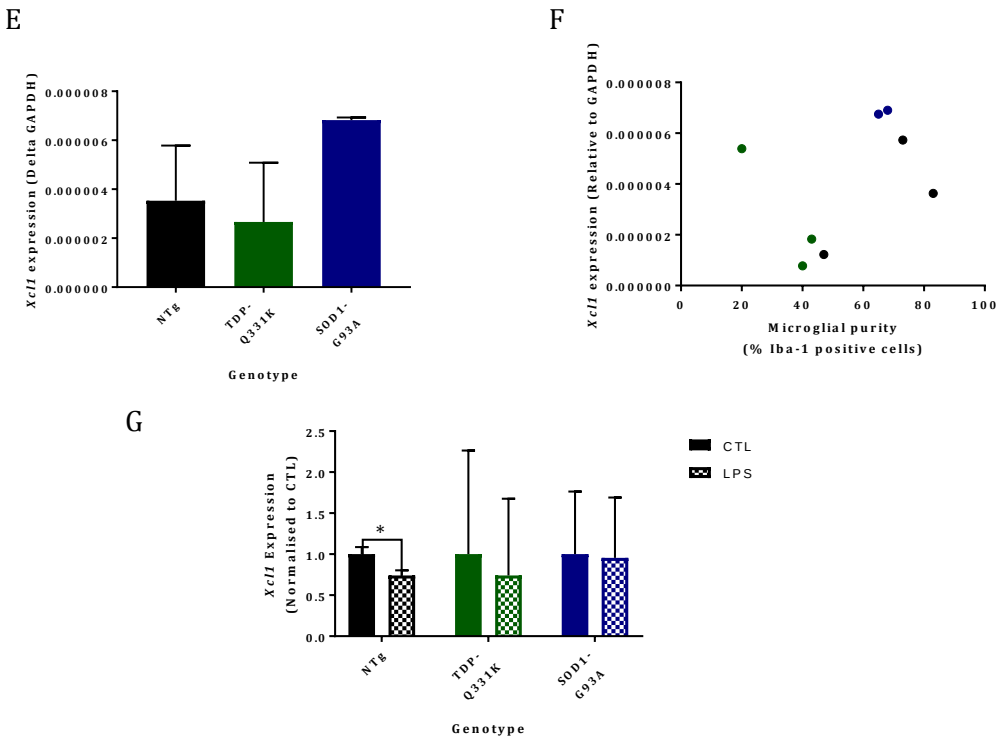

Figure 5.2.14. *Xcl1 expression in primary glial cultures of NTg, SOD1-G93A and TDP-Q331K mice.* Representative images of primary microglial cultures obtained from 10month TDP-Q331K (A) and 90 day SOD1-G93A (B) mice (for NTg cultures see figure 3.2.5). Microglia and astrocytes were identified by immunocytochemical detection of Iba-1 (red) and GFAP (green), respectively. C) Quantification of Iba-1 positive and GFAP positive cells in relation to total cell number was used to estimate microglia cell purity. Cultures prepared from TDP-Q331K mice demonstrate a low abundance (34%) of Iba-1 positive cells in comparison to NTg (68%) and G93A (67%) preparations. D) LPS treatment induces an increase of Iba-1 reactivity, relative to control conditions, by a mean of 50%, 18% and 166% in cultures prepared from NTg, TDP-Q331K and SOD1-G93A mice, respectively. E) Absolute levels of *Xcl1* expression, relative to internal *GAPDH* control, are presented for each of the primary microglial cultures (Control conditions) prepared from each genotype. No statistical difference was observed in the level of *Xcl1* expression between genotypes. F) Scatter graph of *Xcl1* expression vs Microglial purity of untreated primary microglial cultures from NTg (Black), TDP-Q331K (green) and SOD1-G93A (blue) mice. G) No difference in *Xcl1* expression was observed for TDP-Q331K or SOD1-G93A primary microglial cultures as a consequence of LPS treatment in comparison to control conditions. A significant decrease was observed for *Xcl1* expression by NTg microglial cultures (*, p = 0.01) as detailed in figure 3.2.5. Comparisons between control and LPS treatments were made according to calculations recommended by Willems 2008.

Treatment with LPS was demonstrated to induce an inflammatory response by primary microglial cells, as evidenced by the morphology and increased reactivity of Iba-1 positive cells (Figure 5.2.14, A, B, D). However, this did vary between cultures from TDP-Q331K and SOD1-G93A mice. For TDP-Q331K cultures this corresponded to a mean increase in Iba-1 reactivity of 18% by cells treated with LPS in comparison to untreated, control cells. For SOD1-G93A cells, this increase was particularly prominent, with Iba-1 reactivity of LPS treated primary cell cultures increasing by a mean of 166% in comparison to untreated cells. This increase was reflected by the adoption of an activated, amoeboid-like morphology of Iba-1 positive cells following LPS treatment. Again, this feature appeared to be more prominent within SOD1-G93A cultures in comparison to TDP-Q331K cultures. However, these observations together support the capacity of LPS treatment to induce an inflammatory response by microglial cells in primary culture.

Following LPS treatment, qPCR was performed to assess the impact of the induced activation of primary microglial cells on *Xcl1* expression. In order to provide a more accurate quantification of the effect of LPS treatment on *Xcl1* expression, qPCR data obtained from untreated and LPS treated primary cultures from independent experiments was standardised to account for variation between replicates. In accordance with previous recommendations (Willems, Leyns and Vandesompele, 2008), data therefore underwent a log transformation and mean centering prior to comparison of normalised values between control and LPS treated cultures.

As can be observed from Figure 5.2.14, G, LPS treatment had very little impact on the expression of *Xcl1* within primary microglial cultures obtained from TDP-Q331K and SOD1-G93A mice. Moreover, the effect of LPS treatment was inconsistent between replicates. Due to the variability of this effect of LPS treatment on *Xcl1* expression, in comparison to untreated cells, the standardised data demonstrates a high variability in the relative *Xcl1* expression of LPS and untreated primary cultures from TDP-Q331K and SOD1-G93A mice. Consequently, there is no evidence to support the capacity for the induction of microglial activation by LPS treatment to affect *Xcl1* expression.

5.2.2 XCR1 expression in cervical cord of ALS patients and neurological controls

In the absence of an antibody that was able to reliably detect Xcr1, it has not been possible to evaluate the presence of the Xcr1 protein within the CNS of mice. However, according to the success of identifying an antibody that can reliably and specifically detect human XCR1 (Chapter 4), it was possible to evaluate XCR1 expression within the human CNS. Therefore, to evaluate XCR1 expression within CNS and to provide an additional insight to the impact

of ALS on the expression of this chemokine receptor, XCR1 expression was evaluated within the cervical region of spinal cords collected from sALS patients and neurological controls.

5.2.2.1 Optimisation of HPA013169 for the detection of XCR1 *within the human cervical cord*

The optimisation of the immunohistochemistry protocol for the detection of XCR1 by HPA013169 was performed using sections of cervical spinal cord obtained from a sALS patient. HPA013169 reactivity was optimised by testing a series of antibody concentrations between 0.5μg/ml and 4μg/ml in combination with alternative antigen retrieval conditions. Exemplary images from this optimisation are provided in figure 5.2.15.

Preliminary tests demonstrated weak reactivity of HPA013169 to localise to cells located within the lateral and medioventral regions of cervical cord white matter. Reactivity was also observed within endothelial cells of blood vessels, a feature that was expected according to the observed reactivity described by the antibody manufacturer (https://www.proteinatlas.org/ENSG00000173578-XCR1/tissue/primary+data). No reactivity was observed within the grey matter of cervical cord. Further refinement of the immunohistochemistry procedure provided greater HPA013169 reactivity, which was observed to be greatest following microwave-induced HIER at pH6 (Figure 5.2.15, A). The optimised protocol was in good agreement with the recommended protocol provided by the manufacturer, which suggested an antibody concentration of 1:20-1:50 (10μg-4μg/ml) to be used following HIER at pH 6.

The morphology of reactive cells suggested HPA013169 to localise to glial cells of the white matter. Figure 5.2.15 demonstrates this reactivity within the medioventral white matter, a region that corresponds to the ventral corticospinal tracts (VCSTs). A similar pattern of reactivity was also observed within the lateral regions of the cervical cord white matter (not shown). The reactivity observed in VCSTs was not uniform however, with a bias of reactivity observed within the VCSTs of one side of the cervical cord (Figure 5.2.15, c). Higher magnification of this region demonstrates numerous cells to exhibit HPA013169 reactivity within the cervical cord VCSTs of this sALS patient (Figure 5.2.15, A, d). Based on this evidence of HPA013169, it was decided to expand the investigation to compare HPA013169 reactivity within the cervical spinal cord of sALS patients and neurological controls.

5.2.2.2 XCR1 presence within the cervical cord of sALS patients and neurological controls

For comparison of XCR1 presence, HPA013169 reactivity was analysed within the cervical cord of 5 neurological controls and 6 sALS patients. Qualitative and quantitative assessment of HPA01369 reactivity was performed whilst blinded to the diagnosis of sALS or control.

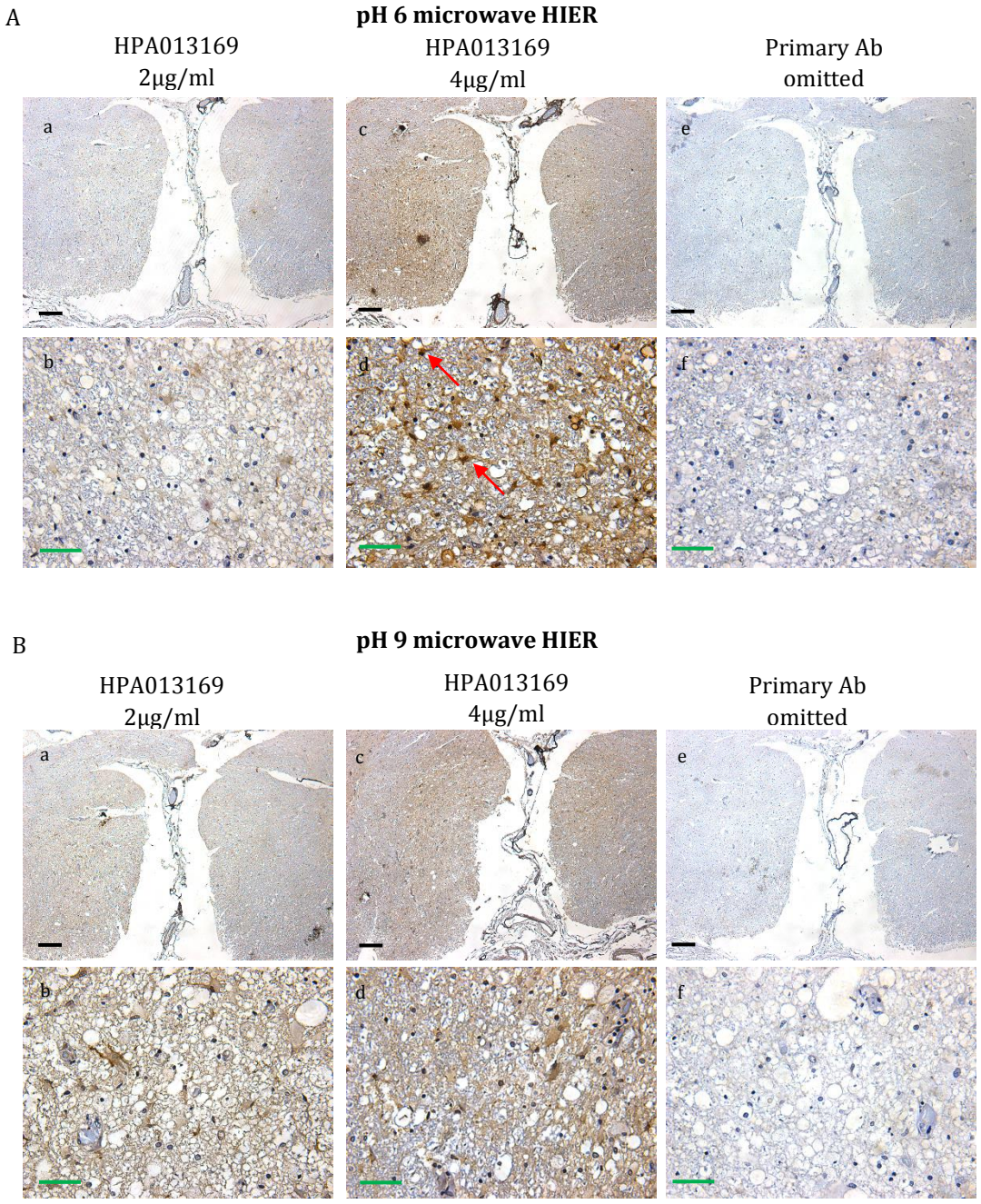

Figure 5.2.15. *Optimisation of HPA013169 (Atlas Anti-XCR1) reactivity within human cervical cord.* HPA013169 was tested at concentrations between 0.5µg/ml and 4µg/ml following HIER antigen retrieval. Representative images of the ventral corticospinal tracts of cervical cord treated with HPA013169 at 2µg/ml or 4µg/ml, and their respective negative controls, following microwave HIER in pH6 (A) or pH9 (B) buffer. Exemplary detection of XCR1-positive cells is highlighted by red arrows in A, d. Scale bars: Black = 200µm; Green = 50µm.

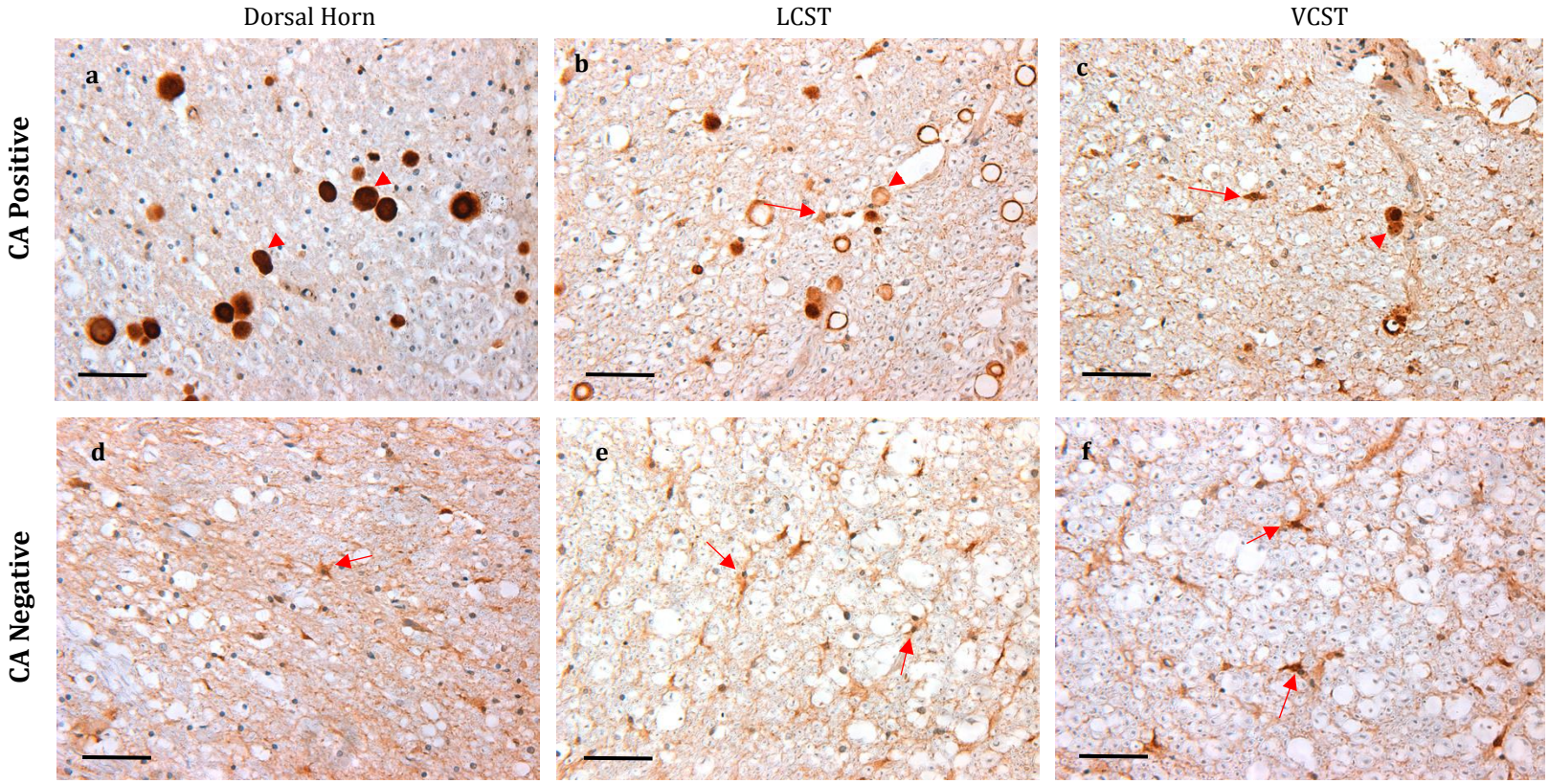

Figure 5.2.16. *Atlas anti-XCR1 immunoreactivity within the cervical cord of Control and sALS patients.* Images of Dorsal Horn, LCST and VCST of sections demonstrating HPA013169 reactivity in sections that were positive or negative for Corpora Amylacea (CA). CA inclusions demonstrate strong DAB reactivity (Red arrowheads) whereas HPA013169-positive cells (red arrows) are less reactive but prominent within white matter. Scale bars = 50μm.

A

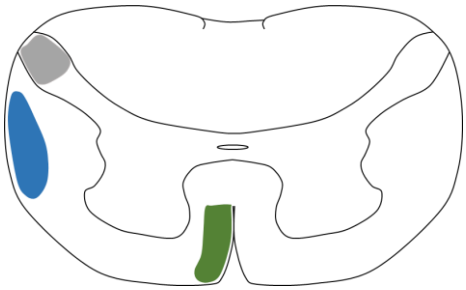

B

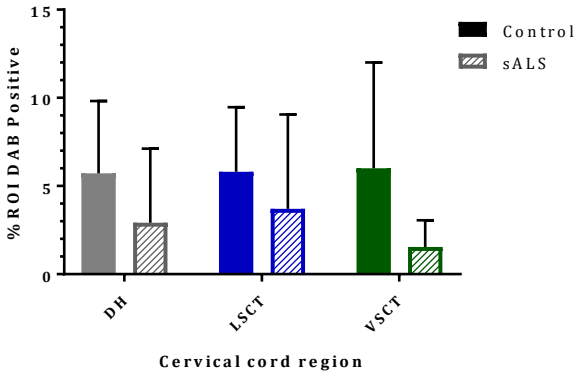

C

Presence of Corpora Amylacea

	Control	sALS
DH	2/4 (50%)	5/5 (100%)
LCST	2/5 (40%)	4/6 (66%)
VCST	2/5 (40%)	5/6 (83%)

D

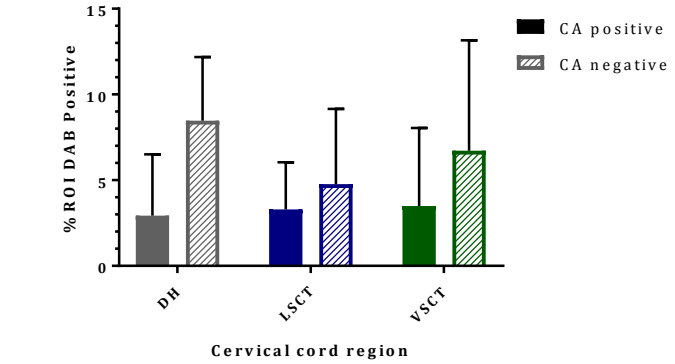

Figure 5.2.17. *Semi-quantitative analysis of Corpora Amylacea presence within cervical cord of ALS patients and controls*. A) Schematic illustration of cervical cord and regions analysed. Grey = Dorsal Horn (DH); Blue = Lateral corticospinal tracts (LCST); Green = Ventral Corticospinal Tracts (VCST). B) Quantification of DAB positive area within Dorsal Horn, LSCT and VCST of control and sALS samples. Error bars = ±SD. C) Incidence of HPA013169-positive CA within DH, LCST or VCST within Control and sALS sample sections. D) Quantification of DAB positive area within Dorsal Horn, LSCT and VCST that are positive or negative for the presence of CA. Error bars = ±SD. For N of each group see table in C.

Examination of HPA013169 reactivity within these cervical cords sections indicated XCR1 expression at variable levels, but for all samples evaluated. HPA013169 reactivity was again observed to predominate within the white matter of cervical cord. However, a feature that was not observed for the cervical cord sections used for optimisation, was the prevalent reactivity which localised to corpora amylacea (CA) inclusions that were distributed among the lateral regions of cervical cord white matter. CA also predominated within the dorsal horn of several cervical cord samples. The prevalence of these inclusions varied amongst both control and sALS samples and were either localised to the VCSTs, Lateral Corticospinal Tracts (LCSTs), dorsal horn, or, to a lesser extent, mediodorsal white matter. For one cervical cord examined (LP094/09) however, this reactivity localised to almost the entire perimeter of the cervical cord. Examples of HPA013169 reactivity within the VCST, LCST or Dorsal horn that exhibit the presence or absence of CA is presented in figure 5.2.16. A consistent feature that was observed within all sections was reactivity by blood vessels and also by cells resembling the morphology of astrocytes. For these cells, reactivity is observed at the cell soma, as indicated by the presence of counterstained nuclei. In addition, some cells demonstrate reactivity along processes which appear to surround an internal structure.

According to these initial observations, analysis of HPA013169 reactivity was decided to focus on the VCSTs, LCSTs and dorsal horn of cervical cord. Within these regions, analysis was performed on two factors: i) the presence or absence of HPA013169 reactivity by CA and ii) quantitative examination of HPA013169 reactivity area.

Following this analysis of each of the cervical cords, samples were categorised to sALS or control following removal of the study blind. As displayed in figure 5.2.17, B, the area of HPA013169 reactivity was indicated to demonstrate a high variability between samples. However, overall the presence of HPA013169 reactivity was indicated to be reduced in all 3 regions of the cervical cord examined for sALS samples in comparison to neurological controls.

Importantly, the presence of CA that demonstrated HPA013169 reactivity did not distinguish between control and sALS samples, suggesting these HPA013169-positive inclusions to exist within the cervical cord, independent to the diagnosis of ALS. However, qualitative analysis suggests the presence of CA was more prevalent in the sections of sALS patients than controls (figure 5.2.17, C).

In a further attempt to investigate the correspondence of HPA013169 reactivity to the presence of CA, the area of DAB reactivity within each cervical cord region was categorised according to the presence or absence of CA (Figure 5.2.17, D). Following this classification, regions in which there were HPA01369-positive CA inclusions were observed to

demonstrate a consistent decrease in DAB area, suggesting that the presence of these inclusions reduced the overall area of HPA01369 reactivity. Indeed, as can be seen from figure 5.2.16, HPA013169 reactivity within CA-negative sections demonstrates more extensive HPA013169 reactivity of lower intensity than that observed in CA-positive sections.

Overall, these results suggest that HPA013169 reactivity, and hence XCR1 presence, is consistent within the cervical cord of both sALS and control patients. Whilst the reactivity indicates the presence of XCR1-positive cells, the extensive HPA013169 reactivity that localises to CA inclusions appears to affect the quality of HPA01369 binding and hence influence the assessment of XCR1 presence between CA-positive and CA-negative cervical cord.

5.3 Discussion

In this study it was aimed to evaluate the expression of *Xcr1* and its cognate ligand, *Xcl1,* within the context of a prominent neuroinflammatory response. This was based on prior data suggesting the expression of this chemokine signalling axis to contribute to the central pathophysiology following peripheral nerve injury (Bird *et al.,* 2018) and, more recently, diabetic neuropathy (Zychowska *et al.*, 2016). In order to extend this evidence, the expression of the human XCR1 protein has also been tested within the human cervical cord of healthy neurological controls and sALS patients, utilising an antibody that has been independently validated to exhibit specificity to the human XCR1 protein.

5.3.1 Murine ALS models demonstrate a consistent neuroinflammatory response within the spinal cord

In order to provide a valid assessment of *Xcr1* and *Xcl1* expression in the context of a prominent neuroinflammatory response, the expression of Iba-1 and GFAP within the thoracic cord of two murine models of ALS has been investigated to assess the activation of microglia and astrocytes, respectively.

5.3.1.1 SOD-1-G93A mice demonstrate glial activation most prominently within the lateral and ventral regions of thoracic cord

The use of the established SOD1-G93A mouse model was in keeping with prior reports demonstrating the prolific activation of microglia and astrocytes within the spinal cord of rodent models expressing mutant *SOD1* (Gurney *et al.*, 1994; Hall, Oostveen and Gurney, 1998; Graber, Hickey and Harris, 2010; Joyce *et al.*, 2015). Moreover, for the model studied here, the high copy number of mutant *SOD1* expression exacerbates the disease phenotype and increases glial activation, in comparison to models expressing a lower copy number of the transgene or expressing an endogenous mutation within the mouse *Sod1* gene (Joyce *et al.*, 2015; McGoldrick *et al.*, 2013).

The examination of astrocyte and microglia features at 90 and 120 days provided an indication of the temporal changes of glial behaviour with disease progression and are considered to represent the symptomatic and end-stage of disease, respectively (Hall, Oostveen and Gurney, 1998). Iba-1 reactivity identified the enhanced microglial reactivity throughout the thoracic cord, demonstrated by the consistent presence of hypertrophic and hyper-ramified Iba-1 positive cells. In tandem with the increased area of Iba-1 coverage, this is consistent with the proliferation and activation of resident microglia, a characteristic that has been demonstrated for these cells in the SOD1-G93A model at these time points (Dibaj *et al.*, 2011) and is consistent with the analysis methods used for the identification of activated microglial from several pathologies (Korzhevskiy and Kirik, 2015; Beynon and

Walker, 2012). Moreover, the prevalence of Iba-1 reactivity that was observed to be most extensive within the lateral and ventral regions of white and grey matter is supportive of prior reports suggesting a lower microglial activation within the dorsal region of spinal cord for rat and mouse SOD1-G93A models (Dibaj *et al.*, 2011; Graber, Hickey and Harris, 2010). This is consistent with the demonstration of the relative sparing of afferent sensory neurons that innervate the dorsal horn in this model (Gurney *et al.*, 1994). Iba-1 positive aggregates were also observed in multiple thoracic cord regions. Observation of increased microglial aggregates has been described previously within a rat model expressing SOD1-G93A (Fendrick, Xue and Streit, 2007) and suggested to represent the formation of atypical giant multinucleated following microglial fusion. Subsequent analysis has also suggested that these formations represent the aggregation of independent microglia that migrate to sites containing high concentrations of extracellular, pro-inflammatory stimuli such as SOD1 protein aggregates (Graber, Hickey and Harris, 2010). This activation was particularly evident within the lateral and ventral regions of white matter, with notably high numbers of Iba-1 positive cells observed within the ventral horn of the grey matter. These features were observed to progress between 90 and 120 days and clearly illustrated the extensive induction of microglial activation within this mouse model.

The activation of glia at 90 and 120 days was further evidenced by the pronounced increase of GFAP reactivity and coverage within the thoracic cord, indicative of astrogliosis (Philips and Rothstein, 2014). This feature was most evident in the medial and ventral regions of the grey matter, in comparison to age-matched NTg controls. The response of astrocytes during ALS is distinct from that of microglia in that the activation of astrocytes is associated exclusively with a change in phenotype and morphology of resident cells, and not with concomitant cellular proliferation (Philips and Rothstein, 2014). Astrocytes provide essential support to neurons, particularly at the level of the synapse, where the formation of the tripartite synapse by astrocyte processes mediates the maintenance of extracellular neurotransmitter levels (Schousboe, 2003). Indeed, a diminished capacity of astrocytes to maintain physiological glutamate is heavily implicated in the development of excitotoxic mechanisms that contribute to motor neuron death during ALS (Morel *et al.*, 2013; Rothstein *et al.*, 1996; Shaw and Ince, 1997). The increase of GFAP reactivity within the grey matter, along with the comparatively lower increases observed within the white matter is indicative of pathology at the level of the synapse and neuronal somas. This is supported by prior observations in human spinal cord that demonstrates astrogliosis particularly within the medial and ventral spinal cord laminae of the grey matter with little to no GFAP reactivity observed within the cortiospinal tracts (CSTs) (Schiffer *et al.*, 1996) and also consistent with previous evidence of astrogliosis within the spinal cord of the SOD1-G93A model (Hall, Oostveen and Gurney, 1998). Moreover, astrocyte activation within the spinal

cord of murine models of ALS is associated with disease onset (Yamanaka *et al.*, 2008) and *in vivo* monitoring of GFAP expression has clearly illustrated the association of increased GFAP expression with the onset of motor neuron degeneration within these mice (Keller, Gravel and Kriz, 2009). Indeed, despite early reports suggesting astrocyte reactivity to indicate an attempt to ameliorate the toxic environment induced by activated microglia (Hall, Oostveen and Gurney, 1998) it has since become apparent that mutant *SOD1*-expressing astrocytes are detrimental to motor neuron survival. Hence, increased GFAP reactivity is associated with the production of a more toxic neuronal environment, although the exact mechanisms of this remain unclear (Clement *et al.*, 2003; Di Giorgio *et al.*, 2007; Marchetto *et al.*, 2008).

Importantly, the investigation of glial reactivity in this study focussed on the thoracic cord of SOD1-G93A mice and provides a characterisation that diverges from the typical focus on the ventral horn of the lumbar spinal cord. However, pathology within this region of SOD1-G93A mice has been demonstrated and is associated with the degeneration of motor neurons in the ventral horn and also of pre-ganglionic sympathetic motor neurons that are located within the intermediolateral nucleus found between T1 and L2 vertebral regions (Llewellyn-Smith, 2009; Kandinov *et al.*, 2011; Kandinov *et al.*, 2013). The evidence of microglial and GFAP reactivity therefore supports the presence of pathology within this region but also underscores this mouse model to provide samples of spinal cord that exibits prevalent neuroinflammation.

5.3.1.2 TDP-Q331K mice demonstrate distinct patterns of microglial activation to SOD1-G93A mice

In contrast to the widely characterised SOD1-G93A model, the mouse TDP-Q331K model is more recent and has relatively little characterisation. Following the original description of this model (Arnold *et al.*, 2013) a subsequent analysis provided additional insights to the development of pathology by TDP-Q331K mice (Mitchell *et al.*, 2015). From these two descriptions, the presence of microglia and astrocytes, according to Iba-1 and GFAP reactivity, was observed to increase at 10 months within the ventral horn of mice expressing TDP-Q331K in comparison to NTg controls (Arnold *et al.*, 2013). Later characterisation provided evidence of glial activation at 2 months and 24 months, however characterisation of microglia was made by the detection of CD68 (Mitchell *et al.*, 2015). At 2 months, GFAP reactivity demonstrated increased astrocyte presence within the ventral horn, but evidence of CD68 reactivity was absent for TDP-Q331K mice, as observed for NTg mice. By 24 months, GFAP reactivity indicated the sustained increase of astrocyte presence and activation within the ventral horn, however microglial presence demonstrated little changes to that observed

for NTg animals within the same region. Instead, CD68 reactivity was significantly increased within the dorsal columns, lateral and ventral tracts of the white matter of TDP-Q331K mice.

Importantly, the genetic background of the TDP-Q331K mice investigated here (C57BL/6NJ) is different to that used for the original generation of the TDP-Q331K model (C57BL/6NCrl, Arnold *et al.,* 2013). However, behavioural and functional measures of the motor phenotype of the TDP-Q331K mice investigated here have been extensively characterised by Dr Jodie Stephenson (Stephenson 2017). This demonstrated the progressive development of mild motor symptoms by TDP-Q331K mice, including the development of motor tremor by 10 weeks, abnormal gait by 3 months and evidence of increased microglial and astrocyte presence in the ventral horn by Iba-1 and GFAP immunohistochemistry. In conclusion, it was suggested that a plateau of symptoms was achieved by 10 months, but by 6 months the development of the motor phenotype was clearly evident. Thus, this model, despite being on a different genetic background demonstrated consistent functional and pathological features to that described by Arnold et al., 2013.

The evidence gathered by this investigation has therefore provided a considerable extension to the evidence of microglial and astrocyte reactivity within the spinal cord of TDP-Q331K mice. In particular, it has demonstrated that the major area of microglia activation is located within the white matter of thoracic cord at 6 months and 10 months of age for TDP-Q331K mice. Interestingly, the pattern of microglia reactivity within the white matter of TDP-331K is distinct to that observed for SOD1-G93A mice. This is most evident by the prominent Iba-1 reactivity within the dorsal columns of TDP43-Q331K mice, a feature that is not seen for SOD1-G93A mice (Figure 5.2.4; Figure 5.2.10; Dibaj *et al.,* 2011). In addition, this reactivity becomes more prevalent along the entire rostrocaudal axis of the thoracic cord with age (Appendix 4 vs Appendix 5). Notably, previous characterisation of CD68 reactivity, a marker for the presence of activated, phagocytic microglia (Graber, Hickey and Harris, 2010; Korzhevskiy and Kirik, 2015) did not suggest microglial activation within the lateral tracts by 2 months of age for TDP-Q331K mice, despite evidence of motor neuron loss. However, by 24 months, microglial activation within the dorsal and lateral tracts was prevalent (Arnold *et al.*, 2013). Therefore, the evidence provided here within the thoracic cord provides an insight of microglial activity within the lateral and dorsal regions of white matter during an intermediary time period to that described previously. In addition, it also provides an insight in to the activity of microglia during a time that mice are observed to achieve a phenotypic plateau (Arnold *et al.*, 2013); Stephenson 2017). Together, this suggests that the predominant microglial activation within the spinal cord of TDP-Q331K is localised to the lateral and dorsal white matter of TDP-Q331K mice.

Despite receiving little focus within the literature for murine ALS models (Yamanaka *et al.*, 2006), pathology of the lateral and dorsal white matter regions are an important consideration for the interpretation of pathology within murine models of ALS mice. This is due to these regions represents the location of descending CSTs. Within mice, the majority (~80%) of CSTs are located within medial dorsal region of white matter, whilst the remaining ~20% are located within the lateral white matter. These lateral corticospinal CSTs descend throughout the thoracic cord and have been described to extensively innervate both dorsal and ventral grey matter, contributing to the polysynaptic control of lower motor neurons along the rostrocaudal axis (Steward *et al.*, 2004). This is in contrast to the prominence of the descending corticospinal tracts that exist within the dorsal lateral region of spinal cord in primates and humans, a region synonymous with the pathology of ALS. A further reason for the importance of this observed pathology is that CSTs within the lateral regions of mouse spinal cord have been demonstrated to degenerate in a mouse model expressing mutant SOD1-G85R (Yamanaka *et al.*, 2006), whilst the dorsal column CSTs are observed to be spared (Song *et al.*, 2012). Furthermore, pathology within the lateral white matter is also associated with significant disruption to the blood-spinal cord barrier. In several murine models expressing mutant *SOD1* this leads to vascular leakage and extensive microvascular haemorrhage that is evident at presymptomatic stages, prior to motor neuron loss, and preceding the neurovascular inflammatory response (Zhong *et al.*, 2008). This evidence has recently been furthered to demonstrate the significant swelling and degeneration of axons, accompanied by prominent microglial activation, within the lateral CSTs of the SOD1-G93A mouse model at 90 days with a continual decline to 120 days (Dibaj *et al.*, 2011).

In addition to the evidence within dorsal and lateral CSTs of the white matter, analysis of microglial presence, as determined by Iba-1 area, also suggested distinct microglial pathology within the ventral horn grey matter TDP-Q331K mice in comparison to SOD1-G93A mice. For TDP-Q331K mice at 10 months the microglial presence within the ventral horn was increased to a lower extent to that observed at 6 months, in comparison to age-matched NTg controls. Although this evidence is confounded by the low number of animals used for the characterisation at 6 months, this is in line with the evidence from Mitchell 2015. Specifically, Mitchell *et al*., 2015 showed that the presence of CD68 was not changed between NTg and TDP-Q331K mice in ventral horn by 24 months. This indicates that the presence of phagocytic microglia was not any different between NTg and TDP-Q331K mice, even at this late stage and despite the significant loss of lower motor neurons. This is in contrast to SOD1-G93A mice that demonstrate prevalent CD68 reactivity within the ventral horn (Frakes *et al.*, 2014) and were also observed here to provoke a significant increase of Iba-1 reactivity within this region of thoracic cord.

Taken together, the evidence of Iba-1 reactivity within the white and grey matter of these two mouse models demonstrates qualitative differences in microglial reactivity and phenotype. In conjunction with the prior description of CD68 reactivity (Frakes *et al.*, 2014; Mitchell *et al.*, 2015), the microglial reaction within the two models is distinguished by the adoption of phagocytic phenotype within the ventral horn of SOD1-G93A mice that is not seen for TDP-Q331K mice. The reason for this remains speculative, however it is intriguing to note that the aggregation of cytoplasmic ubiquitinated inclusions was not observed for TDP-Q331K mice either within motor neurons or within the neuropil (Mitchell *et al.*, 2015). In contrast, ubiquitinated aggregates of SOD1 protein is prevalent in mice overexpressing SOD1-G93A and prevails within the neuropil before aggregation within motor neurons (Stieber, Gonatas and Gonatas, 2000). Therefore, this distinction in the phagocytic phenotype of microglia may be a consequence of the distinctive presence of aggregated proteins within these two models. In addition, the Iba-1 reactivity observed here suggests the activation of microglia within both regions of CSTs of thoracic cord for TDP-Q331K, whilst reactivity of Iba-1 in SOD1-G93A mice is confined to the lateral CSTs only. This observation is in line with reports from an independent mouse model that expresses a distinct mutation of the human TDP-43 protein (TDP43-A315T) in which axonal degeneration within both dorsal and lateral CSTs was confirmed within the lower thoracic cord (Wegorzewska *et al.*, 2009). Whist focus on CST pathology in mouse models in the literature is less prevalent than that within the grey matter, this region highlights a distinctive pathophysiology of ALS related to TDP-43 or SOD1 mutations and supports the greater involvement of upper motor neuron degeneration, as well as degeneration in other cortical areas, of TDP-Q331K mice. Thus, the pathology observed within the lateral and dorsal CTSs of thoracic cord from TDP-Q331K mice may be more representative of the pathology observed in the broader human ALS population, in which microglial activation within the CSTs of human ALS patients demonstrates a correspondence to disease progression (Brettschneider *et al.*, 2012), but is also suggestive of broader cortical degeneration of patients suffering from ALS associated TDP-43 mutation, as discussed in section 5.1. This is supported by the observation of TDP-Q331K mice to demonstrate symptoms that correlate with a dementia-like phenotype (Stephenson 2017).

5.3.2 The expression of Xcl1, but not Xcr1, is upregulated within the spinal cord of ALS mouse models

A recent investigation demonstrated the expression of Xcr1 and Xcl1 proteins within the lumbar spinal cord of mice by western blot. Furthermore, this expression was found to be influenced by streptozotocin treatment - a treatment used to model diabetic neuropathy in mice (Zychowska *et al.*, 2016). However, no characterisation of the respective gene

expression was carried out within the spinal cord. This project also aimed to evaluate Xcr1 protein expression within the mouse CNS and evaluate this within the context of ALS models, but unfortunately this was not possible due to the unreliability of antibody specificity (Chapter 4). Consequently, the evidence of Xcr1 and Xcl1 expression has relied on qPCR analysis of gene expression. Of particular importance to the evidence gathered here, was that the evaluations of *Xcr1* and *Xcl1* expression were made within a mouse model that demonstrated the activation of microglia, due to the suggestion of these cells being the primary contributor of *Xcl1* in the CNS of mice (Zychowska *et al.*, 2016). As described above and demonstrated in section 5.2, both TDP-Q331K and SOD1-G93A mice demonstrate prolific activation of microglia.

Evaluations of *Xcr1* expression within the spinal cord of NTg mice was previously described to demonstrate low expression (Chapter 3). Here, comparisons of *Xcr1* expression in the spinal cord of NTg mice with that of TDP-Q331K mice, at both 6 and 10 months, also demonstrated low expression and illustrated no change in expression between diseased mice and NTg controls. Comparisons of *Xcr1* expression also demonstrated no changes between SOD1-G93A mice at 90 days with their respective controls. Together, this suggests that *Xcr1* expression is not influenced within the spinal cord of these transgenic mice, despite the distinct pathophysiology that they present.

Evaluation of *Xcl1* expression however, suggested a consistent upregulation of expression in all transgenic mice and ages, in comparison to their NTg controls. This was only observed to be statistically significant however for TDP-Q331K mice at 6 months of age where a mean increase of 102% and 79% was observed in male and female TDP-Q331K mice, respectively. In addition, there was a large range of *Xcl1* expression observed for male TDP-Q331K mice at 10 months, suggesting a potential influence of TDP-Q331K expression on *Xcl1* expression that lacks consistency, a feature that was not observed for female mice. Interestingly, a trend was observed to suggest an increased expression of *Xcr1* by male mice at 10 months in comparison to their female counterparts, irrespective of genotype. A similar trend was also observed for *Xcl1* expression.

Xcl1 expression may also be considered to be increased in SOD1-G93A mice at 90 days. For the three replicates performed, two SOD1-G93A mice demonstrated consistently elevated levels. However one sample demonstrated particularly low expression, a feature that was also observed for *Xcr1* expression from the same mouse. Due to all quality control assessments suggesting this data to be valid the low expression could not be excluded, but does suggest that *Xcl1* expression is elevated in SOD1-G93A mice. Moreover, the level of *Xcl1* expression in SOD1-G93A mice was the highest level of *Xcl1* expression observed from any sample.

The features of *Xcr1* and *Xcl1* expression therefore demonstrate several features that are consistent with the contribution of chemokines and, more broadly, cytokines to the immune response of CNS disease. Firstly, the increased expression within TDP-Q331K mice was most prominent at 6 months of age, whilst evaluation of expression was performed for SOD1-G93A mice at a time point considered to reflect the prominent onset of motor neuron loss (Keller, Gravel and Kriz, 2009). These time points are therefore suggestive of *Xcl1* expression to contribute to an early innate immune response, a feature for which the expression of *Xcl1* has been suggested to be characteristic of (Moser and Loetscher, 2001). In addition, the innate immune response is recognised as a symptom of ALS (Phani, Re and Przedborski, 2012) and is suggested to continue within the SOD1-G93A mouse from the pre-symptomatic to end-stage disease, at which point an adaptive cytotoxic response is suggested to prevail (Beers *et al.*, 2008; Jara *et al.*, 2017; Komine *et al.*, 2018). Specific descriptions of the innate immune response within mice expressing TDP-43 mutations isn't available, yet considering the observed increases of Iba-1 throughout the thoracic cord observed here and the widely documented role of microglia to contribute to the immune response of the CNS (Philips and Rothstein, 2014; Phani, Re and Przedborski, 2012; Lewis *et al.*, 2012) it would seem plausible to recognise an innate immune response within the spinal cords of TDP-Q331K mice, as observed for SOD1-G93A mice.

A second reason for the patterns of *Xcr1* and *Xcl1* expression to resemble features of other cytokines and chemokines is the effect of sex on the expression of these mediators and the broader immune response in general (Klein and Schwarz, 2018). The separation of analysis performed in this study of TDP-Q331K mice was made according to the observation that males demonstrated a more variable disease course than females (Stephenson 2017). However, several cellular components of the immune system are known to vary between males and females. Notably, the higher expression of Toll-like receptors, including TLR4, by peripheral immune cells from males is suggested to be responsible for the increased expression of certain chemokine and cytokines following particular immune challenges, such as LPS (Torcia *et al.*, 2012; Moxley *et al.*, 2002; Rettew and Marriott, 2007; Rettew, Huet and Marriott, 2009). Microglia are also suggested to exhibit sexually dimorphic activation patterns that are linked to the differential expression of estradiol receptors on the microglia obtained from female and male mice (Nissen, 2017). Further sex-based differences between the immune response of males and females have also been documented, including the suggestion of a difference of CD4+ to CD8+ T-cell ratios (Klein and Schwarz, 2018).

Hence, whilst the precise reasons for the differences in *Xcr1* and *Xcl1* expression between mice as a consequence of sex and genotype are unclear, the features of these differences are

indicative of this chemokine signalling axis to participate in some way to the immune response observed in these transgenic models of ALS. However, due to the source of the RNA samples arising from whole spinal cords of mouse and the documented migration of peripheral immune cells, including dendritic cells, to the CNS parenchyma in ALS (Henkel *et al.*, 2004; Henkel *et al.*, 2006; Beers *et al.*, 2008) further refinement to the cellular source of this expression is required.

5.3.3 Xcl1 is expressed at a low level by primary adult mouse microglia and is not influenced as a consequence of ALS-associated mutation or LPS treatment

A further source of evidence to the expression of *Xcl1* within the CNS that arose from the publication by Zychowska *et al.,* was the dramatic increase (~400 fold) of *Xcl1* expression by primary microglia obtained from P1 rat pups as a consequence of LPS treatment for 24 hours (Zychowska *et al.*, 2016). In order to further investigate this possibility in mice, this study has replicated the method used by Zychowska *et al.,* 2016 for the treatment of primary adult mouse microglia. Furthermore, the isolation of primary microglia from NTg, TDP-Q331K and SOD1-G93A mice provided an opportunity to refine the potential cellular source of the observed differences of *Xcl1* expression within the CNS of these mice.

No evidence has been found to here to suggest that primary microglia obtained from adult mice display an increased *Xcl1* expression following LPS treatment. Instead, the only consistent and significant difference observed was a slight decrease (~25%) in *Xcl1* expression by NTg cultures following LPS treatment. This is despite the clear activation of these microglia as demonstrated by quantitative and qualitative assessment of Iba-1 reactivity suggesting across. No differences in *Xcl1* expression were observed for primary cell cultures prepared from TDP-Q331K mice or SOD1-G93A mice following LPS treatment. This is again despite the demonstrated activation of these cells, a feature that was particularly prominent for microglia obtained from SOD1-G93A mice and in line with the description of these mice to exhibit to enhanced activation state (Dibaj *et al.*, 2011).

The expression of *Xcl1* within primary microglial cultures was also observed to be similar between the three genotypes examined. However, the reliability of this assessment to accurately reflect *Xcl1* expression in microglia is confounded by the lack of these cells in cultures from TDP-Q331K mice. In contrast, the consistency of Iba-1 positive cells in NTg and SOD1-G93A does suggest a reasonable assessment of microglia within these cultures. Considering this, the identified similarity of *Xcl1* expression, irrespective of microglial presence between the different cultures, suggests a negligible expression of *Xcl1* expression by microglia from mice of all three genotypes. These results are therefore in contrast to that described for *Xcl1* expression within primary microglia, as described by Zychowska *et al.,* 2016, and suggest a low expression of *Xcl1* by adult mouse microglia, both in resting and

activated states. In addition it also suggests that, unlike other chemokines, including Ccl2, Ccl5, Cxcl10 and Cxcl12 (Swarup *et al.*, 2011; Sargsyan *et al.*, 2009; Komine *et al.*, 2018), the expression of *Xcl1* by microglia is not influenced by the presence of ALS-associated mutations, nor by the treatment of LPS.

Exquisite profiling of microglia isolated from SOD1-G93A mice have demonstrated the unique phenotype adopted by these cells *in vivo* (Chiu *et al.*, 2013). Furthermore, this also demonstrated a distinct expression profile of microglia obtained from SOD1-G93A mice in comparison to microglia treated with LPS (Chiu *et al.*, 2013). Given the spectrum of pathology that the primary microglia cultures studies here have been subject to within the SOD1-G93A mice and TDP-Q331K mice and the demonstration of prominent activation following LPS treatment, this evidence would suggest that microglial expression of *Xcl1* is negligible under physiological and several pathophysiological states. Moreover, it suggests that the differences of *Xcl1* expression observed within spinal cord RNA from TDP-Q331K and SOD1-G93A mice does not arise as a consequence of microglial expression.

5.3.4 HPA013169 reactivity localises to glial cells and detects the presence of Corpora Amylacea

The independent validation of the Atlas HPA013169 antibody to demonstrate specificity to human XCR1 provided an opportunity to investigate the expression of XCR1 within the human CNS and extend the investigation of the expression of this chemokine receptor in ALS.

Initial optimisation of HPA013169 demonstrated the antibody to detect cells within the lateral and ventromedial white matter of cervical cord of an sALS patient. Lateral regions of the cervical cord contain the axons of descending CSTs from cortical neurons, particularly those from upper motor neurons of the motor cortex, within the contralateral brain hemisphere. The ventromedial white matter, also contains CSTs although these arise from cortical neurons of the ipsilateral hemisphere (Charles Watson, 2009). Therefore, the reactivity of HPA013169 to indicate the expression of XCR1 within these regions was particularly interesting considering the prevalent pathology observed within these regions of ALS patients. Consultation with a neuropathologist suggested that HPA013169 reactivity localised to astrocyte cells.

Subsequent analysis was performed in cervical cord from a cohort of Control and sALS patients to determine if HPA013169 reactivity exhibited specific patterns of reactivity as a consequence of disease. This analysis was confounded by the presence of HPA013169 reactivity which localised to CA inclusions. These inclusions were observed for both control and sALS patients and exhibited a high HPA013169 reactivity. The presence of CA was also

demonstrated to reduce the overall area of HPA013169 reactivity, suggesting the higher ffinity of HPA013169 to CA inclusions was capable of inhibiting antibody binding to surrounding XCR1 epitopes.

CA inclusions have been demonstrated to exist within the CNS particularly as a consequence of age and are more prevalent within patients suffering from neurodegenerative diseases including Alzheimer's diseases, Parkinsons Disease and ALS (Pisa *et al.*, 2016). They are characterised by a spherical structure that has a diameter typically between 10-50μm. The composition of CA has been demonstrated to contain mostly polyglucans with small component of protein (Sfanos *et al.*, 2009). The origin of these inclusions is unknown, but the presence of protein components including mitochondrial Heme-oxygenase 1 (Song *et al.*, 2014), ubiquitin, heat shock proteins, the anti-apoptotic protein Bcl2 (Botez and Rami, 2001), several complement factors and other innate immune proteins such as α-defensins, is suggestive of cellular origins that arise as a consequence of chronic inflammation and subsequent cellular death (Meng *et al.*, 2009; Singhrao *et al.*, 1995; Sfanos *et al.*, 2009). Indeed, one theory for the prevalence within patients suffering from neurodegenerative disease is that chronic inflammation within the CNS along with the concomitant presence of pathogens including numerous bacteria, virus and potentially fungi, can lead to a chronic inflammatory reaction to such pathogens and the aggregation of cellular and pathogenic products within the CNS (Meng *et al.*, 2009; Pisa *et al.*, 2016).

The reactivity of HPA013169 to CA inclusions may therefore indicate significant aggregation of XCR1 within these inclusions. However, this can only considered a possibility and cannot be considered certain, due in no small part to the significant non-specific binding of several antibodies to CA inclusions (Auge *et al.*, 2018). Despite this, the quantification of CA presence within the cervical cord of sALS and control patients, according to HPA013169 reactivity, demonstrated a higher prevalence of these inclusions within sALS patients. This is in line with a recent systematic quantification of CA within the CNS and spinal cord of ALS and control patients (Pisa *et al.*, 2016).

Excluding the reactivity to CA, HPA013169 was observed to identify numerous cells within the white matter of cervical cord. These cells were often observed to encapsulate axonal-like structures (Figure 5.2.16, e) and therefore in addition to their identification as astrocytes it is possible that these cells may also represent oligodendrocytes. This provides an intriguing point for further investigation of XCR1 reactivity within the CNS. Indeed numerous chemokine receptors have been described to be expressed by astrocytes and oligodendrocytes and this appears to be particularly prevalent as a consequence of inflammatory lesions in multiple sclerosis and include chemokine receptor CCR2, CCR3, CCR5, CXCR1, CXCR2 and CXCR3 (Simpson *et al.*, 1998; Simpson *et al.*, 2000; Omari *et al.*,

2005; Omari *et al.*, 2006). In line with the dogmatic principle of chemokine receptor function, the expression of chemokine receptors by astrocytes is associated with the migration of these cells to sites of injury and may also influence their capacity for proliferation. The importance of oligodendrocytes to the pathology of ALS is underscored by the prominent degeneration of descending CSTs that is characteristic of the disease. Moreover, oligodendrocyte pathology has begun to be appreciated in murine ALS models. In these models, oligodendrocytes are thought to contribute to disease by the decreased provision of trophic support to neurons due to decreased expression of monocarboxylate transporters. Oligodendrocytes and their precursors also display disrupted maturation which likely contributes to dysfunctional myelination of axons, particularly within the ventral grey and white matter of mutant SOD1 mice (Hughes *et al.*, 2013; Nonneman, Robberecht and Van Den Bosch, 2014).

However, without conformation of the cellular identity responsible for this reactivity, the implications of HPA013169 reactivity and hence XCR1 expression by these cells is difficult to comment upon. In particular, due to the documented exclusivity of XCR1 expression by tissue and lymphoid resident cross-presenting DCs (Dorner *et al.*, 2009; Bachem *et al.*, 2010) and the documented evidence for DC recruitment to the spinal cord of ALS patients (Henkel *et al.*, 2004) the possibility of HPA013169 reactivity to reflect DCs in the spinal cord can also not be excluded. Unfortunately, time restrictions have not made the characterisation of HPA013169 reactive cells possible, however plans are underway to achieve this.

5.3.5 Summary

In this study the expression of *Xcr1* and *Xcl1* has been sought to be investigated within a model of prominent neuroinflammation. This is in line with previous evidence to demonstrate the expression of chemokines and their receptors within the CNS as a consequence of disease. Moreover, it was also sought to specifically evaluate the expression of *Xcl1* within primary microglia according to recent suggestions suggesting the expression of this chemokine by these cells. This has been achieved by the utilisation of two distinct murine models of ALS that were demonstrated to present prolific activation of resident microglia and astrocytes. This has demonstrated a small but noticeable increase of *Xcl1* expression within the spinal cord of these murine models, however further repeats will be required to validate these differences.

The preparation of primary microglia from SOD1-G93A and TDP-Q331K mice also demonstrated a lack of change to the expression of *Xcl1* in comparison to NTg controls and also following LPS treatment. Together, this evidence supports a contribution of the class C chemokine receptor and its ligand to the immune response that is generated in the SOD1-

G93A and TDP-Q331K models of ALS, however this is not contributed to by the expression of *Xcl1* by microglia.

In an attempt to provide further clarity to the expression of XCR1 within the CNS, we have, to the best of our knowledge, provided the first comparison of XCR1 presence within the spinal cord of neurological controls and sALS patients. Unfortunately, this evidence has suggested the HPA013169 antibody to also demonstrate reactivity to CA inclusions, despite previous validation of specificity to the XCR1 protein. This has confounded a clear interpretation of XCR1 presence. However, HPA013169 reactivity indicates the expression of XCR1 by glial cells, particularly within the white matter of cervical cord that contain the axons of descending corticospinal tracts. The identity of these cells has yet to be confirmed but warrants further investigation to characterise the expression of XCR1 within the CNS.

6.0 Conclusions and Future Work

This project has sought to provide an insight to the emerging role of the Class C Chemokine Receptor, Xcr1 and its ligand, Xcl1, within the CNS (Bird *et al.*, 2018; Zychowska *et al.*, 2016). One of the primary aims of this project was to establish the presence and localisation of Xcr1 protein within the CNS. Consequently, a significant portion of time has been used for the testing of antibodies to validate their specificity to Xcr1. In doing so, a reliable technique involving the overexpression of myc-tagged target Xcr1 and XCR1 proteins *in vitro* has shown to provide a reliable source of antigen for the testing of antibody specificity. In particular, the C-terminal myc tag allowed clear illustration of the antibody specificity through colocalisation with a validated monoclonal anti-myc antibody. This is in line with previous and contemporary work that has demonstrated the validity of *in vitro* characterisation of antibody specificity to GPCRs and other proteins via the transient or stable expression of target protein in cell culture (Grimsey *et al.*, 2008; Skogs *et al.*, 2017). Based on the evidence from this method, unfortunately it has not been possible to reliably evaluate the expression of Xcr1 protein within the CNS due to a lack of specificity of all tested antibodies.

There is evidence to suggest that the lack of antibody reliability has made a considerable contribution to the lack of reproducibility in life science research. Several studies have been shown to base conclusions upon results that arose from non-specific binding of antibody. One estimate has suggested ~50% of all commercially available antibodies to be non-specific and hence provide unreliable detection of their target protein (Baker, 2015). Along with others (Bordeaux *et al.*, 2010; Skogs *et al.*, 2017; Grimsey *et al.*, 2008) the results from this study therefore provide a relatively economical and reproducible protocol that should be used for the in-house validation of antibodies prior to their use on test specimens.

6.1 Does an alternative composition of Xcr1 mRNA exist?

The investigation of *Xcr1* mRNA composition has focussed on the potential for an alternative structure to mature *Xcr1* mRNA. Use of 5'RACE provided clear evidence to support the existence of *Xcr1* mRNA composed of both exon 1 and exon 2. However, the retention of intron 1 sequences remains inconclusive. A lack of clarity regarding this has arisen from the fact that the two potential Xcr1 ORFs that have been proposed lie in-frame within one another. Without clarification of the actual amino acid sequence of the Xcr1 protein, confirming the actual *Xcr1* mRNA sequence is made problematic as the original description of Xcr1 protein (referred to as Xcr1S in this study, (Yoshida *et al.*, 1998)) could theoretically arise from either mRNA isoform. In testing the expression of each potential isoform it was consistently observed that for both spleen and spinal cord tissue evaluation of RNA arising from exon 1 and exon 2 or exon 2 only demonstrated similar levels of expression. However,

it was intriguing to note that for the evaluation of RNA from mESC-derived motor neurons the expression of RNA containing exon 2 only was considerably higher than RNA composed of exon 1 and exon 2. Retrospective microarray analysis of the immortalised NSC-34 murine motor neuron-like cell line further supported the higher presence of RNA derived from exon-2 of *Xcr1,* in comparison to exon 1.

Given the documented alternative splicing and the use of alternative promoters by other chemokine receptors such as CXCR3 (Lasagni *et al.*, 2003) and CCR5 (Mummidi *et al.*, 2007), the capacity for alternative expression of mRNA arising from *Xcr1* warrants further investigation. In particular, the functional capacity of predicted promoter regions within intron 1 should be assessed. This will provide important insights in to the regulation of *Xcr1* mRNA that may prove important for translating the evidence of Xcr1 between mouse and human.

6.2 Evaluation of Xcr1 *protein isoforms supports the function of the* Xcr1S *protein*

An essential and fundamental aspect to the investigation of any protein is to be sure of its identity. Since the discovery of the Xcr1 protein as the murine homologue of human XCR1, a considerable lack of clarity has arisen regarding the identity of the Xcr1 protein. This has primarily arisen from the more recent discovery of *Xcr1* exon 1, and led to the prediction of an alternative ORF site within *Xcr1* mRNA, as discussed. Consequently, two protein isoforms remain theoretically plausible translations of the mRNA sequence, differing by 16 amino acids within the N-Terminal domain. This study has provided the first direct functional comparison of these potential isoforms by evaluating their interaction with β-arrestin, a ubiquitous intracellular protein that interacts with all GPCRs. This evidence has provided further support to the original description of the Xcr1 protein and adds credence to the suggestion that the functional Xcr1 protein arises from a coding sequence residing exclusively within exon 2. This evidence is given further support from the observation that the human XCR1 ORF is also confined to a single exon (Shinkai *et al.*, 2005). This has important implications for future investigations of this protein, particularly for the development of specific antibodies. Given the observation that the only antibody with a validated specificity in this study targeted the N-terminal domain of the human XCR1 protein, defining the actual sequence of the Xcr1 N-terminal will hopefully enable the fruitful outcome of subsequent antibody development.

6.3 Microglia display a low Xcl1 expression that is not induced by inflammatory stimuli

During the course of this project, evidence emerged to support the expression of Xcr1 and Xcl1 within the CNS of mice in a mouse model of diabetic neuropathy (Zychowska *et al.*, 2016). The authors suggested Xcr1 to be expressed by neurons of the spinal cord and the

expression of Xcl1 by microglia. The expression of *Xcl1* was also suggested in response to the inflammatory stimulus, LPS. Two methodological flaws were identified for this study. Firstly, the antibody used for the detection of Xcr1 within the spinal cord was raised to an immunogen from the human XCR1 protein and had not been validated for specificity to mouse Xcr1. Secondly, evidence to support the expression of *Xcl1* in mouse microglia arose from the use of primary cells obtained from rat pups (Zychowska *et al.*, 2016). The evidence gathered from this project has therefore provided contrasting evidence to these suggestions based on i) a demonstrated lack of specificity of Abcam 188896 to mouse Xcr1 and ii) the observed lack of response by primary adult mouse microglial cells to express *Xcl1* following LPS administration. The expression of *Xcl1* was also not observed to be upregulated within a primary cell culture enriched with microglia obtained from SOD1-G93A and TDP-Q331K mice. This is despite the upregulated expression of *Xcl1* observed within RNA collected from the spinal cord of these mice. Furthermore, prolific microglial activation was observed in these spinal cords. This evidence therefore suggests that *Xcl1* is not expressed by mouse microglia. Conformation of Xcr1 expression by spinal cord neurons will require further investigation utilising a reliable antibody with a demonstrated specificity to Xcr1.

In the process of confirming the use of mouse models that demonstrate consistent microglial activation, this project has identified distinct glial pathology within the spinal cords of SOD1-G93A and TDP-Q331K mice. This is in support of the work of others that demonstrate alternative sites of pathology within the spinal cord of these mouse models. Moreover, it supports the use of these models to provide a more comprehensive reflection of pathophysiology that is observed for ALS patients with distinct genetic pathogenesis.

6.4 The expression of XCR1 *by resident cells of the human CNS remains inconclusive*

In line with the ultimate objective of this project to assess the expression and potential function of the class C chemokine receptor and ligand within the human CNS, the expression of human XCR1 has been evaluated within the spinal cord of control and ALS patients by immunohistochemistry. This preliminary investigation has provided evidence to suggest the low expression of this chemokine receptor by cells of the CNS, particularly within the white matter of cervical cord. The observed reactivity is supported by the independent validation of the antibody used for XCR1 detection. Unfortunately, due to circumstances beyond our control, it has not been possible to clarify the identity of the cells which demonstrate XCR1 expression. Furthermore, the detection of XCR1 using this validated antibody within a wider population may be confounded by reactivity to CA bodies that often display the non-specific accumulation of antibody. Plans to identify the cellular identity of cells demonstrating XCR1-reactivity are underway.

6.5 Conclusion

The class C chemokine receptor, XCR1, and its ligand(s) in mice and human represents a highly conserved chemokine signalling axis. The strong homology of this axis, from the level of DNA sequence to the observed physiological function, suggests a clear translational capacity for the observations made in mice to predict that carried out in humans. Technical limitations, including access to reliable antibodies, have prevented the application of consistent methodologies to the investigation of XCR1 and XCL1 between both mouse and human samples of CNS tissue. However, analysis of samples from mouse models of human disease has permitted the examination of prior suggestions regarding the function of Xcr1 and Xcl1 in the CNS. This has suggested that *Xcl1* is not a component of the microglial inflammatory response and that the current evidence of Xcr1 expression by neurons can only be considered preliminary. Furthermore, this study has provided the first examination of XCR1 protein expression within the spinal cord of humans following the independent validation of antibody specificity. Preliminary results from this would further suggest that the current observations made by others in mice are not representative of the true expression pattern of Xcr1 within the CNS.

A central ethos of this PhD project has been to provide reliable and reproducible evidence that will serve as a cornerstone for future investigations of this chemokine ligand and receptor, particularly in relation to the mouse and human homologues of XCR1. Key to this evidence has been the attempt to clarify the molecular identity of mRNA and protein species that arise from the *Xcr1* gene. This study has gone some way to provide this. With further refinement, the techniques and tools developed here should provide a reliable underpinning to gain further clarity of this chemokine signalling axis and its potential role in CNS health and disease.

References

Abbadie, C., Lindia, J. A., Cumiskey, A. M., Peterson, L. B., Mudgett, J. S., Bayne, E. K., DeMartino, J. A., MacIntyre, D. E. and Forrest, M. J. (2003) 'Impaired neuropathic pain responses in mice lacking the chemokine receptor CCR2', *Proceedings of the National Academy of Sciences of the United States of America,* 100(13), pp. 7947-7952.

Abbott, N. J., Patabendige, A. A. K., Dolman, D. E. M., Yusof, S. R. and Begley, D. J. (2010) 'Structure and function of the blood-brain barrier', *Neurobiology of Disease,* 37(1), pp. 13-25.

Absinta, M., Ha, S. K., Nair, G., Sati, P., Luciano, N. J., Palisoc, M., Louveau, A., Zaghloul, K. A., Pittaluga, S., Kipnis, J. and Reich, D. S. (2017) 'Human and nonhuman primate meninges harbor lymphatic vessels that can be visualized noninvasively by MRI', *Elife,* 6.

Adler, M. W. and Rogers, T. J. (2005) 'Are chemokines the third major system in the brain?', *Journal of Leukocyte Biology,* 78(6), pp. 1204-1209.

Al-Chalabi, A. and Hardiman, O. (2013) 'The epidemiology of ALS: a conspiracy of genes, environment and time', *Nature Reviews Neurology,* 9(11), pp. 617-628.

Alken, M., Schmidt, A., Rutz, C., Furkert, J., Kleinau, G., Rosenthal, W. and Schuelein, R. (2009) 'The Sequence after the Signal Peptide of the G Protein-Coupled Endothelin B Receptor Is Required for Efficient Translocon Gating at the Endoplasmic Reticulum Membrane', *Molecular Pharmacology,* 75(4), pp. 801-811.

Allen, S. J., Crown, S. E. and Handel, T. M. (2007) 'Chemokine: Receptor structure, interactions, and antagonism', *Annual Review of Immunology,* 25, pp. 787-820.

Altschul, S. F., Gish, W., Miller, W., Myers, E. W. and Lipman, D. J. (1990) 'Basic Local Alignment Search Tool', *Journal of Molecular Biology,* 215(3), pp. 403-410.

Araki-Sasaki, K., Tanaka, T., Ebisuno, Y., Kanda, H., Umemoto, E., Hayashi, K. and Miyasaka, M. (2006) 'Dynamic expression of chemokines and the infiltration of inflammatory cells in the HSV-infected cornea and its associated tissues', *Ocular Immunology and Inflammation,* 14(5), pp. 257-266.

Arnold, E. S., Ling, S.-C., Huelga, S. C., Lagier-Tourenne, C., Polymenidou, M., Ditsworth, D., Kordasiewicz, H. B., McAlonis-Downes, M., Platoshyn, O., Parone, P. A., Da Cruz, S., Clutario, K. M., Swing, D., Tessarollo, L., Marsala, M., Shaw, C. E., Yeo, G. W. and Cleveland, D. W. (2013) 'ALS-linked TDP-43 mutations produce aberrant RNA splicing and adult-onset motor neuron disease without aggregation or loss of nuclear TDP-43', *Proceedings of the National Academy of Sciences of the United States of America,* 110(8), pp. E736-E745.

Auge, E., Duran, J., Guinovart, J. J., Pelegri, C. and Vilaplana, J. (2018) 'Exploring the elusive composition of corpora amylacea of human brain', *Scientific Reports,* 8.

Babcock, A. A., Kuziel, W. A., Rivest, S. and Owens, T. (2003) 'Chemokine expression by glial cells directs leukocytes to sites of axonal injury in the CNS', *Journal of Neuroscience,* 23(21), pp. 7922-7930.

Bachem, A., Guettler, S., Hartung, E., Ebstein, F., Schaefer, M., Tannert, A., Salama, A., Movassaghi, K., Opitz, C., Mages, H. W., Henn, V., Kloetzel, P.-M., Gurka, S. and Kroczek, R. A.

(2010) 'Superior antigen cross-presentation and XCR1 expression define human CD11c(+)CD141(+) cells as homologues of mouse CD8(+) dendritic cells', *Journal of Experimental Medicine,* 207(6), pp. 1273-1281.

Bajetto, A., Bonavia, R., Barbero, S., Florio, T. and Schettini, G. (2001) 'Chemokines and their receptors in the central nervous system', *Frontiers in Neuroendocrinology,* 22(3), pp. 147-184.

Baker, M. (2015) 'blame it on the antibodies', *Nature,* 521(7552), pp. 274-276.

Banci, L., Bertini, I., Boca, M., Girotto, S., Martinelli, M., Valentine, J. S. and Vieru, M. (2008) 'SOD1 and Amyotrophic Lateral Sclerosis: Mutations and Oligomerization', *Plos One,* 3(2).

Banisadr, G., Gosselin, R. D., Mechighel, P., Kitabgi, P., Rosene, W. and Parsadaniantz, S. P. M. (2005) 'Highly regionalized neuronal expression of monocyte chemoattractant protein-1 (MCP-1/CCL2) in rat brain: Evidence for its colocalization with neurotransmitters and neuropeptides', *Journal of Comparative Neurology,* 489(3), pp. 275-292.

Banisadr, G., Skrzydelski, D., Kitabgi, P., Rostene, W. and Parsadaniantz, S. M. (2003) 'Highly regionalized distribution of stromal cell-derived factor-1/CXCL12 in adult rat brain: constitutive expression in cholinergic, dopaminergic and vasopressinergic neurons', *European Journal of Neuroscience,* 18(6), pp. 1593-1606.

Barber, S. C. and Shaw, P. J. (2010) 'Oxidative stress in ALS: Key role in motor neuron injury and therapeutic target', *Free Radical Biology and Medicine,* 48(5), pp. 629-641.

Baron, P., Bussini, S., Cardin, V., Corbo, M., Conti, G., Galimberti, D., Scarpini, E., Bresolin, N., Wharton, S. B., Shaw, P. J. and Silani, V. (2005) 'Production of monocyte chemoattractant protein-1 in amyotrophic lateral sclerosis', *Muscle & Nerve,* 32(4), pp. 541-544.

Bechmann, I., Kwidzinski, E., Kovac, A. D., Simburger, E., Horvath, T., Gimsa, U., Dirnagl, U., Priller, J. and Nitsch, R. (2001) 'Turnover of rat brain perivascular cells', *Experimental Neurology,* 168(2), pp. 242-249.

Bedoui, S., Whitney, P. G., Waithman, J., Eidsmo, L., Wakim, L., Caminschi, I., Allan, R. S., Wojtasiak, M., Shortman, K., Carbone, F. R., Brooks, A. G. and Heath, W. R. (2009) 'Cross-presentation of viral and self antigens by skin-derived CD103(+) dendritic cells', *Nature Immunology,* 10(5), pp. 488-495.

Beers, D. R., Henkel, J. S., Zhao, W., Wang, J. and Appel, S. H. (2008) 'CD4+T cells support glial neuroprotection, slow disease progression, and modify glial morphology in an animal model of inherited ALS', *Proceedings of the National Academy of Sciences of the United States of America,* 105(40), pp. 15558-15563.

Belmer, A., Doly, S., Setola, V., Banas, S. M., Moutkine, I., Boutourlinsky, K., Kenakin, T. and Maroteaux, L. (2014) 'Role of the N-Terminal Region in G Protein-Coupled Receptor Functions: Negative Modulation Revealed by 5-HT2B Receptor Polymorphisms', *Molecular Pharmacology,* 85(1), pp. 127-138.

Bennett, M. L., Bennett, F. C., Liddelow, S. A., Ajami, B., Zamanian, J. L., Fernhoff, N. B., Mulinyawe, S. B., Bohlen, C. J., Adil, A., Tucker, A., Weissman, I. L., Chang, E. F., Li, G., Grant, G. A., Gephart, M. G. H. and Barres, B. A. (2016) 'New tools for studying microglia in the mouse and human CNS', *Proceedings of the National Academy of Sciences of the United States of America,* 113(12), pp. E1738-E1746.

Beynon, S. B. and Walker, F. R. (2012) 'microglial activation in the injured and healthy brain: what are we really talking about? practical and theoretical issues associated with the measurement of changes in microglial morphology', *Neuroscience,* 225, pp. 162-171.

Biber, K., Tsuda, M., Tozaki-Saitoh, H., Tsukamoto, K., Toyomitsu, E., Masuda, T., Boddeke, H. and Inoue, K. (2011) 'Neuronal CCL21 up-regulates microglia P2X4 expression and initiates neuropathic pain development', *Embo Journal,* 30(9), pp. 1864-1873.

Bird, E. V., Iannitti, T., Christmas, C. R., Obara, I., Andreev, V. I., King, A. E. and Boissonade, F. M. (2018) 'A Novel Role for Lymphotactin (XCL1) Signaling in the Nervous System: XCL1 Acts via its Receptor XCR1 to Increase Trigeminal Neuronal Excitability', *Neuroscience,* 379, pp. 334-349.

Bohm, S. K., Grady, E. F. and Bunnett, N. W. (1997) 'Regulatory mechanisms that modulate signalling by G-protein-coupled receptors', *Biochemical Journal,* 322, pp. 1-18.

Boillee, S., Vande Velde, C. and Cleveland, D. W. (2006) 'ALS: A disease of motor neurons and their nonneuronal neighbors', *Neuron,* 52(1), pp. 39-59.

Boismenu, R., Feng, L. L., Xia, Y. Y., Chang, J. C. C. and Havran, W. L. (1996) 'Chemokine expression by intraepithelial gamma delta T cells - Implications for the recruitment of inflammatory cells to damaged epithelia', *Journal of Immunology,* 157(3), pp. 985-992.

Bordeaux, J., Welsh, A. W., Agarwal, S., Killiam, E., Baquero, M. T., Hanna, J. A., Anagnostou, V. K. and Rimm, D. L. (2010) 'Antibody validation', *Biotechniques,* 48(3), pp. 197-209.

Bose, S. and Cho, J. (2013) 'Role of chemokine CCL2 and its receptor CCR2 in neurodegenerative diseases', *Archives of Pharmacal Research,* 36(9), pp. 1039-1050.

Botez, G. and Rami, A. (2001) 'Immunoreactivity for Bcl-2 and C-Jun/AP1 in hippocampal corpora amylacea after ischaemia in humans', *Neuropathology and Applied Neurobiology,* 27(6), pp. 474-480.

Bradley, L. M., Asensio, V. C., Schioetz, L. K., Harbertson, J., Krahl, T., Patstone, G., Woolf, N., Campbell, I. L. and Sarvetnick, N. (1999) 'Islet-specific Th1, but not Th2, cells secrete multiple chemokines and promote rapid induction of autoimmune diabetes', *Journal of Immunology,* 162(5), pp. 2511-2520.

Brettschneider, J., Toledo, J. B., Van Deerlin, V. M., Elman, L., McCluskey, L., Lee, V. M. Y. and Trojanowski, J. Q. (2012) 'Microglial Activation Correlates with Disease Progression and Upper Motor Neuron Clinical Symptoms in Amyotrophic Lateral Sclerosis', *Plos One,* 7(6).

Bruijn, L. I., Houseweart, M. K., Kato, S., Anderson, K. L., Anderson, S. D., Ohama, E., Reaume, A. G., Scott, R. W. and Cleveland, D. W. (1998) 'Aggregation and motor neuron toxicity of an ALS-linked SOD1 mutant independent from wild-type SOD1', *Science,* 281(5384), pp. 1851-1854.

Cairns, C. M., Gordon, J. R., Li, F., Baca-Estrada, M. E., Moyana, T. and Xiang, J. (2001) 'Lymphotactin expression by engineered myeloma cells drives tumor regression: Mediation by CD4(+) and CD8(+) T cells and neutrophils expressing XCR1 receptor', *Journal of Immunology,* 167(1), pp. 57-65.

Callewaere, C., Fernette, B., Raison, D., Mechighel, P., Burlet, A., Calas, A., Kitabgi, P., Melik-Parsadaniantz, S. and Rostene, W. (2008) 'Cellular and subcellular evidence for neuronal interaction between the chemokine stromal cell-derived factor-1/CXCL 12 and

vasopressin: Regulation in the hypothalamo-neurohypophysial system of the Brattleboro rats', *Endocrinology,* 149(1), pp. 310-319.

Cardona, A. E., Pioro, E. P., Sasse, M. E., Kostenko, V., Cardona, S. M., Dijkstra, I. M., Huang, D., Kidd, G., Dombrowski, S., Dutta, R., Lee, J.-C., Cook, D. N., Jung, S., Lira, S. A., Littman, D. R. and Ransohoff, R. M. (2006) 'Control of microglial neurotoxicity by the fractalkine receptor', *Nature Neuroscience,* 9(7), pp. 917-924.

Charles Watson, G. P., Gulgun Kayalioglu (2009) *The Spinal Cord.* 1 edn. (I vols). UK: Academic Press.

Chen, C. G., Li, J., Bot, G., Szabo, I., Rogers, T. J. and Liu-Chen, L. Y. (2004) 'Heterodimerization and cross-desensitization between the mu-opioid receptor and the chemokine CCR5 receptor', *European Journal of Pharmacology,* 483(2-3), pp. 175-186.

Chen, X. H., Geller, E. B., Rogers, T. J. and Adler, M. W. (2007) 'The chemokine CX3CL1/fractalkine interferes with the antinociceptive effect induced by opioid agonists in the periaqueductal grey of rats', *Brain Research,* 1153, pp. 52-57.

Chhor, V., Le Charpentier, T., Lebon, S., Ore, M.-V., Celador, I. L., Josserand, J., Degos, V., Jacotot, E., Hagberg, H., Saevman, K., Mallard, C., Gressens, P. and Fleiss, B. (2013) 'Characterization of phenotype markers and neuronotoxic potential of polarised primary microglia in vitro', *Brain Behavior and Immunity,* 32, pp. 70-85.

Chiang, C.-H., Grauffel, C., Wu, L.-S., Kuo, P.-H., Doudeva, L. G., Lim, C., Shen, C.-K. J. and Yuan, H. S. (2016) 'Structural analysis of disease-related TDP-43 D169G mutation: linking enhanced stability and caspase cleavage efficiency to protein accumulation', *Scientific Reports,* 6.

Chiu, I. M., Morimoto, E. T. A., Goodarzi, H., Liao, J. T., O'Keeffe, S., Phatnani, H. P., Muratet, M., Carroll, M. C., Levy, S., Tavazoie, S., Myers, R. M. and Maniatis, T. (2013) 'A Neurodegeneration-Specific Gene-Expression Signature of Acutely Isolated Microglia from an Amyotrophic Lateral Sclerosis Mouse Model', *Cell Reports,* 4(2), pp. 385-401.

Clark, A. K. and Malcangio, M. (2012) 'Microglial signalling mechanisms: Cathepsin S and Fractalkine', *Experimental Neurology,* 234(2), pp. 283-292.

Clarkson, B. D., Walker, A., Harris, M. G., Rayasam, A., Hsu, M., Sandor, M. and Fabry, Z. (2017) 'CCR7 deficient inflammatory Dendritic Cells are retained in the Central Nervous System', *Scientific Reports,* 7.

Clement, A. M., Nguyen, M. D., Roberts, E. A., Garcia, M. L., Boillee, S., Rule, M., McMahon, A. P., Doucette, W., Siwek, D., Ferrante, R. J., Brown, R. H., Julien, J. P., Goldstein, L. S. B. and Cleveland, D. W. (2003) 'Wild-type nonneuronal cells extend survival of SOD1 mutant motor neurons in ALS mice', *Science,* 302(5642), pp. 113-117.

Coleman, J. U., Ngo, T. and Smith, N. J. (2017) 'The G protein-coupled receptor N-terminus and receptor signalling: N-tering a new era', *Cellular Signalling,* 33, pp. 1-9.

Conductier, G., Blondeau, N., Guyon, A., Nahon, J.-L. and Rovere, C. (2010) 'The role of monocyte chemoattractant protein MCP1/CCL2 in neuroinflammatory diseases', *Journal of Neuroimmunology,* 224(1-2), pp. 93-100.

Cooper-Knock, J., Hewitt, C., Highley, J. R., Brockington, A., Milano, A., Man, S., Martindale, J., Hartley, J., Walsh, T., Gelsthorpe, C., Baxter, L., Forster, G., Fox, M., Bury, J., Mok, K., McDermott, C. J., Traynor, B. J., Kirby, J., Wharton, S. B., Ince, P. G., Hardy, J. and Shaw, P. J.

(2012) 'Clinico-pathological features in amyotrophic lateral sclerosis with expansions in C9ORF72', *Brain,* 135, pp. 751-764.

Cowell, R. M. and Silverstein, F. S. (2003) 'Developmental changes in the expression of chemokine receptor CCR1 in the rat cerebellum', *Journal of Comparative Neurology,* 457(1), pp. 7-23.

Crozat, K., Guiton, R., Contreras, V., Feuillet, V., Dutertre, C.-A., Ventre, E., Manh, T.-P. V., Baranek, T., Storset, A. K., Marvel, J., Boudinot, P., Hosmalin, A., Schwartz-Cornil, I. and Dalod, M. (2010) 'The XC chemokine receptor 1 is a conserved selective marker of mammalian cells homologous to mouse CD8 alpha(+) dendritic cells', *Journal of Experimental Medicine,* 207(6), pp. 1283-1292.

Crozat, K., Tamoutounour, S., Thien-Phong Vu, M., Fossum, E., Luche, H., Ardouin, L., Guilliams, M., Azukizawa, H., Bogen, B., Malissen, B., Henri, S. and Dalod, M. (2011) 'Cutting Edge: Expression of XCR1 Defines Mouse Lymphoid-Tissue Resident and Migratory Dendritic Cells of the CD8 alpha(+) Type', *Journal of Immunology,* 187(9), pp. 4411-4415.

Cruz-Orengo, L., Holman, D. W., Dorsey, D., Zhou, L., Zhang, P., Wright, M., McCandless, E. E., Patel, J. R., Luker, G. D., Littman, D. R., Russell, J. H. and Klein, R. S. (2011) 'CXCR7 influences leukocyte entry into the CNS parenchyma by controlling abluminal CXCL12 abundance during autoimmunity', *Journal of Experimental Medicine,* 208(2), pp. 327-339.

de Jong, E. K., Dijkstra, I. M., Hensens, M., Brouwer, N., van Amerongen, M., Liem, R. S. B., Boddeke, H. and Biber, K. (2005) 'Vesicle-mediated transport and release of CCL21 in endangered neurons: A possible explanation for microglia activation remote from a primary lesion', *Journal of Neuroscience,* 25(33), pp. 7548-7557.

DeJesus-Hernandez, M., Mackenzie, I. R., Boeve, B. F., Boxer, A. L., Baker, M., Rutherford, N. J., Nicholson, A. M., Finch, N. A., Flynn, H., Adamson, J., Kouri, N., Wojtas, A., Sengdy, P., Hsiung, G.-Y. R., Karydas, A., Seeley, W. W., Josephs, K. A., Coppola, G., Geschwind, D. H., Wszolek, Z. K., Feldman, H., Knopman, D. S., Petersen, R. C., Miller, B. L., Dickson, D. W., Boylan, K. B., Graff-Radford, N. R. and Rademakers, R. (2011) 'Expanded GGGGCC Hexanucleotide Repeat in Noncoding Region of C9ORF72 Causes Chromosome 9p-Linked FTD and ALS', *Neuron,* 72(2), pp. 245-256.

Di Giorgio, F. P., Boulting, G. L., Bobrowicz, S. and Eggan, K. C. (2008) 'Human Embryonic Stem Cell-Derived Motor Neurons Are Sensitive to the Toxic Effect of Glial Cells Carrying an ALS-Causing Mutation', *Cell Stem Cell,* 3(6), pp. 637-648.

Di Giorgio, F. P., Carrasco, M. A., Siao, M. C., Maniatis, T. and Eggan, K. (2007) 'Non-cell autonomous effect of glia on motor neurons in an embryonic stem cell-based ALS model', *Nature Neuroscience,* 10(5), pp. 608-614.

Dibaj, P., Steffens, H., Zschuentzsch, J., Nadrigny, F., Schomburg, E. D., Kirchhoff, F. and Neusch, C. (2011) 'In Vivo Imaging Reveals Distinct Inflammatory Activity of CNS Microglia versus PNS Macrophages in a Mouse Model for ALS', *Plos One,* 6(3).

Dong, C., Filipeanu, C. M., Duvernay, M. T. and Wu, G. (2007) 'Regulation of G protein-coupled receptor export trafficking', *Biochimica Et Biophysica Acta-Biomembranes,* 1768(4), pp. 853-870.

Dorner, B. G., Dorner, M. B., Zhou, X., Opitz, C., Mora, A., Guettler, S., Hutloff, A., Mages, H. W., Ranke, K., Schaefer, M., Jack, R. S., Henn, V. and Kroczek, R. A. (2009) 'Selective Expression of the Chemokine Receptor XCR1 on Cross-presenting Dendritic Cells Determines Cooperation with CD8(+) T Cells', *Immunity,* 31(5), pp. 823-833.

Dorner, B. G., Scheffold, A., Rolph, M. S., Huser, M. B., Kaufmann, S. H. E., Radbruch, A., Flesch, I. E. A. and Kroczek, R. A. (2002) 'MIP-1 alpha, MIP-1 beta, RANTES, and ATAC/lymphotactin function together with IFN-gamma as type 1 cytokines', *Proceedings of the National Academy of Sciences of the United States of America,* 99(9), pp. 6181-6186.

Dorner, B. G., Smith, H. R. C., French, A. R., Kim, S., Poursine-Laurent, J., Beckman, D. L., Pingel, J. T., Kroczek, R. A. and Yokoyama, W. M. (2004) 'Coordinate expression of cytokines and chemokines by NK cells during murine cytomegalovirus infection', *Journal of Immunology,* 172(5), pp. 3119-3131.

Drapkin, R., von Horsten, H. H., Lin, Y. F., Mok, S. C., Crum, C. P., Welch, W. R. and Hecht, J. L. (2005) 'Human epididymis protein 4 (HE4) is a secreted glycoprotein that is overexpressed by serous and endometriold ovarian carcinomas', *Cancer Research,* 65(6), pp. 2162-2169.

Endres, M., Andreas, K., Kalwitz, G., Freymann, U., Neumann, K., Ringe, J., Sittinger, M., Haeupl, T. and Kaps, C. (2010) 'Chemokine profile of synovial fluid from normal, osteoarthritis and rheumatoid arthritis patients: CCL25, CXCL10 and XCL1 recruit human subchondral mesenchymal progenitor cells', *Osteoarthritis and Cartilage,* 18(11), pp. 1458-1466.

Engelhardt, B. (2006) 'Molecular mechanisms involved in T cell migration across the blood-brain barrier', *Journal of Neural Transmission,* 113(4), pp. 477-485.

Engelhardt, B., Carare, R. O., Bechmann, I., Flugel, A., Laman, J. D. and Weller, R. O. (2016) 'Vascular, glial, and lymphatic immune gateways of the central nervous system', *Acta Neuropathologica,* 132(3), pp. 317-338.

Ersoy, B. A., Pardo, L., Zhang, S., Thompson, D. A., Millhauser, G., Govaerts, C. and Vaisse, C. (2012) 'Mechanism of N-terminal modulation of activity at the melanocortin-4 receptor GPCR', *Nature Chemical Biology,* 8(8), pp. 725-730.

Fendrick, S. E., Xue, Q.-S. and Streit, W. J. (2007) 'Formation of multinucleated giant cells and microglial degeneration in rats expressing a mutant Cu/Zn superoxide dismutase gene', *Journal of Neuroinflammation,* 4.

Fernandez, E. J. and Lolis, E. (2002) 'Structure junction, and inhibition of chemokines', *Annual Review of Pharmacology and Toxicology,* 42, pp. 469-499.

Ferraiuolo, L., Kirby, J., Grierson, A. J., Sendtner, M. and Shaw, P. J. (2011) 'Molecular pathways of motor neuron injury in amyotrophic lateral sclerosis', *Nature Reviews Neurology,* 7(11), pp. 616-630.

Flad, H. D. and Brandt, E. (2010) 'Platelet-derived chemokines: pathophysiology and therapeutic aspects', *Cellular and Molecular Life Sciences,* 67(14), pp. 2363-2386.

Foran, E. and Trotti, D. (2009) 'Glutamate Transporters and the Excitotoxic Path to Motor Neuron Degeneration in Amyotrophic Lateral Sclerosis', *Antioxidants & Redox Signaling,* 11(7), pp. 1587-U6.

Forster, R., Davalos-Misslitz, A. C. and Rot, A. (2008) 'CCR7 and its ligands: balancing immunity and tolerance', *Nature Reviews Immunology,* 8(5), pp. 362-371.

Fox, J. C., Nakayama, T., Tyler, R. C., Sander, T. L., Yoshie, O. and Volkman, B. F. (2015) 'Structural and agonist properties of XCL2, the other member of the C-chemokine subfamily', *Cytokine,* 71(2), pp. 302-311.

Frakes, A. E., Ferraiuolo, L., Haidet-Phillips, A. M., Schmelzer, L., Braun, L., Miranda, C. J., Ladner, K. J., Bevan, A. K., Foust, K. D., Godbout, J. P., Popovich, P. G., Guttridge, D. C. and Kaspar, B. K. (2014) 'Microglia Induce Motor Neuron Death via the Classical NF-kappa B Pathway in Amyotrophic Lateral Sclerosis', *Neuron,* 81(5), pp. 1009-1023.

Gao, Y.-J., Zhang, L., Samad, O. A., Suter, M. R., Yasuhiko, K., Xu, Z.-Z., Park, J.-Y., Lind, A.-L., Ma, Q. and Ji, R.-R. (2009) 'JNK-Induced MCP-1 Production in Spinal Cord Astrocytes Contributes to Central Sensitization and Neuropathic Pain', *Journal of Neuroscience,* 29(13), pp. 4096-4108.

Gilliland, C. T., Salanga, C. L., Kawamura, T., Trejo, J. and Handel, T. M. (2013) 'The Chemokine Receptor CCR1 Is Constitutively Active, Which Leads to G Protein-independent, beta-Arrestin-mediated Internalization', *Journal of Biological Chemistry,* 288(45), pp. 32194-32210.

Gosselin, R. D., Varela, C., Banisadr, G., Mechighel, P., Rostene, W., Kitabgi, P. and Melik-Parsadaniantz, S. (2005) 'Constitutive expression of CCR2 chemokine receptor and inhibition by MCP-1/CCL2 of GABA-induced currents in spinal cord neurones', *Journal of Neurochemistry,* 95(4), pp. 1023-1034.

Graber, D. J., Hickey, W. F. and Harris, B. T. (2010) 'Progressive changes in microglia and macrophages in spinal cord and peripheral nerve in the transgenic rat model of amyotrophic lateral sclerosis', *Journal of Neuroinflammation,* 7.

Graves, M. C., Fiala, M., Dinglasan, L. A. V., Liu, N. Q., Sayre, J., Chiappelli, F., van Kooten, C. and Vinters, H. V. (2004) 'Inflammation in amyotrophic lateral sclerosis spinal cord and brain is mediated by activated macrophages, mast cells and T cells', *Amyotrophic Lateral Sclerosis and Other Motor Neuron Disorders,* 5(4), pp. 213-219.

Grimsey, N. L., Goodfellow, C. E., Scotter, E. L., Dowie, M. J., Glass, M. and Graham, E. S. (2008) 'Specific detection of CB(1) receptors; cannabinoid CB(1) receptor antibodies are not all created equal!', *Journal of Neuroscience Methods,* 171(1), pp. 78-86.

Gurney, M. E., Pu, H. F., Chiu, A. Y., Dalcanto, M. C., Polchow, C. Y., Alexander, D. D., Caliendo, J., Hentati, A., Kwon, Y. W., Deng, H. X., Chen, W. J., Zhai, P., Sufit, R. L. and Siddique, T. (1994) 'motor-neuron degeneration in mice that express a human cu,zn superoxide-dismutase mutation', *Science,* 264(5166), pp. 1772-1775.

Guyon, A., Skrzydelski, D., De Giry, I., Rovere, C., Conductier, G., Trocello, J. M., Dauge, V., Kitabgi, P., Rostene, W., Nahon, J. L. and Parsadaniantz, S. M. (2009) 'long term exposure to the chemokine ccl2 activates the nigrostriatal dopamine system: a novel mechanism for the control of dopamine release', *Neuroscience,* 162(4), pp. 1072-1080.

Haidet-Phillips, A. M., Hester, M. E., Miranda, C. J., Meyer, K., Braun, L., Frakes, A., Song, S., Likhite, S., Murtha, M. J., Foust, K. D., Rao, M., Eagle, A., Kammesheidt, A., Christensen, A., Mendell, J. R., Burghes, A. H. M. and Kaspar, B. K. (2011) 'Astrocytes from familial and sporadic ALS patients are toxic to motor neurons', *Nature Biotechnology,* 29(9), pp. 824-U79.

Hall, E. D., Oostveen, J. A. and Gurney, M. E. (1998) 'Relationship of microglial and astrocytic activation to disease onset and progression in a transgenic model of familial ALS', *Glia,* 23(3), pp. 249-256.

Heinisch, S., Palma, J. and Kirby, L. G. (2011) 'Interactions between chemokine and mu-opioid receptors: Anatomical findings and electrophysiological studies in the rat periaqueductal grey', *Brain Behavior and Immunity,* 25(2), pp. 360-372.

Henkel, J. S., Beers, D. R., Siklos, L. and Appel, S. H. (2006) 'The chemokine MCP-1 and the dendritic and myeloid cells it attracts are increased in the mSOD1 mouse model of ALS', *Molecular and Cellular Neuroscience,* 31(3), pp. 427-437.

Henkel, J. S., Engelhardt, J. I., Siklos, L., Simpson, E. P., Kim, S. H., Pan, T. H., Goodman, J. C., Siddique, T., Beers, D. R. and Appel, S. H. (2004) 'Presence of dendritic cells, MCP-1, and activated microglia/macrophages in amyotrophic lateral sclerosis spinal cord tissue', *Annals of Neurology,* 55(2), pp. 221-235.

Hensley, K., Abdel-Moaty, H., Hunter, J., Mhatre, M., Mou, S., Nguyen, K., Potapova, T., Pye, Q. N., Qi, M., Rice, H., Stewart, C., Stroukoff, K. and West, M. (2006) 'Primary glia expressing the G93A-SOD1 mutation present a neuroinflammatory phenotype and provide a cellular system for studies of glial inflammation', *Journal of Neuroinflammation,* 3.

Hoglund, R. A. and Maghazachi, A. A. (2014) 'Multiple sclerosis and the role of immune cells', *World journal of experimental medicine,* 4(3), pp. 27-37.

Holman, D. W., Klein, R. S. and Ransohoff, R. M. (2011) 'The blood-brain barrier, chemokines and multiple sclerosis', *Biochimica Et Biophysica Acta-Molecular Basis of Disease,* 1812(2), pp. 220-230.

Holmes, W. E., Lee, J., Kuang, W. J., Rice, G. C. and Wood, W. I. (1991) 'structure and functional expression of a human interleukin-8 receptor', *Science,* 253(5025), pp. 1278-1280.

Hu, Y., Cao, C., Qin, X.-Y., Yu, Y., Yuan, J., Zhao, Y. and Cheng, Y. (2017) 'Increased peripheral blood inflammatory cytokine levels in amyotrophic lateral sclerosis: a meta-analysis study', *Scientific Reports,* 7.

Huang, H., Li, F., Cairns, C. M., Gordon, J. R. and Xiang, J. (2001) 'Neutrophils and B cells express XCR1 receptor and chemotactically respond to lymphotactin', *Biochemical and Biophysical Research Communications,* 281(2), pp. 378-382.

Hughes, E. G., Kang, S. H., Fukaya, M. and Bergles, D. E. (2013) 'Oligodendrocyte progenitors balance growth with self-repulsion to achieve homeostasis in the adult brain', *Nature Neuroscience,* 16(6), pp. 668-+.

Huising, M. O., Stet, R. J. M., Kruiswijk, C. P., Savelkoul, H. F. J. and Verburg-van Kemenade, B. M. L. (2003a) 'Molecular evolution of CXC chemokines: extant CXC chemokines originate from the CNS', *Trends in Immunology,* 24(6), pp. 307-313.

Huising, M. O., Stet, R. J. M., Kruiswijk, C. P., Savelkoul, H. F. J. and Verburg-van Kemenade, B. M. L. (2003b) 'Response to Shields: Molecular evolution of CXC chemokines and receptors', *Trends in Immunology,* 24(7), pp. 356-357.

Ilieva, H., Polymenidou, M. and Cleveland, D. W. (2009) 'Non-cell autonomous toxicity in neurodegenerative disorders: ALS and beyond', *Journal of Cell Biology,* 187(6), pp. 761-772.

Jahnsen, J. A. and Uhlen, S. (2012) 'The predicted N-terminal signal sequence of the human alpha(2C)-adrenoceptor does not act as a functional cleavable signal peptide', *European Journal of Pharmacology,* 684(1-3), pp. 51-58.

Jara, J. H., Gen, B., Stanford, M. J., Pytel, P., Roos, R. P., Weintraub, S., Mesulam, M. M., Bigio, E. H., Miller, R. J. and Ozdinler, P. H. (2017) 'Evidence for an early innate immune response in the motor cortex of ALS', *Journal of Neuroinflammation,* 14.

Ji, R.-R., Xu, Z.-Z. and Gao, Y.-J. (2014) 'Emerging targets in neuroinflammation-driven chronic pain', *Nature Reviews Drug Discovery,* 13(7), pp. 533-548.

Johnson, B. S., McCaffery, J. M., Lindquist, S. and Gitler, A. D. (2008) 'A yeast TDP-43 proteinopathy model: Exploring the molecular determinants of TDR-43 aggregation and cellular toxicity', *Proceedings of the National Academy of Sciences of the United States of America,* 105(17), pp. 6439-6444.

Joyce, P. I., McGoldrick, P., Saccon, R. A., Weber, W., Fratta, P., West, S. J., Zhu, N., Carter, S., Phatak, V., Stewart, M., Simon, M., Kumar, S., Heise, I., Bros-Facer, V., Dick, J., Corrochano, S., Stanford, M. J., Tu Vinh, L., Nolan, P. M., Meyer, T., Brandner, S., Bennett, D. L. H., Ozdinler, P. H., Greensmith, L., Fisher, E. M. C. and Acevedo-Arozena, A. (2015) 'A novel SOD1-ALS mutation separates central and peripheral effects of mutant SOD1 toxicity', *Human Molecular Genetics,* 24(7), pp. 1883-1897.

Jung, H., Toth, P. T., White, F. A. and Miller, R. J. (2008) 'Monocyte chemoattractant protein-1 functions as a neuromodulator in dorsal root ganglia neurons', *Journal of Neurochemistry,* 104(1), pp. 254-263.

Kadi, L., Selvaraju, R., de Lys, P., Proudfoot, A. E. I., Wells, T. N. C. and Boschert, U. (2006) 'Differential effects of chemokines on oligodendrocyte precursor proliferation and myelin formation in vitro', *Journal of Neuroimmunology,* 174(1-2), pp. 133-146.

Kalkonde, Y. V., Morgan, W. W., Sigala, J., Maffi, S. K., Condello, C., Kuziel, W., Ahuja, S. S. and Ahuja, S. K. (2007) 'Chemokines in the MPTP model of Parkinson's disease: Absence of CCL2 and its receptor CCR2 does not protect against striatal neurodegeneration', *Brain Research,* 1128(1), pp. 1-11.

Kandinov, B., Grigoriadis, N. C., Touloumi, O., Drory, V. E., Offen, D. and Korczyn, A. D. (2013) 'Immunohistochemical analysis of sympathetic involvement in the SOD1-G93A transgenic mouse model of amyotrophic lateral sclerosis', *Amyotrophic Lateral Sclerosis and Frontotemporal Degeneration,* 14(5-6), pp. 424-433.

Kandinov, B., Korczyn, A. D., Rabinowitz, R., Nefussy, B. and Drory, V. E. (2011) 'Autonomic impairment in a transgenic mouse model of amyotrophic lateral sclerosis', *Autonomic Neuroscience-Basic & Clinical,* 159(1-2), pp. 84-89.

Kawasaki, Y., Zhang, L., Cheng, J. K. and Ji, R. R. (2008) 'Cytokine mechanisms of central sensitization: Distinct and overlapping role of interleukin-1 beta, interleukin-6, and tumor necrosis factor-beta in regulating synaptic and neuronal activity in the superficial spinal cord', *Journal of Neuroscience,* 28(20), pp. 5189-5194.

Keller, A. F., Gravel, M. and Kriz, J. (2009) 'Live Imaging of Amyotrophic Lateral Sclerosis Pathogenesis: Disease Onset is Characterized by Marked Induction of GFAP in Schwann Cells', *Glia,* 57(10), pp. 1130-1142.

Kelner, G. S., Kennedy, J., Bacon, K. B., Kleyensteuber, S., Largaespada, D. A., Jenkins, N. A., Copeland, N. G., Bazan, J. F., Moore, K. W., Schall, T. J. and Zlotnik, A. (1994) 'Lymphotactin - a cytokine that represents a new class of chemokine', *Science,* 266(5189), pp. 1395-1399.

Kida, S., Pantazis, A. and Weller, R. O. (1993) 'CSF drains directly from the subarachnoid space into nasal lymphatics in the rat - anatomy, histology and immunological significance', *Neuropathology and Applied Neurobiology,* 19(6), pp. 480-488.

Kim, B. O., Liu, Y., Zhou, B. Y. and He, J. J. (2004) 'Induction of C chemokine XCL1 (lymphotactin/single C motif-1 alpha/activation-induced, T cell-derived and chemokine-

related cytokine) expression by HIV-1 Tat protein', *Journal of Immunology,* 172(3), pp. 1888-1895.

Klein, M., Paul, R., Angele, B., Popp, B., Pfister, H. W. and Koedel, U. (2006) 'Protein expression pattern in experimental pneumococcal meningitis', *Microbes and Infection,* 8(4), pp. 974-983.

Klein, S. L. and Schwarz, J. M. 2018. Sex-Specific Regulation of Peripheral and Central Immune Responses. Oxford University Press.

Kochl, R., Alken, M., Rutz, C., Krause, G., Oksche, A., Rosenthal, W. and Schulein, R. (2002) 'The signal peptide of the G protein-coupled human endothelin B receptor is necessary for translocation of the N-terminal tail across the endoplasmic reticulum membrane', *Journal of Biological Chemistry,* 277(18), pp. 16131-16138.

Kokovay, E., Goderie, S., Wang, Y., Lotz, S., Lin, G., Sun, Y., Roysam, B., Shen, Q. and Temple, S. (2010) 'Adult SVZ Lineage Cells Home to and Leave the Vascular Niche via Differential Responses to SDF1/CXCR4 Signaling', *Cell Stem Cell,* 7(2), pp. 163-173.

Komine, O., Yamashita, H., Fujimori-Tonou, N., Koike, M., Jin, S., Moriwaki, Y., Endo, F., Watanabe, S., Uematsu, S., Akira, S., Uchiyama, Y., Takahashi, R., Misawa, H. and Yamanaka, K. (2018) 'Innate immune adaptor TRIF deficiency accelerates disease progression of ALS mice with accumulation of aberrantly activated astrocytes', *Cell death and differentiation*.

Korzhevskiy, D. E. and Kirik, O. V. (2015) 'cerebral microglia and microglial markers', *Morfologiia (Saint Petersburg, Russia),* 147(3), pp. 37-44.

Kremlev, S. G., Roberts, R. L. and Palmer, C. (2004) 'Differential expression of chemokines and chemokine receptors during microglial activation and inhibition', *Journal of Neuroimmunology,* 149(1-2), pp. 1-9.

Kroczek, R. A. and Henn, V. (2012) 'The role of XCR1 and its liganc XCL1 in antigen cross-presentation by murine and human dendritic cells', *Frontiers in Immunology,* 3.

Kuhle, J., Lindberg, R. L. P., Regeniter, A., Mehling, M., Steck, A. J., Kappos, L. and Czaplinski, A. (2009) 'Increased levels of inflammatory chemokines in amyotrophic lateral sclerosis', *European Journal of Neurology,* 16(6), pp. 771-774.

Kuloglu, E. S., McCaslin, D. R., Kitabwalla, M., Pauza, C. D., Markley, J. L. and Volkman, B. F. (2001) 'Monomeric solution structure of the prototypical 'C' chemokine lymphotactin', *Biochemistry,* 40(42), pp. 12486-12496.

Kuloglu, E. S., McCaslin, D. R., Markley, J. L. and Volkman, B. F. (2002) 'Structural rearrangement of human lymphotactin, a C chemokine, under physiological solution conditions', *Journal of Biological Chemistry,* 277(20), pp. 17863-17870.

Kurt, R. A., Bauck, M., Harma, S., McCulloch, K., Baher, A. and Urba, W. J. (2001) 'Role of C chemokine lymphotactin in mediating recruitment of antigen-specific CD62L(lo) cells in vitro and in vivo', *Cellular Immunology,* 209(2), pp. 83-88.

La Spada, A. R. and Taylor, J. P. (2010) 'Repeat expansion disease: progress and puzzles in disease pathogenesis', *Nature Reviews Genetics,* 11(4), pp. 247-258.

Lasagni, L., Francalanci, M., Annunziato, F., Lazzeri, E., Giannini, S., Cosmi, L., Sagrinati, C., Mazzinghi, B., Orlando, C., Maggi, E., Marra, F., Romagnani, S., Serio, M. and Romagnani, P. (2003) 'An alternatively spliced variant of CXCR3 mediates the inhibition of endothelial

cell growth induced by IP-10, Mig, and I-TAC, and acts as functional receptor for platelet factor 4', *Journal of Experimental Medicine,* 197(11), pp. 1537-1549.

Latremoliere, A. and Woolf, C. J. (2009) 'Central Sensitization: A Generator of Pain Hypersensitivity by Central Neural Plasticity', *Journal of Pain,* 10(9), pp. 895-926.

Laudanna, C., Kim, J. Y., Constantin, G. and Butcher, E. C. (2002) 'Rapid leukocyte integrin activation by chemokines', *Immunological Reviews,* 186, pp. 37-46.

Lazarini, F., Tham, T. N., Casanova, P., Arenzana-Seisdedos, F. and Dubois-Dalcq, M. (2003) 'Role of the alpha-chemokine stromal cell-derived factor (SDF-1) in the developing and mature central nervous system', *Glia,* 42(2), pp. 139-148.

Lee, Y. B., Nagai, A. and Kim, S. U. (2002) 'Cytokines, chemokines, and cytokine receptors in human microglia', *Journal of Neuroscience Research,* 69(1), pp. 94-103.

Lei, Y., Ripen, A. M., Ishimaru, N., Ohigashi, I., Nagasawa, T., Jeker, L. T., Boesl, M. R., Hollaender, G. A., Hayashi, Y., Malefyt, R. d. W., Nitta, T. and Takahama, Y. (2011) 'Aire-dependent production of XCL1 mediates medullary accumulation of thymic dendritic cells and contributes to regulatory T cell development', *Journal of Experimental Medicine,* 208(2), pp. 383-394.

Lei, Y. and Takahama, Y. (2012) 'XCL1 and XCR1 in the immune system', *Microbes and Infection,* 14(3), pp. 262-267.

Lein, E. S. and Hawrylycz, M. J. and Ao, N. and Ayres, M. and Bensinger, A. and Bernard, A. and Boe, A. F. and Boguski, M. S. and Brockway, K. S. and Byrnes, E. J. and Chen, L. and Chen, L. and Chen, T.-M. and Chin, M. C. and Chong, J. and Crook, B. E. and Czaplinska, A. and Dang, C. N. and Datta, S. and Dee, N. R. and Desaki, A. L. and Desta, T. and Diep, E. and Dolbeare, T. A. and Donelan, M. J. and Dong, H.-W. and Dougherty, J. G. and Duncan, B. J. and Ebbert, A. J. and Eichele, G. and Estin, L. K. and Faber, C. and Facer, B. A. and Fields, R. and Fischer, S. R. and Fliss, T. P. and Frensley, C. and Gates, S. N. and Glattfelder, K. J. and Halverson, K. R. and Hart, M. R. and Hohmann, J. G. and Howell, M. P. and Jeung, D. P. and Johnson, R. A. and Karr, P. T. and Kawal, R. and Kidney, J. M. and Knapik, R. H. and Kuan, C. L. and Lake, J. H. and Laramee, A. R. and Larsen, K. D. and Lau, C. and Lemon, T. A. and Liang, A. J. and Liu, Y. and Luong, L. T. and Michaels, J. and Morgan, J. J. and Morgan, R. J. and Mortrud, M. T. and Mosqueda, N. F. and Ng, L. L. and Ng, R. and Orta, G. J. and Overly, C. C. and Pak, T. H. and Parry, S. E. and Pathak, S. D. and Pearson, O. C. and Puchalski, R. B. and Riley, Z. L. and Rockett, H. R. and Rowland, S. A. and Royall, J. J. and Ruiz, M. J. and Sarno, N. R. and Schaffnit, K. and Shapovalova, N. V. and Sivisay, T. and Slaughterbeck, C. R. and Smith, S. C. and Smith, K. A. and Smith, B. I. and Sodt, A. J. and Stewart, N. N. and Stumpf, K.-R. and Sunkin, S. M. and Sutram, M. and Tam, A. and Teemer, C. D. and Thaller, C. and Thompson, C. L. and Varnam, L. R. and Visel, A. and Whitlock, R. M. and Wohnoutka, P. E. and Wolkey, C. K. and Wong, V. Y. and Wood, M. and Yaylaoglu, M. B. and Young, R. C. and Youngstrom, B. L. and Yuan, X. F. and Zhang, B. and Zwingman, T. A. and Jones, A. R. (2007) 'Genome-wide atlas of gene expression in the adult mouse brain', *Nature,* 445(7124), pp. 168-176.

Lewis, C.-A., Manning, J., Rossi, F. and Krieger, C. (2012) 'The Neuroinflammatory Response in ALS: The Roles of Microglia and T Cells', *Neurology research international,* 2012, pp. 803701-803701.

Ling, S.-C., Polymenidou, M. and Cleveland, D. W. (2013) 'Converging Mechanisms in ALS and FTD: Disrupted RNA and Protein Homeostasis', *Neuron,* 79(3), pp. 416-438.

Liu, C., Cui, G., Zhu, M., Kang, X. and Guo, H. (2014) 'Neuroinflammation in Alzheimer's disease: chemokines produced by astrocytes and chemokine receptors', *International Journal of Clinical and Experimental Pathology,* 7(12), pp. 8342-8355.

Llewellyn-Smith, I. J. (2009) 'Anatomy of synaptic circuits controlling the activity of sympathetic preganglionic neurons', *Journal of Chemical Neuroanatomy,* 38(3), pp. 231-239.

Louveau, A., Smirnov, I., Keyes, T. J., Eccles, J. D., Rouhani, S. J., Peske, J. D., Derecki, N. C., Castle, D., Mandell, J. W., Lee, K. S., Harris, T. H. and Kipnis, J. (2015) 'Structural and functional features of central nervous system lymphatic vessels', *Nature,* 523(7560), pp. 337-+.

Louyeau, A., Harris, T. H. and Kipnis, J. (2015) 'Revisiting the Mechanisms of CNS Immune Privilege', *Trends in Immunology,* 36(10), pp. 569-577.

Lu, Y.-C., Yeh, W.-C. and Ohashi, P. S. (2008) 'LPS/TLR4 signal transduction pathway', *Cytokine,* 42(2), pp. 145-151.

Luttichau, H. R. (2008) 'The herpesvirus 8 encoded chemokines vCCL2 (vMIP-II) and vCCL3 (vMIP-III) target the human but not the murine lymphotactin receptor', *Virology Journal,* 5.

Ma, Q., Jones, D., Borghesani, P. R., Segal, R. A., Nagasawa, T., Kishimoto, T., Bronson, R. T. and Springer, T. A. (1998) 'Impaired B-lymphopoiesis, myelopoiesis, and derailed cerebellar neuron migration in CXCR4- and SDF-1-deficient mice', *Proceedings of the National Academy of Sciences of the United States of America,* 95(16), pp. 9448-9453.

Ma, Q. L., Ineichen, B. V., Detmar, M. and Proulx, S. T. (2017) 'Outflow of cerebrospinal fluid is predominantly through lymphatic vessels and is reduced in aged mice', *Nature Communications,* 8.

Mackenzie, I. R. A., Bigio, E. H., Ince, P. G., Geser, F., Neumann, M., Cairns, N. J., Kwong, L. K., Forman, M. S., Ravits, J., Stewart, H., Eisen, A., McClusky, L., Kretzschmar, H. A., Monoranu, C. M., Highley, J. R., Kirby, J., Siddique, T., Shaw, P. J., Lee, V. M. Y. and Trojanowski, J. Q. (2007) 'Pathological TDP-43 distinguishes sporadic amyotrophic lateral sclerosis from amyotrophic lateral sclerosis with SOD1 mutations', *Annals of Neurology,* 61(5), pp. 427-434.

Majounie, E., Renton, A. E., Mok, K., Dopper, E. G. P., Waite, A., Rollinson, S., Chio, A., Restagno, G., Nicolaou, N., Simon-Sanchez, J., van Swieten, J. C., Abramzon, Y., Johnson, J. O., Sendtner, M., Pamphlett, R., Orrell, R. W., Mead, S., Sidle, K. C., Houlden, H., Rohrer, J. D., Morrison, K. E., Pall, H., Talbot, K., Ansorge, O., Hernandez, D. G., Arepalli, S., Sabatelli, M., Mora, G., Corbo, M., Giannini, F., Calvo, A., Englund, E., Borghero, G., Foris, G. L., Remes, A. M., Laaksovirta, H., McCluskey, L., Trojanowski, J. Q., Van Deerlin, V. M., Schellenberg, G. D., Nalls, M. A., Drory, V. E., Lu, C.-S., Yeh, T.-H., Ishiura, H., Takahashi, Y., Tsuji, S., Le Ber, I., Brice, A., Drepper, C., Williams, N., Kirby, J., Shaw, P., Hardy, J., Tienari, P. J., Heutink, P., Morris, H. R., Pickering-Brown, S., Traynor, B. J., Chromosome, A. L. S. F. T. D. C., French Res Network, F. F. A. and Consortium, I. (2012) 'Frequency of the C9orf72 hexanucleotide repeat expansion in patients with amyotrophic lateral sclerosis and frontotemporal dementia: a cross-sectional study', *Lancet Neurology,* 11(4), pp. 323-330.

Mantovani, S., Garbelli, S., Pasini, A., Alimonti, D., Perotti, C., Melazzini, M., Bendotti, C. and Mora, G. (2009) 'Immune system alterations in sporadic amyotrophic lateral sclerosis patients suggest an ongoing neuroinflammatory process', *Journal of Neuroimmunology,* 210(1-2), pp. 73-79.

Marchetto, M. C. N., Muotri, A. R., Mu, Y., Smith, A. M., Cezar, G. G. and Gage, F. H. (2008) 'Non-Cell-Autonomous Effect of Human SOD1(G37R) Astrocytes on Motor Neurons Derived from Human Embryonic Stem Cells', *Cell Stem Cell,* 3(6), pp. 649-657.

Markovic, D. and Challiss, R. A. J. (2009) 'Alternative splicing of G protein-coupled receptors: physiology and pathophysiology', *Cellular and Molecular Life Sciences,* 66(20), pp. 3337-3352.

McCall, M. N., McMurray, H. R., Land, H. and Almudevar, A. (2014) 'On non-detects in qPCR data', *Bioinformatics,* 30(16), pp. 2310-2316.

McCandless, E. E., Piccio, L., Woerner, B. M., Schmidt, R. E., Rubin, J. B., Cross, A. H. and Klein, R. S. (2008) 'Pathological expression of CXCL12 at the blood-brain barrier correlates with severity of multiple sclerosis', *American Journal of Pathology,* 172(3), pp. 799-808.

McCandless, E. E., Wang, Q., Woerner, B. M., Harper, J. M. and Klein, R. S. (2006) 'CXCL12 limits inflammation by localizing mononuclear infiltrates to the perivascular space during experimental autoimmune encephalomyelitis', *Journal of Immunology,* 177(11), pp. 8053-8064.

McCulloch, C. V., Morrow, V., Milasta, S., Comerford, I., Milligan, G., Graham, G. J., Isaacs, N. W. and Nibbs, R. J. B. (2008) 'Multiple roles for the C-terminal tail of the chemokine scavenger D6', *Journal of Biological Chemistry,* 283(12), pp. 7972-7982.

McGoldrick, P., Joyce, P. I., Fisher, E. M. C. and Greensmith, L. (2013) 'Rodent models of amyotrophic lateral sclerosis', *Biochimica Et Biophysica Acta-Molecular Basis of Disease,* 1832(9), pp. 1421-1436.

Mead, R. J., Bennett, E. J., Kennerley, A. J., Sharp, P., Sunyach, C., Kasher, P., Berwick, J., Pettmann, B., Battaglia, G., Azzouz, M., Grierson, A. and Shaw, P. J. (2011) 'Optimised and Rapid Pre-clinical Screening in the SOD1(G93A) Transgenic Mouse Model of Amyotrophic Lateral Sclerosis (ALS)', *Plos One,* 6(8).

Menetski, J., Mistry, S., Lu, M., Mudgett, J. S., Ransohoff, R. M., Demartino, J. A., Macintyre, D. E. and Abbadie, C. (2007) 'Mice overexpressing chemokine ligand 2 (CCL2) in astrocytes display enhanced nociceptive responses', *Neuroscience,* 149(3), pp. 706-714.

Meng, H., Zhang, X., Blaivas, M. and Wang, M. M. (2009) 'Localization of blood proteins thrombospondin1 and ADAMTS13 to cerebral corpora amylacea', *Neuropathology,* 29(6), pp. 664-671.

Meyer, K., Ferraiuolo, L., Miranda, C. J., Likhite, S., McElroy, S., Renusch, S., Ditsworth, D., lagier-Tourenne, C., Smith, R. A., Ravits, J., Burghes, A. H., Shaw, P. J., Cleveland, D. W., Kolb, S. J. and Kaspar, B. K. (2014) 'Direct conversion of patient fibroblasts demonstrates non-cell autonomous toxicity of astrocytes to motor neurons in familial and sporadic ALS', *Proceedings of the National Academy of Sciences of the United States of America,* 111(2), pp. 829-832.

Michel, M. C., Wieland, T. and Tsujimoto, G. (2009) 'How reliable are G-protein-coupled receptor antibodies?', *Naunyn-Schmiedebergs Archives of Pharmacology,* 379(4), pp. 385-388.

Middel, P., Thelen, P., Blaschke, S., Polzien, F., Reich, K., Blaschke, V., Wrede, A., Hummel, K. M., Gunawan, B. and Radzun, H. J. (2001) 'Expression of the T-cell chemoattractant chemokine lymphotactin in Crohn's disease', *American Journal of Pathology,* 159(5), pp. 1751-1761.

Mitchell, J. C., Constable, R., So, E., Vance, C., Scotter, E., Glover, L., Hortobagyi, T., Arnold, E. S., Ling, S.-C., McAlonis, M., Da Cruz, S., Polymenidou, M., Tessarolo, L., Cleveland, D. W. and Shaw, C. E. (2015) 'Wild type human TDP-43 potentiates ALS-linked mutant TDP-43 driven progressive motor and cortical neuron degeneration with pathological features of ALS', *Acta Neuropathologica Communications,* 3.

Miyauchi, S., Hirasawa, A., Iga, T., Liu, N., Itsubo, C., Sadakane, K., Hara, T. and Tsujimoto, G. (2009) 'Distribution and regulation of protein expression of the free fatty acid receptor GPR120', *Naunyn-Schmiedebergs Archives of Pharmacology,* 379(4), pp. 427-434.

Morel, L., Regan, M., Higashimori, H., Seng Kah, N., Esau, C., Vidensky, S., Rothstein, J. and Yang, Y. (2013) 'Neuronal Exosomal miRNA-dependent Translational Regulation of Astroglial Glutamate Transporter GLT1', *Journal of Biological Chemistry,* 288(10), pp. 7105-7116.

Mori, K., Weng, S.-M., Arzberger, T., May, S., Rentzsch, K., Kremmer, E., Schmid, B., Kretzschmar, H. A., Cruts, M., Van Broeckhoven, C., Haass, C. and Edbauer, D. (2013) 'The C9orf72 GGGGCC Repeat Is Translated into Aggregating Dipeptide-Repeat Proteins in FTLD/ALS', *Science,* 339(6125), pp. 1335-1338.

Mortier, A., Gouwy, M., Van Damme, J. and Proost, P. (2011) 'Effect of posttranslational processing on the in vitro and in vivo activity of chemokines', *Experimental Cell Research,* 317(5), pp. 642-654.

Moser, B. and Loetscher, P. (2001) 'Lymphocyte traffic control by chemokines', *Nature Immunology,* 2(2), pp. 123-128.

Moussaud, S. and Draheim, H. J. (2010) 'A new method to isolate microglia from adult mice and culture them for an extended period of time', *Journal of Neuroscience Methods,* 187(2), pp. 243-253.

Moxley, G., Posthuma, D., Carlson, P., Estrada, E., Han, J. F., Benson, L. L. and Neale, M. C. (2002) 'Sexual dimorphism in innate immunity', *Arthritis and Rheumatism,* 46(1), pp. 250-258.

Muller, S., Dorner, B., Korthauer, U., Mages, H. W., Dapuzzo, M., Senger, G. and Kroczek, R. A. (1995) 'cloning of ATAC, an activation-induced, chemokine-related molecule exclusively expressed in cd8(+) t-lymphocytes', *European Journal of Immunology,* 25(6), pp. 1744-1748.

Mummidi, S., Adams, L. M., VanCompernolle, S. E., Kalkonde, M., Camargo, J. F., Kulkarni, H., Bellinger, A. S., Bonello, G., Tagoh, H., Ahuja, S. S., Unutmaz, D. and Ahnja, S. K. (2007) 'Production of specific mRNA transcripts, usage of an alternate promoter, and octamer-binding transcription factors influence the surface expression levels of the HIV cereceptor CCR5 on primary T cells', *Journal of Immunology,* 178(9), pp. 5668-5681.

Murphy, K. J. (2013) 'Neuron - glia crosstalk in health and disease: fractalkine and CX(3)CR1 take centre stage', *Open Biology,* 3(12).

Murphy, P. M. and Tiffany, H. L. (1991) 'cloning of complementary-DNA encoding a functional human interleukin-8 receptor', *Science,* 253(5025), pp. 1280-1283.

Nadim, F. and Bucher, D. (2014) 'Neuromodulation of neurons and synapses', *Current Opinion in Neurobiology,* 29, pp. 48-56.

Neel, N. F., Schutyser, E., Sai, J., Fan, G. H. and Richmond, A. (2005) 'Chemokine receptor internalization and intracellular trafficking', *Cytokine & Growth Factor Reviews,* 16(6), pp. 637-658.

Neumann, M., Sampathu, D. M., Kwong, L. K., Truax, A. C., Micsenyi, M. C., Chou, T. T., Bruce, J., Schuck, T., Grossman, M., Clark, C. M., McCluskey, L. F., Miller, B. L., Masliah, E., Mackenzie, I. R., Feldman, H., Feiden, W., Kretzschmar, H. A., Trojanowski, J. Q. and Lee, V. M. Y. (2006) 'Ubiquitinated TDP-43 in frontotemporal lobar degeneration and amyotrophic lateral sclerosis', *Science,* 314(5796), pp. 130-133.

Nevins, A. M., Subramanian, A., Tapia, J. L., Delgado, D. P., Tyler, R. C., Jensen, D. R., Ouellette, A. J. and Volkman, B. F. (2016) 'A Requirement for Metamorphic Interconversion in the Antimicrobial Activity of Chemokine XCL1', *Biochemistry,* 55(27), pp. 3784-3793.

Nicolai, J., Burbassi, S., Rubin, J. and Meucci, O. (2010) 'CXCL12 inhibits expression of the NMDA receptor's NR2B subunit through a histone deacetylase-dependent pathway contributing to neuronal survival', *Cell Death & Disease,* 1.

Nissen, J. C. (2017) 'Microglial Function across the Spectrum of Age and Gender', *International Journal of Molecular Sciences,* 18(3).

Nomiyama, H., Osada, N. and Yoshie, O. (2010) 'The evolution of mammalian chemokine genes', *Cytokine & Growth Factor Reviews,* 21(4), pp. 253-262.

Nomiyama, H., Osada, N. and Yoshie, O. (2011) 'A family tree of vertebrate chemokine receptors for a unified nomenclature', *Developmental and Comparative Immunology,* 35(7), pp. 705-715.

Nomiyama, H., Osada, N. and Yoshie, O. (2013) 'Systematic classification of vertebrate chemokines based on conserved synteny and evolutionary history', *Genes to Cells,* 18(1), pp. 1-16.

Nonneman, A., Robberecht, W. and Van Den Bosch, L. (2014) 'The role of oligodendroglial dysfunction in amyotrophic lateral sclerosis', *Neurodegenerative disease management,* 4(3), pp. 223-39.

O'Rourke, J. G., Bogdanik, L., Yanez, A., Lall, D., Wolf, A. J., Muhammad, A. K. M. G., Ho, R., Carmona, S., Vit, J. P., Zarrow, J., Kim, K. J., Bell, S., Harms, M. B., Miller, T. M., Dangler, C. A., Underhill, D. M., Goodridge, H. S., Lutz, C. M. and Baloh, R. H. (2016) 'C9orf72 is required for proper macrophage and microglial function in mice', *Science,* 351(6279), pp. 1324-1329.

Ohab, J. J., Fleming, S., Blesch, A. and Carmichael, S. T. (2006) 'A neurovascular niche for neurogenesis after stroke', *Journal of Neuroscience,* 26(50), pp. 13007-13016.

Ohta, T., Sugiyama, M., Hemmi, H., Yamazaki, C., Okura, S., Sasaki, I., Fukuda, Y., Orimo, T., Ishii, K. J., Hoshino, K., Ginhoux, F. and Kaisho, T. (2016) 'Crucial roles of XCR1-expressing dendritic cells and the XCR1-XCL1 chemokine axis in intestinal immune homeostasis', *Scientific Reports,* 6.

Omari, K. M., John, G., Lango, R. and Raine, C. S. (2006) 'Role for CXCR2 and CXCL1 on glia in multiple sclerosis', *Glia,* 53(1), pp. 24-31.

Omari, K. M., John, G. R., Sealfon, S. C. and Raine, C. S. (2005) 'CXC chemokine receptors on human oligodendrocytes: implications for multiple sclerosis', *Brain,* 128, pp. 1003-1015.

Ossovskaya, V. S. and Bunnett, N. W. (2004) 'Protease-activated receptors: Contribution to physiology and disease', *Physiological Reviews,* 84(2), pp. 579-621.

Ousman, S. S. and Kubes, P. (2012) 'Immune surveillance in the central nervous system', *Nature Neuroscience,* 15(8), pp. 1096-1101.

Phani, S., Re, D. B. and Przedborski, S. (2012) 'The role of the innate immune system in ALS', *Frontiers in Pharmacology,* 3.

Phatnani, H. P., Guarnieri, P., Friedman, B. A., Carrasco, M. A., Muratet, M., O'Keeffe, S., Nwakeze, C., Pauli-Behn, F., Newberry, K. M., Meadows, S. K., Tapia, J. C., Myers, R. M. and Maniatis, T. (2013) 'Intricate interplay between astrocytes and motor neurons in ALS', *Proceedings of the National Academy of Sciences of the United States of America,* 110(8), pp. E756-E765.

Philips, T. and Rothstein, J. D. (2014) 'Glial cells in amyotrophic lateral sclerosis', *Experimental Neurology,* 262, pp. 111-120.

Pisa, D., Alonso, R., Rabano, A. and Carrasco, L. (2016) 'Corpora Amylacea of Brain Tissue from Neurodegenerative Diseases Are Stained with Specific Antifungal Antibodies', *Frontiers in Neuroscience,* 10.

Puma, C., Danik, M., Quirion, R., Ramon, F. and Williams, S. (2001) 'The chemokine interleukin-8 acutely reduces Ca2+ currents in identified cholinergic septal neurons expressing CXCR1 and CXCR2 receptor mRNAs', *Journal of Neurochemistry,* 78(5), pp. 960-971.

Qin, X.-Y., Zhang, S.-P., Cao, C., Loh, Y. P. and Cheng, Y. (2016) 'Aberrations in Peripheral Inflammatory Cytokine Levels in Parkinson Disease A Systematic Review and Meta-analysis', *Jama Neurology,* 73(11), pp. 1316-1324.

Ragozzino, D., Di Angelantonio, S., Trettel, F., Bertollini, C., Maggi, L., Gross, C., Charo, I. F., Limatola, C. and Eusebi, F. (2006) 'Chemokine fractalkine/CX(3)CL1 negatively modulates active glutamatergic synapses in rat hippocampal neurons', *Journal of Neuroscience,* 26(41), pp. 10488-10498.

Ransohoff, R. M. (2009) 'Chemokines and Chemokine Receptors: Standing at the Crossroads of Immunobiology and Neurobiology', *Immunity,* 31(5), pp. 711-721.

Ransohoff, R. M., Kivisakk, P. and Kidd, G. (2003) 'Three or more routes for leukocyte migration into the central nervous system', *Nature Reviews Immunology,* 3(7), pp. 569-581.

Rath, A. and Deber, C. M. (2013) 'Correction factors for membrane protein molecular weight readouts on sodium dodecyl sulfate-polyacrylamide gel electrophoresis', *Analytical Biochemistry,* 434(1), pp. 67-72.

Ravits, J., Paul, P. and Jorg, C. (2007) 'Focality of upper and lower motor neuron degeneration at the clinical onset of ALS', *Neurology,* 68(19), pp. 1571-1575.

Reaux-Le Goazigo, A., Van Steenwinckel, J., Rostene, W. and Parsadaniantz, S. M. (2013) 'Current status of chemokines in the adult CNS', *Progress in Neurobiology,* 104, pp. 67-92.

Ren, K. and Dubner, R. (2010) 'Interactions between the immune and nervous systems in pain', *Nature Medicine,* 16(11), pp. 1267-1276.

Rettew, J. and Marriott, I. (2007) 'Testosterone attenuates TLR4 expression on murine macrophages', *Journal of Immunology,* 178.

Rettew, J. A., Huet, Y. M. and Marriott, I. (2009) 'Estrogens Augment Cell Surface TLR4 Expression on Murine Macrophages and Regulate Sepsis Susceptibility in Vivo', *Endocrinology,* 150(8), pp. 3877-3884.

Rhodes, K. J. and Trimmer, J. S. (2006) 'Antibodies as valuable neuroscience research tools versus reagents of mass distraction', *Journal of Neuroscience,* 26(31), pp. 8017-8020.

Rice, P., Longden, I. and Bleasby, A. (2000) 'EMBOSS: The European molecular biology open software suite', *Trends in Genetics,* 16(6), pp. 276-277.

Robin, A. M., Zhang, Z. G., Wang, L., Zhang, R. L., Katakowski, M., Zhang, L., Wang, Y., Zhang, C. L. and Chopp, M. (2006) 'Stromal cell-derived factor 1 alpha mediates neural progenitor cell motility after focal cerebral ischemia', *Journal of Cerebral Blood Flow and Metabolism,* 26(1), pp. 125-134.

Rosen, D. R. (1993) 'mutations in cu/zn superoxide-dismutase gene are associated with familial amyotrophic-lateral-sclerosis (vol 362, pg 59, 1993)', *Nature,* 364(6435), pp. 362-362.

Rostene, W., Kitabgi, P. and Melik-Parsadaniantz, S. (2007) 'Opinion - Chemokines: a new class of neuromodulator?', *Nature Reviews Neuroscience,* 8(11), pp. 895-904.

Rothstein, J. D., DykesHoberg, M., Pardo, C. A., Bristol, L. A., Jin, L., Kuncl, R. W., Kanai, Y., Hediger, M. A., Wang, Y. F., Schielke, J. P. and Welty, D. F. (1996) 'Knockout of glutamate transporters reveals a major role for astroglial transport in excitotoxicity and clearance of glutamate', *Neuron,* 16(3), pp. 675-686.

Salajegheh, M., Pinkus, J. L., Taylor, J. P., Amato, A. A., Nazareno, R., Baloh, R. H. and Greenberg, S. A. (2009) 'sarcoplasmic redistribution of nuclear tdp-43 in inclusion body myositis', *Muscle & Nerve,* 40(1), pp. 19-31.

Saper, C. B. (2009) 'A Guide to the Perplexed on the Specificity of Antibodies', *Journal of Histochemistry & Cytochemistry,* 57(1), pp. 1-5.

Sargsyan, S. A., Blackburn, D. J., Barber, S. C., Monk, P. N. and Shaw, P. J. (2009) 'Mutant SOD1 G93A microglia have an inflammatory phenotype and elevated production of MCP-1', *Neuroreport,* 20(16), pp. 1450-1455.

Saura, J., Tusell, J. M. and Serratosa, J. (2003) 'High-yield isolation of murine microglia by mild trypsinization', *Glia,* 44(3), pp. 183-189.

Scheerert, P. and Sommer, M. E. (2017) 'Structural mechanism of arrestin activation', *Current Opinion in Structural Biology,* 45, pp. 160-169.

Schiffer, D., Cordera, S., Cavalla, P. and Migheli, A. (1996) 'Reactive astrogliosis of the spinal cord in amyotrophic lateral sclerosis', *Journal of the Neurological Sciences,* 139, pp. 27-33.

Schilling, M., Strecker, J.-K., Ringelstein, E. B., Kiefer, R. and Schaebitz, W.-R. (2009) 'Turn-over of meningeal and perivascular macrophages in the brain of MCP-1-, CCR-2-or double knockout mice', *Experimental Neurology,* 219(2), pp. 583-585.

Schindelin, J., Arganda-Carreras, I., Frise, E., Kaynig, V., Longair, M., Pietzsch, T., Preibisch, S., Rueden, C., Saalfeld, S., Schmid, B., Tinevez, J. Y., White, D. J., Hartenstein, V., Eliceiri, K., Tomancak, P. and Cardona, A. (2012) 'Fiji: an open-source platform for biological-image analysis', *Nature Methods,* 9(7), pp. 676-682.

Schousboe, A. (2003) 'Role of astrocytes in the maintenance and modulation of glutamatergic and GABAergic neurotransmission', *Neurochemical Research,* 28(2), pp. 347-352.

Schuelein, R., Westendorf, C., Krause, G. and Rosenthal, W. (2012) 'Functional significance of cleavable signal peptides of G protein-coupled receptors', *European Journal of Cell Biology,* 91(4), pp. 294-299.

Schultheiss, C., Abe, P., Hoffmann, F., Mueller, W., Kreuder, A.-E., Schuetz, D., Haege, S., Redecker, C., Keiner, S., Kannan, S., Claasen, J.-H., Pfrieger, F. W. and Stumm, R. (2013) 'CXCR4 Prevents Dispersion of Granule Neuron Precursors in the Adult Dentate Gyrus', *Hippocampus,* 23(12), pp. 1345-1358.

Seifert, R. and Wenzel-Seifert, K. (2002) 'Constitutive activity of G-protein-coupled receptors: cause of disease and common property of wild-type receptors', *Naunyn-Schmiedebergs Archives of Pharmacology,* 366(5), pp. 381-416.

Sephton, C. F., Cenik, B., Cenik, B. K., Herz, J. and Yu, G. (2012) 'TDP-43 in central nervous system development and function: clues to TDP-43-associated neurodegeneration', *Biological Chemistry,* 393(7), pp. 589-594.

Sfanos, K. S., Wilson, B. A., De Marzo, A. M. and Isaacs, W. B. (2009) 'Acute inflammatory proteins constitute the organic matrix of prostatic corpora amylacea and calculi in men with prostate cancer', *Proceedings of the National Academy of Sciences of the United States of America,* 106(9), pp. 3443-3448.

Shang, Y. and Huang, E. J. (2016) 'Mechanisms of FUS mutations in familial amyotrophic lateral sclerosis', *Brain Research,* 1647, pp. 65-78.

Shaw, P. J. and Ince, P. G. (1997) 'Glutamate, excitotoxicity and amyotrophic lateral sclerosis', *Journal of Neurology,* 244, pp. S3-S14.

Shields, D. C. (2003) 'Molecular evolution of CXC chemokines and receptors', *Trends in Immunology,* 24(7), pp. 355-355.

Shinkai, H., Morozumi, T., Toki, D., Eguchi-Ogawa, T., Muneta, Y., Awata, T. and Uenishi, H. (2005) 'Genomic structure of eight porcine chemokine receptors and intergene sharing of an exon between CCR1 and XCR1', *Gene,* 349, pp. 55-66.

Simpson, J., Rezaie, P., Newcombe, J., Cuzner, M. L., Male, D. and Woodroofe, M. N. (2000) 'Expression of the beta-chemokine receptors CCR2, CCR3 and CCR5 in multiple sclerosis central nervous system tissue', *Journal of Neuroimmunology,* 108(1-2), pp. 192-200.

Simpson, J. E., Newcombe, J., Cuzner, M. L. and Woodroofe, M. N. (1998) 'Expression of monocyte chemoattractant protein-1 and other beta-chemokines by resident glia and inflammatory cells in multiple sclerosis lesions', *Journal of Neuroimmunology,* 84(2), pp. 238-249.

Singhrao, S. K., Morgan, B. P., Neal, J. W. and Newman, G. R. (1995) 'a functional-role for corpora-amylacea based on evidence from complement studies', *Neurodegeneration,* 4(3), pp. 335-345.

Skogs, M., Stadler, C., Schutten, R., Hjelmare, M., Gnann, C., Bjork, L., Poser, I., Hyman, A., Uhlen, M. and Lundberg, E. (2017) 'Antibody Validation in Bioimaging Applications Based on Endogenous Expression of Tagged Proteins', *Journal of Proteome Research,* 16(1), pp. 147-155.

Skrzydelski, D., Guyon, A., Dauge, V., Rovere, C., Apartis, E., Kitabgi, P., Nahon, J. L., Rostene, W. and Melik-Parsadaniantz, S. (2007) 'The chemokine stromal cell-derived factor-1/CXCL12 activates the nigrostriatal dopamine system', *Journal of Neurochemistry,* 102(4), pp. 1175-1183.

Soboleski, M. R., Oaks, J. and Halford, W. P. (2005) 'Green fluorescent protein is a quantitative reporter of gene expression in individual eukaryotic cells', *Faseb Journal,* 19(1), pp. 440-+.

Song, F., Chiang, P., Wang, J., Ravits, J. and Loeb, J. A. (2012) 'Aberrant Neuregulin 1 Signaling in Amyotrophic Lateral Sclerosis', *Journal of Neuropathology and Experimental Neurology,* 71(2), pp. 104-115.

Song, W., Zukor, H., Liberman, A., Kaduri, S., Arvanitakis, Z., Bennett, D. A. and Schipper, H. M. (2014) 'Astroglial heme oxygenase-1 and the origin of corpora amylacea in aging and degenerating neural tissues', *Experimental Neurology,* 254, pp. 78-89.

Sorge, R. E., Mapplebeck, J. C. S., Rosen, S., Beggs, S., Taves, S., Alexander, J. K., Martin, L. J., Austin, J.-S., Sotocinal, S. G., Chen, D., Yang, M., Shi, X. Q., Huang, H., Pillon, N. J., Bilan, P. J., Tu, Y., Klip, A., Ji, R.-R., Zhang, J., Salter, M. W. and Mogil, J. S. (2015) 'Different immune cells mediate mechanical pain hypersensitivity in male and female mice', *Nature Neuroscience,* 18(8), pp. 1081-+.

Sreedharan, J., Blair, I. P., Tripathi, V. B., Hu, X., Vance, C., Rogelj, B., Ackerley, S., Durnall, J. C., Williams, K. L., Buratti, E., Baralle, F., de Belleroche, J., Mitchell, J. D., Leigh, P. N., Al-Chalabi, A., Miller, C. C., Nicholson, G. and Shaw, C. E. (2008) 'TDP-43 mutations in familial and sporadic amyotrophic lateral sclerosis', *Science,* 319(5870), pp. 1668-1672.

Srinivasan, S., Lubrano-Berthelier, C., Govaerts, C., Picard, F., Santiago, P., Conklin, B. R. and Vaisse, C. (2004) 'Constitutive activity of the melanocortin-4 receptor is maintained by its N-terminal domain and plays a role in energy homeostasis in humans', *Journal of Clinical Investigation,* 114(8), pp. 1158-1164.

Stamatovic, S. M., Dimitrijevic, O. B., Keep, R. F. and Andjelkovic, A. V. (2006) 'Protein kinase C alpha-RhoA cross-talk in CCL2-induced alterations in brain endothelial permeability', *Journal of Biological Chemistry,* 281(13), pp. 8379-8388.

Stamatovic, S. M., Keep, R. F., Wang, M. M., Jankovic, I. and Andjelkovic, A. V. (2009) 'Caveolae-mediated Internalization of Occludin and Claudin-5 during CCL2-induced Tight Junction Remodeling in Brain Endothelial Cells', *Journal of Biological Chemistry,* 284(28), pp. 19053-19066.

Stephenson, J (2017), 'Beyond SOD1: Detailed Characterisation of a TDP-43 Transgenic Mouse Model of Motor Neurone Disease', PhD Thesis, University of Sheffield

Steward, O., Zheng, B. H., Ho, C., Anderson, K. and Tessier-Lavigne, M. (2004) 'The dorsolateral corticospinal tract in mice: An alternative route for corticospinal input to caudal segments following dorsal column lesions', *Journal of Comparative Neurology,* 472(4), pp. 463-477.

Stieber, A., Gonatas, J. O. and Gonatas, N. K. (2000) 'Aggregation of ubiquitin and a mutant ALS-linked SOD1 protein correlate with disease progression and fragmentation of the Golgi apparatus', *Journal of the Neurological Sciences,* 173(1), pp. 53-62.

Stopford, M. J., (2016), 'Development of a Cellular Model for C9ORF72-related Amyotrophic Lateral Sclerosis', PhD Thesis, University of Sheffield

Stowe, A. M., Wacker, B. K., Cravens, P. D., Perfater, J. L., Li, M. K., Hu, R., Freie, A. B., Stueve, O. and Gidday, J. M. (2012) 'CCL2 upregulation triggers hypoxic preconditioning-induced protection from stroke', *Journal of Neuroinflammation,* 9.

Strausberg, R. L., Feingold, E. A., Grouse, L. H., Derge, J. G., Klausner, R. D., Collins, F. S., Wagner, L., Shenmen, C. M., Schuler, G. D., Altschul, S. F., Zeeberg, B., Buetow, K. H., Schaefer, C. F., Bhat, N. K., Hopkins, R. F., Jordan, H., Moore, T., Max, S. I., Wang, J., Hsieh, F., Diatchenko, L., Marusina, K., Farmer, A. A., Rubin, G. M., Hong, L., Stapleton, M., Soares, M. B., Bonaldo, M. F., Casavant, T. L., Scheetz, T. E., Brownstein, M. J., Usdin, T. B., Toshiyuki, S., Carninci, P., Prange, C., Raha, S. S., Loquellano, N. A., Peters, G. J., Abramson, R. D., Mullahy, S. J., Bosak, S. A., McEwan, P. J., McKernan, K. J., Malek, J. A., Gunaratne, P. H., Richards, S., Worley, K. C., Hale, S., Garcia, A. M., Gay, L. J., Hulyk, S. W., Villalon, D. K., Muzny, D. M., Sodergren, E. J., Lu, X. H., Gibbs, R. A., Fahey, J., Helton, E., Ketteman, M., Madan, A., Rodrigues, S., Sanchez, A., Whiting, M., Young, A. C., Shevchenko, Y., Bouffard, G. G., Blakesley, R. W., Touchman, J. W., Green, E. D., Dickson, M. C., Rodriguez, A. C., Grimwood, J., Schmutz, J., Myers, R. M., Butterfield, Y. S. N., Kryzywinski, M. I., Skalska, U., Smailus, D. E., Schnerch, A., Schein, J. E., Jones, S. J. M., Marra, M. A. and Mammalian Gene Collection, M. G. C. P. (2002) 'Generation and initial analysis of more than 15,000 full-length human and mouse cDNA sequences', *Proceedings of the National Academy of Sciences of the United States of America,* 99(26), pp. 16899-16903.

Sugiyama, T., Kohara, H., Noda, M. and Nagasawa, T. (2006) 'Maintenance of the hematopoietic stem cell pool by CXCL12-CXCR4 chemokine signaling in bone marrow stromal cell niches', *Immunity,* 25(6), pp. 977-988.

Svec, D., Tichopad, A., Novosadova, V., Pfaffl, M. W. and Kubista, M. (2015) 'How good is a PCR efficiency estimate: Recommendations for precise and robust qPCR efficiency assessments', *Biomolecular detection and quantification,* 3, pp. 9-16.

Swarup, V., Phaneuf, D., Dupre, N., Petri, S., Strong, M., Kriz, J. and Julien, J.-P. (2011) 'Deregulation of TDP-43 in amyotrophic lateral sclerosis triggers nuclear factor kappa B-mediated pathogenic pathways', *Journal of Experimental Medicine,* 208(12), pp. 2429-2447.

Szabo, I., Chen, X. H., Xin, L., Adler, M. W., Howard, O. M. Z., Oppenheim, J. J. and Rogers, T. J. (2002) 'Heterologous desensitization of opioid receptors by chernokines inhibits chemotaxis and enhances the perception of pain', *Proceedings of the National Academy of Sciences of the United States of America,* 99(16), pp. 10276-10281.

Takeshita, Y. and Ransohoff, R. M. (2012) 'Inflammatory cell trafficking across the blood-brain barrier: chemokine regulation and in vitro models', *Immunological Reviews,* 248, pp. 228-239.

Tateishi, T., Yamasaki, R., Tanaka, M., Matsushita, T., Kikuchi, H., Isobe, N., Ohyagi, Y. and Kira, J.-i. (2010) 'CSF chemokine alterations related to the clinical course of amyotrophic lateral sclerosis', *Journal of Neuroimmunology,* 222(1-2), pp. 76-81.

Taylor, J. P., Brown, R. H., Jr. and Cleveland, D. W. (2016) 'Decoding ALS: from genes to mechanism', *Nature,* 539(7628), pp. 197-206.

Torcia, M. G., Nencioni, L., Clemente, A. M., Civitelli, L., Celestino, I., Limongi, D., Fadigati, G., Perissi, E., Cozzolino, F., Garaci, E. and Palamara, A. T. (2012) 'Sex Differences in the Response to Viral Infections: TLR8 and TLR9 Ligand Stimulation Induce Higher IL10 Production in Males', *Plos One,* 7(6).

Tsai, H. H., Frost, E., To, V., Robinson, S., ffrench-Constant, C., Geertman, R., Ransohoff, R. M. and Miller, R. H. (2002) 'The chemokine receptor CXCR2 controls positioning of oligodendrocyte precursors in developing spinal cord by arresting their migration', *Cell,* 110(3), pp. 373-383.

Tuan Leng, T., Savage, J. C., Hui, C. W., Bisht, K. and Tremblay, M.-E. (2017) 'Microglia across the lifespan: from origin to function in brain development, plasticity and cognition', *Journal of Physiology-London,* 595(6), pp. 1929-1945.

Verge, G. M., Milligan, E. D., Maier, S. F., Watkins, L. R., Naevel, G. S. and Foster, A. C. (2004) 'Fractakine (CX3CL1) and fractakine receptor (CX3CR1) distribution in spinal cord and dorsal root ganglia under basal and neuropathic pain conditions', *European Journal of Neuroscience,* 20(5), pp. 1150-1160.

Vincze, T., Posfai, J. and Roberts, R. J. (2003) 'NEBcutter: a program to cleave DNA with restriction enzymes', *Nucleic Acids Research,* 31(13), pp. 3688-3691.

Walz, A., Peveri, P., Aschauer, H., Thelen, M., Kernen, P., Dewald, B. and Baggiolini, M. (1989) 'structure and properties of a novel neutrophil-activating factor (NAF) produced by human-monocytes', *Agents and Actions,* 26(1-2), pp. 148-150.

Watkins, L. R., Milligan, E. D. and Maier, S. F. (2001) 'Glial activation: a driving force for pathological pain', *Trends in Neurosciences,* 24(8), pp. 450-455.

Weber, M., Blair, E., Simpson, C. V., O'Hara, M., Blackburn, P. E., Rot, A., Graham, G. J. and Nibbs, R. J. B. (2004) 'The chemokine receptor D6 constitutively traffics to and from the cell surface to internalize and degrade chemokine', *Molecular Biology of the Cell,* 15(5), pp. 2492-2508.

Wegorzewska, I., Bell, S., Cairns, N. J., Miller, T. M. and Baloh, R. H. (2009) 'TDP-43 mutant transgenic mice develop features of ALS and frontotemporal lobar degeneration', *Proceedings of the National Academy of Sciences of the United States of America,* 106(44), pp. 18809-18814.

White, M. A., Kim, E., Duffy, A., Adalbert, R., Phillips, B. U., Peters, O. M., Stephenson, J., Yang, S., Massenzio, F., Lin, Z., Andrews, S., Segonds-Pichon, A., Metterville, J., Saksida, L. M., Mead, R., Ribchester, R. R., Barhomi, Y., Serre, T., Coleman, M. P., Fallon, J., Bussey, T. J., Brown, R. H. and Sreedharan, J. (2018) 'TDP-43 gains function due to perturbed autoregulation in a Tardbp knock-in mouse model of ALS-FTD', *Nature Neuroscience,* 21(4), pp. 552-+.

Wierda, R. J. and van den Elsen, P. J. (2012) 'Genetic and Epigenetic Regulation of CCR5 Transcription', *Biology,* 1(3), pp. 869-79.

Willems, E., Leyns, L. and Vandesompele, J. (2008) 'Standardization of real-time PCR gene expression data from independent biological replicates', *Analytical Biochemistry,* 379(1), pp. 127-129.

Williams, J. L., Patel, J. R., Daniels, B. P. and Klein, R. S. (2014) 'Targeting CXCR7/ACKR3 as a therapeutic strategy to promote remyelination in the adult central nervous system', *Journal of Experimental Medicine,* 211(5), pp. 791-799.

Wils, H., Kleinberger, G., Janssens, J., Pereson, S., Joris, G., Cuijt, I., Smits, V., Ceuterick-de Groote, C., Van Broeckhoven, C. and Kumar-Singh, S. (2010) 'TDP-43 transgenic mice develop spastic paralysis and neuronal inclusions characteristic of ALS and

frontotemporal lobar degeneration', *Proceedings of the National Academy of Sciences of the United States of America,* 107(8), pp. 3858-3863.

Yamanaka, K., Chun, S. J., Boillee, S., Fujimori-Tonou, N., Yamashita, H., Gutmann, D. H., Takahashi, R., Misawa, H. and Cleveland, D. W. (2008) 'Astrocytes as determinants of disease progression in inherited amyotrophic lateral sclerosis', *Nature Neuroscience,* 11(3), pp. 251-253.

Yamanaka, K., Miller, T. M., McAlonis-Downes, M., Chun, S. J. and Cleveland, D. W. (2006) 'Progressive spinal axonal degeneration and slowness in ALS2-deficient mice', *Annals of Neurology,* 60(1), pp. 95-104.

Yamazaki, C., Miyamoto, R., Hoshino, K., Fukuda, Y., Sasaki, I., Saito, M., Ishiguchi, H., Yano, T., Sugiyama, T., Hemmi, H., Tanaka, T., Hamada, E., Hirashima, T., Amakawa, R., Fukuhara, S., Nomura, S., Ito, T. and Kaisho, T. (2010) 'Conservation of a chemokine system, XCR1 and its ligand, XCL1, between human and mice', *Biochemical and Biophysical Research Communications,* 397(4), pp. 756-761.

Yamazaki, C., Sugiyama, M., Ohta, T., Hemmi, H., Hamada, E., Sasaki, I., Fukuda, Y., Yano, T., Nobuoka, M., Hirashima, T., Iizuka, A., Sato, K., Tanaka, T., Hoshino, K. and Kaisho, T. (2013) 'Critical Roles of a Dendritic Cell Subset Expressing a Chemokine Receptor, XCR1', *Journal of Immunology,* 190(12), pp. 6071-6082.

Ye, J., Coulouris, G., Zaretskaya, I., Cutcutache, I., Rozen, S. and Madden, T. L. (2012) 'Primer-BLAST: A tool to design target-specific primers for polymerase chain reaction', *Bmc Bioinformatics,* 13.

Yoshida, T., Imai, T., Kakizaki, M., Nishimura, M., Takagi, S. and Yoshie, O. (1998) 'Identification of single C motif-1 lymphotactin receptor XCR1', *Journal of Biological Chemistry,* 273(26), pp. 16551-16554.

Yoshida, T., Imai, T., Kakizaki, M., Nishimura, M. and Yoshie, O. (1995) 'molecular-cloning of a novel c-type or gamma-type chemokine, SCM-1', *Febs Letters,* 360(2), pp. 155-159.

Yoshida, T., Izawa, D., Nakayama, T., Nakahara, K., Kakizaki, M., Imai, T., Suzuki, R., Miyasaka, M. and Yoshie, O. (1999) 'Molecular cloning of mXCR1, the murine SCM-1/lymphotactin receptor', *Febs Letters,* 458(1), pp. 37-40.

Yue, F. and Cheng, Y. and Breschi, A. and Vierstra, J. and Wu, W. and Ryba, T. and Sandstrom, R. and Ma, Z. and Davis, C. and Pope, B. D. and Shen, Y. and Pervouchine, D. D. and Djebali, S. and Thurman, R. E. and Kaul, R. and Rynes, E. and Kirilusha, A. and Marinov, G. K. and Williams, B. A. and Trout, D. and Amrhein, H. and Fisher-Aylor, K. and Antoshechkin, I. and DeSalvo, G. and See, L.-H. and Fastuca, M. and Drenkow, J. and Zaleski, C. and Dobin, A. and Prieto, P. and Lagarde, J. and Bussotti, G. and Tanzer, A. and Denas, O. and Li, K. and Bender, M. A. and Zhang, M. and Byron, R. and Groudine, M. T. and McCleary, D. and Pham, L. and Ye, Z. and Kuan, S. and Edsall, L. and Wu, Y.-C. and Rasmussen, M. D. and Bansal, M. S. and Kellis, M. and Keller, C. A. and Morrissey, C. S. and Mishra, T. and Jain, D. and Dogan, N. and Harris, R. S. and Cayting, P. and Kawli, T. and Boyle, A. P. and Euskirchen, G. and Kundaje, A. and Lin, S. and Lin, Y. and Jansen, C. and Malladi, V. S. and Cline, M. S. and Erickson, D. T. and Kirkup, V. M. and Learned, K. and Sloan, C. A. and Rosenbloom, K. R. and De Sousa, B. L. and Beal, K. and Pignatelli, M. and Flicek, P. and Lian, J. and Kahveci, T. and Lee, D. and Kent, W. J. and Santos, M. R. and Herrero, J. and Notredame, C. and Johnson, A. and Vong, S. and Lee, K. and Bates, D. and Neri, F. and Diegel, M. and Canfield, T. and Sabo, P. J. and Wilken, M. S. and Reh, T. A. and Giste, E. and Shafer, A. and Kutyavin, T. and Haugen, E. and Dunn, D. and Reynolds, A. P. and Neph, S. and Humbert, R. and Hansen, R. S. and De Bruijn, M. and Selleri, L. and Rudensky, A. and

Josefowicz, S. and Samstein, R. and Eichler, E. E. and Orkin, S. H. and Levasseur, D. and Papayannopoulou, T. and Chang, K.-H. and Skoultchi, A. and Gosh, S. and Disteche, C. and Treuting, P. and Wang, Y. and Weiss, M. J. and Blobel, G. A. and Cao, X. and Zhong, S. and Wang, T. and Good, P. J. and Lowdon, R. F. and Adams, L. B. and Zhou, X.-Q. and Pazin, M. J. and Feingold, E. A. and Wold, B. and Taylor, J. and Mortazavi, A. and Weissman, S. M. and Stamatoyannopoulos, J. A. and Snyder, M. P. and Guigo, R. and Gingeras, T. R. and Gilbert, D. M. and Hardison, R. C. and Beer, M. A. and Ren, B. and Mouse, E. C. (2014) 'A comparative encyclopedia of DNA elements in the mouse genome', *Nature,* 515(7527), pp. 355-+.

Zeisel, A., Koestler, W. J., Molotski, N., Tsai, J. M., Krauthgamer, R., Jacob-Hirsch, J., Rechavi, G., Soen, Y., Jung, S., Yarden, Y. and Domany, E. (2011) 'Coupled pre-mRNA and mRNA dynamics unveil operational strategies underlying transcriptional responses to stimuli', *Molecular Systems Biology,* 7.

Zhang, Z.-J., Cao, D.-L., Zhang, X., Ji, R.-R. and Gao, Y.-J. (2013) 'Chemokine contribution to neuropathic pain: Respective induction of CXCL1 and CXCR2 in spinal cord astrocytes and neurons', *Pain,* 154(10), pp. 2185-2197.

Zhong, Z., Deane, R., Ali, Z., Parisi, M., Shapovalov, Y., O'Banion, M. K., Stojanovic, K., Sagare, A., Boillee, S., Cleveland, D. W. and Zlokovic, B. V. (2008) 'ALS-causing SOD1 mutants generate vascular changes prior to motor neuron degeneration', *Nature Neuroscience,* 11(4), pp. 420-422.

Zhuang, Z.-Y., Kawasaki, Y., Tan, P.-H., Wen, Y.-R., Huang, J. and Ji, R.-R. (2007) 'Role of the CX3CR1/p38 MAPK pathway in spinal microglia for the development of neuropathic pain following nerve injury-induced cleavage of fractalkine', *Brain Behavior and Immunity,* 21(5), pp. 642-651.

Zlotnik, A. and Yoshie, O. (2000) 'Chemokines: A new classification system and their role in immunity', *Immunity,* 12(2), pp. 121-127.

Zlotnik, A. and Yoshie, O. (2012) 'The Chemokine Superfamily Revisited', *Immunity,* 36(5), pp. 705-716.

Zlotnik, A., Yoshie, O. and Nomiyama, H. (2006) 'The chemokine and chemokine receptor superfamilies and their molecular evolution', *Genome Biology,* 7(12).

Zychowska, M., Rojewska, E., Piotrowska, A., Kreiner, G. and Mika, J. (2016) 'Microglial Inhibition Influences XCL1/XCR1 Expression and Causes Analgesic Effects in a Mouse Model of Diabetic Neuropathy', *Anesthesiology,* 125(3), pp. 573-589.

> Ensembl Xcr1 gene sequence (ENSMUST00000182350.1)

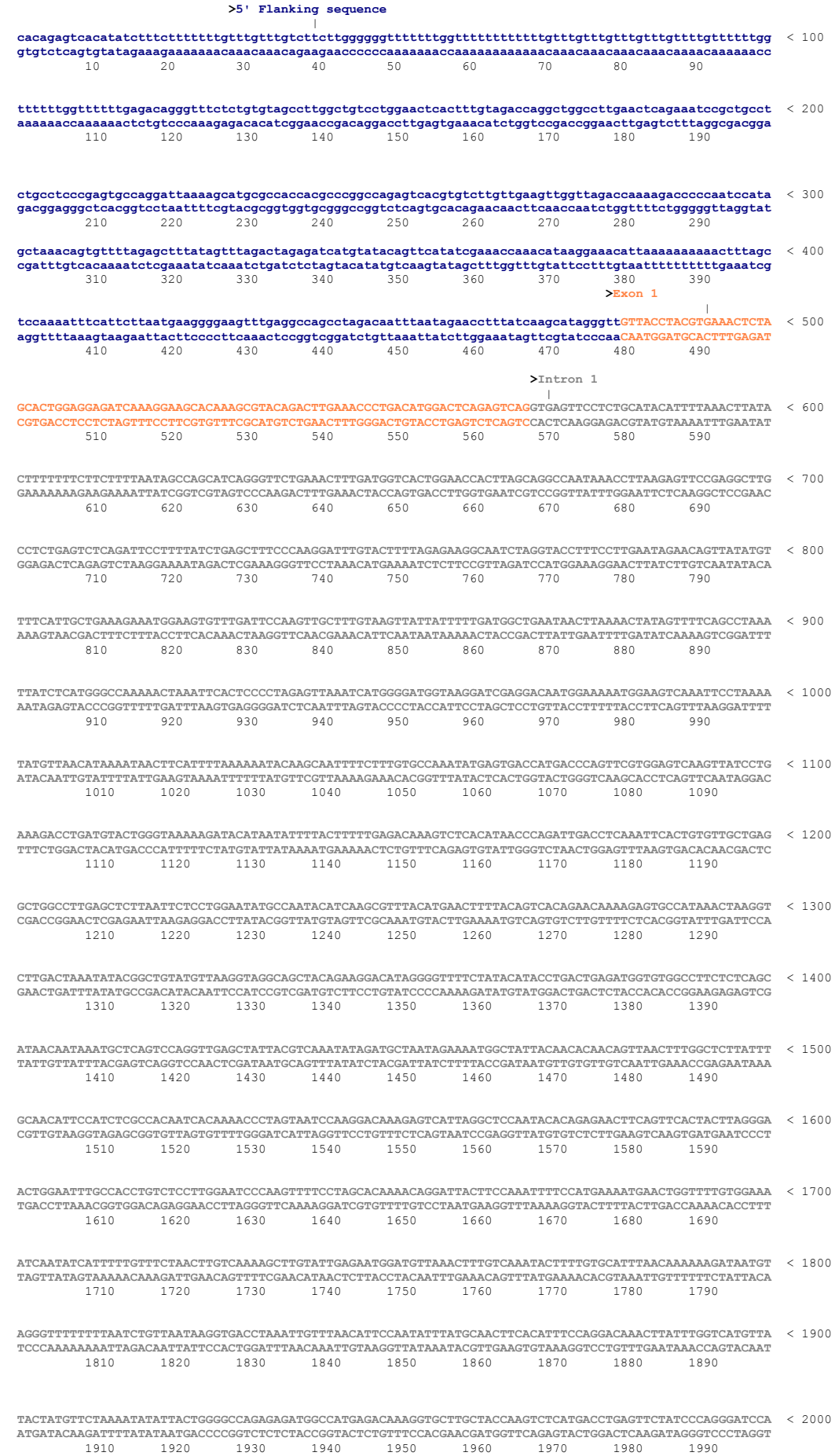

```
CCTCGTAGAAGGAGAAAACCAACTTCTACAGGTTGTCCTCCGGCATCCAAATGCATAGCATGGCAAATATATGAGTATATACTCATAAACTCAAATAAAT  < 2100
GGAGCATCTTCCTCTTTTGGTTGAAGATGTCCAACAGGAGGCCGTAGGTTTACGTATCGTACCGTTTATATACTCATATATGAGTATTTGAGTTTATTTA
         2010      2020      2030      2040      2050      2060      2070      2080      2090

AAATAAATAAATAAATAAATAAATAAATAAATAAATGTAATAAATATTTTAAATGTATTATTGAACTTGACTCAACCTATAATTTGGAAAGAATGTTTGT  < 2200
TTTATTTATTTATTTATTTATTTATTTATTTATTTACATTATTTATAAAATTTACATAATAACTTGAACTGAGTTGGATATTAAACCTTTCTTACAAACA
         2110      2120      2130      2140      2150      2160      2170      2180      2190

GTTGAGATAAAGCTGTAGCTCAGCATTTATCAAAAGCTGACAAAGTTCTGGATTTATTCAGTCCCCAGCACTGAATAAATCTGGTGTGATGACACAGGCC  < 2300
CAACTCTATTTCGACATCGAGTCGTAAATAGTTTTCGACTGTTTCAAGACCTAAATAAGTCAGGGGTCGTGACTTATTTAGACCACACTACTGTGTCCGG
         2210      2220      2230      2240      2250      2260      2270      2280      2290

TTGAATCTTAGCAGTTTCAAAGTAGAACCAGGAGGATCAGAGGCCTCAAAATCTTTGGCTTATAAAGAGGCCAGCCTGTTTCAAAAAATAAAAGAATTTT  < 2400
AACTTAGAATCGTCAAAGTTTCATCTTGGTCCTCCTAGTCTCCGGAGTTTTAGAAACCGAATATTTCTCCGGTCGGACAAAGTTTTTTATTTTCTTAAAA
         2310      2320      2330      2340      2350      2360      2370      2380      2390

TGTATCTGTATTCATAAATAATATTAGCCCGTGGTTTTTGTTTATTGTAAATTTTTCATCTGATTTTGGAATCGTGGGTATATTTTCCTTATAAAGCAAG  < 2500
ACATAGACATAAGTATTTATTATAATCGGGCACCAAAAACAAATAACATTTAAAAAGTAGACTAAAACCTTAGCACCCATATAAAAGGAATATTTCGTTC
         2410      2420      2430      2440      2450      2460      2470      2480      2490

TTGAAGGGGATATTTGTGTAATATTGATGTTATTTTTTCCTCAAATATTTGAGAACAATTTCTAACAGTAAGCTCTGCCTCCCTTTCAGGGGCAGCACTT  < 2600
AACTTCCCCTATAAACACATTATAACTACAATAAAAAAGGAGTTTATAAACTCTTGTTAAAGATTGTCATTCGAGACGGAGGGAAAGTCCCCGTCGTGAA
         2510      2520      2530      2540      2550      2560      2570      2580      2590

CAAATATCAATTTAGTTCTTTCAGGTATTGCTAGCACATTTACAGTTCAAGGACAACCATTTGAGCAAGATATATGGGCGAAATATGGAACTTTCTATCT  < 2700
GTTTATAGTTAAATCAAGAAAGTCCATAACGATCGTGTAAATGTCAAGTTCCTGTTGGTAAACTCGTTCTATATACCCGCTTTATACCTTGAAAGATAGA
         2610      2620      2630      2640      2650      2660      2670      2680      2690

TTTTTTTTCTTTCCTTTATTTATACCTCTTACTTTCTAGTACTTTTAGTTGCCCTAAACCTGGCTATCTGGTTCTTCAAAATGGAAAAAAAAATGCACTA  < 2800
AAAAAAAAGAAAGGAAATAAATATGGAGAATGAAAGATCATGAAAATCAACGGGATTTGGACCGATAGACCAAGAAGTTTTACCTTTTTTTTTACGTGAT
         2710      2720      2730      2740      2750      2760      2770      2780      2790

TTTGTCTAGCTTATTTTATTTAACACAATAATCTCAAATTGCATCCATTTTCCAGCAAATGAGAATAAAAGTCCATTGGGTTATGCCTTAGTTACTGTTT  < 2900
AAACAGATCGAATAAAATAAATTGTGTTATTAGAGTTTAACGTAGGTAAAAGGTCGTTTACTCTTATTTTCAGGTAACCCAATACGGAATCAATGACAAA
         2810      2820      2830      2840      2850      2860      2870      2880      2890

TGTTGCTGTGAAGAGAAACCATGATAGAGGCAACACAAAAGCATTTAATTGGGGACTTATTTGACAGTTTTAGAGAGTTAGTCCATGATCATCATGGTGG  < 3000
ACAACGACACTTCTCTTTGGTACTATCTCCGTTGTGTTTTCGTAAATTAACCCCTGAATAAACTGTCAAAATCTCTCAATCAGGTACTAGTAGTACCACC
         2910      2920      2930      2940      2950      2960      2970      2980      2990

AAGTAGGCATGATATTGGAGTAATAACTGAGAGTTTTACATTCTGATTTACAGGCATCACTCAGGGGGGGGGGGAGAGAGAGAGTCAGACAGAGACAGAGA  < 3100
TTCATCCGTACTATAACCTCATTATTGACTCTCAAAATGTAAGACTAAATGTCCGTAGTGAGTCCCCCCCCCCTCTCTCTCTCAGTCTGTCTCTGTCTCT
         3010      3020      3030      3040      3050      3060      3070      3080      3090

CAGAGACAGAGAGACAGAGAGACTGGACCTAATTTGTGCTTTTGAAAACTCACACCCTACTTCCAGTGACACACCAACTCCAATAAGACCATACTTCCTA  < 3200
GTCTCTGTCTCTCTGTCTCTCTGACCTGGATTAAACACGAAAACTTTTGAGTGTGGGATGAAGGTCACTGTGTGGTTGAGGTTATTCTGGTATGAAGGAT
         3110      3120      3130      3140      3150      3160      3170      3180      3190

ATTCTTTGAAACTCTTCCACTAACTGGTGTCTAAGCATTCAAATATAAGCATTCAAATATATGCCCCTCTGGGGCCACTCTCATTCAAACCACCACAGTA  < 3300
TAAGAAACTTTGAGAAGGTGATTGACCACAGATTCGTAAGTTTATATTCGTAAGTTTATATACGGGGAGACCCCGGTGAGAGTAAGTTTGGTGGTGTCAT
         3210      3220      3230      3240      3250      3260      3270      3280      3290

TACAAGCCACTGTTTTTCTTTATCAATTCATCAGTTGACAGATAATTGTTGGCTTATTCTGAACAGTGTTATAAGAAACATAGATGTTCAGGTATCTCTG  < 3400
ATGTTCGGTGACAAAAAGAAATAGTTAAGTAGTCAACTGTCTATTAACAACCGAATAAGACTTGTCACAATATTCTTTGTATCTACAAGTCCATAGAGAC
         3310      3320      3330      3340      3350      3360      3370      3380      3390

TATCATAGACTTAGAGACCTTTGGGCATATACACAGGAATGGGTCGTGTGGTAGAGGAACCTCTATAATGATTTCCATAGTGCTAAACCACTTTATATCC  < 3500
ATAGTATCTGAATCTCTGGAAACCCGTATATGTGTCCTTACCCAGCACACCATCTCCTTGGAGATATTACTAAAGGTATCACGATTTGGTGAAATATAGG
         3410      3420      3430      3440      3450      3460      3470      3480      3490

TACAAGCAGTGATAAAGGTTCCTCTTTCCCACACCCTCACTACCATTTGTTGTTTTTATAATAACAAACCCTCTGACTTGAGGGGTAAAATATTAATATG  < 3600
ATGTTCGTCACTATTTCCAAGGAGAAAGGGTGTGGGAGTGATGGTAAACAACAAAAATATTATTGTTTGGGAGACTGAACTCCCCATTTTATAATTATAC
         3510      3520      3530      3540      3550      3560      3570      3580      3590

GTTTTAATTTTCATTTCTTTGATCCCTAAAGATGTTAAATATTCTTTATGGTCTTGGCCATTTGCACTTCATCTTTTTGAGAACTGTCTTTCATTTCATT  < 3700
CAAAATTAAAAGTAAAGAAACTAGGGATTTCTACAATTTATAAGAAATACCAGAACCGGTAAACGTGAAGTAGAAAAACTCTTGACAGAAAGTAAAGTAA
         3610      3620      3630      3640      3650      3660      3670      3680      3690

AGCCTATTTATTGATTGAATTGTTTGAGTTTTAAAATTTAATTACTAAAAATTCTTTGTATATCCTATTATTAATCTTCTGTCAAATGTATAACTAGCAA  < 3800
TCGGATAAATAACTAACTTAACAAACTCAAAATTTTAAATTAATGATTTTTAAGAAACATATAGGATAATAATTAGAAGACAGTTTACATATTGATCGTT
         3710      3720      3730      3740      3750      3760      3770      3780      3790

AGATTTTTTTTCTCCCATCCTATAGACCATCTCTTCATCTGATTGCTTCCATGGCTATGCAGAGGCTTTTAATTTCAATCTATCCCACTTATCTATTCT  < 3900
TCTAAAAAAAAGAGGGTAGGATATCTGGTAGAGAAGTAGACTAACGAAGGTACCGATACGTCTCCGAAAAATTAAAGTTAGATAGGGTGAATAGATAAGA
         3810      3820      3830      3840      3850      3860      3870      3880      3890

TGTATTATTTTCTGAGCTACTGGAGTCCTTTTCTAAAAGGGCTCCTATGCCAAATCTTAAAATGTTTTCTTTATTTTTCTCTAAAATTTTCAGAAGTTCA  < 4000
ACATAATAAAAGACTCGATGACCTCAGGAAAAGATTTTCCCGAGGATACGGTTTAGAATTTTACAAAAGAAATAAAAAGAGATTTTAAAAGTCTTCAAGT
         3910      3920      3930      3940      3950      3960      3970      3980      3990

TGTCATACATTAAAGTCTTTAGTCCACTTTGAACTGTTTTATATTGGAGTTTAGTTTATTTTTCTATATGTAGATAACCAGTTTTCCCAGCACAATTTGT  < 4100
ACAGTATGTAATTTCAGAAATCAGGTGAAACTTGACAAAATATAACCTCAAATCAAATAAAAAGATATACATCTATTGGTCAAAAGGGTCGTGTTAAACA
```

```
         4010      4020      4030      4040      4050      4060      4070      4080      4090

TGAAAAGGCTGACTTTTTAACACATATGTTTTGATATTTTTGTCAAAAATCTAGTAGGTAGCTATAGCTGTGTGGGTTCTTTATCTATCCCGCTAATCTG  < 4200
ACTTTTCCGACTGAAAAATTGTGTATACAAAACTATAAAAACAGTTTTTAGATCATCCATCGATATCGACACACCCAAGAAATAGATAGGGCGATTAGAC
         4110      4120      4130      4140      4150      4160      4170      4180      4190

CATGTCTTTTTTTTTTTTTAGTTTTTTTTAATTAGGTATTTATTTCATTTACATTTCCAATGCTATCCCAAAAATCCCCCACACGCTCCCCCACCCACTCC  < 4300
GTACAGAAAAAAAAAAAAATCAAAAAAAAATTAATCCATAAATAAAGTAAATGTAAAGGTTACGATAGGGTTTTTAGGGGGTGTGCGAGGGGGTGGGTGAGG
         4210      4220      4230      4240      4250      4260      4270      4280      4290

CCTACCCACCCACTCCCACTTCTTGGCCCTGGCGTTCCCCTGTACTGAGGCATATAAAGTTTGCAAGACCAAGGGGCCTCTCTTTCCAATGATGGCCGAC  < 4400
GGATGGGTGGGTGAGGGTGAAGAACCGGGACCGCAAGGGGACATGACTCCGTATATTTCAAACGTTCTGGTTCCCCGGAGAGAAAGGTTACTACCGGCTG
         4310      4320      4330      4340      4350      4360      4370      4380      4390

TAGGCCATCTTCTGATACATATGCAGCTAGAGACACGAGCTCTGCGGGGGGGTGGGGGTACTGGTTAGTTCATATTGTTGTTCCACCTACAGGGTTGCAGA  < 4500
ATCCGGTAGAAGACTATGTATACGTCGATCTCTGTGCTCGAGACGCCCCCCACCCCCATGACCAATCAAGTATAACAACAAGGTGGATGTCCCAACGTCT
         4410      4420      4430      4440      4450      4460      4470      4480      4490

TCTCTTTAGCTCCTTGGGTACTTTCTCTAGCTCCTTCATTGGGGGCCCTGTGATCCATCCAATAGCTGACTGTGAGCATCCACTTCTGTGTTTGCTAGGC  < 4600
AGAGAAATCGAGGAACCCATGAAAGAGATCGAGGAAGTAACCCCCGGGACACTAGGTAGGTTATCGACTGACACTCGTAGGTGAAGACACAAACGATCCG
         4510      4520      4530      4540      4550      4560      4570      4580      4590

CCCGGCATAGTCTCACAAGAGACAGCTATATCTGGGTCCTTTCAGCAAAATCTTGCTAGTGTATGCAATGGTGTCAGCGTTTGGAAGCTGATTATGGGAT  < 4700
GGGCCGTATCAGAGTGTTCTCTGTCGATATAGACCCAGGAAAGTCGTTTTAGAACGATCACATACGTTACCACAGTCGCAAACCTTCGACTAATACCCTA
         4610      4620      4630      4640      4650      4660      4670      4680      4690

GGATCCCCGGATATGGCAGTTTCTAGATGGTCCATCCTTTCGTCTCAGCTCCAAACTTTGTCTCTGTAACTCCTTCCATGGGTGTTTTGTTCTCAATTCT  < 4800
CCTAGGGGCCTATACCGTCAAAGATCTACCAGGTAGGAAAGCAGAGTCGAGGTTTGAAACAGAGACATTGAGGAAGGTACCCACAAAACAAGAGTTAAGA
         4710      4720      4730      4740      4750      4760      4770      4780      4790

AAGAAGGGGCAAAGTGTCCACACTTTGGTCTTCATTCTTCTTGAGTTTCGTGTGTTTTGCAAATTGTATCTTATATCTTGGGTATTCTAAGTTTCTGGAC  < 4900
TTCTTCCCCGTTTCACAGGTGTGAAACCAGAAGTAAGAAGAACTCAAAGCACACAAAACGTTTAACATAGAATATAGAACCCATAAGATTCAAAGACCTG
         4810      4820      4830      4840      4850      4860      4870      4880      4890

TAATATCCACTTATCAGTGAGTAAGCATGTCTTTTTTTTTTTTTTTTTTTTTTGCCACAACCATGATGTTTCATTATGACACAACACATTTTTTAAAAT  < 5000
ATTATAGGTGAATAGTCACTCATTCGTACAGAAAAAAAAAAAAAAAAAAAAAAACGGTGTTGGTACTACAAAGTAATACTGTGTTGTGTAAAAAATTTA
         4910      4920      4930      4940      4950      4960      4970      4980      4990

AAAGAACAAAACAGAAAACCCTGGCTGACTTCAAACTCATGATATTCTTAACATAGTTCCCCAGTAGCCAAATCATAGGCATTTACTACCATCCCCAGCT  < 5100
TTTCTTGTTTTGTCTTTTGGGACCGACTGAAGTTTGAGTACTATAAGAATTGTATCAAGGGGTCATCGGTTTAGTATCCGTAAATGATGGTAGGGGTCGA
         5010      5020      5030      5040      5050      5060      5070      5080      5090

TATTTCAATTATAATATCTGAGAAGCTCAGGCAATTTCTCTAATTATCTTCCTCAAAATACAAGAGTATAGAATTTTGCATTGCAGTCTTAGATGTTCAA  < 5200
ATAAAGTTAATATTATAGACTCTTCGAGTCCGTTAAAGAGATTAATAGAAGGAGTTTTATGTTCTCATATCTTAAAACGTAACGTCAGAATCTACAAGTT
         5110      5120      5130      5140      5150      5160      5170      5180      5190

GCTTCCTGGTTTTATAATGCTGAAAAGTATTTTCACTAGACTGAACCACCACCCTCCTATCCTATGAGATTTTTTTTCAATGAAAGCCTGCTATGAAGAT  < 5300
CGAAGGACCAAAATATTACGACTTTTCATAAAAGTGATCTGACTTGGTGGTGGGAGGATAGGATACTCTAAAAAAAAAGTTACTTTCGGACGATACTTCTA
         5210      5220      5230      5240      5250      5260      5270      5280      5290

CTATGCAGTTTATGAAGAGAGAATAGAGAAAGTGATAGCCAGAAAGGGAGGGGAAAGAGAGACAGGGAAGACAAAACATTCTCTAGACATTTATTGAATG  < 5400
GATACGTCAAATACTTCTCTCTTATCTCTTTCACTATCGGTCTTTCCCTCCCCTTTCTCTCTGTCCCTTCTGTTTTGTAAGAGATCTGTAAATAACTTAC
         5310      5320      5330      5340      5350      5360      5370      5380      5390

ACTGAACAAATGAATCTGGGAACTTGAGTCCTTTTGTAAATAAGAAACTAAGGCTCAGAAAGGTTAAAAAAATTTGCACAAGGGCACAGTAGTGGGATCC  < 5500
TGACTTGTTTACTTAGACCCTTGAACTCAGGAAAACATTTATTCTTTGATTCCGAGTCTTTCCAATTTTTTTAAACGTGTTCCCGTGTCATCACCCTAGG
         5410      5420      5430      5440      5450      5460      5470      5480      5490

ACTTTGATTTCAAGCCTTTCGGTCTAGTTCCACTTCTCTTTTCTCCTACATCTACTGCGAGCCTATCTTAAGATTTCTCAGGGCCAGTCTACCAGGAGAA  < 5600
TGAAACTAAAGTTCGGAAAGCCAGATCAAGGTGAAGAGAAAAGAGGATGTAGATGACGCTCGGATAGAATTCTAAAGAGTCCCGGTCAGATGGTCCTCTT
         5510      5520      5530      5540      5550      5560      5570      5580      5590

ATGGGGCTTGGGACAGATGTAAATCAATGTGTGTCCTTGGTTGAGAAAGTCTTTCTACAGGAAAAAAAAAATGTTCCTTAATGACTTTATGTAGTAGCCC  < 5700
TACCCCGAACCCTGTCTACATTTAGTTACACACAGGAACCAACTCTTTCAGAAAGATGTCCTTTTTTTTTTTACAAGGAATTACTGAAATACATCATCGGG
         5610      5620      5630      5640      5650      5660      5670      5680      5690

AATTCTCAATCTTGTTATAAATAGTTCACTAGTGGAATCTGGCCCACAGACTTTACTTTTTTGCAGCATGGATAATAATGATCCCTATTCCAACTATGTG  < 5800
TTAAGAGTTAGAACAATATTTATCAAGTGATCACCTTAGACCGGGTGTCTGAAATGAAAAAACGTCGTACCTATTATTACTAGGGATAAGGTTGATACAC
         5710      5720      5730      5740      5750      5760      5770      5780      5790

                          >Exon 2
                            |
GATTTAAACCCAACATGTCTATCATTTCAGATGCTCTCAGTATCCCTGCATCCCGCGTCCAGATGGAGTCCTCTACAGCCTTTTATGATTATCATGATAA  < 5900
CTAAATTTGGGTTGTACAGATAGTAAAGTCTACGAGAGTCATAGGGACGTAGGGCGCAGGTCTACCTCAGGAGATGTCGGAAAATACTAATAGTACTATT
         5810      5820      5830      5840      5850      5860      5870      5880      5890

ATTGAGTCTTCTATGTGAGAACAATGTCATCTTCTTTTCCACCATCTCTACCATTGTCCTGTACTCTCTGGTATTTCTCCTCAGCCTTGTGGGTAACAGC  < 6000
TAACTCAGAAGATACACTCTTGTTACAGTAGAAGAAAAGGTGGTAGAGATGGTAACAGGACATGAGAGACCATAAAGAGGAGTCGGAACACCCATTGTCG
         5910      5920      5930      5940      5950      5960      5970      5980      5990

CTGGTTTTGTGGGTCTTGGTGAAGTATGAGAATCTAGAGTCACTCACCAATATCTTCATCCTCAACCTGTGTCTCTCAGACCTGATGTTCTCCTGTCTAC  < 6100
GACCAAAACACCCAGAACCACTTCATACTCTTAGATCTCAGTGAGTGGTTATAGAAGTAGGAGTTGGACACAGAGAGTCTGGACTACAAGAGGACAGATG
         6010      6020      6030      6040      6050      6060      6070      6080      6090

TGCCTGTGTTGATCTCAGCACAATGGAGTTGGTTTCTAGGTGACTTCTTCTGCAAGTTCTTCAACATGATCTTCGGCATCAGCCTCTACAGCAGCATCTT  < 6200
```

```
ACGGACACAACTAGAGTCGTGTTACCTCAACCAAAGATCCACTGAAGAAGACGTTCAAGAAGTTGTACTAGAAGCCGTAGTCGGAGATGTCGTCGTAGAA
         6110      6120      6130      6140      6150      6160      6170      6180      6190

CTTCCTTACCATCATGACCATCCACCGATACCTGTCTGTAGTGAGCCCCATCTCTACTCTGGGTATCCATACCCTCCGCTGCCGTGTGCTGGTGACATCA  < 6300
GAAGGAATGGTAGTACTGGTAGGTGGCTATGGACAGACATCACTCGGGGTAGAGATGAGACCCATAGGTATGGGAGGCGACGGCACACGACCACTGTAGT
         6210      6220      6230      6240      6250      6260      6270      6280      6290

TGTGTGTGGGCAGCCAGCATCCTGTTCTCCATCCCTGATGCTGTCTTCCACAAAGTGATCTCCTTAAATTGTAAATATTCTGAACATCATGGGTTCTTGG  < 6400
ACACACACCCGTCGGTCGTAGGACAAGAGGTAGGGACTACGACAGAAGGTGTTTCACTAGAGGAATTTAACATTTATAAGACTTGTAGTACCCAAGAACC
         6310      6320      6330      6340      6350      6360      6370      6380      6390

CCTCAGTCTACCAGCACAACATCTTCTTCCTCCTCTCCATGGGAATCATCCTATTCTGTTATGTACAGATTCTCAGGACTTTGTTTCGCACAAGGTCCAG  < 6500
GGAGTCAGATGGTCGTGTTGTAGAAGAAGGAGGAGGTACCCTTAGTAGGATAAGACAATACATGTCTAAGAGTCCTGAAACAAAGCGTGTTCCAGGTC
         6410      6420      6430      6440      6450      6460      6470      6480      6490

ACAGAGACACCGAACAGTCAGGCTCATCTTCACCGTCGTGGTAGCATACTTCCTCAGCTGGGCTCCCTACAACCTCACACTCTTCCTGAAAACTGGAATC  < 6600
TGTCTCTGTGGCTTGTCAGTCCGAGTAGAAGTGGCAGCACCATCGTATGAAGGAGTCGACCCGAGGGATGTTGGAGTGTGAGAAGGACTTTTGACCTTAG
         6510      6520      6530      6540      6550      6560      6570      6580      6590

ATCCAGCAGAGCTGTGAGAGCCTTCAGCAACTGGACATTGCTATGATTATCTGTCGCCATTTGGCCTTCTCTCATTGCTGTTTCAACCCAGTGCTTTATG  < 6700
TAGGTCGTCTCGACACTCTCGGAAGTCGTTGACCTGTAACGATACTAATAGACAGCGGTAAACCGGAAGAGAGTAACGACAAAGTTGGGTCACGAAATAC
         6610      6620      6630      6640      6650      6660      6670      6680      6690

TCTTTGTTGGGATCAAGTTCCGCAGACACCTAAAACATCTCTTCCAGCAGGTCTGGCTGTGCCGGAAGACATCCAGCACTGTTCCCTGCTCCCCTGGTAC  < 6800
AGAAACAACCCTAGTTCAAGGCGTCTGTGGATTTTGTAGAGAAGGTCGTCCAGACCGACACGGCCTTCTGTAGGTCGTGACAAGGGACGAGGGGACCATG
         6710      6720      6730      6740      6750      6760      6770      6780      6790

CTTTACATATGAGGGACCCTCCTTCTACTGAGAGGAGAGGATGGGCACATGGAGATGACTATGGGAGGTAAAGGAAGACAAGGAGAAGTGGATCAGGAAG  < 6900
GAAATGTATACTCCCTGGGAGGAAGATGACTCTCCTCTCCTACCCGTGTACCTCTACTGATACCCTCCATTTCCTTCTGTTCCTCTTCACCTAGTCCTTC
         6810      6820      6830      6840      6850      6860      6870      6880      6890

GAAAATATAACTGAAGATACTACAGAGTGTGGAGGAAAGACATGATACCCATGGGGAAGTGGCTTCCAGCTGGGCAAGCCAAAGCAACACTTCGTGCACT  < 7000
CTTTTATATTGACTTCTATGATGTCTCACACCTCCTTTCTGTACTATGGGTACCCCTTCACCGAAGGTCGACCCGTTCGGTTTCGTTGTGAAGCACGTGA
         6910      6920      6930      6940      6950      6960      6970      6980      6990

CAGTTCATCATTTATTCTCTTACTTAGACATAGATTGCTTGTTAGTGATGGTCAGAAGATCCTAAATAGAAGGATTTCTAGACTTTAGGAGGGCTTGAAG  < 7100
GTCAAGTAGTAAATAAGAGAATGAATCTGTATCTAACGAACAATCACTACCAGTCTTCTAGGATTTATCTTCCTAAAGATCTGAAATCCTCCCGAACTTC
         7010      7020      7030      7040      7050      7060      7070      7080      7090

CTTATAGTATGTGCTAACTGTGCAGTGATGTTGCTGGTACATAGGGTTGCCCCAAACTATTTTTTTTTCACCTTGGTGATAGCTGACTCTGTGATTCTTA  < 7200
GAATATCATACACGATTGACACGTCACTACAACGACCATGTATCCCAACGGGGTTTGATAAAAAAAAAGTGGAACCACTATCGACTGAGACACTAAGAAT
         7110      7120      7130      7140      7150      7160      7170      7180      7190

GCAGCTACAGAAAGAAAAAAAACTCTCTTCAGGACAAGAATAATCACATCTTTAAATAAGTACAGTCACAATGAAGTCTATACCATAAAATCCCACTAAA  < 7300
CGTCGATGTCTTTCTTTTTTTTGAGAGAAGTCCTGTTCTTATTAGTGTAGAAATTTATTCATGTCAGTGTTACTTCAGATATGGTATTTTAGGGTGATTT
         7210      7220      7230      7240      7250      7260      7270      7280      7290

ATGAAGATGGTTCTGAGCCGGGTGTGGTGGCGCATGCCTTTAATCCCAGCACTCAGGAGGCAGAGACAGGCAGATTTCTGAGTTTGAGGCCAGCCTGGTC  < 7400
TACTTCTACCAAGACTCGGCCCACACCACCGCGTACGGAAATTAGGGTCGTGAGTCCTCCGTCTCTGTCCGTCTAAAGACTCAAACTCCGGTCGGACCAG
         7310      7320      7330      7340      7350      7360      7370      7380      7390

TACAGAGTGAGTTCCAGGACAGCCAGGGCTACACAGAGAAACCCTGTCTTGAAAAACAAAACAAAACAAAACAAAACAAAAAAACAACAACAACA  < 7500
ATGTCTCACTCAAGGTCCTGTCGGTCCCGATGTGTCTCTTTGGGACAGAACTTTTTGTTTTGTTTTGTTTTGTTTTGTTTTTTTGTTGTTGTTGT
         7410      7420      7430      7440      7450      7460      7470      7480      7490

AAGATGGTTCCATATTCTGGCAACAGCTGCTAACACATAAGCTGGCTTTTAAATATTTAGCTCATAACTGAAAGAAAAAATACAATATGTGCTACTGTCT  < 7600
TTCTACCAAGGTATAAGACCGTTGTCGACGATTGTGTATTCGACCGAAAATTTATAAATCGAGTATTGACTTTCTTTTTTATGTTATACACGATGACAGA
         7510      7520      7530      7540      7550      7560      7570      7580      7590

GCACTAAGTAATTATTTGGACAATACAAAGATGAATAGGATATTGCTGCTAACTTTCAGTTGACACCAATCCATCCAAGAAGGTCCAGATAAGAAAAGTC  < 7700
CGTGATTCATTAATAAACCTGTTATGTTTCTACTTATCCTATAACGACGATTGAAAGTCAACTGTGGTTAGGTAGGTTCTTCCAGGTCTATTCTTTTCAG
         7610      7620      7630      7640      7650      7660      7670      7680      7690

CACTTAACAGAGGCATTCAGGTTGAATATTCCTGTCATTTCATCTCTTCCAGATTGAGAGAAAGATGACTTCCTTACATGTGGATAATAATGCCAGCATT  < 7800
GTGAATTGTCTCCGTAAGTCCAACTTATAAGGACAGTAAAGTAGAGAAGGTCTAACTCTCTTTCTACTGAAGGAATGTACACCTATTATTACGGTCGTAA
         7710      7720      7730      7740      7750      7760      7770      7780      7790

CCCCTCTTAACCATTCTCCAGAGCTAAATTCTCCTCATGCACCACATTCCCTTTCGCAGAGCCAGGTCCCGTGGATTCTGCCTTCCCAACATCTCTCCAG  < 7900
GGGGAGAATTGGTAAGAGGTCTCGATTTAAGAGGAGTACGTGGTGTAAGGGAAAGCGTCTCGGTCCAGGGCACCTAAGACGGAAGGGTTGTAGAGAGGTC
         7810      7820      7830      7840      7850      7860      7870      7880      7890

CTTATGAGCACATACCCTTGACTTCATCTTTATAGTGCCCTCTGTTCCATAGTATCTTCCTTTTGCTTCTATTTTTCCTCTGTTACATCTTCCTCCTTCA  < 8000
GAATACTCGTGTATGGGAACTGAAGTAGAAATATCACGGGAGACAAGGTATCATAGAAGGAAAACGAAGATAAAAAGGAGACAATGTAGAAGGAGGAAGT
         7910      7920      7930      7940      7950      7960      7970      7980      7990

GGAAGCTGCCTGCCTGAGATTTATCTTTTATTTTACAGCTCCTCTGCCTAGAGTCTGTCTTTGACGCTTTAATAAAATTGTCCTCAAGCTCCCTTCTGAG  < 8100
CCTTCGACGGACGGACTCTAAATAGAAAATAAAATGTCGAGGAGACGGATCTCAGACAGAAACTGCGAAATTATTTTAACAGGAGTTCGAGGGAAGACTC
         8010      8020      8030      8040      8050      8060      8070      8080      8090

TTACTTCTTAAATTCTTTTATTAATAAAACTAGTAACACAAAAGAGGGCCCAGATTTCCCTGGTAATATAAGGTTACTCCATCAGAATGCTCCAGAATTT  < 8200
AATGAAGAATTTAAGAAAATAATTATTTTGATCATTGTGTTTTCTCCCGGGTCTAAAGGGACCATTATATTCCAATGAGGTAGTCTTACGAGGTCTTAAA
         8110      8120      8130      8140      8150      8160      8170      8180      8190

CAGGTAACATTATTACCTTTGGGGCAGTTTAGACTGTTATATCTGCATCCAGGGCCAAAGACAGAACTCAGATCCTGTTCTTTCAACCAAAAATAAATAC  < 8300
```

```
GTCCATTGTAATAATGGAAACCCCGTCAAATCTGACAATATAGACGTAGGTCCCGGTTTCTGTCTTGAGTCTAGGACAAGAAAGTTGGTTTTTATTTATG
         8210      8220      8230      8240      8250      8260      8270      8280      8290

ATAAAAACATATAACAGTAGACTTTAAAGAATTAATGAAAAAATTAAAAGACATAAAATAGTTATGGATTACCCAGAAGAAGTAACTTTCAAGTGGATAG  < 8400
TATTTTTGTATATTGTCATCTGAAATTTCTTAATTACTTTTTTAATTTTCTGTATTTTATCAATACCTAATGGGTCTTCTTCATTGAAAGTTCACCTATC
         8310      8320      8330      8340      8350      8360      8370      8380      8390

AGGGATGGCTCAGCAGTTAAGAGCACTGGCTACTCCTCCAGAGGGCCTAAATTCAGTTCCCAAAGCCCACATGGTATCTCCCAACCATTTTAACTGCAGT  < 8500
TCCCTACCGAGTCGTCAATTCTCGTGACCGATGAGGAGGTCTCCCGGATTTAAGTCAAGGGTTTCGGGTGTACCATAGAGGGTTGGTAAAATTGACGTCA
         8410      8420      8430      8440      8450      8460      8470      8480      8490

TCCAAGGGAATCCATTGCCCTCTTCTGGCCTCCTTTCCTTTGTACACGAAGATGAACATTTCATATATCTTACAATGTGTCGGTTAGAGATCCCTCGGGC  < 8600
AGGTTCCCTTAGGTAACGGGAGAAGACCGGAGGAAAGGAAACATGTGCTTCTACTTGTAAAGTATATAGAATGTTACACAGCCAATCTCTAGGGAGCCCG
         8510      8520      8530      8540      8550      8560      8570      8580      8590

ACCTTACACTTCATCCTAGTTTATATCTCTGCCCATTAGCCAGGTGGGCTTGAAATTCCTTTTCTTCTAAAAGCCTCAATTTCATCTTTGAAGTTCAGAA  < 8700
TGGAATGTGAAGTAGGATCAAATATAGAGACGGGTAATCGGTCCACCCGAACTTTAAGGAAAAGAAGATTTTCGGAGTTAAAGTAGAAACTTCAAGTCTT
         8610      8620      8630      8640      8650      8660      8670      8680      8690

ATGAACCCTACCTATAGCACAGAGCTGTGTTGAGTTTTAAACATAACATTATATAGGCTTTTGGTTAGGGTATGACATATTAGGTTTTTAATATATACAA  < 8800
TACTTGGGATGGATATCGTGTCTCGACACAACTCAAAATTTGTATTGTAATATATCCGAAAACCAATCCCATACTGTATAATCCAAAAATTATATATGTT
         8710      8720      8730      8740      8750      8760      8770      8780      8790

TAATCTACTGCACAATATTTTGGTCAATGTTGGACCACATATCACTGTGCTCCCTTAAGACTAAATCATCTAGTGATGTCATAGTCATCTTAATTTATCT  < 8900
ATTAGATGACGTGTTATAAAACCAGTTACAACCTGGTGTATAGTGACACGAGGGAATTCTGATTTAGTAGATCACTACAGTATCAGTAGAATTAAATAGA
         8810      8820      8830      8840      8850      8860      8870      8880      8890

AACTATACTCCAGATGAATTGTCTATGAAATTCTCAAAATACATCATTGCCCTTAAATAACCCATGATTGCTTGAGACCTGTCTTCCTCTTCTCTGTAAA  < 9000
TTGATATGAGGTCTACTTAACAGATACTTTAAGAGTTTTATGTAGTAACGGGAATTTATTGGGTACTAACGAACTCTGGACAGAAGGAGAAGAGACATTT
         8910      8920      8930      8940      8950      8960      8970      8980      8990

TTTATTTGGGATCTAAGTTTCAAACAAGGGTGTTTGAAATCCCTTTTGTGGGAACAGGACTGAGGATGGGCATTTAGAGGCGACAGAGTCACGTGACAAC  < 9100
AAATAAACCCTAGATTCAAAGTTTGTTCCCACAAACTTTAGGGAAAACACCCTTGTCCTGACTCCTACCCGTAAATCTCCGCTGTCTCAGTGCACTGTTG
         9010      9020      9030      9040      9050      9060      9070      9080      9090

TCCTGGTAAATAAAGCTCCAGAGATCAGTATCAGTGTGCAGATCTGCATTTATTGCCAAGCACATAAGCTTATATACAGTATTTGAGCCAATCCCAAGCC  < 9200
AGGACCATTTATTTCGAGGTCTCTAGTCATAGTCACACGTCTAGACGTAAATAACGGTTCGTGTATTCGAATATATGTCATAAACTCGGTTAGGGTTCGG
         9110      9120      9130      9140      9150      9160      9170      9180      9190

CCTAAATCCTTGGCCAAGCATAACTTACTACATCTCACCATATCCCAATAAAAGCTGTGACTGATGAGGTAACTCAGAGAGAAGGGGTGTGGCGAGCATT  < 9300
GGATTTAGGAACCGGTTCGTATTGAATGATGTAGAGTGGTATAGGGTTATTTTCGACACTGACTACTCCATTGAGTCTCTCTTCCCCACACCGCTCGTAA
         9210      9220      9230      9240      9250      9260      9270      9280      9290

GTCACCTGTAGGGACTTTTGTGAAGACTCAGAAGCAGCCACTGTCTTGACCTTAGTTCCTTTTTGCTGTCTCACTGGTGTCCCGGGAGCCATCTTAGATC  < 9400
CAGTGGACATCCCTGAAAACACTTCTGAGTCTTCGTCGGTGACAGAACTGGAATCAAGGAAAAACGACAGAGTGACCACAGGGCCCTCGGTAGAATCTAG
         9310      9320      9330      9340      9350      9360      9370      9380      9390

TGACACCATGTACAGCAGATCAGGACTCTGTGGCACAGTGCTCTCCACCCCACATATTCCTTCACAAGGTTGTCTTCCACATGCCTCACACTCTCAATCT  < 9500
ACTGTGGTACATGTCGTCTAGTCCTGAGACACCGTGTCACGAGAGGTGGGGTGTATAAGGAAGTGTTCCAACAGAAGGTGTACGGAGTGTGAGAGTTAGA
         9410      9420      9430      9440      9450      9460      9470      9480      9490

TAACATCCCAAAGCTGTTCAGGCTGTAGTCAGAGCAAGTTTTTCTTAGTTCACTCTATTGATAAATCTTTATTTCTGATGTCATTTCCTCCCACTTCTTC  < 9600
ATTGTAGGGTTTCGACAAGTCCGACATCAGTCTCGTTCAAAAAGAATCAAGTGAGATAACTATTTAGAAATAAAGACTACAGTAAAGGAGGGTGAAGAAG
         9510      9520      9530      9540      9550      9560      9570      9580      9590

CCTTTTTTTTGTTTTCCTTTGTTAACAGAAAGGGGAATCATTTCTCTTCGTGAGGTTTTTTTTATCCTCATCCACAAACTGACAACTCCATCAAGTTAAT  < 9700
GGAAAAAAAACAAAAGGAAACAATTGTCTTTCCCCTTAGTAAAGAGAAGCACTCCAAAAAAAATAGGAGTAGGTGTTTGACTGTTGAGGTAGTTCAATTA
         9610      9620      9630      9640      9650      9660      9670      9680      9690

ATGTTGTCTCATATACCTCCAGTATAAAATATGAAATTAACTTAAAAGATTTCTTTTCCTTCCTGTATGAATTTATCCTGAGAACCTGGAATGCTGAAGT  < 9800
TACAACAGAGTATATGGAGGTCATATTTTATACTTTAATTGAATTTTCTAAAGAAAAGGAAGGACATACTTAAATAGGACTCTTGGACCTTACGACTTCA
         9710      9720      9730      9740      9750      9760      9770      9780      9790

CTGGCAGATGCCACTATTAGCTAAGTCCTGTAAGGTACACAAGCATTTCTAGCTAACATGATGAAAATAAGGCAGTGTGAGGAGCCAGCCAGAGCTAAGA  < 9900
GACCGTCTACGGTGATAATCGATTCAGGACATTCCATGTGTTCGTAAAGATCGATTGTACTACTTTTATTCCGTCACACTCCTCGGTCGGTCTCGATTCT
         9810      9820      9830      9840      9850      9860      9870      9880      9890



AGCGAACCTAATCATGGGCTGACATTCCTATGTACTGTCCCCTGTCTTTAGCATGTTCATCCATACTGGACTTGGAATGCAGTGTTCTATTGCACCAGGC  < 10000
TCGCTTGGATTAGTACCCGACTGTAAGGATACATGACAGGGGACAGAAATCGTACAAGTAGGTATGACCTGAACCTTACGTCACAAGATAACGTGGTCCG
         9910      9920      9930      9940      9950      9960      9970      9980      9990

TTCAGGGTGCTTTGCAACTCAGCAACAAGCAAACACGGGACTGAGGAAGCTAAGCATGGTAGTTCTTTAGCACATATTTTCAAACACTGTTTTTTAAGTG  < 10100
AAGTCCCACGAAACGTTGAGTCGTTGTTCGTTTGTGCCCTGACTCCTTCGATTCGTACCATCAAGAAATCGTGTATAAAAGTTTGTGACAAAAAATTCAC
         10010     10020     10030     10040     10050     10060     10070     10080     10090

TCTGTTAATGAGGGGGAAACAAAAACTGAGAACTTAGGTCCAGCAGTACATACTAAGTTCATTTTTTTTTAGCTTCATAAATAAAACGTAATAGT  < 10195
AGACAATTACTCCCCCTTTGTTTTTGACTCTTGAATCCAGGTCGTCATGTATGATTCAAGTAAAAAAAAATCGAAGTATTTATTTTGCATTATCA
         10110     10120     10130     10140     10150     10160     10170     10180     10190
```

Appendix 1. *Xcr1 gene sequence containing 5' flanking region, exon 1, intron 1 and exon 2.* Sequence obtained from Ensembl. Transcript ID ENSMUST00000182350.1.

```
RC221929          1 AACAAAATATTAACGCTTACAATTTCCATTCGCCATTCAGGCTGCGCAAC     50
RC221929seq       1 --------------------------------------------------      0
RC221929         51 TGTTGGGAAGGGCGATCGGTGCGGGCCTCTTCGCTATTACGCCAGCTGGC    100
RC221929seq       1 --------------------------------------------------      0
RC221929        101 GAAAGGGGGATGTGCTGCAAGGCGATTAAGTTGGGTAACGCCAGGGTTTT    150
RC221929seq       1 --------------------------------------------------      0
RC221929        151 CCCAGTCACGACGTTGTAAAACGACGGCCAGTGCCAAGCTGATCTATACA    200
RC221929seq       1 --------------------------------------------------      0
RC221929        201 TTGAATCAATATTGGCAATTAGCCATATTAGTCATTGGTTATATAGCATA    250
RC221929seq       1 --------------------------------------------------      0
RC221929        251 AATCAATATTGGCTATTGGCCATTGCATACGTTGTATCTATATCATAATA    300
RC221929seq       1 --------------------------------------------------      0
RC221929        301 TGTACATTTATATTGGCTCATGTCCAATATGACCGCCATGTTGACATTGA    350
RC221929seq       1 --------------------------------------------------      0
RC221929        351 TTATTGACTAGTTATTAATAGTAATCAATTACGGGGTCATTAGTTCATAG    400
RC221929seq       1 --------------------------------------------------      0
RC221929        401 CCCATATATGGAGTTCCGCGTTACATAACTTACGGTAAATGGCCCGCCTG    450
RC221929seq       1 --------------------------------------------------      0
RC221929        451 GCTGACCGCCCAACGACCCCCGCCCATTGACGTCAATAATGACGTATGTT    500
RC221929seq       1 --------------------------------------------------      0
RC221929        501 CCCATAGTAACGCCAATAGGGACTTTCCATTGACGTCAATGGGTGGAGTA    550
RC221929seq       1 --------------------------------------------------      0
RC221929        551 TTTACGGTAAACTGCCCACTTGGCAGTACATCAAGTGTATCATATGCCAA    600
RC221929seq       1 --------------------------------------------------      0
RC221929        601 GTCCGCCCCCTATTGACGTCAATGACGGTAAATGGCCCGCCTGGCATTAT    650
RC221929seq       1 --------------------------------------------------      0
RC221929        651 GCCCAGTACATGACCTTACGGGACTTTCCTACTTGGCAGTACATCTACGT    700
RC221929seq       1 --------------------------------------------------      0
RC221929        701 ATTAGTCATCGCTATTACCATGGTGATGCGGTTTTGGCAGTACACCAATG    750
RC221929seq       1 --------------------------------------------------      0
RC221929        751 GGCGTGGATAGCGGTTTGACTCACGGGGATTTCCAAGTCTCCACCCCATT    800
RC221929seq       1 --------------------------------------------------      0
RC221929        801 GACGTCAATGGGAGTTTGTTTTGGCACCAAAATCAACGGGACTTTCCAAA    850
RC221929seq       1 --------------------------------------------------      0
RC221929        851 ATGTCGTAATAACCCCGCCCCGTTGACGCAAATGGGCGGTAGGCGTGTAC    900
```

```
RC221929seq       1 --------------------------------------------------      0

RC221929        901 GGTGGGAGGTCTATATAAGCAGAGCTCGTTTAGTGAACCGTCAGAATTTT    950

RC221929seq       1 --------------------------------------------------      0

RC221929        951 GTAATACGACTCACTATAGGGCGGCCGGGAATTCGTCGACTGGATC----    996

RC221929seq       1 ------------------------------------------------NNNN      4

RC221929        997 -----------CGGTACCGAGGAGATCTGCCGCCGCGATCGCCATGGAGT   1035
                            ||||||||||||||||||||||||||||||||||||||||
RC221929seq       5 NNNNNNNNGNNCGGTACCGAGGAGATCTGCCGCCGCGATCGCCATGGAGT     54

RC221929       1036 CCTCAGGCAACCCAGAGAGCACCACCTTTTTTTACTATGACCTTCAGAGC   1085
                    ||||||||||||||||||||||||||||||||||||||||||||||||||||
RC221929seq      55 CCTCAGGCAACCCAGAGAGCACCACCTTTTTTTACTATGACCTTCAGAGC    104

RC221929       1086 CAGCCGTGTGAGAACCAGGCCTGGGTCTTTGCTACCCTCGCCACCACTGT   1135
                    ||||||||||||||||||||||||||||||||||||||||||||||||||||
RC221929seq     105 CAGCCGTGTGAGAACCAGGCCTGGGTCTTTGCTACCCTCGCCACCACTGT    154

RC221929       1136 CCTATACTGCCTGGTGTTTCTCCTCAGCCTAGTGGGCAACAGCCTGGTCC   1185
                    ||||||||||||||||||||||||||||||||||||||||||||||||||||
RC221929seq     155 CCTATACTGCCTGGTGTTTCTCCTCAGCCTAGTGGGCAACAGCCTGGTCC    204

RC221929       1186 TGTGGGTCCTGGTGAAGTATGAGAGCCTGGAGTCCCTCACCAACATCTTC   1235
                    ||||||||||||||||||||||||||||||||||||||||||||||||||||
RC221929seq     205 TGTGGGTCCTGGTGAAGTATGAGAGCCTGGAGTCCCTCACCAACATCTTC    254

RC221929       1236 ATCCTCAACCTGTGCCTCTCAGACCTGGTGTTCGCCTGCTTGTTGCCTGT   1285
                    ||||||||||||||||||||||||||||||||||||||||||||||||||||
RC221929seq     255 ATCCTCAACCTGTGCCTCTCAGACCTGGTGTTCGCCTGCTTGTTGCCTGT    304

RC221929       1286 GTGGATCTCCCCATACCACTGGGGCTGGGTGCTGGGAGACTTCCTCTGCA   1335
                    ||||||||||||||||||||||||||||||||||||||||||||||||||||
RC221929seq     305 GTGGATCTCCCCATACCACTGGGGCTGGGTGCTGGGAGACTTCCTCTGCA    354

RC221929       1336 AACTCCTCAATATGATCTTCTCCATCAGCCTCTACAGCAGCAGCTTCTTC   1385
                    ||||||||||||||||||||||||||||||||||||||||||||||||||||
RC221929seq     355 AACTCCTCAATATGATCTTCTCCATCAGCCTCTACAGCAGCAGCTTCTTC    404

RC221929       1386 CTGACCATCATGACCATCCACCGCTACCTGTCGGTAGTGAGCCCCCTCTC   1435
                    ||||||||||||||||||||||||||||||||||||||||||||||||||||
RC221929seq     405 CTGACCATCATGACCATCCACCGCTACCTGTCGGTAGTGAGCCCCCTCTC    454

RC221929       1436 CACCCTGCGCGTCCCCACCCTCCGCTGCCGGGTGCTGGTGACCATGGCTG   1485
                    ||||||||||||||||||||||||||||||||||||||||||||||||||||
RC221929seq     455 CACCCTGCGCGTCCCCACCCTCCGCTGCCGGGTGCTGGTGACCATGGCTG    504

RC221929       1486 TGTGGGTAGCCAGCATCCTGTCCTCCATCCTCGACACCATCTTCCACAAG   1535
                    ||||||||||||||||||||||||||||||||||||||||||||||||||||
RC221929seq     505 TGTGGGTAGCCAGCATCCTGTCCTCCATCCTCGACACCATCTTCCACAAG    554

RC221929       1536 GTGCTTTCTTCGGGCTGTGATTATTCCGAACTCACGTGGTACCTCACCTC   1585
                    ||||||||||||||||||||||||||||||||||||||||||||||||||||
RC221929seq     555 GTGCTTTCTTCGGGCTGTGATTATTCCGAACTCACGTGGTACCTCACCTC    604

RC221929       1586 CGTCTACCAGCACAACCTCTTCTTCCTGCTGTCCCTGGGGATTATCCTGT   1635
                    ||||||||||||||||||||||||||||||||||||||||||||||||||||
RC221929seq     605 CGTCTACCAGCACAACCTCTTCTTCCTGCTGTCCCTGGGGATTATCCTGT    654

RC221929       1636 TCTGCTACGTGGAGATCCTCAGGACCCTGTTCCGCTCACGCTCCAAGCGG   1685
                    ||||||||||||||||||||||||||||||||||||||||||||||||||||
RC221929seq     655 TCTGCTACGTGGAGATCCTCAGGACCCTGTTCCGCTCACGCTCCAAGCGG    704

RC221929       1686 CGCCACCGCACGGTCAAGCTCATCTTCGCCATCGTGGTGGCCTACTTCCT   1735
                    ||||||||||||||||||||||||||||||||||||||||||||||||||||
RC221929seq     705 CGCCACCGCACGGTCAAGCTCATCTTCGCCATCGTGGTGGCCTACTTCCT    754
```

```
RC221929        1736 CAGCTGGGGTCCCTACAACTTCACCCTGTTTCTGCAGACGCTGTTTCGGA   1785
                     ||||||||||||||||||||||||||||||||||||||||||||||||||
RC221929seq      755 CAGCTGGGGTCCCTACAACTTCACCCTGTTTCTGCAGACGCTGTTTCGGA    804

RC221929        1786 CCCAGATCATCCGGAGCTGCGAGGCCAAACAGCAGCTAGAATACGCCCTG   1835
                     ||||||||||||||||||||||||||||||||||||||||||||||||||||
RC221929seq      805 CCCAGATCATCCGGAGCTGCGAGGCCAAACAGCAGCTAGAATACGCCCTG    854

RC221929        1836 CTCATCTGCCGCAACCTCGCCTTCTCCCACTGCTGCTTTAACCCGGTGCT   1885
                     ||||||||||||||||||||||||||||||||||||||||||||||||||||
RC221929seq      855 CTCATCTGCCGCAACCTCGCCTTCTCCCACTGCTGCTTTAACCCGGTGCT    904

RC221929        1886 CTATGTCTTCGTGGGGGTCAAGTTCCGCACACACCTGAAACATGTTCTCC   1935
                     ||||||||||||||||||||||||||||||||||||||||||||||||||||
RC221929seq      905 CTATGTCTTCGTGGGGGTCAAGTTCCGCACACACCTGAAACATGTTCTCC    954

RC221929        1936 GGCAGTTCTGGTTCTGCCGGCTGCAGGCACCCAGCCCAGCCTCGATCCCC   1985
                     ||||||||||||||||||||||||||||||||||||||||||||||||||||
RC221929seq      955 GGCAGTTCTGGTTCTGCCGGCTGCAGGCACCCAGCCCAGCCTCGATCCCC   1004

RC221929        1986 CACTCCCCTGGTGCCTTCGCCTATGAGGGCGCCTCCTTCTACACGCGTAC   2035
                     ||||||||||||||||||||||||||||||||||||||||||||||||||||
RC221929seq     1005 CACTCCCCTGGTGCCTTCGCCTATGAGGGCGCCTCCTTCTACACGCGTAC   1054

RC221929        2036 GCGGCCGCTCGAGCAGAAACTCATCTCAGAAGAGGATCTGGCAGCAAATG   2085
                     ||||||||||||||||||||||||||||||||||||||||||||||||||||
RC221929seq     1055 GCGGCCGCTCGAGCAGAAACTCATCTCAGAAGAGGATCTGGCAGCAAATG   1104

RC221929        2086 ATATCCTGGATTACAAGGATGACGACGATAAGGTTTAAACGGCCGGCCGC   2135
                     ||||||||||||||||||||||||||||||||
RC221929seq     1105 ATATCCTGGATTACAAGGATGACGACGATAAGTTNNNN------------   1132

RC221929        2136 GGTCATAGCTGTTTCCTGAACAGATCCCGGGTGGCATCCCTGTGACCCCT   2185

RC221929seq     1133 ------------------------------------------------   1132

RC221929        2186 CCCCAGTGCCTCTCCTGGCCCTGGAAGTTGCCACTCCAGTGCCCACCAGC   2235

RC221929seq     1133 ------------------------------------------------   1132

RC221929        2236 CTTGTCCTAATAAAATTAAGTTGCATCATTTTGTCTGACTAGGTGTCCTT   2285

RC221929seq     1133 ------------------------------------------------   1132

RC221929        2286 CTATAATATTATGGGGTGGAGGGGGGTGGTATGGAGCAAGGGGCAAGTTG   2335

RC221929seq     1133 ------------------------------------------------   1132

RC221929        2336 GGAAGACAACCTGTAGGGCCTGCGGGGTCTATTGGGAACCAAGCTGGAGT   2385

RC221929seq     1133 ------------------------------------------------   1132

RC221929        2386 GCAGTGGCACAATCTTGGCTCACTGCAATCTCCGCCTCCTGGGTTCAAGC   2435

RC221929seq     1133 ------------------------------------------------   1132

RC221929        2436 GATTCTCCTGCCTCAGCCTCCCGAGTTGTTGGGATTCCAGGCATGCATGA   2485

RC221929seq     1133 ------------------------------------------------   1132

RC221929        2486 CCAGGCTCAGCTAATTTTTGTTTTTTTGGTAGAGACGGGGTTTCACCATA   2535

RC221929seq     1133 ------------------------------------------------   1132

RC221929        2536 TTGGCCAGGCTGGTCTCCAACTCCTAATCTCAGGTGATCTACCCACCTTG   2585

RC221929seq     1133 ------------------------------------------------   1132

RC221929        2586 GCCTCCCAAATTGCTGGGATTACAGGCGTGAACCACTGCTCCCTTCCCTG   2635
```

```
RC221929seq    1133 --------------------------------------------------   1132
RC221929       2636 TCCTTCTGATTTTAAAATAACTATACCAGCAGGAGGACGTCCAGACACAG   2685
RC221929seq    1133 --------------------------------------------------   1132
RC221929       2686 CATAGGCTACCTGGCCATGCCCAACCGGTGGGACATTTGAGTTGCTTGCT   2735
RC221929seq    1133 --------------------------------------------------   1132
RC221929       2736 TGGCACTGTCCTCTCATGCGTTGGGTCCACTCAGTAGATGCCTGTTGAAT   2785
RC221929seq    1133 --------------------------------------------------   1132
RC221929       2786 TGGGTACGCGGCCAGCGGCGAGCGGTATCAGCTCACTCAAAGGCGGTAAT   2835
RC221929seq    1133 --------------------------------------------------   1132
RC221929       2836 ACGGTTATCCACAGAATCAGGGGATAACGCAGGAAAGAACATGTGAGCAA   2885
RC221929seq    1133 --------------------------------------------------   1132
RC221929       2886 AAGGCCAGCAAAAGGCCAGGAACCGTAAAAAGGCCGCGTTGCTGGCGTTT   2935
RC221929seq    1133 --------------------------------------------------   1132
RC221929       2936 TTCCATAGGCTCCGCCCCCCTGACGAGCATCACAAAAATCGACGCTCAAG   2985
RC221929seq    1133 --------------------------------------------------   1132
RC221929       2986 TCAGAGGTGGCGAAACCCGACAGGACTATAAAGATACCAGGCGTTTCCCC   3035
RC221929seq    1133 --------------------------------------------------   1132
RC221929       3036 CTGGAAGCTCCCTCGTGCGCTCTCCTGTTCCGACCCTGCCGCTTACCGGA   3085
RC221929seq    1133 --------------------------------------------------   1132
RC221929       3086 TACCTGTCCGCCTTTCTCCCTTCGGGAAGCGTGGCGCTTTCTCATAGCTC   3135
RC221929seq    1133 --------------------------------------------------   1132
RC221929       3136 ACGCTGTAGGTATCTCAGTTCGGTGTAGGTCGTTCGCTCCAAGCTGGGCT   3185
RC221929seq    1133 --------------------------------------------------   1132
RC221929       3186 GTGTGCACGAACCCCCCGTTCAGCCCGACCGCTGCGCCTTATCCGGTAAC   3235
RC221929seq    1133 --------------------------------------------------   1132
RC221929       3236 TATCGTCTTGAGTCCAACCCGGTAAGACACGACTTATCGCCACTGGCAGC   3285
RC221929seq    1133 --------------------------------------------------   1132
RC221929       3286 AGCCACTGGTAACAGGATTAGCAGAGCGAGGTATGTAGGCGGTGCTACAG   3335
RC221929seq    1133 --------------------------------------------------   1132
RC221929       3336 AGTTCTTGAAGTGGTGGCCTAACTACGGCTACACTAGAAGAACAGTATTT   3385
RC221929seq    1133 --------------------------------------------------   1132
RC221929       3386 GGTATCTGCGCTCTGCTGAAGCCAGTTACCTTCGGAAAAAGAGTTGGTAG   3435
RC221929seq    1133 --------------------------------------------------   1132
RC221929       3436 CTCTTGATCCGGCAAACAAACCACCGCTGGTAGCGGTGGTTTTTTTGTTT   3485
RC221929seq    1133 --------------------------------------------------   1132
```

```
RC221929        3486 GCAAGCAGCAGATTACGCGCAGAAAAAAAGGATCTCAAGAAGATCCTTTG   3535
RC221929seq     1133 --------------------------------------------------   1132
RC221929        3536 ATCTTTTCTACGGGGTCTGACGCTCAGTGGAACGAAAACTCACGTTAAGG   3585
RC221929seq     1133 --------------------------------------------------   1132
RC221929        3586 GATTTTGGTCATGAGATTATCAAAAAGGATCTTCACCTAGATCCTTTTAA   3635
RC221929seq     1133 --------------------------------------------------   1132
RC221929        3636 ATTAAAAATGAAGTTTTAAATCAATCTAAAGTATATATGAGTAACCTGAG   3685
RC221929seq     1133 --------------------------------------------------   1132
RC221929        3686 GCTATGGCAGGGCCTGCCGCCCCGACGTTGGCTGCGAGCCCTGGGCCTTC   3735
RC221929seq     1133 --------------------------------------------------   1132
RC221929        3736 ACCCGAACTTGGGGGGTGGGGTGGGGAAAAGGAAGAAACGCGGGCGTATT   3785
RC221929seq     1133 --------------------------------------------------   1132
RC221929        3786 GGCCCCAATGGGGTCTCGGTGGGGTATCGACAGAGTGCCAGCCCTGGGAC   3835
RC221929seq     1133 --------------------------------------------------   1132
RC221929        3836 CGAACCCCGCGTTTATGAACAAACGACCCAACACCGTGCGTTTTATTCTG   3885
RC221929seq     1133 --------------------------------------------------   1132
RC221929        3886 TCTTTTTATTGCCGTCATAGCGCGGGTTCCTTCCGGTATTGTCTCCTTCC   3935
RC221929seq     1133 --------------------------------------------------   1132
RC221929        3936 GTGTTTCAGTTAGCCTCCCCCTAGGGTGGGCGAAGAACTCCAGCATGAGA   3985
RC221929seq     1133 --------------------------------------------------   1132
RC221929        3986 TCCCCGCGCTGGAGGATCATCCAGCCGGCGTCCCGGAAAACGATTCCGAA   4035
RC221929seq     1133 --------------------------------------------------   1132
RC221929        4036 GCCCAACCTTTCATAGAAGGCGGCGGTGGAATCGAAATCTCGTGATGGCA   4085
RC221929seq     1133 --------------------------------------------------   1132
RC221929        4086 GGTTGGGCGTCGCTTGGTCGGTCATTTCGAACCCCAGAGTCCCGCTCAGA   4135
RC221929seq     1133 --------------------------------------------------   1132
RC221929        4136 AGAACTCGTCAAGAAGGCGATAGAAGGCGATGCGCTGCGAATCGGGAGCG   4185
RC221929seq     1133 --------------------------------------------------   1132
RC221929        4186 GCGATACCGTAAAGCACGAGGAAGCGGTCAGCCCATTCGCCGCCAAGCTC   4235
RC221929seq     1133 --------------------------------------------------   1132
RC221929        4236 TTCAGCAATATCACGGGTAGCCAACGCTATGTCCTGATAGCGATCCGCCA   4285
RC221929seq     1133 --------------------------------------------------   1132
RC221929        4286 CACCCAGCCGGCCACAGTCGATGAATCCAGAAAAGCGGCCATTTTCCACC   4335
RC221929seq     1133 --------------------------------------------------   1132
RC221929        4336 ATGATATTCGGCAAGCAGGCATCGCCATGGGTCACGACGAGATCCTCGCC   4385
```

```
RC221929seq    1133 --------------------------------------------------   1132
RC221929       4386 GTCGGGCATGCTCGCCTTGAGCCTGGCGAACAGTTCGGCTGGCGCGAGCC   4435
RC221929seq    1133 --------------------------------------------------   1132
RC221929       4436 CCTGATGCTCTTCGTCCAGATCATCCTGATCGACAAGACCGGCTTCCATC   4485
RC221929seq    1133 --------------------------------------------------   1132
RC221929       4486 CGAGTACGTGCTCGCTCGATGCGATGTTTCGCTTGGTGGTCGAATGGGCA   4535
RC221929seq    1133 --------------------------------------------------   1132
RC221929       4536 GGTAGCCGGATCAAGCGTATGCAGCCGCCGCATTGCATCAGCCATGATGG   4585
RC221929seq    1133 --------------------------------------------------   1132
RC221929       4586 ATACTTTCTCGGCAGGAGCAAGGTGAGATGACAGGAGATCCTGCCCCGGC   4635
RC221929seq    1133 --------------------------------------------------   1132
RC221929       4636 ACTTCGCCCAATAGCAGCCAGTCCCTTCCCGCTTCAGTGACAACGTCGAG   4685
RC221929seq    1133 --------------------------------------------------   1132
RC221929       4686 CACAGCTGCGCAAGGAACGCCCGTCGTGGCCAGCCACGATAGCCGCGCTG   4735
RC221929seq    1133 --------------------------------------------------   1132
RC221929       4736 CCTCGTCTTGCAGTTCATTCAGGGCACCGGACAGGTCGGTCTTGACAAAA   4785
RC221929seq    1133 --------------------------------------------------   1132
RC221929       4786 AGAACCGGGCGCCCCTGCGCTGACAGCCGGAACACGGCGGCATCAGAGCA   4835
RC221929seq    1133 --------------------------------------------------   1132
RC221929       4836 GCCGATTGTCTGTTGTGCCCAGTCATAGCCGAATAGCCTCTCCACCCAAG   4885
RC221929seq    1133 --------------------------------------------------   1132
RC221929       4886 CGGCCGGAGAACCTGCGTGCAATCCATCTTGTTCAATCATGCGAAACGAT   4935
RC221929seq    1133 --------------------------------------------------   1132
RC221929       4936 CCTCATCCTGTCTCTTGATCGATCTTTGCAAAAGCCTAGGCCTCCAAAAA   4985
RC221929seq    1133 --------------------------------------------------   1132
RC221929       4986 AGCCTCCTCACTACTTCTGGAATAGCTCAGAGGCCGAGGCGGCCTCGGCC   5035
RC221929seq    1133 --------------------------------------------------   1132
RC221929       5036 TCTGCATAAATAAAAAAAATTAGTCAGCCATGGGGCGGAGAATGGGCGGA   5085
RC221929seq    1133 --------------------------------------------------   1132
RC221929       5086 ACTGGGCGGAGTTAGGGGCGGGATGGGCGGAGTTAGGGGCGGGACTATGG   5135
RC221929seq    1133 --------------------------------------------------   1132
RC221929       5136 TTGCTGACTAATTGAGATGCATGCTTTGCATACTTCTGCCTGCTGGGGAG   5185
RC221929seq    1133 --------------------------------------------------   1132
RC221929       5186 CCTGGGGACTTTCCACACCTGGTTGCTGACTAATTGAGATGCATGCTTTG   5235
RC221929seq    1133 --------------------------------------------------   1132
```

```
RC221929        5236 CATACTTCTGCCTGCTGGGGAGCCTGGGGACTTTCCACACCCTAACTGAC   5285
RC221929seq     1133 --------------------------------------------------   1132
RC221929        5286 ACACATTCCACAGCTGGTTCTTTCCGCCTCAGGACTCTTCCTTTTTCAAT   5335
RC221929seq     1133 --------------------------------------------------   1132
RC221929        5336 ATTATTGAAGCATTTATCAGGGTTATTGTCTCATGAGCGGATACATATTT   5385
RC221929seq     1133 --------------------------------------------------   1132
RC221929        5386 GAATGTATTTAGAAAAATAAACAAATAGGGGTTCCGCGCACATTTCCCCG   5435
RC221929seq     1133 --------------------------------------------------   1132
RC221929        5436 AAAAGTGCCACCTGACGCGCCCTGTAGCGGCGCATTAAGCGCGGCGGGTG   5485
RC221929seq     1133 --------------------------------------------------   1132
RC221929        5486 TGGTGGTTACGCGCAGCGTGACCGCTACACTTGCCAGCGCCCTAGCGCCC   5535
RC221929seq     1133 --------------------------------------------------   1132
RC221929        5536 GCTCCTTTCGCTTTCTTCCCTTCCTTTCTCGCCACGTTCGCCGGCTTTCC   5585
RC221929seq     1133 --------------------------------------------------   1132
RC221929        5586 CCGTCAAGCTCTAAATCGGGGGCTCCCTTTAGGGTTCCGATTTAGTGCTT   5635
RC221929seq     1133 --------------------------------------------------   1132
RC221929        5636 TACGGCACCTCGACCCCAAAAAACTTGATTAGGGTGATGGTTCACGTAGT   5685
RC221929seq     1133 --------------------------------------------------   1132
RC221929        5686 GGGCCATCGCCCTGATAGACGGTTTTTCGCCCTTTGACGTTGGAGTCCAC   5735
RC221929seq     1133 --------------------------------------------------   1132
RC221929        5736 GTTCTTTAATAGTGGACTCTTGTTCCAAACTGGAACAACACTCAACCCTA   5785
RC221929seq     1133 --------------------------------------------------   1132
RC221929        5786 TCTCGGTCTATTCTTTTGATTTATAAGGGATTTTGCCGATTTCGGCCTAT   5835
RC221929seq     1133 --------------------------------------------------   1132
RC221929        5836 TGGTTAAAAAATGAGCTGATTTAACAAAAATTTAACGCGAATTTT   5880
RC221929seq     1133 ------------------------------------------   1132
```

Appendix 2. *Alignment of sequenced region of RC221929 to complete plasmid sequence.* RC221929 was amplified by *E.Coli* transformation. Plasmids were isolated and sequenced as described in section 5.2.2. Start and stop codons are highlighted in green and red, respectively.

```
Predicted          1 AACAAAATATTAACGCTTACAATTTCCATTCGCCATTCAGGCTGCGCAAC     50
MR225748Seq        1 --------------------------------------------------      0
Predicted         51 TGTTGGGAAGGGCGATCGGTGCGGGCCTCTTCGCTATTACGCCAGCTGGC    100
MR225748Seq        1 --------------------------------------------------      0
Predicted        101 GAAAGGGGGATGTGCTGCAAGGCGATTAAGTTGGGTAACGCCAGGGTTTT    150
MR225748Seq        1 --------------------------------------------------      0
Predicted        151 CCCAGTCACGACGTTGTAAAACGACGGCCAGTGCCAAGCTGATCTATACA    200
MR225748Seq        1 --------------------------------------------------      0
Predicted        201 TTGAATCAATATTGGCAATTAGCCATATTAGTCATTGGTTATATAGCATA    250
MR225748Seq        1 --------------------------------------------------      0
Predicted        251 AATCAATATTGGCTATTGGCCATTGCATACGTTGTATCTATATCATAATA    300
MR225748Seq        1 --------------------------------------------------      0
Predicted        301 TGTACATTTATATTGGCTCATGTCCAATATGACCGCCATGTTGACATTGA    350
MR225748Seq        1 --------------------------------------------------      0
Predicted        351 TTATTGACTAGTTATTAATAGTAATCAATTACGGGGTCATTAGTTCATAG    400
MR225748Seq        1 --------------------------------------------------      0
Predicted        401 CCCATATATGGAGTTCCGCGTTACATAACTTACGGTAAATGGCCCGCCTG    450
MR225748Seq        1 --------------------------------------------------      0
Predicted        451 GCTGACCGCCCAACGACCCCCGCCCATTGACGTCAATAATGACGTATGTT    500
MR225748Seq        1 --------------------------------------------------      0
Predicted        501 CCCATAGTAACGCCAATAGGGACTTTCCATTGACGTCAATGGGTGGAGTA    550
MR225748Seq        1 --------------------------------------------------      0
Predicted        551 TTTACGGTAAACTGCCCACTTGGCAGTACATCAAGTGTATCATATGCCAA    600
MR225748Seq        1 --------------------------------------------------      0
Predicted        601 GTCCGCCCCCTATTGACGTCAATGACGGTAAATGGCCCGCCTGGCATTAT    650
MR225748Seq        1 --------------------------------------------------      0
Predicted        651 GCCCAGTACATGACCTTACGGGACTTTCCTACTTGGCAGTACATCTACGT    700
MR225748Seq        1 --------------------------------------------------      0
Predicted        701 ATTAGTCATCGCTATTACCATGGTGATGCGGTTTTGGCAGTACACCAATG    750
MR225748Seq        1 --------------------------------------------------      0
Predicted        751 GGCGTGGATAGCGGTTTGACTCACGGGGATTTCCAAGTCTCCACCCCATT    800
MR225748Seq        1 --------------------------------------------------      0
Predicted        801 GACGTCAATGGGAGTTTGTTTTGGCACCAAAATCAACGGGACTTTCCAAA    850
MR225748Seq        1 --------------------------------------------------      0
Predicted        851 ATGTCGTAATAACCCCGCCCCGTTGACGCAAATGGGCGGTAGGCGTGTAC    900
MR225748Seq        1 --------------------------------------------------      0
Predicted        901 GGTGGGAGGTCTATATAAGCAGAGCTCGTTTAGTGAACCGTCAGAATTTT    950
MR225748Seq        1 --------------------------------------------------      0
```

```
Predicted        951 GTAATACGACTCACTATAGGGCGGCCGGGAATTCGTCGACTGGATCCGGT   1000
                                                                ||||
MR225748Seq        1 ----------------------------------------------CGGT      4

Predicted       1001 ACCGAGGAGATCTGCCGCCGCGATCGCCATGGACTCAGAGTCAGATGCTC   1050
                     ||||||||||||||||||||||||||||||||||||||||||||||||||
MR225748Seq        5 ACCGAGGAGATCTGCCGCCGCGATCGCCATGGACTCAGAGTCAGATGCTC     54

Predicted       1051 TCAGTATCCCTGCATCCCGCGTCCAGATGGAGTCCTCTACAGCCTTTTAT   1100
                     ||||||||||||||||||||||||||||||||||||||||||||||||||
MR225748Seq       55 TCAGTATCCCTGCATCCCGCGTCCAGATGGAGTCCTCTACAGCCTTTTAT    104

Predicted       1101 GATTATCATGATAAATTGAGTCTTCTATGTGAGAACAATGTCATCTTCTT   1150
                     ||||||||||||||||||||||||||||||||||||||||||||||||||
MR225748Seq      105 GATTATCATGATAAATTGAGTCTTCTATGTGAGAACAATGTCATCTTCTT    154

Predicted       1151 TTCCACCATCTCTACCATTGTCCTGTACTCTCTGGTATTTCTCCTCAGCC   1200
                     ||||||||||||||||||||||||||||||||||||||||||||||||||
MR225748Seq      155 TTCCACCATCTCTACCATTGTCCTGTACTCTCTGGTATTTCTCCTCAGCC    204

Predicted       1201 TTGTGGGTAACAGCCTGGTTTTGTGGGTCTTGGTGAAGTATGAGAATCTA   1250
                     ||||||||||||||||||||||||||||||||||||||||||||||||||
MR225748Seq      205 TTGTGGGTAACAGCCTGGTTTTGTGGGTCTTGGTGAAGTATGAGAATCTA    254

Predicted       1251 GAGTCACTCACCAATATCTTCATCCTCAACCTGTGTCTCTCAGACCTGAT   1300
                     ||||||||||||||||||||||||||||||||||||||||||||||||||
MR225748Seq      255 GAGTCACTCACCAATATCTTCATCCTCAACCTGTGTCTCTCAGACCTGAT    304

Predicted       1301 GTTCTCCTGTCTACTGCCTGTGTTGATCTCAGCACAATGGAGTTGGTTTC   1350
                     ||||||||||||||||||||||||||||||||||||||||||||||||||
MR225748Seq      305 GTTCTCCTGTCTACTGCCTGTGTTGATCTCAGCACAATGGAGTTGGTTTC    354

Predicted       1351 TAGGTGACTTCTTCTGCAAGTTCTTCAACATGATCTTCGGCATCAGCCTC   1400
                     ||||||||||||||||||||||||||||||||||||||||||||||||||
MR225748Seq      355 TAGGTGACTTCTTCTGCAAGTTCTTCAACATGATCTTCGGCATCAGCCTC    404

Predicted       1401 TACAGCAGCATCTTCTTCCTTACCATCATGACCATCCACCGATACCTGTC   1450
                     ||||||||||||||||||||||||||||||||||||||||||||||||||
MR225748Seq      405 TACAGCAGCATCTTCTTCCTTACCATCATGACCATCCACCGATACCTGTC    454

Predicted       1451 TGTAGTGAGCCCCATCTCTACTCTGGGTATCCATACCCTCCGCTGCCGTG   1500
                     ||||||||||||||||||||||||||||||||||||||||||||||||||
MR225748Seq      455 TGTAGTGAGCCCCATCTCTACTCTGGGTATCCATACCCTCCGCTGCCGTG    504

Predicted       1501 TGCTGGTGACATCATGTGTGTGGGCAGCCAGCATCCTGTTCTCCATCCCT   1550
                     ||||||||||||||||||||||||||||||||||||||||||||||||||
MR225748Seq      505 TGCTGGTGACATCATGTGTGTGGGCAGCCAGCATCCTGTTCTCCATCCCT    554

Predicted       1551 GATGCTGTCTTCCACAAAGTGATCTCCTTAAATTGTAAATATTCTGAACA   1600
                     ||||||||||||||||||||||||||||||||||||||||||||||||||
MR225748Seq      555 GATGCTGTCTTCCACAAAGTGATCTCCTTAAATTGTAAATATTCTGAACA    604

Predicted       1601 TCATGGGTTCTTGGCCTCAGTCTACCAGCACAACATCTTCTTCCTCCTCT   1650
                     ||||||||||||||||||||||||||||||||||||||||||||||||||
MR225748Seq      605 TCATGGGTTCTTGGCCTCAGTCTACCAGCACAACATCTTCTTCCTCCTCT    654

Predicted       1651 CCATGGGAATCATCCTATTCTGTTATGTACAGATTCTCAGGACTTTGTTT   1700
                     ||||||||||||||||||||||||||||||||||||||||||||||||||
MR225748Seq      655 CCATGGGAATCATCCTATTCTGTTATGTACAGATTCTCAGGACTTTGTTT    704

Predicted       1701 CGCACAAGGTCCAGACAGAGACACCGAACAGTCAGGCTCATCTTCACCGT   1750
                     ||||||||||||||||||||||||||||||||||||||||||||||||||
MR225748Seq      705 CGCACAAGGTCCAGACAGAGACACCGAACAGTCAGGCTCATCTTCACCGT    754

Predicted       1751 CGTGGTAGCATACTTCCTCAGCTGGGCTCCCTACAACCTCACACTCTTCC   1800
                     ||||||||||||||||||||||||||||||||||||||||||||||||||
MR225748Seq      755 CGTGGTAGCATACTTCCTCAGCTGGGCTCCCTACAACCTCACACTCTTCC    804

Predicted       1801 TGAAAACTGGAATCATCCAGCAGAGCTGTGAGAGCCTTCAGCAACTGGAC   1850
                     ||||||||||||||||||||||||||||||||||||||||||||||||||
MR225748Seq      805 TGAAAACTGGAATCATCCAGCAGAGCTGTGAGAGCCTTCAGCAACTGGAC    854

Predicted       1851 ATTGCTATGATTATCTGTCGCCATTTGGCCTTCTCTCATTGCTGTTTCAA   1900
                     ||||||||||||||||||||||||||||||||||||||||||||||||||
MR225748Seq      855 ATTGCTATGATTATCTGTCGCCATTTGGCCTTCTCTCATTGCTGTTTCAA    904

Predicted       1901 CCCAGTGCTTTATGTCTTTGTTGGGATCAAGTTCCGCAGACACCTAAAAC   1950
                     ||||||||||||||||||||||||||||||||||||||||||||||||||
MR225748Seq      905 CCCAGTGCTTTATGTCTTTGTTGGGATCAAGTTCCGCAGACACCTAAAAC    954
```

```
Predicted       1951 ATCTCTTCCAGCAGGTCTGGCTGTGCCGGAAGACATCCAGCACTGTTCCC   2000
                     ||||||||||||||||||||||||||||||||||||||||||||||||||
MR225748Seq      955 ATCTCTTCCAGCAGGTCTGGCTGTGCCGGAAGACATCCAGCACTGTTCCC   1004

Predicted       2001 TGCTCCCCTGGTACCTTTACATATGAGGGACCCTCCTTCTACACGCGTAC   2050
                     ||||||||||||||||||||||||||||||||||||||||||||||||||
MR225748Seq     1005 TGCTCCCCTGGTACCTTTACATATGAGGGACCCTCCTTCTACACGCGTAC   1054

Predicted       2051 GCGGCCGCTCGAGCAGAAACTCATCTCAGAAGAGGATCTGGCAGCAAATG   2100
                     ||||||||||||||||||||||||||||||||||||||||||||||||||
MR225748Seq     1055 GCGGCCGCTCGAGCAGAAACTCATCTCAGAAGAGGATCTGGCAGCAAATG   1104

Predicted       2101 ATATCCTGGATTACAAGGATGACGACGATAAGGTTTAAA-------CGGC   2143
                     ||||||||||||||||||||||||||||||||||..|       .
MR225748Seq     1105 ATATCCTGGATTACAAGGATGACGACGATAAGGTTTNNANNNNNNNN---   1151

Predicted       2144 CGGCCGCGGTCATAGCTGTTTCCTGAACAGATCCCGGGTGGCATCCCTGT   2193

MR225748Seq     1152 --------------------------------------------------   1151

Predicted       2194 GACCCCTCCCCAGTGCCTCTCCTGGCCCTGGAAGTTGCCACTCCAGTGCC   2243

MR225748Seq     1152 --------------------------------------------------   1151

Predicted       2244 CACCAGCCTTGTCCTAATAAAATTAAGTTGCATCATTTTGTCTGACTAGG   2293

MR225748Seq     1152 --------------------------------------------------   1151

Predicted       2294 TGTCCTTCTATAATATTATGGGGTGGAGGGGGGTGGTATGGAGCAAGGGG   2343

MR225748Seq     1152 --------------------------------------------------   1151

Predicted       2344 CAAGTTGGGAAGACAACCTGTAGGGCCTGCGGGGTCTATTGGGAACCAAG   2393

MR225748Seq     1152 --------------------------------------------------   1151

Predicted       2394 CTGGAGTGCAGTGGCACAATCTTGGCTCACTGCAATCTCCGCCTCCTGGG   2443

MR225748Seq     1152 --------------------------------------------------   1151

Predicted       2444 TTCAAGCGATTCTCCTGCCTCAGCCTCCCGAGTTGTTGGGATTCCAGGCA   2493

MR225748Seq     1152 --------------------------------------------------   1151

Predicted       2494 TGCATGACCAGGCTCAGCTAATTTTTGTTTTTTTGGTAGAGACGGGGTTT   2543

MR225748Seq     1152 --------------------------------------------------   1151

Predicted       2544 CACCATATTGGCCAGGCTGGTCTCCAACTCCTAATCTCAGGTGATCTACC   2593

MR225748Seq     1152 --------------------------------------------------   1151

Predicted       2594 CACCTTGGCCTCCCAAATTGCTGGGATTACAGGCGTGAACCACTGCTCCC   2643

MR225748Seq     1152 --------------------------------------------------   1151

Predicted       2644 TTCCCTGTCCTTCTGATTTTAAAATAACTATACCAGCAGGAGGACGTCCA   2693

MR225748Seq     1152 --------------------------------------------------   1151

Predicted       2694 GACACAGCATAGGCTACCTGGCCATGCCCAACCGGTGGGACATTTGAGTT   2743

MR225748Seq     1152 --------------------------------------------------   1151

Predicted       2744 GCTTGCTTGGCACTGTCCTCTCATGCGTTGGGTCCACTCAGTAGATGCCT   2793

MR225748Seq     1152 --------------------------------------------------   1151

Predicted       2794 GTTGAATTGGGTACGCGGCCAGCGGCGAGCGGTATCAGCTCACTCAAAGG   2843

MR225748Seq     1152 --------------------------------------------------   1151

Predicted       2844 CGGTAATACGGTTATCCACAGAATCAGGGGATAACGCAGGAAAGAACATG   2893

MR225748Seq     1152 --------------------------------------------------   1151

Predicted       2894 TGAGCAAAAGGCCAGCAAAAGGCCAGGAACCGTAAAAAGGCCGCGTTGCT   2943
```

MR225748Seq	1152	----------	1151
Predicted	2944	GGCGTTTTTCCATAGGCTCCGCCCCCCTGACGAGCATCACAAAAATCGAC	2993
MR225748Seq	1152	----------	1151
Predicted	2994	GCTCAAGTCAGAGGTGGCGAAACCCGACAGGACTATAAAGATACCAGGCG	3043
MR225748Seq	1152	----------	1151
Predicted	3044	TTTCCCCCTGGAAGCTCCCTCGTGCGCTCTCCTGTTCCGACCCTGCCGCT	3093
MR225748Seq	1152	----------	1151
Predicted	3094	TACCGGATACCTGTCCGCCTTTCTCCCTTCGGGAAGCGTGGCGCTTTCTC	3143
MR225748Seq	1152	----------	1151
Predicted	3144	ATAGCTCACGCTGTAGGTATCTCAGTTCGGTGTAGGTCGTTCGCTCCAAG	3193
MR225748Seq	1152	----------	1151
Predicted	3194	CTGGGCTGTGTGCACGAACCCCCCGTTCAGCCCGACCGCTGCGCCTTATC	3243
MR225748Seq	1152	----------	1151
Predicted	3244	CGGTAACTATCGTCTTGAGTCCAACCCGGTAAGACACGACTTATCGCCAC	3293
MR225748Seq	1152	----------	1151
Predicted	3294	TGGCAGCAGCCACTGGTAACAGGATTAGCAGAGCGAGGTATGTAGGCGGT	3343
MR225748Seq	1152	----------	1151
Predicted	3344	GCTACAGAGTTCTTGAAGTGGTGGCCTAACTACGGCTACACTAGAAGAAC	3393
MR225748Seq	1152	----------	1151
Predicted	3394	AGTATTTGGTATCTGCGCTCTGCTGAAGCCAGTTACCTTCGGAAAAAGAG	3443
MR225748Seq	1152	----------	1151
Predicted	3444	TTGGTAGCTCTTGATCCGGCAAACAAACCACCGCTGGTAGCGGTGGTTTT	3493
MR225748Seq	1152	----------	1151
Predicted	3494	TTTGTTTGCAAGCAGCAGATTACGCGCAGAAAAAAAGGATCTCAAGAAGA	3543
MR225748Seq	1152	----------	1151
Predicted	3544	TCCTTTGATCTTTTCTACGGGGTCTGACGCTCAGTGGAACGAAAACTCAC	3593
MR225748Seq	1152	----------	1151
Predicted	3594	GTTAAGGGATTTTGGTCATGAGATTATCAAAAAGGATCTTCACCTAGATC	3643
MR225748Seq	1152	----------	1151
Predicted	3644	CTTTTAAATTAAAAATGAAGTTTTAAATCAATCTAAAGTATATATGAGTA	3693
MR225748Seq	1152	----------	1151
Predicted	3694	ACCTGAGGCTATGGCAGGGCCTGCCGCCCCGACGTTGGCTGCGAGCCCTG	3743
MR225748Seq	1152	----------	1151
Predicted	3744	GGCCTTCACCCGAACTTGGGGGGTGGGGTGGGGAAAAGGAAGAAACGCGG	3793
MR225748Seq	1152	----------	1151
Predicted	3794	GCGTATTGGCCCCAATGGGGTCTCGGTGGGGTATCGACAGAGTGCCAGCC	3843
MR225748Seq	1152	----------	1151
Predicted	3844	CTGGGACCGAACCCCGCGTTTATGAACAAACGACCCAACACCGTGCGTTT	3893
MR225748Seq	1152	----------	1151
Predicted	3894	TATTCTGTCTTTTTATTGCCGTCATAGCGCGGGTTCCTTCCGGTATTGTC	3943

```
MR225748Seq     1152 --------------------------------------------------   1151

Predicted       3944 TCCTTCCGTGTTTCAGTTAGCCTCCCCCTAGGGTGGGCGAAGAACTCCAG   3993

MR225748Seq     1152 --------------------------------------------------   1151

Predicted       3994 CATGAGATCCCCGCGCTGGAGGATCATCCAGCCGGCGTCCCGGAAAACGA   4043

MR225748Seq     1152 --------------------------------------------------   1151

Predicted       4044 TTCCGAAGCCCAACCTTTCATAGAAGGCGGCGGTGGAATCGAAATCTCGT   4093

MR225748Seq     1152 --------------------------------------------------   1151

Predicted       4094 GATGGCAGGTTGGGCGTCGCTTGGTCGGTCATTTCGAACCCCAGAGTCCC   4143

MR225748Seq     1152 --------------------------------------------------   1151

Predicted       4144 GCTCAGAAGAACTCGTCAAGAAGGCGATAGAAGGCGATGCGCTGCGAATC   4193

MR225748Seq     1152 --------------------------------------------------   1151

Predicted       4194 GGGAGCGGCGATACCGTAAAGCACGAGGAAGCGGTCAGCCCATTCGCCGC   4243

MR225748Seq     1152 --------------------------------------------------   1151

Predicted       4244 CAAGCTCTTCAGCAATATCACGGGTAGCCAACGCTATGTCCTGATAGCGA   4293

MR225748Seq     1152 --------------------------------------------------   1151

Predicted       4294 TCCGCCACACCCAGCCGGCCACAGTCGATGAATCCAGAAAAGCGGCCATT   4343

MR225748Seq     1152 --------------------------------------------------   1151

Predicted       4344 TTCCACCATGATATTCGGCAAGCAGGCATCGCCATGGGTCACGACGAGAT   4393

MR225748Seq     1152 --------------------------------------------------   1151

Predicted       4394 CCTCGCCGTCGGGCATGCTCGCCTTGAGCCTGGCGAACAGTTCGGCTGGC   4443

MR225748Seq     1152 --------------------------------------------------   1151

Predicted       4444 GCGAGCCCCTGATGCTCTTCGTCCAGATCATCCTGATCGACAAGACCGGC   4493

MR225748Seq     1152 --------------------------------------------------   1151

Predicted       4494 TTCCATCCGAGTACGTGCTCGCTCGATGCGATGTTTCGCTTGGTGGTCGA   4543

MR225748Seq     1152 --------------------------------------------------   1151

Predicted       4544 ATGGGCAGGTAGCCGGATCAAGCGTATGCAGCCGCCGCATTGCATCAGCC   4593

MR225748Seq     1152 --------------------------------------------------   1151

Predicted       4594 ATGATGGATACTTTCTCGGCAGGAGCAAGGTGAGATGACAGGAGATCCTG   4643

MR225748Seq     1152 --------------------------------------------------   1151

Predicted       4644 CCCCGGCACTTCGCCCAATAGCAGCCAGTCCCTTCCCGCTTCAGTGACAA   4693

MR225748Seq     1152 --------------------------------------------------   1151

Predicted       4694 CGTCGAGCACAGCTGCGCAAGGAACGCCCGTCGTGGCCAGCCACGATAGC   4743

MR225748Seq     1152 --------------------------------------------------   1151

Predicted       4744 CGCGCTGCCTCGTCTTGCAGTTCATTCAGGGCACCGGACAGGTCGGTCTT   4793

MR225748Seq     1152 --------------------------------------------------   1151

Predicted       4794 GACAAAAAGAACCGGGCGCCCCTGCGCTGACAGCCGGAACACGGCGGCAT   4843

MR225748Seq     1152 --------------------------------------------------   1151

Predicted       4844 CAGAGCAGCCGATTGTCTGTTGTGCCCAGTCATAGCCGAATAGCCTCTCC   4893

MR225748Seq     1152 --------------------------------------------------   1151
```

```
Predicted       4894 ACCCAAGCGGCCGGAGAACCTGCGTGCAATCCATCTTGTTCAATCATGCG   4943
MR225748Seq     1152 --------------------------------------------------   1151
Predicted       4944 AAACGATCCTCATCCTGTCTCTTGATCGATCTTTGCAAAAGCCTAGGCCT   4993
MR225748Seq     1152 --------------------------------------------------   1151
Predicted       4994 CCAAAAAAGCCTCCTCACTACTTCTGGAATAGCTCAGAGGCCGAGGCGGC   5043
MR225748Seq     1152 --------------------------------------------------   1151
Predicted       5044 CTCGGCCTCTGCATAAATAAAAAAAATTAGTCAGCCATGGGGCGGAGAAT   5093
MR225748Seq     1152 --------------------------------------------------   1151
Predicted       5094 GGGCGGAACTGGGCGGAGTTAGGGGCGGGATGGGCGGAGTTAGGGGCGGG   5143
MR225748Seq     1152 --------------------------------------------------   1151
Predicted       5144 ACTATGGTTGCTGACTAATTGAGATGCATGCTTTGCATACTTCTGCCTGC   5193
MR225748Seq     1152 --------------------------------------------------   1151
Predicted       5194 TGGGGAGCCTGGGGACTTTCCACACCTGGTTGCTGACTAATTGAGATGCA   5243
MR225748Seq     1152 --------------------------------------------------   1151
Predicted       5244 TGCTTTGCATACTTCTGCCTGCTGGGGAGCCTGGGGACTTTCCACACCCT   5293
MR225748Seq     1152 --------------------------------------------------   1151
Predicted       5294 AACTGACACACATTCCACAGCTGGTTCTTTCCGCCTCAGGACTCTTCCTT   5343
MR225748Seq     1152 --------------------------------------------------   1151
Predicted       5344 TTTCAATATTATTGAAGCATTTATCAGGGTTATTGTCTCATGAGCGGATA   5393
MR225748Seq     1152 --------------------------------------------------   1151
Predicted       5394 CATATTTGAATGTATTTAGAAAAATAAACAAATAGGGGTTCCGCGCACAT   5443
MR225748Seq     1152 --------------------------------------------------   1151
Predicted       5444 TTCCCCGAAAAGTGCCACCTGACGCGCCCTGTAGCGGCGCATTAAGCGCG   5493
MR225748Seq     1152 --------------------------------------------------   1151
Predicted       5494 GCGGGTGTGGTGGTTACGCGCAGCGTGACCGCTACACTTGCCAGCGCCCT   5543
MR225748Seq     1152 --------------------------------------------------   1151
Predicted       5544 AGCGCCCGCTCCTTTCGCTTTCTTCCCTTCCTTTCTCGCCACGTTCGCCG   5593
MR225748Seq     1152 --------------------------------------------------   1151
Predicted       5594 GCTTTCCCCGTCAAGCTCTAAATCGGGGGCTCCCTTTAGGGTTCCGATTT   5643
MR225748Seq     1152 --------------------------------------------------   1151
Predicted       5644 AGTGCTTTACGGCACCTCGACCCCAAAAAACTTGATTAGGGTGATGGTTC   5693
MR225748Seq     1152 --------------------------------------------------   1151
Predicted       5694 ACGTAGTGGGCCATCGCCCTGATAGACGGTTTTTCGCCCTTTGACGTTGG   5743
MR225748Seq     1152 --------------------------------------------------   1151
Predicted       5744 AGTCCACGTTCTTTAATAGTGGACTCTTGTTCCAAACTGGAACAACACTC   5793
MR225748Seq     1152 --------------------------------------------------   1151
Predicted       5794 AACCCTATCTCGGTCTATTCTTTTGATTTATAAGGGATTTTGCCGATTTC   5843
MR225748Seq     1152 --------------------------------------------------   1151
Predicted       5844 GGCCTATTGGTTAAAAAATGAGCTGATTTAACAAAAATTTAACGCGAATT   5893
MR225748Seq     1152 --------------------------------------------------   1151
```

```
Predicted       5894 TT   5895
MR225748Seq     1152 --   1151
```

Appendix 3. *Alignment of sequenced region of MR225748 to complete plasmid sequence.* MR225748 was amplified by *E.Coli* transformation. Plasmids were isolated and sequenced as described in section 5.2.2. Start and stop codons are highlighted in green and red, respectively.

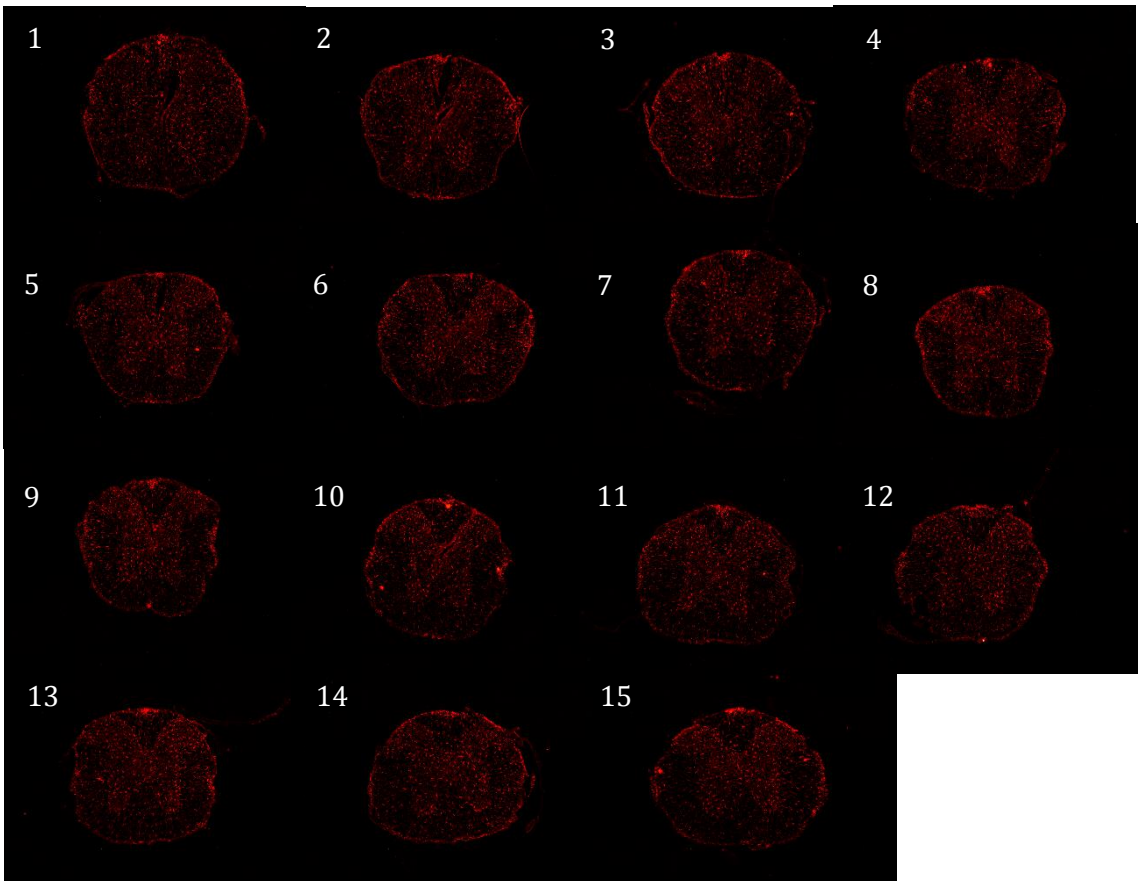

Appendix 4. *Iba-1 reactivity along the rostrocaudal axis of the thoracic cord of a 6 month female TDP-Q331K mouse.* 30µm sections were made along the collected thoracic cord samples. Sections are numbered in ascending order from the most rostral to most caudal segment. Images presented represent sections at intervals of approximately 450-540µm and are estimated to originate between levels T7 and T13.

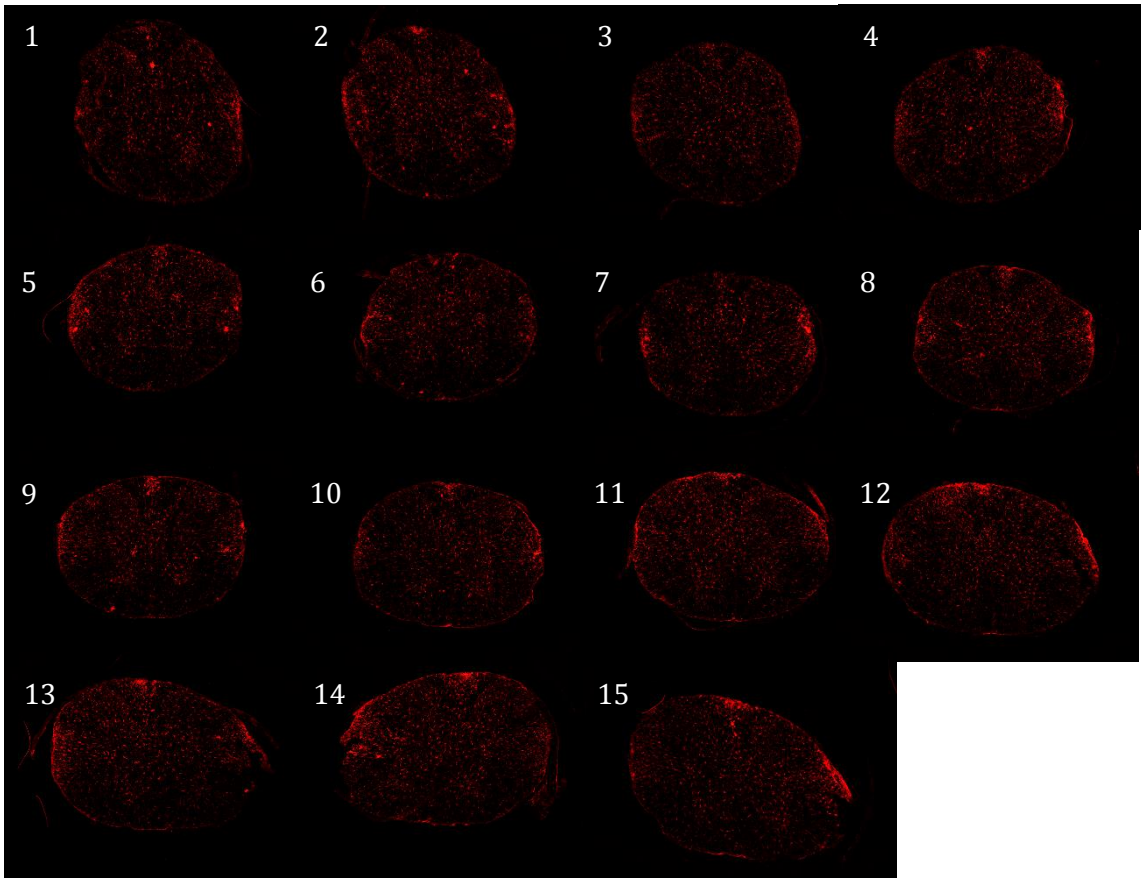

Appendix 5. *Iba-1 reactivity along the rostrocaudal axis of the thoracic cord of a 10 month female TDP-Q331K mouse.* 30μm sections were made along the collected thoracic cord samples. Sections are numbered in ascending order from the most rostral to most caudal segment. Images presented represent sections at intervals of approximately 450-540μm and are estimated to originate between levels T7 and T13.

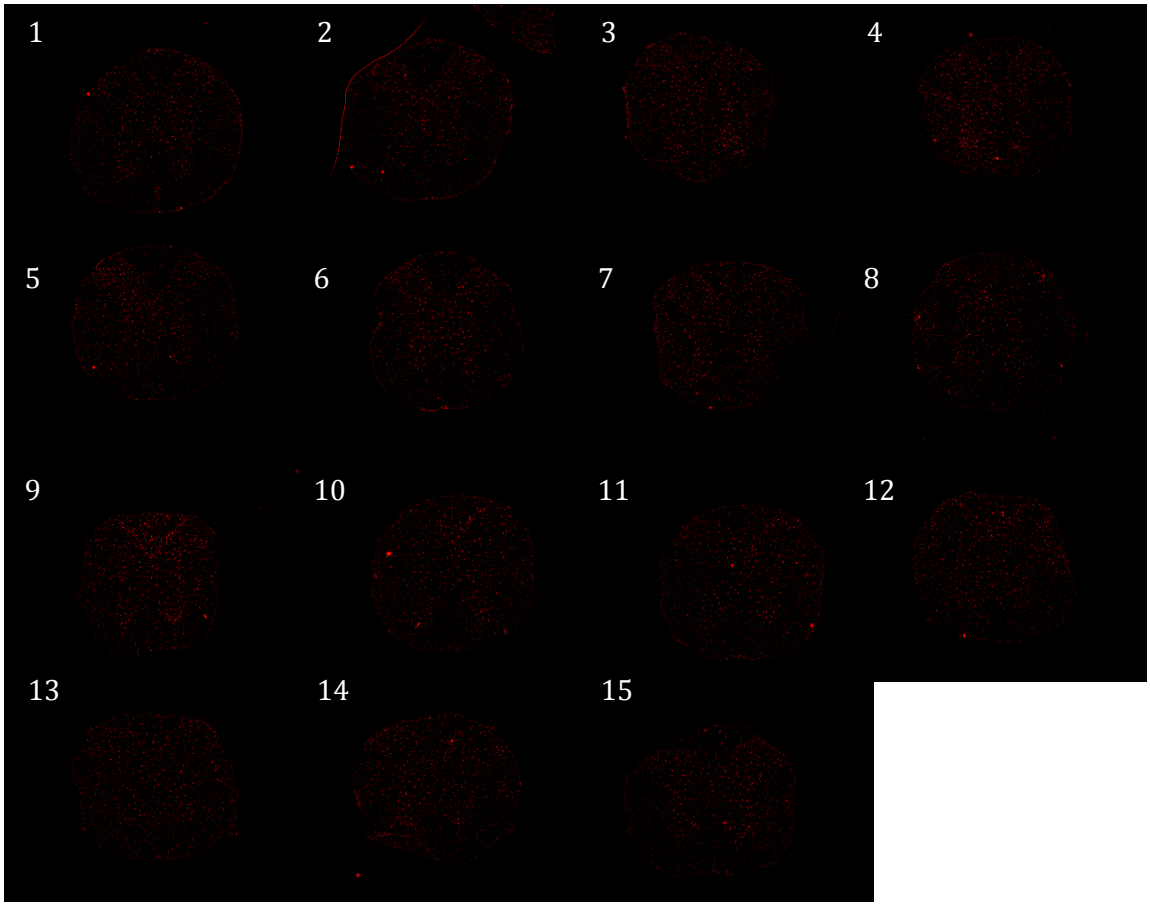

Appendix 6. *Iba-1 reactivity along the rostrocaudal axis of the thoracic cord of a 10 month female NTg mouse.* 30μm sections were made along the collected thoracic cord samples. Sections are numbered in ascending order from the most rostral to most caudal segment. Images presented represent sections at intervals of approximately 450-540μm and are estimated to originate between levels T7 and T13.

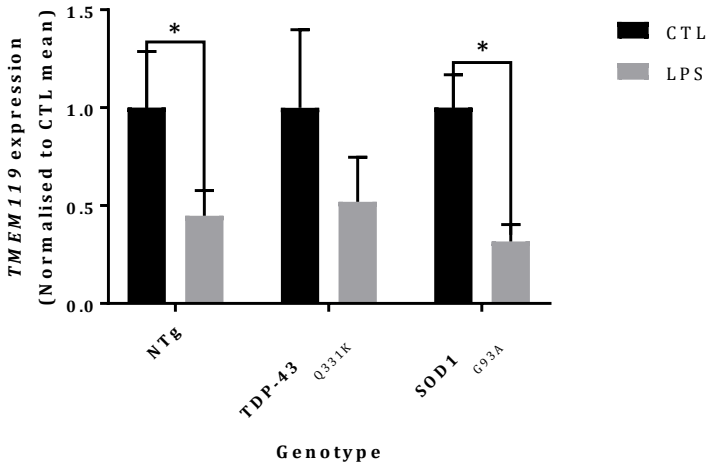

Appendix 7. *Evaluation of TMEM119 in primary microglial cultures obtained from NTg, TDP-Q331K and SOD1-G93A mice following LPS treatment.* LPS treatment results in the consistent decrease of TMEM119 expression within primary microglial cultures, irrespective of genotype. This decrease was considered significant for the evaluations performed of NTg and SOD1-G93A cultures (*, $p<0.05$).